IMAGE-BASED SOIL PARTICLE SIZE AND SHAPE CHARACTERIZATION

by

Hyon-Sohk Ohm

A dissertation submitted in partial fulfillment
of the requirements for the degree of
Doctor of Philosophy
(Civil Engineering)
in the University of Michigan
2013

Doctoral Committee:

Professor Roman D. Hryciw, Chair
Professor Radoslaw Michalowski
Assistant Professor Silvio Savarese
Assistant Professor Dimitrios Zekkos

DEDICATION

To my wife Hyesung and my son Henry

ACKNOWLEDGEMENTS

First of all, I would like to thank to my advisor, Dr. Hryciw, who supported me throughout this long journey by offering me motivation and encouragement. I would like to thank to the other committee members, Dr. Michalowski, Dr. Savarese, and Dr. Zekkos for their invaluable advice. I would like to thank to Mr. Rick Burch and Mr. Bob Fischer for their advice on design and construction of two laboratory devices. I would like to thank to all of the other members in geotechnical engineering group including Dr. Athanasopoulos-Zekkos, Dr. Gray, Dr. Woods and my colleagues for sharing their expertise and friendship. Lastly, Hyesung and I would like to thank to our parents for always trusting in us and for their unconditional love toward us.

TABLE OF CONTENTS

LIST OF TABLES

LIST OF FIGURES

Figure

LIST OF APPENDICES

ABSTRACT

Two laboratory tests using image-based methods to determine particle size distribution of soil were developed. The Sediment Imaging or “Sedimaging” test determines size distribution of soil having particle diameters between 0.075 mm and 2 mm. A Translucent Segregation Table (TST) test determines size distribution of soil having particle diameter larger than 2 mm. Both tests produce particle size distributions that compare well with results by sieving.

The Sedimaging test utilizes a statistical method based on wavelet transformation of images to produce a particle size distribution. The wavelet transformation method requires images of relatively uniform particle sizes, thus sedimentation of a soil specimen through a column filled with water is implemented in the Sedimaging test device to segregate particles by size. An image of the sedimented soil is analyzed incrementally by overlapping 128 pixel × 128 pixel areas yielding thousands of values of a wavelet index (*CA*). The *CA* values are converted to particle sizes in units of pixels per particle diameter (*PPD*) through a previously established calibration curve. The calibration curve is an empirical fit to *CA* versus *PPD* data obtained from images of pre-sieved soils. The *PPD* is converted to sieve opening size using the known camera magnification.

The TST test utilizes a deterministic method facilitated by watershed segmentation. The watershed segmentation requires thresholded images, thus a translucent plate and a backlight table are implemented in the TST system to provide a bright and uniform grayscale contrast to

the soil particles. Particles are introduced at the top of the inclined TST and are allowed to pass beneath the series of bridges having decreasing underpass heights. The bridges prevent small particles from hiding beneath large particles. After capturing an image of roughly segregated particles from above, touching particles in the image are segmented by the watershed segmentation. For each segmented particle, the largest and intermediate dimensions are computed by fitting an ellipse to the particle. The smallest dimension, which is not shown in the TST image, is estimated from the average of two bounding bridge heights between which each particle comes to rest on the TST. To correct the intermediate dimension to sieve opening size, a correction factor is derived based on the ratio between the intermediate and smallest dimensions.

CHAPTER I

Introduction: Advantages of Image-Based Methods Over Sieving

1.1 Introduction

Traditionally, grain size distribution of soil particles larger than U.S. Standard Sieve No. 200 (0.075 mm openings) is determined by a sieving test. While it would be impossible to accurately estimate the number of sieve tests performed annually worldwide, the number must surely be at least in the tens of thousands. With the possible exception of water content tests, it is the most common soil test performed. Along with the Atterberg limits tests, sieving is requisite for soil classification of coarse-grained soils. It is also the basis for quality control of aggregate materials placed beneath pavements and for concrete.

However, sieving is energy intensive, time consuming and relatively costly in terms of equipment maintenance and replacement of damaged or worn sieves. Sieving is also unattractive from the perspective of the laboratory environment; it is noisy, dusty, consumes water and generates vibrations which may affect nearby operations of sensitive laboratory equipment. By contrast, image-based techniques are rapid, environmentally friendly and sustainable as they do not wear out of damage hardware and require less water and energy consumption.

1.2 The Sieving Sequence and Testing Time

A typical sieve test sequence begins with specimen drying to obtain its dry weight. The specimen is then washed over a No. 200 sieve to obtain the percentage of fines and, or to collect the fines for hydrometer testing. The wash times for samples can range from 5 minutes for uniform clean sands to more than an hour for well graded silty of clayey materials or crushed concrete. After washing, the specimen must again be dried to compute the "percentage loss by wash". Drying is performed in ovens or in pans over gas burners or electric coils. The duration of drying may range from 20 minutes for sand to several hours for slags. After drying, the soils must cool to room temperature prior to sieving to prevent sieve damage and heat injuries to lab personnel. The actual sieving through a stack of 6 sieves takes 10 to 11 minutes. Each sieve is then weighed and the weights are recorded. Each sieve must be cleaned with a brush appropriate for its mesh to remove lodged particles. The cleaning and weighing requires 2 to 3 minutes per sieve.

Overall, the minimum time required for performing a sieve test is easily more than 30 minutes excluding the time required for drying, cooling, initial weighing, washing, re-drying and re-cooling. With these additional steps, the average test time easily exceeds 1 hour per test.

1.3 Damage to Sieves and System Maintenance

Damage to sieves commonly occurs during cleaning by brushing. No. 200 sieves are the mostly commonly damaged as they have the finest thread diameters. However, sieves as large as the No. 30 sieves (0.600 mm openings) also become damaged with time. Besides damage during brushing, sieve openings may be stretched due to overloading. To prevent overloading, scalper screens (sieves placed between specification sieves) are occasionally used to reduce the

maximum weight retained on any one sieve. Specimens with very poor gradations may need to be broken up into smaller portions and hand shaken.

Maintaining the sieves' dimensional specifications for accuracy of results is essential. Thus, sieve tolerances are checked every six months or whenever there is a question regarding accuracy. Sieves not meeting specifications must be discarded and replaced. The costs of sieving must also include maintenance of shakers and annual (or more frequent if there is a question of accuracy) calibration of laboratory scales.

1.4 Environmental Concerns Associated with Sieving

Besides the obvious power consumption associated with running sieve shakers, the volume of water required for washing ranges from 7.56 liters (2 gallons) to more than 37.8 liters (10 gallons) per specimen depending on soil type. Thus, both energy and considerable water is consumed in sieving. There is also a potential health hazard from emission and inhalation of dust. Even pre-washed specimens can generate dust due to abrasion and breakage of fines from coarser particles during shaking. Using enclosed shakers, ventilation systems or respirators may somewhat abate the concern for dust inhalation. However, the production of dust also raises the question of test accuracy. Simply put, if the dust particles are a result of the abrasion of coarser particles then the resulting grain size distribution is slightly inaccurate. This may be particularly important in crushed limestones and crushed concretes to be used for aggregate. This problem is exacerbated by the fact that sieve analysis typically provides only eight points for a gradation curve and that modification of a single point on the curve could significantly amplify inaccurate classifications of soils.

1.5 Evaluation of Vibration and Noise due to Sieving

The levels of vibration and noise due to typical sieve shaking in a laboratory were evaluated in the Geotechnical Engineering Laboratory at the University of Michigan. Figure 1.1 illustrates the testing setup.

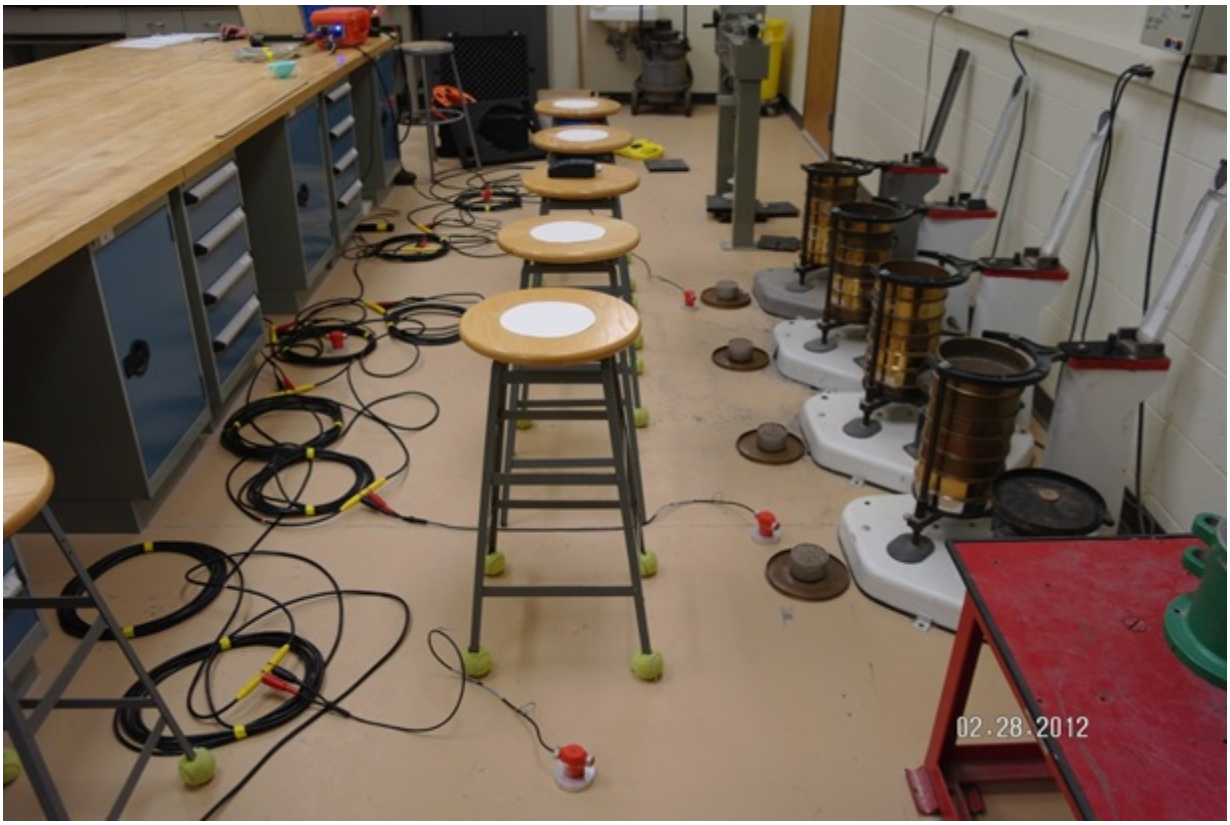

Figure 1.1 Testing setup to evaluate vibration and noise from sieve shakers

Four sieve shakers were used. To measure vibrations from the sieve shakers, nine 4.5 Hz geophones were placed in a radial pattern (Figure 1.2). Additionally, a digital sound meter was used to measure noise levels. Peak ground velocity (PGV) and noise were recorded from the simultaneous use of four sieve shakers. The PGV at about 3 feet from 4 shakers operating simultaneously was measured as 0.04 cm/sec (0.016 in/sec) and noise levels were measured as 89 to 90 dB. Considering that construction vibration damage criteria is 0.5 in/sec in PGV for

reinforced-concrete building and 0.12 in/sec in PGV for buildings extremely susceptible to vibration damage (Hanson et al. 2006), the vibrations from sieve shakers would not cause any damage to buildings.

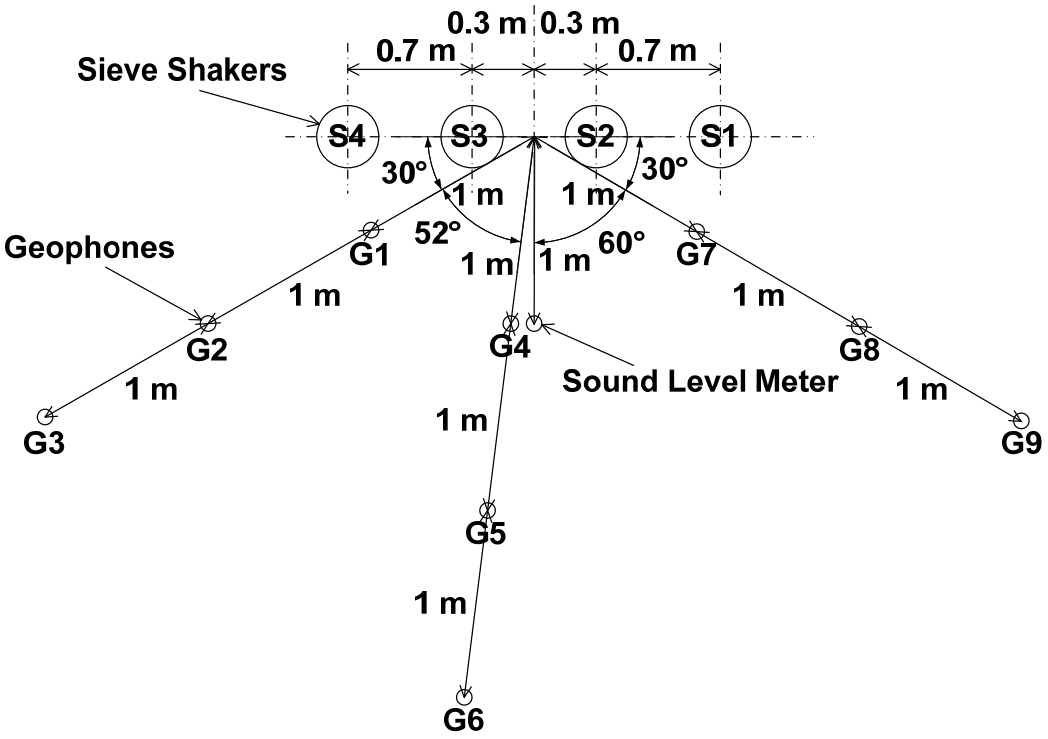

Figure 1.2 A plan view of the testing setup for vibration monitoring

However, the vibration and noise from sieve shakers to human perception may not be insignificant. Even relatively low levels of vibration may be problematic in extremely sensitive laboratory situations in which vibration-sensitive equipment such as electron microscopes are used. Also, noise pollution can cause health problems such as hearing damage, cardiovascular disease, sleep disorder, and metal health.

1.6 Grain Size Distribution by Image Analysis

Image analysis is widely adopted by pharmaceutical industries, powder technology, and food industries to determine particle size distributions for quality control purposes. This dissertation presents two tests using image-based methods to determine particle size distribution of soil. *Sediment Imaging* or *Sedimaging* test determines particle size distribution for particles in the range between U.S. Standard Sieve No. 200 (0.075 mm openings) and U.S. Standard Sieve No. 10 (2.00 mm openings). *Translucent Segregation Table* or *TST* test determines particle size distribution for particles in the range between U.S. Standard Sieve No. 10 (2.00 mm openings) and U.S. Standard Sieve 1 ½ in. (35 mm openings) or more.

The advantages of determination of grain size distribution by image analysis over sieving include shorter testing time, lower energy consumption and improvement to the laboratory environment. The Sedimaging test takes a total 15 to 20 minutes to perform. If the percentage of fines does not need to be determined the soil sample does not have to be dried or weighed and the testing time is even less. If, however, the percent of fines must be determined, the soil sample does have to be dried (but only once) and weighed. Preparation of the soil for the Sedimaging test requires much less time than what the sieve test requires for drying, cooling, washing, drying and cooling again, all prior to actual sieving.

By contrast to sieving, the Sedimaging test creates no noise or vibration. Also by contrast to sieving and subsequent cleaning of the sieves, there is no dust created during Sedimaging. The Sedimaging test is also much more efficient than the sieve test in terms of energy. The only power consumption is by a computer controlled camera. Only about 7.56 liters (2 gallons) of water are used in the Sedimaging test to fill a sedimentation column, make a soil-water mixture,

and clean the column. This is much less than the amount of water consumed in determining loss by wash in the sieve test. A 5 cent rubber balloon is used to create a vacuum inside the pre-segregation tube. This is the only material consumed in the Sedimaging test, but even it can be reused several times. There is no wear on the aluminum sedimentation column and an aluminum sediment accumulator when cleaning the device.

Sedimaging also improves significantly the quality assurance of the data by minimizing the potential for measurement, copying or calculation errors as well as other errors associated with transportation and handling of the samples from the sieves to the scales. Another advantage of Sedimaging over sieving is that it provides a permanent visual record of the soil. The image provides a visible profile of the segregated soil column which shows particle colors, shapes and textures. About 5,000 data points are obtained in a Sedimaging test compared to typically 8 by sieving. The Sedimaging software automatically computes grain size distribution metrics including the coefficients of uniformity and gradation without interpolation between points. Eventually, Sedimaging software may yield information on particle shapes and fabric, neither of which is obtainable by sieving.

Finally, while sieving systems come in a variety of arrangements and features such that their system costs are somewhat variable, the typical average cost is certainly higher than that of a Sedimaging system. In the future, as the price of digital cameras continues to drop the economic advantage of Sedimaging will continue to increase.

1.7 Scope of Study

Chapter I compares the sieving and Sedimaging tests in terms of time, cost, environmental issues including noise and vibration. This work resulted in a paper titled "Sustainable Soil Particle Size Characterization through Image Analysis" (Ohm et al. 2012) and published in the Proceedings of the 17th Great Lakes Geotechnical and Geoenvironmental Conference.

Chapter II includes evaluation of commercial systems for grain size distribution determination of soil and image analysis methods to determine particle size and shape of soil. This work was part of a report titled "Feasibility of Digital Imaging to Characterize Earth Materials" (Hryciw and Ohm 2012).

Chapter III covers the Sedimaging apparatus, test procedures, and wavelet transformation for image analysis. Particle size distributions obtained from sieving and the Sedimaging are compared. Effects of surface textures on a calibration curve, correlation between energy ratio and particle orientation, and segmentation using mean-shift clustering are also discussed. This chapter resulted in several papers including "Particle Shape Determination in a Sedimaging Device" (Ohm and Hryciw 2012) published in the Proceedings of the 2012 World Congress on Advances in Civil, Environmental, and Materials Research, "The Theoretical Basis for Optical Granulometry by Wavelet Transformation" (Hryciw et al. 2013) submitted to the Journal of Computing in Civil Engineering, "Size Distribution of Coarse-Grained Soil by Sedimaging" (Ohm and Hryciw 2013b) submitted to the Journal of Geotechnical and Geoenvironmental Engineering, and "Soil Fabric Characterization by Wavelet Transformation of Images" (Ohm and Hryciw 2014) abstract submitted to Geo-Congress 2014.

Chapter IV covers the Translucent Segragation Table apparatus, test procedure, and watershed segmentation for image analysis. Particle size distributions obtained from sieving and the TST are compared. Over-segmentation from watershed segmentation results, volume-based distribution using bridge heights, and a correction factor applied to the minor axis dimension are also discussed. This work will be published as a paper titled "The Translucent Segregation Table Test for Sand and Gravel Particle Size Distribution" (Ohm and Hryciw 2013c) in the ASTM Geotechnical Testing Journal.

Chapter V suggests future directions including a higher magnification camera on image-based methods, a linear calibration curve by wavelet transformation, and morphological opening as an alternative to wavelet transformation to analyze sedimented soil images. This chapter yielded several papers including "Enhanced Soil Characterization through Advances in Imaging Technology" (Ohm and Hryciw 2013a) submitted to the proceedings of the 18th International Conference on Soil Mechanics and Geotechnical Engineering, and "Morphological Opening to Determine Particle Size Distributions of Sedimented Soil Images" (Ohm et al. 2014) prepared for submission to the Powder Technology.

CHAPTER II

Literature Review

2.1 Commercial Systems for Determination of Particle Size Distributions

In recent decades new particles-sizing techniques have been developed that utilize advanced technologies: 1) x-ray absorption, 2) electrical sensing zone, 3) laser diffraction, 4) single particle optical sizing, and 5) image analysis (Abbireddy and Clayton 2009). Figure 2.1 shows the particle size range that can be determined using various systems that utilize these technologies.

X-ray absorption technique measures the concentration of particles with time as they sediment through liquid (Stein 1985). Particle size is determined based on Stokes' law just as with hydrometer test. One system utilizing x-ray absorption technique (SediGraph III 5120 by micromeritics) determines particle sizes ranging from 0.1 μm to 300 μm.

The electrical sensing zone method measures the change in resistance when a particle passes through a small aperture (Jackson et al. 1995) The volume of the particle passing through the aperture is proportional to the amplitude of the measured electrical impedance. A system utilizing the electrical sensing zone technique (Elzone II 5390 by micromeritics) determines particle sizes ranging from 0.4 μm to 240 μm.

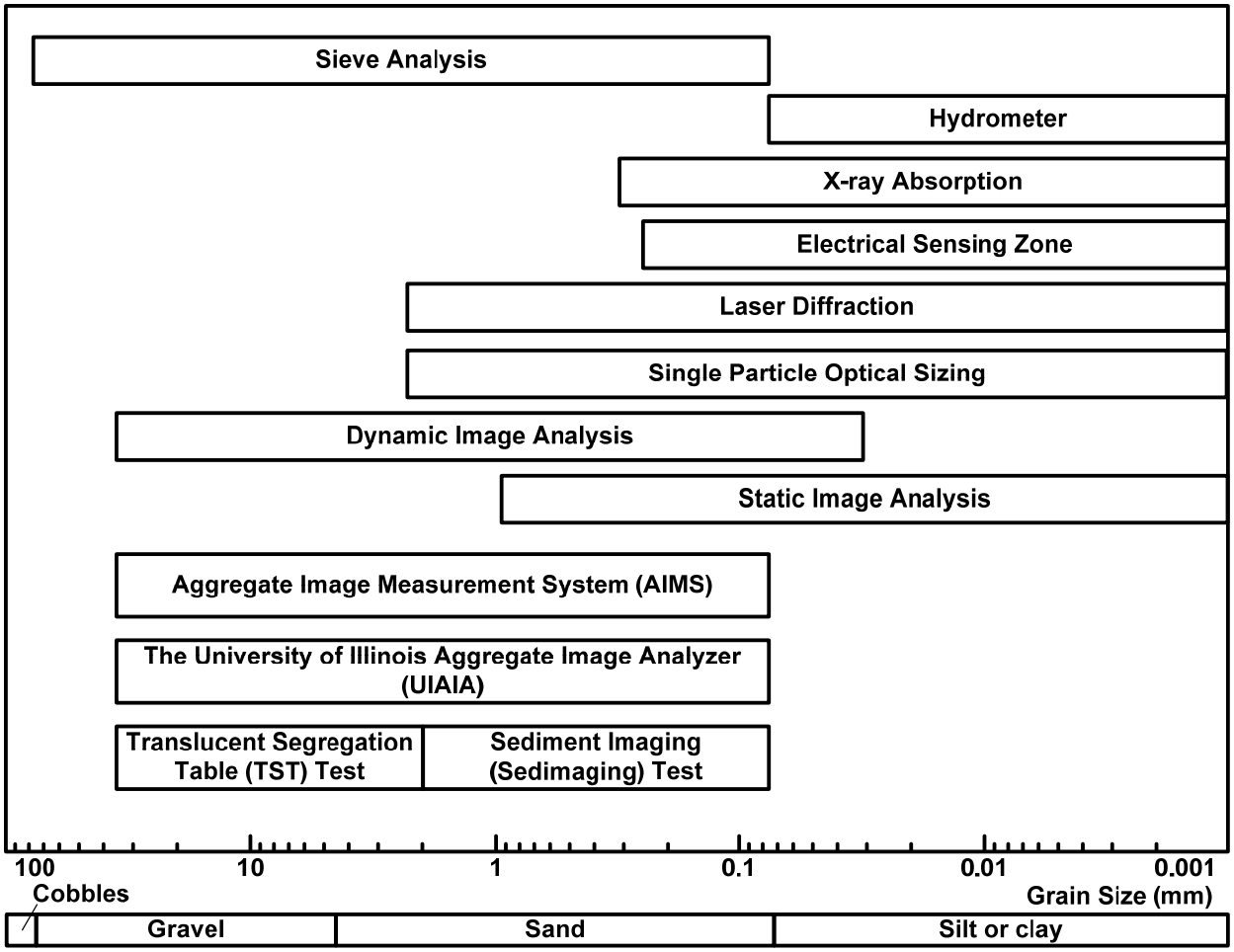

Figure 2.1 Comparison of particle sizing ranges for various systems

The laser diffraction method is based on the principle that particles of a given size diffract light through an angle that increases with decreasing particle size (Hayton et al. 2001). Particle size is then determined by Mie theory that describes the relationship between the angular distribution of light intensity and particle radius (Wen et al. 2002). A system utilizing laser diffraction method (Saturn DigiSizer II by micromeritics) determines particle sizes ranging from 0.04 μm to 2500 μm.

The single particle optical sizing method detects individual particles as they fall through a detection zone and through a laser beam (White 2003). The magnitude of the scattered or blocked light received by the detector is then related to the diameter of the particle. A system utilizing single particle optical sizing method (Agilent 7080 AccuSizer by Agilent Technologies) determines particle sizes ranging from 0.5 μm to 2500 μm.

Some methods based on image analysis utilize cameras to capture images of particles while they fall from a conveyer belt (dynamic image analysis) or while lying down on a flat table (static image analysis). A commercial system utilizing dynamic image analysis (CAMSIZER by Retsch Technology) determines particle sizes ranging from 30 μm to 30 mm and one utilizing static image analysis (PSA300 by HORIBA) determines particle sizes ranging from 0.5 μm to 1000 μm.

One of the main advantages of image analysis over other particles-sizing techniques described here is that not only particle size but also particle shape can be determined. Because of that, researchers working in pavement applications developed a system utilizing image analysis to characterize particle shape, angularity, and surface roughness and correlate them to pavement performance. The Aggregate Image Measurement System (AIMS) uses a variable magnification microscope-camera system to characterize shape for particles ranging from 0.075 mm to 37.5 mm in size (Gates et al. 2011). The thickness of a particle is obtained by focusing on a table first and moving the camera up to focus on the particle surface (Fletcher et al. 2003). The particle shape, angularity, and surface roughness were quantified by AIMS and correlated to pavement performance (Masad et al. 2000; Masad et al. 2001; Fletcher et al. 2002; Chandan et al. 2004; Al-Rousan et al. 2005; Al-Rousan et al. 2007; Mahmoud and Masad 2007; Mahmoud et al. 2010).

The University of Illinois Aggregate Image Analyzer (UIAIA) uses three orthogonally captured images to characterize shape for particles ranging from 0.075 mm to 25 mm size (Tutumluer et al. 2005). The particle shape, angularity, and surface roughness were quantified by the UIAIA and correlated to pavement performance (Rao and Tutumluer 2000; Tutumluer et al. 2000; Rao et al. 2001; Rao et al. 2002; Tutumluer et al. 2005; Pan and Tutumluer 2006; Pan et al. 2006; Tutumluer and Pan 2008; Mishra et al. 2010). A review of imaging methods for characterizing aggregates shape texture and angularity based on test repeatability, reproducibility, accuracy and applicability is provided by Masad and Tutumluer (2007).

The new image-based particle size analyzers, Sedimaging and TST, developed at the University of Michigan aim to reduce costs compared to the CAMSIZER and to reduce the time required for sample preparation compared to the AIMS or UIAIA systems. It should be noted that the AIMS and UIAIA systems characterize individual particles whereas Sedimaging and TST do not require physical separation of particles by taking advantage of uniquely developed image analysis methods.

2.2 Image-Based Methods for Determination of Particle Size Distributions

Image-based methods for determination of soil particle size distribution are divided into two broad categories: deterministic methods and statistical methods (Shin and Hryciw 2004). Deterministic methods use edge detection or gray scale thresholding for segmenting particles and counting the pixels in the segmented particles, whereas statistical methods represent an image by index values based on image texture. Texture is defined by the repeating patterns in an image.

When deterministic methods are used for non-contacting particles, the particles are placed on a translucent flat surface and a backlight intensity is adjusted so that the background of the soil image is pure white (Raschke and Hryciw 1997). This enables easy thresholding to segment the soil particles. Prior to photographing, the soil particles have to be detached from one another, otherwise touching particles would be interpreted as larger single particles.

To eliminate the need for detaching the particles, watershed segmentation was proposed to segment the particles when they are touching each other (Ghalib and Hryciw 1999). To increase the sample size, images of adjacent fields of view may be stitched along their image boundaries to create a single global mosaic image (Ghalib and Hryciw 1999).

Still, the particle size distribution in an assembly of soil images containing contacting and overlapping soil particles cannot be easily determined by deterministic methods and the problem may be impossible to overcome if the particles have a significant size range. Statistical methods were therefore developed to determine particle size distribution in a 3-D assembly of particles. One of the statistical methods called wavelet transformation decomposes a soil image of $2^n \times 2^n$ pixels size into n decomposition levels (Shin and Hryciw 2004). The energy of a transform coefficient matrix represents texture information at each wavelet decomposition level. The number of pixel per particle diameter (*PPD*) was introduced by Ghalib et al. (1998) to express the perceived size of soil particle in an image. As the *PPD* increases, the concentration of energy moves toward higher decomposition levels. The centroid of the area beneath the normalized energy profiles with respect to the vertical axis or wavelet index (*CA*) was correlated to *PPD* to produce a calibration curve (Hryciw et al. 2006; Hryciw et al. 2009). The TST utilizes a deterministic method for image analysis based on watershed analysis while the Sedimaging test utilizes a statistical method for image analysis based on wavelet transformation.

Other statistical methods, edge pixel density (EPD) and mathematical morphology, were proposed for determination of soil particle size from images of relatively uniform contacting particles (Jung 2010). EPD is defined as the ratio of edge pixels to total pixels in an image. The edge pixels are obtained by utilizing the Canny edge detection modified by removal of short false edges caused by internal texture. A correlation between EPD and *PPD* was found just as between *CA* and *PPD* from wavelet transformation. Morphological opening is defined as erosion followed by dilation in mathematical morphology. The morphological opening removes objects smaller than a structuring element. The pattern spectrum value (PSV) is defined as the difference of the summation of all pixel values in an image obtained by opening the original image using a consecutive structuring element size (SES). SES corresponding to a peak PSV was correlated with *PPD*. Chapter 5.4 will discuss mathematical morphology in more detail.

2.3 Conventional Particle Shape Determination

As mentioned earlier, one of the main advantages of use of image analysis on particle sizing might be its capability of determining particle shape. Particle shape can be characterized by its scale into three categories: form, roundness, and surface texture (Barrett 1980) as shown in Figure 2.3. Form is the largest scale property that reflects variations at the particle level. Roundness is the intermediate scale property that reflects variations at the particle corners. Surface texture is the smallest scale property that reflects variations at the particle surfaces between corners or superimposed on corners. Form, roundness, and surface texture are essentially independent measures of shape that can vary widely without affecting the other two properties.

The form and the roundness of the particle can be described by two common dimensionless parameters: sphericity and roundness (Wadell 1932). Sphericity is defined as the ratio of the diameter of a sphere of equal volume to the diameter of a circumscribing sphere, while roundness is defined as the ratio of the average radius of curvature of surface features to the radius of the maximum sphere that can be inscribed within a particle's perimeter.

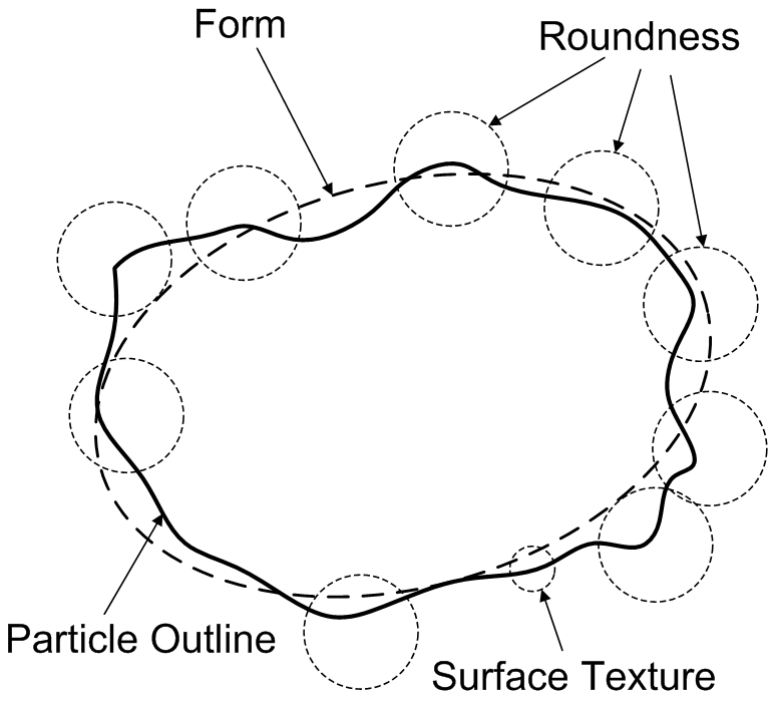

Figure 2.2 Particle shape characterized at three orders of scale (After Mitchell and Soga 2005)

Particle shape also been described by observing individual particles and comparing their geometry against a chart such as shown in Figure 2.4 (Krumbein and Sloss 1963). This chart has organized particle shapes with respect to sphericity and roundness. The charts are a rapid method to identify the particle shape of a few particles, but it would not be practical to repeat this method for many particles at many sizes. Furthermore, observational subjectivity might not be avoided.

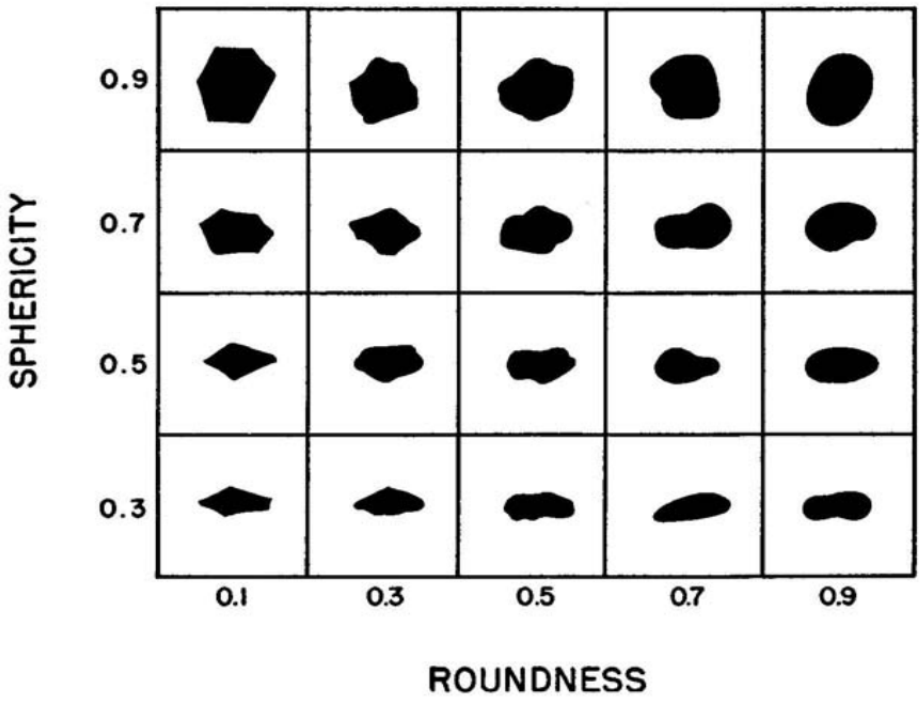

Figure 2.3 Chart for visual estimation of sphericity and roundness of particles (Krumbein and Sloss 1963)

2.4 Image-Based Particle Shape Determination

To remove the observational subjectivity associated with using a particle shape chart, several methods for the quantification of particle shape using image analysis have been proposed (Clark 1981; Kuo and Freeman 2000; Sukumaran and Ashmawy 2001; Bowman et al. 2001). Kuo and Freeman (2000) have proposed imaging indices such as *formfactor*, *angularity*, and *roughness*. The formfactor is defined as the square of the ratio of the *perimeter of an equivalent circle* to the *perimeter of the particle*. The equivalent circle is defined as a circle having the same area as the particle. The area of the particle is the sum of pixels present within the particle boundary (Figure 2.5(a)). The perimeter of the particle is defined as the sum of pixels on the particle boundary (Figure 2.5(b)). The angularity is defined as the square of the ratio of the *perimeter of the bounding polygon* to the *perimeter of an equivalent ellipse*. The bounding polygon is found using

the *feret* diameter. The feret diameter refers to a straight line measurement made between two tangents (Figure 2.5(c)). By rotating the coordinate axes, the feret diameter in any direction can be found. For instance, with 16 rotation steps, a bounding polygon with 32 corners and sides can be obtained (Figure 2.5(d)). The equivalent ellipse is defined as an ellipse having the same area and aspect ratio as the particle. Finally, the roughness is defined as the square of the ratio of the perimeter of the particle to the perimeter of the bounding polygon.

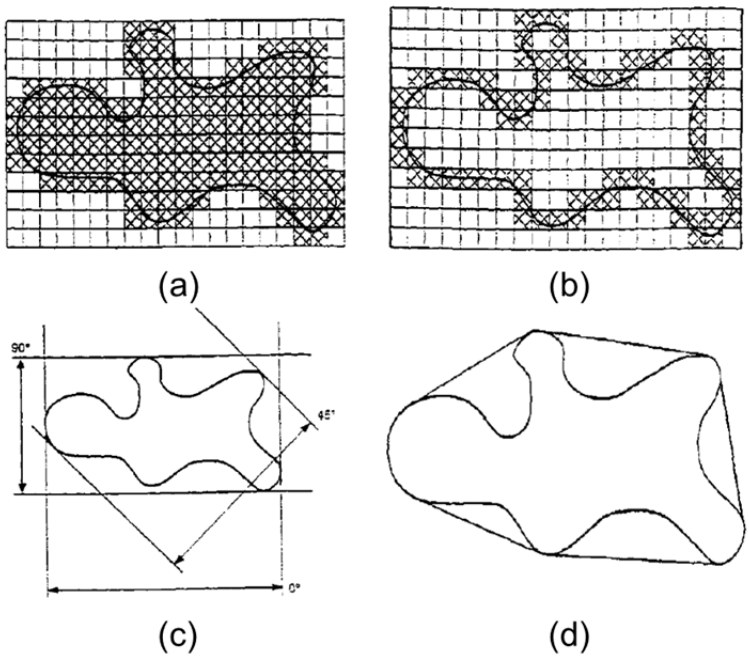

Figure 2.4 Measurements for imaging indices: (a) a projected particle area, (b) a boundary of a projected particle, (c) typical feret measurements, (d) perimeter of a bounding polygon (Kuo and Freeman 2000)

Sukumaran and Ashmawy (2001) have proposed a method that compares the discretized particle outline with a circle (Figure 2.5). The projection of a particle and a circle around the particle are discretized using the same sampling interval. Then the distortion angles α between each corresponding pair of chords for the particle and the circle and the internal angles β of the particle are obtained. *Shape factor* is defined as the sum of the absolute values of the distortion

angles, which is an indication of the particle outline's deviation from the circular shape. *Angularity factor* is defined as the sum of the difference between 180 degrees and the internal angles.

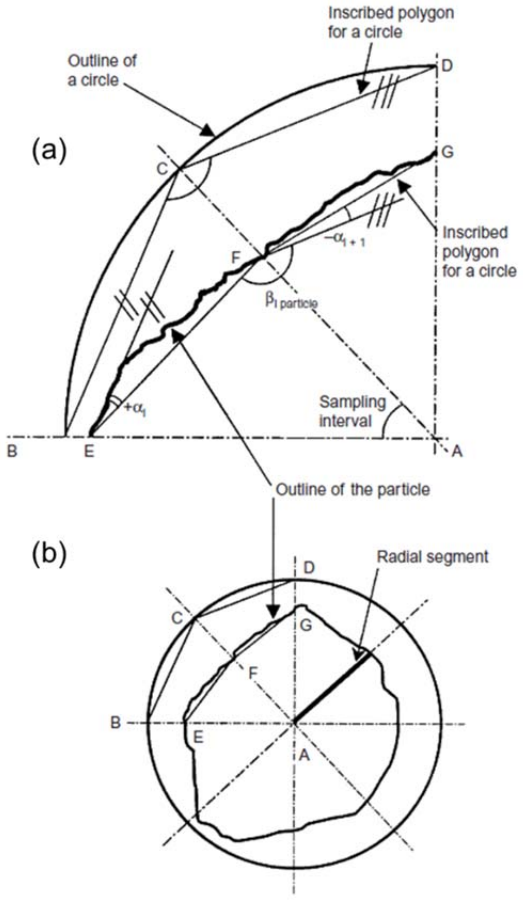

Figure 2.5 Measurements for shape and angularity factor: (a) a particle and a circle discretized with same sampling interval, (b) distortion angle α and internal angle β (Sukumaran and Ashmawy 2001)

Fourier series has been used to describe particle shape by unrolling an outline of a particle and expressing the discrete points on the polar coordinates R and θ (Clark 1981; Bowman et al. 2001). However, if the particle outline has a concave shape, two possible values of $R(\theta)$ can exist. To solve this problem, *Fourier shape descriptors* have been proposed where the outline of the

particle is considered to be a complex function generated by a point moving around the boundary. Bowman et al. (2001) have shown that lower order descriptor numbers provide the measures of elongation, trignularity, squareness and particle irregularity, while higher order descriptor numbers provide measures of local roughness.

2.5 Engineering Properties from Particle Size and Shape

Particle size and shape determined from image analysis are correlated with performance of pavement in transportation engineering as well as engineering properties such as minimum and maximum densities, critical state friction angle, and groutability in geotechnical engineering. Koerner (1969) proposed an empirical expression for maximum and minimum densities of dry quartz powders in terms of effective particle size D_{10}, particle size distribution defined by coefficient of uniformity C_u, particle shape defined by sphericity. Koerner (1970) also proposed an angle of shear resistance of cohesionless soils in terms of particle shape, effective particle size, particle size distribution, relative density, and type of mineral. Chang and Woods (1992) found that effective particle size and coefficient of uniformity are the most important properties of soils controlling the number of inter-particle contacts in sand. Kuo et al. (1996) captured a projection of three dimensions of a gravel size particle using a sample tray that can hold the particle and rotate it 90 degrees. Later using this device, particle shape, angularity and surface roughness of particles were quantified (Kuo and Freeman 2000) and Kuo (2002) found strong correlation between the permanent deformation properties of Hot Mix Asphalt (HMA) mixtures and particle shape indices. Sukumaran and Ashmawy (2001) used a sand size particle's two-dimensional projection to quantify particle shape and angularity. Later, they correlated particle shape and

angularity obtained from particle images with hopper flow rate as well as pluviated void ratio (Sukumaran and Ashmawy 2003). Bowman et al. (2001) also used two dimensional morphological characteristics of a sand size particle to quantify particle shape based on Fourier shape descriptors. Later, this method was used to quantify change in particle shape from microstructure of dense sands during one-dimensional creep obtained from an optical microscopy (Bowman and Soga 2003). Kokusho et al. (2004) performed a series of undrained triaxial tests on granular soils with different particle size distributions to investigate the effect of the particle gradation on the undrained shear characteristics. Ozgurel and Vipulanandan (2005) found that particle size distribution and fines content influenced the strength, modulus, and stress-strain relationship of grouted sand. Also, Vipulanandan and Ozgurel (2009) proposed a model to predict the grouting pressures required to grout the soils based on particle size distribution and fines content. Cho et al. (2006) quantified sphericity and roundness of a sand size particle based on a chart for visual estimation of particle shape proposed by Krumbein and Sloss (1963). They found that decrease in sphericity or roundness leads to increase in minimum and maximum void ratios, decrease in small strain stiffness, increase in compressibility, increase in constant volume critical state friction angle, and increase in critical state line intercept (Cho et al. 2006). Bareither et al. (2008) proposed a regression model that can be used to predict friction angle of compacted sands based on effective particle size, maximum dry unit weight, and roundness.

Particle shape obtained from image analysis is also used in Discrete Element Method (DEM) simulations to correlate particle shape with engineering properties. Ashmawy et al. (2003) obtained images of representative particles from different types of soils and built a corresponding shape library for each material. The liquefaction response of different particle shapes was

compared by numerical analysis utilizing the shape library. Mahmoud et al. (2010) combined DEM and image processing techniques where DEM input parameters such as particle shape and gradation were determined by imaging and were correlated with pavement resistance to fracture. Qian et al. (2011) proposed an image-aided DEM approach to quantify individual effects of various geogrid products on particles with different size and shape.

CHAPTER III

Sedimaging

3.1 Introduction

This chapter describes a rapid, clean, low-energy image-based test for determining the grain size distribution of soil. The test is called *sediment imaging* or *sedimaging*. It develops the grain size distribution for particles in the range between 2.0 mm (No. 10 sieve opening) and 0.075 mm (No. 200 sieve opening). In addition, the percentage of fines (particles passing the No. 200 sieve) is also determined. The system utilizes a sedimentation column for rapidly sorting a soil specimen by particle size, a high resolution digital SLR camera for capturing an image of the sedimented soil column and software for interpreting the soil image and producing its particle size distribution.

3.2 Sedimaging Apparatus

The sedimaging hardware consists of eight major parts shown in Figure 3.1: (1) a sedimentation column, (2) a support tower and base, (3) a positioning system, (4) a pre-segregation tube and its adaptor, (5) a connector and drainage system, (6) a sediment accumulator, (7) a camera, and (8) computer.

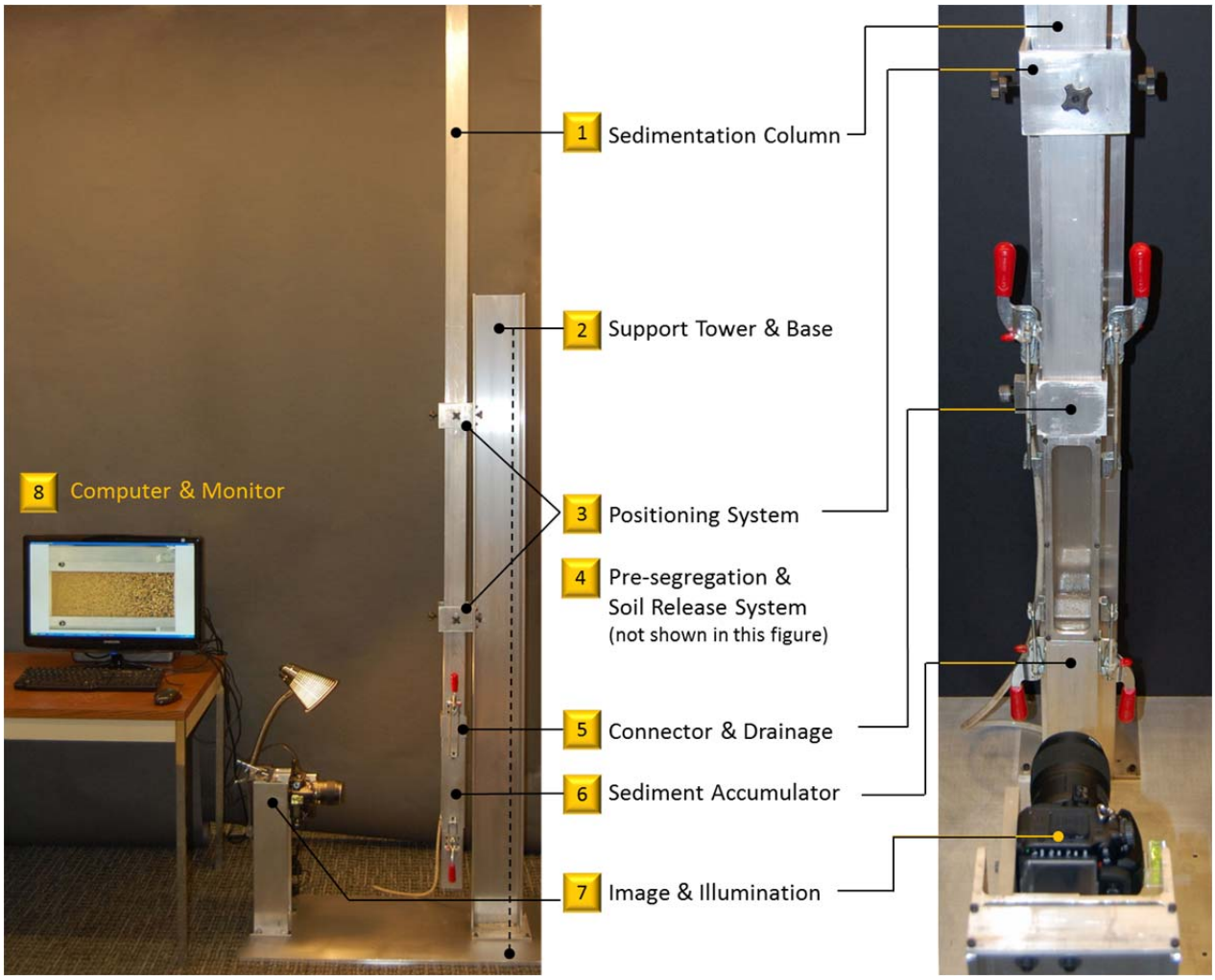

Figure 3.1 Sedimaging hardware

The sedimentation column is a 64 mm (2.5 in.) × 64 mm (2.5 in.) × 2134 mm (7 ft.) aluminum square tube of 6.4 mm (0.25 in.) wall thickness. The sedimentation column is filled with water and the soil specimen is introduced at its top. The particles settle down through this column and into a sediment accumulator below. The support tower is a 102 mm (4 in.) × 152 mm (6 in.) × 1981 mm (6.5 ft.) aluminum I-beam bolted to a 457 mm (1.5 ft.) × 914 mm (3 ft.) × 13 mm (0.5 in.) aluminum base plate. Together, they provide resistance to overturning of the sedimentation column.

The positioning system consists of 2 brackets and 5 positioning clamp screws per bracket (Figure 3.2). The two brackets are 102 mm (4 in.) × 102 mm (4 in.) × 76 mm (3 in.) long aluminum square tubes of 6.4 mm (0.25 in.) wall thickness. Two 6.4 mm (0.25 in.) diameter positioning clamp screws attach each bracket to the support tower. Three other positioning clamp screws have 16 mm (0.625 in.) diameter hard rubber contact pads on their ends to position the sedimentation column vertically and immobilize it. The sedimentation column could also be wall-mounted to eliminate the support tower and base.

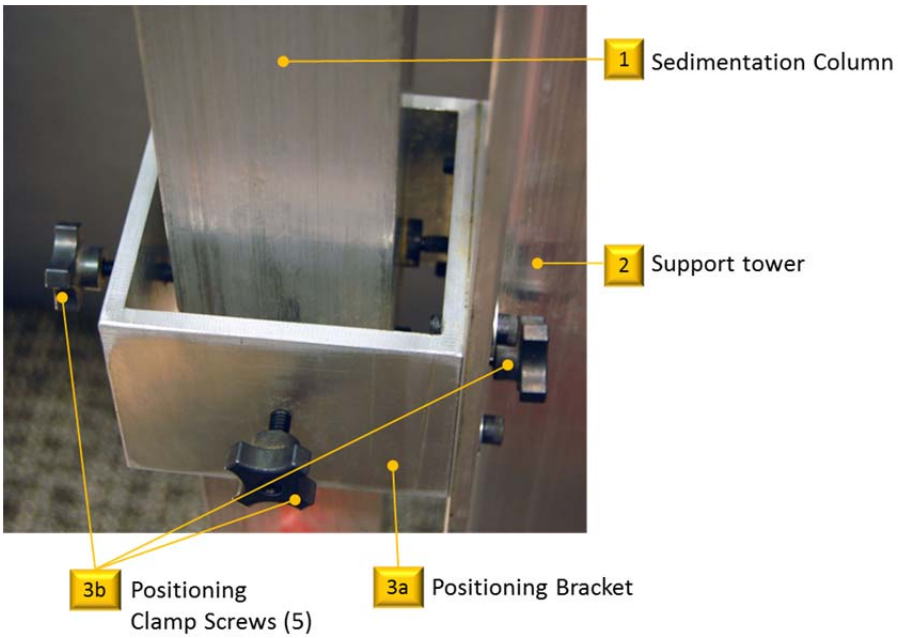

Figure 3.2 The positioning system

An acrylic “pre-segregation tube” is used to mix a soil sample with water, to have soil particles roughly segregated by size in the tube, and to release soil-water mixture into the column (Figure 3.3 and 3.4). It is 457 mm (18 in.) long with a 64 mm (2.5 in.) outside diameter and 6.4 mm (0.25 in.) wall thickness. One end of the tube is open and the other end is permanently capped by an acrylic circular disk of 13 mm (0.5 in.) thickness and 76 mm (3 in.) diameter. A 13

mm (0.5 in.) diameter vacuum vent and its cap are located at the center of the circular disk. A pre-segregation tube adaptor mates the circular pre-segregation tube to the square sedimentation column.

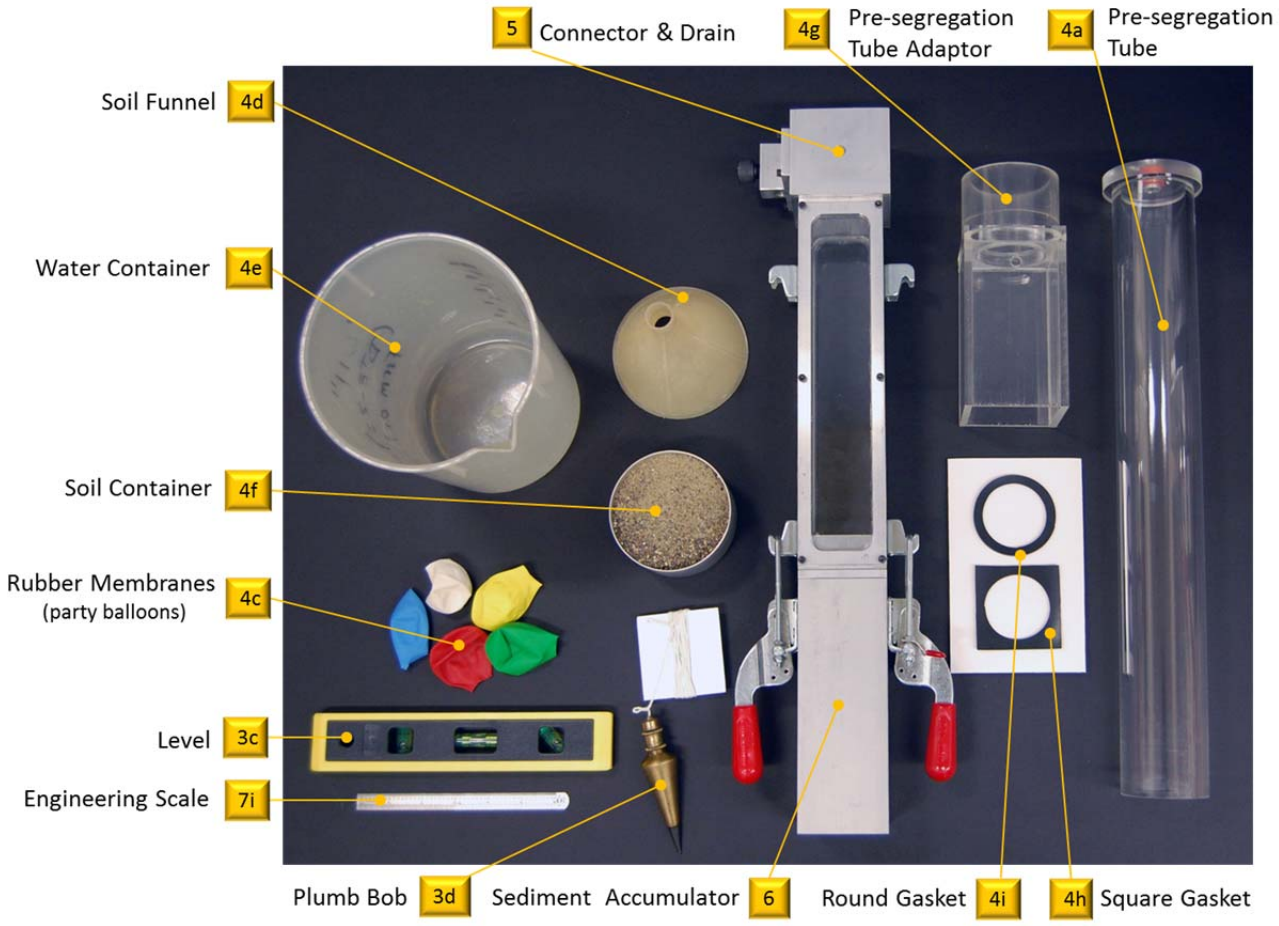

Figure 3.3 Ancillary tools for the sedimaging

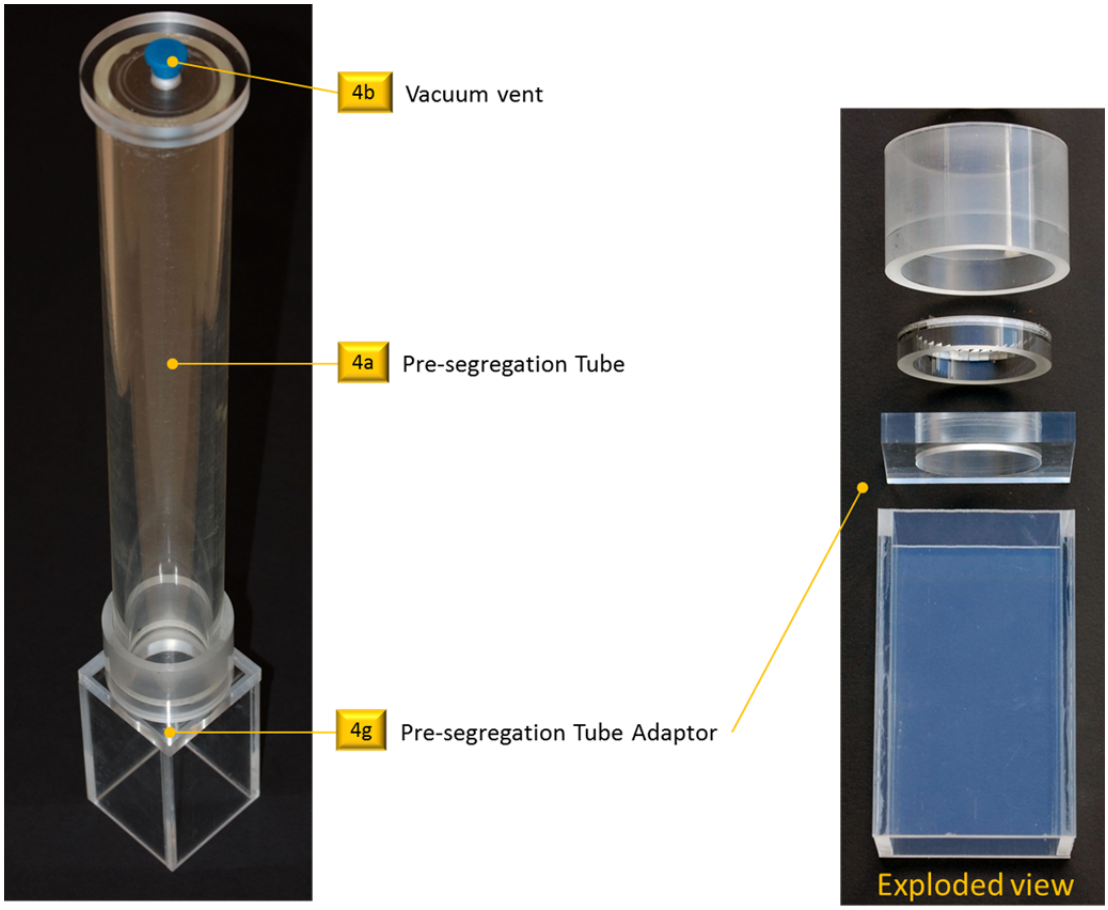

Figure 3.4 The pre-segregation tube and its adaptor

The connector which is located between the sedimentation column and the sediment accumulator, consists of a 76mm (3 in.) × 76 mm (3 in.) outer square aluminum tube of 6.4 mm (0.25 in.) wall thickness and a 64 mm (2.5 in.) × 64 mm (2.5 in.) inner square aluminum tube with the same wall thickness (Figure 3.5). A drainage valve with a socket cap screw for a valve stem has a 13 mm (0.5 in.) thread diameter and 44 mm (1.75 in.) length. The valve stem passes through the connector and the tip of the stem is flush with the inside wall of the connector when in the closed position. When the valve is opened by unscrewing it, water drains from the system through a flexible tube.

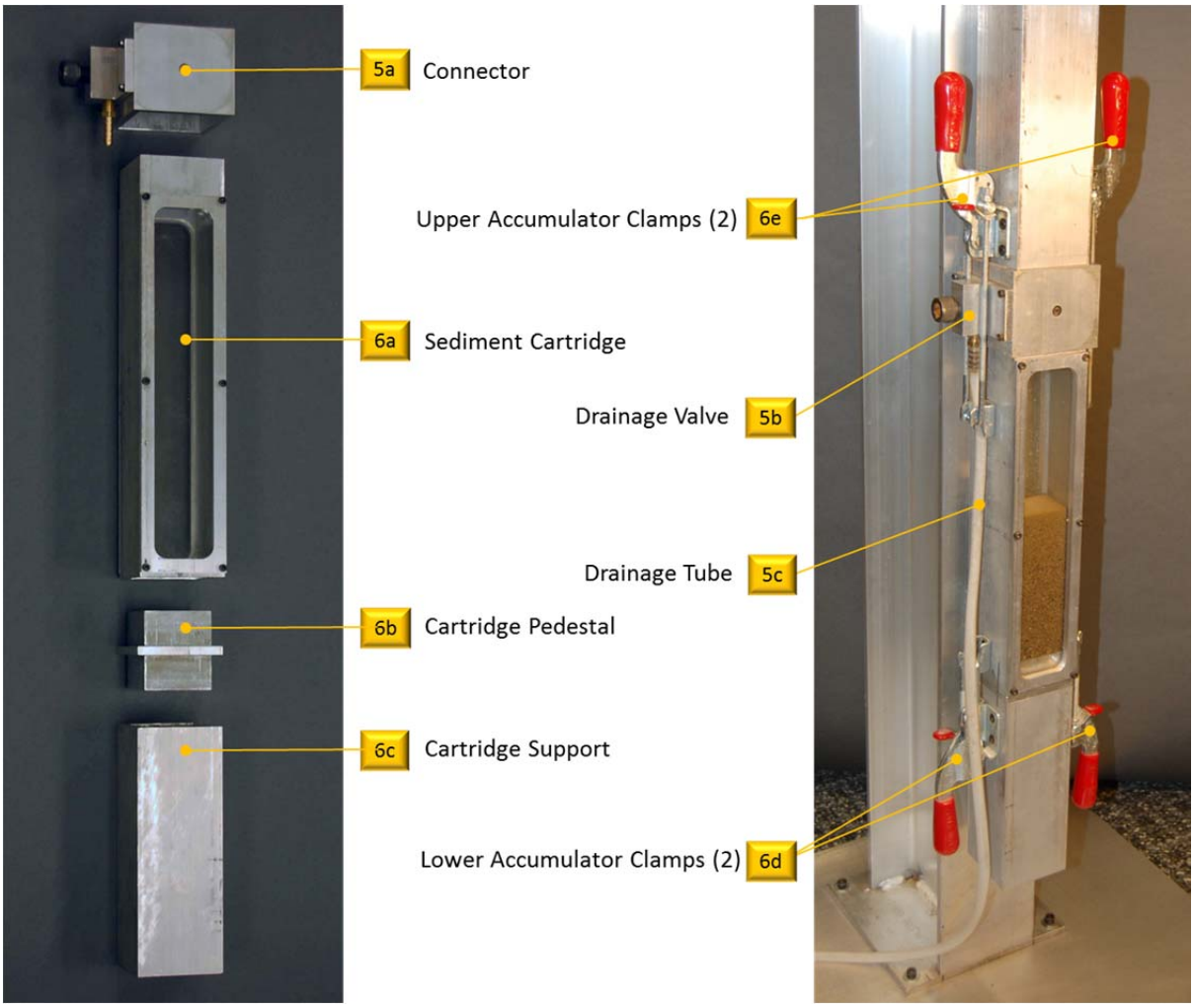

Figure 3.5 The connector and the sediment cartridge

The sediment accumulator, shown in Figure 3.5, consists of a sediment cartridge, a cartridge pedestal, a cartridge support and lower and upper accumulator clamps. The sediment cartridge is a 64 mm (2.5 in.) × 64 mm (2.5 in.) × 305 mm (1 ft.) long aluminum tube of 6.4 mm (0.25 in.) wall thickness. It has two 3.2 mm (0.125 in.) thick glass windows attached over openings on opposite sides of the sediment cartridge. Images of the sedimented soils are taken through these windows. The largest soil particles which settle at the bottom of the sediment cartridge sit on top of the cartridge pedestal which is milled down from a 64 mm (2.5 in.) × 64 mm (2.5 in.) × 57 mm (2.25 in.) square aluminum bar. The cartridge pedestal sits atop the

cartridge support which is a 64 mm (2.5 in.) × 64 mm (2.5 in.) × 178 mm (7 in.) aluminum tube of 6.4 mm (0.25 in.) wall thickness. The two lower accumulator clamps hold the sediment cartridge, the cartridge pedestal, and the cartridge support together while the two upper accumulator clamps hold the sediment column, connector and the sediment cartridge together during a test.

A 16.2 megapixels Nikon D7000 camera with an AF-S Micro Nikkor 60 mm f/2.8G ED camera lens is used to capture the images (Figure 3.6). The camera is connected to a computer and is controlled remotely by NKRemote software be Breeze Systems. Design drawings of the Sedimaging device can be found in Appendix B.

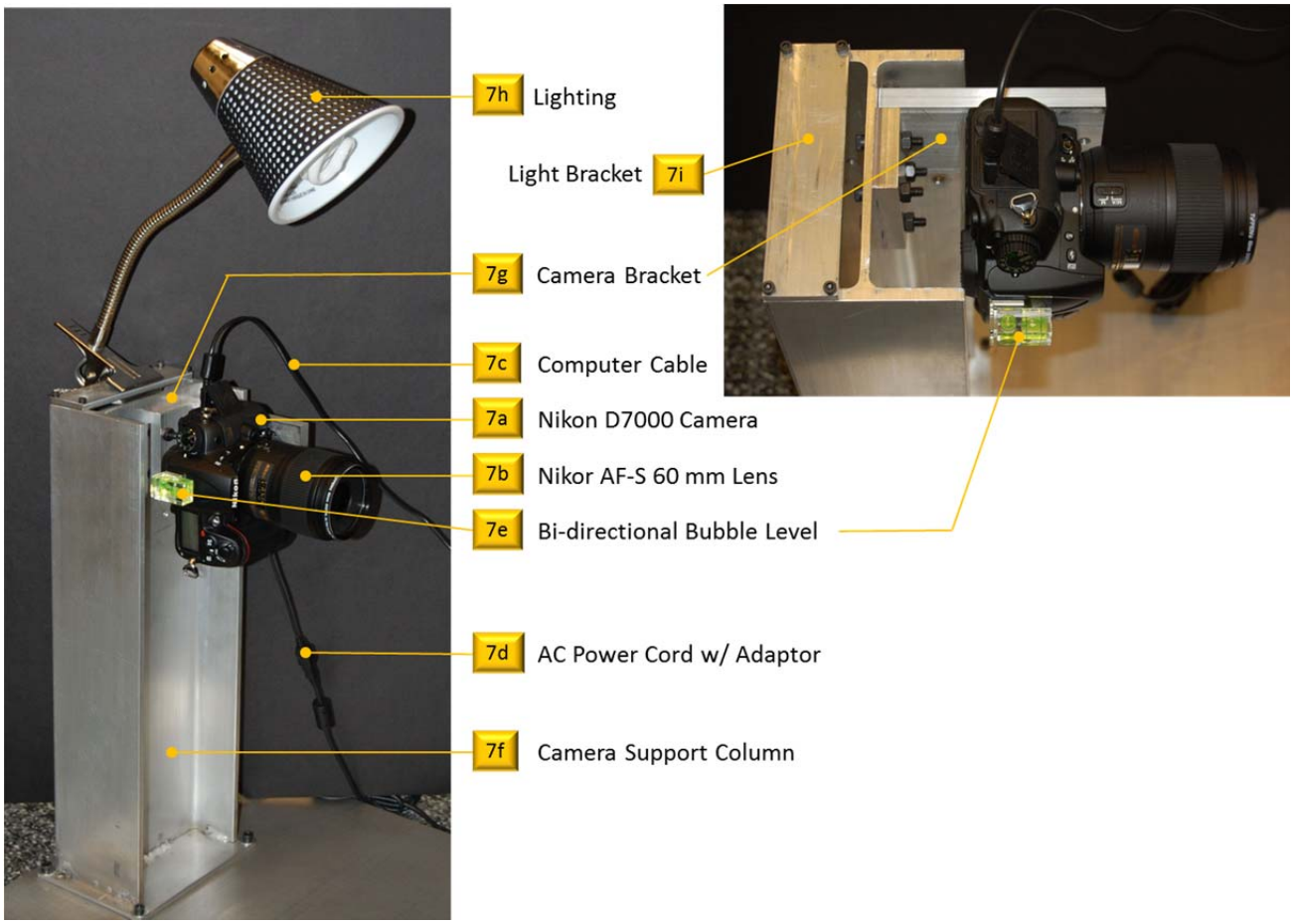

Figure 3.6 The camera system

3.3 Test Procedures

A sedimaging test typically takes 15 minutes when the percentage of fines needs to be determined and 10 min when there are no fines in the soil. The test is performed in ten steps: (1) filling the column with water, (2) pre-segregation, (3) sedimentation, (4) column drainage, (5) tapping the accumulator to level the soil surface, (6) image capture, (7) removal of dirty water from the accumulator and refilling it to a specific height, (8) weighing the accumulator, (9) analyzing the image and printing the results, (10) emptying, rinsing and reattaching the accumulator.

Soil and the sedimentation column preparation are shown in Figure 3.7 and 3.8. A soil canister is filled with a dry specimen. For soils with a typical specific gravity of 2.65 this will be approximately 450 g. The weight of soil is then recorded. The sedimentation column is filled with 6000 mL of water. The square gasket, the pre-segregation tube adaptor, and the circular gasket are placed on top of the sedimentation column.

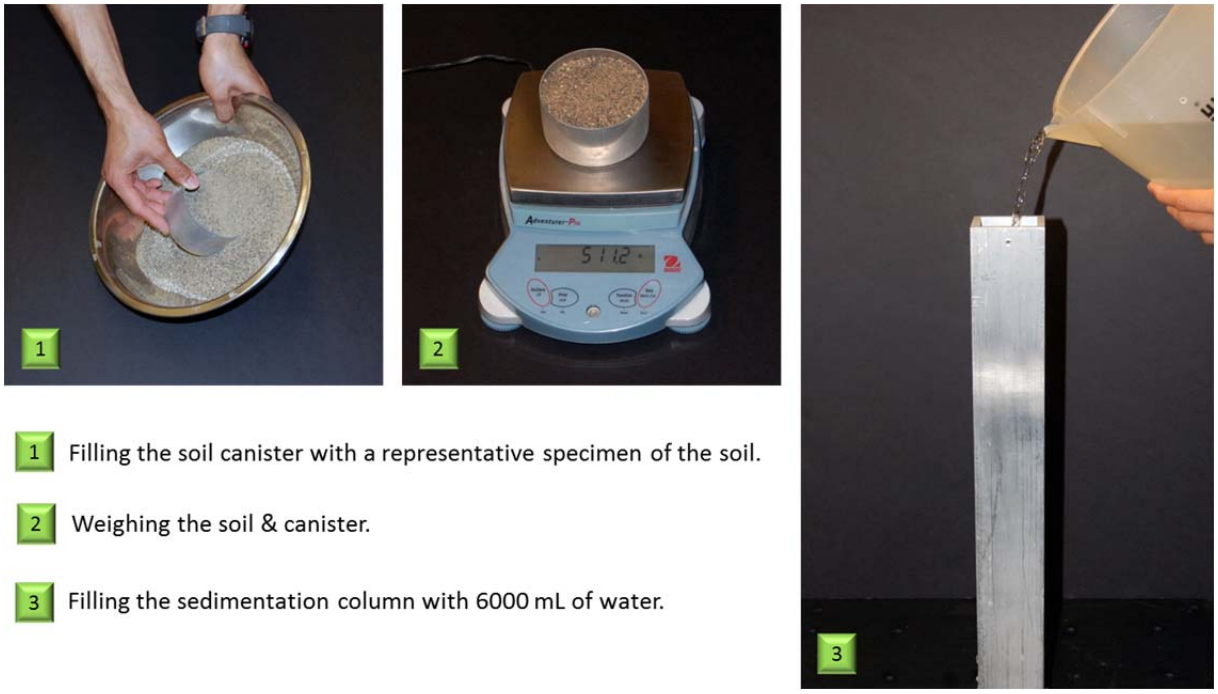

Figure 3.7 Soil and sedimentation column preparation

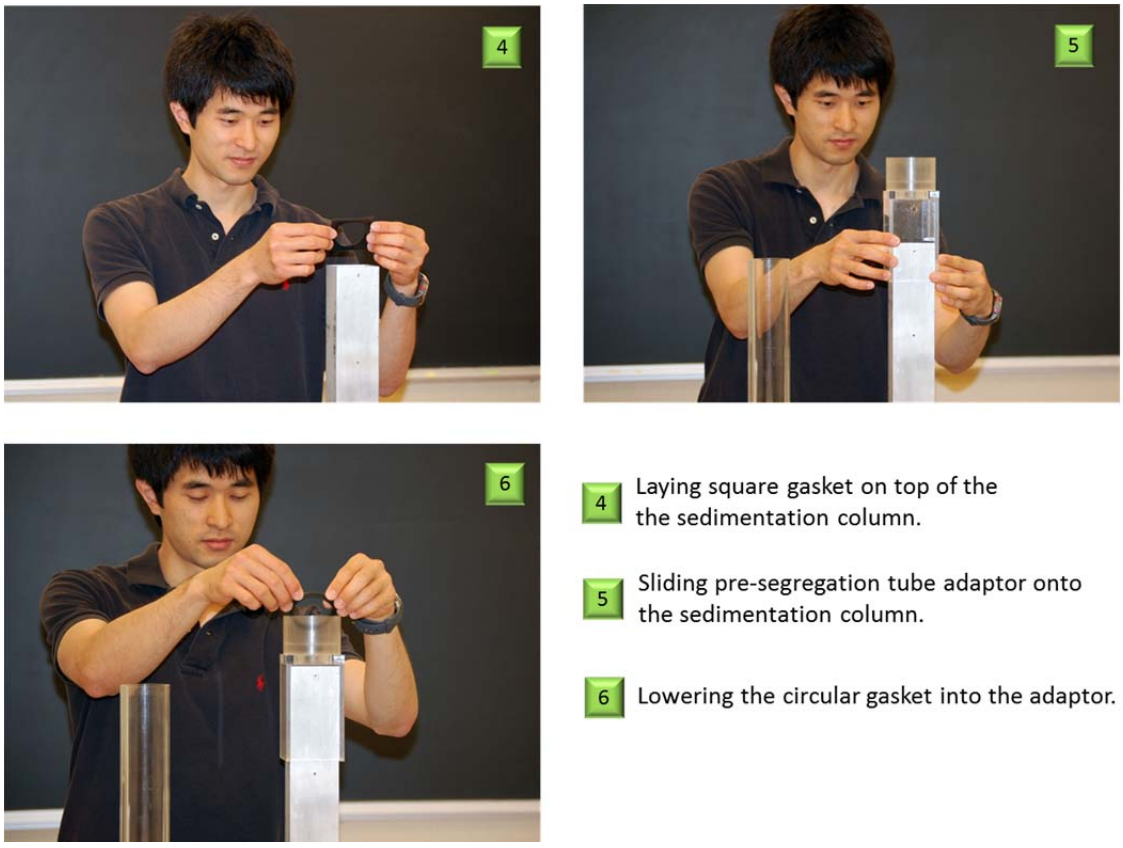

Figure 3.8 Assembling the pre-segregation tube adaptor

The pre-segregation procedure is illustrated in Figure 3.9, 3.10, 3.11 and 3.12. To begin a test, water and soil are placed into the pre-segregation tube. The open end of the pre-segregation tube is covered by a stretched rubber membrane. A small vacuum is created in the tube by pressing down on the center of the stretched membrane thereby allowing some air to escape. This results in a concave membrane surface. The pre-segregation tube containing the soil-water mixture is shaken several times until the particles are well mixed. While holding the tube vertically with the membrane on the bottom, the membrane is rolled off of the end of the tube. The vacuum in the tube prevents the soil from slipping out. The pre-segregation tube is then placed into the adaptor on top of the sedimentation column. Lastly, the soil-water mixture is released into the sedimentation column by opening the pre-segregation tube's vent cap.

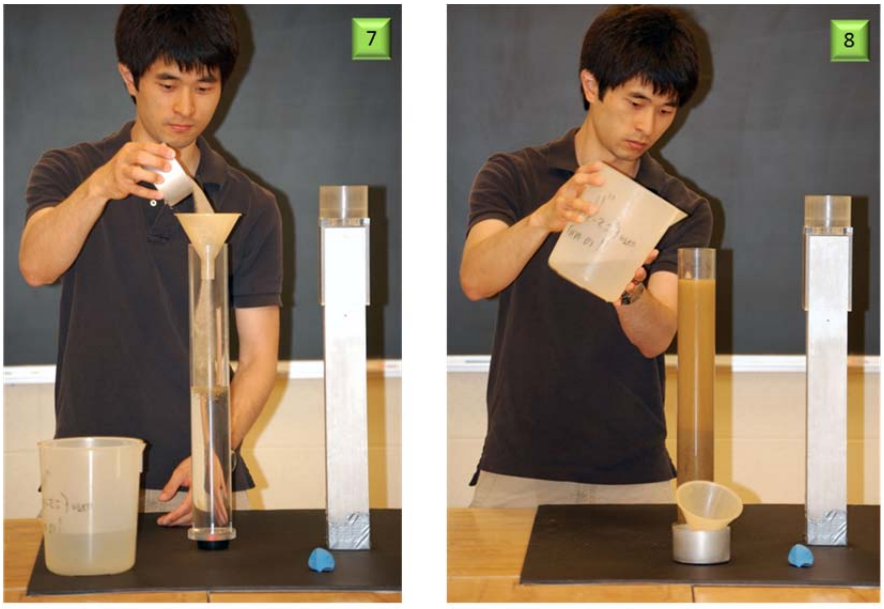

Figure 3.9 Placing water and soil into the pre-segregation tube

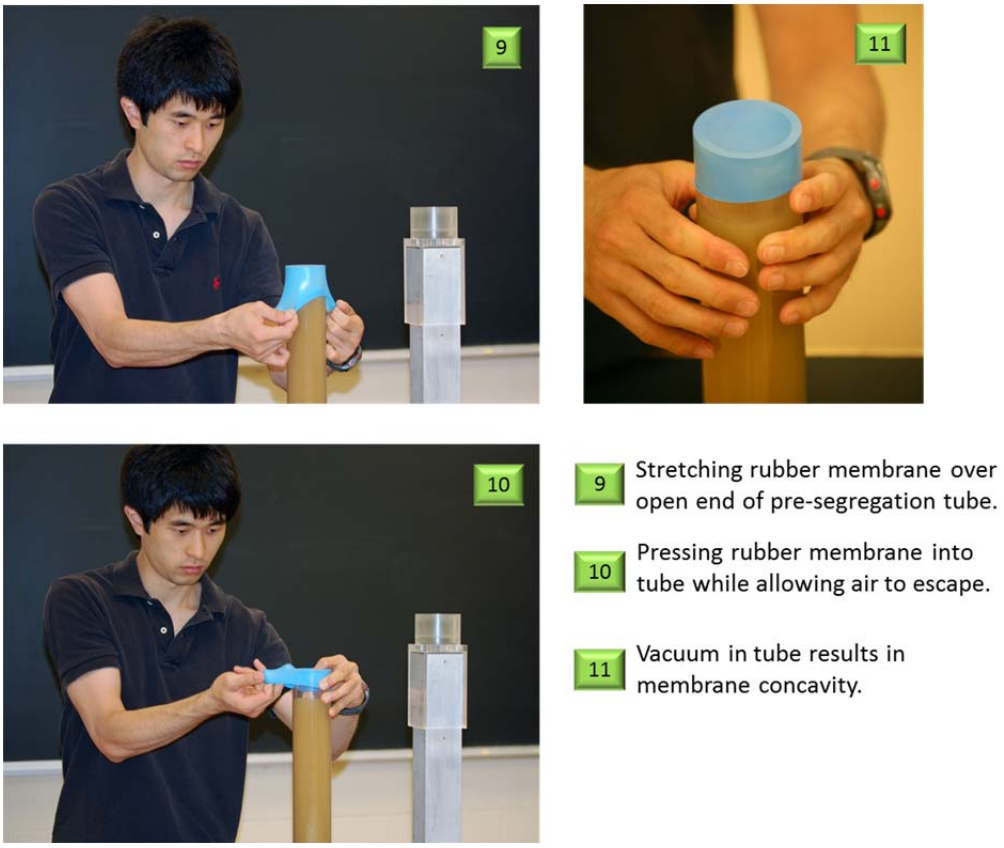

Figure 3.10 Installing the rubber membrane on the pre-segregation tube

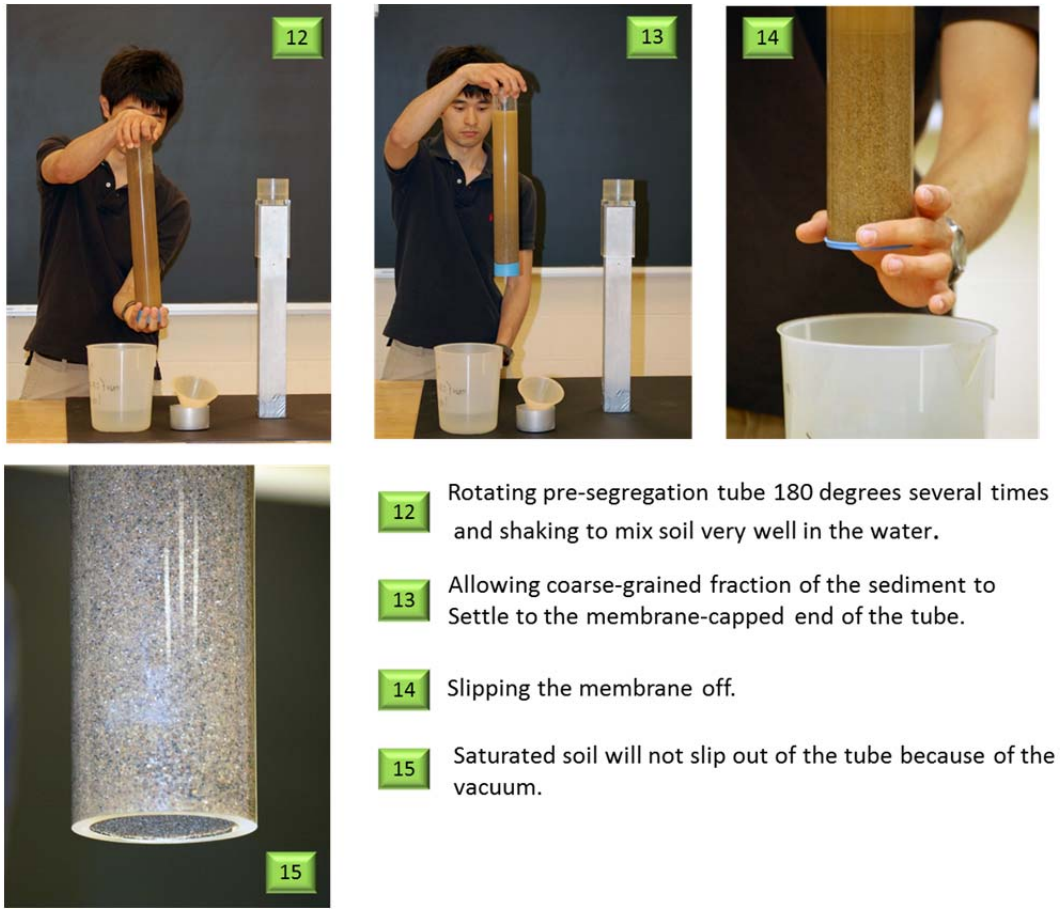

Figure 3.11 Soil pre-segregation

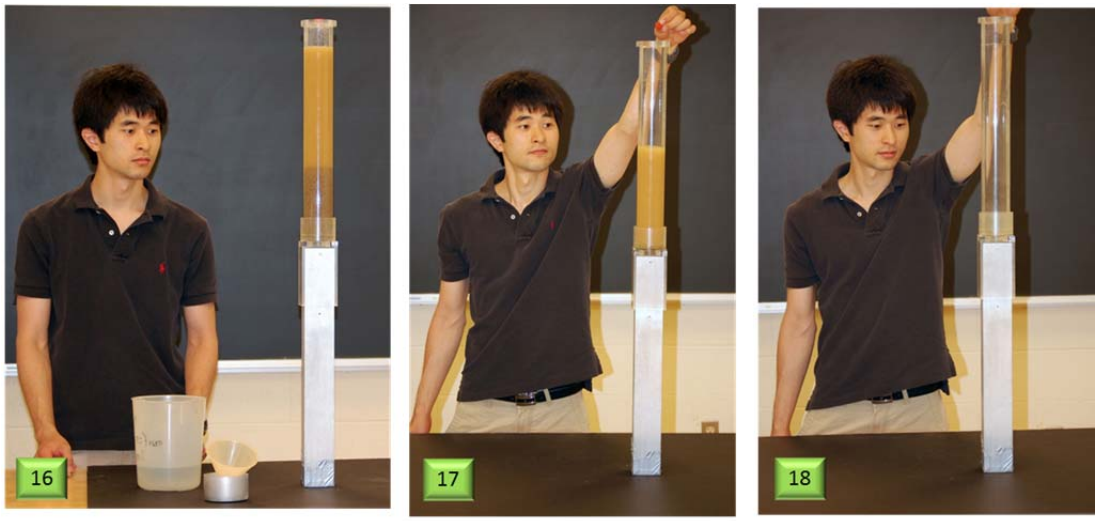

16 Pre-segregation tube with soil placed in adaptor.

17 Opening vent releases soil into the sedimentation column.

18 Soil-water mixture enters column in 1 to 2 seconds.

Figure 3.12 Soil release into sedimentation column

Sedimentation of the soil particles takes about 5 minutes if the specimen contains only sands and 10 minutes if fines are present. The operator can observe a magnified view of the soil accumulation on a monitor so he knows when it has been completed. After the requisite time for sedimentation passes, the water from the sedimentation column is released by opening the drainage valve (Figure 3.13). Since the drainage valve is located above the accumulator the soil remains saturated. Following drainage, the top surface of the accumulated soil is leveled with one sharp tap applied to the accumulator which liquefies the loose soil (Figure 3.14). This leveling is necessary to capture a rectangular image of the soil but it has no effect on the test results. The image is captured (Figure 3.15) and the accumulator is immediately detached from the column by pulling down the two upper accumulator clamps (Figure 3.16). The fines in suspension that have not settled down inside the accumulator are removed using a syringe and

the accumulator is refilled with water to a mark (Figure 3.17). The accumulator with the soil-water mixture is weighed. It is then emptied and reattached to the column for the next test.

19 Opening drainage valve.

20 Emptying through drainage line.

Figure 3.13 Draining the sedimentation column

21 Taping the side of the sedimented column (once) to flatten the surface (if necessary).

22 Image of sedimented soil before the tap.

23 Image of sedimented soil after the tap.

Figure 3.14 Tapping the column

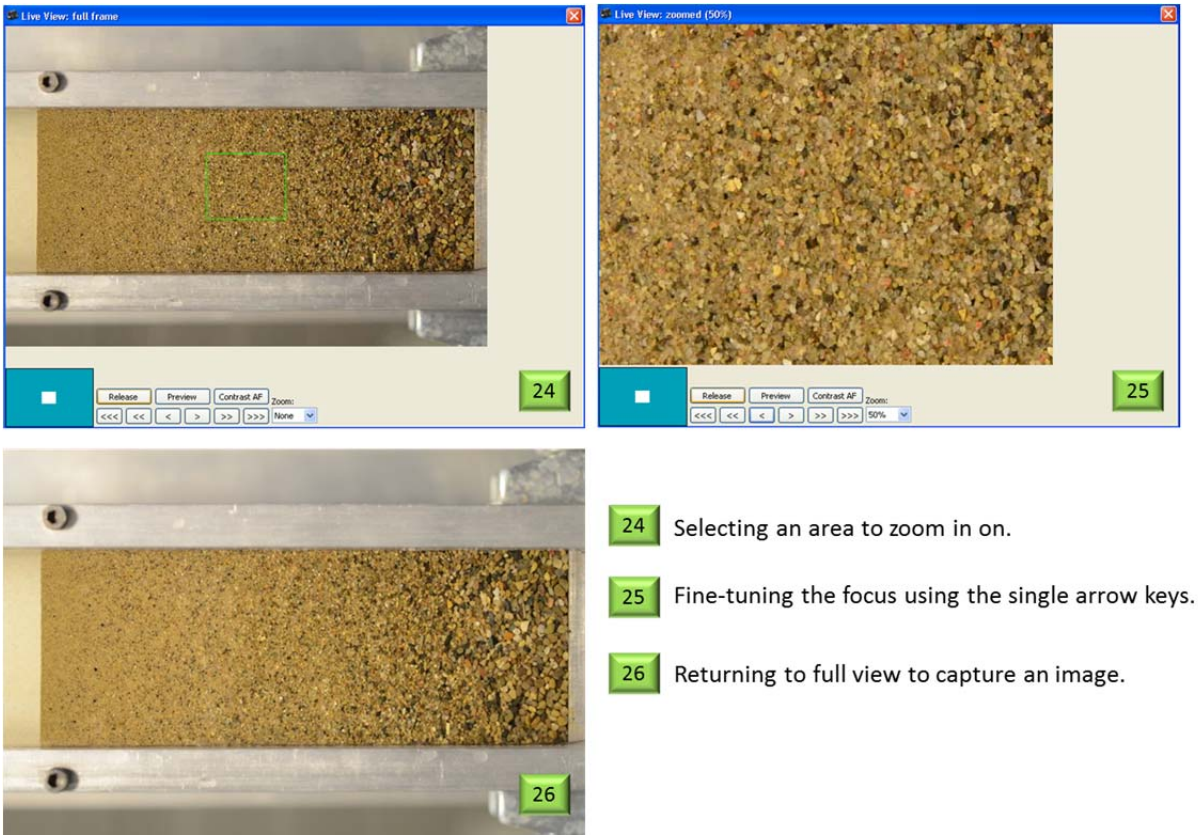

Figure 3.15 Focusing and capturing an image

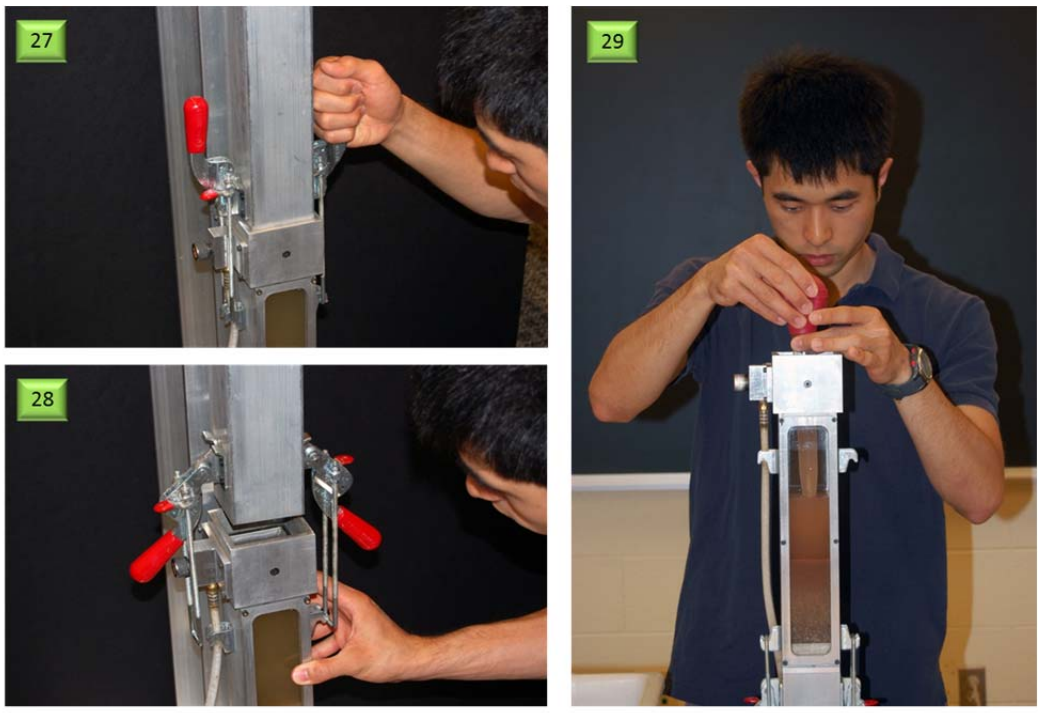

27 Releasing the clamps.

28 Detaching the connector & accumulator.

29 Removing some dirty water.

Figure 3.16 Detaching connector and accumulator, removing water with fines

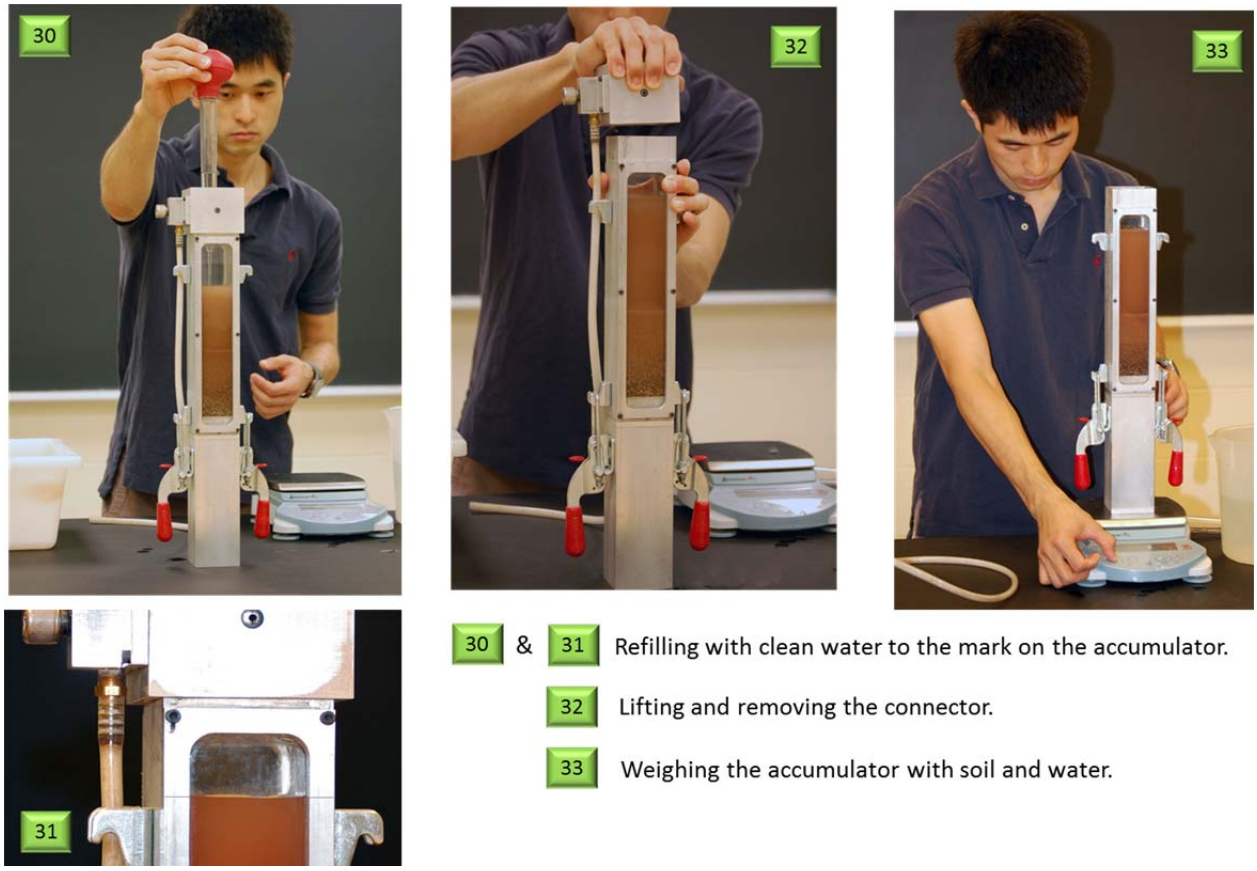

Figure 3.17 Refilling with clean water, removing connector and weighing

3.4 Wavelet Transformation

3.4.1 Wavelet Transformation in Optical Granulometry

Sedimaging utilizes wavelet transformation to analyze the image of the sedimented soil and determine its grain size distribution. Wavelet transformation has previously been employed to characterize the shape, angularity and surface texture of individual aggregate or percentage of fines from assemblies of contacting particles. Kim et al. (2002) laser-scanned 22 mm to 58 mm particles dispersed on a flat surface. They obtained descriptors of shape, angularity and texture based on the wavelet energies computed at different scales (decomposition levels) for each descriptor. Chandan et al. (2004) used wavelet decomposition for surface texture analysis of aggregate. They observed different "energy signatures" for highly textured blast furnace slag than for natural rounded gravel. Amankwah and Aldrich (2011) used wavelet transforms along with morphological operations to extract features (objects) from images of assemblies of contacting particles. Their goal was to detect the percentage of fines on conveyor belts carrying mined coal. However, they found that standard segmentation of image features to be difficult when a large range of particle sizes was encountered in a contacting assembly. Therefore they recommended an approach using multivariate image analysis methods instead of wavelet transformation alone.

The research efforts of Shin and Hryciw (2004); Jung et al. (2008); Hryciw et al. (2009) and the present work are somewhat related to Amankwah and Aldrich's in that the analysis is performed on images of contacting three-dimensional particle assemblies. However, there is one major fundamental difference: The wavelet transformation method described in this paper is used

on images or parts of images containing nearly uniform-sized particles such as shown in Figure 3.18.

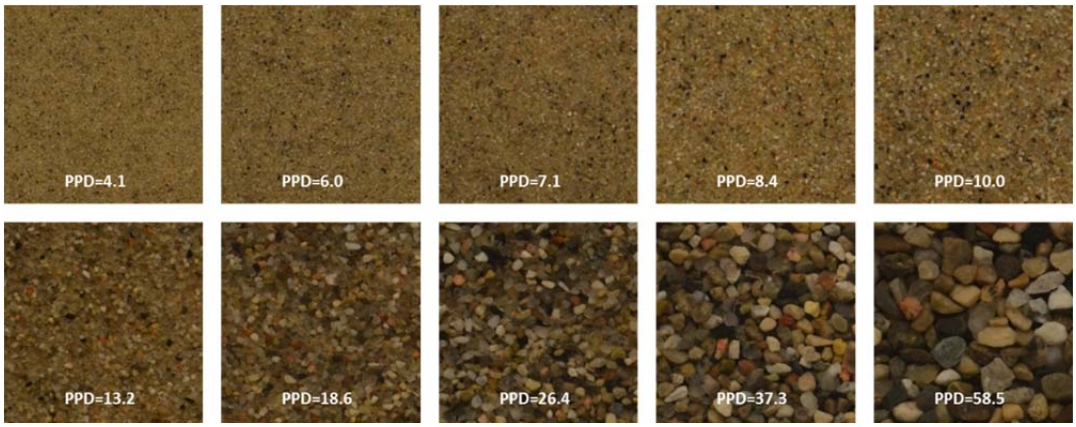

Figure 3.18 Images of 10 nearly uniform-grained soil specimens with *PPD* ranging from 4.1 to 58.5

Since most natural soils contain a range of particle sizes typically spanning at least an order of magnitude or more in diameter, a hydraulic sedimentation system initially suggested by Hryciw and Jung (2009) and improved by Hryciw and Ohm (2012) is used to rapidly sort the particles by size. Three soil specimens sorted this way are shown in Figure 3.19. The images are analyzed piece-wise by small areas having the size of the colored squares at the bottom of the images. By virtue of their small size relative to the overall specimen, each analysis square contains particles of relatively uniform size. Empirical calibration curves originally proposed by Shin and Hryciw (2004) and later updated by Hryciw et al. (2009) relate a "wavelet index" to the average particle size in an analysis square. The information from thousands of overlapping squares are combined to yield the particle size distribution of the entire specimen. Fortunately, Hryciw and Jung (2008) found that there are no significant variations in porosity through the sedimented soil columns. As such, each square analysis area represents an equal percentage of the total volume of solids. This greatly simplifies the analysis to produce grain size distributions.

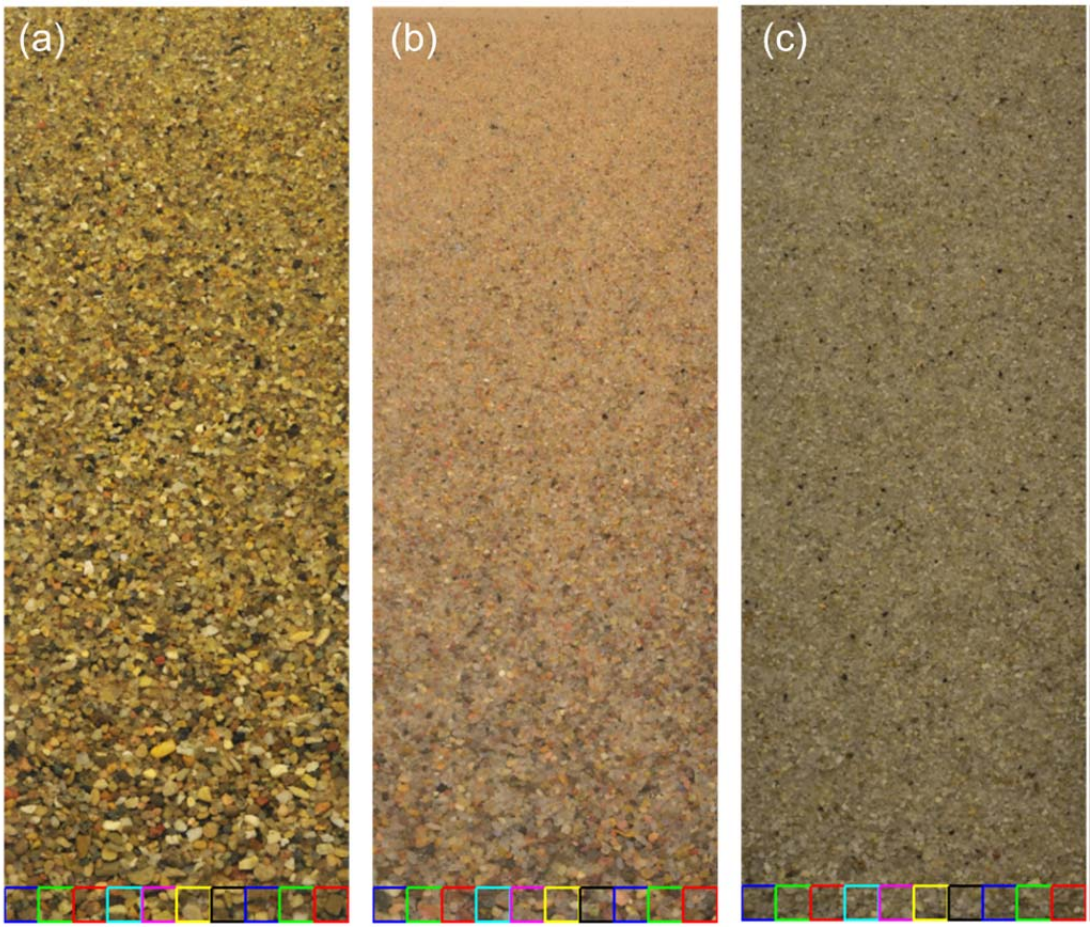

Figure 3.19 Soil specimens sorted by sedimentation through water: (a) Griffin, IN, (b) Rincon, NM, (c) Scotts Valley, CA

3.4.2 Normalized Energy Distribution and Soil Particle Size

Wavelet transformation decomposes a soil image of $2^k \times 2^k$ pixel size into *k decomposition levels*.

The seven successive levels for a $2^7 \times 2^7$ pixel image are shown in Figure 3.20.

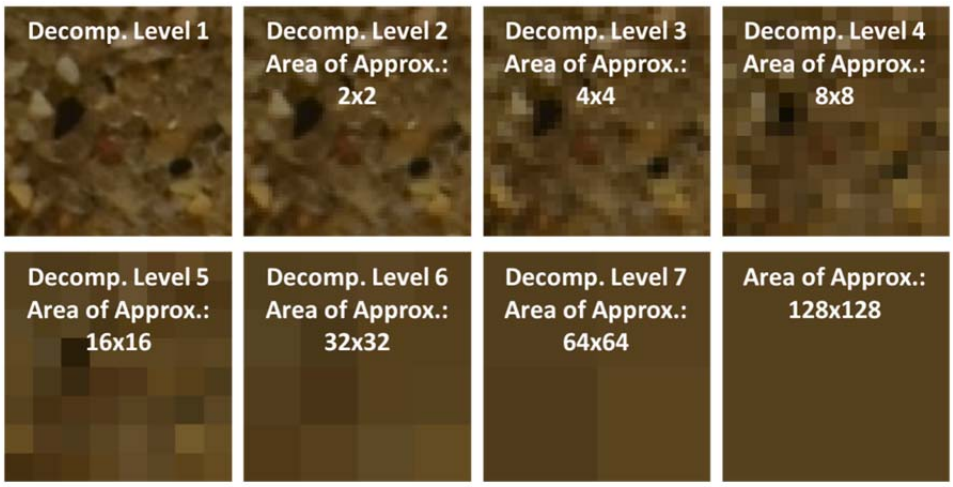

Figure 3.20 Seven levels of downscaling beginning with a 128 × 128 image at *PPD* = 13.2

The sum of the *Energies* in the three directions at each level is computed as:

$$E_i = \sum E_{Hi} + \sum E_{Vi} + \sum E_{Di} \tag{3.1}$$

where E_i is the Energy of the i-th decomposition, E_{Hi}, E_{Vi}, and E_{Di} are Energies in horizontal, vertical, and diagonal directions, respectively. This Energy is a measure of the magnitude of the differences between average grayscale values of adjacent regions in an image. At the first decomposition level, each pixel is compared to its nearest neighbors. At the second level, each 2 × 2 pixel region is compared to its neighboring 2 × 2 regions; at the third level, 4 × 4 regions are compared, then 8 × 8 regions and so on. For very large images the values of E_i become correspondingly very large. The actual E_i values are obviously not very useful since they merely increase with image size. However, the distribution of Energy by decomposition level is. Recognizing this, Shin and Hryciw (2004) expressed the Energy at each level as a percentage of the sum of Energies at all levels and termed it the *Normalized Energy*, E_{ni}:

$$E_{ni} = \frac{E_i}{\sum_{i=1}^{n} E_i} \tag{3.2}$$

where n = number of decomposition levels. Figure 3.21 shows the resulting Normalized Energies by decomposition level corresponding to Figure 3.20.

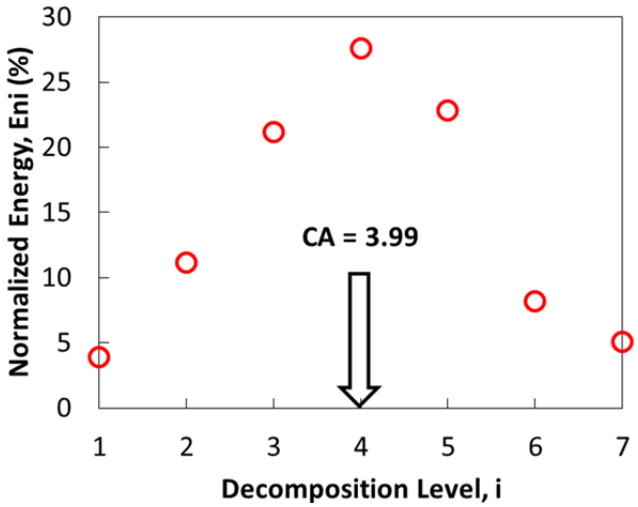

Figure 3.21 Normalized energy distribution for the soil in Figure 3.20

Shin and Hryciw (2004) sought a single parameter or index value to represent the complete Normalized Energy distribution for correlation to *PPD*. They defined a wavelet index, *CA* as the first moment of the Normalized Energy distribution with respect to the Normalized Energy axis. In other words, *CA* is the average weighted decomposition level where the weighting factor is the Normalized Energy ("*CA*" is also the "center of area" beneath the Normalized Total Energy curve as shown in Figure 3.21):

$$CA = \sum_{i=1}^{N} iE_{ni} \tag{3.3}$$

Shin and Hryciw (2004) showed that as the average number of pixels per soil particle diameter (*PPD*) (Ghalib et al. 1998) increases, the concentration of Energy shifts to higher decomposition levels (Figure 3.22).

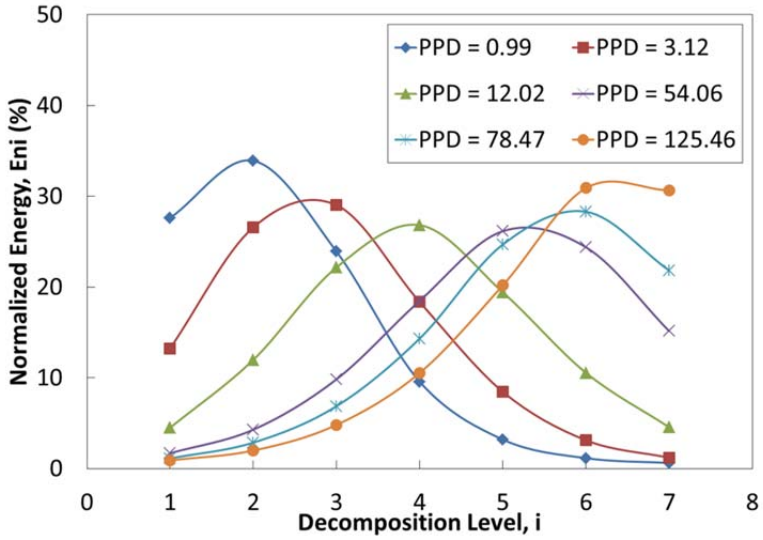

Figure 3.22 Normalized Energies for various *PPD*s (Jung 2012)

As more data became available for a larger number of sands over a wider range of *PPD* values, an apparent nonlinear relationship between *CA* and *PPD* developed as shown in Figure 3.23. Remarkably, the data in Figure 3.23 is based on images of sands with various particle sizes, angularities, grain colors, color uniformities and camera magnifications. Later, it was found that when images are taken of saturated soil contained behind a 0.125 in. glass pane, as opposed to dry soil on a flat surface, the curve shifts upward slightly, particularly at higher *PPD* levels as shown in Figure 3.24. An empirical fit to the *CA* vs *PPD* data or a *calibration curve* was given by Hryciw et al. (2009):

$$PPD = \left(\frac{CA}{2.4}\right)^{A} \tag{3.4}$$

where the coefficient A is 5.1 for saturated soil behind a glass window and 5.9 for dry soil.

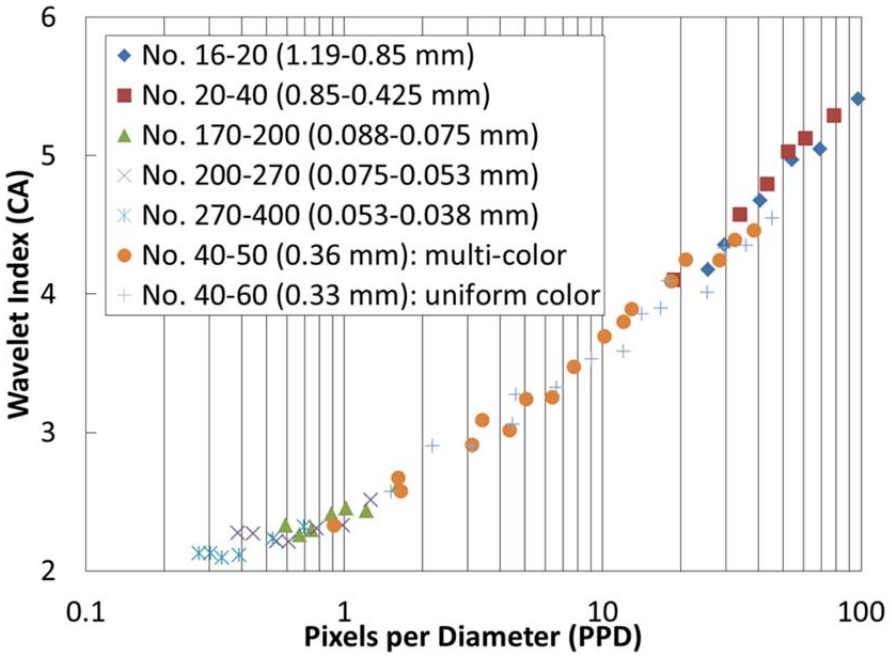

Figure 3.23 *CA* vs *PPD* for various soils (Jung 2010)

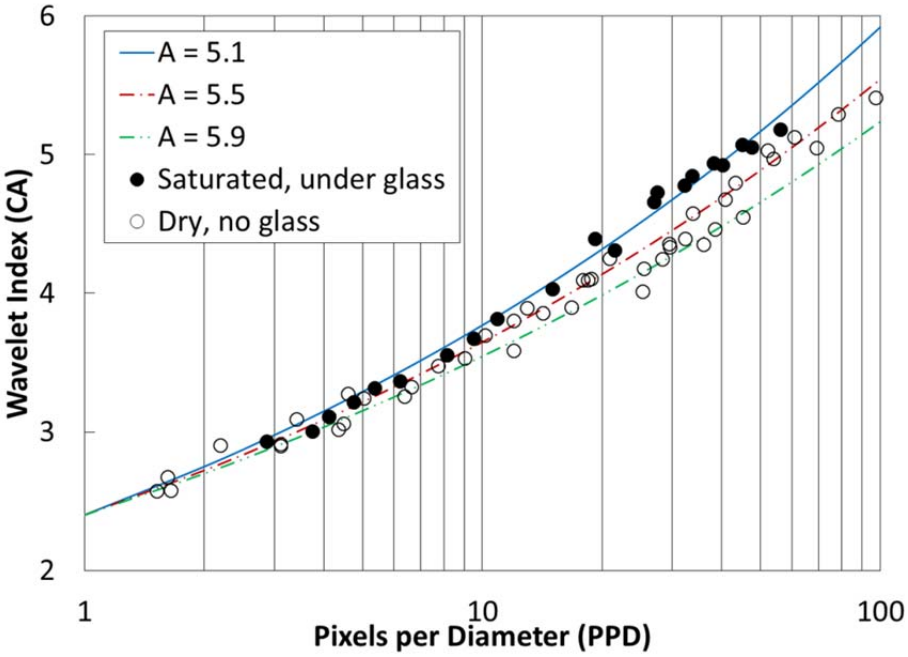

Figure 3.24 *CA* vs *PPD* for saturated soil (Hryciw et al. 2009)

Once the *CA* is determined for an image containing nearly uniform sized grains, the *PPD* is computed by Equation (3.4) and the actual particle size can be computed as:

$$D = \frac{PPD}{M} \tag{3.5}$$

where D is the average actual diameter of soil particles (mm) and M is the camera magnification (pix/mm).

3.4.3 CA vs PPD Calibration and Particle Size Distribution

It is noted that the data for calibration (Figure 3.23 and 3.24) was collected using 128 × 128 areas of relatively uniform sized particles that were obtained by pre-sieving the soil through successive sieves with closely spaced opening sizes. Nevertheless, even the particles retained between two successive standard US sieves vary by 50% to 100% in diameter. Furthermore, even for an assembly of "uniform sized" soil grains, the observed *CA* values show some scatter due to the random fabric, pore spaces, particle angularities etc. Therefore, there will naturally be some statistical variation in computed particle sizes between different 128 × 128 regions of the same "uniform sized" soil specimen. Figure 3.25 illustrates the *CA* versus *PPD* data scatter for a soil called "2NS" by the Michigan Department of Transportation. The rectangular blocks have horizontal dimensions corresponding to the range between sieve openings from which specimens were collected and the vertical dimension of each rectangle represents plus or minus one standard deviation (σ) of observed *CA* values for each size range.

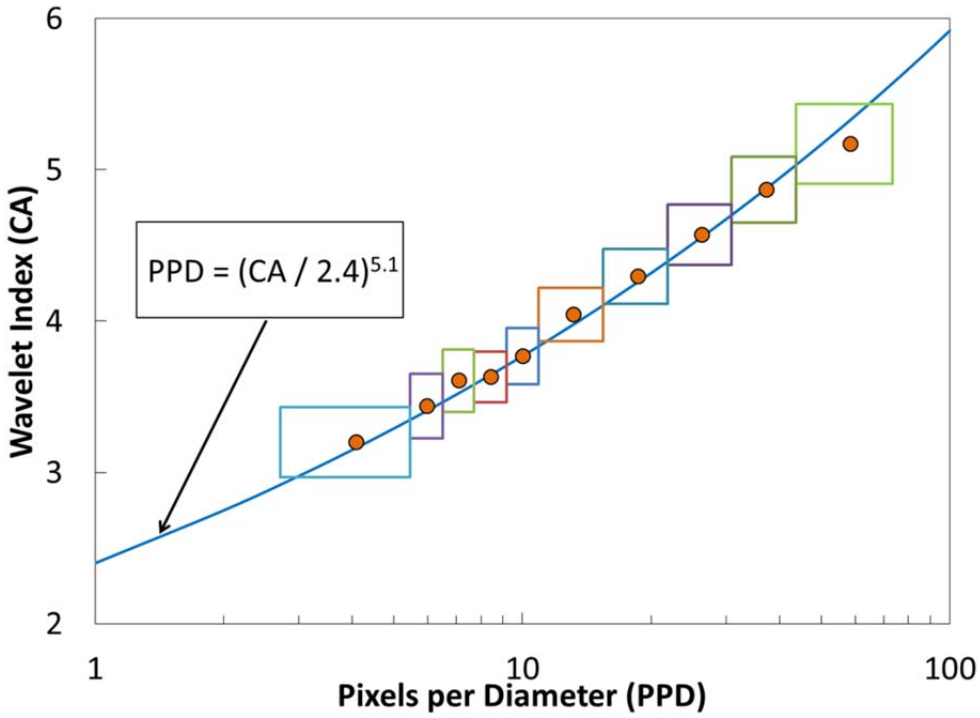

Figure 3.25 Ranges of *CA* and *PPD* values for 2NS soil

In light of the statistical variations in *CA* values, to obtain a reasonable estimate of the particle size distribution of a soil specimen, a large number of 128 × 128 areas of an image must be analyzed. For example, for each of the images in Figure 3.19 approximately 5000 overlapping 128 × 128 areas were used to develop the particle size distributions. The 10 colored squares at the bottoms of the sorted soil columns in Figure 3.19 show the size of the 128 × 128 areas which scan vertically through the specimen. Because of their small size relative to the full image, the analysis areas contain soil grains of similar size. *CA* is computed for each analysis area and converted to *PPD* and *D* by Equations (3.4) and (3.5) respectively. All of the data is then sorted by particle size to produce the final grain size distribution shown in Figure 3.26.

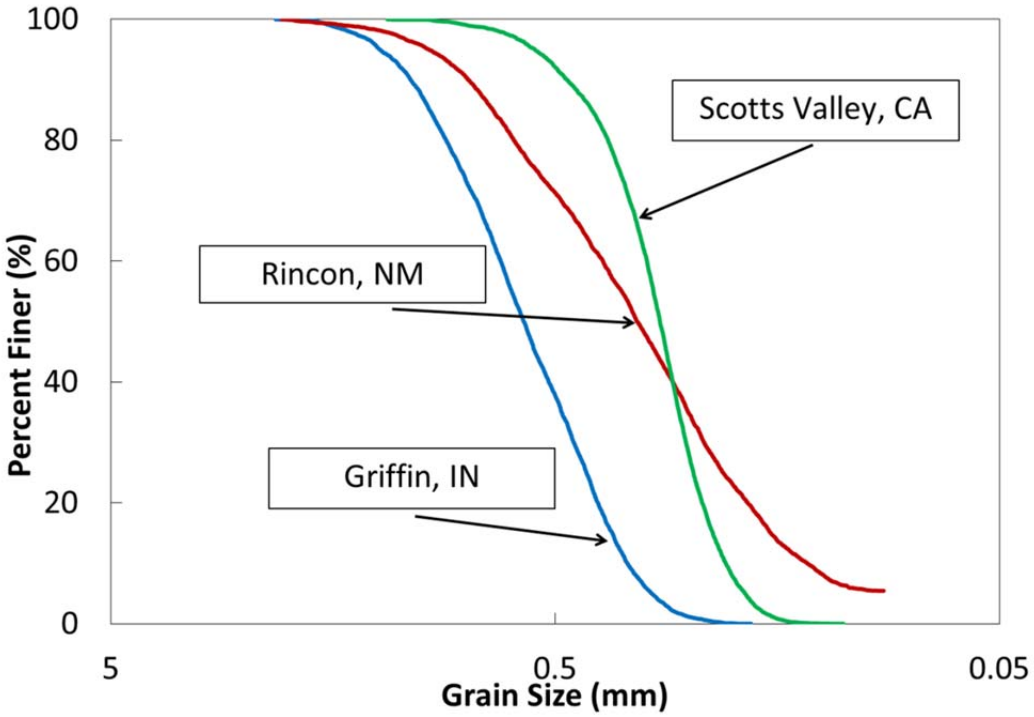

Figure 3.26 Particle size distributions of soils in Figure 3.19

3.5 Percentage of Fines Determination

With future advances in DSLR camera technology, a single sedimaging photographic will be able to size particles over a larger range than the current 2.0 mm to 0.075 mm. Indeed, at their current development trajectory, commercial DSLR cameras could size particles down to 0.020 mm within five to ten years (Ohm and Hryciw 2013a).

For now, the percentage of fines in a soil specimen can still be determined in the Sedimaging test. The procedure combines some small volume of fines observed in the image (soil particles in the sedimented soil column found above the level at which 0.075 mm particles are detected) with the weight of soil solids removed during sedimentation column drainage (see Chapter 3.3). The latter component is termed the partial percentage of fines (*P%F*) and computed by:

$$P\%F = \left(\frac{W_s - W_{sa}}{W_s} \right) \times 100(\%) \tag{3.6}$$

where W_s is the dry weight of the test specimen and W_{sa} is the weight of soil deposited in the accumulator. W_{sa} is computed by:

$$W_{sa} = \frac{G_s \left[W_{s+wf+a} - W_{a+w} \right]}{G_s - 1} \tag{3.7}$$

where W_{s+wf+a} is the combined weight of the soil in the accumulator, the water in the accumulator and accumulator itself; W_{a+w} is the weight of the accumulator filled with water; and G_s is the specific gravity of the specimen solids.

3.6 Comparison of Sieving and Sedimaging Particle Size Distribution

Tests were performed on nine different soils to compare Sedimaging grain size distributions to sieving. The soil colors and particle shapes were determined by visual observation and are listed in Table 3.1 and sample images are shown in Figure 3.27.

Table 3.1 Soil description of different soils

Soil Name	Soil Color	Particle Shape	Color Uniformity
2NS	Light brown	Subrounded to subangular	Uniform to non-uniform
Capitola, CA	Light brown	Subrounded to subangular	Uniform to non-uniform
Class IIA	Very light brown	Subangular	Uniform
Costa Rica	Black	Subrounded	Non-Uniform
Griffin, IN	Light brown	Subrounded to subangular	Non-Uniform
Rincon, NM	Light reddish	Subrounded to subangular	Uniform
Scotts Valley, CA	Grey	Subangular	Uniform to non-uniform
Upper Peninsula, MI	Reddish	Subrounded to subangular	Uniform to non-uniform
Oakland Co., MI	Light brown	Subangular	Uniform

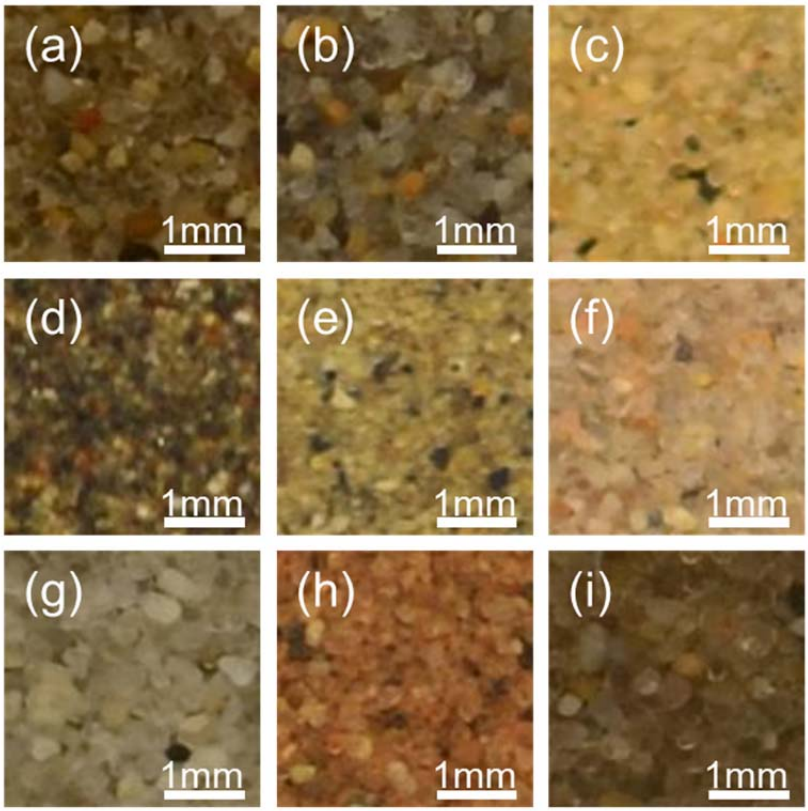

Figure 3.27 Sample soil images: (a) 2NS, (b) Capitola, (c) ClassIIA, (d) Costa Rica, (e) Griffin, (f) Rincon, (g) Scotts Valley, (h) Upper Peninsula, and (i) Oakland Co.

Typical Sedimaging results are shown in Figure 3.28 and 3.29. Since Sedimaging images such as shown on Figure 3.28 (*a*) and 3.29 (*a*) contain particles sorted by size, the image is analyzed incrementally with height to produce the complete grain size distribution. The areas of analysis are 128 pixels × 128 pixels as shown by the colorful squares at the bottom of the image. Because of their small size relative to the full image, the analysis areas contain soil grains of similar size. The analysis squares scan up through the image in 10 adjacent non-overlapping columns moving vertically eight pixels at a time. At each elevation the *CA* is computed and successively converted to *PPD* and *D*. This yields about 5,500 values of *D* from the 1,280 (H) × 4,500 (V) pixels image. The vertical dimension is the full height of the soil column but the horizontal dimension is cropped down from a slightly wider image of the full accumulator

window. A random but representative 20% of the data points are shown in Figure 3.28 (*b*) and 3.29 (*b*). All of the data is then sorted by particle size to produce the final grain size distribution shown in Figure 3.28 (*c*) and 3.29 (*c*). Since variations in void ratio in the column have been shown to be insignificant (Hryciw and Jung 2008; Hryciw and Jung 2009), each data point represents an equal percentage of the specimen by volume.

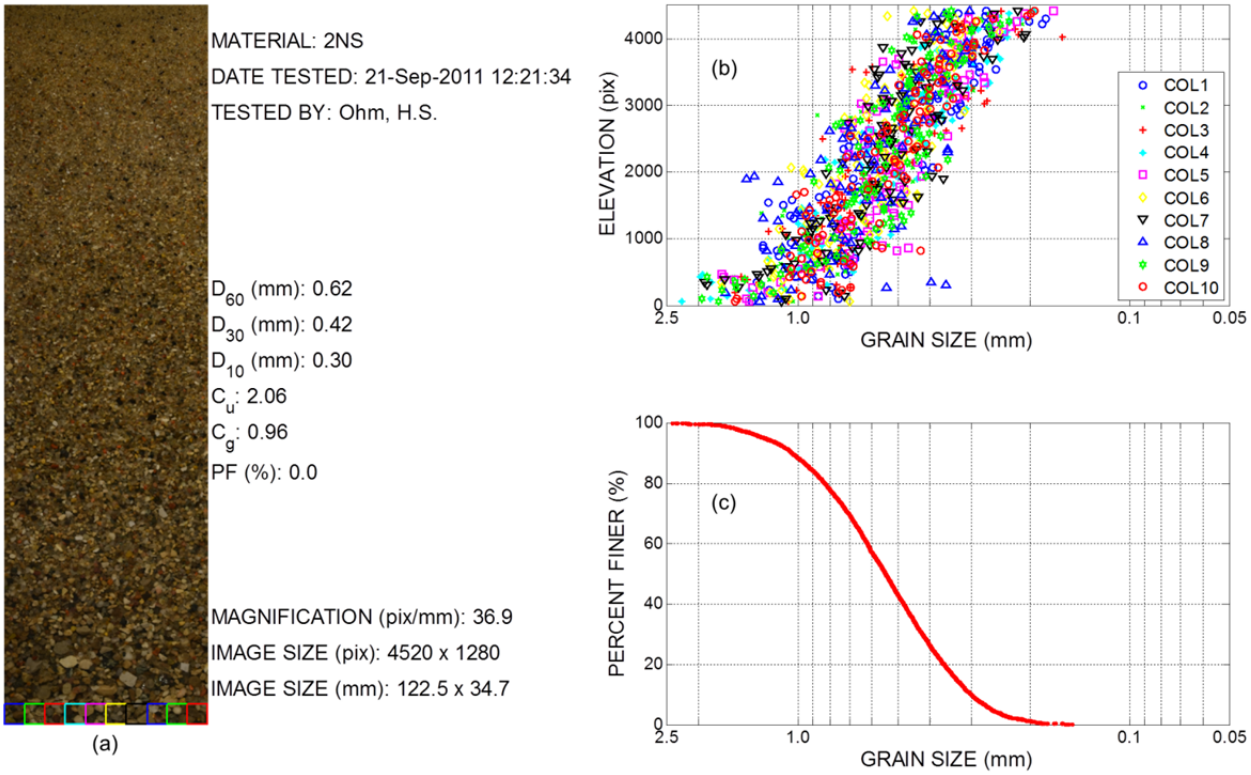

Figure 3.28 Typical Sedimaging result: 2NS soil

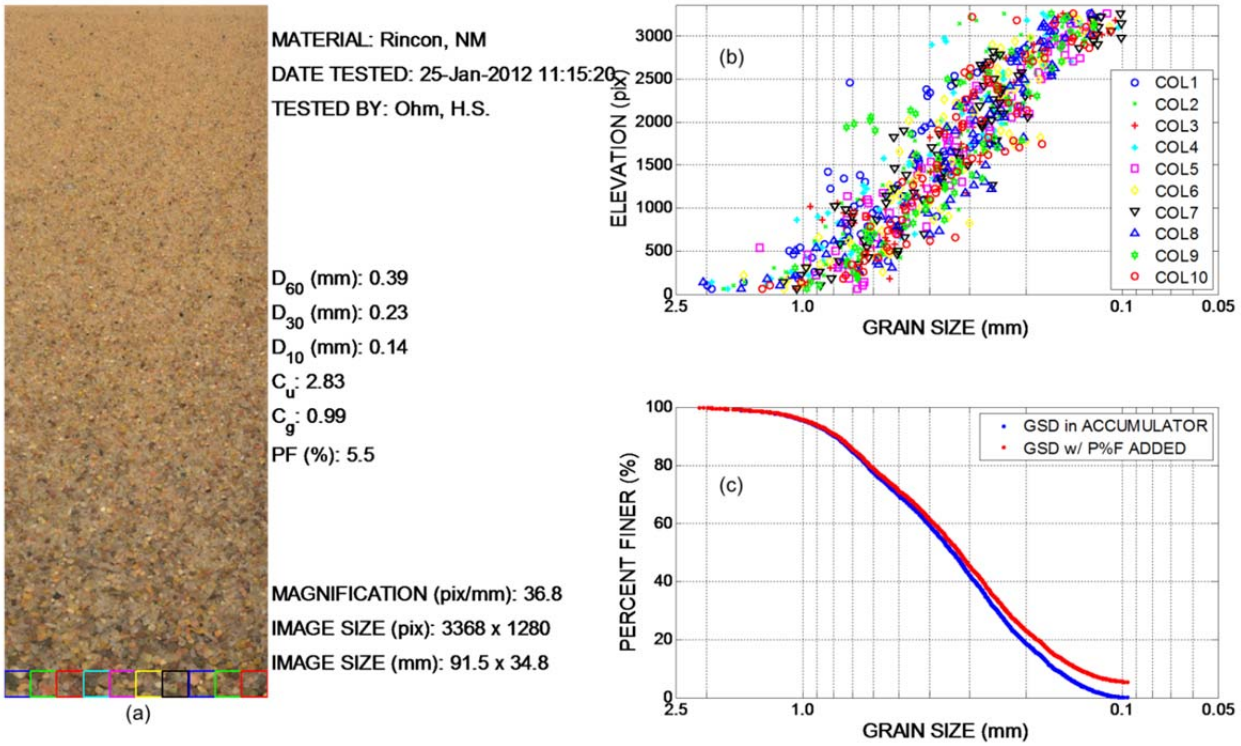

Figure 3.29 Typical Sedimaging result: Rincon soil

The values of D_{85}, D_{60}, D_{50}, D_{30}, D_{10} and the coefficient of uniformity, D_{60}/D_{10} determined by sieving and Sedimaging are tabulated in Table 3.2. The weights of the soil specimens used both in Sedimaging and sieving ranged from 400 g to 500 g. The same soil specimens were used for both tests to eliminate any randomness that could result from soil splitting. The results are compared graphically in Figure 3.30. For both tests only the data points are shown with no curve fitting. The differences in appearance of the two data sets is due to the fact that sieving provides only 10 to 11 data points compared to over 5,000 by Sedimaging. Finally, the data from Table 3.2 is compared graphically in Figure 3.31. Complete Sedimaging results can be found in Appendix C.

Table 3.2 Comparisons between sieve and Sedimaging results of different soils

Soil Name	Sieving						Sedimaging					
	D_{85} (mm)	D_{60} (mm)	D_{50} (mm)	D_{30} (mm)	D_{10} (mm)	C_u	D_{85} (mm)	D_{60} (mm)	D_{50} (mm)	D_{30} (mm)	D_{10} (mm)	C_u
2NS	1.00	0.57	0.50	0.38	0.25	2.28	0.92	0.62	0.54	0.42	0.30	2.07
Capitola, CA	0.47	0.36	0.35	0.30	0.23	1.57	0.56	0.44	0.4	0.35	0.29	1.52
Class IIA	0.38	0.26	0.24	0.18	0.11	2.36	0.34	0.22	0.19	0.15	0.11	2.00
Costa Rica	0.18	0.16	0.15	0.12	0.10	1.60	0.20	0.16	0.14	0.12	0.11	1.45
Griffin, IN	1.00	0.68	0.60	0.45	0.30	2.27	0.96	0.67	0.59	0.45	0.34	1.97
Rincon, NM	0.74	0.42	0.36	0.26	0.14	3.00	0.69	0.39	0.33	0.23	0.14	2.79
Scotts Valley, CA	0.45	0.34	0.33	0.27	0.22	1.55	0.41	0.31	0.29	0.25	0.21	1.48
Upper Peninsula, MI	1.10	0.68	0.60	0.41	0.24	2.83	0.91	0.58	0.45	0.32	0.20	2.90
Oakland Co., MI	0.48	0.35	0.31	0.26	0.22	1.59	0.46	0.31	0.28	0.23	0.19	1.63

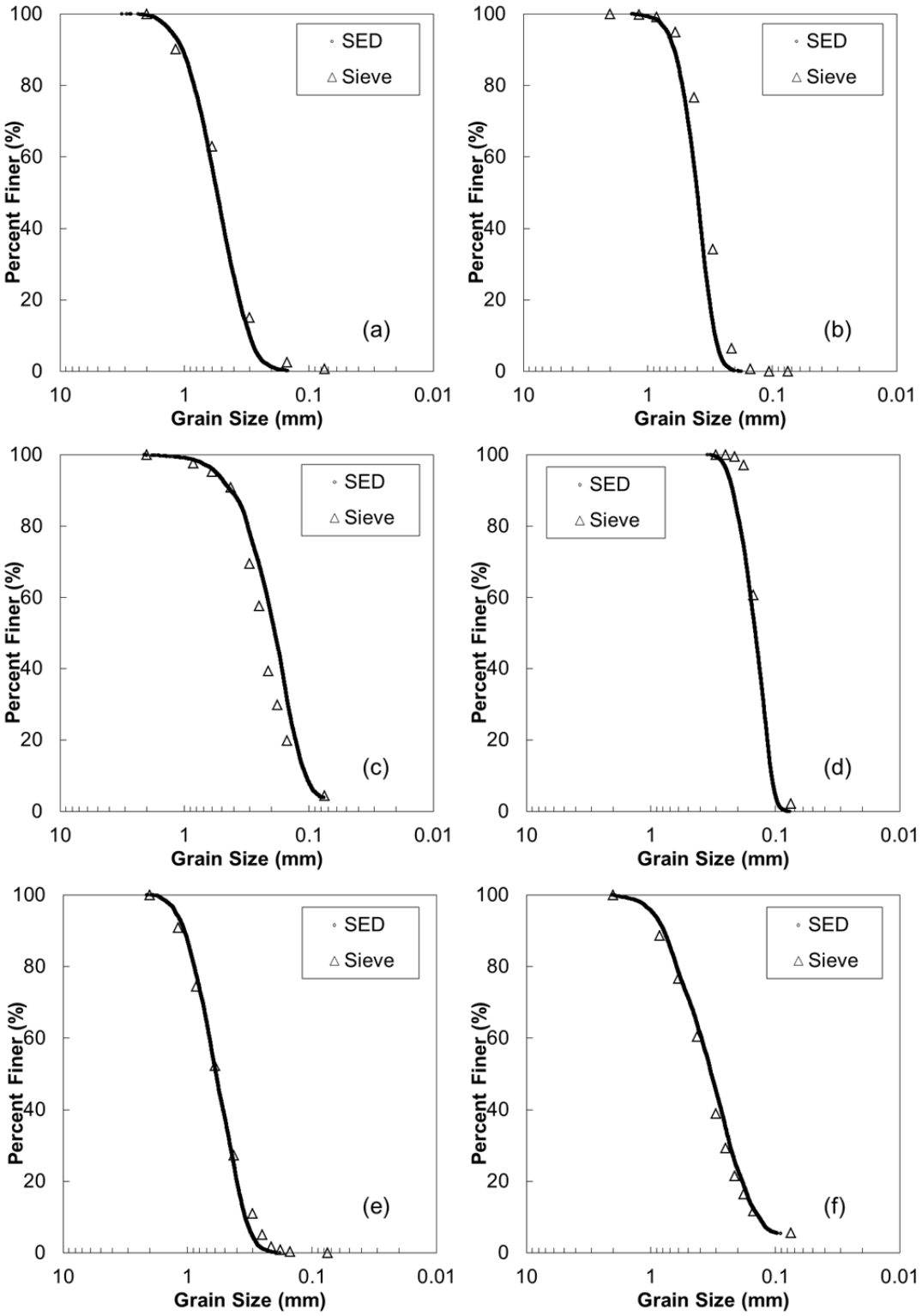

Figure 3.30 Sedimaging test results: (a) 2NS, (b) Capitola, (c) ClassIIA, (d) Costa Rica, (e) Griffin, (f) Rincon

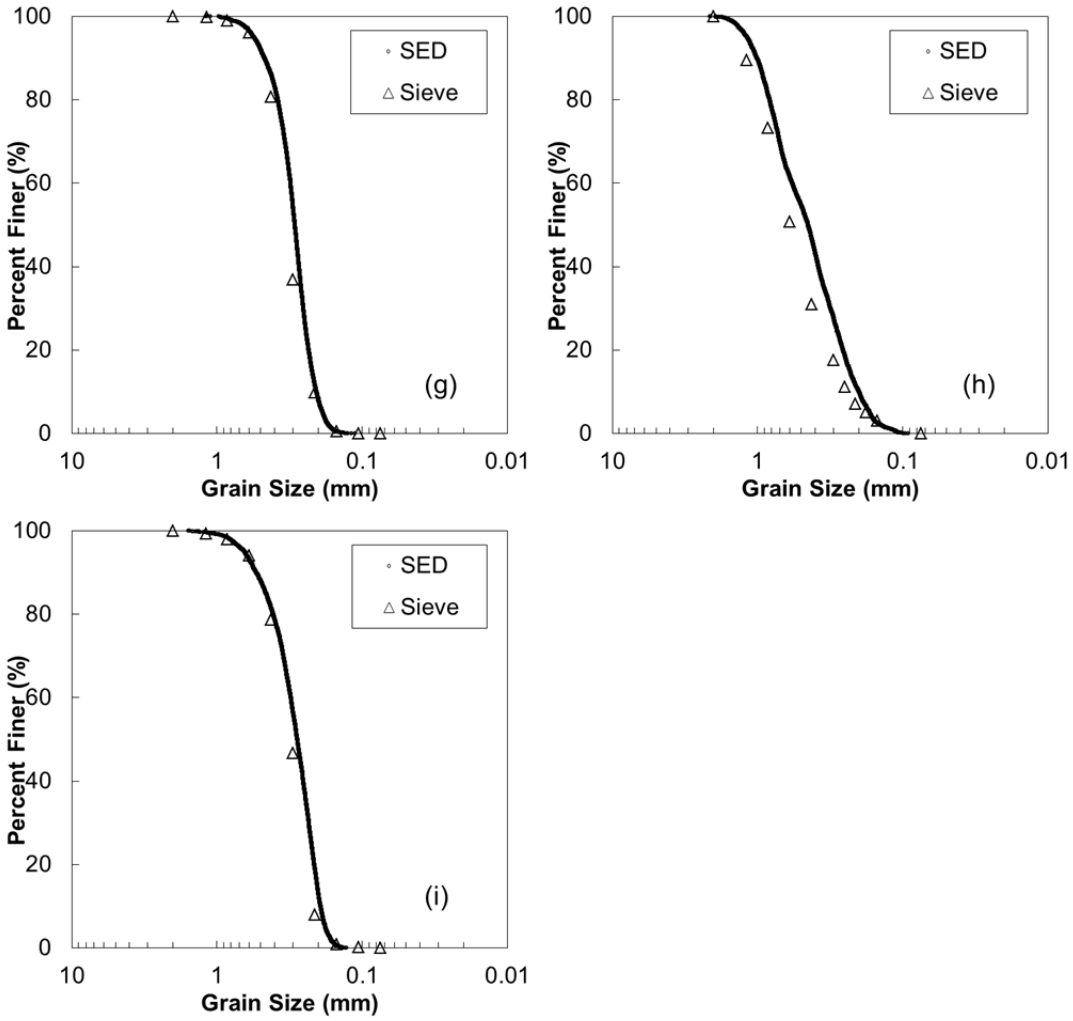

Figure 3.30 (Continued) Sedimaging test results: (g) Scotts Valley, (h) Upper Peninsula, (i) Oakland Co.

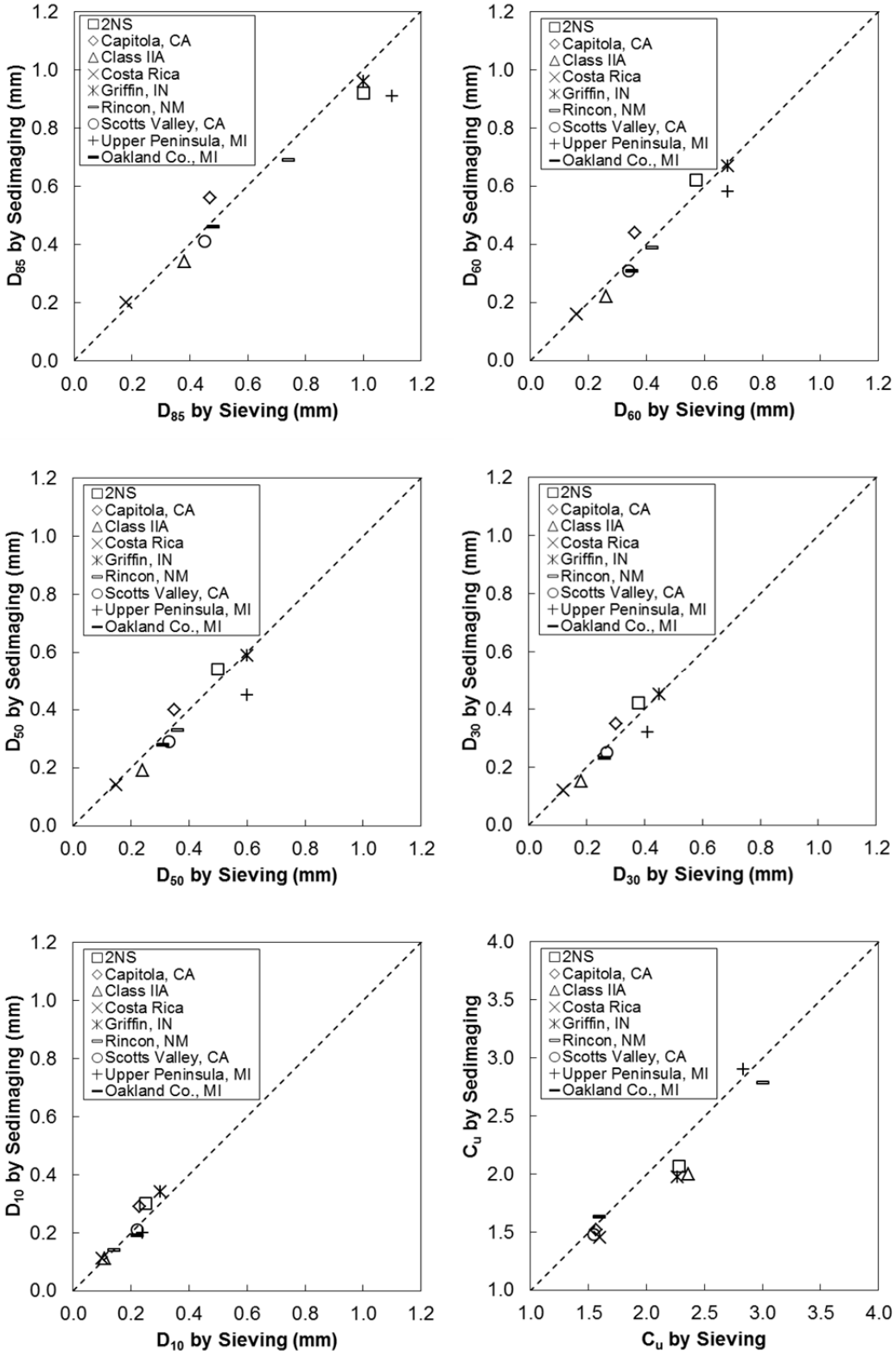

Figure 3.31 Comparison between Sedimaging and sieving

Because the *CA* versus *PPD* calibration curve was developed from images of pre-sieved soils and because their *PPD*s were computed from known sieve openings, the Sedimaging test does not redefine particle size. Instead, it essentially mimics sieving. As such, despite some slight variations, excellent agreement was observed between Sedimaging and sieving results in almost all nine tests. This is only surprising given that the colors, shapes and gradations of the tested soils were chosen based on their variability. The image processing for all nine Sedimaging tests used the same calibration curve that was developed on entirely different soils some years ago. Nevertheless, if Sedimaging is to be used for quality control purposes where soil with the same geological origin were to be tested repeatedly (such as for borrow from a quarrying operation), it is recommended that a site (geology) specific calibration curve be used to insure a perfect match between sieve and Sedimaging results and it will be discussed in Chapter 3.7.

3.7 Effects of Surface Textures on a Calibration Curve

For the majority of natural soils the relationship between *CA* and *PPD* can be expressed by Equation (3.4). However, for soils with rough, pitted or mottled particles, the size distribution by Sedimaging when using Equation (3.4) tends to deviate from the size distribution by sieving. Figure 3.32 and 3.33 show calibration curves for "30A" and "Gabbro" soils that have rough, pitted or mottled particles. Each data point represents the average *CA* at the average *PPD*. The error bars in the vertical direction indicate plus or minus one standard deviation in *CA*, while the error bars in the horizontal direction indicate the two bounding sieve sizes.

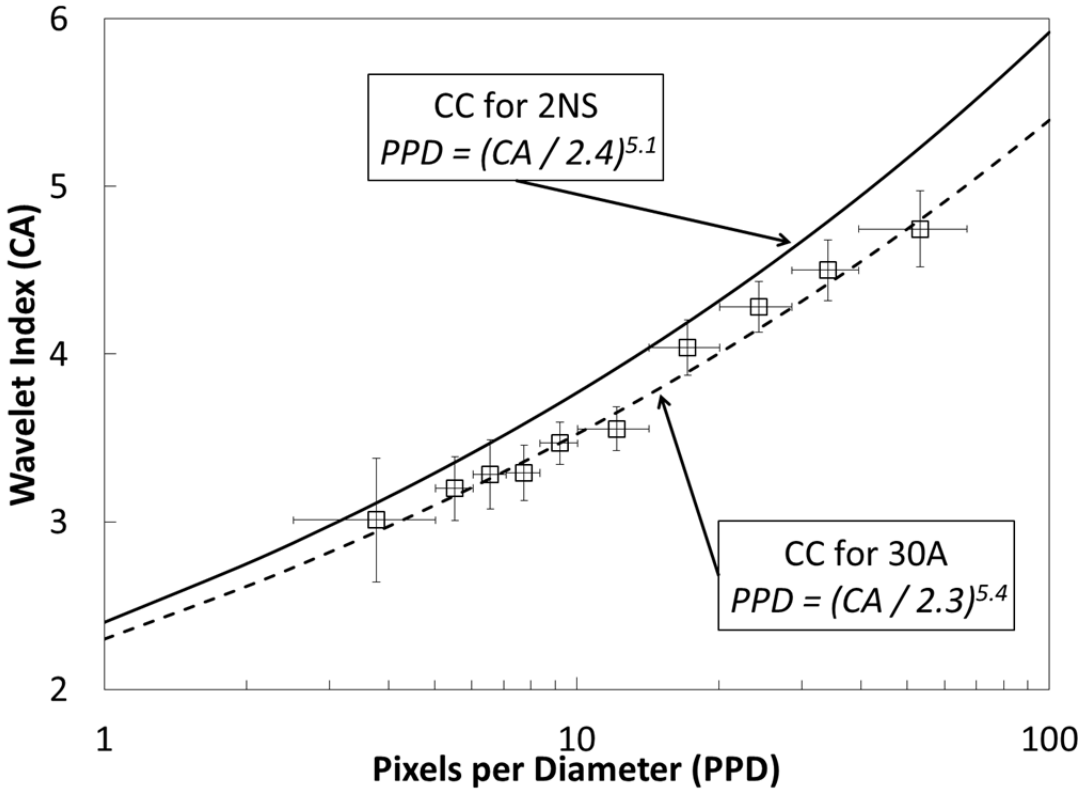

Figure 3.32 A calibration curve for 30A soil

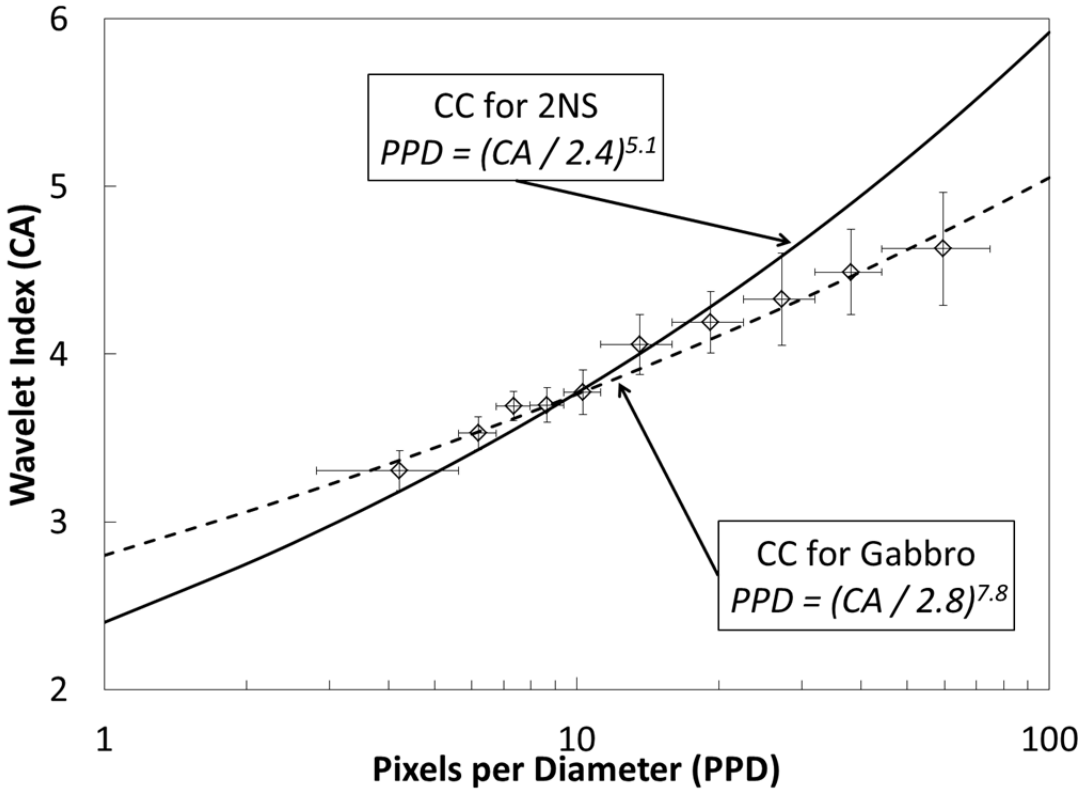

Figure 3.33 A calibration curve for Gabbro soil

Figure 3.32 and 3.33 show that data points obtained from 10 different pre-sieved 30A and Gabbro soils deviate from the calibration curve for 2NS soil. For 30A soil, all of the data points shift downward, while for Gabbro soils more deviation from the calibration curve for 2NS is observed at higher *PPD*. Figure 3.34 shows particles at about the same size for the three soils. The 30A and Gabbro soil particles have more internal texture than 2NS particles. Internal particle texture is interpreted as smaller particles by image analysis thereby causing Sedimaging to underestimate the actual particle sizes. Therefore, at the same *PPD*, *CA* will be smaller for soil with more internal texture causing a shift in the calibration curve downward.

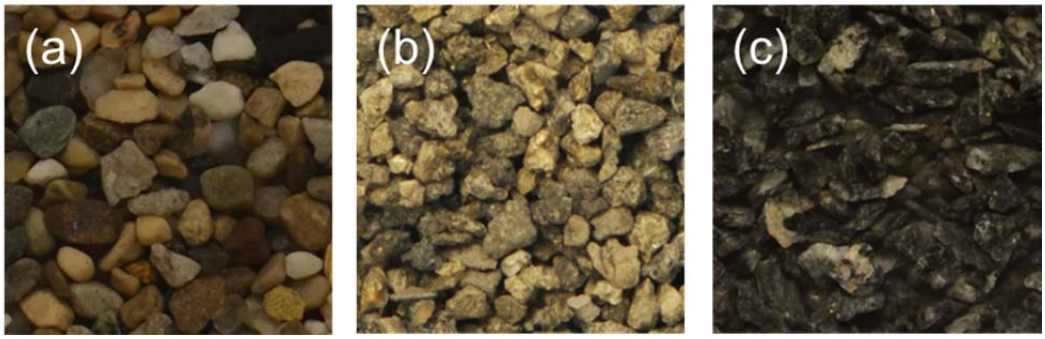

Figure 3.34 Soil image of different soils: (a) 2NS, (b) 30A, (c) Gabbro (*PPD* = 53.3 ~ 59.6)

If Sedimaging is to be used for quality control purposes for soil particles with erratic internal textures (intraparticle color variations or particle roughnesses), soil-specific calibration curves should be developed to insure a better match between sieve and Sedimaging results such as Figure 3.32 and 3.33. Modified Sedimaging results using these soil-specific calibration curves (Figure 3.32 and 3.33) are shown in Figure 3.35 and 3.36.

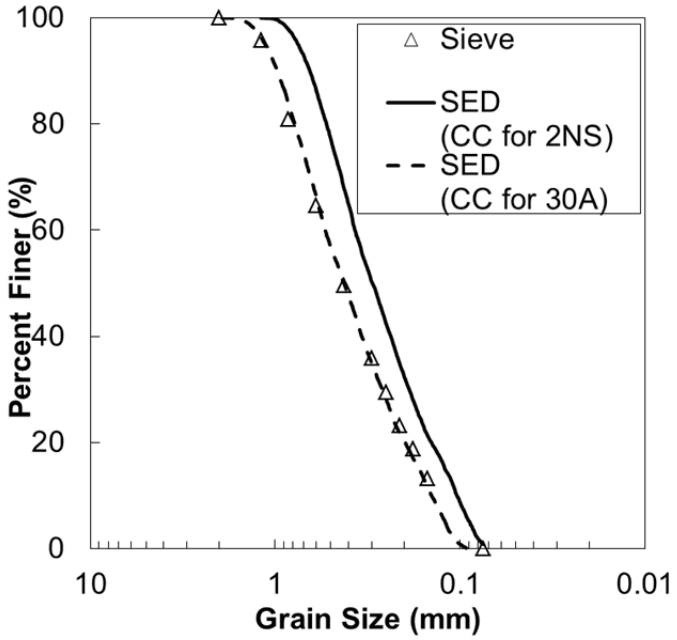

Figure 3.35 Grain size distributions using the calibration curve for 2NS and 30A

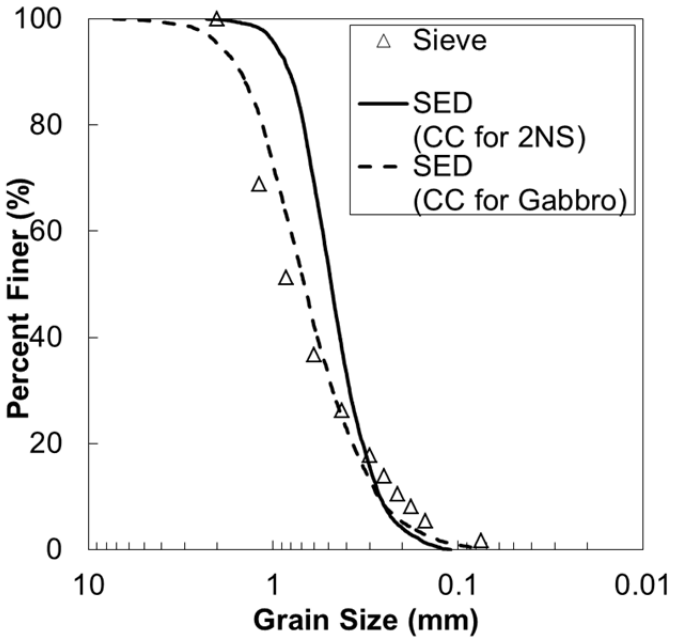

Figure 3.36 Grain size distributions using the calibration curve for 2NS and Gabbro

3.8 Correlation between Energy Ratio and Particle Orientation

As discussed earlier in Chapter 3.4, Energy is defined as a measure of the magnitude of the differences between average grayscale values of adjacent regions in an image. Since the Energy can be considered separately for horizontal, vertical, and diagonal directions, more information about the soil such as particle shape, particle orientation and fabric can be obtained. To this end, an *Energy Ratio* (*F*) is defined to compare wavelet decomposition Energies in the horizontal and vertical directions:

for $E_{Hi} > E_{Vi}$

$$F = \frac{\sum_{i=1}^{n} E_{Hi}}{\sum_{i=1}^{n} E_{Vi}} \tag{3.8}$$

for $E_{Hi} < E_{Vi}$

$$F = -\frac{\sum_{i=1}^{n} E_{Vi}}{\sum_{i=1}^{n} E_{Hi}} \tag{3.9}$$

where *F* is the *Energy Ratio* and E_{Hi} and E_{Vi} are Energies in the horizontal and vertical directions, respectively. Thus, *F* values greater than +1 are indicative of particles oriented with their long axes horizontally, while *F* values smaller than -1 indicate vertical orientation of the long axes. The absolute value of *F* is an indicator of overall particle sphericity with $|F| \approx 1$ for very spherical particles.

Images of 2NS soil of different size ranges were taken with different camera magnifications in the Sedimaging accumulator and on a flat surface. Values of *F* were computed to analyze the effects of particle shape and orientation on *F*. Figure 3.37 and 3.38 show typical results obtained from the Sedimaging and the flat surface tests.

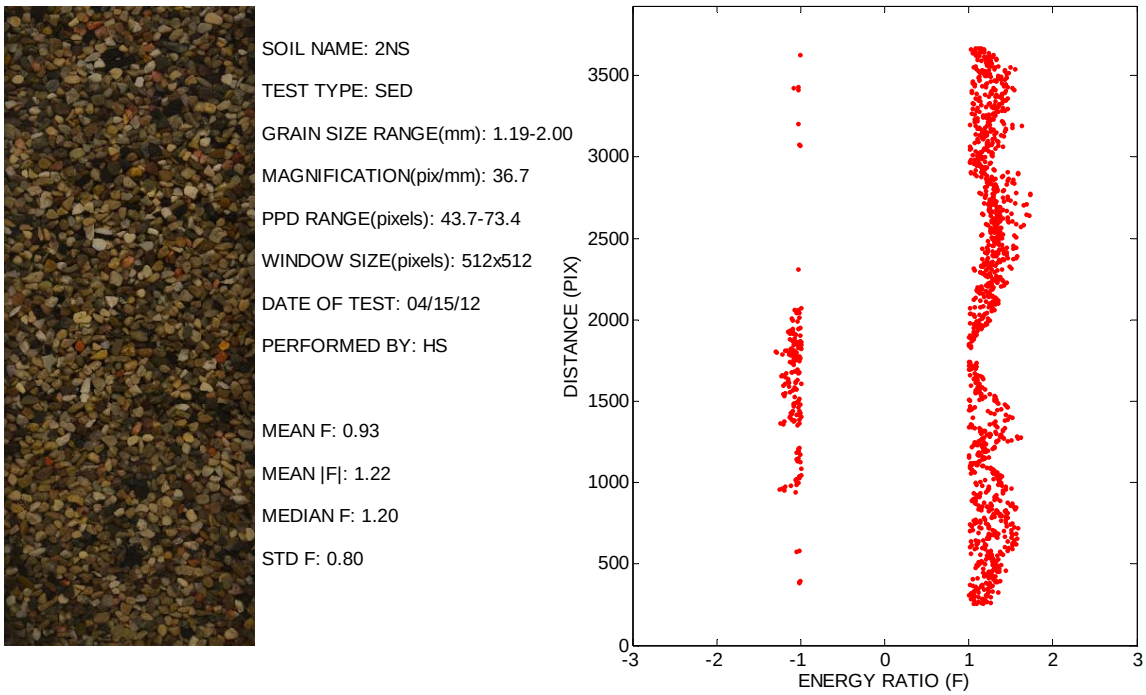

Figure 3.37 Typical *Energy Ratio* distributions of soils in the Sedimaging soil accumulator

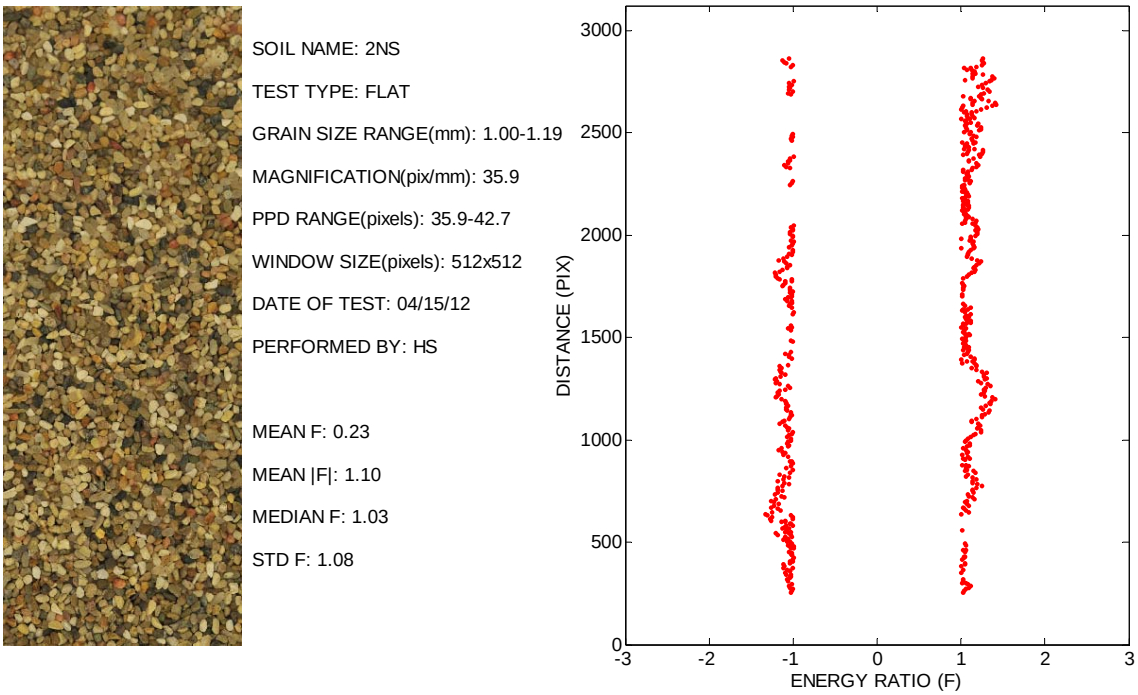

Figure 3.38 Typical *Energy Ratio* distributions of soils in the flat surface test

As shown in Figure 3.37 and 3.38, more F values greater than +1 were observed in the Sedimaging accumulator, while F values are distributed in both greater than +1 and less than -1 in the flat surface test. Obviously, soil particles in the Sedimaging are oriented with their long axes horizontally ($F > 1$), whereas soil particles placed on the flat surface are randomly oriented because there is no sedimentation through water. 15 tests were performed (Table 3.3) and the mean value of F and the mean absolute value of F were compared (Figure 3.39 and 3.40).

Table 3.3 Energy Ratio analysis on 15 tests

Different Soil Sizes with Same Camera Magnification in Sedimaging Test					
PPD	58.6	37.3	26.4	18.6	13.2
Mean F	0.93	1.21	1.23	1.22	1.16
Mean Absolute F	1.22	1.26	1.23	1.22	1.18
Same Soil Sizes with Different Camera Magnifications in Sedimaging Test					
PPD	71.0	56.5	46.8	39.9	34.8
Mean F	0.98	1.11	1.29	1.25	1.30
Mean Absolute F	1.28	1.19	1.29	1.25	1.30
Same Soil Sizes with Different Camera Magnifications on a Flat Surface					
PPD	39.3	28.9	23.0	18.9	16.3
Mean F	0.23	-0.27	-0.14	-0.33	-0.12
Mean Absolute F	1.10	1.06	1.07	1.05	1.05

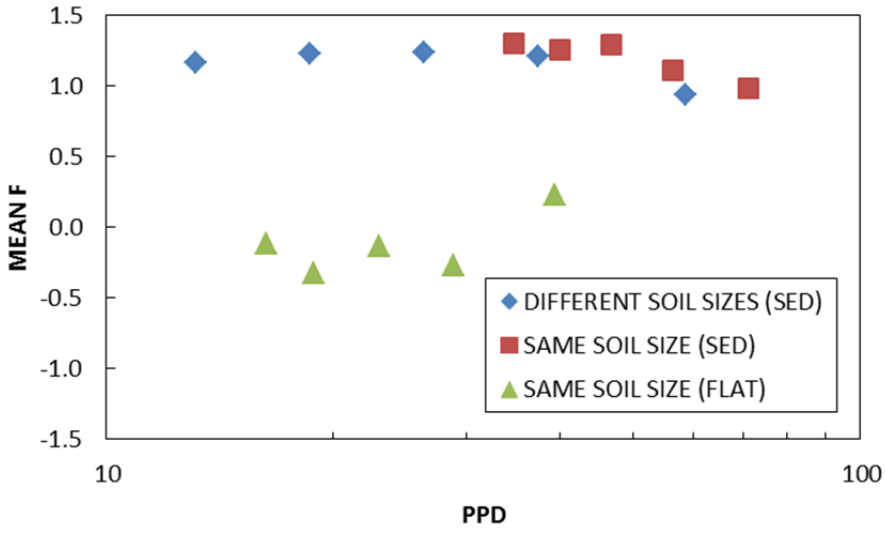

Figure 3.39 The mean value of *F* from the Sedimaging and the flat test

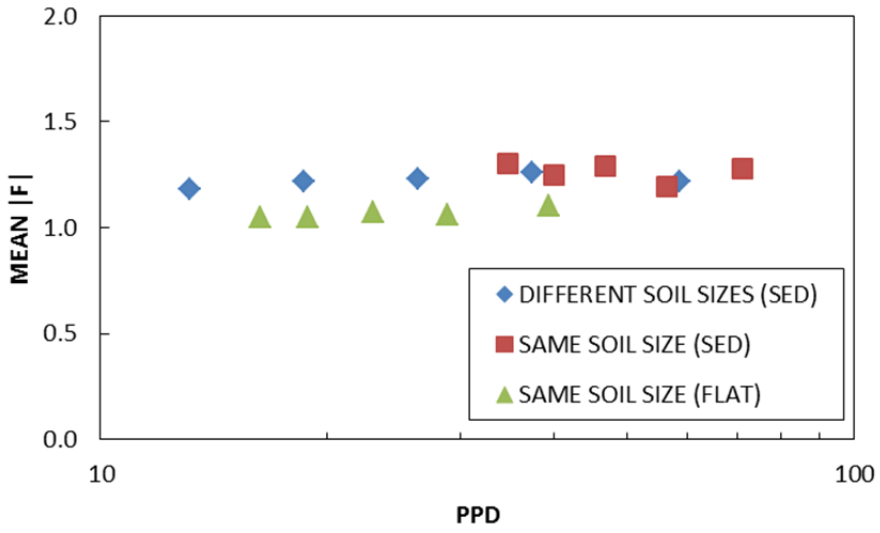

Figure 3.40 The mean value of absolute *F* from the Sedimaging and the flat test

Different sizes of sieved 2NS soil (1.19 ~ 2.00 mm, 0.84 ~ 1.19 mm, 0.60 ~ 0.84 mm, 0.42 ~ 0.60 mm and 0.30 ~ 0.42 mm) were used with the same magnification (36.7 pix/mm) in the Sedimaging test, while same sizes of sieved 2NS soil (1.19 ~ 2.00 mm in the Sedimaging test and 1.00 ~ 1.19 mm in the flat surface test) were used with different magnifications (44.5, 35.4,

29.3, 25.0 and 21.8 pix/mm in the Sedimaging and 35.9, 26.4, 21.0, 17.2 and 14.9 pix/mm in the flat test). The mean value of F in the Sedimaging test is around 1.2, while the mean value of F in the flat surface test is around -0.1. The mean of the absolute F in the Sedimaging test is around 1.24, while the absolute value of F in the flat surface test is around 1.07. As discussed earlier, soil particles are oriented with their longest axes horizontally in the Sedimaging apparatus making the mean F values larger than 1, while soil particles spread on a flat surface have randomly distributed orientations making the mean F values around 0. Soil particles in the Sedimaging test will typically show their longest and shortest axis, while in the flat surface test will typically show their longest and intermediate axis. Thus, the mean absolute value of F in the Sedimaging test is higher than the mean absolute value of F in the flat surface test. These observations show that the mean of F could be an indicator of particle orientation or fabric, whereas the mean of absolute F could be an indicator of particle shape or sphericity. Overall, the F values obtained by the Sedimaging could be an excellent indicator of particle shape and the potential for development of an oriented soil fabric. It needs to be correlated with particle sphericity and more fundamental soil properties such as anisotropic stiffness and strength.

3.9 Segmentation Using Mean-Shift Clustering

3.9.1 Image Segmentation

Not only image-based methods for particle size distribution determination but also for particle shape determination can be categorized into deterministic methods and statistical methods. Statistical approach to determine particle shape such as the method using Energy Ratio gives an overall trend in particle shape within an image analysis area. Deterministic approach to determine particle shape may need to delineate individual particles prior to determining the particle shape. A potential deterministic method to quantify particle shapes from the images of the sedimented soil is discussed in this chapter. *Image segmentation* is used to delineate individual particles by dividing the image into components sharing a common characteristic such as a gray scale value. Two image segmentation methods, *k-means clustering* and *mean-shift clustering* are introduced. Then, a method for particle segmentation in an image is proposed.

3.9.2 k-means Clustering

Digital images consist of a matrix of pixels in the x-y coordinate space. For black and white photos, each pixel has a gray scale intensity value from 0 to 255 (in 8-bit images). Pixel intensity values can be plotted as the z-coordinate for an image location defined by the x-y spatial coordinates. Image segmentation methods then assign these x-y-z points to a group whose coordinates are relatively close to each other in the three dimensional space. *k*-means clustering shown in Figure 3.41 is one of these image segmentation methods (Forsyth and Ponce 2003). The steps for *k*-means clustering are:

1) A *k*-value is chosen equal to the number of objects (particles) expected in an image. These are called "seeds" (Figure 3.41 (*a*)).
2) The *k* number of seeds are placed at random locations on the image.
3) The distances between each seed and all pixel points in the image are computed (Figure 3.41 (*b*)).
4) Each pixel in the image is assigned to a group containing the seed nearest to the image pixel. In other words, all image points "cluster" around their nearest seed.
5) The location of the seed is moved to the geometric centroid of its cluster (Figure 3.41 (*c*)).
6) The distances between each seed in its new location and all pixel points in the image are computed.
7) All image points are reassigned to their nearest seed.
8) The location of the seed is moved to the new geometric centroid of its cluster.
9) Step 6) to 8) are repeated until the differences between the new centroid location and the precious centroid location are negligible.

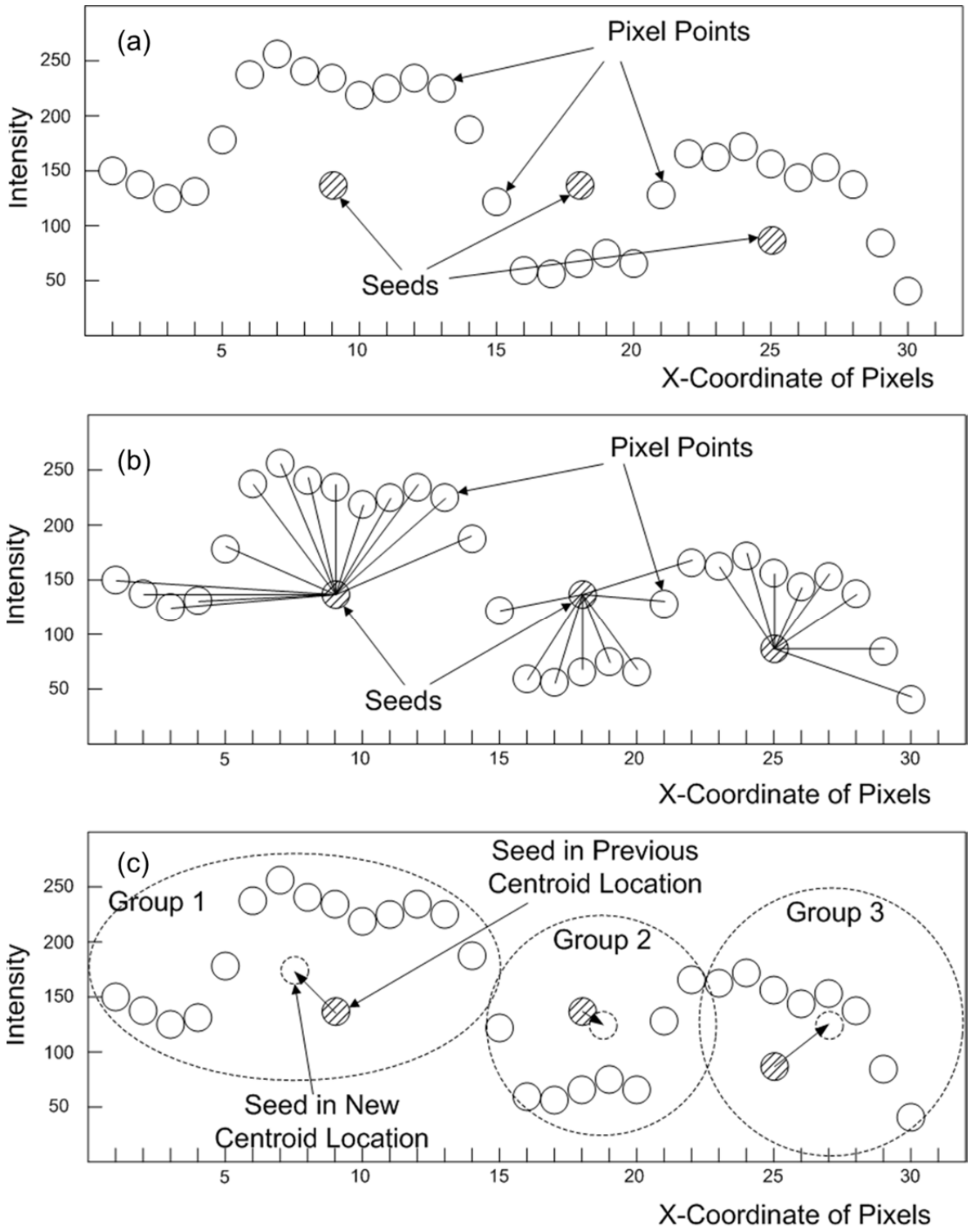

Figure 3.41 The concept of *k*-means clustering

3.9.3 Mean-shift Clustering

The main drawbacks of *k*-means clustering are the need to pre-estimate the number of required seeds (*k*) and the effect of the initial placement of the seeds on the segmentation results. To solve these problems, mean-shift clustering shown in Figure 3.42 was proposed by Comaniciu and Meer (2002). Mean-shift clustering finds locations of the highest densities of points in the three dimensional space where the z-coordinates are again the gray-scale intensity values. The steps for mean-shift clustering are:

1) A pixel point in the three dimensional space of an image is randomly chosen (Figure 3.42 (*a*)).
2) A centroid (an old centroid) of pixel points that are located within a radius *R* from the selected pixel point is computed. Note that the radius *R* is selected arbitrary.
3) A centroid (a new centroid) of pixel points that are located within a radius *R* from the old centroid is computed (Figure 3.42 (*b*)).
4) Step 2) and 3) are repeated until the difference between the old centroid and the new centroid is negligible (Figure 3.42 (*c*)).
5) This process is then repeated using every point in the entire image.
6) All of the original image points that ultimately end up having the same (common) final centroid are assigned to their own unique "group".

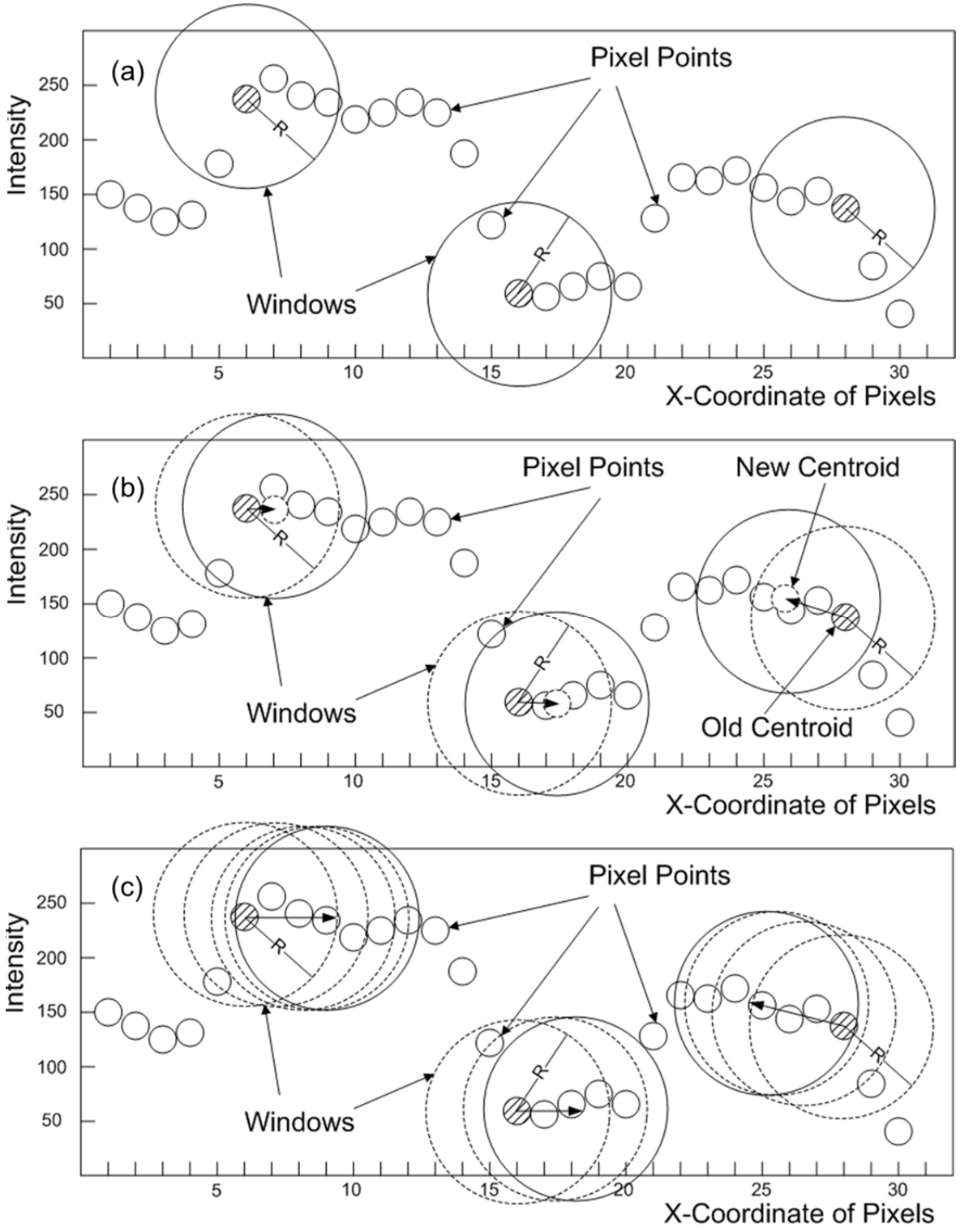

Figure 3.42 The concept of mean-shift clustering

The groups of pixel points reveal zones of similar gray scale value. In a sedimented soil image from the Sedmaging, these may be parts of a particle having similar internal shades of gray, voids between soil particles, entire individual soil particles, or combinations of two (or more) adjacent soil particles having similar gray scales. Obviously, it would be best if the group reflected only "entire particles" rather than parts of particles, voids or agglomerations of adjoining particles.

3.9.4 Window Radius R and Particle Shape Determination

Mean-shift clustering requires one parameter that a user needs to select – the window radius *R* which may also be termed as the "resolution of the analysis". Figure 3.43 shows a soil image and the results of segmentation of the image by the mean-shift clustering using different *R* values.

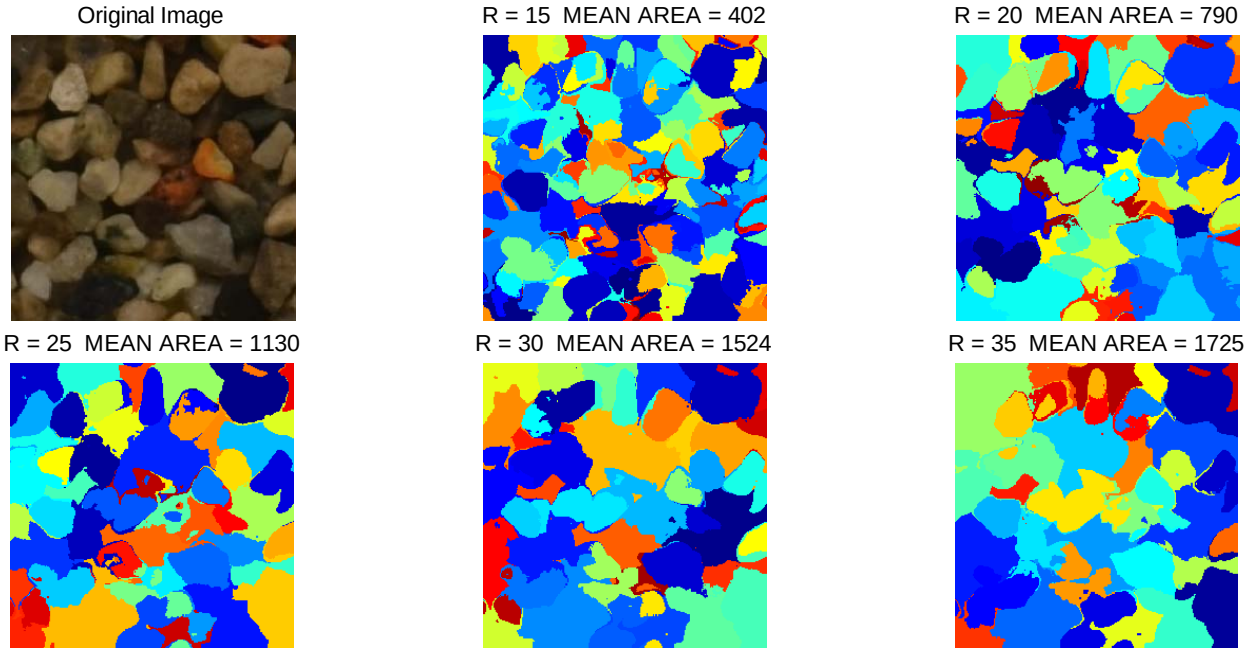

Figure 3.43 Results of mean-shift clustering on a 256 × 256 soil image

A small *R* causes over-segmentation of the soil particles, while a large *R* causes under-segmentation. Also, as discussed earlier, segmented objects in an over-segmented image are mostly internal textures, voids, or color variations within soil particles, whereas segmented objects in an under-segmented image are mostly combined two adjacent soil particles that have similar gray scale values. In order to obtain good segmentation reflecting the actual particles, an estimate of *R* may be obtained by wavelet transformation.

Because the average particle size in every 256 pixels by 256 pixels area of the original image is known from the wavelet transformation, an *R* value can be estimated as half of the diameter of a soil particle i.e. the *PPD*. After the first estimate of *R* is used, mean-shift clustering is performed using a range of *R* values close to the first estimate. Even though an appropriate *R* value is determined from wavelet transformation, manual selection of well-segmented particles is required. After selecting well-segmented particles, the aspect ratio of those particles is computed as shown in Figure 3.44.

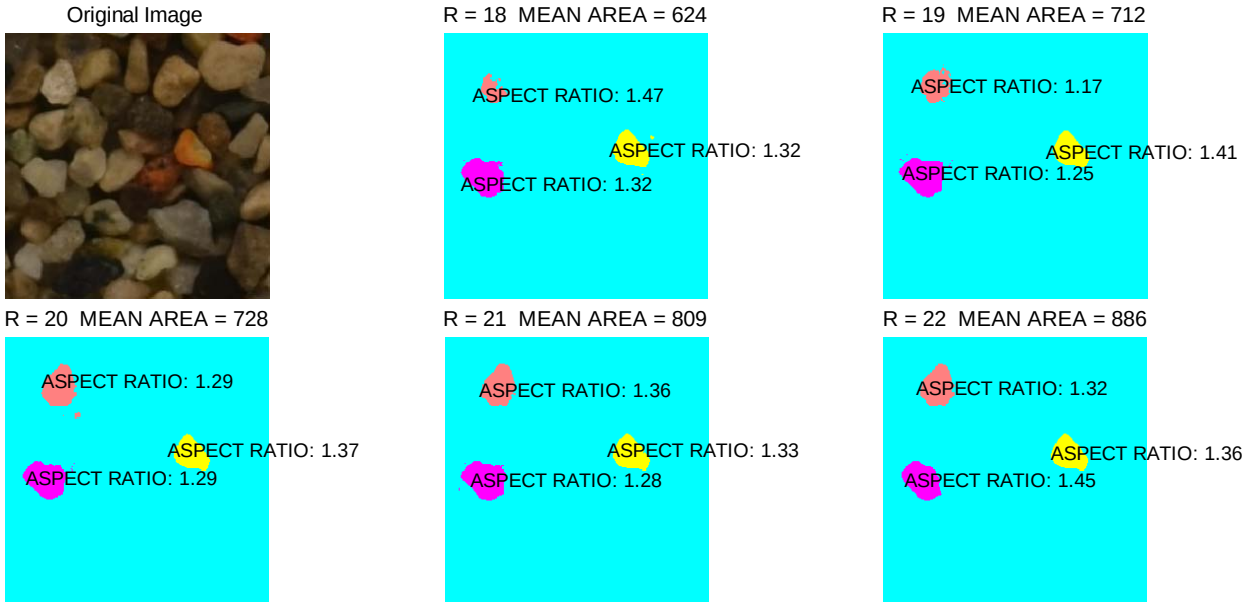

Figure 3.44 Aspect ratios of manually selected well-segmented particles

Manual selection of the well-segmented particles can be automated by knowing that: 1) the most visible particles will generally have the largest exposed areas at their given elevations in the sediment accumulator, 2) they will also generally contain a high percentage of edges that are concave with respect to the center of the particle, and 3) they will be better illuminated if they are in contact with the glass pane.

CHAPTER IV

Translucent Segregation Table

4.1 Introduction

A complementary image-based system that determines particle size distributions of soils in the range between 2.0 mm (No. 10 sieve opening) and 35 mm (1½ in. sieve opening) is described in this chapter. The test is called the *Translucent Segregation Table* (TST) test. The TST is conceptually simple: coarse sand and gravel is spread out on a well backlit translucent surface and photographed from above. To insure that all particles are in camera view, the TST is designed to provide rapid segregation of particles by size so that small particles cannot be hidden from view behind larger ones. However, most importantly for TST test expediency and practicality, the particles need not be physically separated from one another since the image analysis methods will delineate all particle boundaries and therefore "digitally detach" the particles. This chapter details the TST system hardware, test procedures and image analysis methods for developing particle size distributions. TST results are compared with sieving results. Particle shape will be addressed only to the extent needed for determining "sieve-equivalent" particle size distributions.

4.2 Translucent Segregation Table Apparatus

The Translucent Segregation Table (TST) hardware consists of: 1) a camera system, 2) a computer and monitor, 3) the Translucent Segregation Table (TST), and 4) ancillary supplies which is shown in Figure 4.1. The camera system is a 16.2 megapixels Nikon D7000 SLR camera with a 60 mm macro lens (AF-S Micro NIKKOR 60 mm f/2.8G ED). The camera is mounted on the laboratory ceiling as shown in Figure 4.2. The vertical distance between the ceiling-mounted camera lens and the surface of the TST is 7.6 ft (2.3 m). At this distance, the field of view is 3 ft. (0.9 m) by 2 ft. (0.6 m) corresponding to the bottom two-thirds of the TST. The camera is leveled using a bi-directional bubble level attached on the camera's flash shoe. A computer and monitor are used to control the camera and remotely capture images using NKRemote software by Breeze Systems. The computer system also analyzes the images and produces the particle size distribution.

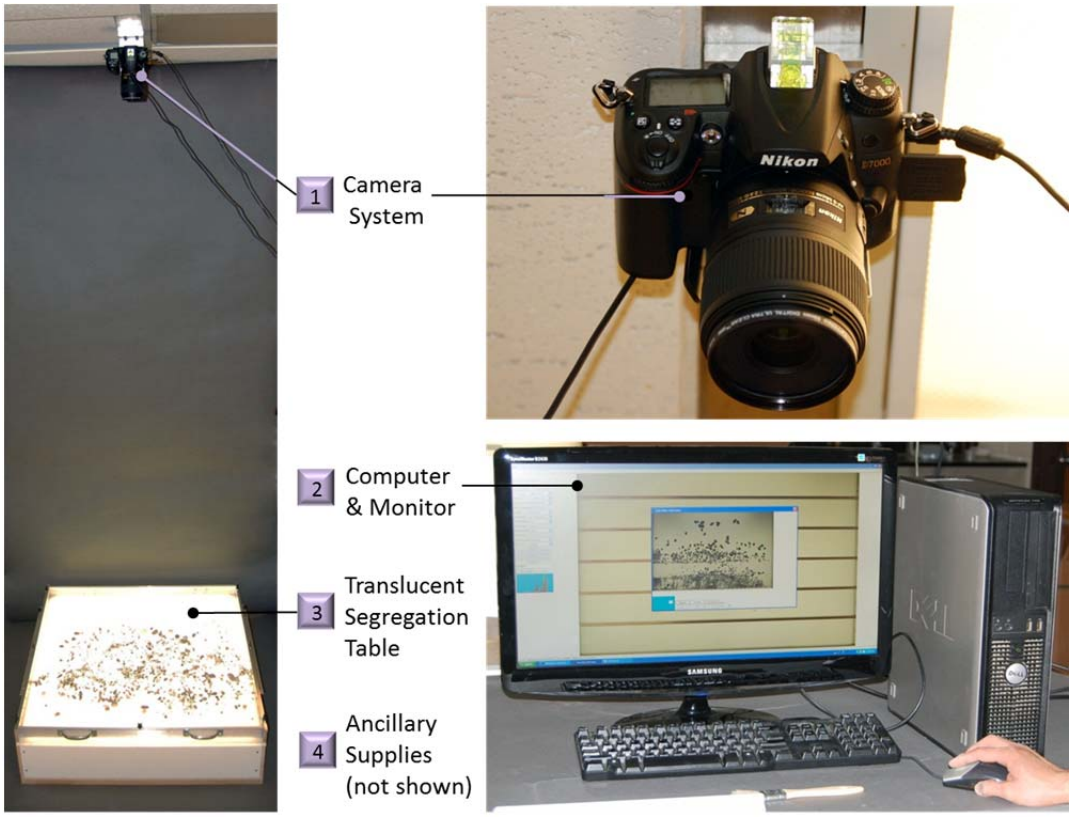

Figure 4.1 Translucent Segregation Table (TST) system overview

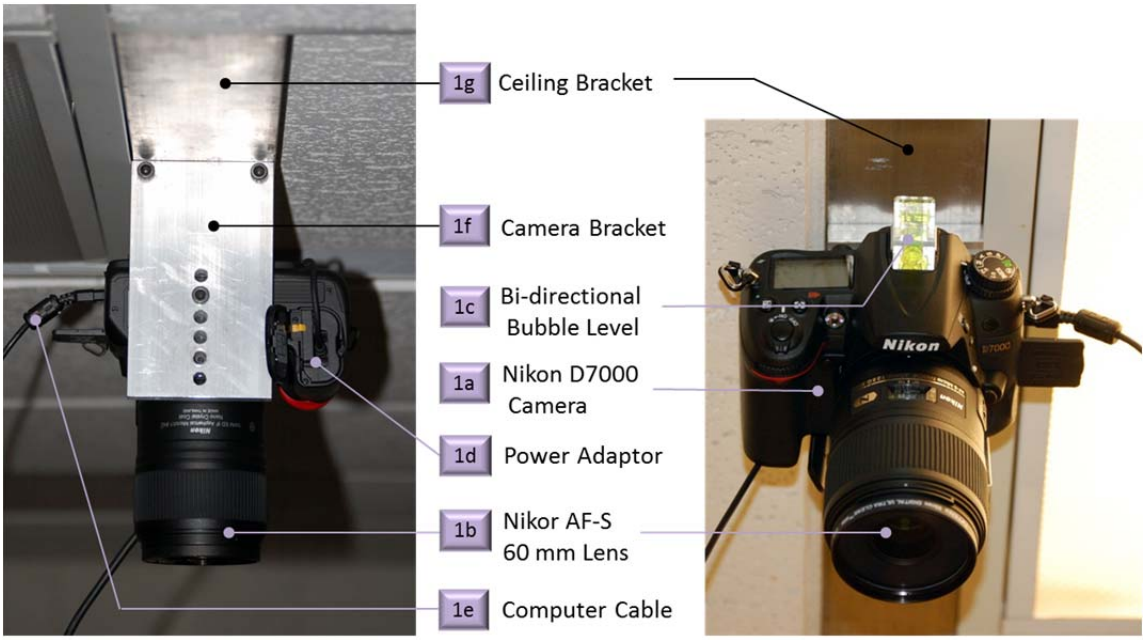

Figure 4.2 TST camera system

The Translucent Segregation Table (TST) is the centerpiece of the system (Figure 4.3). Its main component is a 3 ft (0.9 m) by 3 ft (0.6 m) translucent plate made of white acrylic having a 0.375 in. (9.5 mm) thickness. The plate is fixed atop a 3 ft (0.9 m) by 3 ft (0.6 m) transparent base of a clear acrylic with a 0.5 in. (12.7 mm) thickness. The transparent base stiffens the plate system. By increasing the plate rigidity, displacements of the translucent plate caused by its self-weight and the weight of soil are minimized. The translucent plate acts as a diffuser for light coming from a light box below to provide a bright and uniform background for the soil image.

Figure 4.3 Translucent segregation table and bridges

Attached above and around the perimeter of the translucent plate are a top wall, a bottom wall and two side walls. The top and bottom walls are 35 in. (889.0 mm) by 2 in. (50.8 mm) aluminum plates of 0.5 in. (12.7 mm) thickness. The top wall has two handles for lifting and

inclining the plate assembly. The top wall can be removed to allow the soil to be swept out after testing. The bottom wall has two hinges that connect it to a light box and allow the plate assembly to incline while remaining attached to the light box. The two side walls are 36 in. (914.4 mm) by 2 in. (50.8 mm) slotted aluminum plates with a 0.5 in. (12.7 mm) thickness.

The side walls contain nine matched pairs of slots to hold a series of bridges as shown in Figure 4.4. The bridges have different underpass clearances to allow different sized particles to pass beneath them. Not all of the bridge slots must be used in any one test but the large number of available slots and bridge affords the flexibility to collect comparable volumes of soil in the areas between bridges. The six bridges are 36 in. (914.4 mm) by 0.375 in. (9.5 mm) aluminum plates with underpass heights equivalent to sieve opening sizes of: 1 in. (25.4 mm), 0.75 in. (19.1 mm), 0.5 in. (12.7 mm), 0.375 in. (9.5 mm), No. 4 (4.75 mm) and No. 8 (2.36 mm). After being placed into the slots, the bridges are immobilized using two cover bars. Two 23 in. (584.2 mm) long L-channels serve as support feet for the inclined plate assembly.

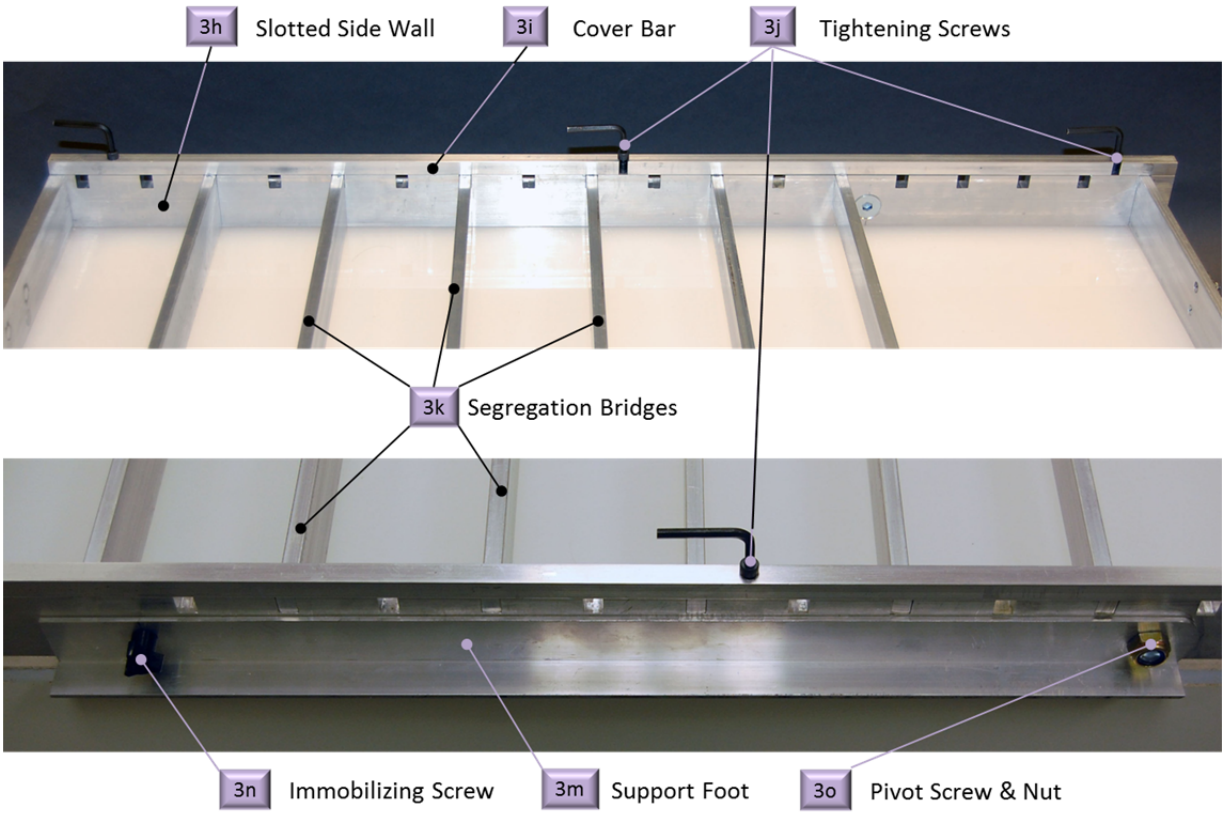

Figure 4.4 TST side walls

Once the specimen is introduced at the top of the slope as shown in Figure 4.5, the translucent plate is inclined. The particles slide and roll down the incline passing beneath the series of bridges having decreasing underpass heights on the way down the incline. This allows the particles to segregate by size. Design drawings of the TST device can be found in Appendix B.

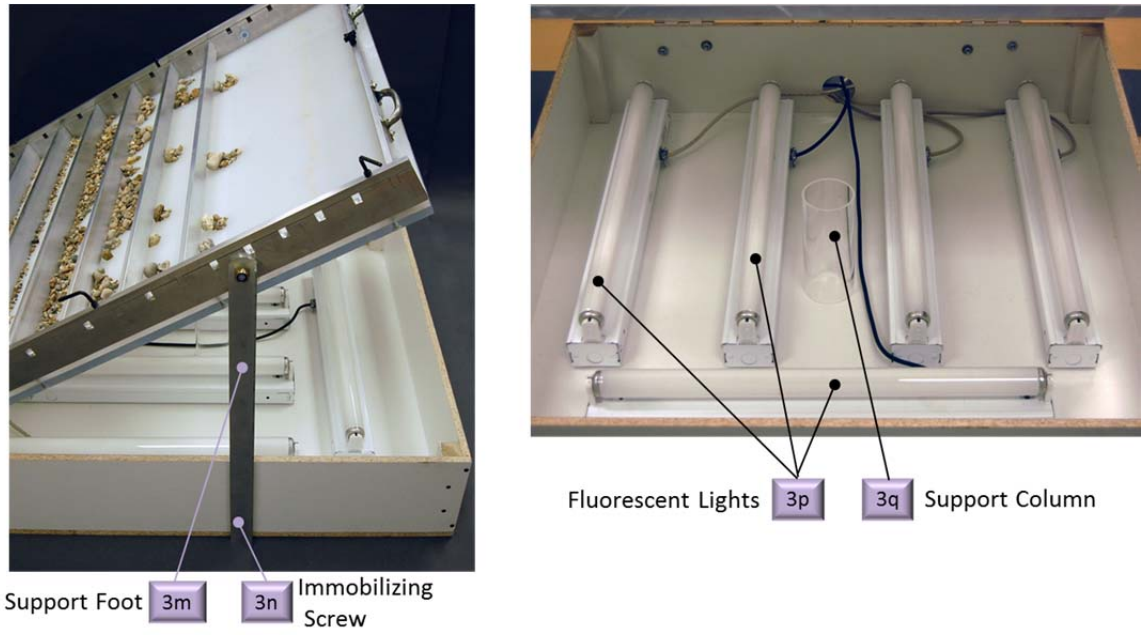

Figure 4.5 Raised TST and lighting system

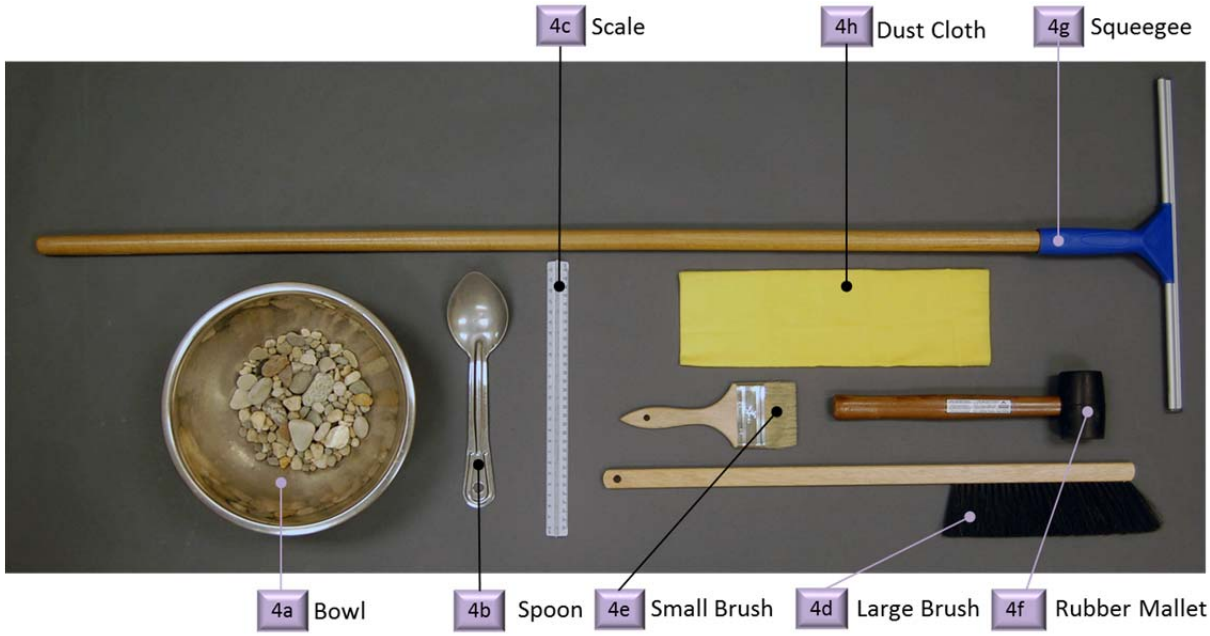

Figure 4.6 TST system supplies

4.3 Test Procedures

Preparation of a soil specimen by the TST consists of the 6 steps: (1) placing soil on the translucent plate above the topmost bridge (Figure 4.7), (2) lifting the top end of the TST plate and immobilizing the inclined plate, thereby allowing the soil particles to slide or roll down the incline (Figure 4.8), (3) lightly brushing beneath the bridges to break soil blockages (Figure 4.9), (4) lowering the plate and distributing the soil particles over the area between the segregation bridges (Figure 4.10), (5) removing the segregation bridges (Figure 4.11), and (6) capturing the image (Figure 4.12).

To elaborate on step 4, after lowering the plate to its horizontal position, the soil particles may still be piled up behind some bridges. Therefore, they must be distributed over the area between the bridges so that none sit on top of one another. This takes only a few minutes and is accomplished by tapping the TST with a rubber mallet and, or gently brushing the particles. After the image is captured, the soil particles can be swept out through an opening created by removal of the top wall of the TST (Figure 4.13). The maximum amount of soil that the TST can test is about 1.3 kg. This amount of soil occupies about 30% of an image. For reference, 1.3 kg corresponds to about 400 particles of 25 mm (1 in.) diameter or about 44,000 particles of 2.36 mm (No. 8 sieve) diameter. If more than 1.3 kg of soil is to be sized, it is split for into two or more lifts and the collected data is combined to produce one composite size distribution.

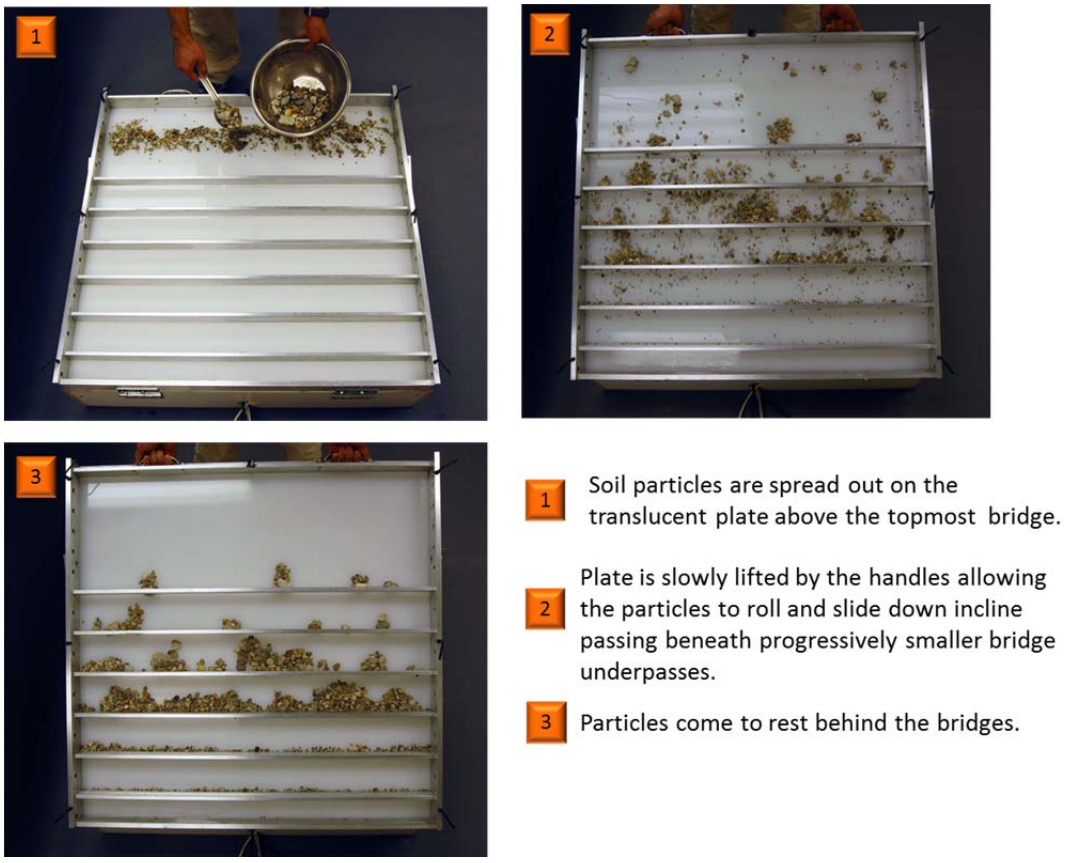

Figure 4.7 Introducing specimen and table raising

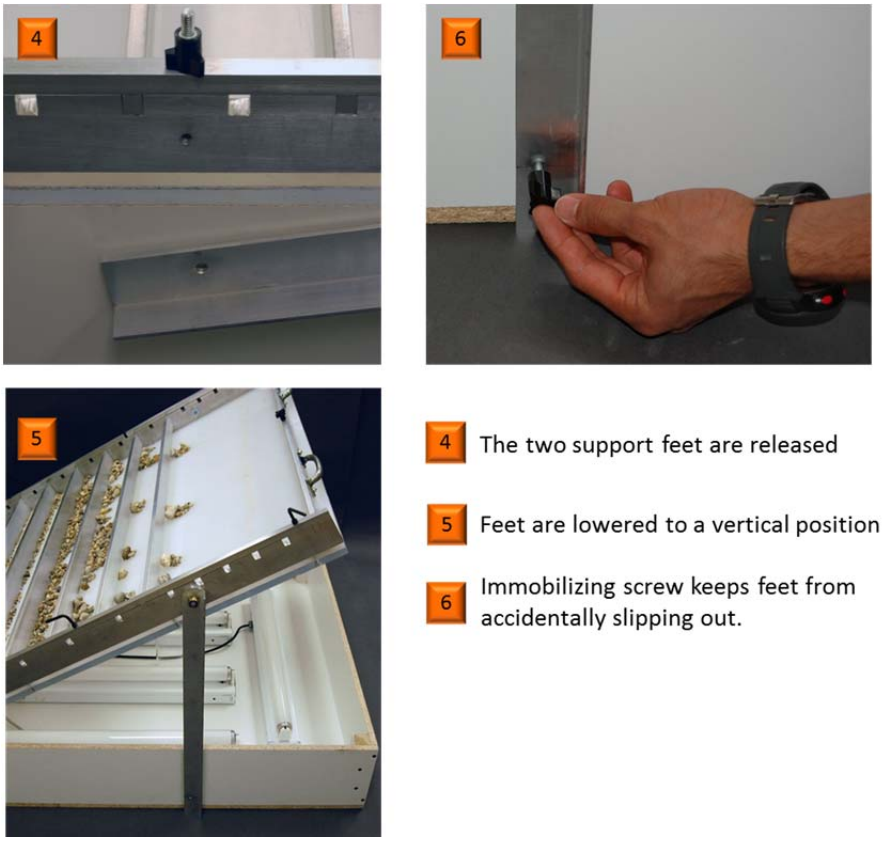

Figure 4.8 Immobilizing the inclined table

Figure 4.9 Brushing

Figure 4.10 Tapping down

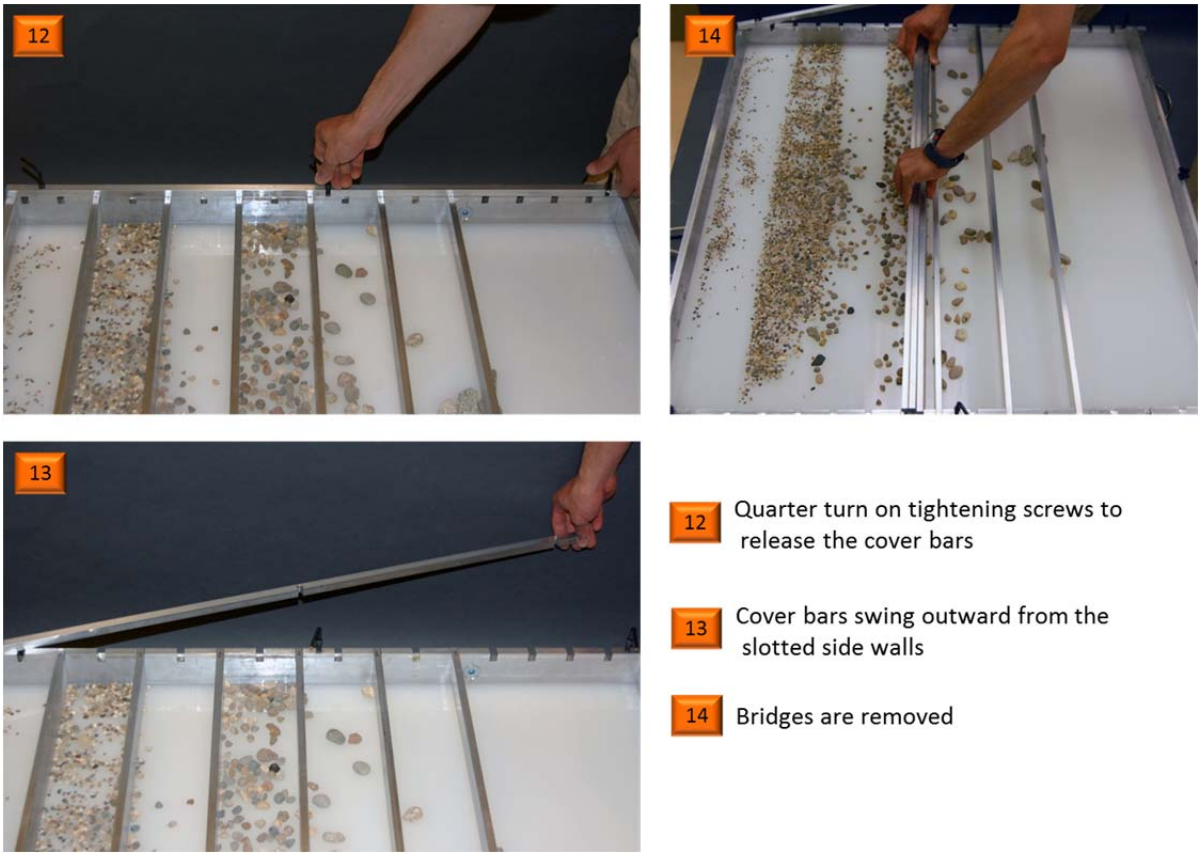

Figure 4.11 Removing the bridges

Figure 4.12 Image capture

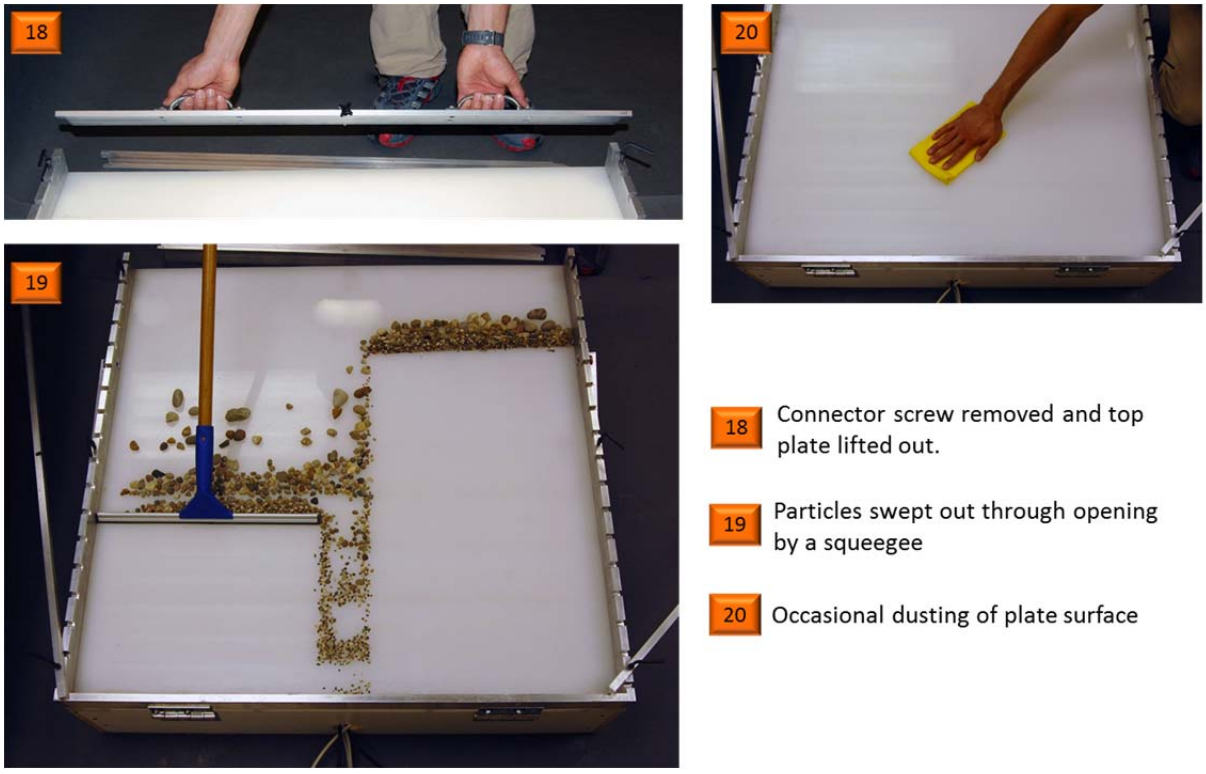

Figure 4.13 Specimen removal and cleaning

4.4 Watershed Segmentation

Following particle segregation and image capture, a TST image is analyzed to "segment" the particles. Segmentation is the process of identifying individual objects (i.e. particles) in an image. Ghalib and Hryciw (1999) showed how this can be accomplished for contacting soil particles using a multistep process termed *watershed segmentation* (Beucher and Lantuejoul 1979; Meyer and Beucher 1990; Vincent and Soille 1991). Today, the popular public domain image processing program developed at the National Institute of Health (NIH) called ImageJ contains a watershed segmentation routine. Because of its ease of use and universal acceptance, ImageJ was adopted for this research.

To illustrate the watershed segmentation procedure, Figure 4.14 zooms in on a small section of a TST image. Because of the bright TST backlighting, the particles appear black in the original image as shown in Figure 4.14 (*a*). The original color image is converted to an 8-bit grayscale image (not shown). Because of the bright back-illumination from five 24 in. (609.6 mm) fluorescent light bulbs in the box beneath the translucent plate, the grayscale image can easily be converted to a binary image (Figure 4.14 (*b*)) using an automatic thresholding feature in ImageJ. Next, a *Euclidian distance map* (EDM) is created (Figure 4.14 (*c*)) by replacing each foreground (particle) pixel with a pixel value equal to that pixel's distance from the nearest background (light table) pixel. The EDMs can be viewed as concave drainage basins or "watersheds" with each drainage basin representing the projected area of a particle. Each basin possesses local minima or *ultimate eroded points* (UEPs) shown in Figure 4.14 (*d*). At each UEP, water is envisioned to begin filling the drainage basin in a process called dilation. An intermediate step in the dilation process is illustrated in Figure 4.14 (*e*). The watersheds continue to expand (dilate) until a previously known edge of the particle is reached or until the dilating

object hits the edge of the region of another UEP. The final result of the watershed segmentation is shown in Figure 4.14 (*f*). Following watershed segmentation, the perimeters, projected areas and locations of every individual particle in the TST image are known.

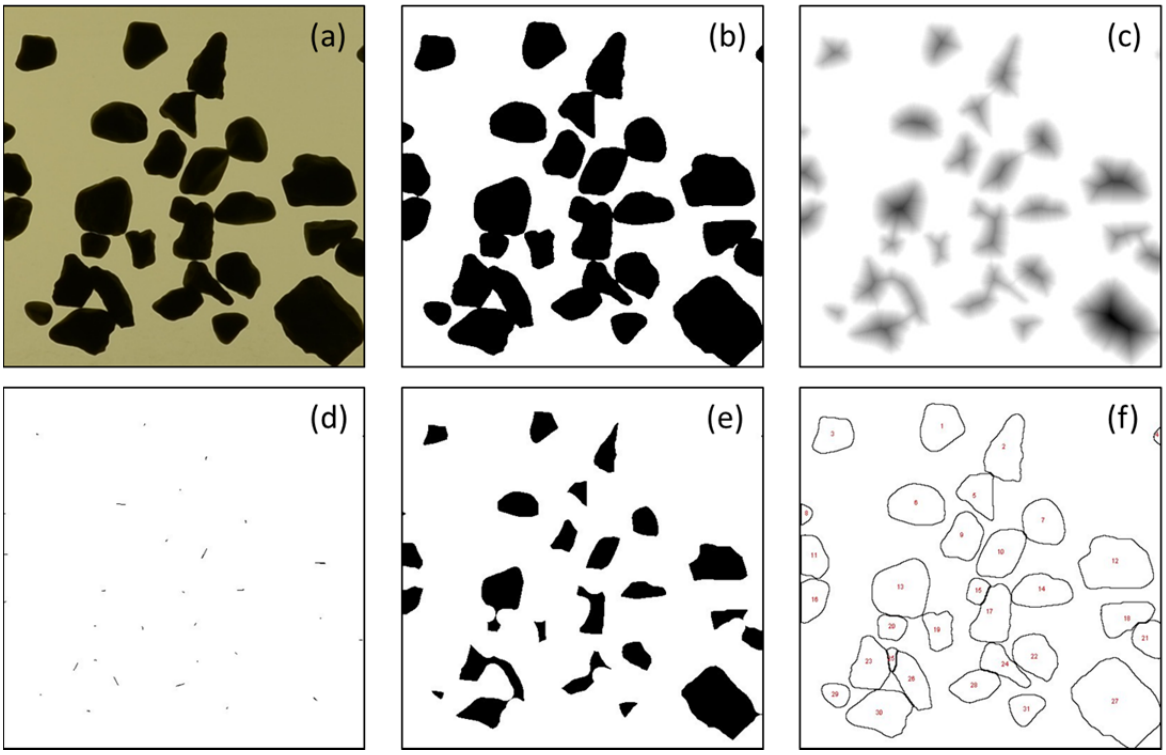

Figure 4.14 Watershed segmentation in ImageJ: (a) section of a TST image, (b) binary image, (c) Euclidean Distance Map, (d) Ultimate Eroded Points, (e) dilation, and (f) completed segmentation

4.5 Volume-Based Size Distribution by TST Using Bridge Heights

It should be recognized that the particle size found by sieving will generally be different from that found by the TST as illustrated in Figure 4.15.

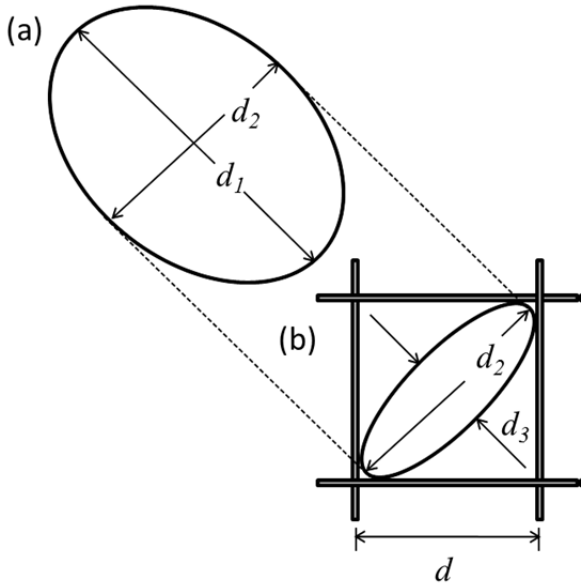

Figure 4.15 Difference in grain size as defined by sieving compared to the TST: (a) typical TST view, (b) particle passing through sieve opening

In Figure 4.15, particles are idealized as ellipsoids having axial dimensions $d_1 > d_2 > d_3$. Since particles in the TST are more likely to lie with the short dimension (d_3) vertical, the d_1 and d_2 dimensions dictate the apparent area of particles observed in TST images (Figure 4.15 (*a*)). By contrast, the sieve-based particle size is most closely related to d_2 (Figure 4.15 (*b*)). For this reason, particle sizes defined by image-based method and sieve analysis are different and will be discussed in Chapter 4.6. Another main difference between image-based method and sieving is that image-based method determines volume-based particle size distribution, whereas sieving determines weight-based particle size distribution. Therefore, the specific gravity of soil particles

is assumed to be constant over the particle size range to compare volume-based particle size distribution by the TST to weight-based particle size distribution by sieving.

As mentioned earlier, the TST bridges were designed to prevent small particles from hiding beneath large particles. To illustrate their importance two initial tests were performed. In the first test, a soil specimen was spread out on the light table without passing beneath the bridges prior to image capture. The same soil specimen was then allowed to segregate using the TST bridges. A comparison of the test results shown in Figure 4.16 confirms that some smaller particles must have been hidden and therefore unaccounted for. The particle size distribution curve shifted in the finer soil direction when the bridges were used. In these two preliminary tests, for purposes of computing particle volumes it was assumed that the smallest particle dimension (d_3) was the same as d_2. Particle volumes were therefore computed as $d_1 \times d_2^2$. This is an obvious initial oversimplification. To better match sieving results, a better estimate for d_3 was needed.

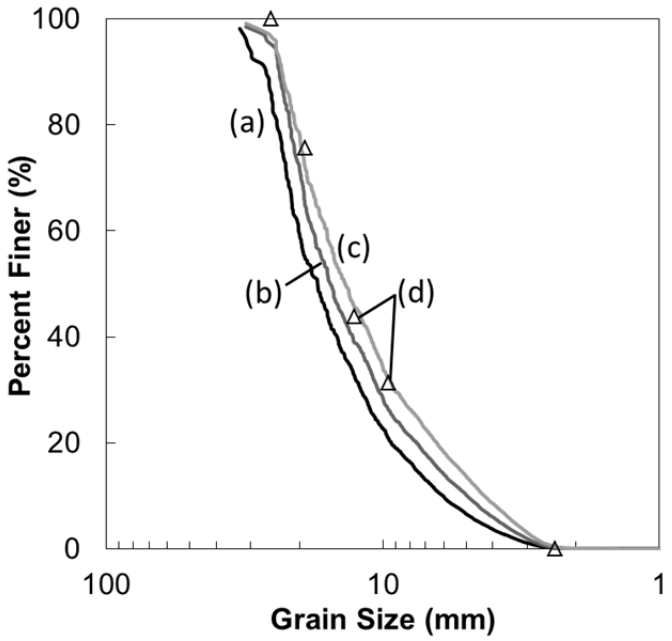

Figure 4.16 Comparison of grain size distribution by sieving and by TST: (a) TST without segregation by bridges, (b) TST with segregation by bridges, (c) TST with segregation and volume computation using the third dimension (d_3), and (d) sieving

Since the smallest particle dimension (d_3) would generally be the height of the particle as it rested on the TST, it could not be determined from the images. However, d_3 can be estimated from the average underpass height of the two bridges between which each particle comes to rest on the TST. The third grain size distribution shown in Figure 4.16 assumed this average value for d_3 and particle volumes were computed as $d_1 \times d_2 \times d_3$. This resulted in some additional improvement towards matching the sieve results.

4.6 Correction Factor Applied on Minor Axis Dimension (d_2)

As discussed in Chapter 4.5, particle size definitions are different by image-based method and sieving. Ghalib and Hryciw (1999) defined the particle size as the diameter of a circle having the same area as in the projected area of a particle in an image. Their results had to be corrected to match sieving results through an empirical factor based on particle angularity. The same factor was applied to all of the particles in the specimen. Tutumluer et al. (2000) also originally took an "equivalent sphere" approach to define the particle diameter and suggested a shift of the particle size distribution curve to match sieving data. Later, Tutumluer et al. (2005) used the d_2 dimension to define particle size.

Although d_2 is the dimension most closely related to sieve size (d), there will naturally be some effect of d_3 on the sieve opening through which a particle will pass. Kumara et al. (2012) used a correction factor on the d_2 dimension to match the sieve size. They found that the correction factor is controlled by d_3 and is typically 0.86. Altuhafi et al. (2012) used the minimum *feret diameter* as an image-based particle size. The feret diameter is the distance between two tangents on opposite sides of the particle.

Referring again to Figure 4.15 it is easy to see that for perfectly spherical particles ($d_1 = d_2 = d_3$) we will have $d = d_2$. At the other extreme, for a perfectly flat particle ($d_3 \approx 0$) we have $d = d_2/\sqrt{2}$. For intermediate situations ($0 < d_3 < d_2$), the exact relationship between d_2 and d can be determined analytically by fitting an ellipse to the square sieve opening shown in Figure 4.17.

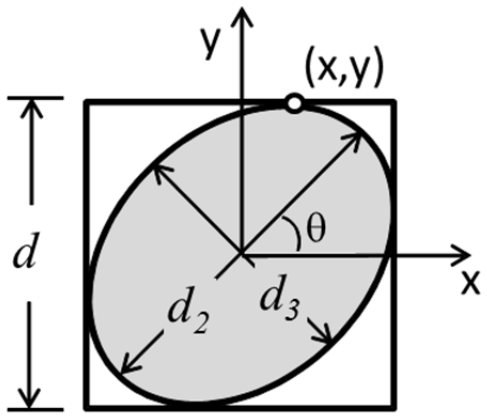

Figure 4.17 Elliptical particle fitted to a square sieve opening

The equation of an ellipse with its longer axis rotated an angle θ counter-clockwise from the x–axis as shown in Figure 4.17 is:

$$\frac{\left(x\cos\theta + y\sin\theta\right)^2}{\left(d_2/2\right)^2} + \frac{\left(x\sin\theta - y\cos\theta\right)^2}{\left(d_3/2\right)^2} = 1 \tag{4.1}$$

The largest ellipse that could pass through a square of dimension $d \times d$, would have an orientation of $\theta = 45°$. Therefore,

$$\frac{\left(x^2 + 2xy + y^2\right)}{d_2^{\,2}} + \frac{\left(x^2 - 2xy + y^2\right)}{d_3^{\,2}} = \frac{1}{2} \tag{4.2}$$

or

$$\left(x^2 + 2xy + y^2\right)d_3^{\,2} + \left(x^2 - 2xy + y^2\right)d_2^{\,2} = \frac{d_2^{\,2}d_3^{\,2}}{2} \tag{4.3}$$

Implicit differentiation of Equation 4.3 yields:

$$d_3^{\,2}\left(2x+2x\frac{dy}{dx}+2y+2y\frac{dy}{dx}\right)+d_2^{\,2}\left(2x-2x\frac{dy}{dx}-2y+2y\frac{dy}{dx}\right)=0 \tag{4.4}$$

which is solved for dy/dx:

$$\frac{dy}{dx}=\frac{d_3^2(x+y)+d_2^2(x-y)}{d_2^2(x-y)-d_3^2(x+y)} \tag{4.5}$$

At point (x, y) in Figure 4.17 the ellipse is tangent to the square. As such, dy/dx is zero here meaning that:

$$d_3^2(x+y)+d_2^2(x-y)=0 \tag{4.6}$$

Solving for x we find:

$$x=\frac{F-1}{F+1}y \tag{4.7}$$

where

$$F=\left(\frac{d_2}{d_3}\right)^2 \tag{4.8}$$

Equation 4.7 may be inserted into Equation 4.3 to give:

$$\frac{4F}{F+1}y^2=\frac{d_2^2}{2} \tag{4.9}$$

Since $d=2y$ Equation 4.9 becomes:

$$\frac{d}{d_2}=\sqrt{\frac{F+1}{2F}} \tag{4.10}$$

Equation 4.10 is plotted in Figure 4.18 and hereafter is referred to as the "d_2 correction factor". Equation 4.10 was also verified by graphically by fitting ellipses with $1 < d_2/d_3 < 8$ to a square. The sieve opening (d), as well as d_2 and d_3 were measured digitally using a 2D object drawing program. The resulting d/d_2 ratios agreed perfectly with the analytical solution as shown by the five data points in Figure 4.18. In summary, the TST image and elliptical fitting of particles provide the d_2 value for each particle in a specimen. The equivalent sieve opening size through which each particle would pass is obtained by multiplying d_2 by the d_2 correction factor. The volume of each particle is again computed as $d_1 \times d_2 \times d_3$.

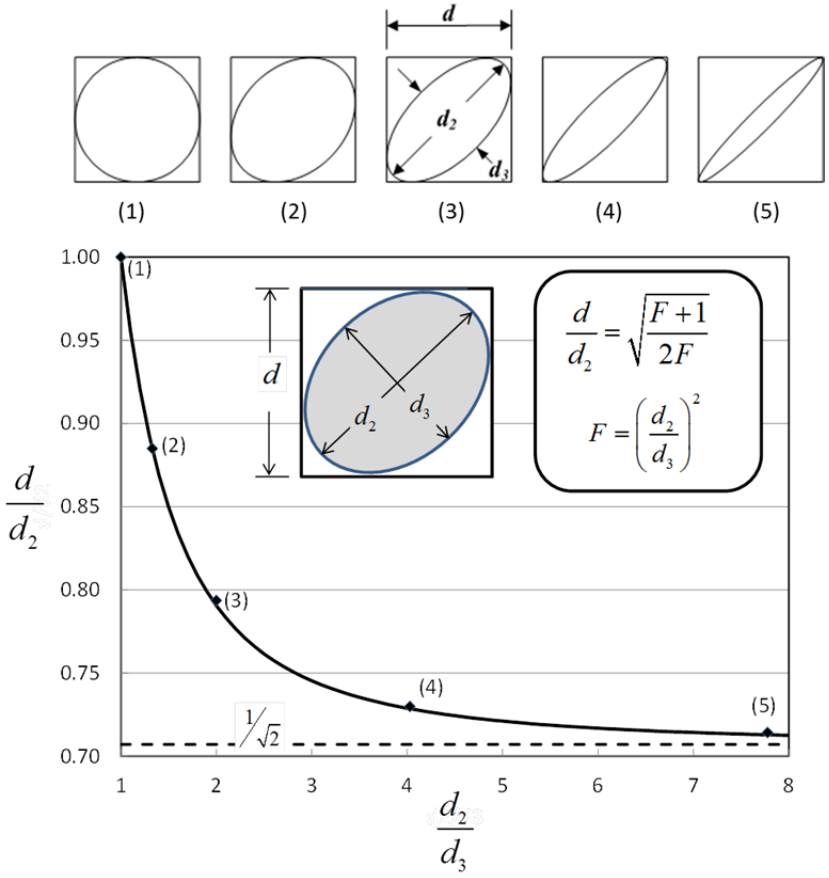

Figure 4.18 Correction factor applied to d_2 to account for effect of the smallest ellipsoid dimension (d_3) on equivalent sieve opening size (d)

4.7 Comparison between Sieving and Translucent Segregation Table

Twenty soil samples provided by the Michigan Department of Transportation (MDOT) were tested by the TST and sieving. The dry weights of the samples varied between 1.9 kg and 2.6 kg. Because these sample weights exceeded the current maximum TST specimen weight of 1.3 kg, each sample was divided and tested in two lifts. The first ten specimens (T1-T10) were made by dividing a large batch of soil into 10 portions, whereas the second ten samples (T11-T20) were made to specific gradations from large batches of pre-sieved material. TST and sieve tests were performed for each sample. Figure 4.19 shows a typical TST test result. Original images obtained from the TST are shown in Figure 4.19 (*a*), the particle aspect ratios (d_1/d_2) are plotted in Figure 4.19 (*b*) and particle size distribution is shown in Figure 4.19 (*c*).

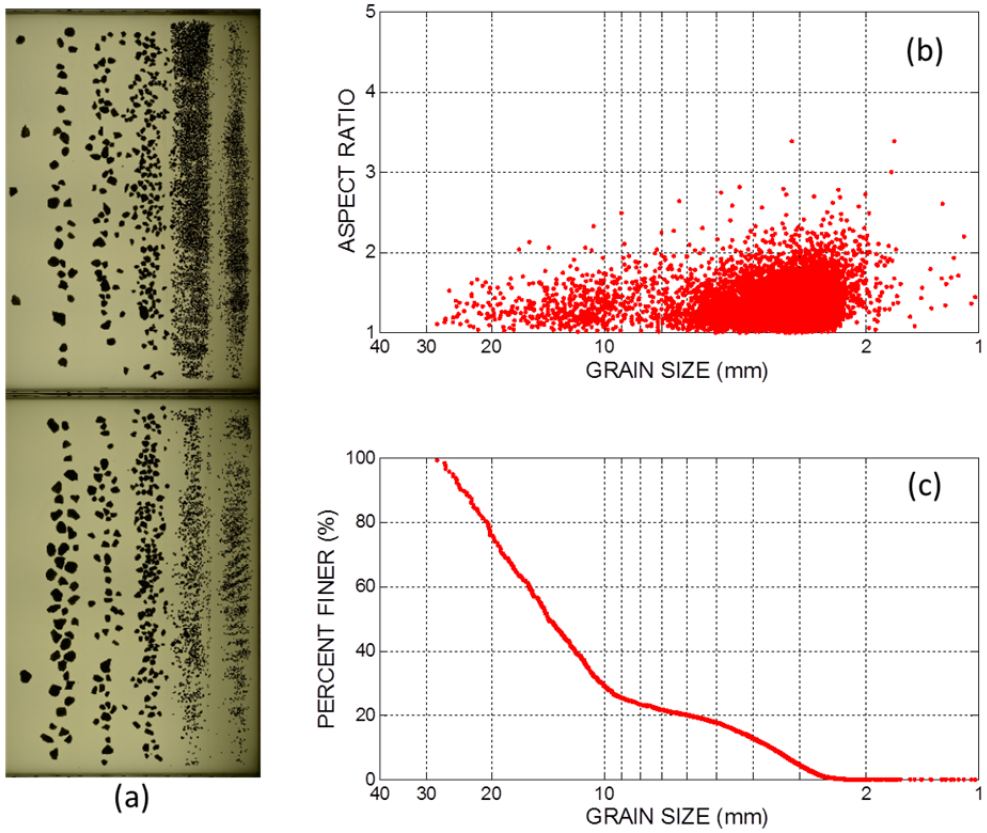

Figure 4.19 A typical TST test result

The results of tests T1 to T20 are compared in Figure 4.20 and 4.21. For comparison, the TST results are plotted both with and without use of the d_2 correction factor. In general, the agreement between sieving and TST results is very good. It is noted that the uncorrected TST curves plot slightly to the left (coarser) than by sieving while the corrected TST curves plot slightly to the right (finer). Most of the sieve points fall between the two TST curves suggesting that the two TST curves bracket the sieve data. At second glance it appears that the corrected TST curve better matches the sieve data for larger particles (d > 10 mm) while the uncorrected TST is a better match for smaller particles (d < 10 mm). Complete TST results can be found in Appendix D.

However, particle distribution curves are "cumulative" and thus a disparity at the top of the curve causes a divergence between the curves that continues as two parallel lines even if there is perfect agreement through the remainder of the size spectrum. Therefore, in Figure 4.22 the data is plotted by particle size increment rather than by the customary cumulative particle size distribution. It confirms that the largest disagreement between sieve results and the uncorrected TST is in the largest (37.5 mm to 25 mm) size range. The d_2 correction by Equation (4.10) brought the TST and sieve results to much better agreement in this size range. It is also noted that for particles larger than about 10 mm, the corrected TST data better agreed with sieve data while the uncorrected TST data was in better agreement with sieve data for particles smaller than about 10 mm. The data used to compare particle size distribution by sieving and TST is listed in Table 4.1, 4.2, 4.3 and 4.4. Table 4.1 and 4.2 correspond to Figure 4.20 and 4.21 while Tables 4.3 and 4.4 provide the numerical values used to create Figure 4.22.

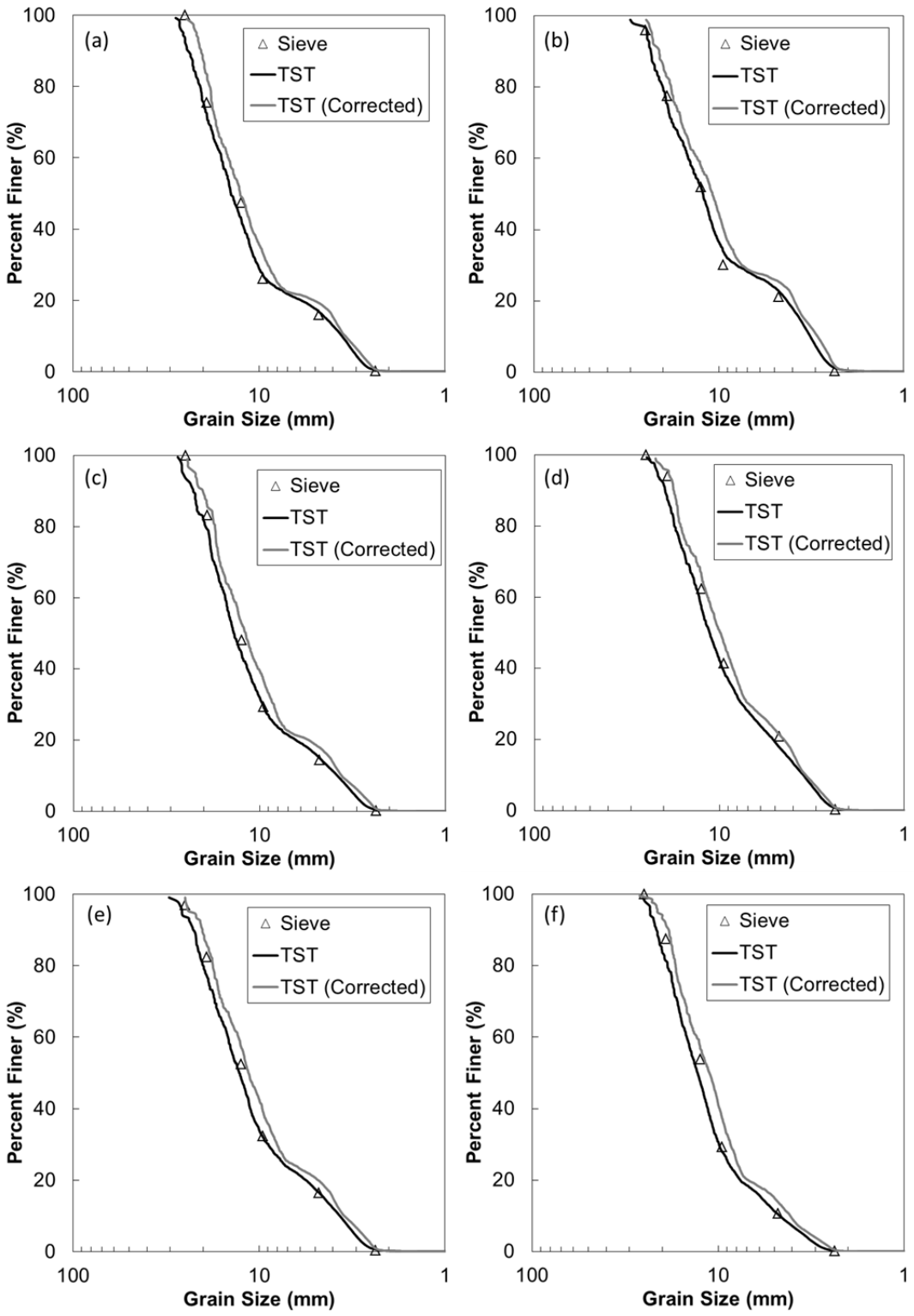

Figure 4.20 Comparison of TST and sieving results: (a) T1, (b) T2, (c) T3, (d) T4, (e) T5, (f) T6

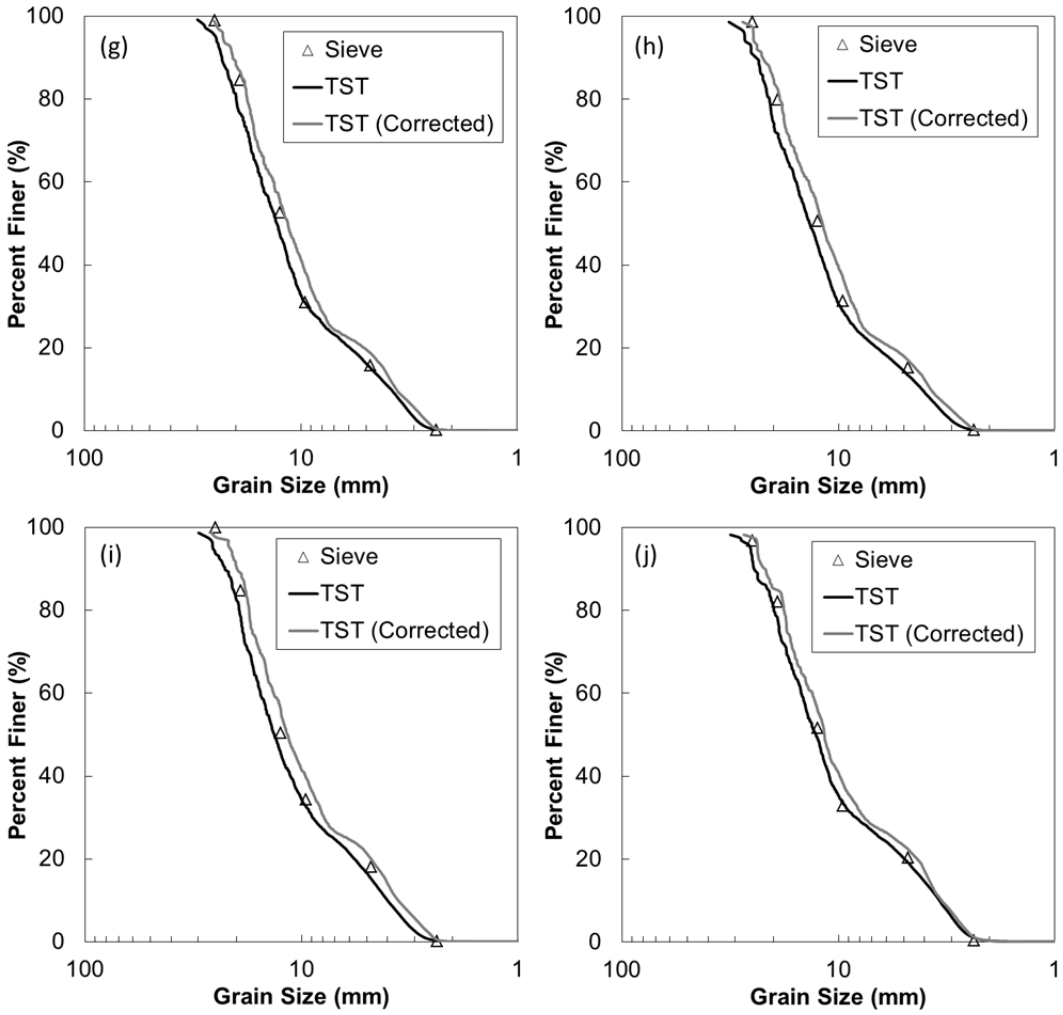

Figure 4.20 (Continued) Comparison of TST and sieving results: (g) T7, (h) T8, (i) T9, (j) T10

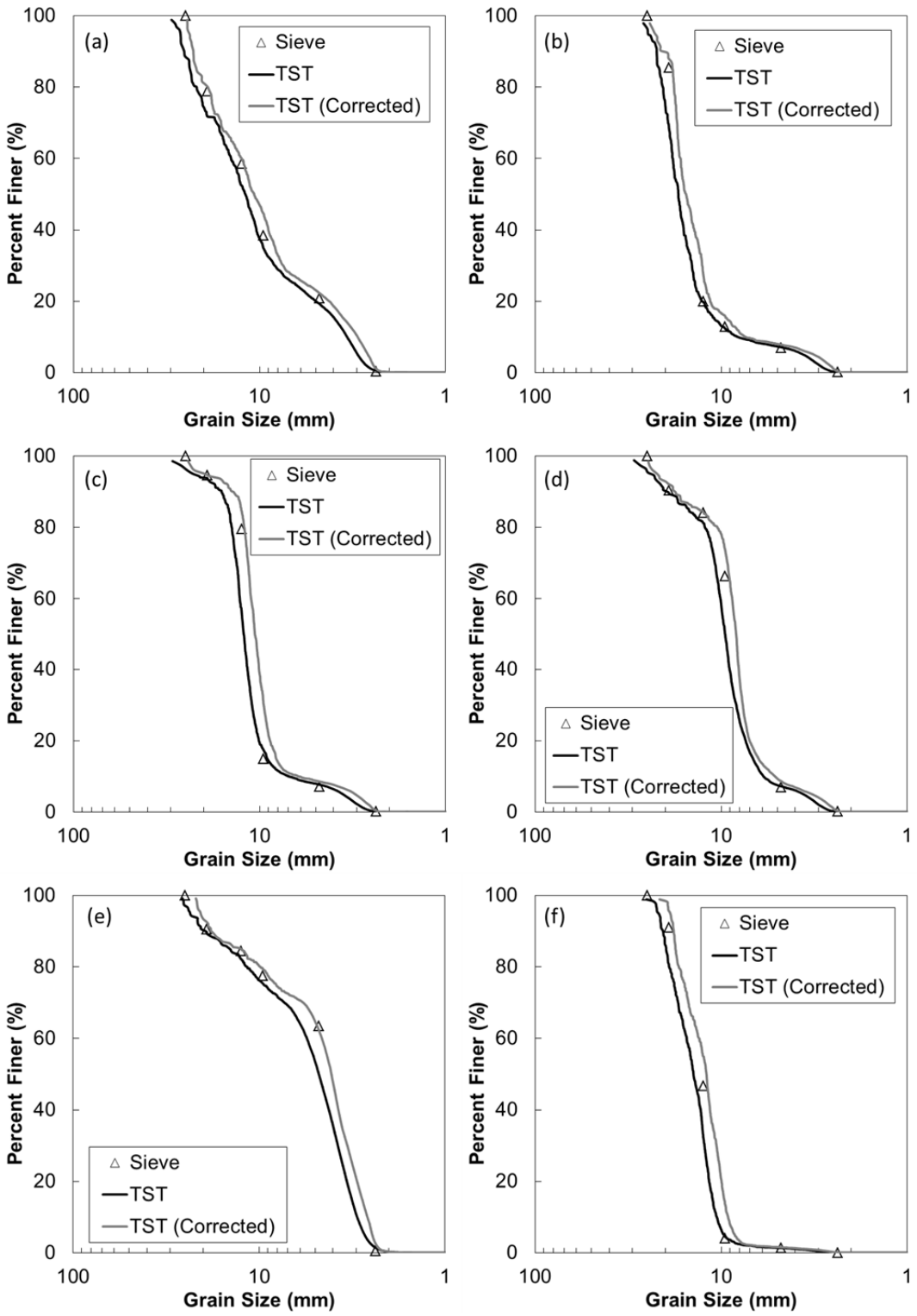

Figure 4.21 Comparison of TST and sieving results: (a) T11, (b) T12, (c) T13, (d) T14, (e) T15, (f) T16

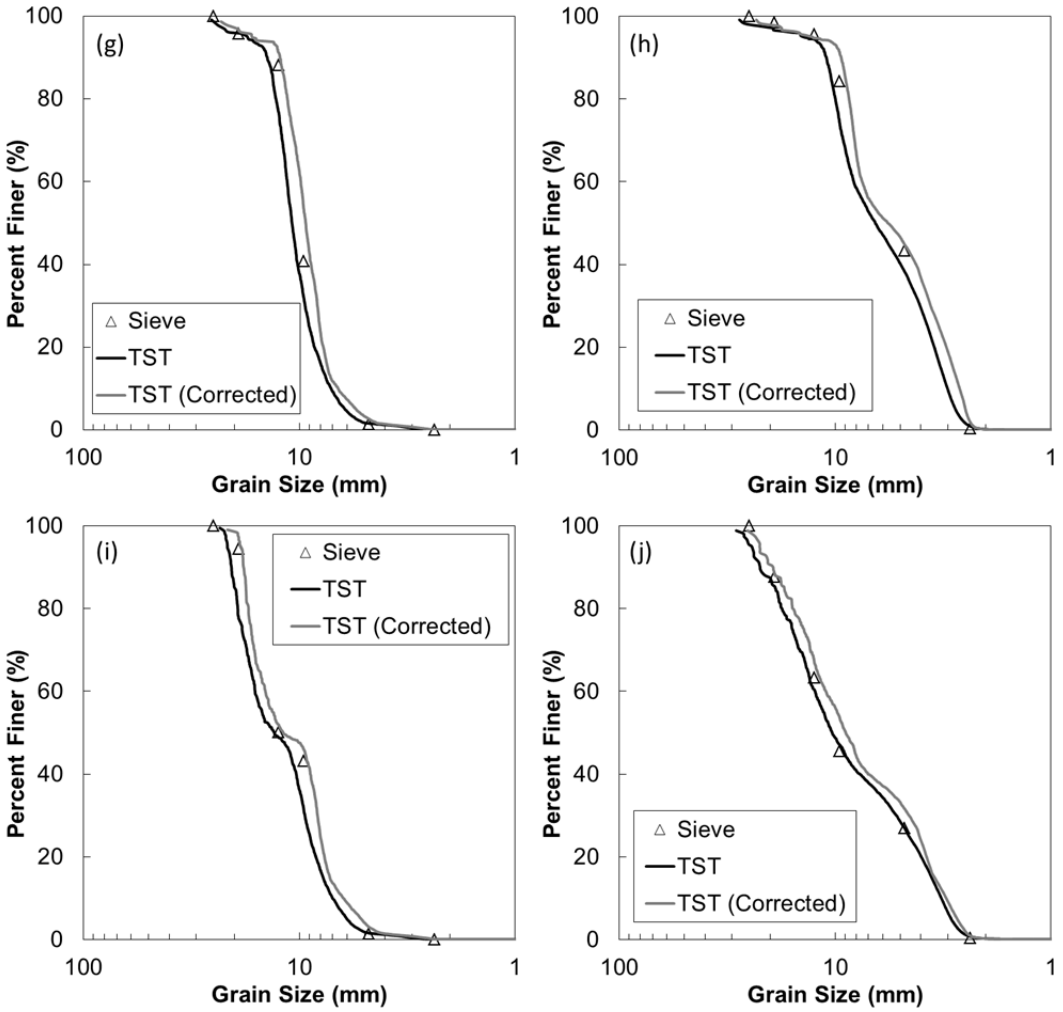

Figure 4.21 (Continued) Comparison of TST and sieving results: (g) T17, (h) T18, (i) T19, (j) T20

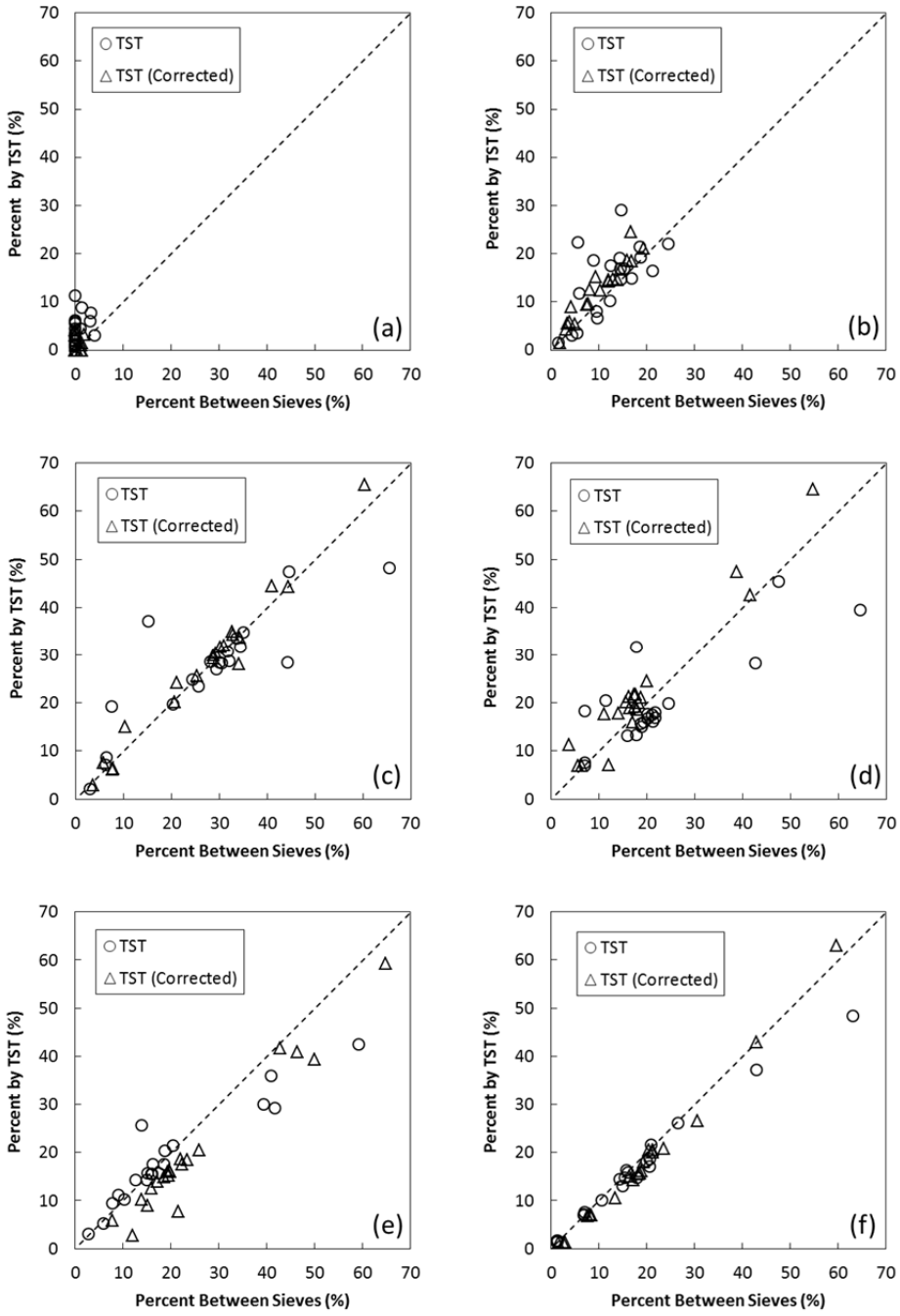

Figure 4.22 Comparison of TST corrected and uncorrected results by size intervals (T1 to T20): (a) 37.5 mm - 25 mm, (b) 25 mm - 19 mm, (c) 19 mm - 12.5 mm, (d) 12.5 mm - 9.5 mm, (e) 9.5 mm - 4.75mm, (f) 4.75 mm - 2.36 mm

Table 4.1 Percent of soil passing different sieve opening sizes

Specimen Number	Opening Size					
	1"	3/4"	1/2"	3/8"	No. 4	No. 8
	25 mm	19 mm	12.5 mm	9.5 mm	4.75 mm	2.36 mm
T1	100.0	75.5	47.3	26.0	15.8	0.1
T2	95.9	77.4	51.9	30.1	21.2	0.3
T3	100.0	83.2	48.3	29.3	14.5	0.2
T4	100.0	94.1	62.4	41.3	20.8	0.3
T5	96.9	82.4	52.4	32.3	16.3	0.3
T6	100.0	87.5	53.8	29.2	10.7	0.1
T7	98.9	84.6	52.6	30.9	15.7	0.2
T8	98.6	79.9	50.5	31.2	15.2	0.2
T9	100.0	84.7	50.4	34.4	18.2	0.2
T10	96.8	82.1	51.6	32.9	20.3	0.3
T11	100.0	78.8	58.6	38.4	20.9	0.3
T12	100.0	85.4	19.9	12.9	7.0	0.1
T13	100.0	94.6	79.5	14.9	7.2	0.1
T14	100.0	90.4	84.0	66.2	7.0	0.1
T15	100.0	90.6	84.4	77.4	63.5	0.5
T16	100.0	91.1	46.6	4.0	1.3	0.0
T17	100.0	95.7	88.1	40.7	1.3	0.1
T18	100.0	98.4	95.6	84.2	43.3	0.3
T19	100.0	94.4	50.1	43.1	1.4	0.0
T20	100.0	87.7	63.3	45.6	26.9	0.4

Table 4.2 Percent passing different equivalent opening sizes by the TST

Specimen Number	Opening Size					
	1"	3/4"	1/2"	3/8"	No. 4	No. 8
	25 mm	19 mm	12.5 mm	9.5 mm	4.75 mm	2.36 mm
T1	100.0	83.4	49.3	33.1	19.2	0.6
T2	100.0	83.1	57.8	40.5	25.4	1.8
T3	100.0	85.6	52.9	36.5	17.9	0.7
T4	100.0	96.1	66.0	47.3	21.4	1.0
T5	100.0	86.1	57.4	39.2	19.8	0.9
T6	99.5	91.4	57.2	37.2	13.8	0.4
T7	98.8	86.8	55.9	38.2	18.7	0.4
T8	98.6	82.7	54.0	36.6	16.8	0.4
T9	98.7	89.4	56.6	39.6	19.9	0.5
T10	98.2	85.3	56.1	38.2	22.3	1.1
T11	100.0	80.7	60.1	44.5	22.2	1.0
T12	100.0	88.1	27.7	15.7	7.9	0.3
T13	100.0	95.0	84.7	30.0	8.5	0.4
T14	100.0	92.2	84.5	73.4	8.6	0.3
T15	100.0	92.6	85.0	79.4	62.2	2.5
T16	100.0	95.9	55.0	13.5	1.6	0.1
T17	100.0	97.0	91.3	52.6	2.7	0.1
T18	100.0	98.2	94.7	91.0	44.7	1.8
T19	100.0	96.6	52.2	45.8	3.0	0.1
T20	98.8	88.5	67.5	53.5	31.5	0.9

Table 4.3 Percent of specimen found between different sieve opening sizes

Specimen Number	Opening Size					
	> 1"	1" - 3/4"	3/4" - 1/2"	1/2" - 3/8"	3/8" - No. 4	No. 4 - No. 8
	> 25 mm	25-19 mm	19-12.5 mm	12.5-9.5 mm	9.5-4.75 mm	4.75-2.36 mm
T1	0.0	24.5	28.2	21.3	10.2	15.7
T2	4.1	18.5	25.6	21.7	9.0	20.8
T3	0.0	16.8	35.0	18.9	14.9	14.3
T4	0.0	5.9	31.6	21.1	20.5	20.5
T5	3.1	14.5	30.0	20.1	15.9	16.1
T6	0.0	12.5	33.7	24.6	18.5	10.6
T7	1.1	14.3	32.0	21.7	15.2	15.5
T8	1.4	18.7	29.4	19.3	16.0	15.0
T9	0.0	15.3	34.4	15.9	16.2	17.9
T10	3.2	14.7	30.5	18.7	12.6	20.0
T11	0.0	21.2	20.2	20.2	17.5	20.6
T12	0.0	14.6	65.5	7.1	5.9	6.9
T13	0.0	5.4	15.1	64.6	7.8	7.0
T14	0.0	9.6	6.4	17.8	59.3	6.9
T15	0.0	9.4	6.2	7.0	13.9	63.0
T16	0.0	8.9	44.5	42.6	2.7	1.3
T17	0.0	4.3	7.5	47.5	39.4	1.3
T18	0.0	1.6	2.9	11.4	40.9	42.9
T19	0.0	5.6	44.3	7.0	41.7	1.4
T20	0.0	12.3	24.3	17.8	18.7	26.5

Table 4.4 Percent found between different equivalent opening sizes by the TST

Specimen Number	Sieve Opening Size					
	> 1"	1" - 3/4"	3/4" - 1/2"	1/2" - 3/8"	3/8" - No. 4	No. 4 - No. 8
	> 25 mm	25-19 mm	19-12.5 mm	12.5-9.5 mm	9.5-4.75 mm	4.75-2.36 mm
T1	0.0	16.6	34.1	16.2	13.9	18.6
T2	0.0	16.9	25.3	17.3	15.1	23.6
T3	0.0	14.4	32.7	16.4	18.6	17.2
T4	0.0	3.9	30.1	18.7	25.9	20.4
T5	0.0	13.9	28.7	18.2	19.4	18.9
T6	0.5	8.1	34.2	20.0	23.4	13.4
T7	1.2	12.0	30.9	17.7	19.5	18.3
T8	1.4	15.9	28.7	17.4	19.8	16.4
T9	1.3	9.3	32.8	17.0	19.7	19.4
T10	1.8	12.9	29.2	17.9	15.9	21.2
T11	0.0	19.3	20.6	15.6	22.3	21.2
T12	0.0	11.9	60.4	12.0	7.8	7.6
T13	0.0	5.0	10.3	54.7	21.5	8.1
T14	0.0	7.8	7.7	11.1	64.8	8.3
T15	0.0	7.4	7.6	5.6	17.2	59.7
T16	0.0	4.1	40.9	41.5	11.9	1.5
T17	0.0	3.0	5.7	38.7	49.9	2.6
T18	0.0	1.8	3.5	3.7	46.3	42.9
T19	0.0	3.4	44.4	6.4	42.8	2.9
T20	1.2	10.3	21.0	14.0	22.0	30.6

In addition to the d_2/d_3 ratio effect, there are additional factors that could contribute to differences in particle size distributions determined by sieving and by the TST. First, the assumption that the thickness (d_3) of a particle is the average of two bounding bridge heights is approximate. All of the particles are effectively assumed to have one of only five possible d_3 values. Both the AIMS and UI-AIA systems do a better job of resolving d_3. In the AIMS system, the thickness of aggregates is determined by the amount of required auto-focusing. In the UI-AIA system three video cameras are used to obtain three orthogonal views of each particle. Naturally, both methods will analyze many fewer particles per unit time than the TST does.

Therefore, even an approximate assumption for d_3 achieves the TST objective of obtaining particle size distributions of coarse sand and gravel inexpensively and rapidly compared to traditional sieving and other imaging techniques. Nevertheless, to improve the d_3 estimate, more bridges can be used to narrow the ranges between successive bridges.

Secondly, in the present work no consideration was given to the effect that d_1 may have on passage of particles through sieve openings. Longer particles are likely to find it more difficult to pass through a tight opening than shorter particles possessing the same d_2 and d_3. Next, soil particles come in an endless variety of shapes and few are ideally ellipsoidal as was assumed for the derivation of the d_2 correction factor.

Finally, even the highest resolution cameras do have a finite resolution. In the present testing program the largest particles contained 135 pixels per particle diameter (*PPD*) while the smallest particles contained only 10.8 *PPD*. Thus, the elliptical fitting to obtain d_1 and d_2 is less precise for the smaller particles than for the largest ones. Ohm and Hryciw (2013a) discuss how future advances in camera technology will eliminate this possible problem and lead to more accurate particle sizing over a larger range of sizes. Regardless of the differences between the TST and sieving, the test results compared in Figure 4.20 and 4.21 demonstrate that the TST provides a consistent and reasonable size distribution for coarse sand and gravel.

4.8 Over-Segmentation from Watershed Segmentation Results

TST images should require little additional segmentation beyond the previously mentioned watershed analysis. However, there is an occasional segmentation problem associated with elongated particles, particularly if they have both convex and concave perimeter segments. Such "peanut shaped" particles are occasionally over-segmented by the watershed method. The result is that a single particle is interpreted as being two as shown in Figure 4.23.

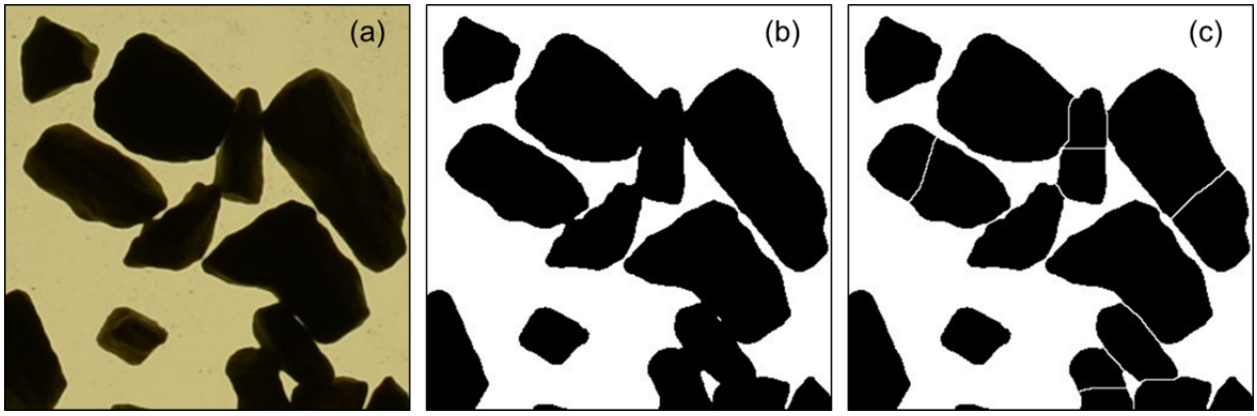

Figure 4.23 Over-segmentation: (a) an original image from the TST, (b) a binary image, and (c) watershed segmentation of a binary image

This problem has only a small effect on grain size distributions. However, its impact on assessment of particle shapes would be more significant and therefore needs to be rectified. Meyer and Beucher (1990) proposed "marker-controlled" watershed segmentation by identifying foreground objects and background objects. Unfortunately, it is not easy to identify or "mark" foreground particles from complex soil grains.

For the TST, a method that handles the over-segmentation problem manually is proposed (Figure 4.24). From the results of watershed segmentation shown in Figure 4.23 (*c*), pairs of over-segmented particles are selected by clicking each object manually. Then, each pair of

selected objects is assigned as the same particle number. Finally, one-pixel line that separates the pair of over-segmented particles is removed by applying the morphological *closing* operation.

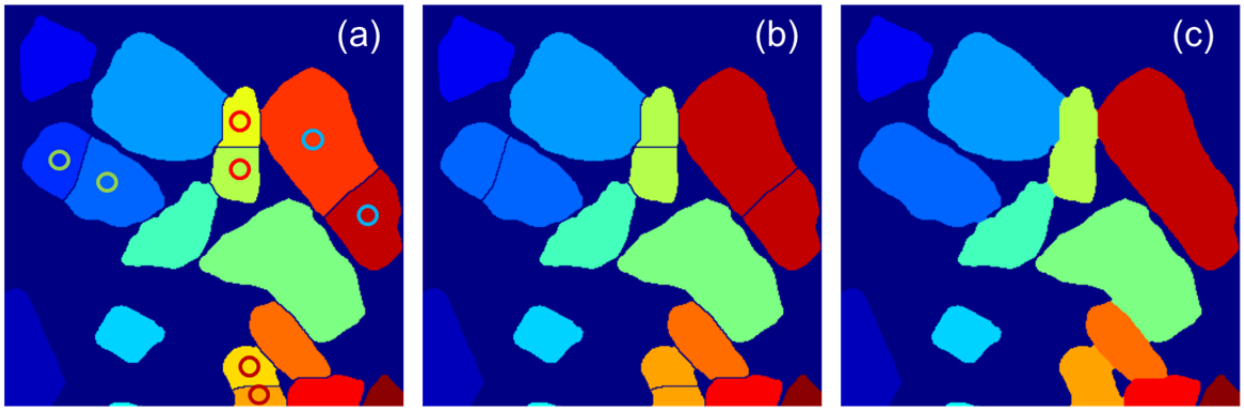

Figure 4.24 Handling over-segmentation: (a) selecting over-segmented particles, (b) assigning same numbers, (c) removing one-pixel line by closing

Both the watershed segmentation and the proposed modified watershed segmentation method were performed on particles retained between the 25.4 mm and 4.75 mm height bridges from T11, T12 and T13 for the comparison. The percentages of number of over-segmented particles were 1.2 %, 3.1 % and 2.6% for tests T11, T12 and T13 respectively. However, when comparing TST results with and without corrections for over-segmentation, almost no differences between the grain size distribution curves were found. Still, automated image processing method must be developed to identify and correct the over-segmentation in the watershed segmentation more efficiently and less subjectively.

CHAPTER V

New Research Directions

5.1 A Higher Magnification Camera on Image-Based Methods

5.1.1 Recent Advances in Imaging Technology

Since their commercial introduction in the late 1990's digital single lens reflex (DSLR) cameras have rapidly increased in resolution as measured by image megapixels (MP). Figure 5.1 shows the resolution history of two commercial lines, DSLR cameras by Nikon and medium format digital camera back (DCB) cameras by Leaf. DSLR cameras reached 36 MP in 2012, while DCB cameras had already achieved 80 MP in 2010. Since DCBs cameras are very expensive, DSLR cameras are currently used in the Sedimaging and TST systems.

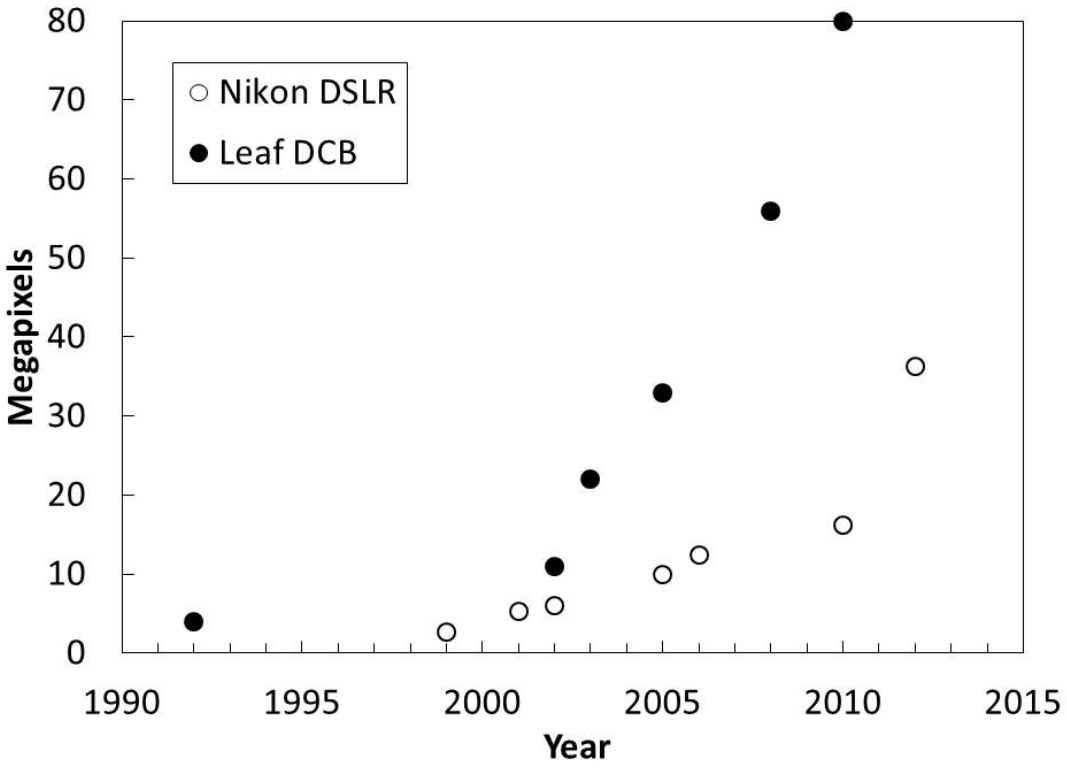

Figure 5.1 Advances in DSLR and DCB camera resolutions over time

Many particulates such as pills, agricultural products and even biological cells are digitally imaged. However, they do not possess a very wide range of sizes and therefore, advances in image resolution is not as critical for their respective industries. By contrast, silt, sand and gravel particles range from 0.002 mm to 75 mm.

With pre-2010 lower resolution DSLR cameras, images had to be taken at several magnifications to capture different particle size ranges. Also, multiple images had to be taken at different specimen locations and digitally "stitched" so that a combined image would be a statistically valid representation of the soil. By contrast, using a post-2010 higher resolution camera, a single photo taken at a fixed magnification can produce particle size distributions for soil particles ranging over 2 orders of magnitude in diameter.

5.1.2 Minimum PPDs for the Sedimaging and the TST

Based on the Sedimaging tests of sands containing known percentages of silt, the minimum *PPD* that can be analyzed by the wavelet method was found to be 2.7. However, for simplicity a more conservative minimum *PPD* of 3.0 will be assumed. To explain why so few pixels are apparently needed to size the particles, it is pointed out that the wavelet method does not determine the sizes of every particle individually. It merely analyzes the overall "texture" in each 128 pixel × 128 pixel analysis subarea.

The minimum *PPD* for the TST test is dictated by the watershed segmentation method and the need to adequately define the particles' projected areas. To find this minimum *PPD*, different quantities of coffee beans were placed on the TST and photographed. The percentage of the image area covered by the coffee beans was varied from 20% to 70% as shown in Figure 5.2.

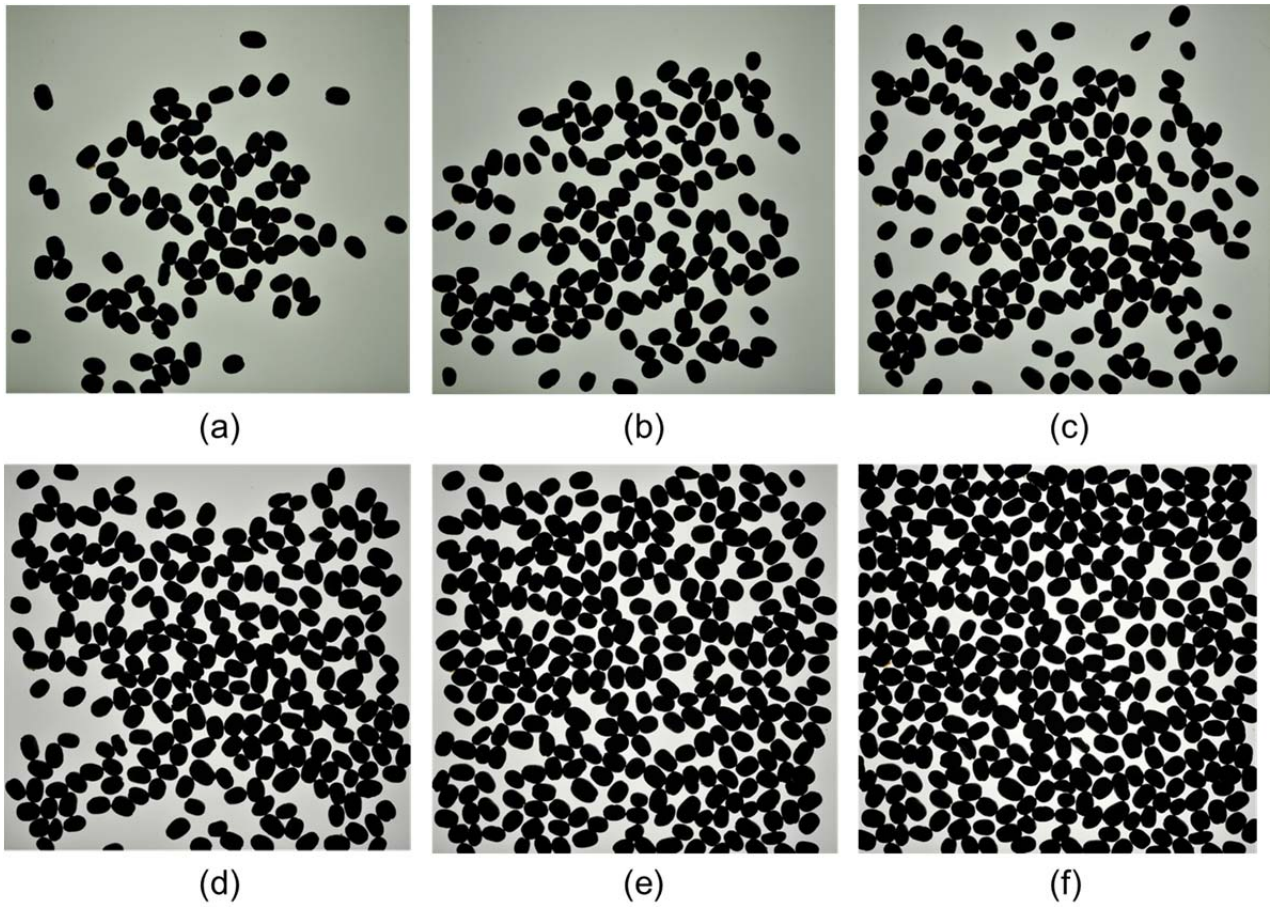

Figure 5.2 Different image coverage by coffee beans: (a) 20%, (b) 30%, (c) 40%, (d) 50%, (e) 60%, (f) 70%

Different *PPD*s were generated by digital downscaling of the original images. Figure 5.3 compares the number of segmented particles by watershed analysis at different *PPD*s to the number of actual coffee beans. Conservatively, the minimum *PPD* to detect all of the particles appears to be 9. It is also noted that even with a coverage area of 70% (i.e. very high contact between particles) watershed segmentation successfully identified virtually all of the beans. Note that the minimum *PPD* for the TST is three times larger than the minimum *PPD* for the Sedimaging. This is because the TST uses a deterministic method that requires good particle

perimeter resolution for watershed analysis while the Sedimaging uses a statistical method that does not require such high resolution.

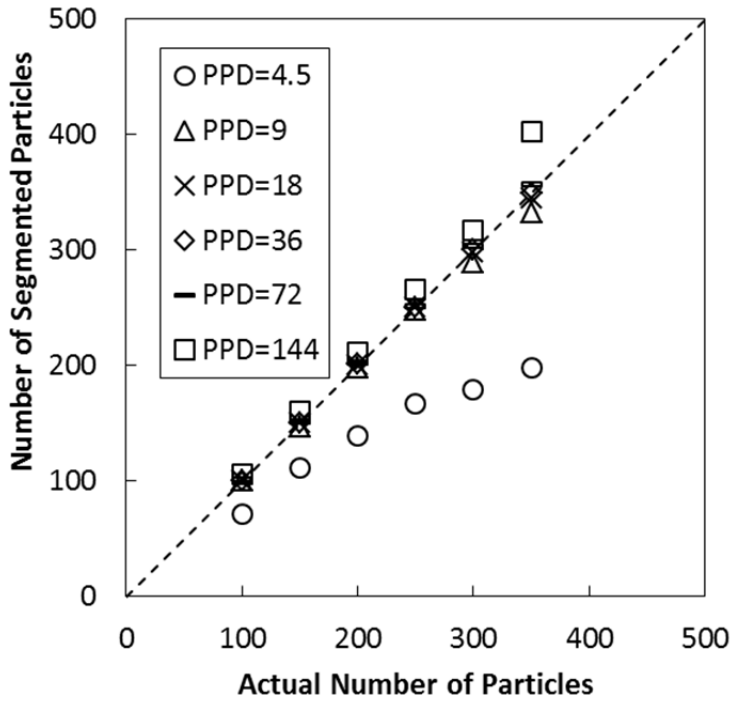

Figure 5.3 Comparison of segmented versus actual number of coffee beans in the TST for various *PPD*

5.1.3 Discussion

The minimum required *PPD*s for the Sedimaging and TST tests are dictated by their respective image analysis methods. However, this is only one factor that will control the minimum particle size that can be determined in each test with a given camera. The other factor is the area to be photographed. The Sedimaging test requires a specimen weight of 450 g to 500 g. This weight yields a loose sedimented soil column height of no more than 135 mm. For the TST, the longer dimension of the table that must appear in the image is 910 mm. This allows for single image

testing of 1.0 to 1.5 kg specimens. With these requisite parameters and the minimum *PPD* requirements of 3 for the Sedimaging and 9 for the TST, the capabilities of four cameras with different resolutions are compared in Table 5.1. The cameras were selected to represent digital capabilities of the early 2000's (6.1 MP), the presently used Nikon D7000 (16.2 MP) and potential usage of higher resolution Nikon D800 (36.3 MP) and Leaf Credo (80 MP) cameras. While the actual costs of digital cameras decrease regularly, if the current (2013) D100 cost was set at 100 arbitrary currency units, the other three cameras would cost 800, 2500 and 40000 respectively.

Table 5.1 Smallest resolved particle sizes by Sedimaging and TST for different camera resolutions

Camera Model	D100	D7000	D800	Credo 80
Year Introduced	2002	2010	2012	2012
Resolution (MP)	6.1	16.2	36.3	80
Resolution (pixels × pixels)	3008 × 2000	4928 × 3264	7360 × 4912	10320 × 7752
Sedimaging				
Soil Column Height (mm)	135	135	135	135
Required Magnification (pixels/mm)	22.3	36.5	54.5	76.4
Minimum *PPD* for Wavelet Analysis (pixels)	3	3	3	3
Smallest Particle Resolved (mm)	0.135	0.082	0.055	0.039
Translucent Segregation Table (TST)				
Longer TST Dimension (mm)	910	910	910	910
Required Magnification (pixels/mm)	3.3	5.4	8.1	11.3
Minimum *PPD* for Watershed Analysis (pixels)	9	9	9	9
Smallest Particle Resolved (mm)	2.7	1.7	1.1	0.8

The longer Sedimaging and TST image dimensions and the larger of the two pixel resolution directions dictate the required magnification in units of pixels/mm. The required *PPD* then establishes the smallest particles size that can be resolved. Table 5.1 reveals that the target particle sizes (0.075 mm for the Sedimaging and 2.0 mm for the TST) could not be achieved with DSLR cameras in the 2000's. By contrast, currently available cameras are well suited for characterizing particles well into the silt range by the Sedimaging and below 1.0 mm by the TST. These calculations suggest that particles in the 2.0 mm to 1.0 mm range could be tested in the TST rather than by the Sedimaging. Such a seemingly small decrease in the maximum particle size for the Sedimaging would have profound implications to the size and cost of the system. By reducing the maximum particle diameter by 50% the cross section of the sedimentation column could be reduced from $(50\ mm)^2$ to $(25\ mm)^2$. At the same time, the column height could be reduced by more than 50% since settling velocity is proportional to the square of the particle diameter and settling velocity controls particle segregation. The presently large Sedimaging system could become a portable device.

Continuing advances in image sensor technology will yield ever-increasing camera resolutions. This will gradually increase the range of particle sizes that could be analyzed from a single image. At the same time, improvements in optics will gradually increase image magnifications. Common current methods for increasing magnification include macro lenses, diopter rings and extension tubes. Table 5.2 lists the smallest soil particle sizes that could theoretically be detected by wavelet analysis using various combinations of these magnifying systems.

Table 5.2 Smallest resolved particles by various magnifying systems

	[1)]Macro Low Mag.	Macro High Mag.	[2)]Macro & Diopters	[3)]Macro & Extension
Magnification (pixels/mm)	36.7	209.8	238.1	254.2
Minimum *PPD* (pixels)	3	3	3	3
Minimum Particle Size (mm)	0.082	0.014	0.013	0.012

1) AF-S Micro Nikkor 60 mm f/2.8 G ED
2) Tiffen 62 mm close-up lens +1, +2 and +4
3) Kenko extension tube 12 mm, 20 mm and 36 mm

A 60 mm macro lens provides magnifications approaching 210 pixels/mm. At this magnification the field of view will be too small for Sedimaging but it demonstrates that particles as small as 0.014 mm can be detected. It is also worth noting that a magnification of 1500 pixels/mm would be able to detect 0.002 mm particles, the commonly cited silt/clay threshold. Smaller, clay-sized particles would not be detected. The use of diopter rings and extension tubes adds very little to the magnification achieved by the macro lens alone. Furthermore, diopter rings and extension tubes decrease the image quality to the point that measures of particle size are noticeably affected. As such, the use of diopter rings and extension tubes is not recommended. Higher magnifications can also be achieved with photomicroscopy at the expense of having a very limited field of view.

5.2 Linear Calibration Curve

5.2.1 Theoretical CA Versus $\log_{10}$(PPD) Relationships

It was earlier observed that the Normalized Energy distribution peaks at the decomposition level at which the approximations are at the size of the features in an image. Each doubling of *PPD* should increase *CA* by 1.0. Thus, the *CA* versus $log_{10}PPD$ relationship should theoretically be linear. This is demonstrated using images of perfect checkerboards shown in Figure 5.4.

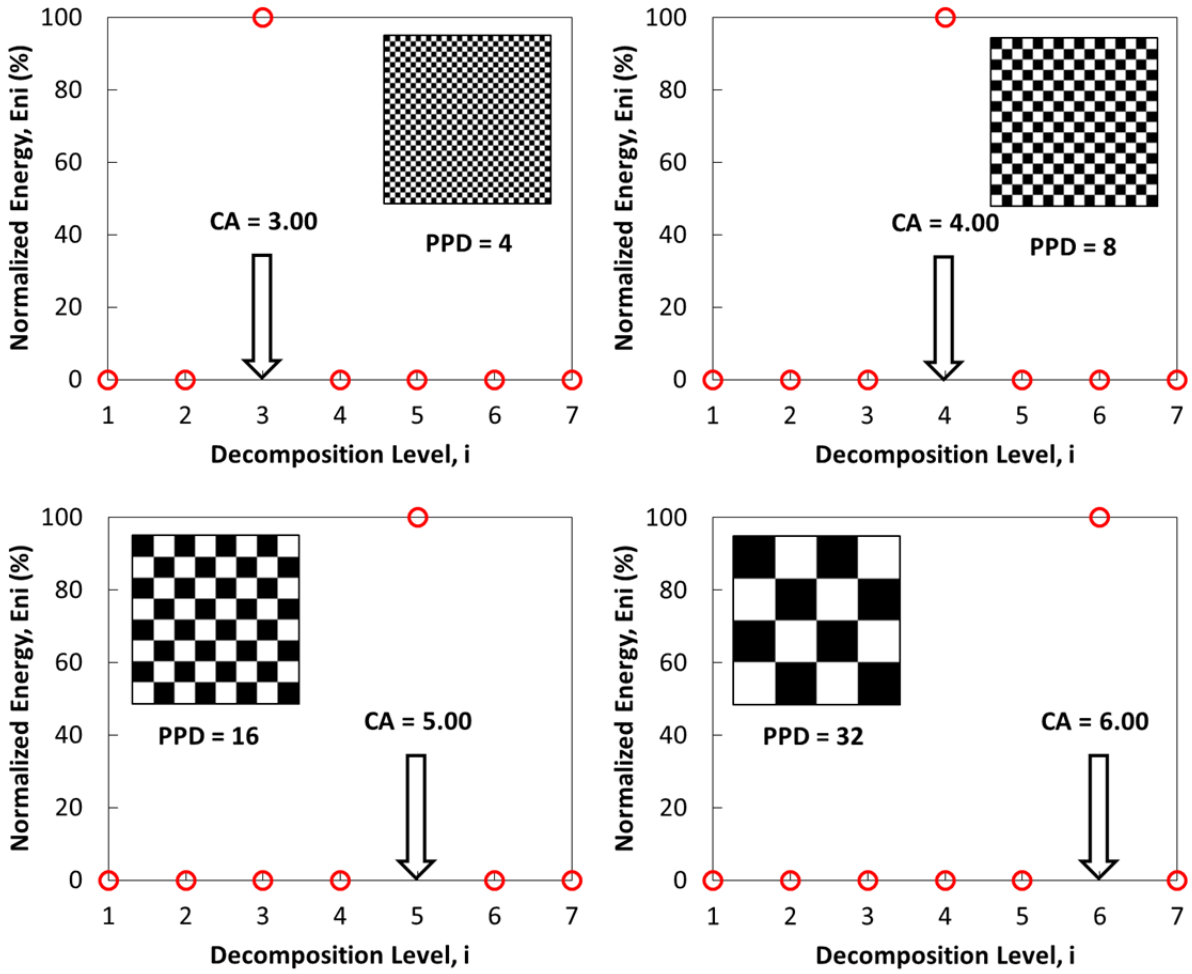

Figure 5.4 *CA* for ideal checkerboards

A checkerboard of 1 × 1 pixels contains all of its energy at the 1st decomposition level and accordingly *CA*=1.00; a checkerboard of 2 × 2 squares contains all of its energy at the 2nd level (*CA*=2.00); a checkerboard of 4 × 4 squares contains all of its energy at the 3rd level (*CA*=3.00) and so on. This idealized "checkerboard relationship" is shown in Figure 5.5 and expressed by:

$$PPD = 2^{CA-1} \tag{5.1}$$

Figure 5.5 also compares Equation (5.1) to the empirically established *CA* vs $log_{10}PPD$ calibrations for saturated soils behind glass. The differences are obviously large but explainable.

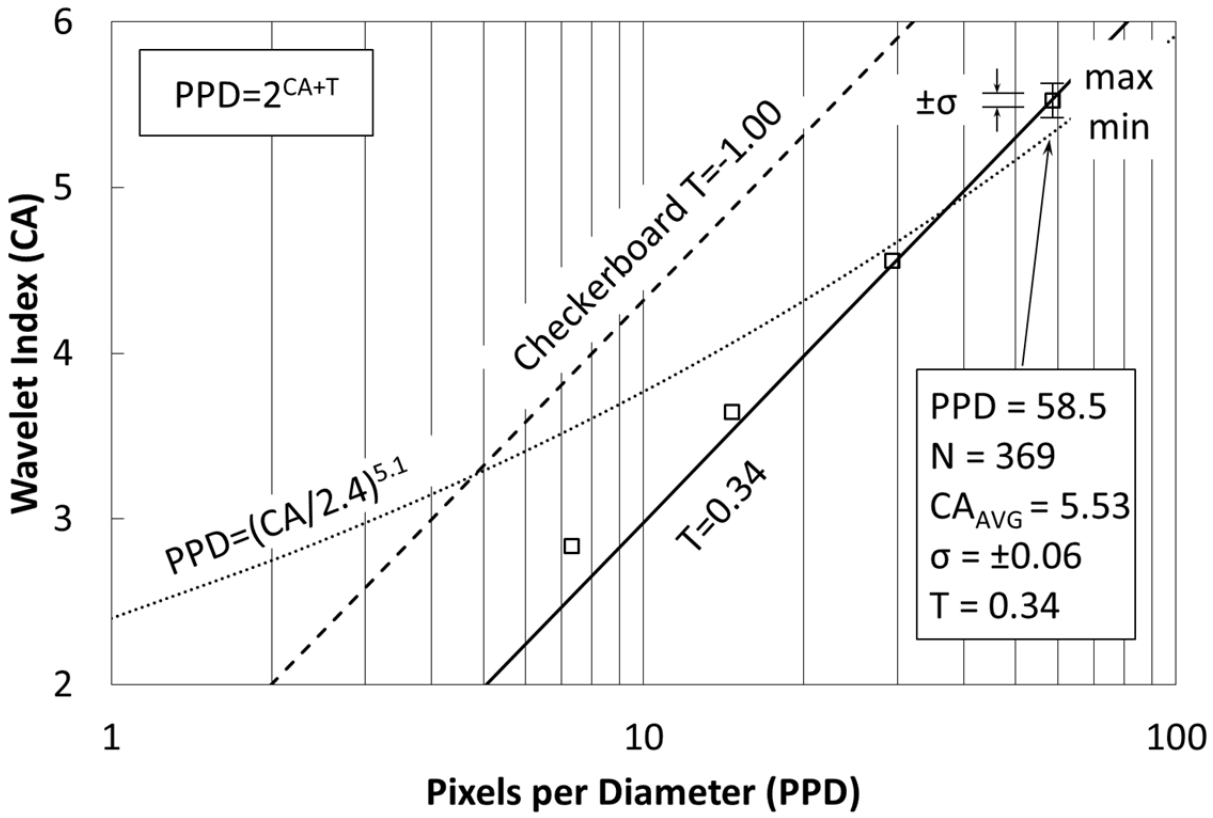

Figure 5.5 Checkerboard model and downscaling from *n*=10

In the early 2000's, prior to wide availability of high resolution digital SLR cameras, Shin and Hryciw (2004) used an analog CCD camera. The signals were digitized into 640 × 480

images. As such, only 7 (at most 8) levels of decomposition could be used. Today, 7 decomposition levels (128 × 128) continue to be used so that the size of the square analysis areas could be small relative to the specimen size when using the highest resolution cameras commercially available. This leads to a critical observation: of the 6 curves shown in Figure 3.22, only the one for *PPD* = 12, which peaks almost symmetrically at the 4th decomposition, comes close to not being truncated at either the 1st or 7th decomposition level. As a result of the truncations of curves for all other *PPD*s, Equation (3.3) under-predicts the true (un-truncated) *CA* at high *PPD* values and over-predicts the true *CA* at low *PPD*s.

To confirm that the true *CA* versus *PPD* calibration line should be linear, a 1024 × 1024 (n=10) image of 2NS soil retained between the No. 10 and No. 16 sieves was captured at *PPD* = 58.5. Instead of the usual 7, all 10 decomposition levels were used to compute *CA*. As shown by the curve in Figure 5.6 for *PPD* = 58.5, the Normalized Energy distribution was not truncated at either end when 10 decomposition levels were used. The 1024 × 1024 images was then digitally downscaled to 512 × 512 (*PPD* = 29.3). Figure 5.6 shows that this caused each data points to shift to the left by exactly one decomposition level. Therefore, *CA* also decreased by exactly 1.0. The image was then further downscaled to 256 × 256 (*PPD* = 14.6) and finally 128 × 128 (*PPD* = 7.3). The experiment was repeated on 369 overlapping images of the soil specimen and the average *CA* was computed to be 5.53 with a standard deviation (σ) of ± 0.06. The maximum and the minimum *CA* values were 5.69 and 5.40, respectively. The results of one test which produced a *CA* value closest to the average are shown in Figure 5.5. The vertical dimension of the open square data point at *PPD* = 58.5 shows the range occupied by ± σ of the *CA* values and the horizontal bars show the minimum and the maximum values. Figure 5.5 also shows the *CA* points corresponding to *PPD* = 29.3, 14.6 and 7.2. As expected from observation of Figure 5.6,

the points for *PPD* = 58.5 and 29.3 fall on a line parallel to the checkerboard line. The point corresponding to *PPD* = 14.6 begins to rise above the line and the point corresponding to *PPD* = 7.3 is well above it as would be expected given the clear truncation of its energy curve in Figure 5.6.

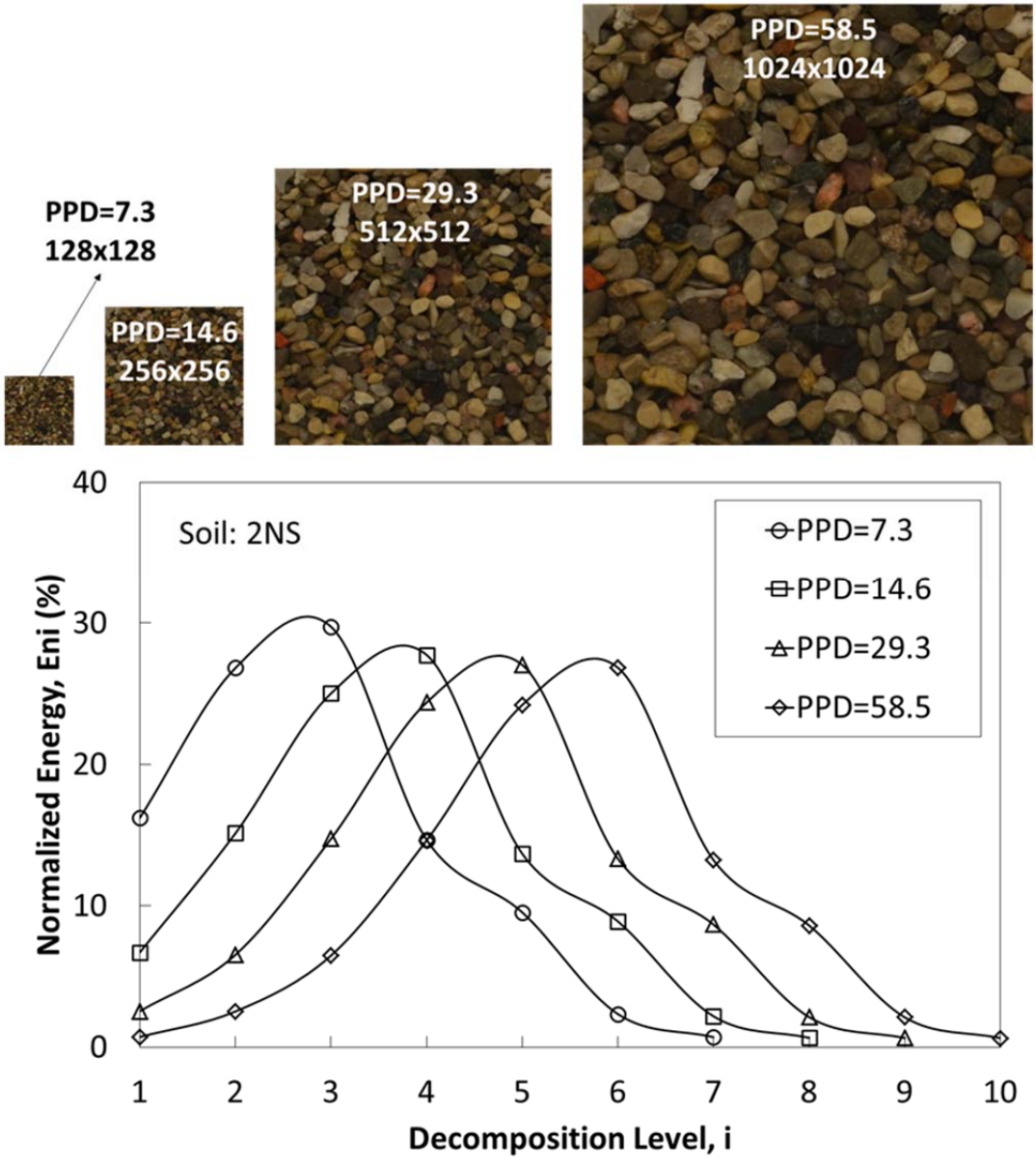

Figure 5.6 Normalized Energies with downscaling from *n*=10

While the "calibration line" for the 2NS in Figure 5.5 is parallel to the checkerboard line, it is offset downward (or to the right) from it. The offset is due to voids, partial particle views, non-square particle geometries and particle surface imperfections. Since such features are smaller than the particles themselves, the *CA* for images of soil assemblies will naturally be lower than for perfect checkerboards.

5.2.2 Discussion of Practical Implications

While current high end camera resolutions and testing system dimensions assure that Equation (3.4) will continue to be used for some years, the prospect of eventually moving to a single-parameter linear calibration is exciting. Since the calibration line would be a simple offset from the checkerboard line, it can be expressed by modification of Equation (5.1) to:

$$PPD = 2^{CA+T} \tag{5.2}$$

The letter *T* is suggested for the shift as it would reflect the soil image's "texture" or "type". For the checkerboard line $T = -1.00$ while for 2NS and many similar alluvial or glacio-fluvial sands, $T = 0.34$ is tentatively recommended. For mottled, roughly textured or translucent soil particles, *T* would be smaller. At any rate, the linear model would be much preferred over the current non-linear calibration as it would require a single empirical parameter (*T*) which for most soils is expected to be about 0.34. Unusual soils would then be characterized by their deviation from the soil baseline of $T = 0.34$.

The eventual implementations of the linear Equation (5.2) would require that the smallest soil particles, ($d = 0.075$ mm) nominally contain at least $PPD = 20$ to 25 to avoid having *CA*

affected by truncation of the Energy distribution at the first decomposition level. This translates to a camera magnification of about 300 pixels/mm which is almost 10 times the currently used magnification. To capture the entire soil column shown in Figure 3.19 with a single image at this magnification would require a 500 to 600 MP camera sensor. Alternatively, it would require high resolution scanning or digital stitching of multiple images which, while technically feasible, are impractical. As such the current 2-parameter non-linear model which yields very good results will continue to be used until higher resolution cameras are developed or an alternate engineering solution is found.

5.3 Morphological Opening to Analyze Sedimented Soil Images

5.3.1 Mathematical Morphology in Optical Granulometry

In this dissertation, for image analysis in the Sedimaging test, a statistical method called 2D wavelet analysis was used and a wavelet index *CA* was correlated to the average particle size as defined by *PPD*. A different approach based on morphological opening to determine particle size distribution of soil from a Sedimaging image is proposed.

Mathematical morphology has previously been employed to characterize particle size and surface texture. Devaux et al. (1997) used two morphological operations, erosion and dilation on steel marbles and ground pea kernels, and found that the erosion or dilation steps can be related to the particle size. Ghalib and Hryciw (1999) used watershed analysis to separate contacted particles from an image captured by a backlit table. Mlynarczuk (2009) used morphological gradient, watershed analysis and morphological filtering to evaluate rock surface roughness from an image obtained by a laser profilometer.

5.3.2 Erosion, Dilation and Structuring Element

Two basic operations in mathematical morphology are *erosion* and *dilation*. Erosion can be described as shrinkage of objects in an image whereas dilation can be described as expansion of objects in an image. It is easy to understand how these two operations work when applied on a binary image. Figure 5.7 shows the results of erosion and dilation on a binary image containing square “objects” of different size. Note that red dots represent locations of pixel points.

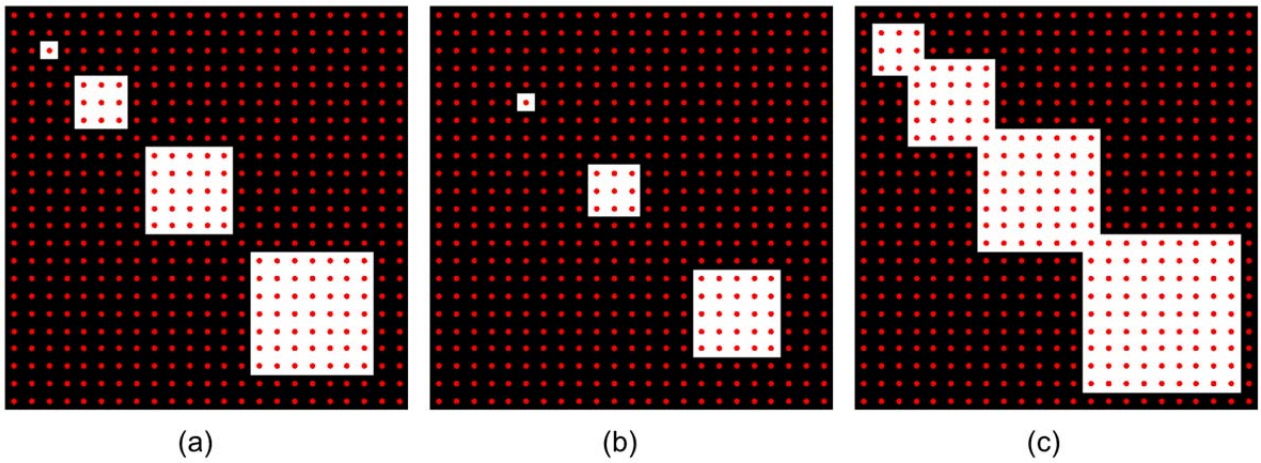

Figure 5.7 Erosion and dilation of a binary image by a 3 x 3 square structuring element: (a) Original image, (b) Erosion, (c) Dilation

To determine how much the area of an object will be shrunk or expanded, a *structuring element* needs to be defined. A Structuring element defines the size of the neighborhood that will be influenced by erosion or dilation, and also defines the center of this neighborhood. The center of the structuring element will progressively be moved to every pixel location in an image. The final products of applying erosion and dilation on an image are entirely dependent on the shape and the size of this structuring element (Solomon and Breckon 2011). As shown in Figure 5.7, an object that is smaller than a 3 by 3 square structuring element is removed by erosion whereas objects that are larger than the structuring element still remain but will be smaller. On the other hand, opening will make every object larger. Mathematically, in both binary and non-binary images the erosion operation replaces the value of each individual pixel in an image by the minimum value of its neighborhood pixels whereas dilation replaces each individual pixel in an image by the maximum value of neighborhood pixels.

5.3.3 Opening and Closing

Now that the two basic operations in mathematical morphology are defined, *opening* and *closing* can be defined based on the sequence of these two basic operations. Opening is defined as erosion followed by dilation, whereas closing is defined as dilation followed by erosion. The easiest way to compare opening and closing is to see the final products of an original image applied by these two operations. Figure 5.8 shows a result of opening an original image using a 3 by 3 square structuring element. One of the square objects from the original image which has a size less than 3 by 3 structuring element is removed as a result of opening. When erosion is first applied on the original image, objects that are smaller than structuring element are removed. When dilation is next applied on the image after erosion, the remaining objects recover their original size. The closing operation is the opposite of the opening operation. Figure 5.9 shows the result of closing an image. Notice that "voids" inside of the square foreground objects that are smaller than the structuring element are removed by closing.

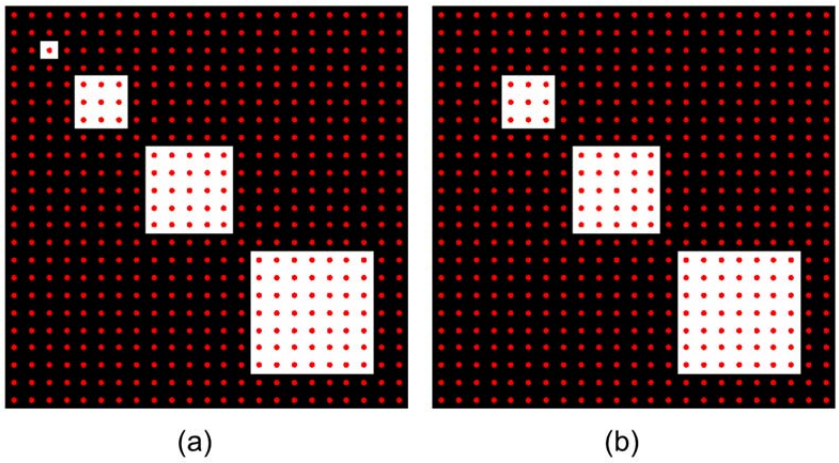

Figure 5.8 Opening of a binary image by a 3 x 3 square structuring element: (a) Original image, (b) After opening

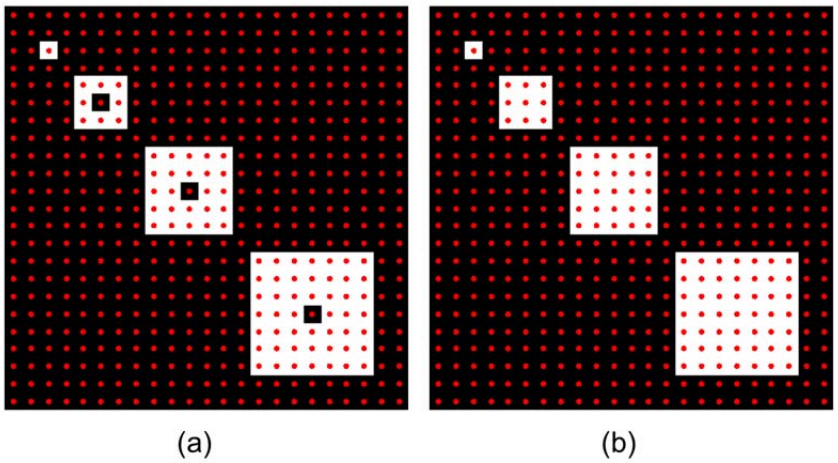

Figure 5.9 Closing of a binary image by a 3 x 3 square structuring element: (a) Original image, (b) After closing

Opening is the operation that is used to determine particle size distribution using morphological processing. The basic premise is that the number of pixels that are removed by opening a binary image with certain sized structuring element corresponds to percentage of objects that are smaller than that structuring element. For a grayscale image, the results of opening may not be as simple to interpret as those for a binary image. The opening operation on a grayscale image tends to suppress bright regions that are smaller than the structuring element (Solomon and Breckon 2011). Figure 5.10 shows opening of a soil image with structuring elements of different sizes. The grayscale image can be plotted in three dimensional space where the x and y axes are the coordinates of each pixel and the z axis is the grayscale value. Thus, the opening operation on a grayscale image can be visualized as removing similar gray scale region that are smaller than structuring element in three dimensional space. Therefore, the result of opening operation on a gray scale image is somewhat different than that on a binary image. In other words, for a binary image objects that are smaller than structuring element are entirely removed from the original

image, whereas for a grayscale image the details of objects that are smaller than the structuring element are removed.

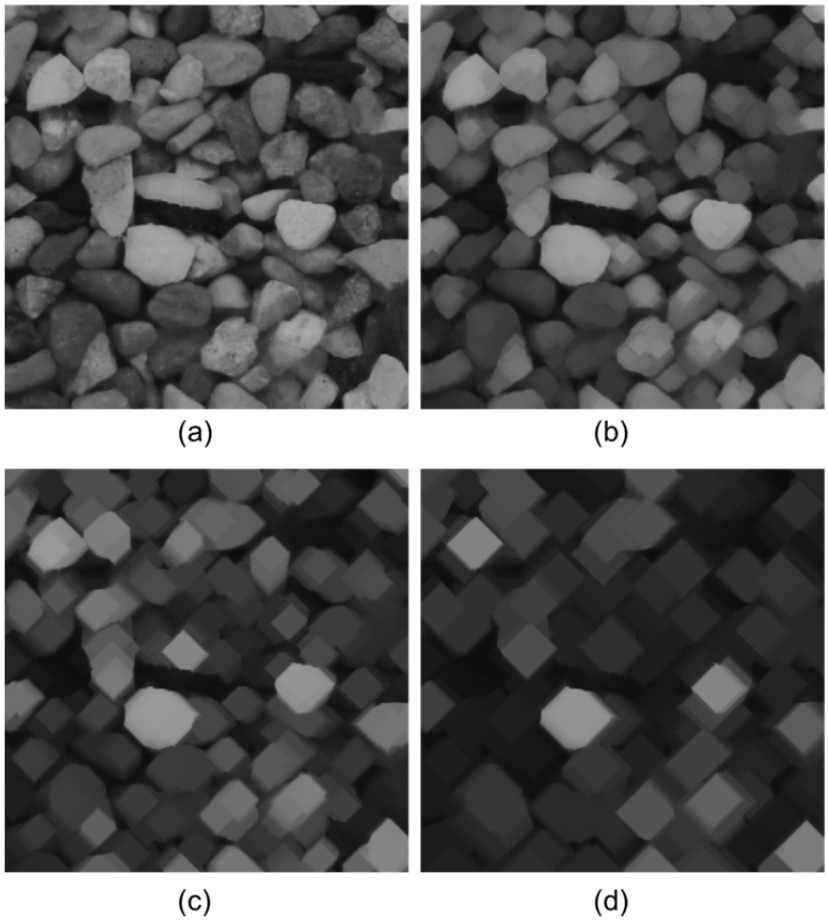

Figure 5.10 Opening of a soil image with different size of diamond shape structuring element: (a) Original image, (b) Opening with *SES*=21, (c) Opening with *SES*=41, (d) Opening with *SES*=61

One could say that the opening operation on a gray scale image can be regarded as blurring the image at different scales. For a soil particle image, details of objects can be parts of a particle having similar internal shades of gray, voids between soil particles, entire individual soil particles, or combinations of two (or more) adjacent soil particles having similar gray scales (Ohm and Hryciw 2012). Therefore, the results of opening a grayscale image cannot be directly

correlated to particle size distribution as can be done for a binary image. Details about how to correlate opening results to particle size distribution follow in next two sections.

5.3.4 Structuring Element Size

As discussed earlier, the structuring element is an assemblage of pixels representing any shape that is to define the neighborhood for the morphological operation. For determination of a distribution of sizes of objects in an image, the structuring element shape is chosen to approximate the shape of objects being sized. For soil particles, a diamond shape was selected. The *Structuring Element Size* (*SES*) was defined by the number of pixels along the diagonal of a diamond structuring element (Jung 2010).

5.3.5 Pattern Spectrum

A *pattern spectrum* is a normalized histogram of the objects found in an image (by opening) versus the *SES* (Matheron 1975). Mathematically, a *pattern spectrum value* (*PSV*) for certain *SES* is defined as a summation of the difference in gray scale values between an image opened by *SES*-2 and an image opened by *SES*. For uniform soils, the *SES* corresponding to the peak of the pattern spectrum correlates well with *PPD* (Jung 2010). For non-uniform soils, the pattern spectrum is flatter than that for uniform soils.

5.3.6 Peak of Pattern Spectrum (PPS) Method

An image of soils of sieve diameter between 0.425 mm (No. 40 sieve) and 0.300 mm (No. 50 sieve) was captured in a Sedimaging test. The pattern spectrum was computed for each vertical 128 pixel height increment from bottom to top of the image. The pattern spectrum for all of the increments and their peak values as marked by blue circle are shown in Figure 5.11.

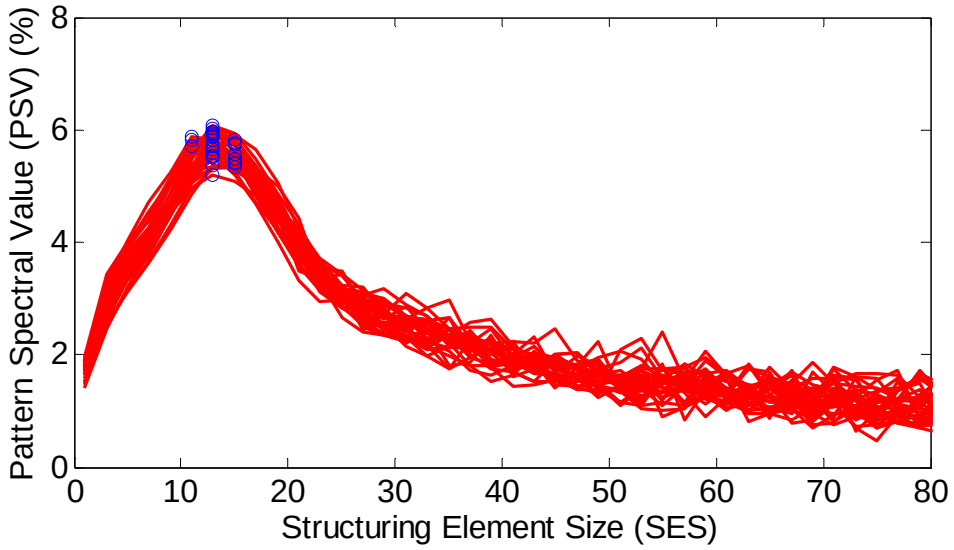

Figure 5.11 Pattern spectrum of pre-sieved soil: No. 40 - No. 50

The *SES* corresponding to the peak of the *PSV* is not exactly equal to *PPD* due to the slightly different shape of the diamond structuring element and typical soil particles (Jung 2010). Therefore, the average of *SES*s corresponding to the peak of the *PSV* and the average *PPD* calculated from the two bounding sieve sizes were plotted to develop a calibration curve. In order to find this curve for a wide range of *PPD*, different particle ranges of sieved soils were prepared and analyzed by the same procedure (Figure 5.12). The relationship between *PPD* and *SES* corresponding to the peak of the *PSV* is as follows:

$$PPD = \left(\frac{SES_p}{1.2} \right)^{1.1} \tag{5.3}$$

where SES_p is the structuring element size corresponding to peak of the *PSV*.

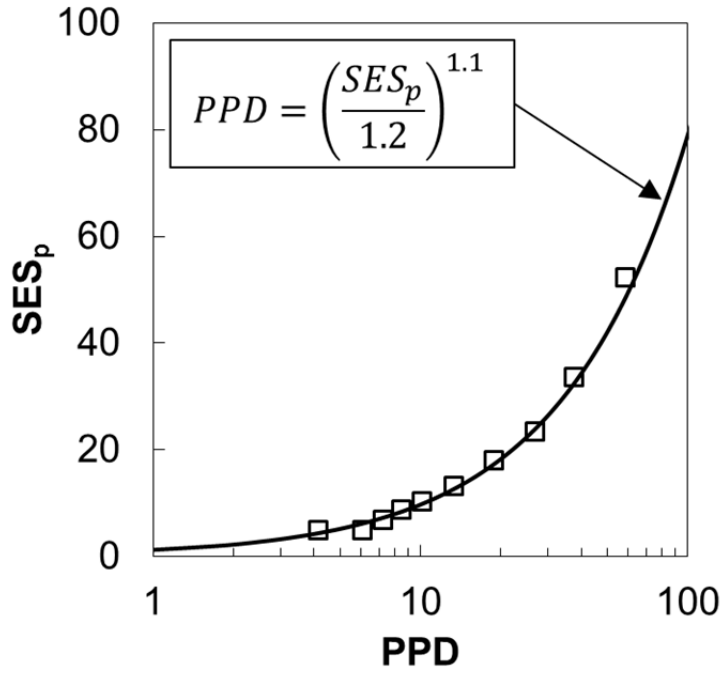

Figure 5.12 Structuring element size corresponding to peak of the *PSV* (SES_p) vs pixels per particle diameter (*PPD*) curve

To summarize, the procedure to analyze an image of a sedimented soil using the *Peak of Pattern Spectrum* (*PPS*) method is as follows. First, a sedimented soil image is obtained in the Sedimaging device. Second, the pattern spectrum for each 128 pixel height increment is computed. Third, the *SES* corresponding to the peak of the *PSV* for each increment is found. Fourth, each *SES* is converted to *PPD* using Equation (5.3) (Figure 5.12). Finally, the particle size distribution of the soil is developed by sorting the *PPD* from each layer by size. A typical result by the *PPS* method is shown in Figure 5.13.

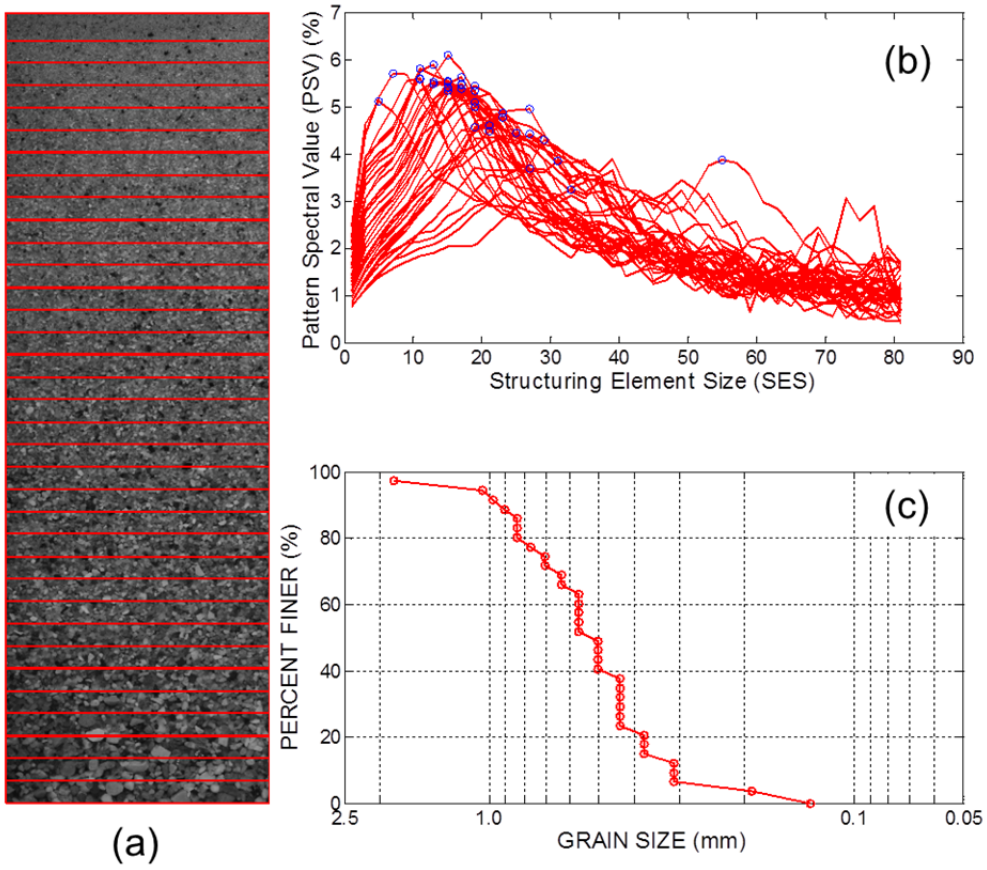

Figure 5.13 Typical result of *PPS* method (S1): (a) Original soil image, (b) Pattern Spectrums for all vertical image increments, (c) Particle size distribution

5.3.7 Pattern Spectrum Matching (PSM) Method

The *PPS* method still requires that soil particles be relatively uniform in size within each 128 pixel high increment of the image. As discussed earlier, this same requirement prompted development of the Sedimaging system to analyze grain sizes of soil using wavelet analysis. In this chapter a method is proposed for analyzing images of for non-uniform soil using a *Pattern Spectrum Matching* (*PSM*) method. In this approach, pattern spectrums for non-uniform soils are created by combining the pattern spectrums of uniform soil particles that are components of the real soil mixture. In other words, the pattern spectrum of a soil "mixture" containing various

sizes is a summation of the weighted contributions of the spectrums of different incremental particle size ranges. The equation describing the pattern spectrum of such soil mixtures is:

$$PSV = C_1 PSV_1 + C_2 PSV_2 + \cdots + C_{i-1} PSV_{i-1} + C_i PSV_i \tag{5.4}$$

$$\sum_{k=1}^{i} C_k = 1 \tag{5.5}$$

where PSV is the pattern spectrum of a soil mixture, PSV_i is the pattern spectrum of the i-th uniform sieved soil constituent, and C_i is the mass (or volume) fraction of the i-th component soil. Unlike the *PPS* method, the entire pattern spectrum from each sieved component soil is used. Figure 5.14 (*a*) shows the pattern spectrum of the sieved component soils. These spectrums are used as a database to create synthetic pattern spectrum of different mass fractions. Figure 5.14 (*b*) shows the range of synthetic pattern spectrums created by assuming various combinations of the nine size increments shown in Figure 5.14 (*a*). Each constituent was assumed to contribute $n \times 10\%$ to the mixture where $0 \leq n \leq 10$. Of course, the sum-of-n's for each synthetic pattern was 10. Figure 5.14 (*b*) also shows the actual pattern spectrum of some real soil mixture. A least-square method is used to find the one synthetic pattern spectrum that best matches the pattern spectrum of the real soil mixture. Figure 5.14 (*c*) shows the synthetic pattern spectrum that matched the pattern spectrum of the real soil mixture shown in Figure 5.14 (*b*). A typical result by the *PSM* method is shown in Figure 5.15.

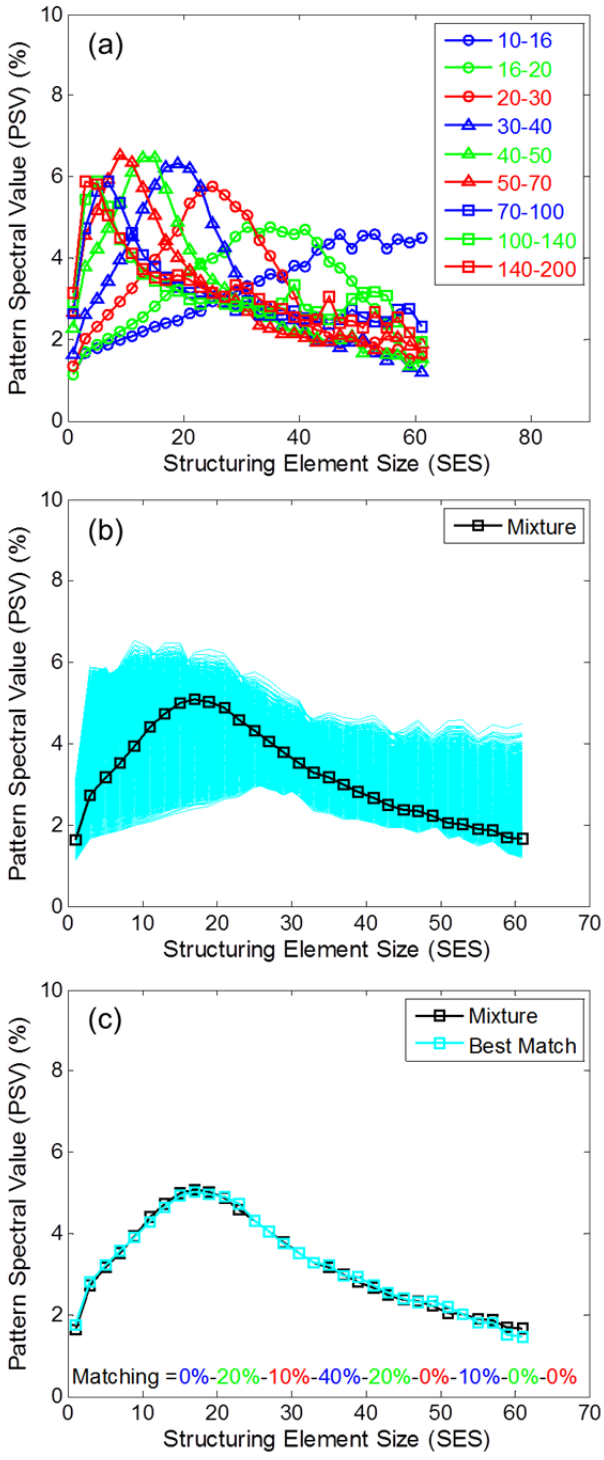

Figure 5.14 Procedure of *PSM* method: (a) Pattern spectrum of sieved soils, (b) Synthetic pattern spectrum using weighted average of pattern spectrum from sieved soils, (c) Matching synthetic spectrum to pattern spectrum of mixture

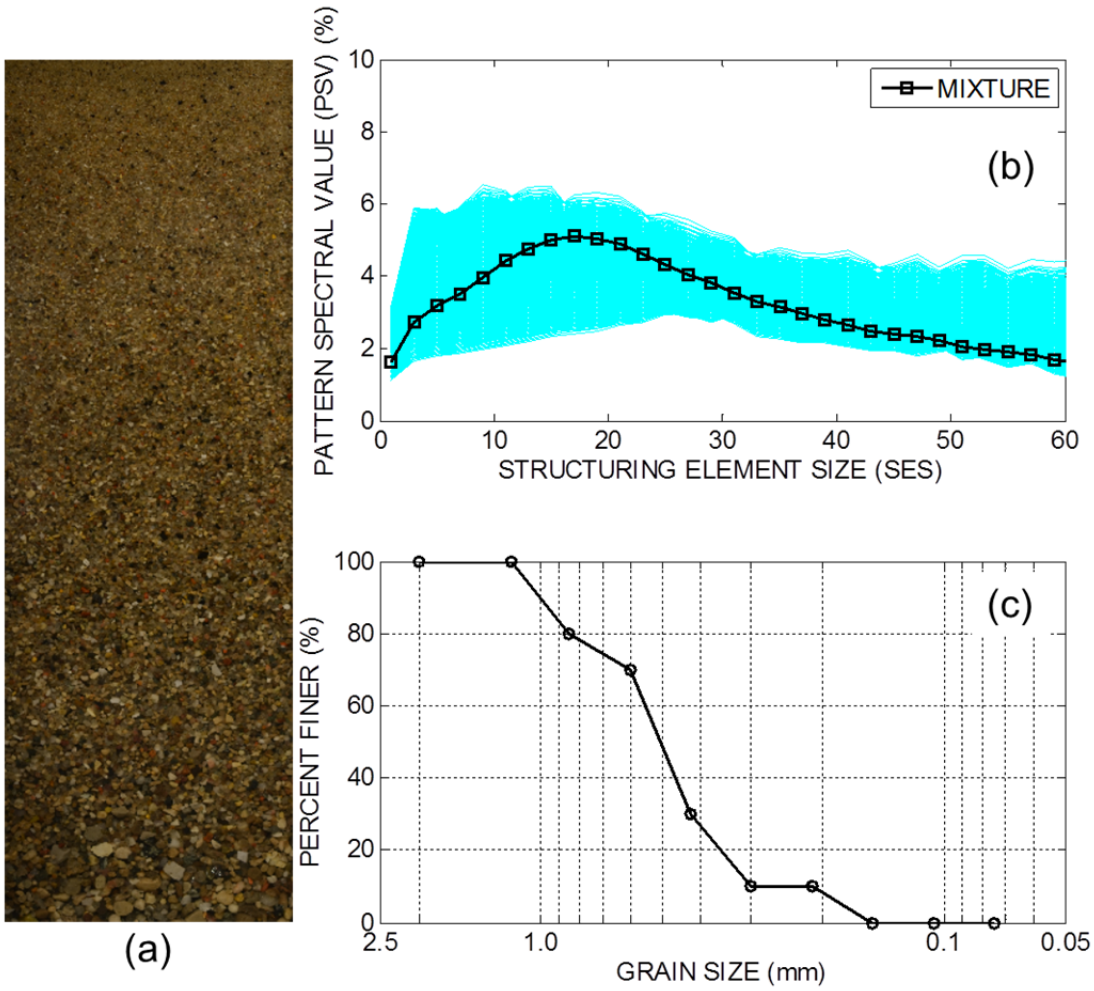

Figure 5.15 Typical result of *PSM* method (S1): (a) Original soil image, (b) Synthetic pattern spectrums and the pattern spectrum of the soil mixture, (c) Particle size distribution

5.3.8 Test Materials

Twenty soil samples were prepared in the Sedimaging system for analysis by the PPS and PSM mathematical morphology methods. The sieve-based size distributions by sieving are shown in Table 5.3. The total weight of each sample varied between 460 g and 510 g listed in Table 5.4. The first ten samples (S1-S10) were made by splitting one large specimen into ten portions then putting each portion through a sample splitter to create two halves. The second ten samples (S11-

S20) were made to specific gradations from large batches of pre-sieved material. The particle size distributions are shown in Figure 5.16.

Table 5.3 Percent passing different sieve opening sizes

Specimen Number	Opening Size				
	No. 16 1.180 mm	No. 30 0.600 mm	No. 50 0.300 mm	No. 100 0.150 mm	No. 200 0.075 mm
S1	90.2	63.0	15.1	2.6	0.7
S2	85.4	57.1	13.7	2.4	0.6
S3	77.7	46.1	11.0	2.4	0.7
S4	83.3	51.6	12.7	2.5	0.6
S5	87.9	58.7	16.1	3.7	0.9
S6	82.7	50.4	11.3	1.9	0.5
S7	82.1	48.3	11.9	2.7	0.7
S8	81.4	48.1	12.0	2.8	0.6
S9	75.3	41.0	9.0	2.0	0.5
S10	78.2	45.2	11.2	2.6	0.6
S11	75.5	52.1	27.5	3.8	1.1
S12	54.1	41.4	27.9	4.1	1.3
S13	86.5	41.4	27.3	4.0	1.4
S14	88.0	75.6	28.0	4.0	1.4
S15	72.6	60.5	48.5	4.2	1.1
S16	87.5	75.8	51.7	28.4	3.2
S17	69.0	38.8	16.0	4.9	3.4
S18	90.6	76.7	44.4	11.7	3.0
S19	89.4	79.5	68.3	37.7	6.6
S20	69.0	63.5	32.3	26.0	1.8

Table 5.4 Total weight of soil specimens

Specimen Number	Total Weight (g)
S1	477.4
S2	484.6
S3	497.8
S4	493.4
S5	487.2
S6	502.6
S7	483.3
S8	498.6
S9	507.3
S10	481.0
S11	475.0
S12	485.0
S13	470.5
S14	486.8
S15	483.2
S16	460.6
S17	481.0
S18	475.3
S19	481.4
S20	465.1

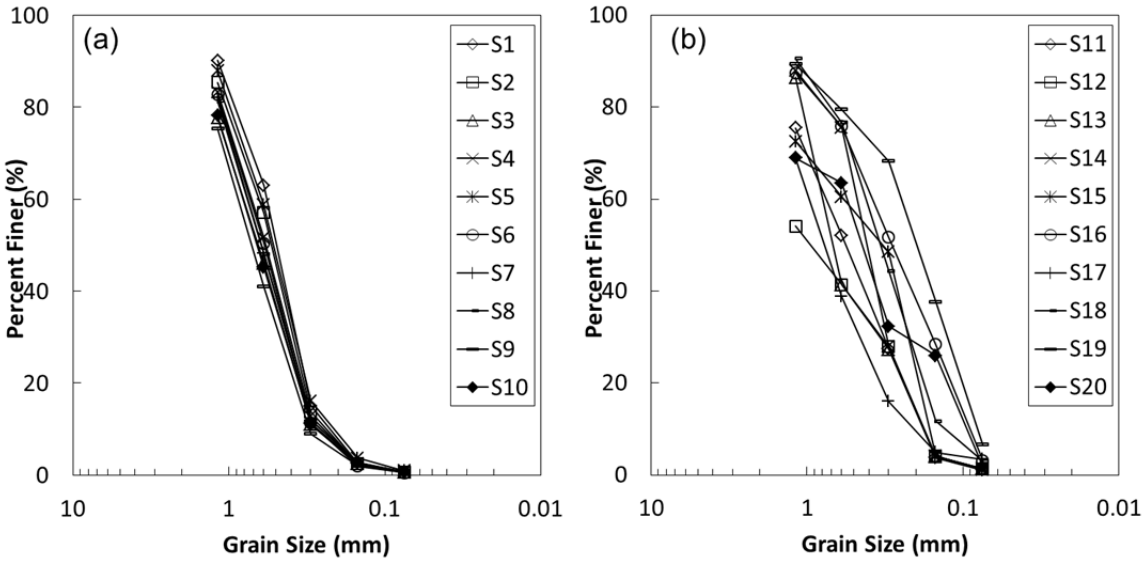

Figure 5.16 Sieve analysis results of 20 soil specimens: (a) S1-S10, (b) S11-S20

5.3.9 Results and Discussions

Figure 5.17 compares the results of the *PPS* image analysis method to sieve analysis. The number of data points obtained by the *PPS* method corresponds to the number of 128 pixel high layers in a sedimented soil image. Figure 5.18 compares the results of the *PSM* method to sieve analysis. The number of data points by the *PSM* method corresponds to the number of pattern spectrums of uniform sized sub-specimens that were used to create the synthetic pattern spectrums. The match between *PPS* method and sieve analysis appears to be as good as the match between the *PSM* method and sieve analysis.

As discussed earlier, both the *PPS* method and wavelet analysis require relatively uniform particle sizes within the area that is being analyzed. If there is a thin layer at the top of a sedimented soil image that is smaller than 128 pixels in height, the average particle size from this thin layer may not be fully calculated by using 128 × 128 pixels windows in wavelet analysis or by the 128 pixel height layers from the *PPS* method. Since morphological opening can analyze an area of any size, the layer thicknesses can be reduced. By contrast, since the window size used for wavelet analysis must be $2^n \times 2^n$, the window size can only be reduced to 64 × 64 pixels, 32 × 32 pixels, and so forth. The flexibility of the *PPS* method can be useful when there is a thin layer that needs to be analyzed.

The purpose of the Sedimaging device is to sort particles by size and therefore insure relative uniformity of particle sizes at certain elevation increments in a sedimented soil. While the *PPS* method requires that the sedimented soil be analyzed incrementally with height, the *PSM* method analyzes the entire sedimented soil column simultaneously. Therefore, the *PSM* method may not need the same degree of particle sorting as the *PPS* requires. Thus, the *PSM*

method may be very useful in analyzing soil mixtures where a large Sedimaging device cannot be utilized, such as in the field. Further study is needed to evaluate how much the Sedimaging system could be scaled down if the *PSM* method is adopted.

However, the PSM results are still very preliminary. They are based on only one soil type. It is not yet known if the synthetic pattern responses determined on the sieved-out mass fractions of one soil will accurately predict the composite pattern response and the particle size distributions of other soils. If this is not the case and if every soil will require that its constituent size fractions be analyzed to create its own unique library of responses then the method may not be as attractive as the present study implies.

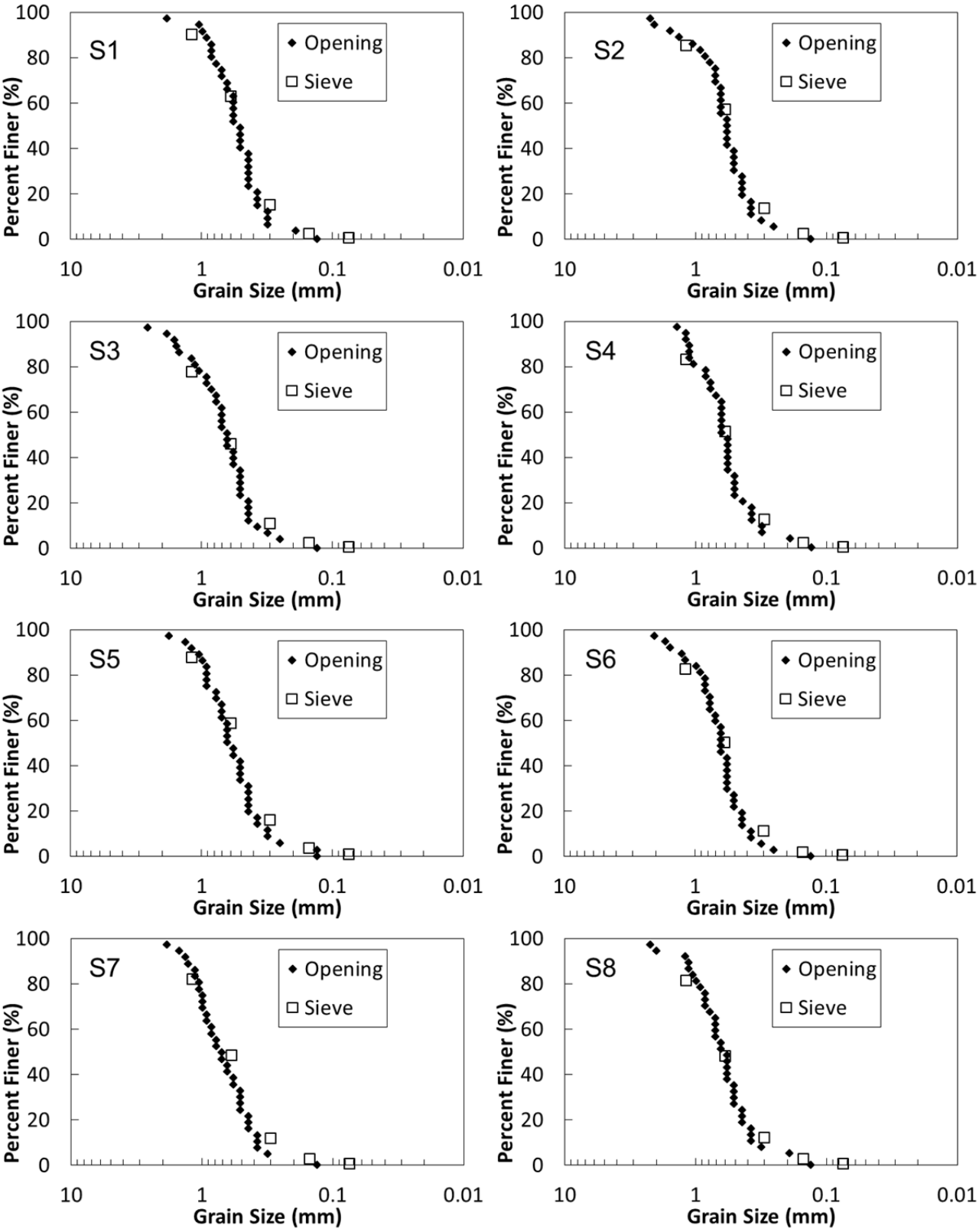

Figure 5.17 Comparison of results from sieve analysis and *PPS* method (S1-S8)

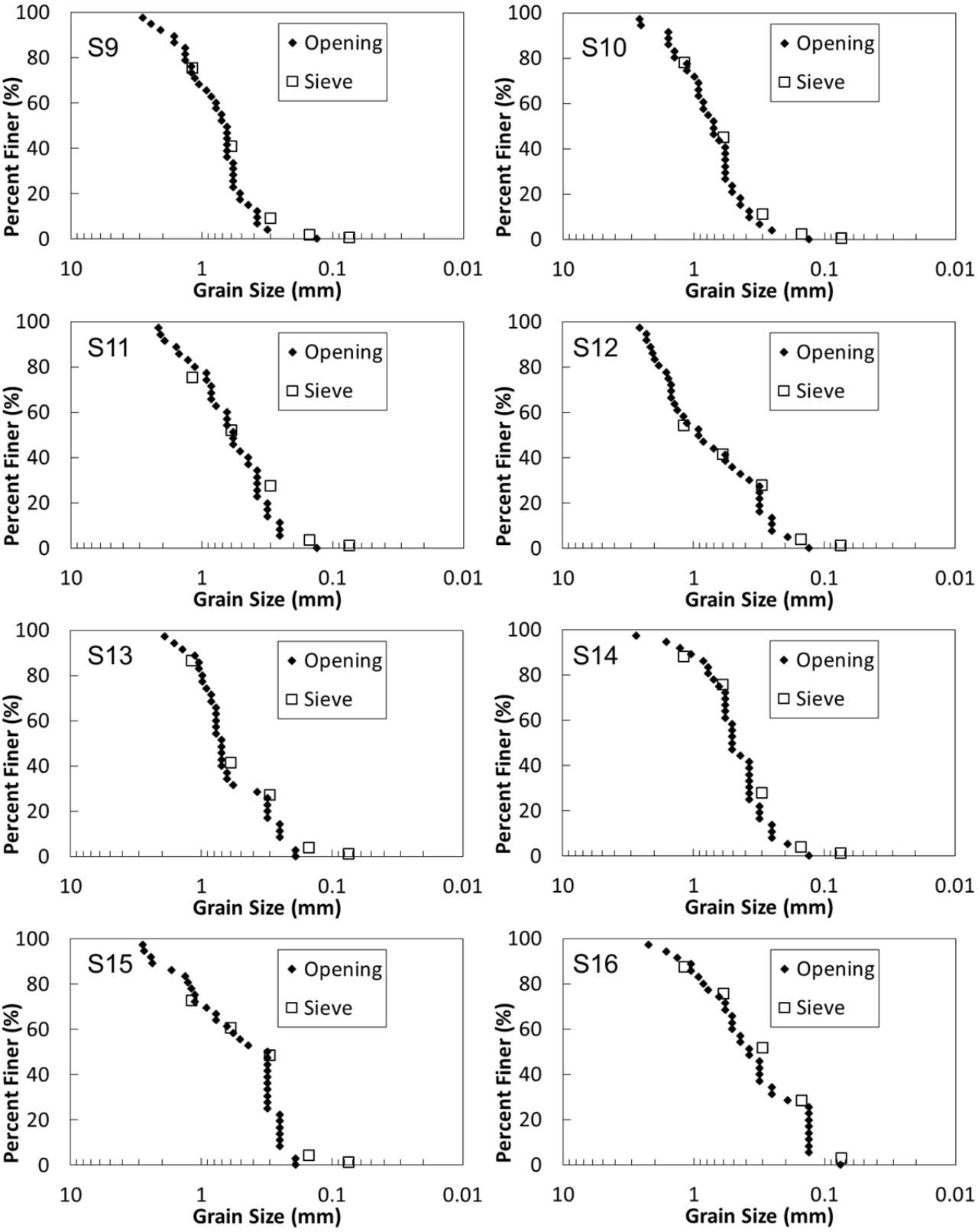

Figure 5.17 (Cont.) Comparison of results from sieve analysis and *PPS* method (S9-S16)

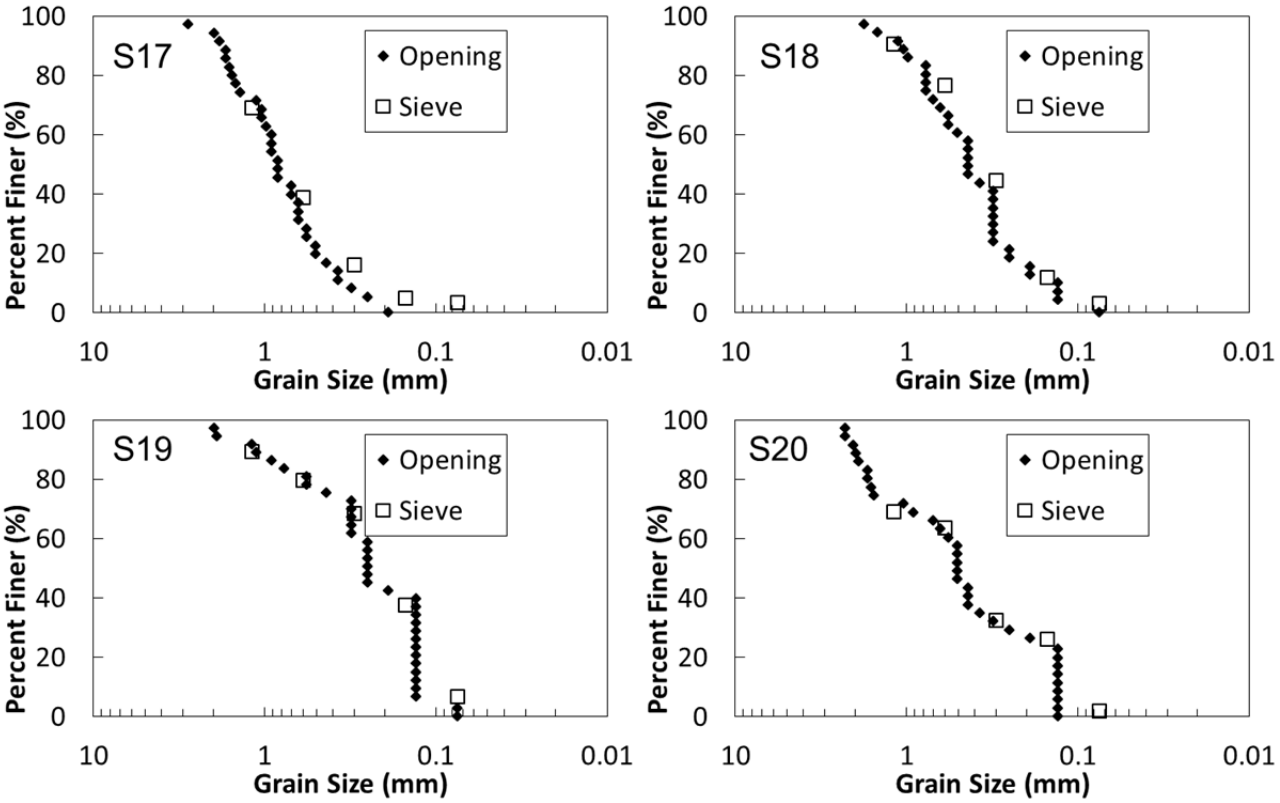

Figure 5.17 (Cont.) Comparison of results from sieve analysis and *PPS* method (S17-S20)

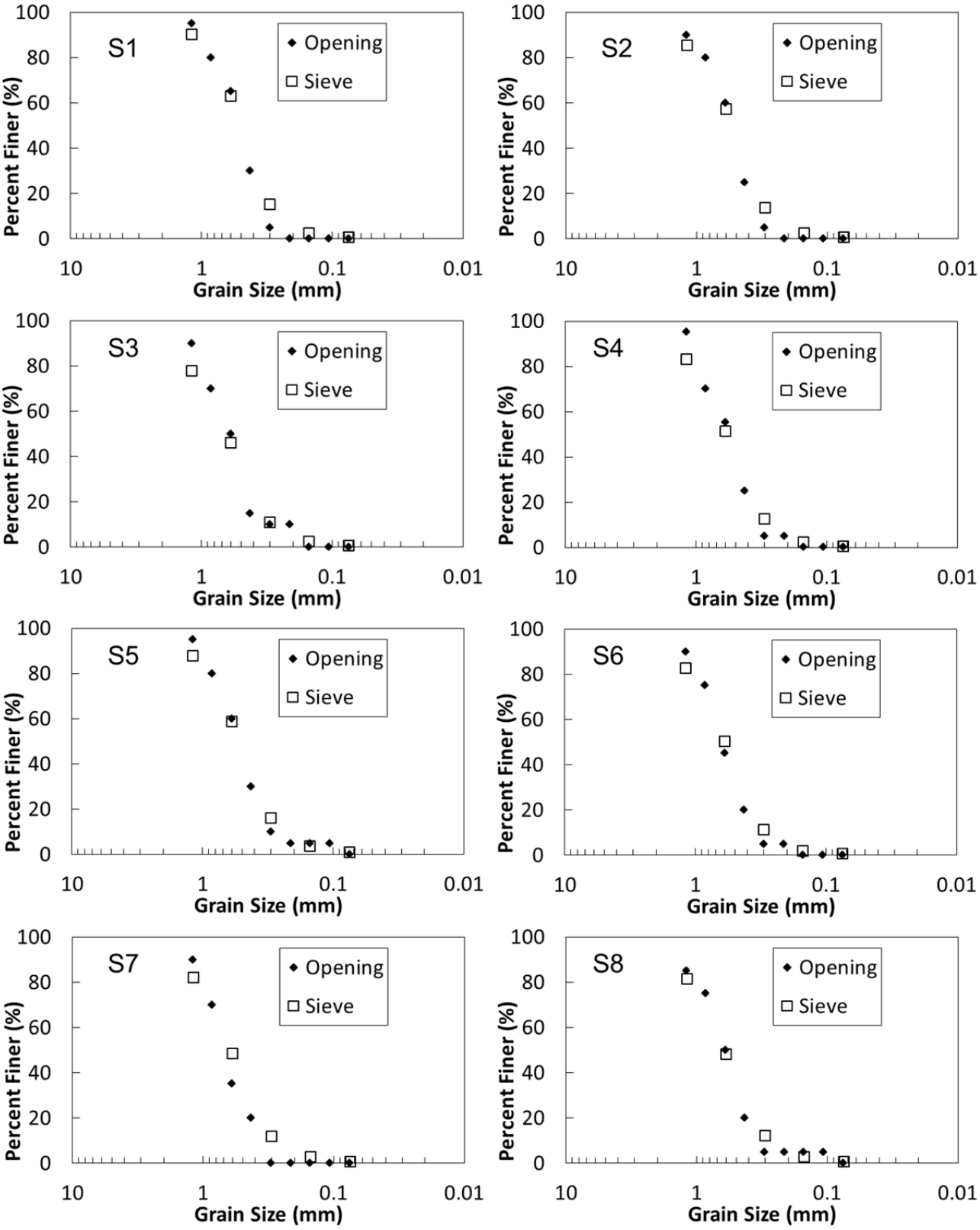

Figure 5.18 Comparison of results from sieve analysis and *PSM* method (S1-S8)

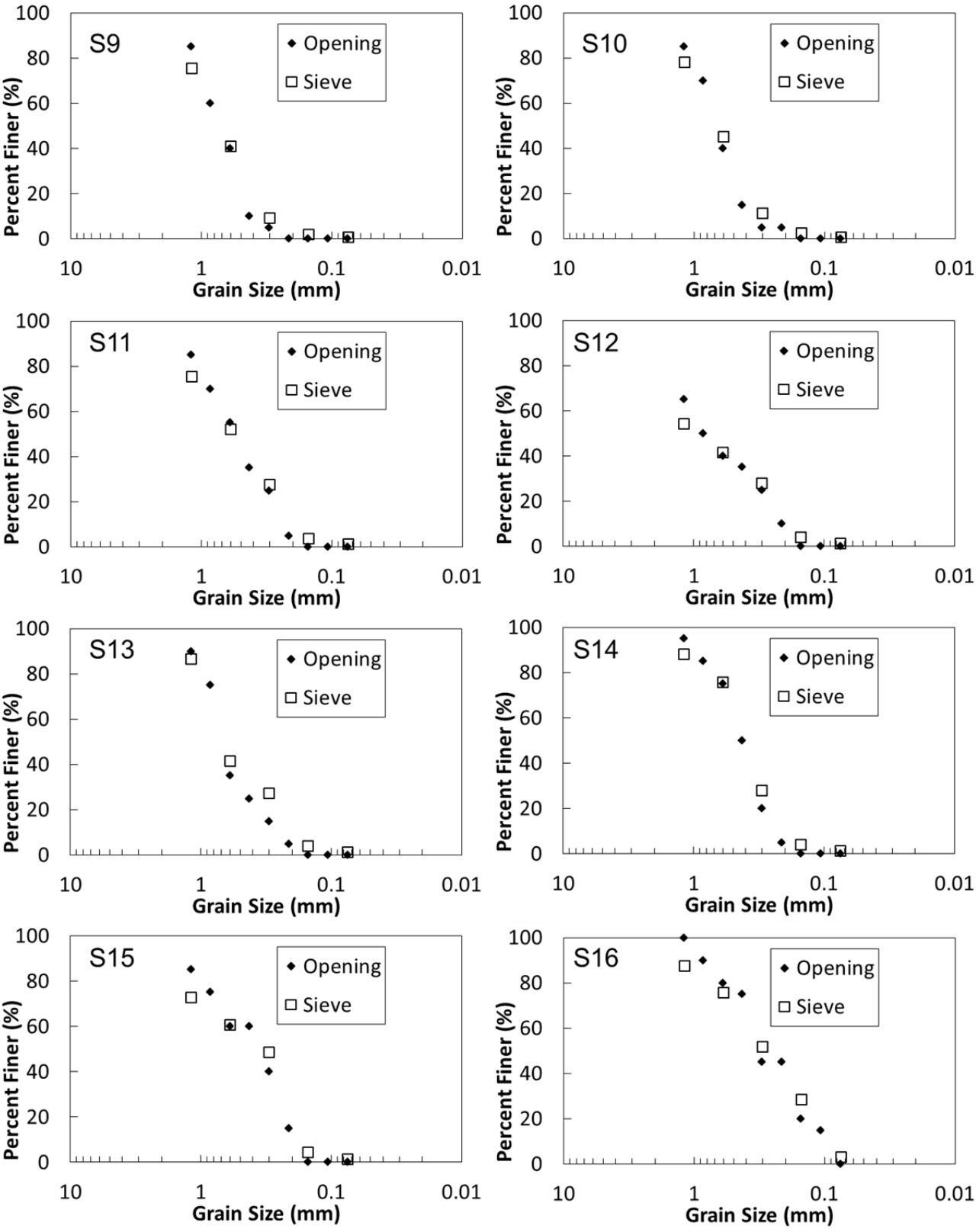

Figure 5.18 (Cont.) Comparison of results from sieve analysis and *PSM* method (S9-S16)

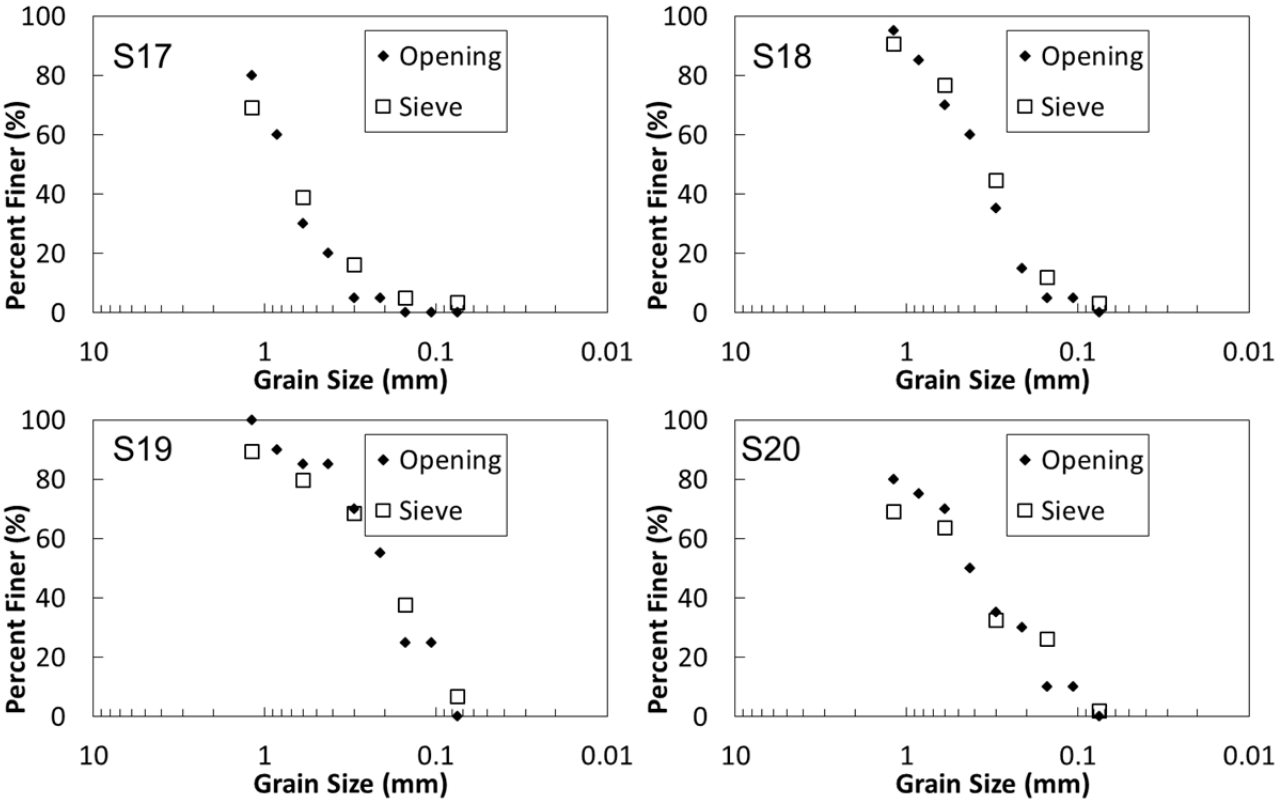

Figure 5.18 (Cont.) Comparison of results from sieve analysis and *PSM* method (S17-S20)

CHAPTER VI

Conclusions

Two tests using image-based methods to determine particle size distribution of soil were developed. Sediment Imaging or Sedimaging test that determines particle size distribution of soil between 0.075 mm and 2 mm utilized a statistical method called wavelet transformation. Translucent Segregation Table or TST test that determines particle size distribution of soil between 2 mm and 35 mm or more utilized a deterministic method called watershed segmentation. Both tests generate particle size distributions of soil that match with sieving results.

For the Sedimaging test, the effects of surface textures on a calibration curve were explored. It was found that internal particle textures may be interpreted as smaller particles thereby causing Sedimaging to underestimate the actual particle sizes. Therefore, development of a soil-specific calibration curves is recommended if Sedimaging is used for quality control purposes for soil particles with erratic internal textures.

A statistical approach which can be used to characterize particle shape and particle orientation or fabric was proposed. An Energy Ratio (F) was defined as the ratio between wavelet decomposition Energies in the horizontal and vertical directions. F values greater than plus 1 are indicative of particles oriented with their long axes horizontally, while F values smaller than minus 1 indicate vertical orientation of axes. The absolute value of F is an indicator

of overall particle sphericity. A deterministic approach utilizing mean-shift clustering was proposed to determine aspect ratios of individual particles. The method requires a first estimate of particle radius that can be obtained by wavelet transformation. Well-segmented particles are still selected manually for computation of the aspect ratios.

For the TST test, over-segmentation from watershed segmentation results was explored. It was found that there is an occasional segmentation problem associated with elongated particles, particularly if they have both convex and concave perimeter segments. This problem has only a small effect on particle size distributions. However, its impact on assessment of particle shapes would be more significant. A method that handles the over-segmentation problem manually was proposed. From the results of watershed segmentation, pairs of over-segmented particles are selected by clicking each object manually. Then, each pair of selected objects is combined to become one particle. Still, an automated image processing method should be developed to identify and correct over-segmentation by watershed segmentation. Bridges used in the TST have two roles: 1) they prevent small particles from hiding beneath large particles and 2) the smallest particle dimension (d_3) can be estimated from the average underpass height of the two bridges between which each particle comes to rest on the TST. The smallest dimension is used to determine the volume-based particle size distribution of a soil. The effects of the minor axis dimension (d_2) and the smallest dimension (d_3) on sieve size (d) were explored. An equation to determine a "d_2 correction factor" based on the ratio between d_2 and d_3 was derived.

For future directions, implementing a higher magnification camera might shift particles between 1 mm and 2 mm in the Sedimaging to the TST. Such a seemingly small decrease in the maximum particle size for Sedimaging would have profound implications to the size and cost of such systems. The presently large Sedimaging system could become a portable device by

reducing the column height by more than 50%. With the higher magnification cameras, single-parameter linear calibration could be developed. The calibration line would be a simple offset from the checkerboard line using a single empirical parameter (*T*). The *T* value would reflect the soil image's texture or type.

Morphological opening could be used to determine particle size distribution from not only uniform particle size images but also non-uniform particle size images. The Peak of Pattern Spectrum (*PPS*) method uses a Structuring Element Size (*SES*) corresponding to the peak of the pattern spectrum of a uniform soil image. A Pattern Spectrum Matching (*PSM*) method uses synthetic pattern spectrums that are created by assuming various combinations of the sieved component soils. A least square method is used to find the one synthetic pattern spectrum that best matches the pattern spectrum of the real soil mixture. It is expected that the *PPS* method can be useful when there is a thin layer in a sedimented soil image that needs to be analyzed while the *PSM* method can be useful to analyze soil mixtures where a Sedimaging device cannot be implemented, such as in the field.

APPENDICES

Appendix A. Software

```
% Sedimaging (SED) Test
% Grain Size Distribution Analysis of Soils
%
% Geotechnical Engineering, Civil and Environmental Engineering
% University of Michigan

clear all;

%% INPUT

prompt={'Enter the Image File Name :  ','Enter the Magnification (pix/mm) :
','Enter the Weight of Canister (W_c) (grams) :  ','Enter the Weight of Dry
Soil and Canister (W_s+c) (grams) :  ','Enter the Weight of Accumulator
filled with Water (W_aw) (grams) :  ','Enter the Weight of: Soil in
Accumulator + Final Water in Accumulator + Empty Accumulator (W_s+wf+a)
(grams):  '};
Ans=inputdlg(prompt,'Input Window');

prompt2={'Enter the Material Name :'};
Ans2=inputdlg(prompt2,'Input Window');

%% LABEL INPUT DATA

I = imread(char(Ans(1)));
Mag = str2double(Ans(2));
W_c = str2double(Ans(3));
W_sc = str2double(Ans(4));
W_aw = str2double(Ans(5));
W_swfa = str2double(Ans(6));

R=dir(char(Ans(1)));
Material = char(Ans2(1));
Date_Tested = R.date;
Tested_By = 'Ohm, H.S.';

%% WEIGHT OF SOIL IN ACCUMULATOR

W_sa = 1.6*(W_swfa - W_aw);
W_s = W_sc - W_c;

if W_sa > W_s
    W_sa = W_s;
end

%% IMAGE CROPPING

I3 = imrotate(I,270,'bilinear');
I2 = imcrop(I3);
Hgt_old = size(I2,1);
Wth_old = size(I2,2);

%% NUMBER OF WINDOWS

n = 8;
```

```
Ver_N = floor((Hgt_old-128)/n)+1;
Hor_N = 10;

Start_Hor = floor((Wth_old - Hor_N * 128)/2);
Hgt_new = 128 + (Ver_N - 1) * n;
Wth_new = 128 * 10;

I3 = I2(Hgt_old - Hgt_new + 1 : Hgt_old , Start_Hor + 1 : Start_Hor +
Wth_new , :);

%% WAVELET ANALYSIS

for i = 1 : Ver_N
    for j = 1 : Hor_N
        I4 = I3(Hgt_new - 127 - n * (i - 1) : Hgt_new - n * (i - 1) , 1 + 128
* (j - 1): 128 + 128 * (j - 1));

[A1 H1 V1 D1]=dwt2(I4,'haar');
[A2 H2 V2 D2]=dwt2(A1,'haar');
[A3 H3 V3 D3]=dwt2(A2,'haar');
[A4 H4 V4 D4]=dwt2(A3,'haar');
[A5 H5 V5 D5]=dwt2(A4,'haar');
[A6 H6 V6 D6]=dwt2(A5,'haar');
[A7 H7 V7 D7]=dwt2(A6,'haar');

E1=H1.^2+V1.^2+D1.^2;
E2=H2.^2+V2.^2+D2.^2;
E3=H3.^2+V3.^2+D3.^2;
E4=H4.^2+V4.^2+D4.^2;
E5=H5.^2+V5.^2+D5.^2;
E6=H6.^2+V6.^2+D6.^2;
E7=H7.^2+V7.^2+D7.^2;

E1=sum(sum(E1));
E2=sum(sum(E2));
E3=sum(sum(E3));
E4=sum(sum(E4));
E5=sum(sum(E5));
E6=sum(sum(E6));
E7=sum(sum(E7));
E=E1+E2+E3+E4+E5+E6+E7;

x=[1:7];
y=[E1/E E2/E E3/E E4/E E5/E E6/E E7/E];
CA(i,j)=dot(x,y);

    end
end

%% CALIBRATION CURVE

PPD = (CA./2.4).^5.1;
Grain_Size = PPD./Mag;
```

```
%% ONE COLUMN GRAIN SIZE

k = 1;

for i = 1: Ver_N
    for j = 1: Hor_N
    Grain_Size_Row(k,1) = Grain_Size(i,j);
    k = k+1;
    end
end

for i = 1:Ver_N
    Locat(i,1) = 64 + 8*(i-1);
end

%% INCREMENT PERCENTAGE

Incre(1) = 8;

for i = 1:15
    Incre(i+1) = Incre(i) - 8/16 + 8/(16-i);
end

Incre_Perc = flipud(Incre'/Hgt_new*100);

for i = 17:Ver_N-16
    Incre_Perc(i) = 8/Hgt_new*100;
end

for i = Ver_N-15:Ver_N
    Incre_Perc(i) = Incre_Perc(Ver_N-i+1);
end

Incre_Perc_Row = Incre_Perc / Hor_N;

for i = 1:Hor_N-1
    Incre_Perc_Row = [Incre_Perc_Row ; Incre_Perc / Hor_N];
end

%% SORTING BY GRAIN SIZE

C = [Grain_Size_Row Incre_Perc_Row];
D = sortrows(C);
E = flipud(D);
Sorted_Grain_Size = E(:,1);
Sorted_Incre_Perc = E(:,2);

%% PASSING PERCENTAGE

for i= 1: Ver_N * Hor_N
    if Sorted_Grain_Size(i,1)>0.075
        Sorted_Grain_Size_Truncated(i,1)=Sorted_Grain_Size(i,1);
        Sorted_Incre_Perc_Truncated(i,1)=Sorted_Incre_Perc(i,1);
```

```
    end
end

Pass_Perc_Truncated(1,1) = 100 - Sorted_Incre_Perc_Truncated(1,1);

for i = 2 : size(Sorted_Incre_Perc_Truncated,1)
    Pass_Perc_Truncated(i,1) = Pass_Perc_Truncated(i-1,1) -
Sorted_Incre_Perc_Truncated(i,1);
end

Sorted_Incre_Perc_Truncated_Added = Sorted_Incre_Perc_Truncated * W_sa / W_s;

Pass_Perc_Truncated_Added(1,1) = 100 - Sorted_Incre_Perc_Truncated_Added(1,1);

for i = 2 : size(Sorted_Incre_Perc_Truncated_Added,1)
    Pass_Perc_Truncated_Added(i,1) = Pass_Perc_Truncated_Added(i-1,1) -
Sorted_Incre_Perc_Truncated_Added(i,1);
end

%% GRAIN SIZE DISTRIBUTION PARAMETERS

if Pass_Perc_Truncated_Added(size(Sorted_Incre_Perc_Truncated_Added,1),1) >
60
    D60 = 0;
    D30 = 0;
    D10 = 0;
    Cu = 0;
    Cg = 0;
else  if  Pass_Perc_Truncated_Added(size(Sorted_Incre_Perc_Truncated_Added,1),1)
> 30
        D30 = 0;
        D10 = 0;
        Cu = 0;
        Cg = 0;
        k = 1;
        for i = 1 : size(Sorted_Incre_Perc_Truncated_Added,1)
            if Pass_Perc_Truncated_Added(i)<=60 &&
Pass_Perc_Truncated_Added(i)>59
                D60(k) = Sorted_Grain_Size_Truncated(i);
                k = k+1;
            end
        end
        D60 = D60(1);
    else if
Pass_Perc_Truncated_Added(size(Sorted_Incre_Perc_Truncated_Added,1),1) > 10
            D10 = 0;
            Cu = 0;
            Cg = 0;
            k = 1;
            m = 1;
            for i = 1 : size(Sorted_Incre_Perc_Truncated_Added,1)
                if Pass_Perc_Truncated_Added(i)<=60 &&
Pass_Perc_Truncated_Added(i)>59
                    D60(k) = Sorted_Grain_Size_Truncated(i);
                    k = k+1;
```

```
                else if Pass_Perc_Truncated_Added(i)<=30 &&
Pass_Perc_Truncated_Added(i)>29
                        D30(m) = Sorted_Grain_Size_Truncated(i);
                        m = m+1;
                    end
                end
            end
            D60 = D60(1);
            D30 = D30(1);
        else
            k = 1;
            m = 1;
            n = 1;
            for i = 1 : size(Sorted_Incre_Perc_Truncated_Added,1)
                if Pass_Perc_Truncated_Added(i)<=60 &&
Pass_Perc_Truncated_Added(i)>59
                    D60(k) = Sorted_Grain_Size_Truncated(i);
                    k = k+1;
                else if Pass_Perc_Truncated_Added(i)<=30 &&
Pass_Perc_Truncated_Added(i)>29
                        D30(m) = Sorted_Grain_Size_Truncated(i);
                        m = m+1;
                    else if Pass_Perc_Truncated_Added(i)<=10 &&
Pass_Perc_Truncated_Added(i)>9
                            D10(n) = Sorted_Grain_Size_Truncated(i);
                            n = n+1;
                        end
                    end
                end
            end
            D60 = D60(1);
            D30 = D30(1);
            D10 = D10(1);
            Cu = D60/D10;
            Cg = (D30)^2/(D10*D60);
        end
    end
end

%% PERCENT FINER BY SIEVE OPENING SIZES

Result_Passing_10 = 100;
Result_Passing_16 = 100;
Result_Passing_20 = 100;
Result_Passing_30 = 100;
Result_Passing_40 = 100;
Result_Passing_50 = 100;
Result_Passing_60 = 100;
Result_Passing_70 = 100;
Result_Passing_80 = 100;
Result_Passing_100 = 100;
Result_Passing_200 = 100;

for i = 1: size(Sorted_Grain_Size_Truncated,1)
    if Sorted_Grain_Size_Truncated(i) >= 2
        Result_Passing_10 = Pass_Perc_Truncated_Added(i);
```

```
    else if Sorted_Grain_Size_Truncated(i) >= 1.19 &&
Sorted_Grain_Size_Truncated(i) < 2
            Result_Passing_16 = Pass_Perc_Truncated_Added(i);

        else if Sorted_Grain_Size_Truncated(i) >= 0.841 &&
Sorted_Grain_Size_Truncated(i) < 1.19
            Result_Passing_20 = Pass_Perc_Truncated_Added(i);

            else if Sorted_Grain_Size_Truncated(i) >= 0.595 &&
Sorted_Grain_Size_Truncated(i) < 0.841
                Result_Passing_30 = Pass_Perc_Truncated_Added(i);

                else if Sorted_Grain_Size_Truncated(i) >= 0.420 &&
Sorted_Grain_Size_Truncated(i) < 0.595
                    Result_Passing_40 = Pass_Perc_Truncated_Added(i);

                    else if Sorted_Grain_Size_Truncated(i) >= 0.297 &&
Sorted_Grain_Size_Truncated(i) < 0.420
                        Result_Passing_50 = Pass_Perc_Truncated_Added(i);

                        else if Sorted_Grain_Size_Truncated(i) >= 0.25 &&
Sorted_Grain_Size_Truncated(i) < 0.297
                            Result_Passing_60 = Pass_Perc_Truncated_Added(i);

                            else if Sorted_Grain_Size_Truncated(i) >= 0.210
&& Sorted_Grain_Size_Truncated(i) < 0.25
                                Result_Passing_70 =
Pass_Perc_Truncated_Added(i);

                                else if Sorted_Grain_Size_Truncated(i) >=
0.177 && Sorted_Grain_Size_Truncated(i) < 0.210
                                    Result_Passing_80 =
Pass_Perc_Truncated_Added(i);

                                    else if Sorted_Grain_Size_Truncated(i) >=
0.149 && Sorted_Grain_Size_Truncated(i) < 0.177
                                        Result_Passing_100 =
Pass_Perc_Truncated_Added(i);

                                        else  if  Sorted_Grain_Size_Truncated(i)
>= 0.074 && Sorted_Grain_Size_Truncated(i) < 0.149
                                            Result_Passing_200 =
Pass_Perc_Truncated_Added(i);
                                            end
                                        end
                                    end
                                end
                            end
                        end
                    end
                end
            end
        end
    end
```

```
end

if min(Sorted_Grain_Size_Truncated) > 0.149 &&
min(Sorted_Grain_Size_Truncated) <= 0.177
    Result_Passing_200 = 0;
else if min(Sorted_Grain_Size_Truncated) > 0.177 &&
min(Sorted_Grain_Size_Truncated) <= 0.210
        Result_Passing_200 = 0;
        Result_Passing_100 = 0;
    else if min(Sorted_Grain_Size_Truncated) > 0.210 &&
min(Sorted_Grain_Size_Truncated) <= 0.25
            Result_Passing_200 = 0;
            Result_Passing_100 = 0;
            Result_Passing_80 = 0;
        else if min(Sorted_Grain_Size_Truncated) > 0.25 &&
min(Sorted_Grain_Size_Truncated) <= 0.297
                Result_Passing_200 = 0;
                Result_Passing_100 = 0;
                Result_Passing_80 = 0;
                Result_Passing_70 = 0;
            else if min(Sorted_Grain_Size_Truncated) > 0.297 &&
min(Sorted_Grain_Size_Truncated) <= 0.420
                    Result_Passing_200 = 0;
                    Result_Passing_100 = 0;
                    Result_Passing_80 = 0;
                    Result_Passing_70 = 0;
                    Result_Passing_60 = 0;
                else if min(Sorted_Grain_Size_Truncated) > 0.420 &&
min(Sorted_Grain_Size_Truncated) <= 0.595
                        Result_Passing_200 = 0;
                        Result_Passing_100 = 0;
                        Result_Passing_80 = 0;
                        Result_Passing_70 = 0;
                        Result_Passing_60 = 0;
                        Result_Passing_50 = 0;
                    else if min(Sorted_Grain_Size_Truncated) > 0.595 &&
min(Sorted_Grain_Size_Truncated) <= 0.841
                            Result_Passing_200 = 0;
                            Result_Passing_100 = 0;
                            Result_Passing_80 = 0;
                            Result_Passing_70 = 0;
                            Result_Passing_60 = 0;
                            Result_Passing_50 = 0;
                            Result_Passing_40 = 0;
                        else if min(Sorted_Grain_Size_Truncated) > 0.841 &&
min(Sorted_Grain_Size_Truncated) <= 1.19
                                Result_Passing_200 = 0;
                                Result_Passing_100 = 0;
                                Result_Passing_80 = 0;
                                Result_Passing_70 = 0;
                                Result_Passing_60 = 0;
                                Result_Passing_50 = 0;
                                Result_Passing_40 = 0;
                                Result_Passing_30 = 0;
                            else if min(Sorted_Grain_Size_Truncated) > 1.19
&& min(Sorted_Grain_Size_Truncated) <= 2
                                    Result_Passing_200 = 0;
```

```
                                    Result_Passing_100 = 0;
                                    Result_Passing_80 = 0;
                                    Result_Passing_70 = 0;
                                    Result_Passing_60 = 0;
                                    Result_Passing_50 = 0;
                                    Result_Passing_40 = 0;
                                    Result_Passing_30 = 0;
                                    Result_Passing_20 = 0;
                                else if min(Sorted_Grain_Size_Truncated) > 2
                                        Result_Passing_200 = 0;
                                    Result_Passing_100 = 0;
                                    Result_Passing_80 = 0;
                                    Result_Passing_70 = 0;
                                    Result_Passing_60 = 0;
                                    Result_Passing_50 = 0;
                                    Result_Passing_40 = 0;
                                    Result_Passing_30 = 0;
                                    Result_Passing_20 = 0;
                                    Result_Passing_16 = 0;
                                    end
                                end
                            end
                        end
                    end
                end
            end
        end
    end
end

Sieve_Size = [2; 1.19; 0.841; 0.595; 0.420; 0.297; 0.25; 0.21; 0.177; 0.149;
0.074];
Result_Passing = [Result_Passing_10; Result_Passing_16; Result_Passing_20;
Result_Passing_30; Result_Passing_40; Result_Passing_50; Result_Passing_60;
Result_Passing_70;  Result_Passing_80;  Result_Passing_100;  Result_Passing_200];

%% OUTPUT

figure(1);
subplot(1,3,1),imshow(I3);

hold on;
mark_color = 'bgrcmykbgrcmykbgrcmykbgrcmyk';
mark_shape = 'ox+*sdv^hox+*sdv^hox+*sdv^ho';

for i = 1 : 1
    for j = 1 : Hor_N
        A = [Hgt_new - 127 - n * (i - 1) Hgt_new - n * (i - 1) Hgt_new - n *
(i - 1) Hgt_new - 127 - n * (i - 1) Hgt_new - 127 - n * (i - 1)];
        B = [1 + 128 * (j - 1) 1 + 128 * (j - 1) 128 + 128 * (j - 1) 128 +
128 * (j - 1) 1 + 128 * (j - 1)];
        plot(B,A,[mark_color(j) '-'],'LineWidth',2);
    end
end

N=floor(Ver_N / 5);
```

```
for i=1:N
    for j=1:Hor_N
        Grain_Size_Red(i,j)=Grain_Size(5*(i-1)+1,j);
        Locat_Red(i)=Locat(5*(i-1)+1);
    end
end

text(1300,Hgt_new/20*1,'SEDIMAGING (SED) TEST','fontsize',15);
text(1300,Hgt_new/20*2,'GEOTECHNICAL ENGINEERING','fontsize',15);
text(1300,Hgt_new/20*3,'UNIVERSITY OF MICHIGAN','fontsize',15);

text(1300,Hgt_new/20*5,['MATERIAL: ',Material],'fontsize',15);
text(1300,Hgt_new/20*6,['DATE TESTED: ',Date_Tested],'fontsize',15);
text(1300,Hgt_new/20*7,['TESTED BY: ',Tested_By],'fontsize',15);

text(1300,Hgt_new/20*10,['D_6_0 (mm): ',sprintf('%1.2f',D60)],'fontsize',15);
text(1300,Hgt_new/20*11,['D_3_0 (mm): ',sprintf('%1.2f',D30)],'fontsize',15);
text(1300,Hgt_new/20*12,['D_1_0 (mm): ',sprintf('%1.2f',D10)],'fontsize',15);
text(1300,Hgt_new/20*13,['C_u: ',sprintf('%1.2f',Cu)],'fontsize',15);
text(1300,Hgt_new/20*14,['C_g: ',sprintf('%1.2f',Cg)],'fontsize',15);
text(1300,Hgt_new/20*15,['PF (%):
',sprintf('%1.1f',abs(Result_Passing_200))],'fontsize',15);

text(1300,Hgt_new/20*17,['MAGNIFICATION (pix/mm):
',sprintf('%2.1f',Mag)],'fontsize',15);
text(1300,Hgt_new/20*18,['IMAGE SIZE (pix): ',num2str(Hgt_new,4),' x
',num2str(Wth_new,4)],'fontsize',15);
text(1300,Hgt_new/20*19,['IMAGE SIZE (mm): ',sprintf('%2.1f',Hgt_new / Mag),'
x ',sprintf('%2.1f',Wth_new / Mag)],'fontsize',15);

subplot(2,2,2),semilogx(Grain_Size_Red(:,1),Locat_Red,'bo','LineWidth',2);
axis([0.05 2.5 0 Hgt_new])
set(gca,'XTick',[0.05,0.06,0.07,0.08,0.09,0.1,0.2,0.3,0.4,0.5,0.6,0.7,0.8,0.9
,1.0,2.0,2.5])
set(gca,'XTickLabel',{'0.05','','','','','0.1','','','','','','','','','1.0',
'','2.5'})
set(gca,'XDir','reverse')
xlabel('GRAIN SIZE (mm)','fontsize',15);
ylabel('ELEVATION (pix)','fontsize',15);
set(gca,'fontsize',15);
hold on;

for i=2:Hor_N
    semilogx(Grain_Size_Red(:,i),Locat_Red,[mark_color(i)
mark_shape(i)],'LineWidth',2);
end

legend('COL1','COL2','COL3','COL4','COL5','COL6','COL7','COL8','COL9','COL10'
,'Location','SouthEast');
grid on;

subplot(2,2,4),semilogx(Sorted_Grain_Size_Truncated,Pass_Perc_Truncated,'b.',
Sorted_Grain_Size_Truncated,Pass_Perc_Truncated_Added,'r.','LineWidth',2);
```

```
axis([0.05 2.5 0 100])
set(gca,'XTick',[0.05,0.06,0.07,0.08,0.09,0.1,0.2,0.3,0.4,0.5,0.6,0.7,0.8,0.9
,1.0,2.0,2.5])
set(gca,'XTickLabel',{'0.05','','','','','0.1','','','','','','','','','1.0',
'','2.5'})
set(gca,'XDir','reverse')
xlabel('GRAIN SIZE (mm)','fontsize',15);
ylabel('PERCENT FINER (%)','fontsize',15);
set(gca,'fontsize',15);

legend('GSD in ACCUMULATOR','GSD w/ P%F ADDED','Location','NorthEast');
grid on;

fig1 = figure(1);
set (fig1, 'Units', 'normalized', 'Position', [0,0,1,1]);
```

```
% Translucent Segregation Table (TST) Test
% Grain Size Distribution Analysis of Soils
%
% Geotechnical Engineering, Civil and Environmental Engineering
% University of Michigan

clear all;

%% INPUT

prompt={'Enter the 1st Image File Name (xxx.jpg):','Enter the 2nd Image File
Name (xxx.jpg):','Enter the 1st Watershed Image File Name (xxx.jpg):','Enter
the 2nd Watershed Image File Name (xxx.jpg):','Enter the Magnification
(pix/mm) :'};
Ans=inputdlg(prompt,'Input Window');

prompt2={'Enter the the 1st Dividing Point (pixel):','Enter the the 2nd
Dividing Point (pixel):','Enter the the 3rd Dividing Point (pixel):','Enter
the the 4th Dividing Point (pixel):','Enter the the 5th Dividing Point
(pixel):'};
Ans2=inputdlg(prompt2,'Dividing Points of 1st Image');

prompt3={'Enter the the 1st Dividing Point (pixel):','Enter the the 2nd
Dividing Point (pixel):','Enter the the 3rd Dividing Point (pixel):','Enter
the the 4th Dividing Point (pixel):','Enter the the 5th Dividing Point
(pixel):'};
Ans3=inputdlg(prompt3,'Dividing Points of 2nd Image');

prompt4={'Enter the Material Name :'};
Ans4=inputdlg(prompt4,'Input Window');

%% LABEL INPUT DATA

I = imread(char(Ans(1)));
I1 = imread(char(Ans(3)));
I2 = im2bw(I1);
I3 = ~I2;
I4 = bwlabel(I3,4);

I_1 = imread(char(Ans(2)));
I1_1 = imread(char(Ans(4)));
I2_1 = im2bw(I1_1);
I3_1 = ~I2_1;
I4_1 = bwlabel(I3_1,4);

I5 = imrotate(I,90);
I6 = imrotate(I_1,90);
I7=[I5;I6];
Mag = str2double(Ans(5));
Hgt_new1 = size(I7,1);
Wth_new1 = size(I7,2);

Material = char(Ans4(1));
R=dir(char(Ans(1)));
Date_Tested = R.date;
```

```
Tested_By = 'Ohm, H.S.';

%% BRIDGE HEIGHTS

e1 = str2double(Ans2(1));
e2 = str2double(Ans2(2));
e3 = str2double(Ans2(3));
e4 = str2double(Ans2(4));
e5 = str2double(Ans2(5));

f1 = str2double(Ans3(1));
f2 = str2double(Ans3(2));
f3 = str2double(Ans3(3));
f4 = str2double(Ans3(4));
f5 = str2double(Ans3(5));

g1 = 25.0;
g2 = 19.0;
g3 = 12.5;
g4 = 9.5;
g5 = 4.75;
g6 = 2.36;

%% DIVIDING IMAGES BY BRIDGES

P1 = I4(1:e1,:);
P2 = I4(e1+1:e2,:);
P3 = I4(e2+1:e3,:);
P4 = I4(e3+1:e4,:);
P5 = I4(e4+1:e5,:);
P6 = I4(e5+1:size(I4,1),:);

O1 = I4_1(1:f1,:);
O2 = I4_1(f1+1:f2,:);
O3 = I4_1(f2+1:f3,:);
O4 = I4_1(f3+1:f4,:);
O5 = I4_1(f4+1:f5,:);
O6 = I4_1(f5+1:size(I4_1,1),:);

%% CLOSING

se = strel('disk',1);

P1_1 = imclose(P1,se);
P2_1 = imclose(P2,se);
P3_1 = imclose(P3,se);
P4_1 = imclose(P4,se);
P5_1 = imclose(P5,se);
P6_1 = imclose(P6,se);

O1_1 = imclose(O1,se);
O2_1 = imclose(O2,se);
O3_1 = imclose(O3,se);
O4_1 = imclose(O4,se);
O5_1 = imclose(O5,se);
```

```
O6_1 = imclose(O6,se);

P=[P1_1;P2_1;P3_1;P4_1;P5_1;P6_1];
O=[O1_1;O2_1;O3_1;O4_1;O5_1;O6_1];

%% MAJOR AXIS AND MINOR AXIS

stats4 = regionprops(P1_1, 'MinorAxisLength');
Minor_Axis1 = [stats4.MinorAxisLength]';
stats4 = regionprops(P2_1, 'MinorAxisLength');
Minor_Axis2 = [stats4.MinorAxisLength]';
stats4 = regionprops(P3_1, 'MinorAxisLength');
Minor_Axis3 = [stats4.MinorAxisLength]';
stats4 = regionprops(P4_1, 'MinorAxisLength');
Minor_Axis4 = [stats4.MinorAxisLength]';
stats4 = regionprops(P5_1, 'MinorAxisLength');
Minor_Axis5 = [stats4.MinorAxisLength]';
stats4 = regionprops(P6_1, 'MinorAxisLength');
Minor_Axis6 = [stats4.MinorAxisLength]';

stats4 = regionprops(O1_1, 'MinorAxisLength');
Minor_Axis1_1 = [stats4.MinorAxisLength]';
stats4 = regionprops(O2_1, 'MinorAxisLength');
Minor_Axis2_1 = [stats4.MinorAxisLength]';
stats4 = regionprops(O3_1, 'MinorAxisLength');
Minor_Axis3_1 = [stats4.MinorAxisLength]';
stats4 = regionprops(O4_1, 'MinorAxisLength');
Minor_Axis4_1 = [stats4.MinorAxisLength]';
stats4 = regionprops(O5_1, 'MinorAxisLength');
Minor_Axis5_1 = [stats4.MinorAxisLength]';
stats4 = regionprops(O6_1, 'MinorAxisLength');
Minor_Axis6_1 = [stats4.MinorAxisLength]';

stats3 = regionprops(P, 'MajorAxisLength');
stats4 = regionprops(P, 'MinorAxisLength');
Major_Axis = [stats3.MajorAxisLength]';
Minor_Axis = [stats4.MinorAxisLength]';

stats3 = regionprops(O, 'MajorAxisLength');
stats4 = regionprops(O, 'MinorAxisLength');
Major_Axis_1 = [stats3.MajorAxisLength]';
Minor_Axis_1 = [stats4.MinorAxisLength]';

X1=[size(Minor_Axis1,1),size(Minor_Axis2,1),size(Minor_Axis3,1),size(Minor_Ax
is4,1),size(Minor_Axis5,1),size(Minor_Axis6,1)];
X2=max(X1)+1;

X1_1=[size(Minor_Axis1_1,1),size(Minor_Axis2_1,1),size(Minor_Axis3_1,1),size(
Minor_Axis4_1,1),size(Minor_Axis5_1,1),size(Minor_Axis6_1,1)];
X2_1=max(X1_1)+1;

Minor_Axis1(X2,1)=0;
Minor_Axis2(X2,1)=0;
Minor_Axis3(X2,1)=0;
Minor_Axis4(X2,1)=0;
```

```
Minor_Axis5(X2,1)=0;
Minor_Axis6(X2,1)=0;

Minor_Axis1_1(X2_1,1)=0;
Minor_Axis2_1(X2_1,1)=0;
Minor_Axis3_1(X2_1,1)=0;
Minor_Axis4_1(X2_1,1)=0;
Minor_Axis5_1(X2_1,1)=0;
Minor_Axis6_1(X2_1,1)=0;

%% ASSIGNING THICKNESS

T1=Minor_Axis1;
for i=1:size(Minor_Axis1,1)
    if Minor_Axis1(i)>0
        T1(i)=(g1+g2)/2*Mag;
    end
end

T2=Minor_Axis2;
for i=1:size(Minor_Axis2,1)
    if Minor_Axis2(i)>0
        T2(i)=(g2+g3)/2*Mag;
    end
end

T3=Minor_Axis3;
for i=1:size(Minor_Axis3,1)
    if Minor_Axis3(i)>0
        T3(i)=(g3+g4)/2*Mag;
    end
end

T4=Minor_Axis4;
for i=1:size(Minor_Axis4,1)
    if Minor_Axis4(i)>0
        T4(i)=(g4+g5)/2*Mag;
    end
end

T5=Minor_Axis5;
for i=1:size(Minor_Axis5,1)
    if Minor_Axis5(i)>0
        T5(i)=(g5+g6)/2*Mag;
    end
end

T6=Minor_Axis6;
for i=1:size(Minor_Axis6,1)
    if Minor_Axis6(i)>0
        T6(i)=(g6+2)/2*Mag;
    end
end

T1_1=Minor_Axis1_1;
```

```
for i=1:size(Minor_Axis1_1,1)
    if Minor_Axis1_1(i)>0
        T1_1(i)=(g1+g2)/2*Mag;
    end
end

T2_1=Minor_Axis2_1;
for i=1:size(Minor_Axis2_1,1)
    if Minor_Axis2_1(i)>0
        T2_1(i)=(g2+g3)/2*Mag;
    end
end

T3_1=Minor_Axis3_1;
for i=1:size(Minor_Axis3_1,1)
    if Minor_Axis3_1(i)>0
        T3_1(i)=(g3+g4)/2*Mag;
    end
end

T4_1=Minor_Axis4_1;
for i=1:size(Minor_Axis4_1,1)
    if Minor_Axis4_1(i)>0
        T4_1(i)=(g4+g5)/2*Mag;
    end
end

T5_1=Minor_Axis5_1;
for i=1:size(Minor_Axis5_1,1)
    if Minor_Axis5_1(i)>0
        T5_1(i)=(g5+g6)/2*Mag;
    end
end

T6_1=Minor_Axis6_1;
for i=1:size(Minor_Axis6_1,1)
    if Minor_Axis6_1(i)>0
        T6_1(i)=(g6+2)/2*Mag;
    end
end

T1a = [T1';T2';T3';T4';T5';T6'];
T2a = [T1_1';T2_1';T3_1';T4_1';T5_1';T6_1'];

Thickness_T1 = max(T1a)';
Thickness_T2 = max(T2a)';
Thickness = [Thickness_T1(1:size(Thickness_T1,1)-
1);Thickness_T2(1:size(Thickness_T2,1)-1)];

Minor = [Minor_Axis;Minor_Axis_1];
Major = [Major_Axis;Major_Axis_1];

%% CORRECTION FACTOR

F=(Minor ./ Thickness).^2;
```

```
F1=(Thickness ./ Minor).^2;

for i=1:size(Minor,1)
    if F(i)>=1
         Correction(i)=sqrt((F(i)+1)./(2*F(i)));
    else Correction(i)=sqrt((F1(i)+1)./(2*F1(i)));
    end
end

Correction=Correction';

%% INCREMENT PERCENTAGE

Vol=Major.*Minor.*Thickness;
Total_Vol = sum(Vol);
Percent_Vol = Vol / Total_Vol * 100;

%% CORRECTED GRAIN SIZE AND ASPECT RATIO

Grain_Size = Minor .* Correction / Mag ;
Aspect_Ratio = Major ./ Minor;

%% SORTING BY GRAIN SIZE

A2 = [Grain_Size Percent_Vol Aspect_Ratio Correction];
B2 = sortrows(A2);
C2 = flipud(B2);

Sorted_Grain_Size = C2(:,1);
Sorted_Incre_Perc = C2(:,2);
Sorted_Aspect_Ratio = C2(:,3);
Sorted_Correction = C2(:,4);

%% PASSING PERCENTAGE

Pass_Perc(1,1) = 100 - Sorted_Incre_Perc(1,1);
for i = 2 : size (Sorted_Grain_Size,1)
    Pass_Perc(i,1) = Pass_Perc(i-1,1) - Sorted_Incre_Perc(i,1);
end

%% OUTPUT

figure(1),subplot(1,3,1),imshow(I7);

text(3300,Hgt_new1/20*1,'TRANSLUCENT SEGREGATION TABLE (TST)','fontsize',15);
text(3300,Hgt_new1/20*2,'GEOTECHNICAL ENGINEERING','fontsize',15);
text(3300,Hgt_new1/20*3,'UNIVERSITY OF MICHIGAN','fontsize',15);

text(3300,Hgt_new1/20*5,['MATERIAL: ',Material],'fontsize',15);
text(3300,Hgt_new1/20*6,['DATE TESTED: ',Date_Tested],'fontsize',15);
text(3300,Hgt_new1/20*7,['TESTED BY: ',Tested_By],'fontsize',15);

text(3300,Hgt_new1/20*17,['MAGNIFICATION (pix/mm):
',sprintf('%2.1f',Mag)],'fontsize',15);
```

```
text(3300,Hgt_new1/20*18,['IMAGE SIZE (pix): ',num2str(Hgt_new1,4),' x
',num2str(Wth_new1,4)],'fontsize',15);
text(3300,Hgt_new1/20*19,['IMAGE SIZE (mm): ',sprintf('%2.1f',Hgt_new1 /
Mag),' x ',sprintf('%2.1f',Wth_new1 / Mag)],'fontsize',15);

subplot(2,2,2),semilogx(Sorted_Grain_Size,Sorted_Aspect_Ratio,'r.','LineWidth
',2);

axis([1 40 1 5])
set(gca,'XTick',[1,2,3,4,5,6,7,8,9,10,20,30,40])
set(gca,'XTickLabel',{'1','2','','','','','','','','10','20','30','40'})
set(gca,'XDir','reverse')

set(gca,'YTick',[1,2,3,4,5])
xlabel('GRAIN SIZE (mm)','fontsize',15);
ylabel('ASPECT RATIO','fontsize',15);

set(gca,'fontsize',15);
grid on;

subplot(2,2,4),semilogx(Sorted_Grain_Size,Pass_Perc,'r.','LineWidth',2);
axis([1 40 0 100])
set(gca,'XTick',[1,2,3,4,5,6,7,8,9,10,20,30,40])
set(gca,'XTickLabel',{'1','2','','','','','','','','10','20','30','40'})
set(gca,'XDir','reverse')
xlabel('GRAIN SIZE (mm)','fontsize',15);
ylabel('PERCENT FINER (%)','fontsize',15);

set(gca,'fontsize',15);

grid on;

fig1 = figure(1);
set (fig1, 'Units', 'Normalized', 'Position', [0,0,1,1]);
```

Appendix B. Design Drawings

Sedimentation Column
(Aluminum, Qty: 1)

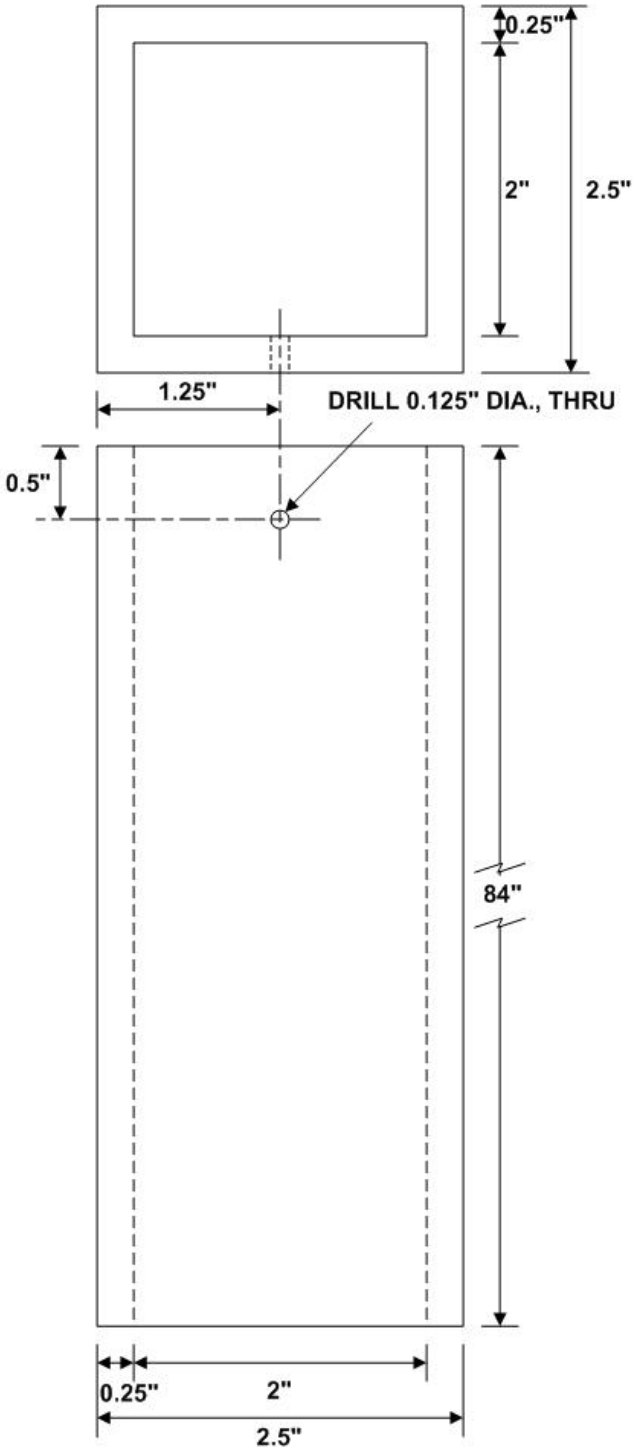

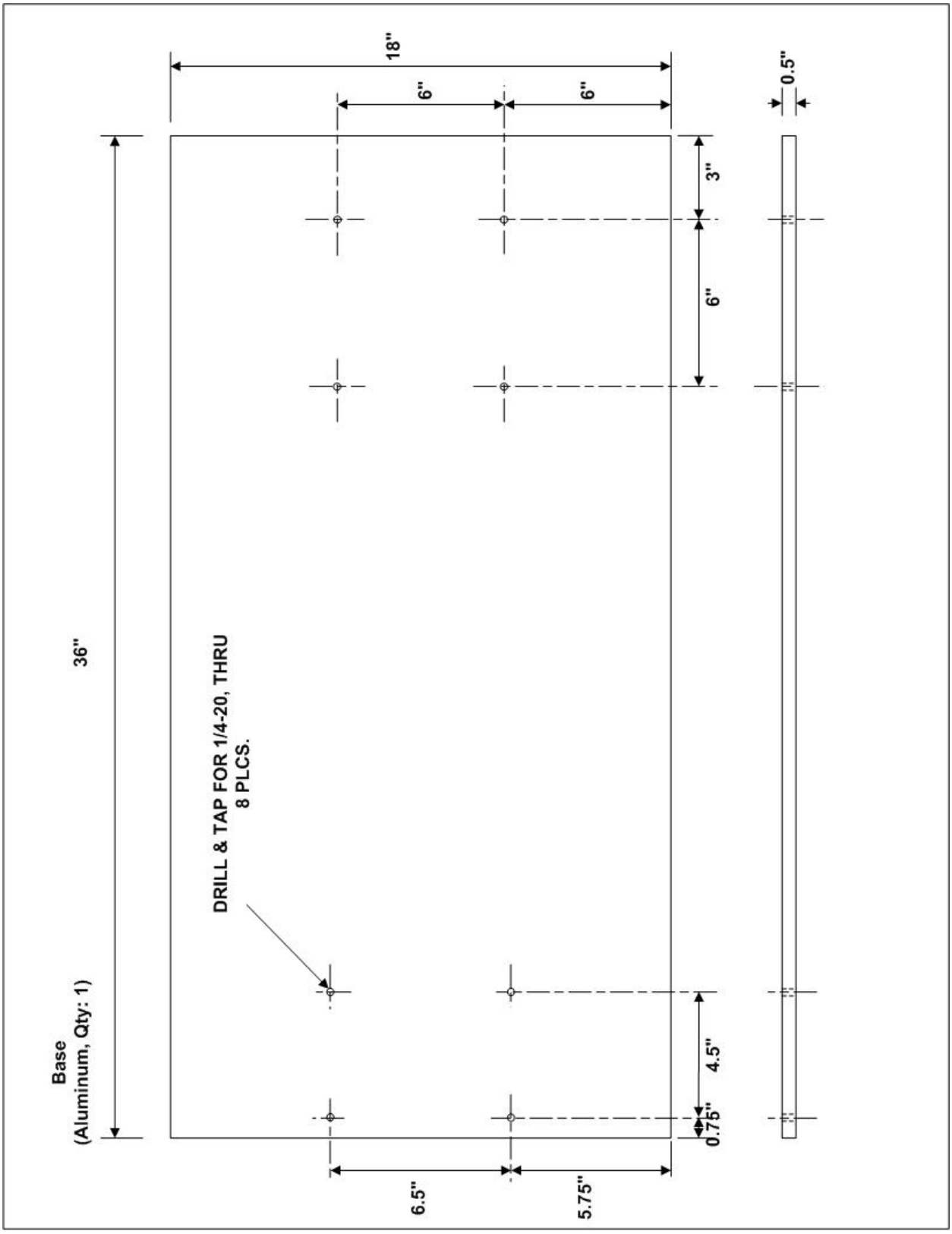
18"
6"
6"
0.5"
3"
6"
36"
DRILL & TAP FOR 1/4-20, THRU
8 PLCS.
Base
(Aluminum, Qty: 1)
4.5"
0.75"
6.5"
5.75"

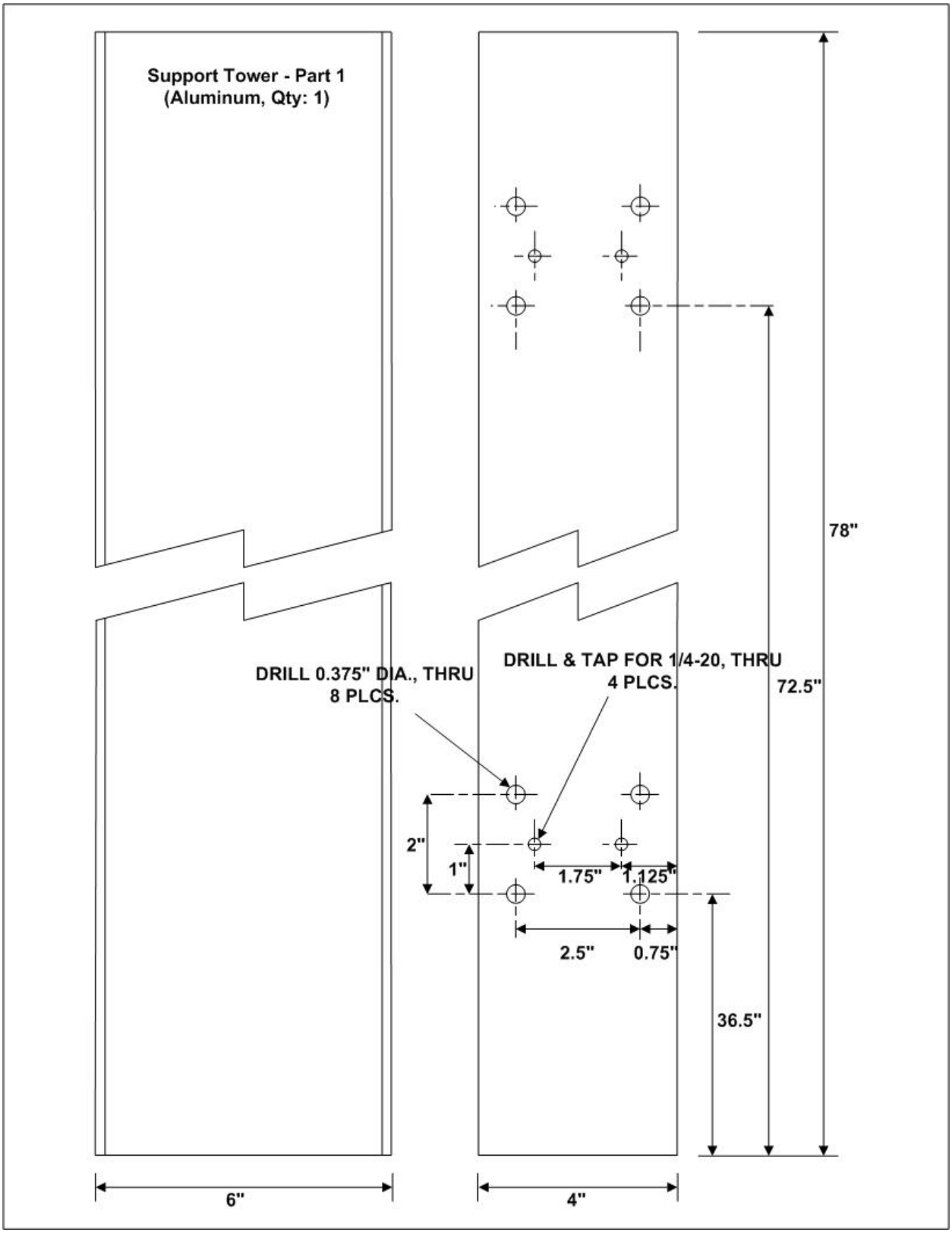
Support Tower - Part 1
(Aluminum, Qty: 1)
78"
72.5"
DRILL 0.375" DIA., THRU
8 PLCS.
DRILL & TAP FOR 1/4-20, THRU
4 PLCS.
2"
1"
1.75"
1.125"
2.5"
0.75"
36.5"
6"
4"

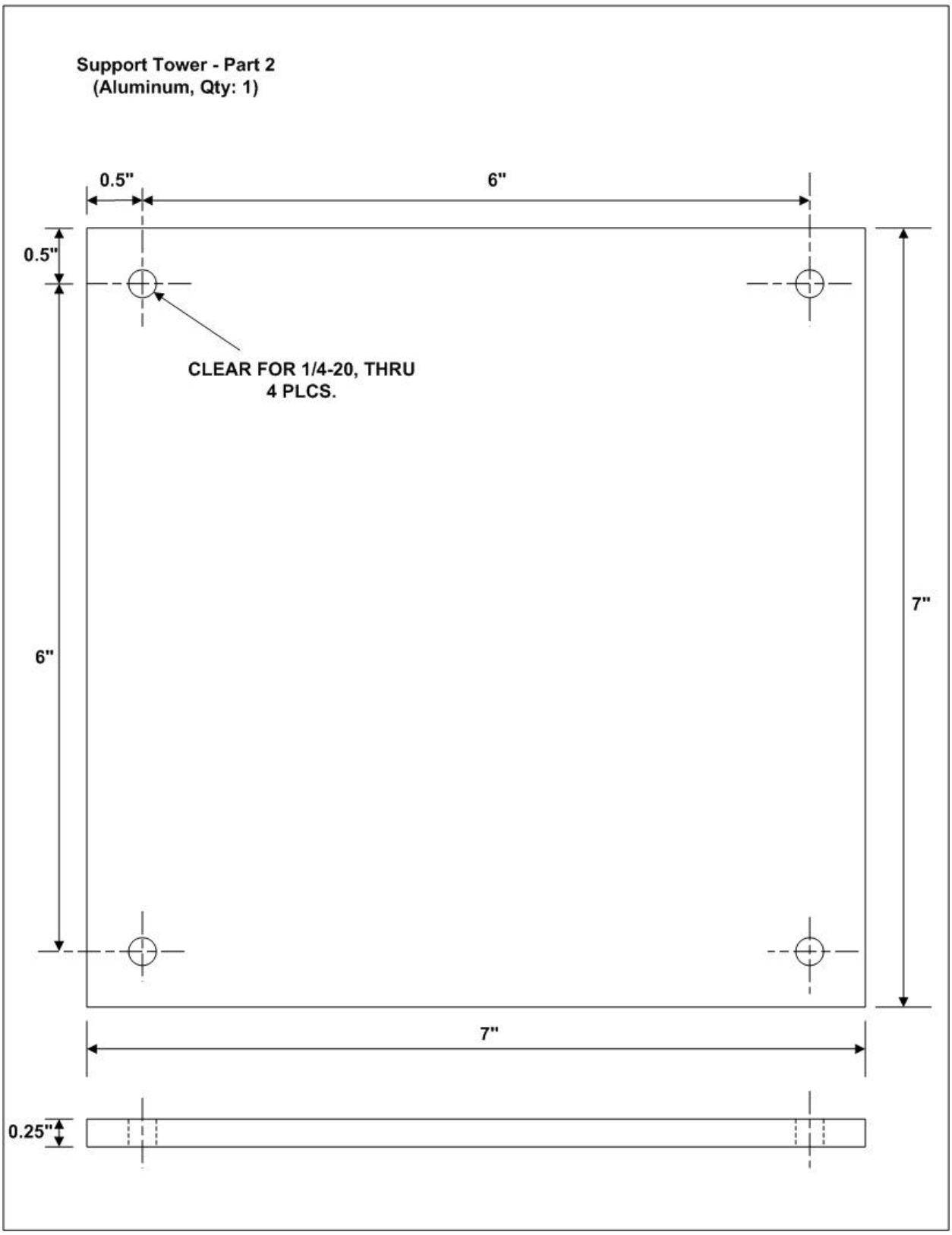
Support Tower - Part 2
(Aluminum, Qty: 1)
0.5"
6"
0.5"
CLEAR FOR 1/4-20, THRU
4 PLCS.
6"
7"
7"
0.25"

Support Tower –
Weldment Drawing
(Aluminum, Qty: 1)

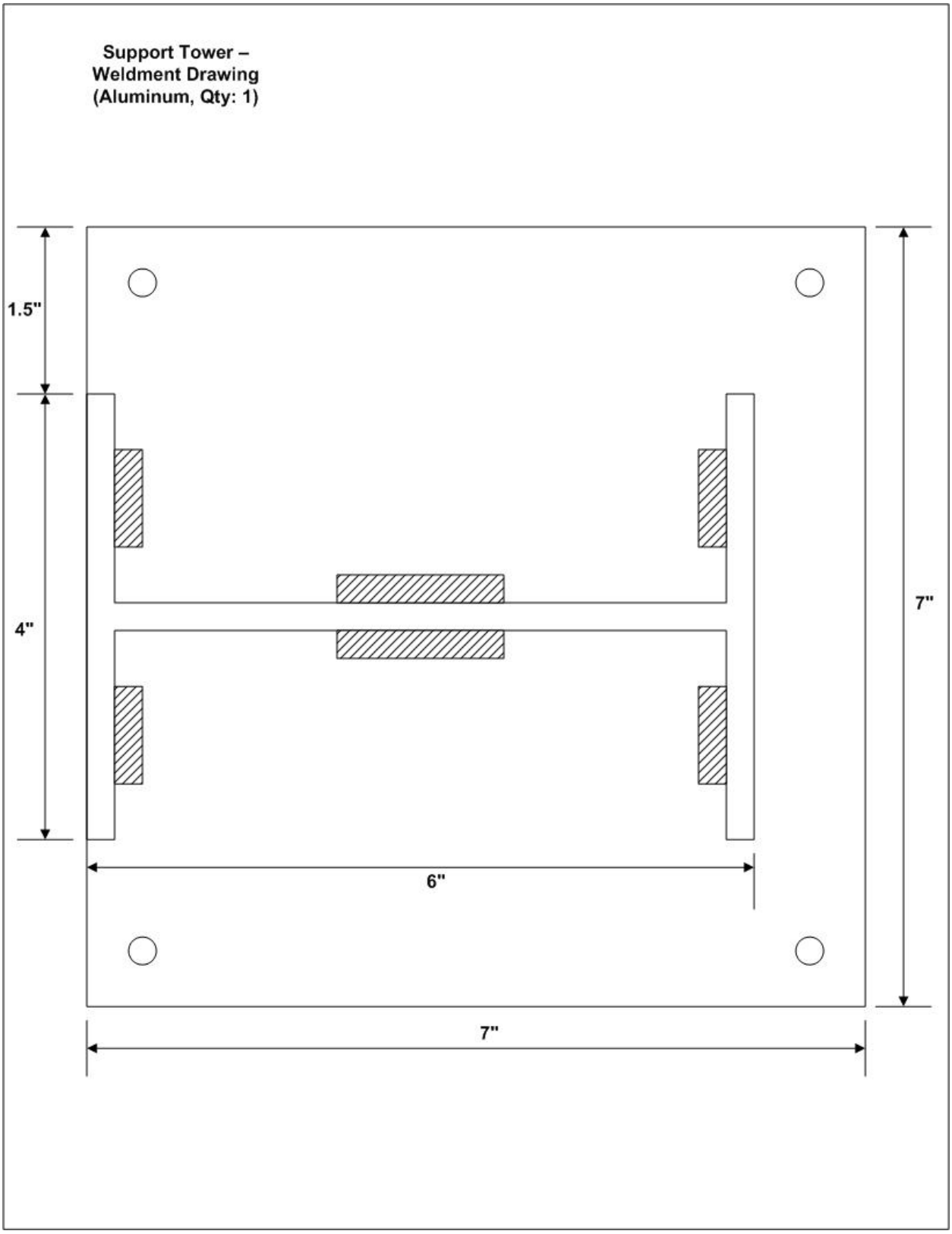

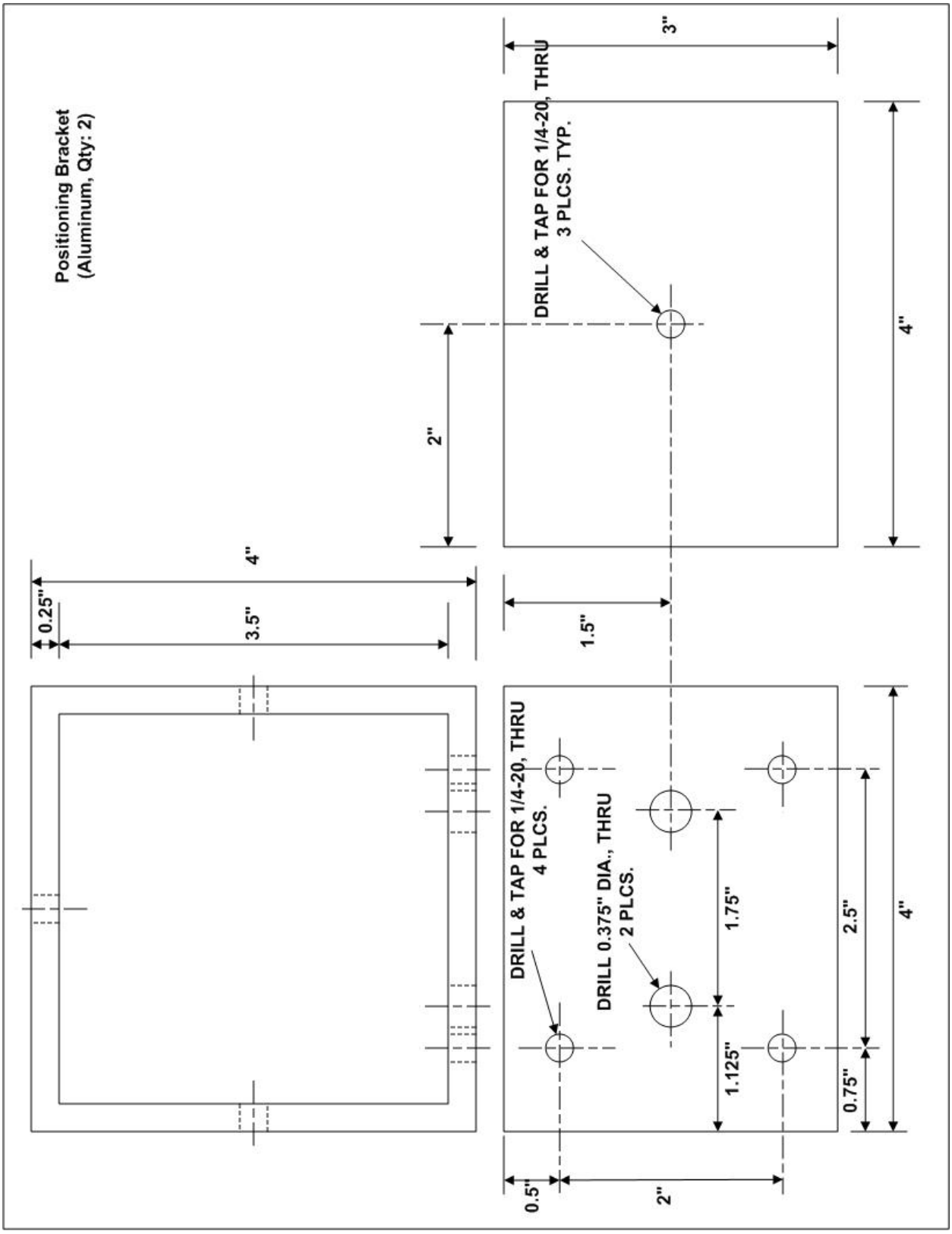
Positioning Bracket
(Aluminum, Qty: 2)
3"
DRILL & TAP FOR 1/4-20, THRU
3 PLCS. TYP.
4"
2"
4"
0.25"
3.5"
1.5"
DRILL & TAP FOR 1/4-20, THRU
4 PLCS.
DRILL 0.375" DIA., THRU
2 PLCS.
1.75"
2.5"
4"
1.125"
0.75"
0.5"
2"

Pre-Segregation Tube
(Acrylic, Qty: 1)

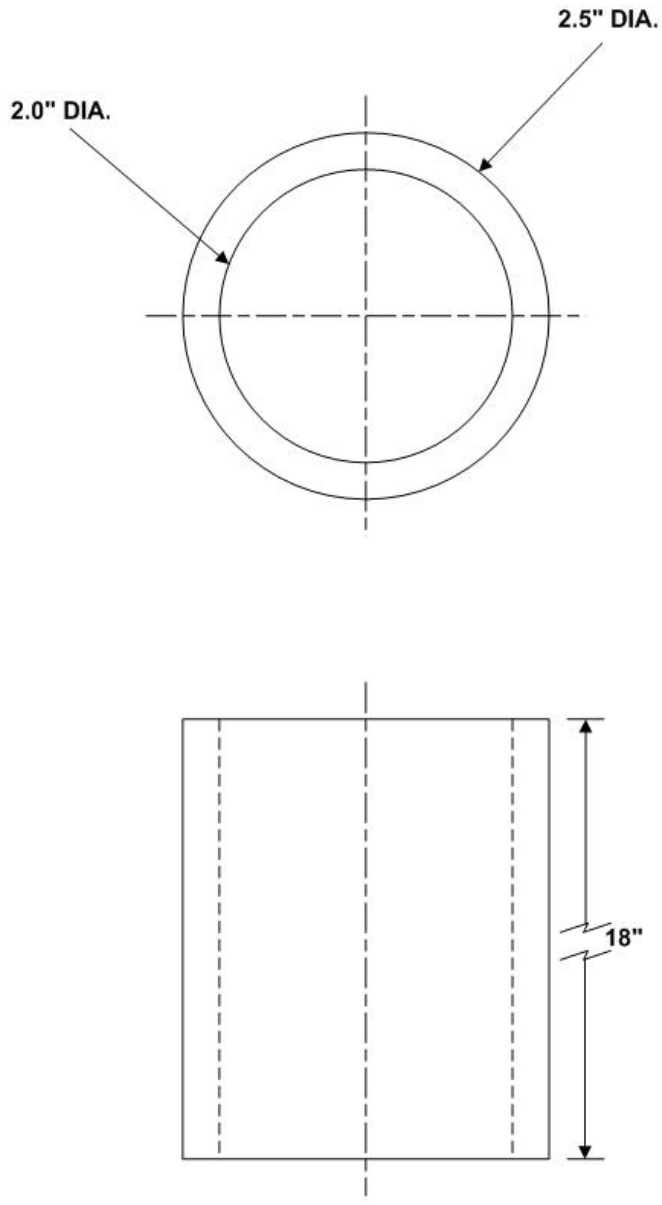

Vacuum Vent
(Acrylic, Qty: 1)

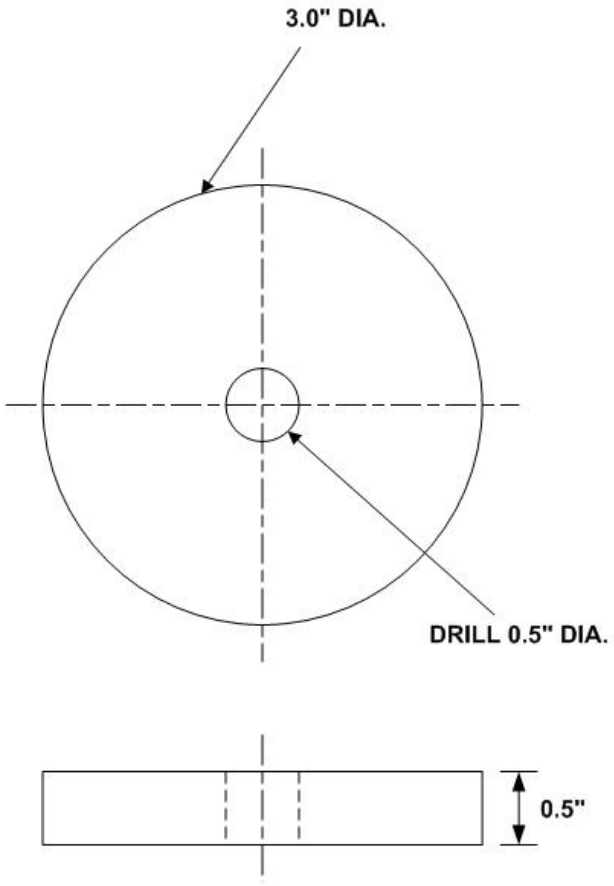

Pre-Segregation Tube
Adaptor - Part 1
(Acrylic, Qty: 1, Assembly View)

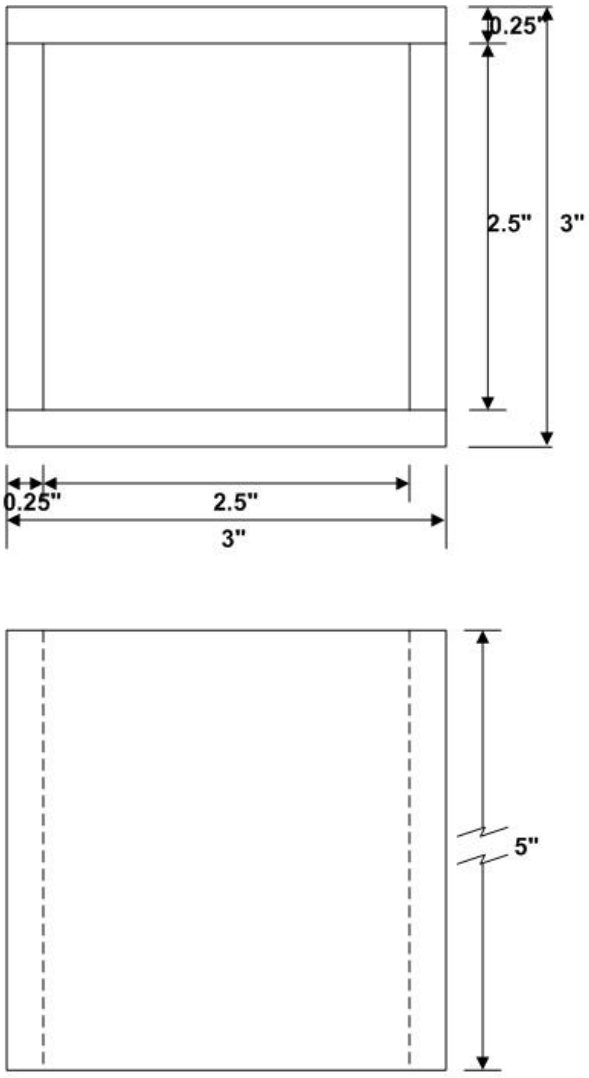

Pre-Segregation Tube
Adaptor - Part 2
(Acrylic, Qty: 1)

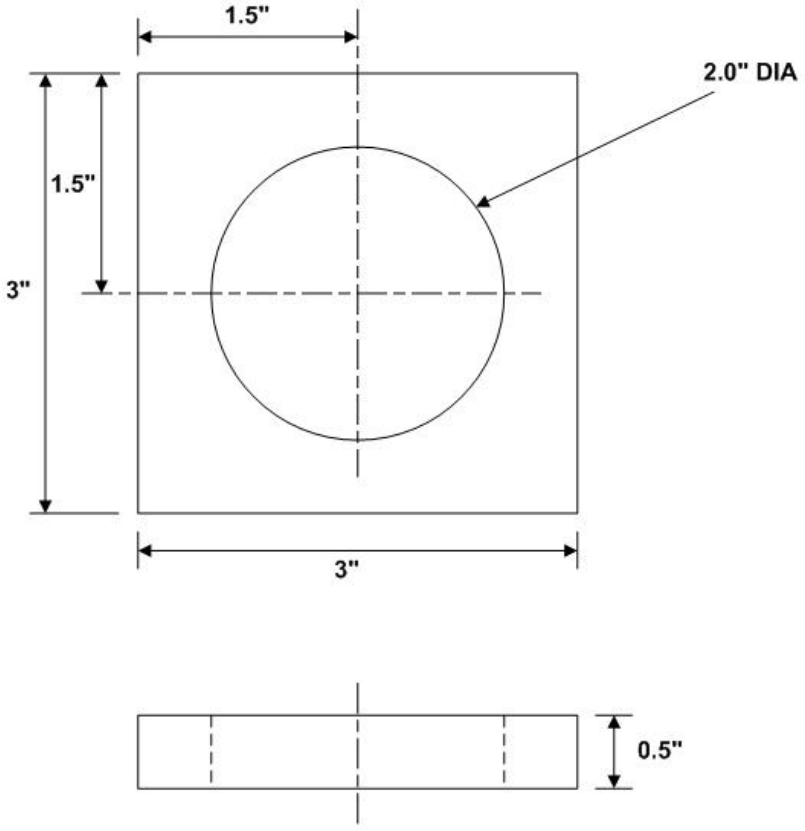

Pre-Segregation Tube
Adaptor - Part 3
(Acrylic, Qty: 1)

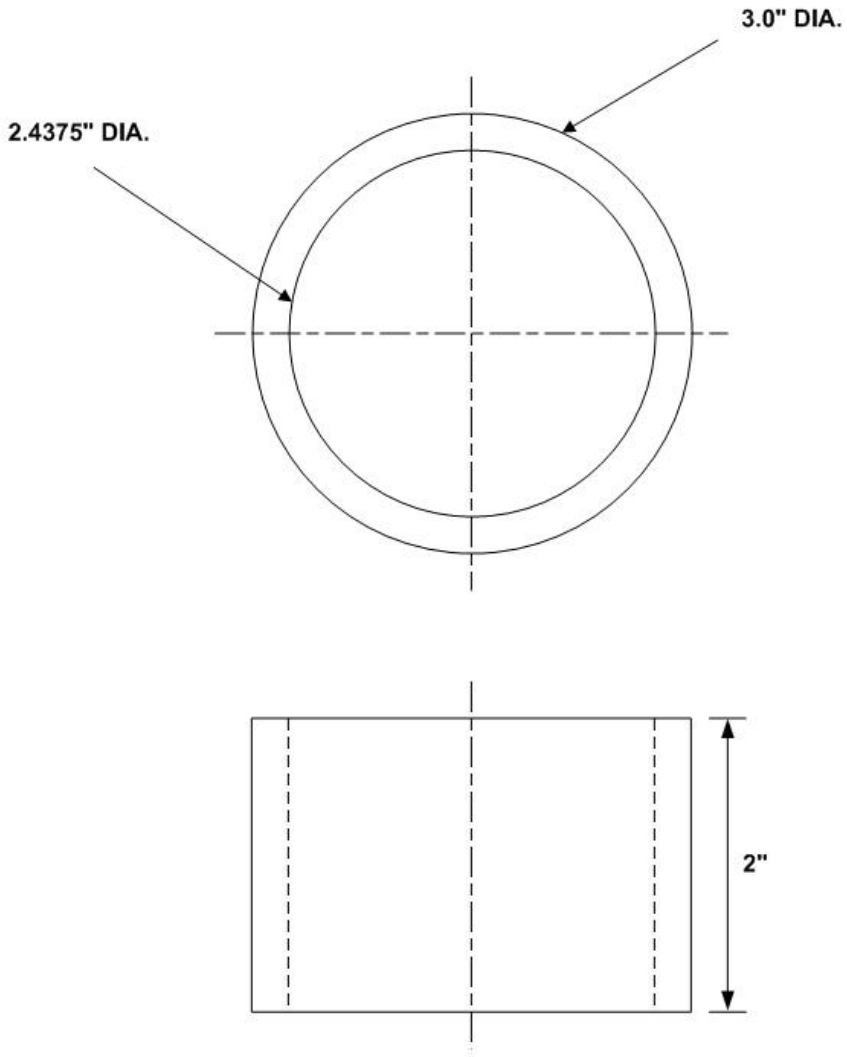

Connector - Part 1
(Aluminum, Qty: 1)

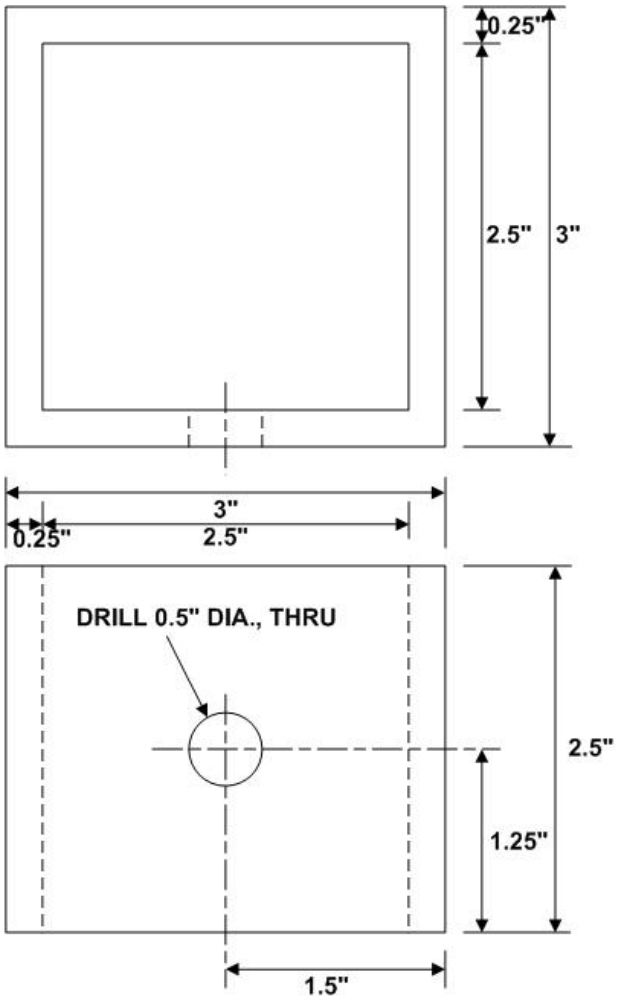

Connector - Part 2
(Aluminum, Qty: 1)

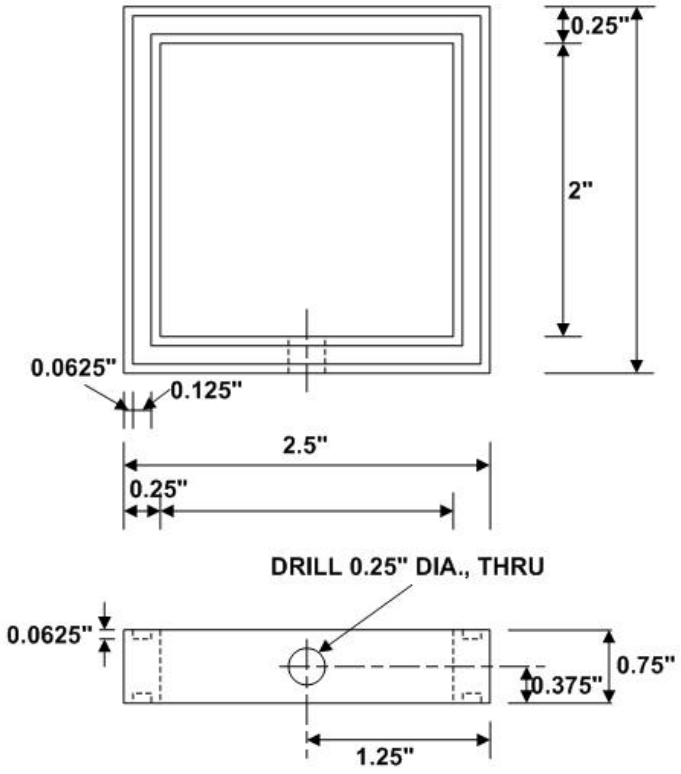

Drainage
(Aluminum, Qty: 1)

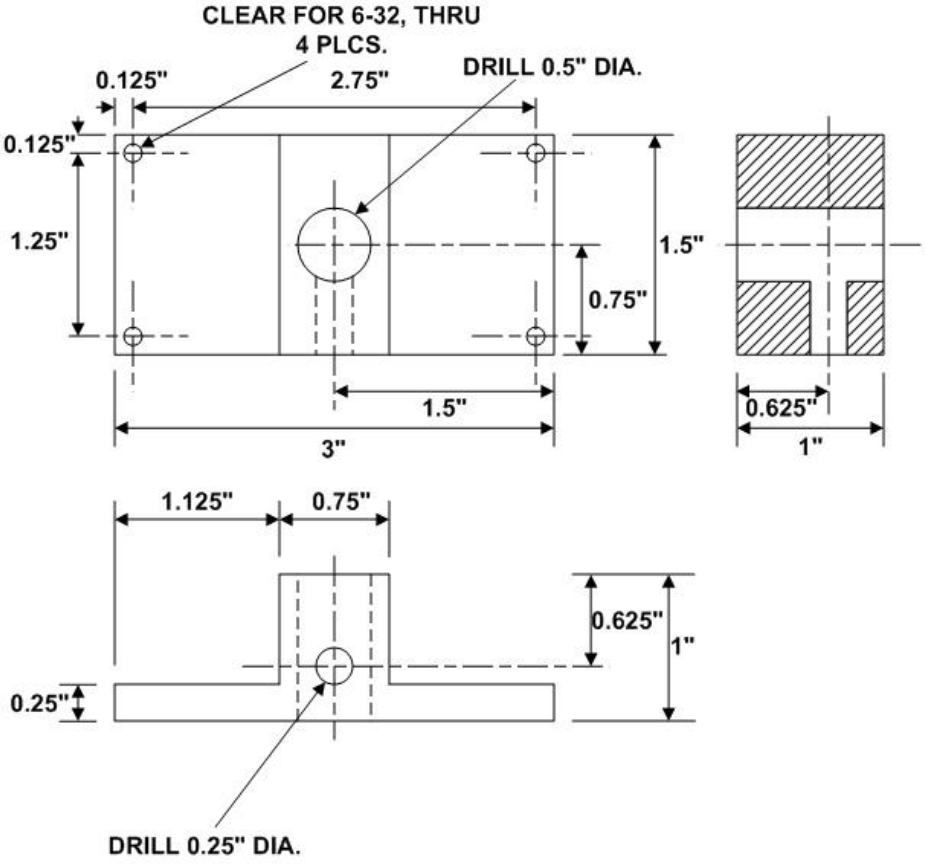

Drainage Valve
(Stainless Steel, Qty: 1)

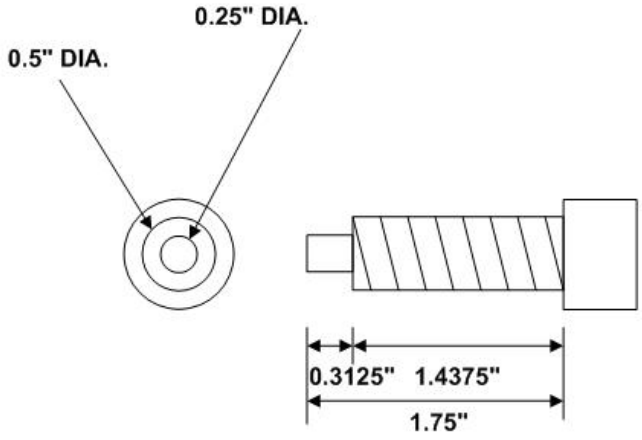

Sediment Cartridge -
Part 1
(Aluminum, Qty: 1)

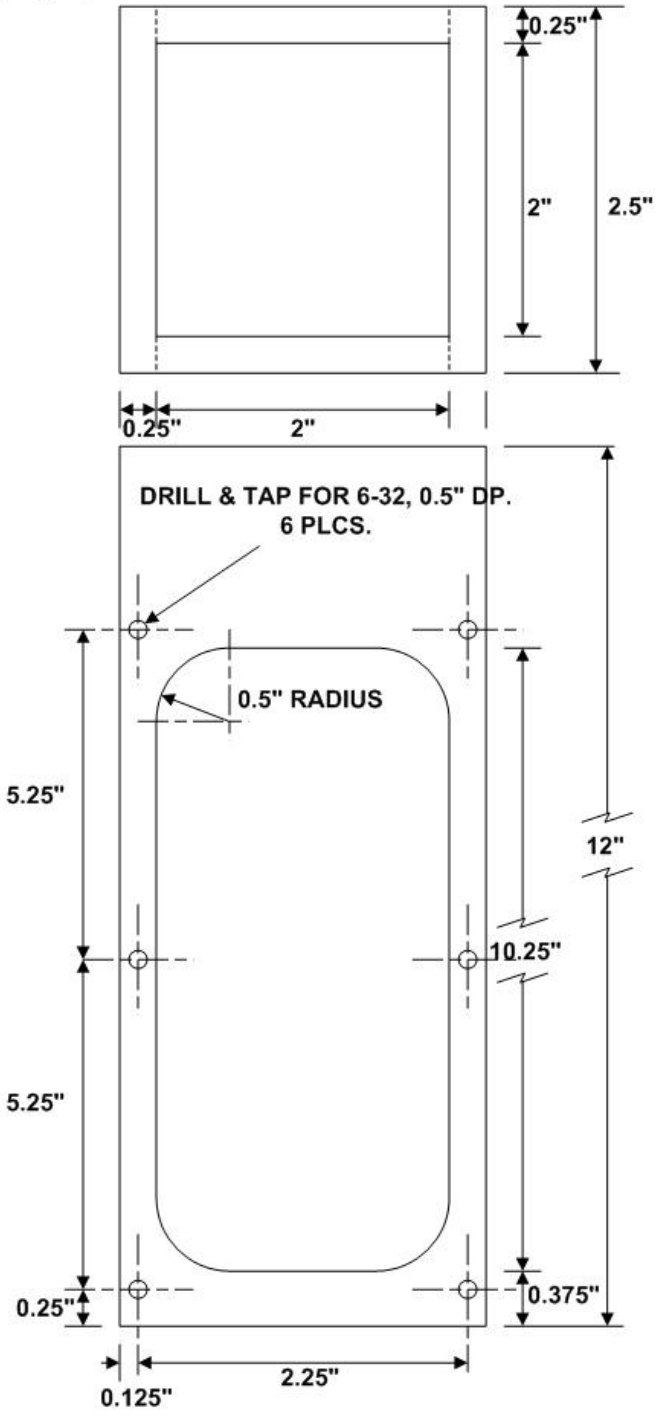

Sediment Cartridge -
Part 2
(Aluminum, Qty: 2)

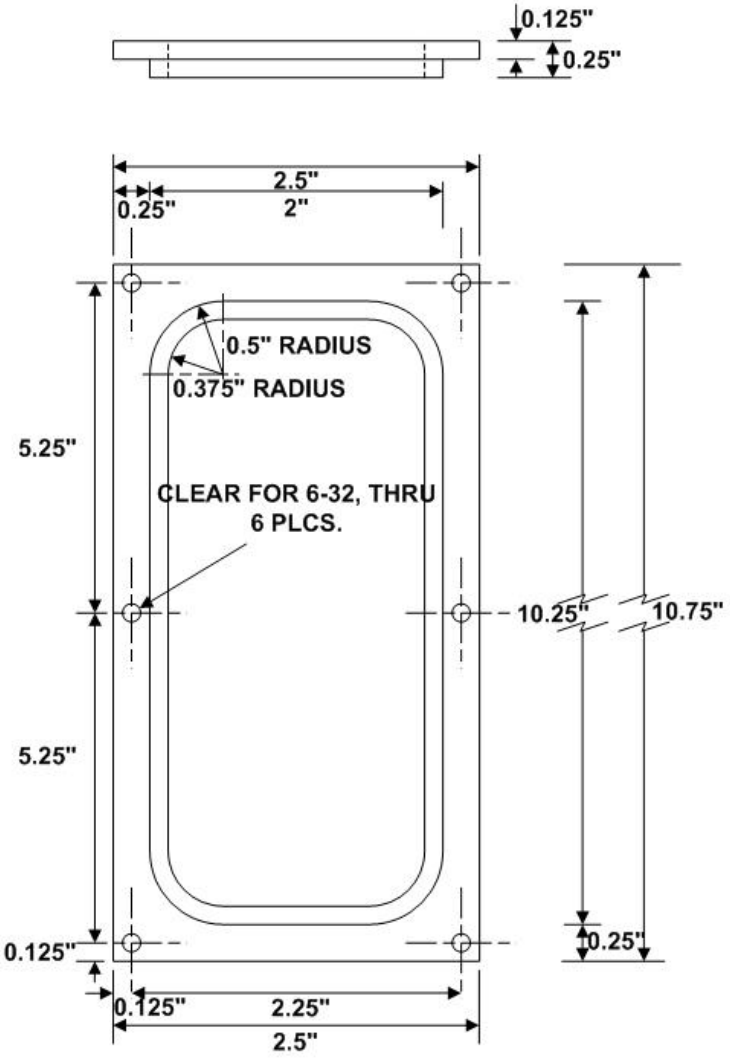

Cartridge Pedestal
(Aluminum, Qty: 1)

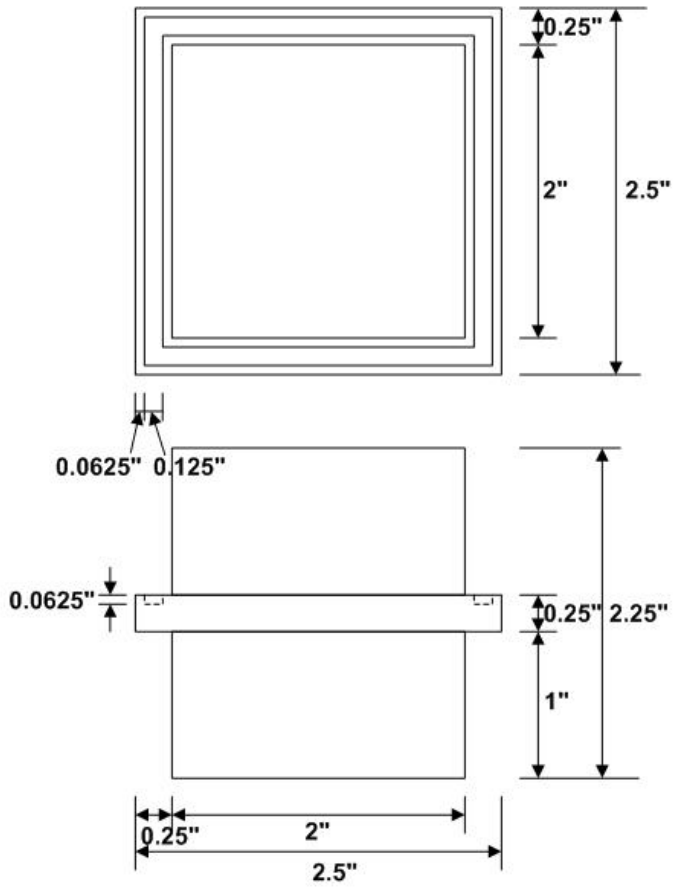

Cartridge Support
(Aluminum, Qty: 1)

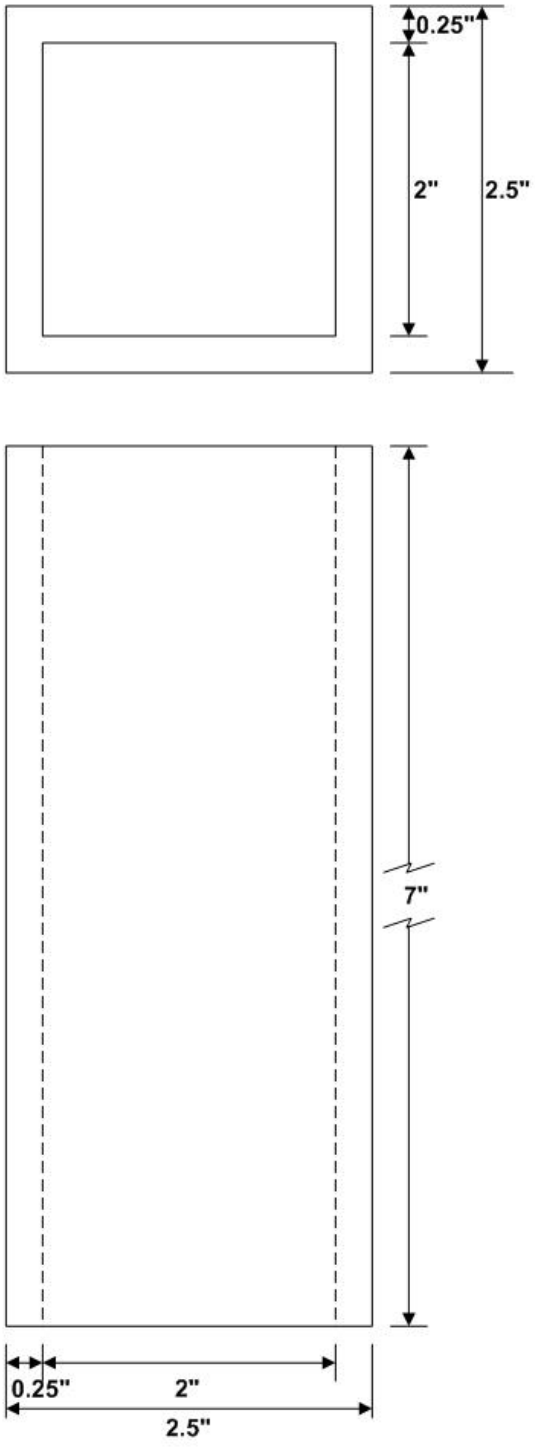

Window
(Borosilicate, Qty: 2)

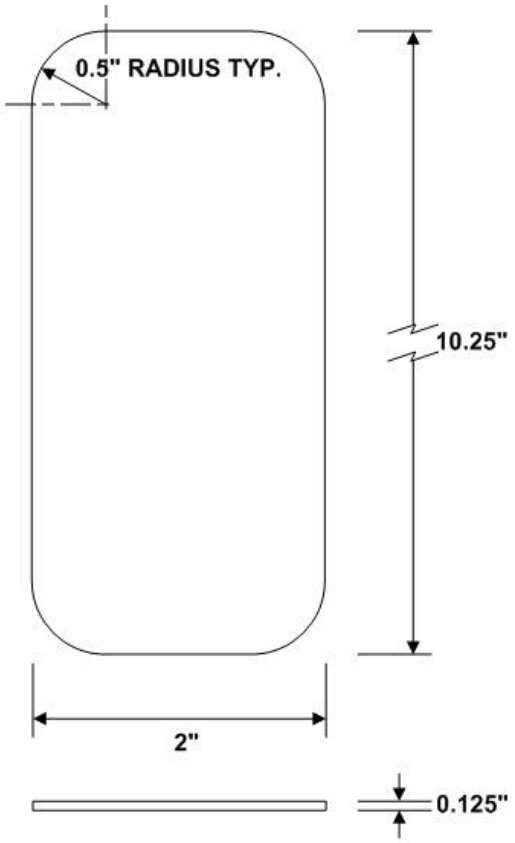

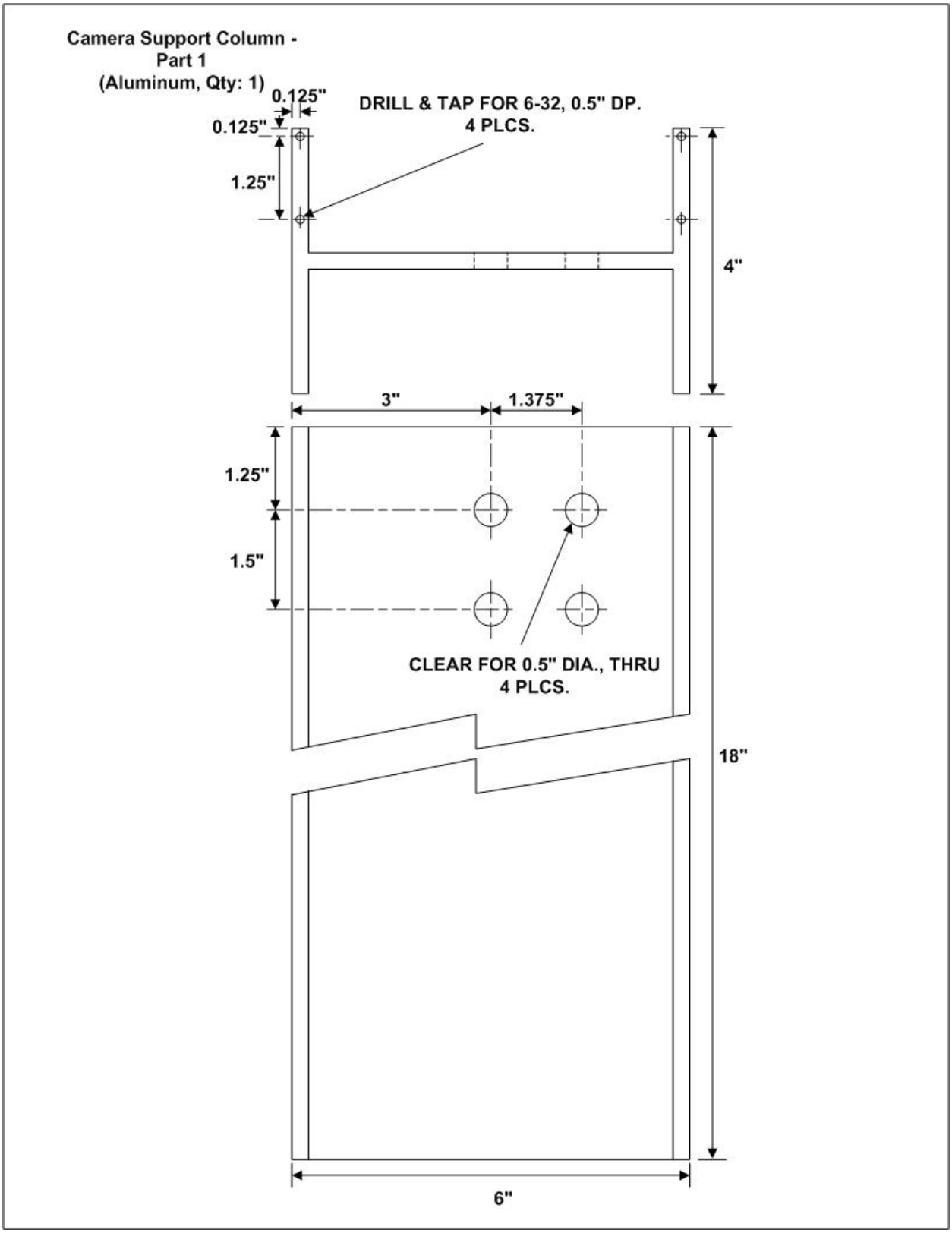
Camera Support Column -
Part 1
(Aluminum, Qty: 1)
0.125"
0.125"
DRILL & TAP FOR 6-32, 0.5" DP.
4 PLCS.
1.25"
4"
3"
1.375"
1.25"
1.5"
CLEAR FOR 0.5" DIA., THRU
4 PLCS.
18"
6"

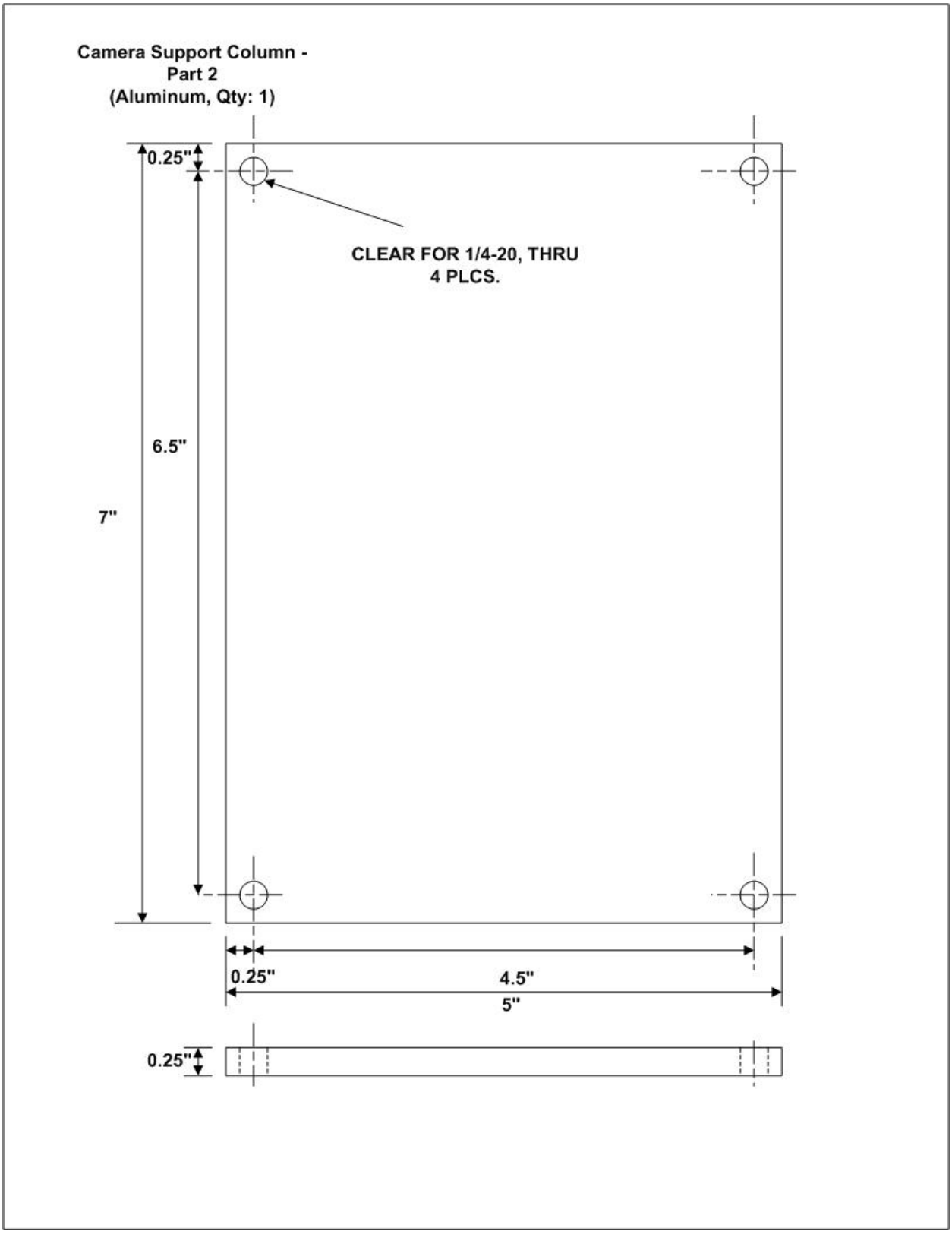
Camera Support Column -
Part 2
(Aluminum, Qty: 1)
0.25"
CLEAR FOR 1/4-20, THRU
4 PLCS.
6.5"
7"
0.25"
4.5"
5"
0.25"

Camera Support Column –
Weldment Drawing
(Aluminum, Qty: 1)

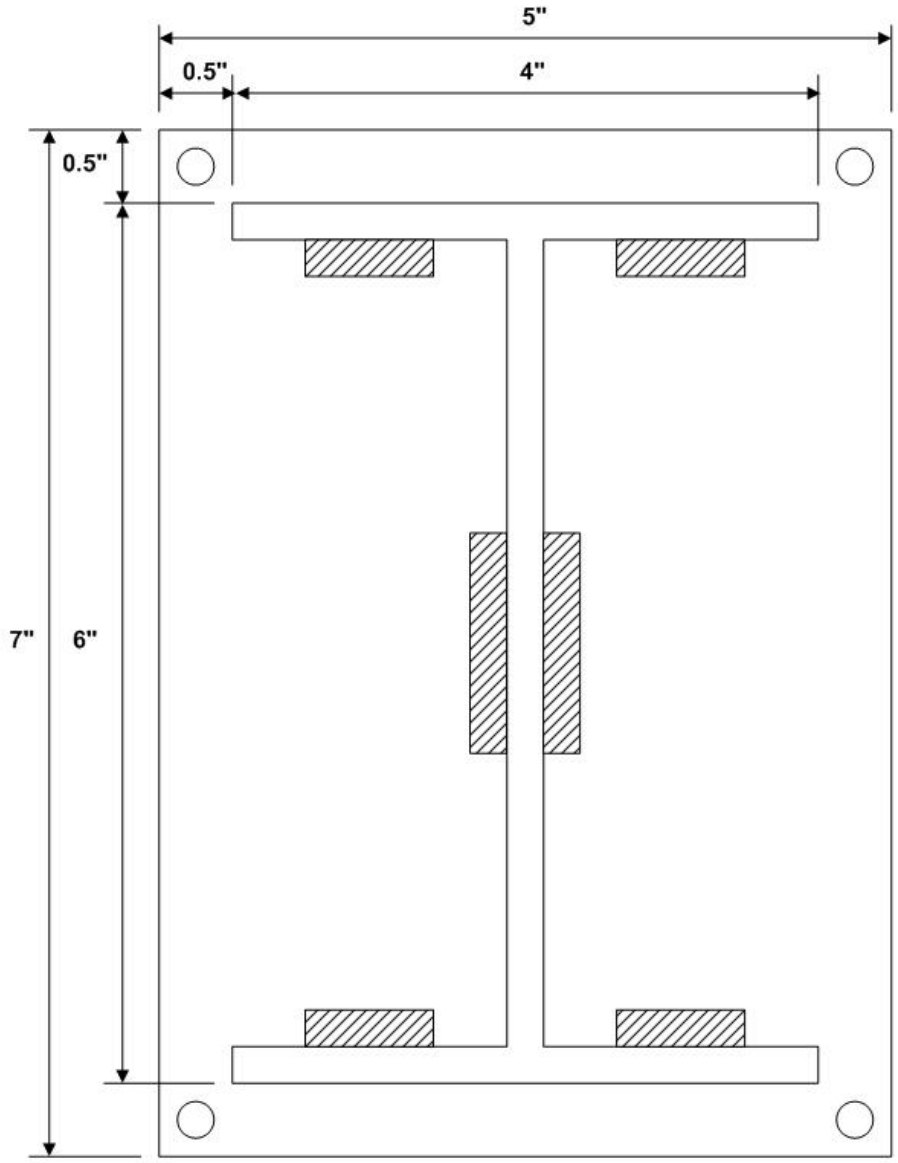

Camera Bracket - Part 1
(Aluminum, Qty: 2)

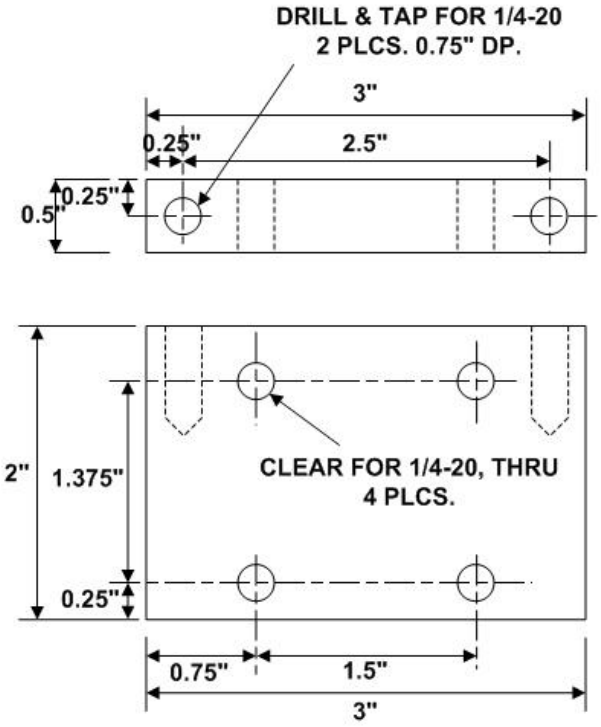

Camera Bracket - Part 2
(Aluminum, Qty: 2)

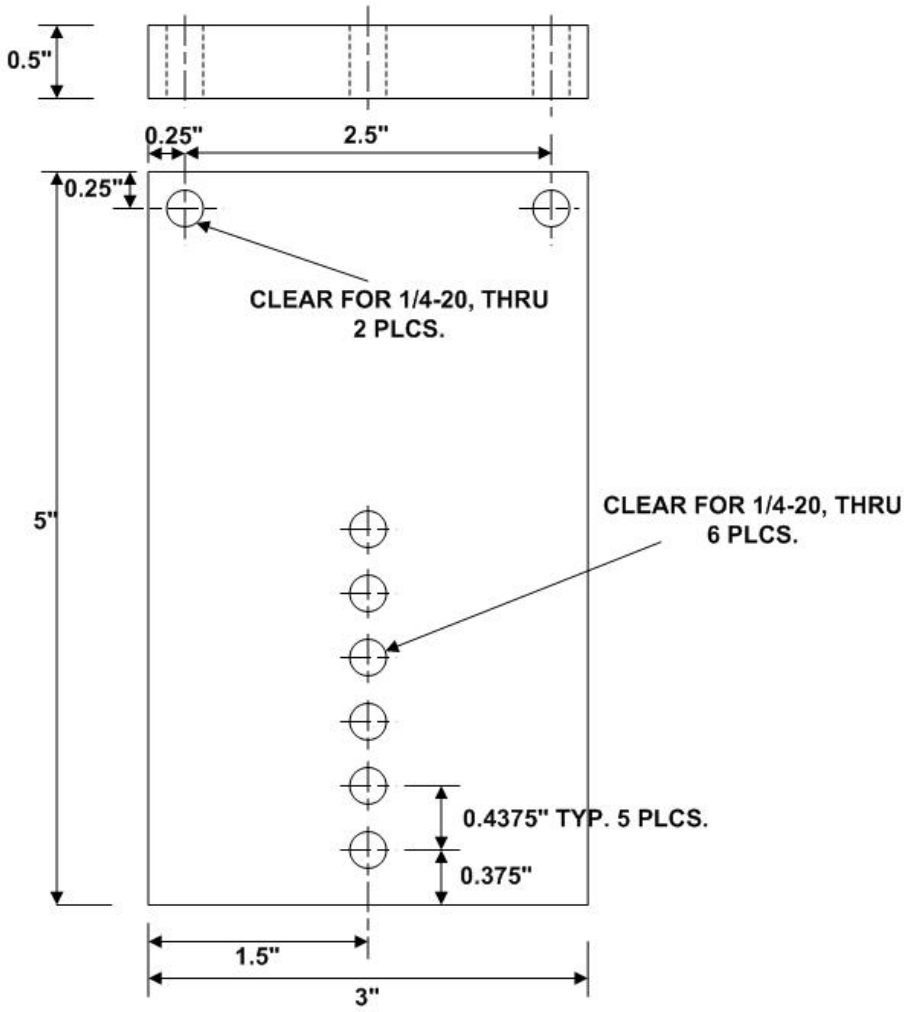

Light Holding
(Aluminum, Qty: 1)

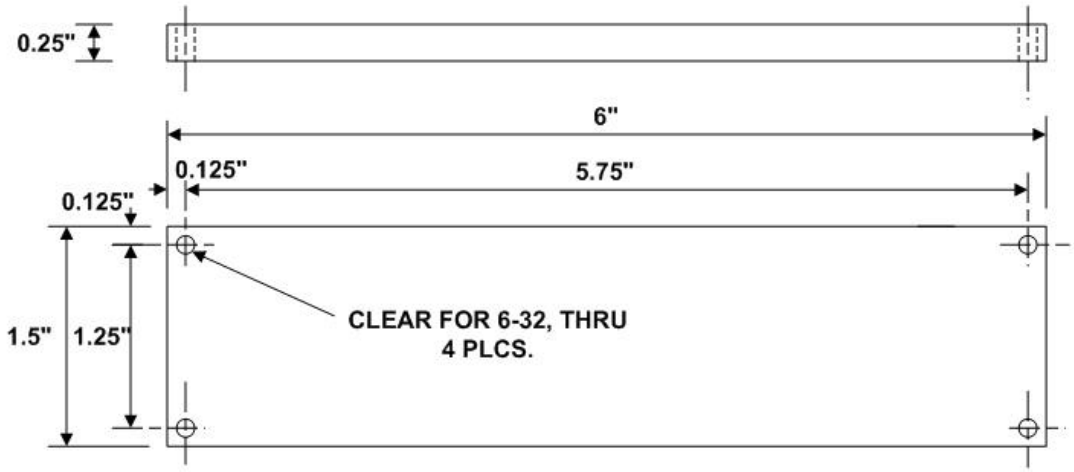

Ceiling Bracket
(Aluminum, Qty: 1)

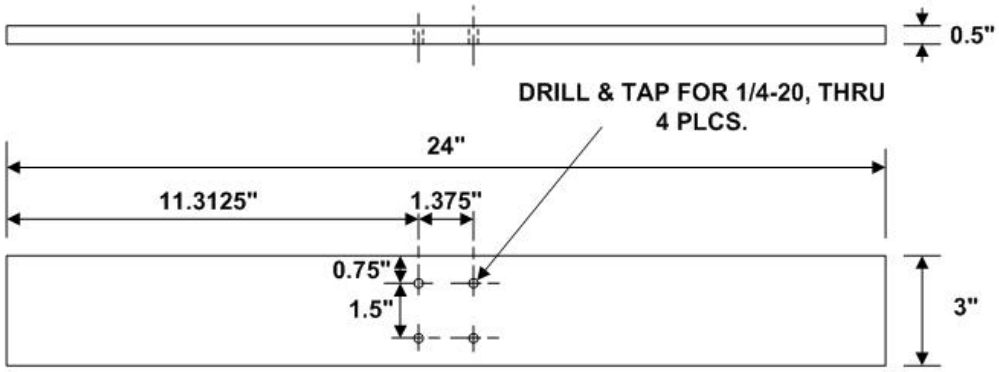

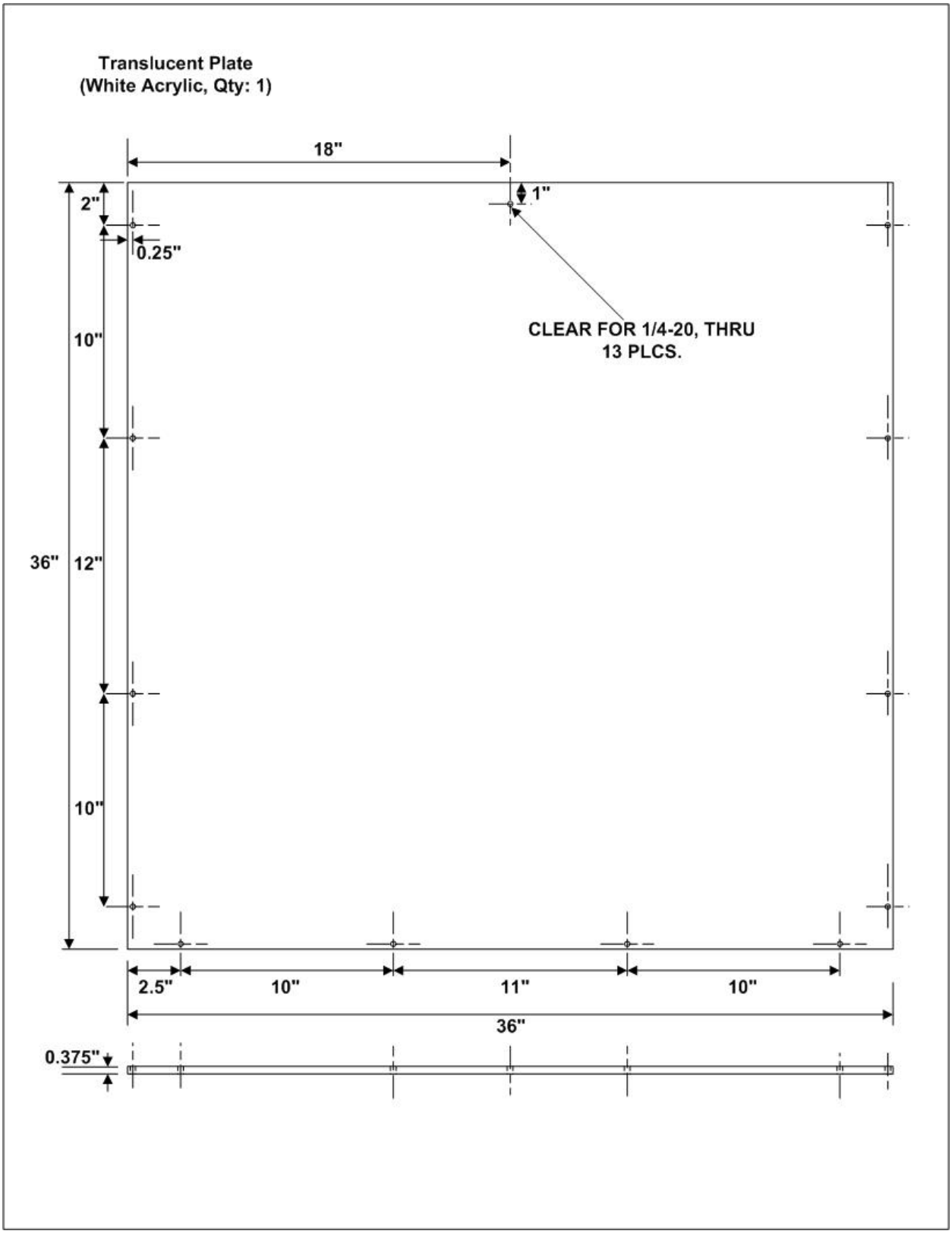
Translucent Plate
(White Acrylic, Qty: 1)
18"
1"
2"
0.25"
CLEAR FOR 1/4-20, THRU
13 PLCS.
10"
36"
12"
10"
2.5"
10"
11"
10"
36"
0.375"

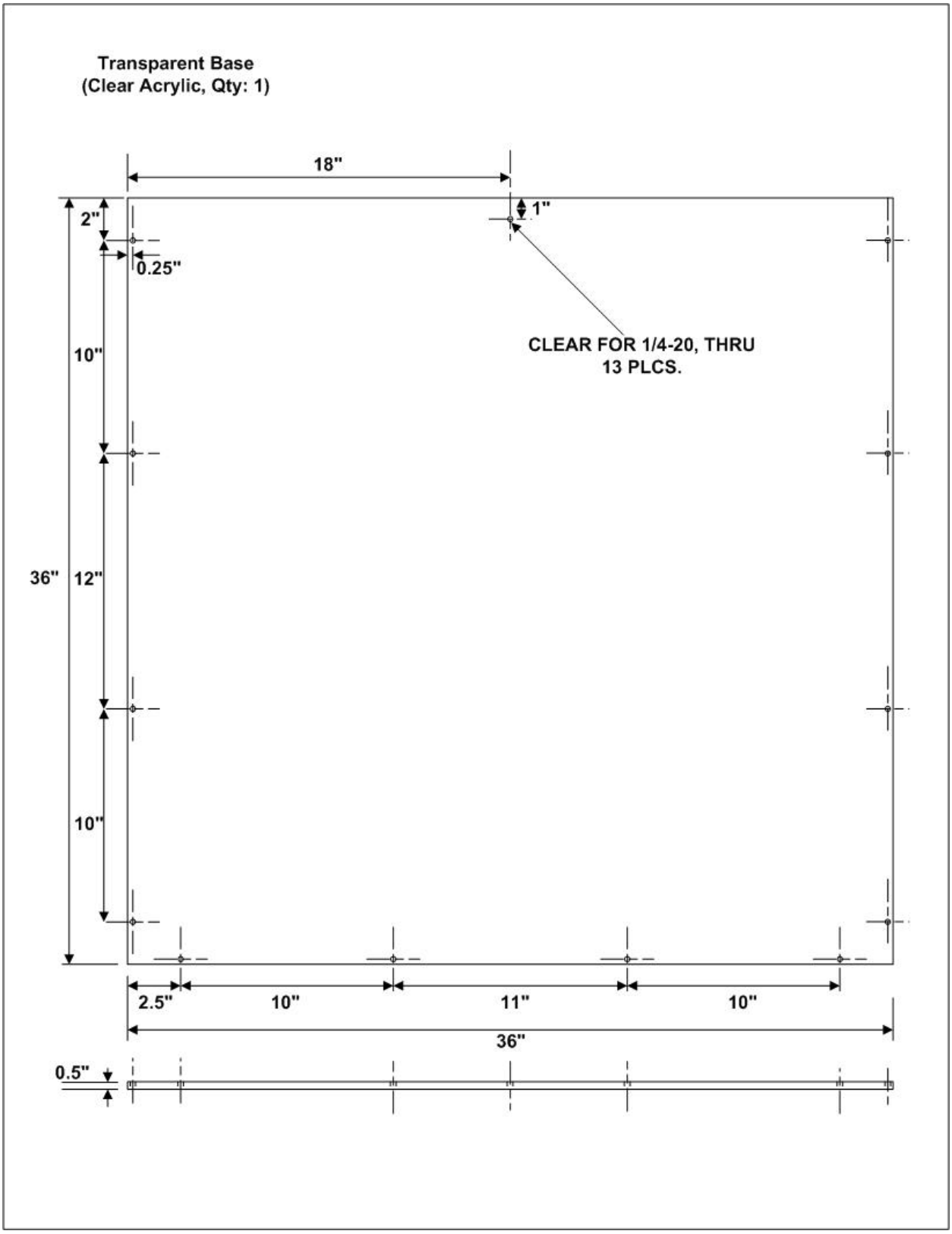
Transparent Base
(Clear Acrylic, Qty: 1)
18"
1"
2"
0.25"
CLEAR FOR 1/4-20, THRU
13 PLCS.
10"
36"
12"
10"
2.5"
10"
11"
10"
36"
0.5"

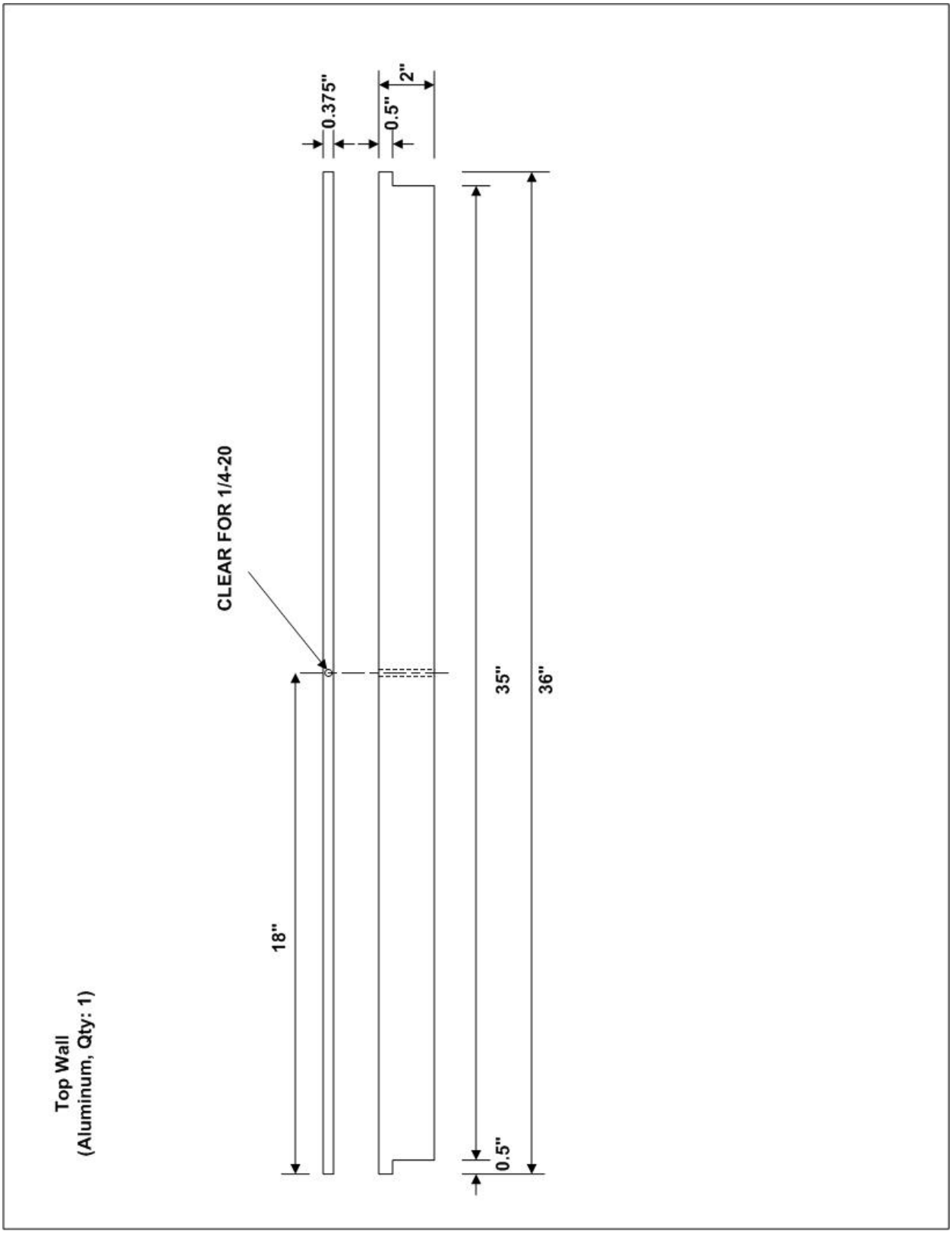
Top Wall
(Aluminum, Qty: 1)
CLEAR FOR 1/4-20
0.375"
0.5"
2"
18"
35"
36"
0.5"

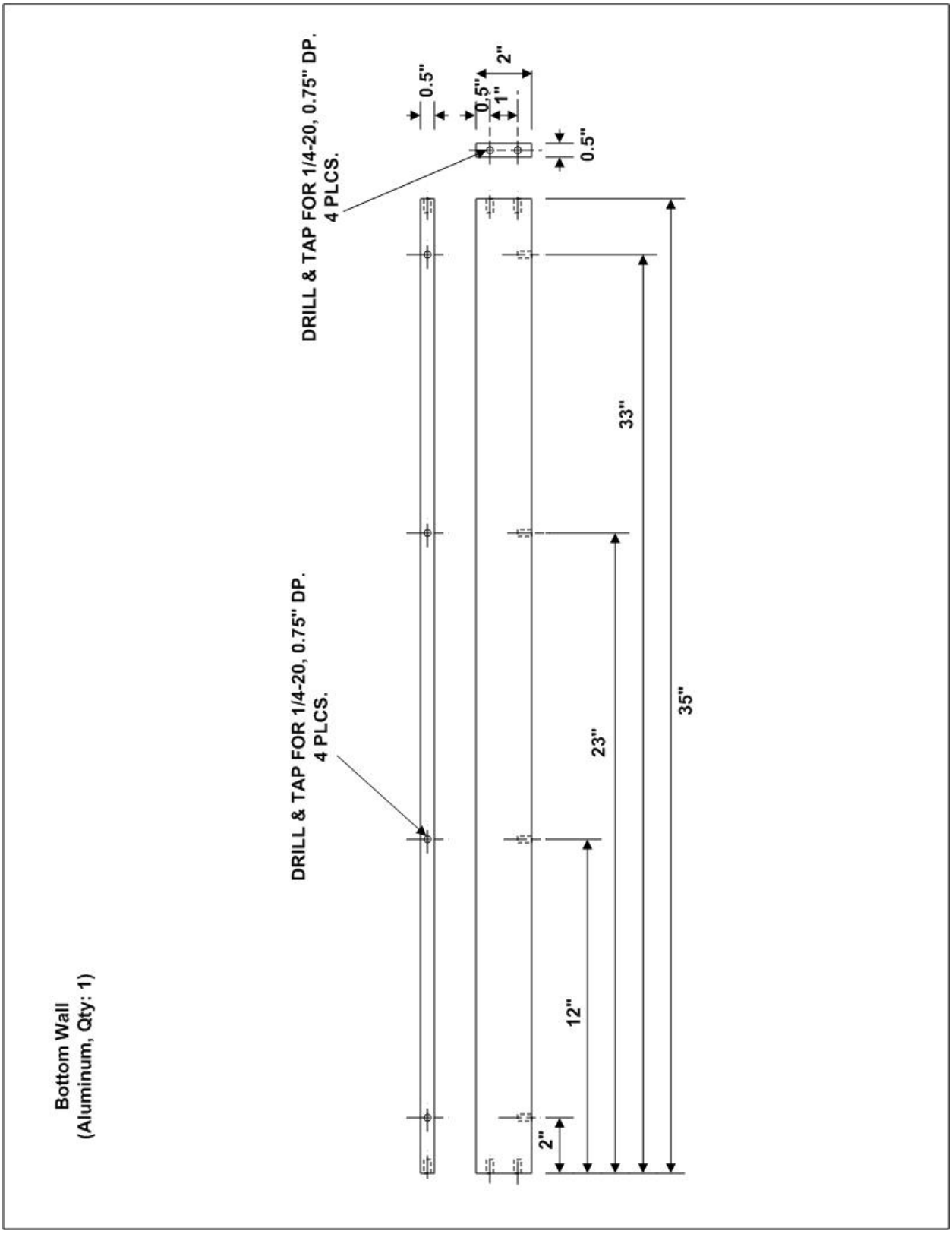
Bottom Wall
(Aluminum, Qty: 1)
DRILL & TAP FOR 1/4-20, 0.75" DP.
4 PLCS.
DRILL & TAP FOR 1/4-20, 0.75" DP.
4 PLCS.
0.5"
0.5"
1"
2"
0.5"
2"
12"
23"
33"
35"

Slotted Side Wall
(Aluminum, Qty: 2)

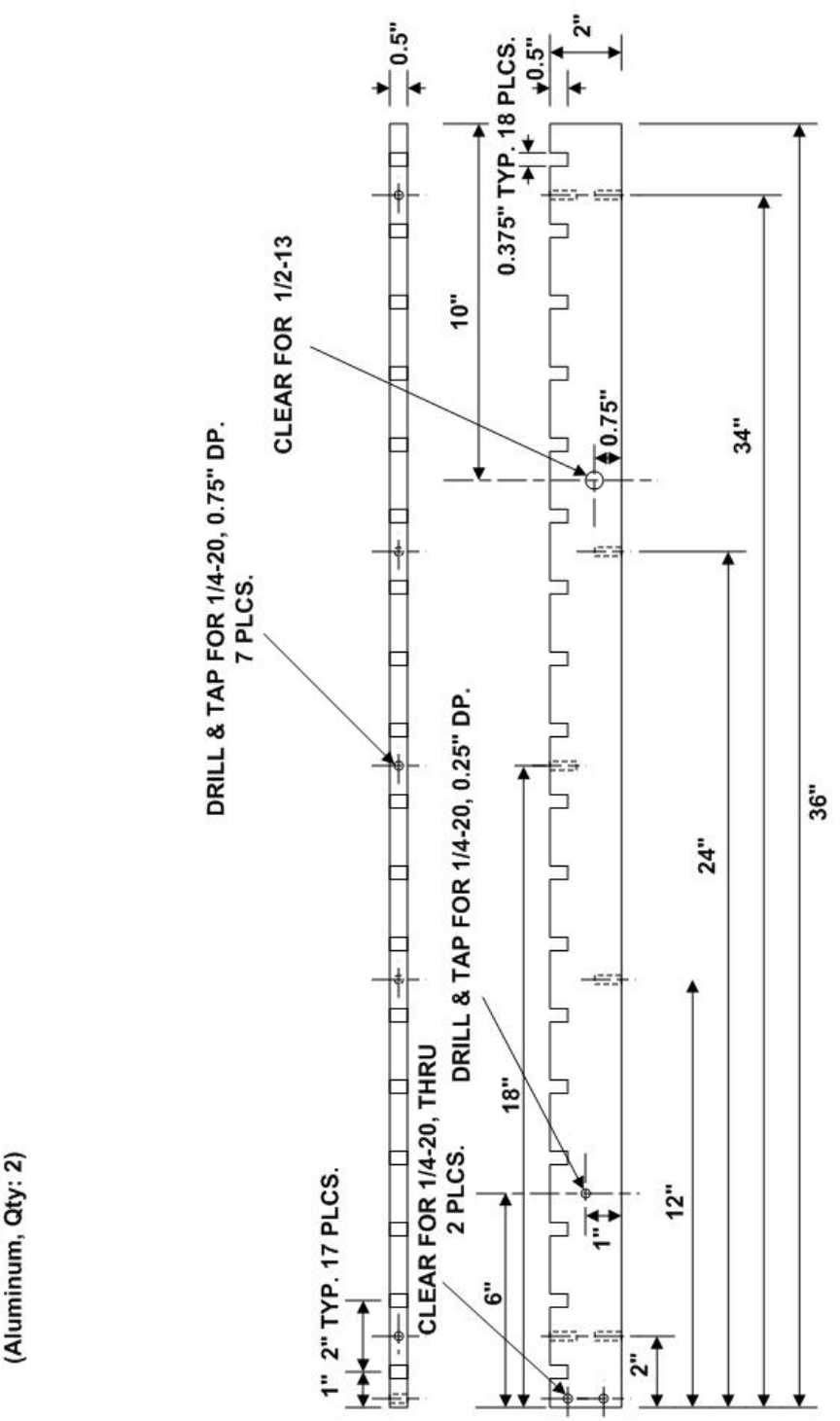

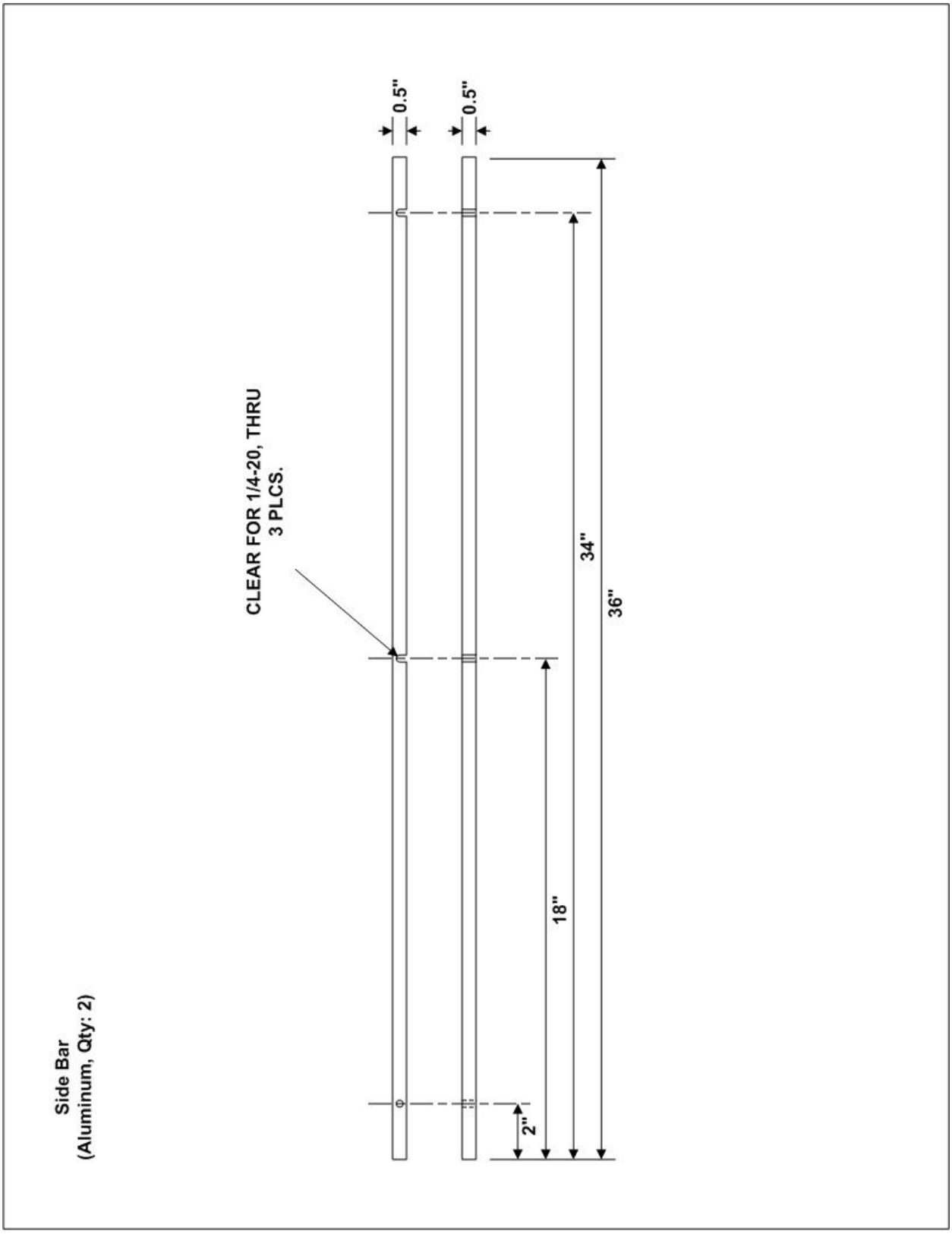
Side Bar
(Aluminum, Qty: 2)
CLEAR FOR 1/4-20, THRU
3 PLCS.
0.5"
0.5"
2"
18"
34"
36"

Segregation Bridge
(Aluminum)

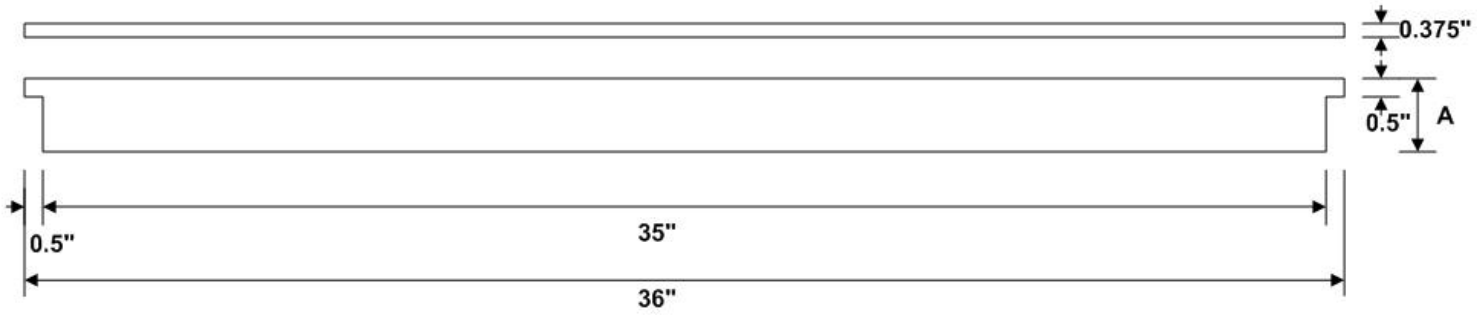

A	Qty
1.2500"	1
1.5000"	1
1.6250"	1
1.8125"	1
1.8750"	1
1.9130"	1

Support Foot
(Aluminum, Qty: 2)

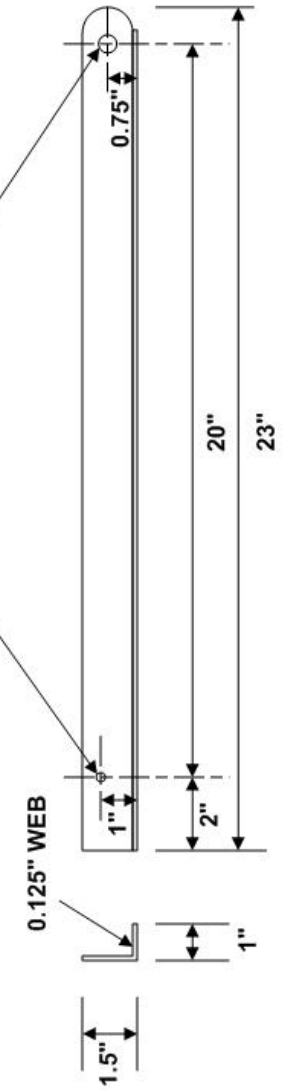

Light Box
(Plywood, Qty: 1, Assembly View)

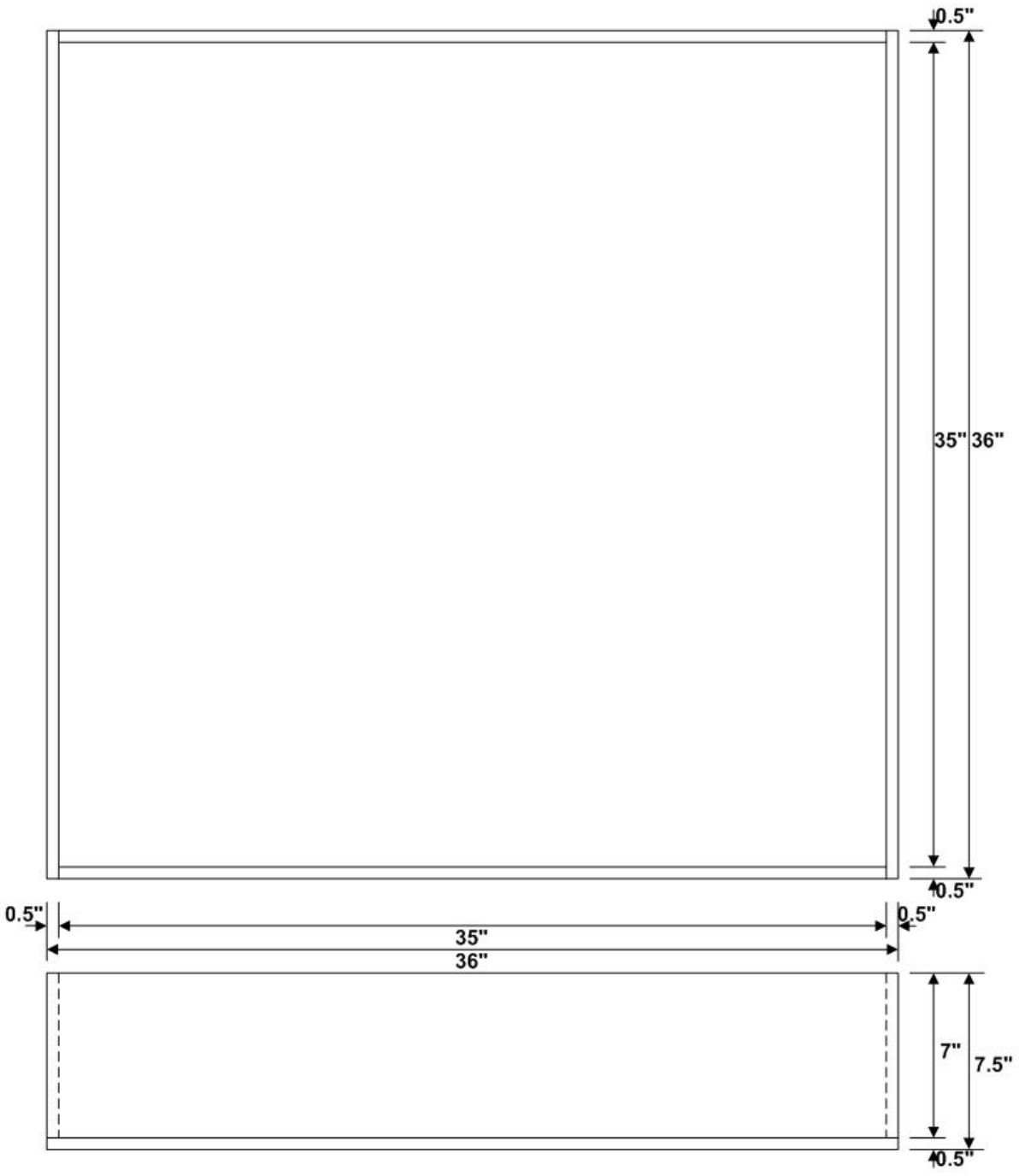

Appendix C. Complete Sedimaging Results

SEDIMAGING (SED) TEST

GEOTECHNICAL ENGINEERING

UNIVERSITY OF MICHIGAN

MATERIAL: 2NS

DATE TESTED: 21-Sep-2011 12:21:34

TESTED BY: Ohm, H.S.

D_{60} (mm): 0.62

D_{30} (mm): 0.42

D_{10} (mm): 0.30

C_u: 2.06

C_g: 0.96

PF (%): 0.0

MAGNIFICATION (pix/mm): 36.9

IMAGE SIZE (pix): 4504 x 1280

IMAGE SIZE (mm): 122.1 x 34.7

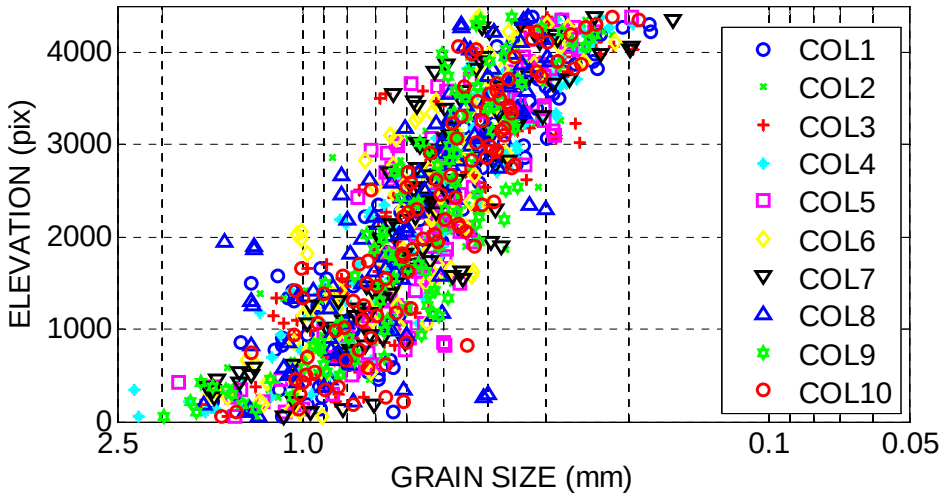

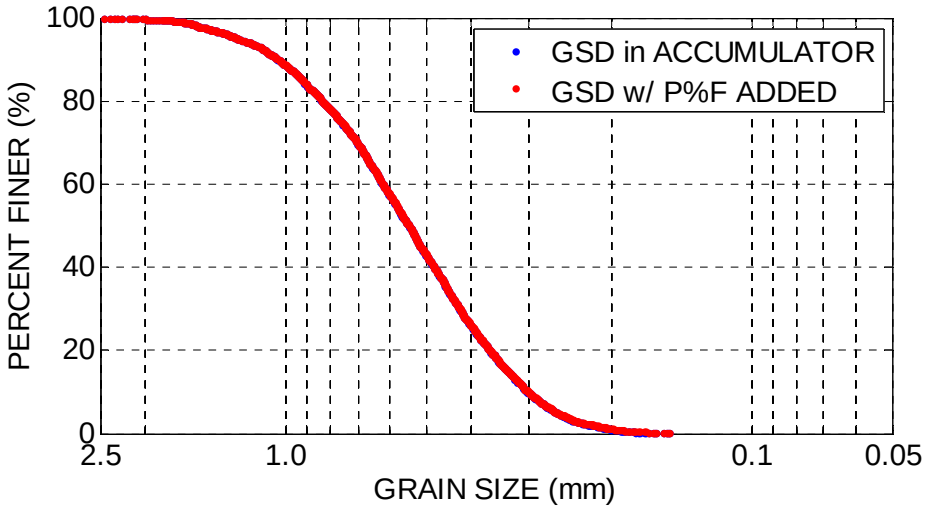

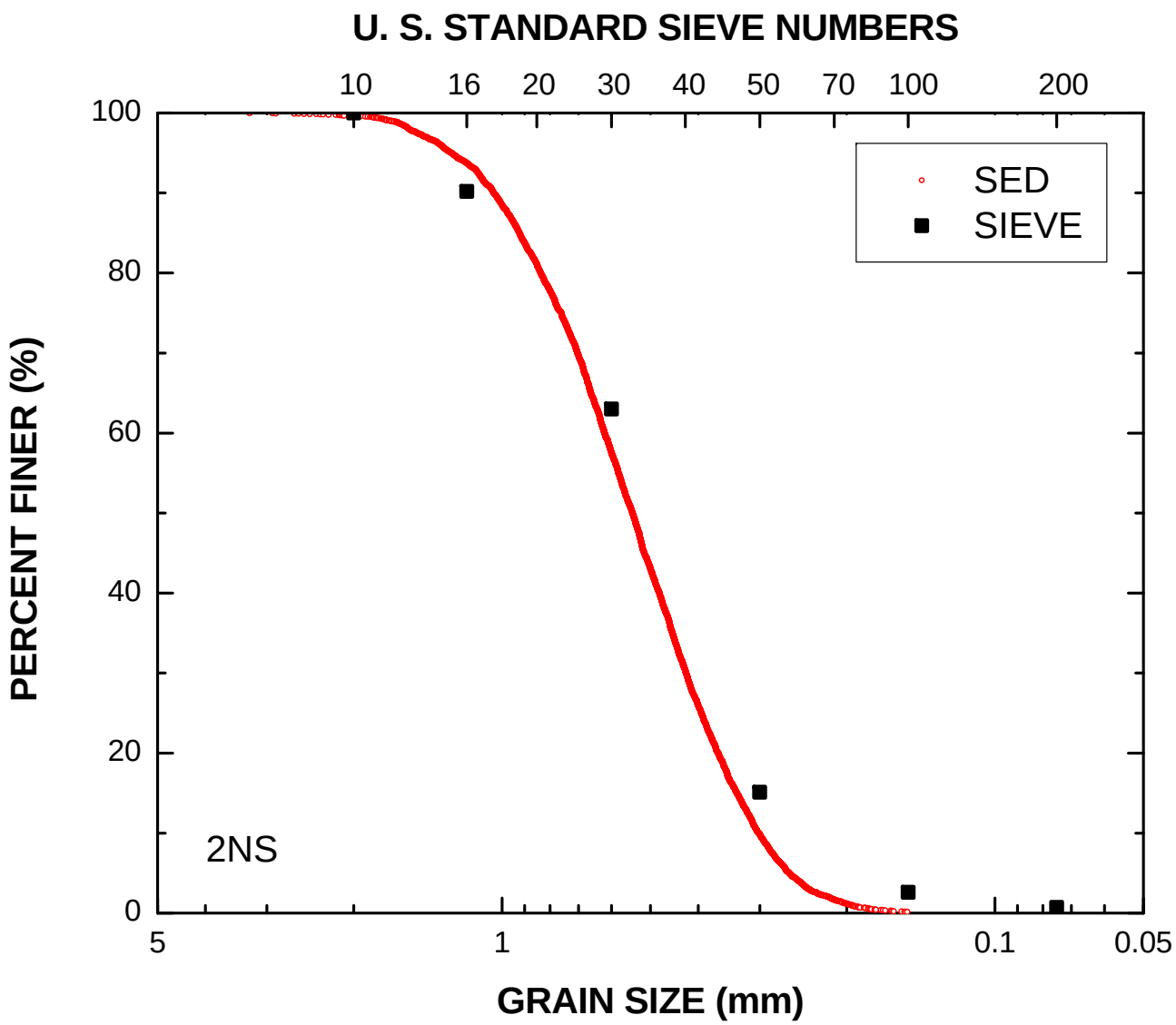
U. S. STANDARD SIEVE NUMBERS
10
16
20
30
40
50
70
100
200
100
80
60
40
20
0
PERCENT FINER (%)
SED
SIEVE
2NS
5
1
0.1
0.05
GRAIN SIZE (mm)

SEDIMAGING (SED) TEST

GEOTECHNICAL ENGINEERING

UNIVERSITY OF MICHIGAN

MATERIAL: Capitola, CA

DATE TESTED: 19-Jun-2012 11:05:24

TESTED BY: Ohm, H.S.

D_{60} (mm): 0.43

D_{30} (mm): 0.35

D_{10} (mm): 0.29

C_u: 1.50

C_g: 0.97

PF (%): 0.0

MAGNIFICATION (pix/mm): 36.7

IMAGE SIZE (pix): 3880 x 1280

IMAGE SIZE (mm): 105.7 x 34.9

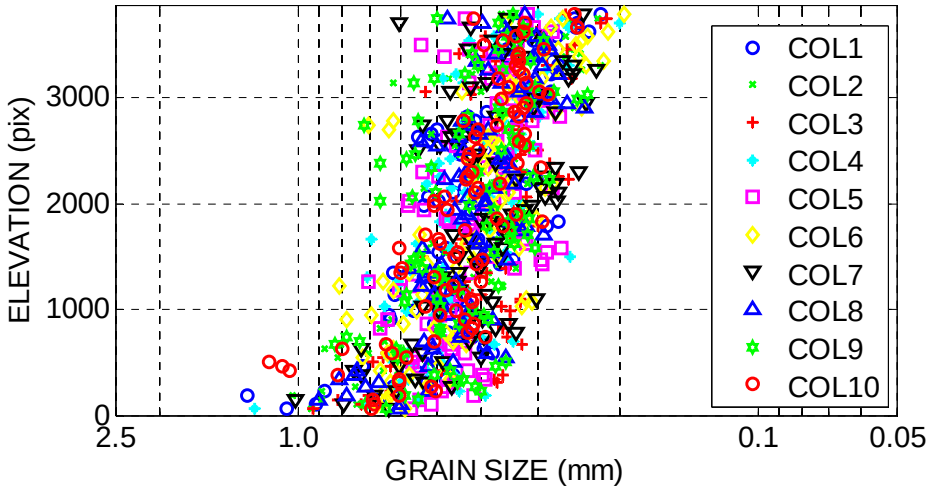

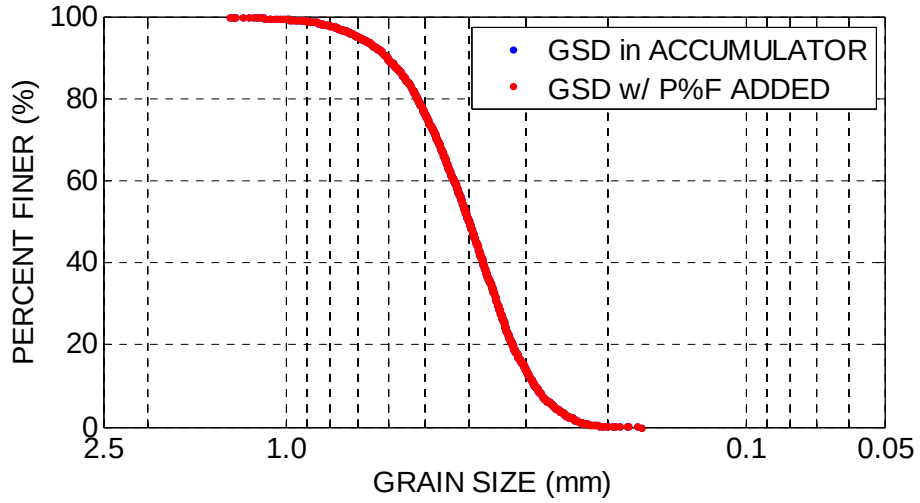

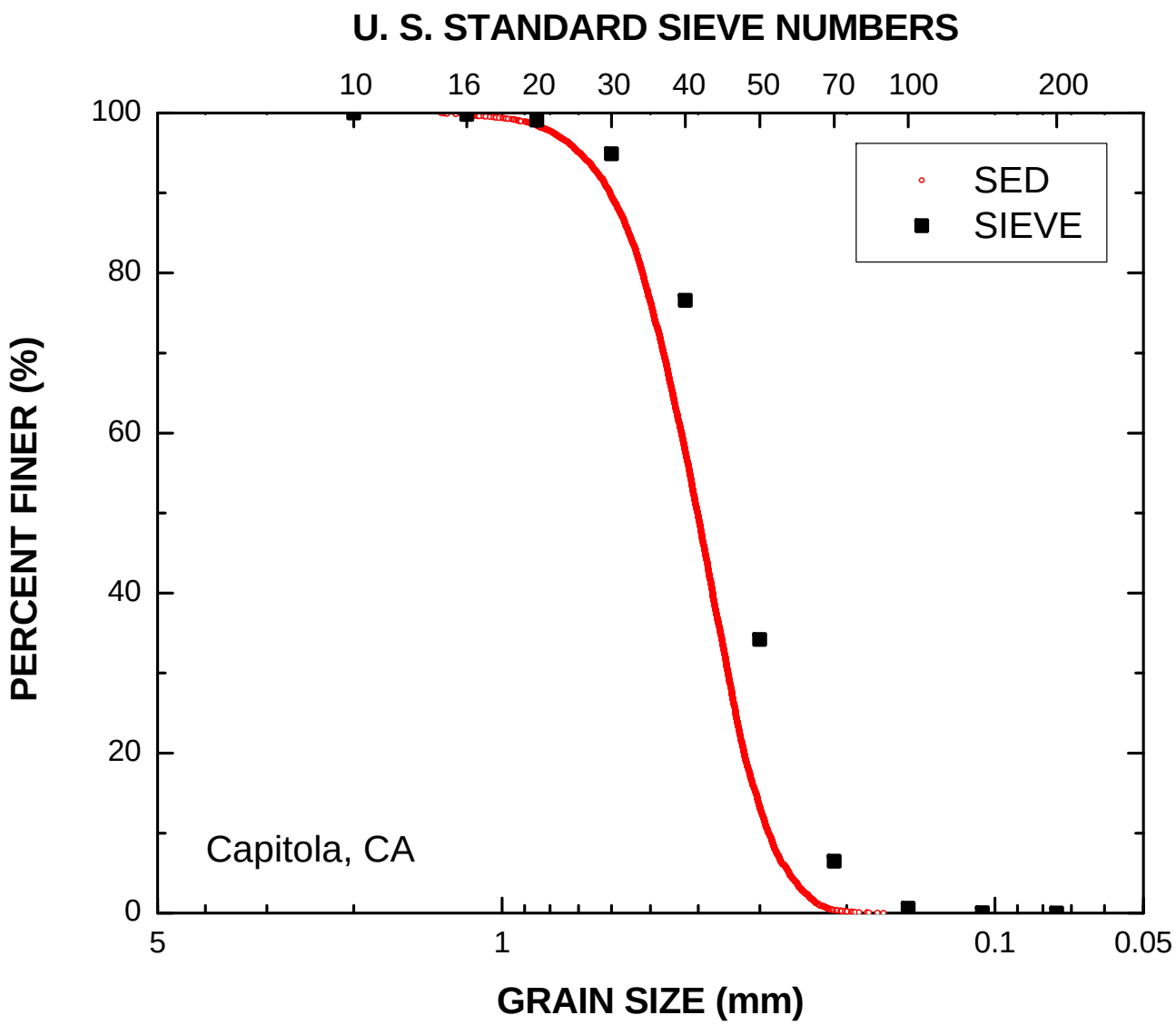
U. S. STANDARD SIEVE NUMBERS
10
16
20
30
40
50
70
100
200
100
80
60
40
20
0
PERCENT FINER (%)
SED
SIEVE
Capitola, CA
5
1
0.1
0.05
GRAIN SIZE (mm)

SEDIMAGING (SED) TEST

GEOTECHNICAL ENGINEERING

UNIVERSITY OF MICHIGAN

MATERIAL: Class IIA

DATE TESTED: 26-Aug-2011 12:31:20

TESTED BY: Ohm, H.S.

D_{60} (mm): 0.22

D_{30} (mm): 0.15

D_{10} (mm): 0.11

C_u: 2.02

C_g: 0.95

PF (%): 3.8

MAGNIFICATION (pix/mm): 36.6

IMAGE SIZE (pix): 4168 x 1280

IMAGE SIZE (mm): 113.9 x 35.0

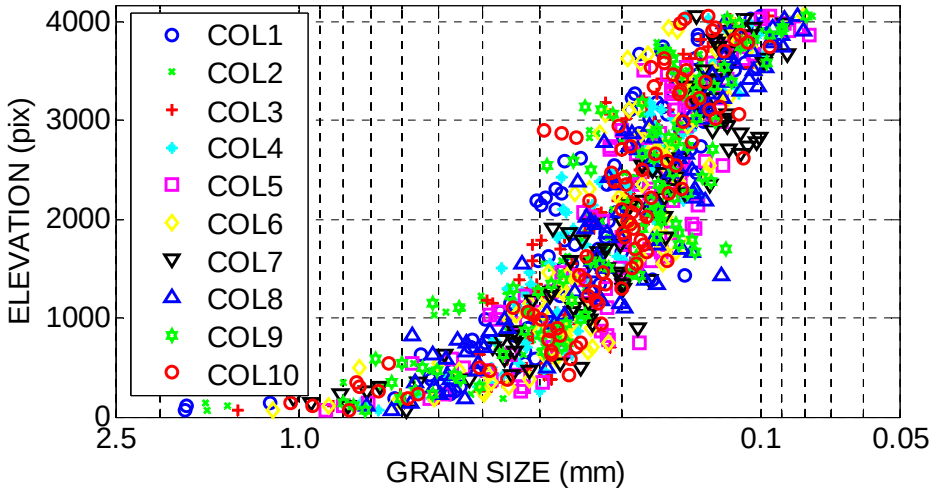

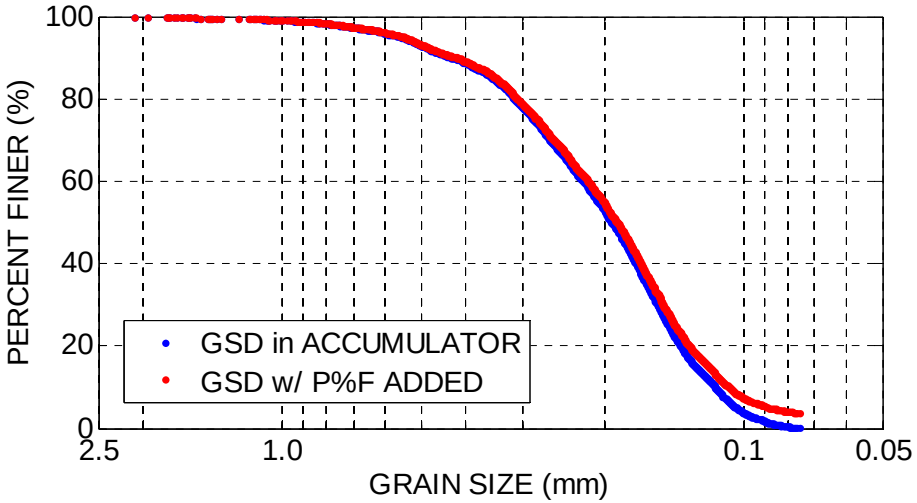

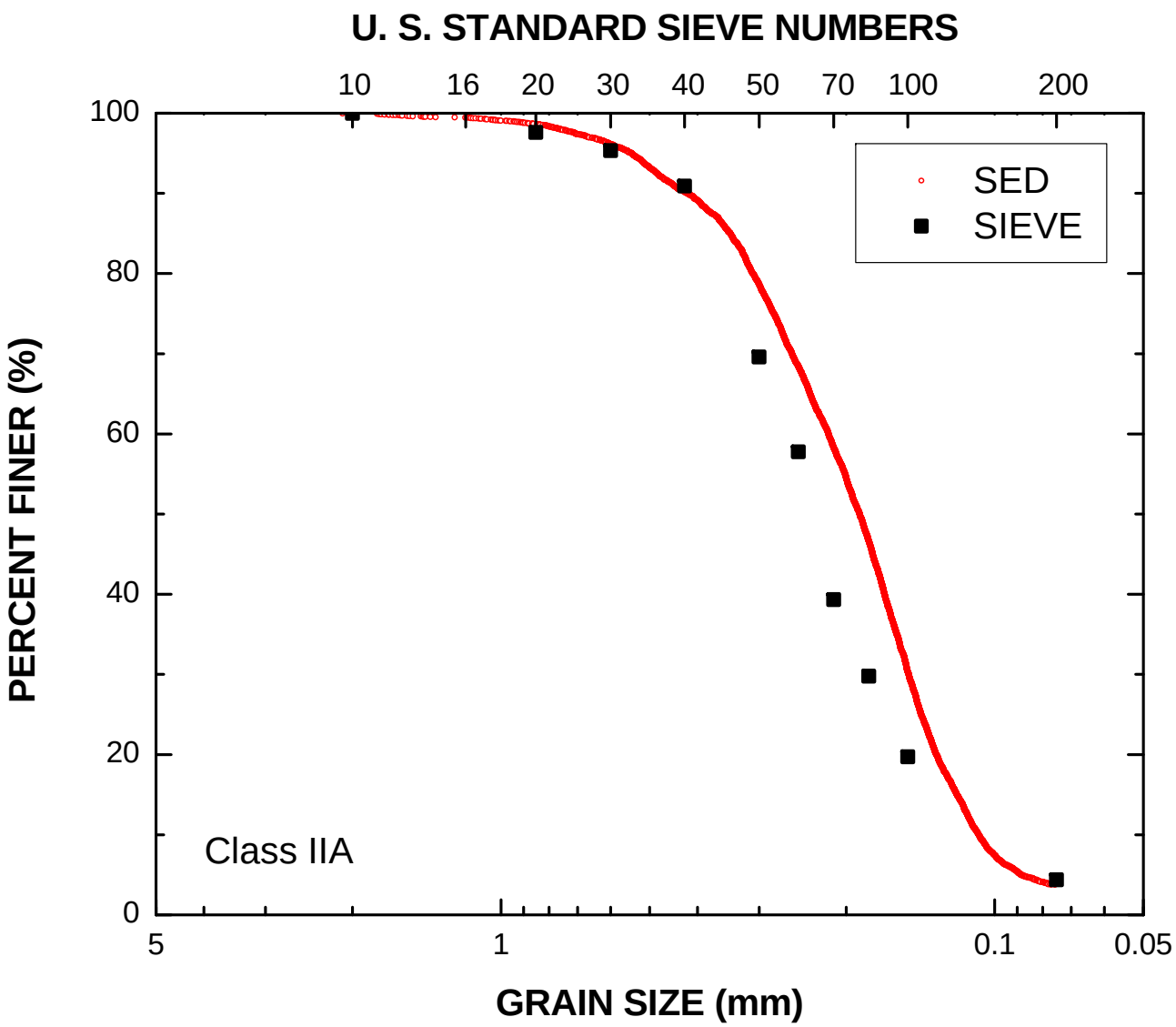
U. S. STANDARD SIEVE NUMBERS
10
16
20
30
40
50
70
100
200
100
80
60
40
20
0
PERCENT FINER (%)
SED
SIEVE
Class IIA
5
1
0.1
0.05
GRAIN SIZE (mm)

SEDIMAGING (SED) TEST

GEOTECHNICAL ENGINEERING

UNIVERSITY OF MICHIGAN

MATERIAL: Costa Rica

DATE TESTED: 04-May-2011 12:53:04

TESTED BY: Ohm, H.S.

D_{60} (mm): 0.16

D_{30} (mm): 0.12

D_{10} (mm): 0.11

C_u: 1.48

C_g: 0.91

PF (%): 0.0

MAGNIFICATION (pix/mm): 33.3

IMAGE SIZE (pix): 4096 x 1280

IMAGE SIZE (mm): 123.0 x 38.4

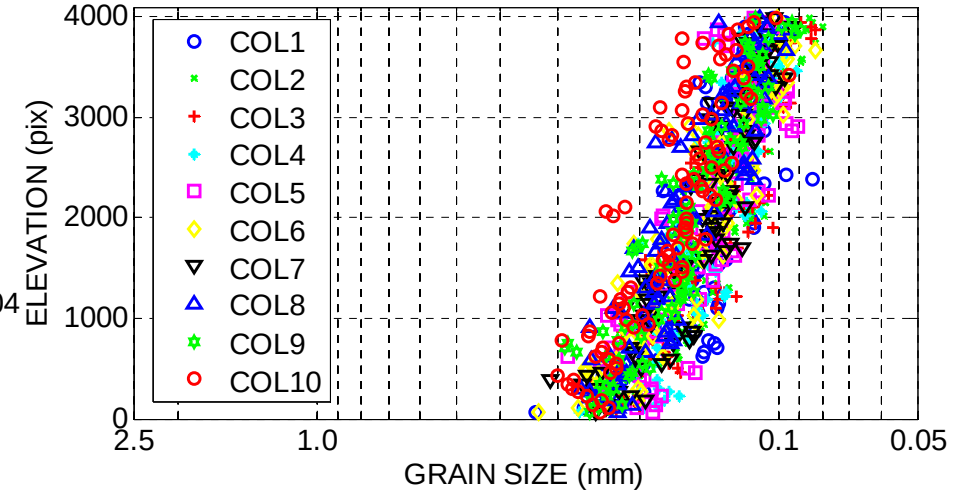

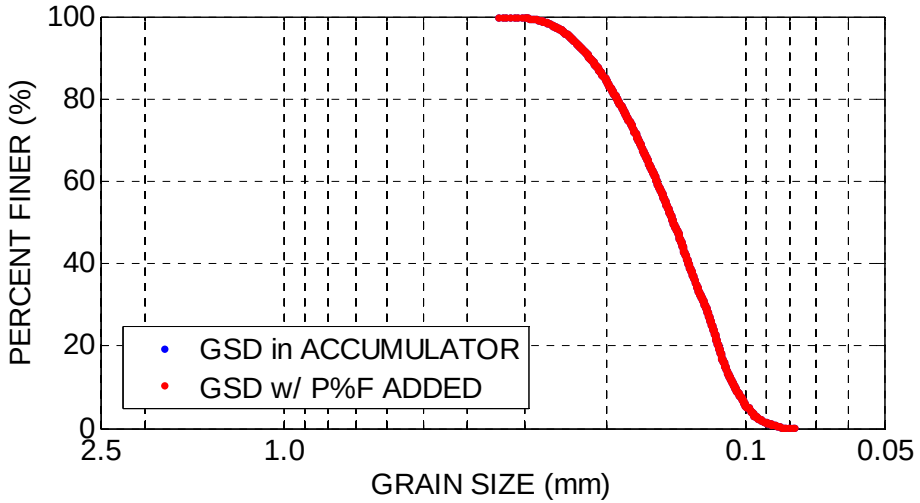

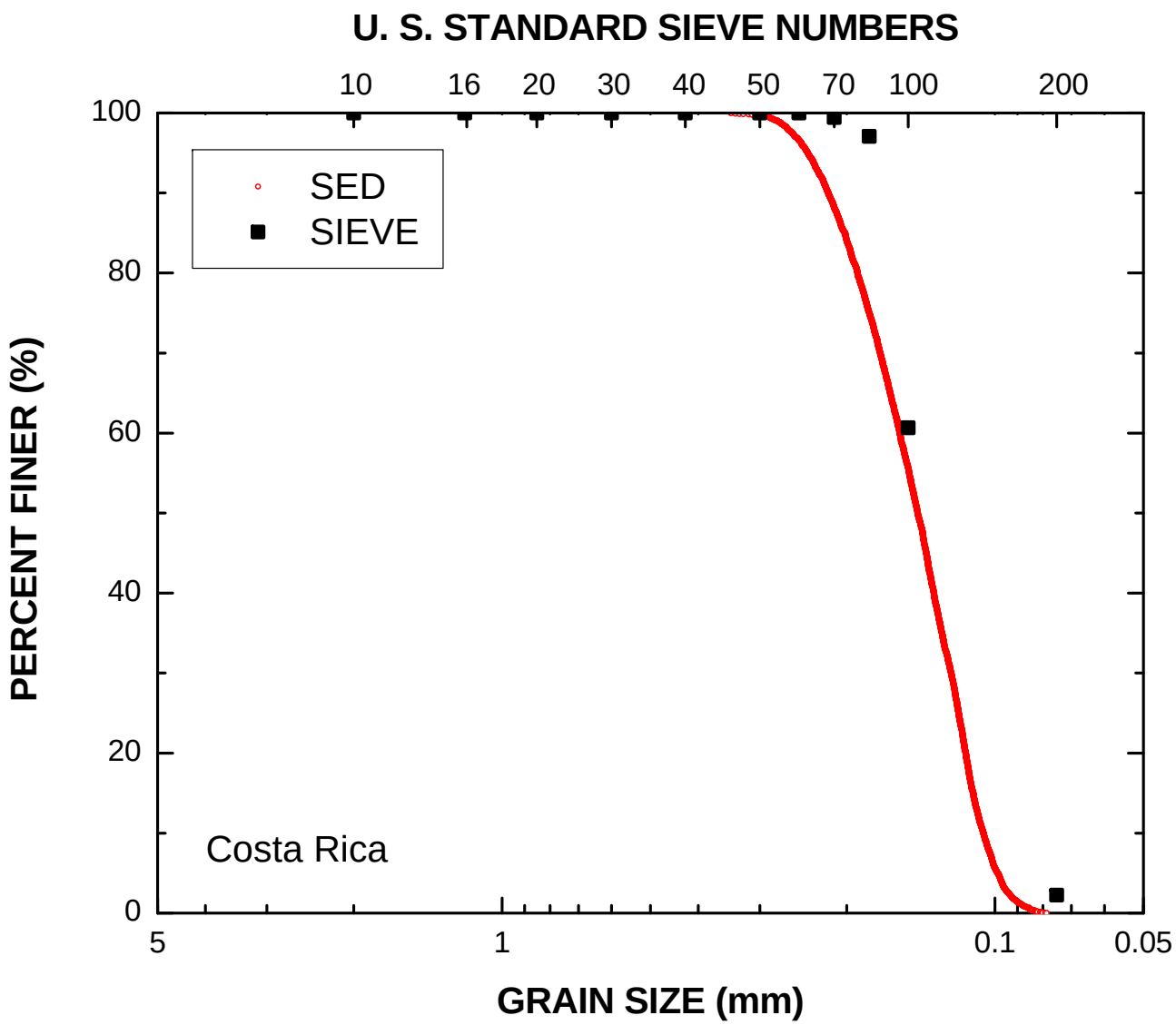
U. S. STANDARD SIEVE NUMBERS
10
16
20
30
40
50
70
100
200
100
80
60
40
20
0
SED
SIEVE
Costa Rica
PERCENT FINER (%)
5
1
0.1
0.05
GRAIN SIZE (mm)

SEDIMAGING (SED) TEST

GEOTECHNICAL ENGINEERING

UNIVERSITY OF MICHIGAN

MATERIAL: Griffin, IN

DATE TESTED: 01-May-2011 09:09:50

TESTED BY: Ohm, H.S.

D_{60} (mm): 0.66

D_{30} (mm): 0.45

D_{10} (mm): 0.35

C_u: 1.92

C_g: 0.90

PF (%): 0.0

MAGNIFICATION (pix/mm): 33.6

IMAGE SIZE (pix): 4136 x 1280

IMAGE SIZE (mm): 123.1 x 38.1

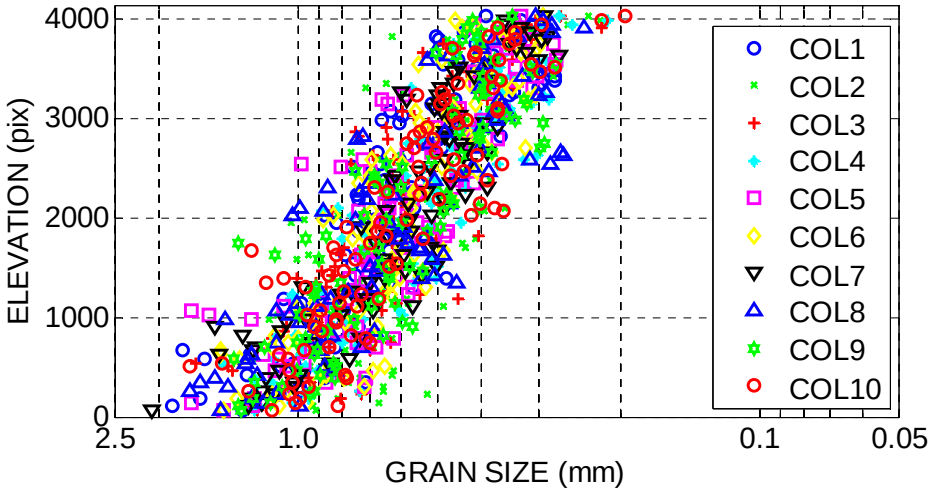

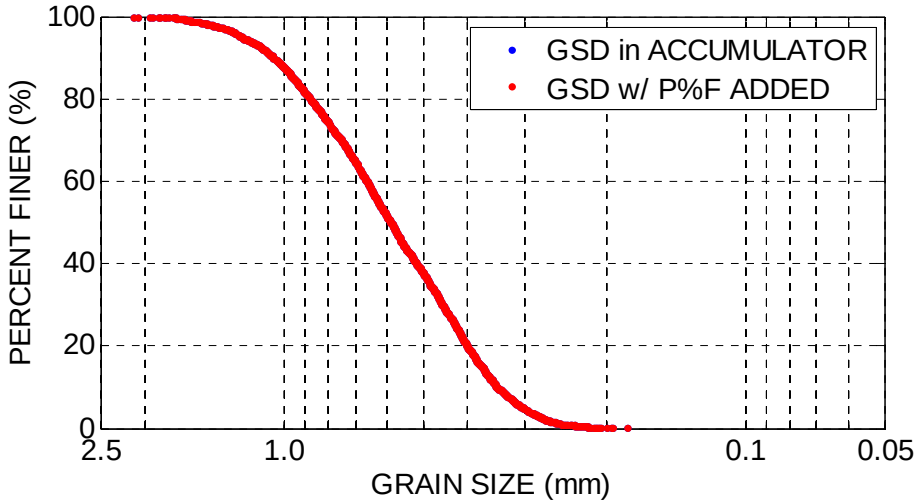

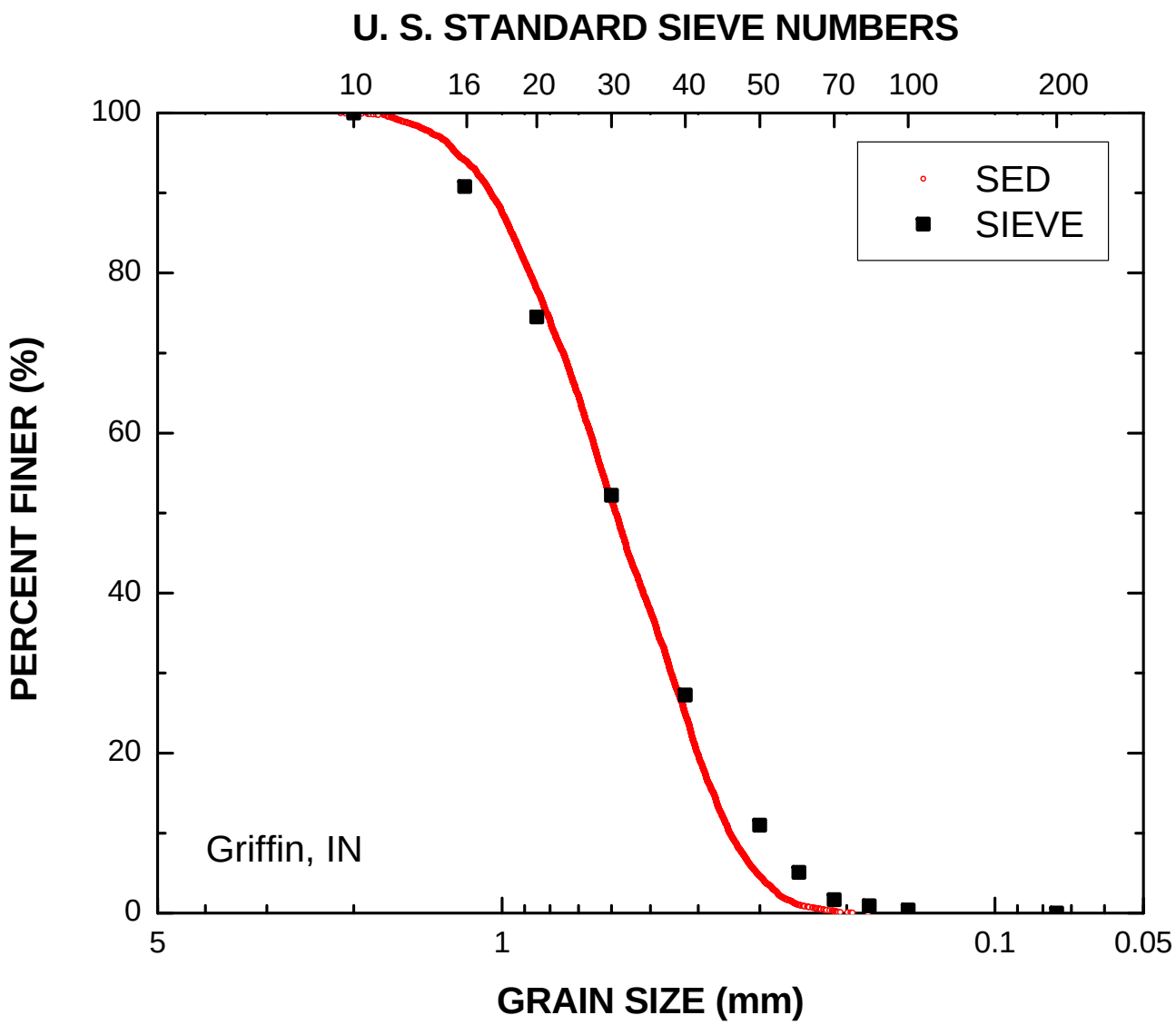
U. S. STANDARD SIEVE NUMBERS
10
16
20
30
40
50
70
100
200
100
80
60
40
20
0
PERCENT FINER (%)
SED
SIEVE
Griffin, IN
5
1
0.1
0.05
GRAIN SIZE (mm)

SEDIMAGING (SED) TEST
GEOTECHNICAL ENGINEERING
UNIVERSITY OF MICHIGAN

MATERIAL: Oakland Co., MI
DATE TESTED: 25-Jun-2012 12:59:02
TESTED BY: Ohm, H.S.

D_{60} (mm): 0.31
D_{30} (mm): 0.23
D_{10} (mm): 0.19
C_u: 1.59
C_g: 0.90
PF (%): 0.0

MAGNIFICATION (pix/mm): 36.7
IMAGE SIZE (pix): 3816 x 1280
IMAGE SIZE (mm): 104.0 x 34.9

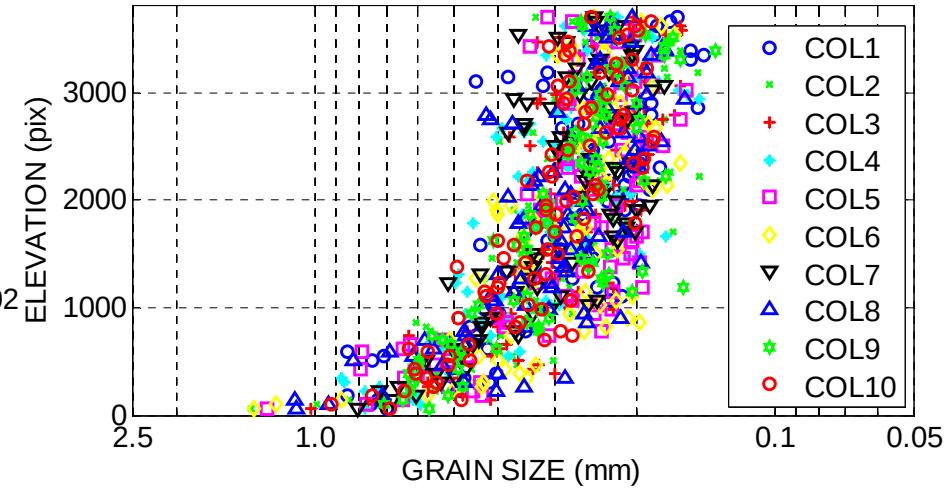

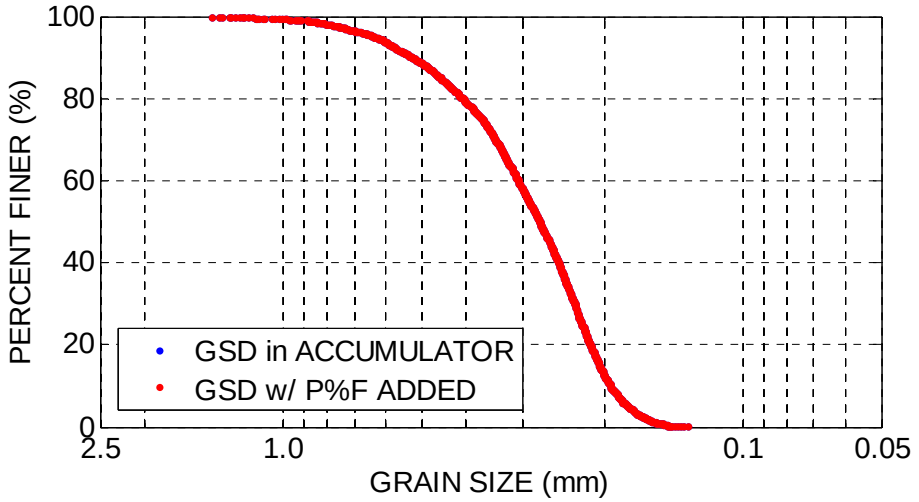

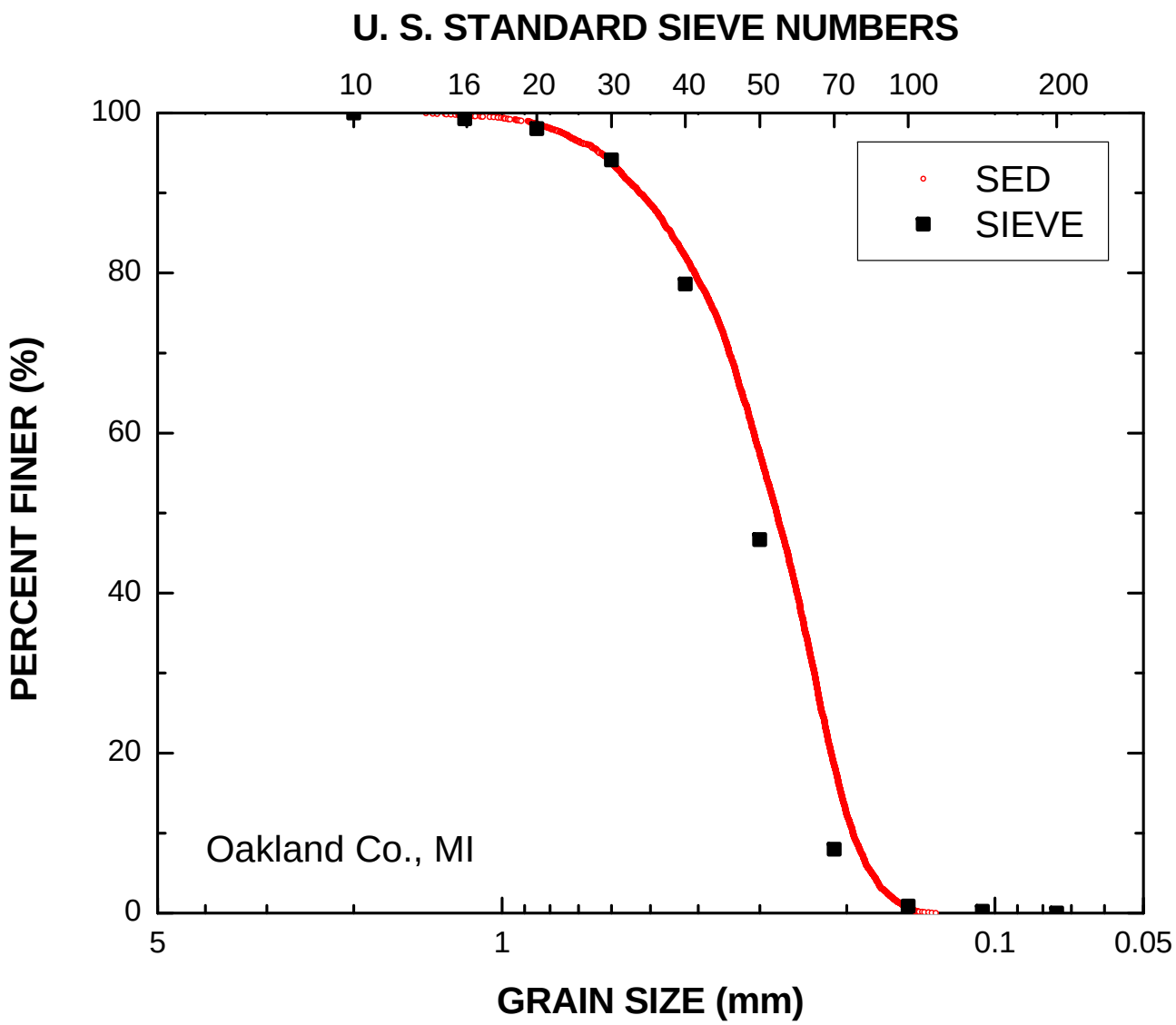
U. S. STANDARD SIEVE NUMBERS
10
16
20
30
40
50
70
100
200
100
80
60
40
20
0
PERCENT FINER (%)
SED
SIEVE
Oakland Co., MI
5
1
0.1
0.05
GRAIN SIZE (mm)

SEDIMAGING (SED) TEST

GEOTECHNICAL ENGINEERING

UNIVERSITY OF MICHIGAN

MATERIAL: Rincon, NM

DATE TESTED: 25-Jan-2012 11:15:22

TESTED BY: Ohm, H.S.

D_{60} (mm): 0.39

D_{30} (mm): 0.23

D_{10} (mm): 0.14

C_u: 2.88

C_g: 0.99

PF (%): 5.5

MAGNIFICATION (pix/mm): 36.8

IMAGE SIZE (pix): 3344 x 1280

IMAGE SIZE (mm): 90.9 x 34.8

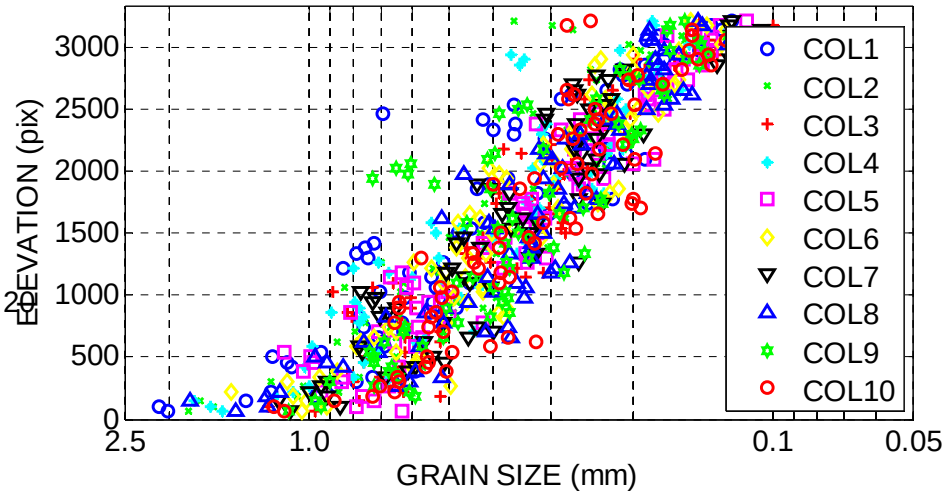

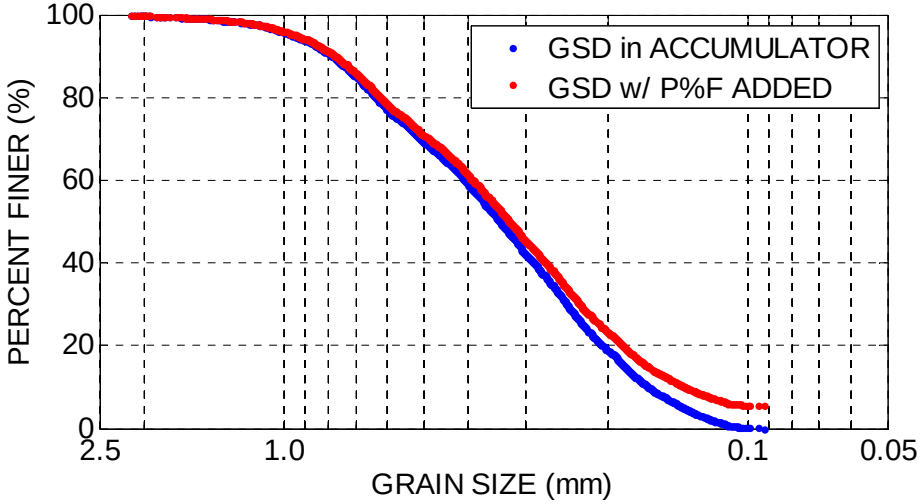

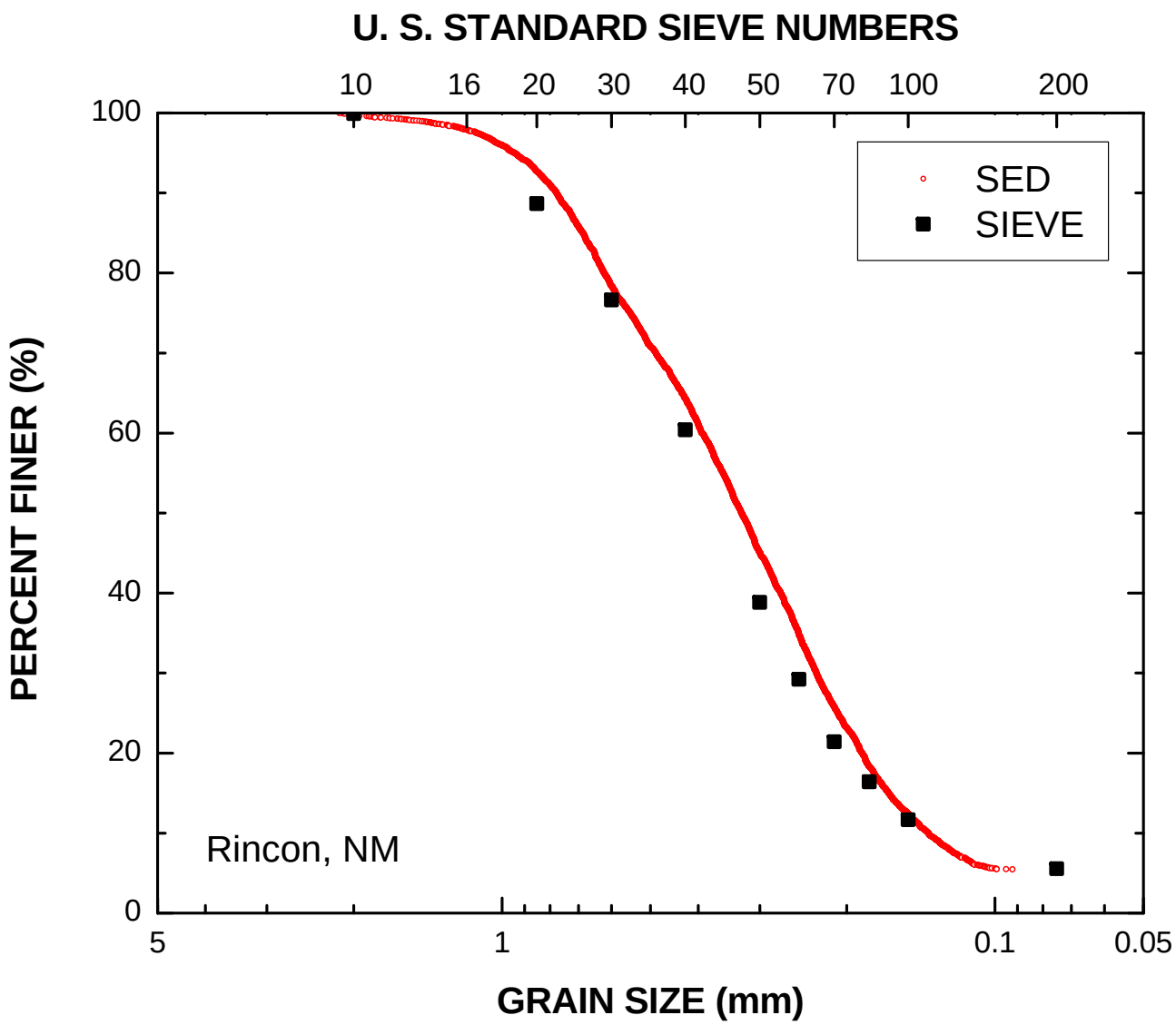
U. S. STANDARD SIEVE NUMBERS
10
16
20
30
40
50
70
100
200
100
80
60
40
20
0
PERCENT FINER (%)
SED
SIEVE
Rincon, NM
5
1
0.1
0.05
GRAIN SIZE (mm)

SEDIMAGING (SED) TEST

GEOTECHNICAL ENGINEERING

UNIVERSITY OF MICHIGAN

MATERIAL: Scotts Valley, CA

DATE TESTED: 13-Jun-2012 12:27:46

TESTED BY: Ohm, H.S.

D_{60} (mm): 0.31

D_{30} (mm): 0.25

D_{10} (mm): 0.21

C_u: 1.51

C_g: 1.00

PF (%): 0.0

MAGNIFICATION (pix/mm): 36.7

IMAGE SIZE (pix): 4256 x 1280

IMAGE SIZE (mm): 116.0 x 34.9

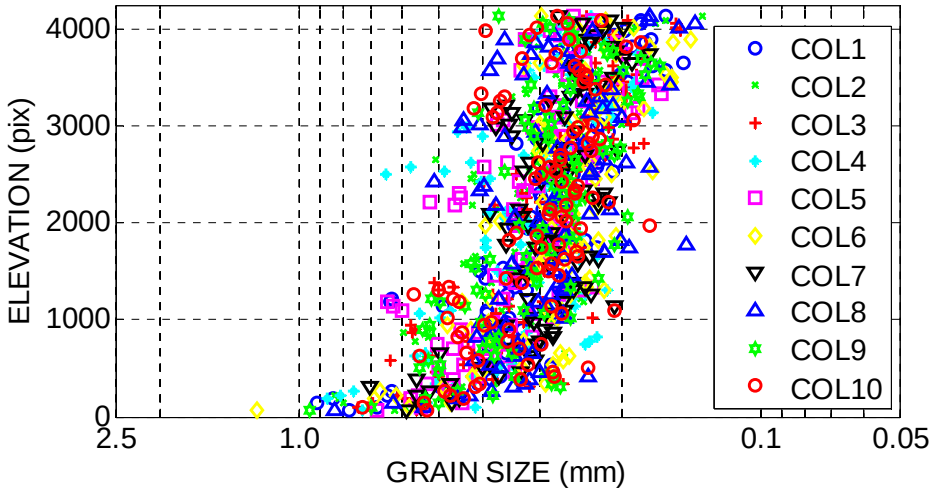

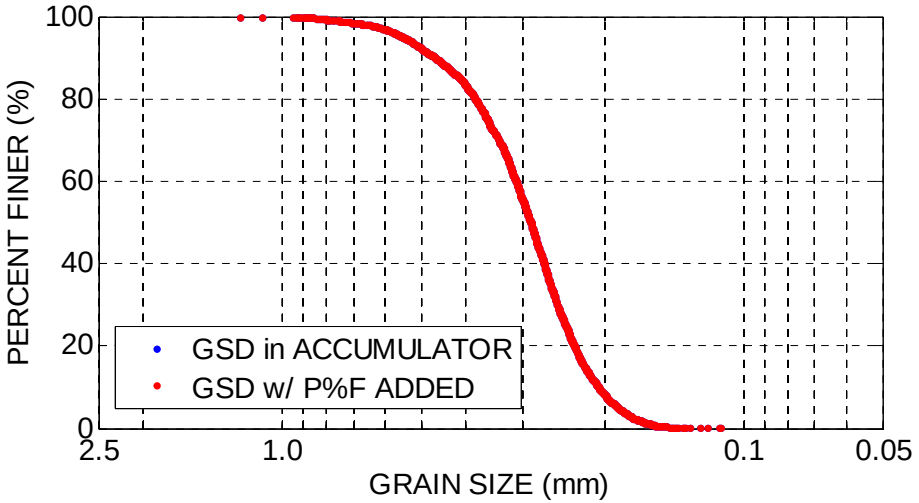

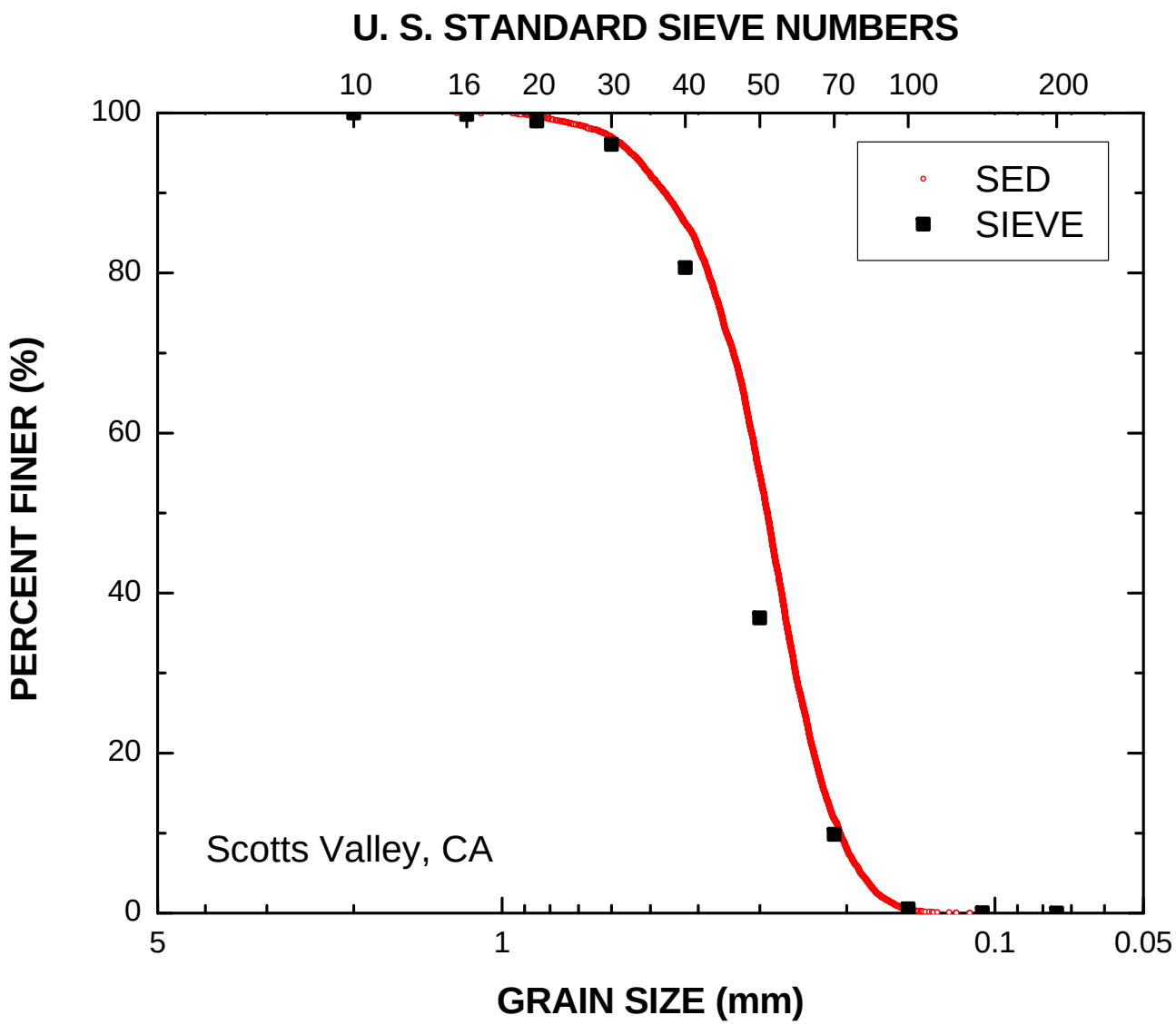
U. S. STANDARD SIEVE NUMBERS
10
16
20
30
40
50
70
100
200
100
80
60
40
20
0
PERCENT FINER (%)
SED
SIEVE
Scotts Valley, CA
5
1
0.1
0.05
GRAIN SIZE (mm)

SEDIMAGING (SED) TEST
GEOTECHNICAL ENGINEERING
UNIVERSITY OF MICHIGAN

MATERIAL: Upper Peninsula, MI
DATE TESTED: 01-May-2011 09:10:08
TESTED BY: Ohm, H.S.

D_{60} (mm): 0.58
D_{30} (mm): 0.31
D_{10} (mm): 0.20
C_u: 2.86
C_g: 0.84
PF (%): 0.0

MAGNIFICATION (pix/mm): 33.5
IMAGE SIZE (pix): 3360 x 1280
IMAGE SIZE (mm): 100.3 x 38.2

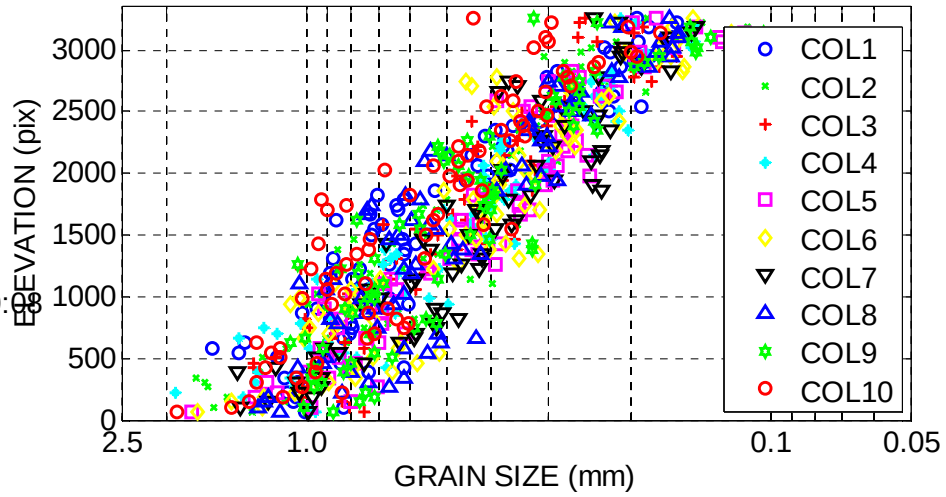

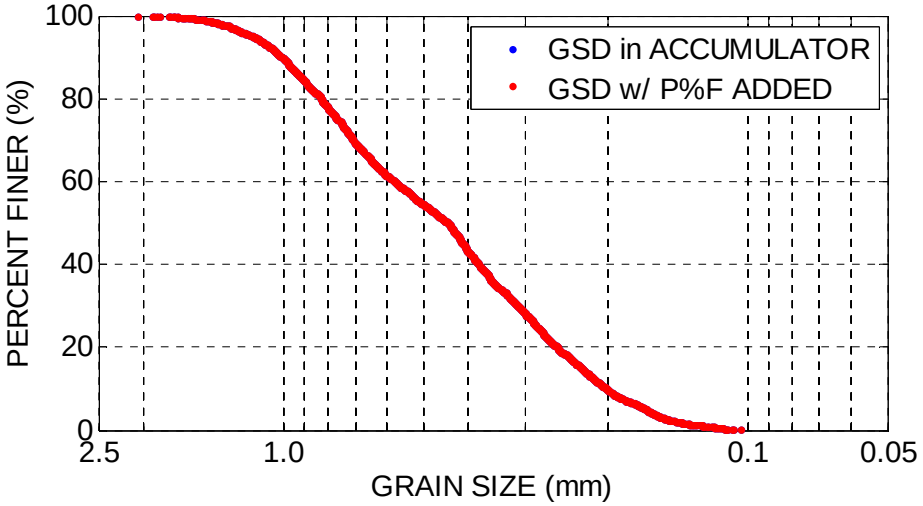

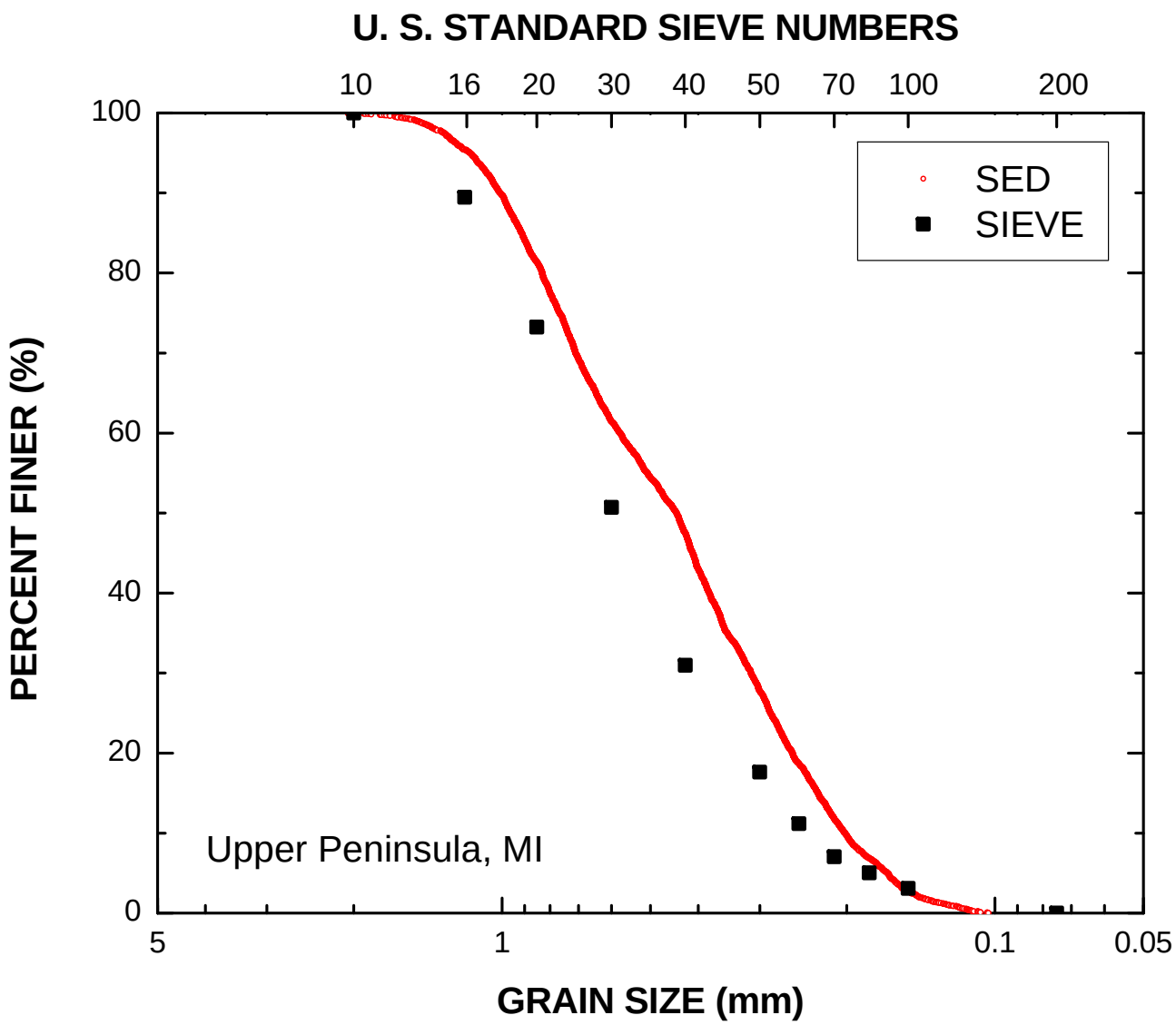
U. S. STANDARD SIEVE NUMBERS
10
16
20
30
40
50
70
100
200
100
80
60
40
20
0
PERCENT FINER (%)
SED
SIEVE
Upper Peninsula, MI
5
1
0.1
0.05
GRAIN SIZE (mm)

SEDIMAGING (SED) TEST

GEOTECHNICAL ENGINEERING

UNIVERSITY OF MICHIGAN

MATERIAL: S1

DATE TESTED: 21-Sep-2011 12:21:34

TESTED BY: Ohm, H.S.

D_{60} (mm): 0.62

D_{30} (mm): 0.42

D_{10} (mm): 0.30

C_u: 2.06

C_g: 0.95

PF (%): 0.1

MAGNIFICATION (pix/mm): 36.9

IMAGE SIZE (pix): 4512 x 1280

IMAGE SIZE (mm): 122.3 x 34.7

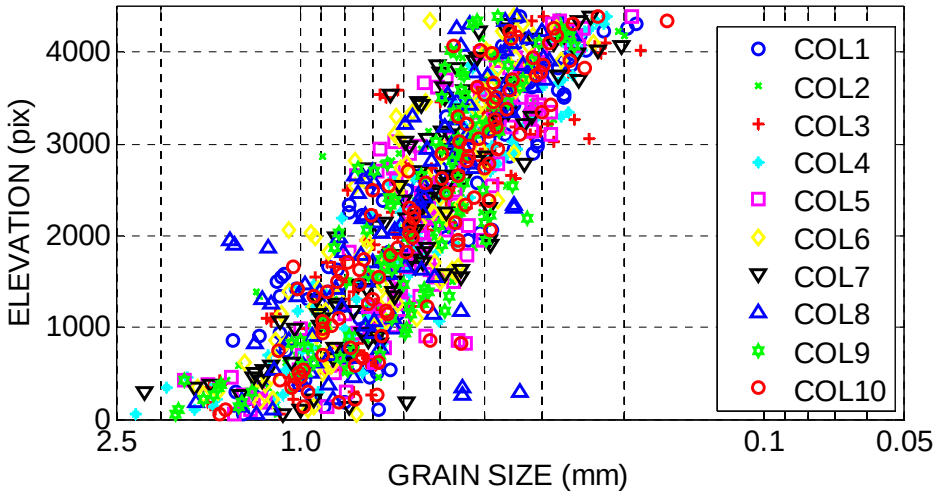

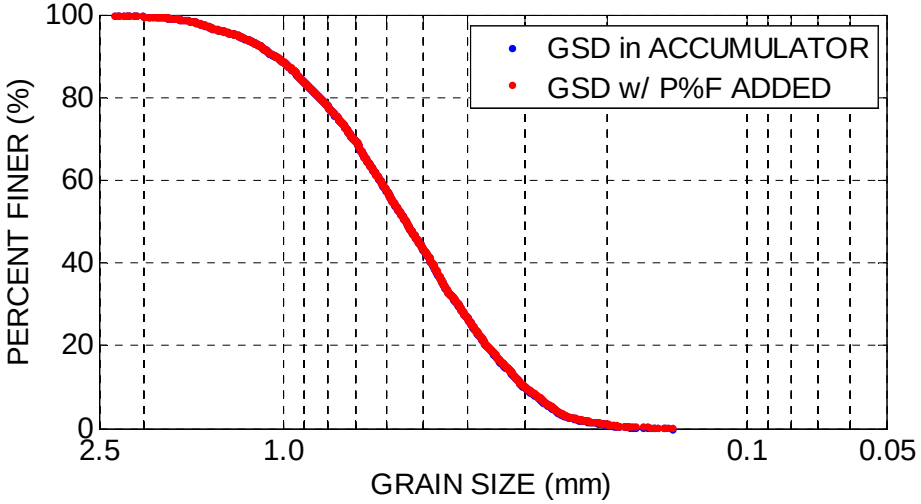

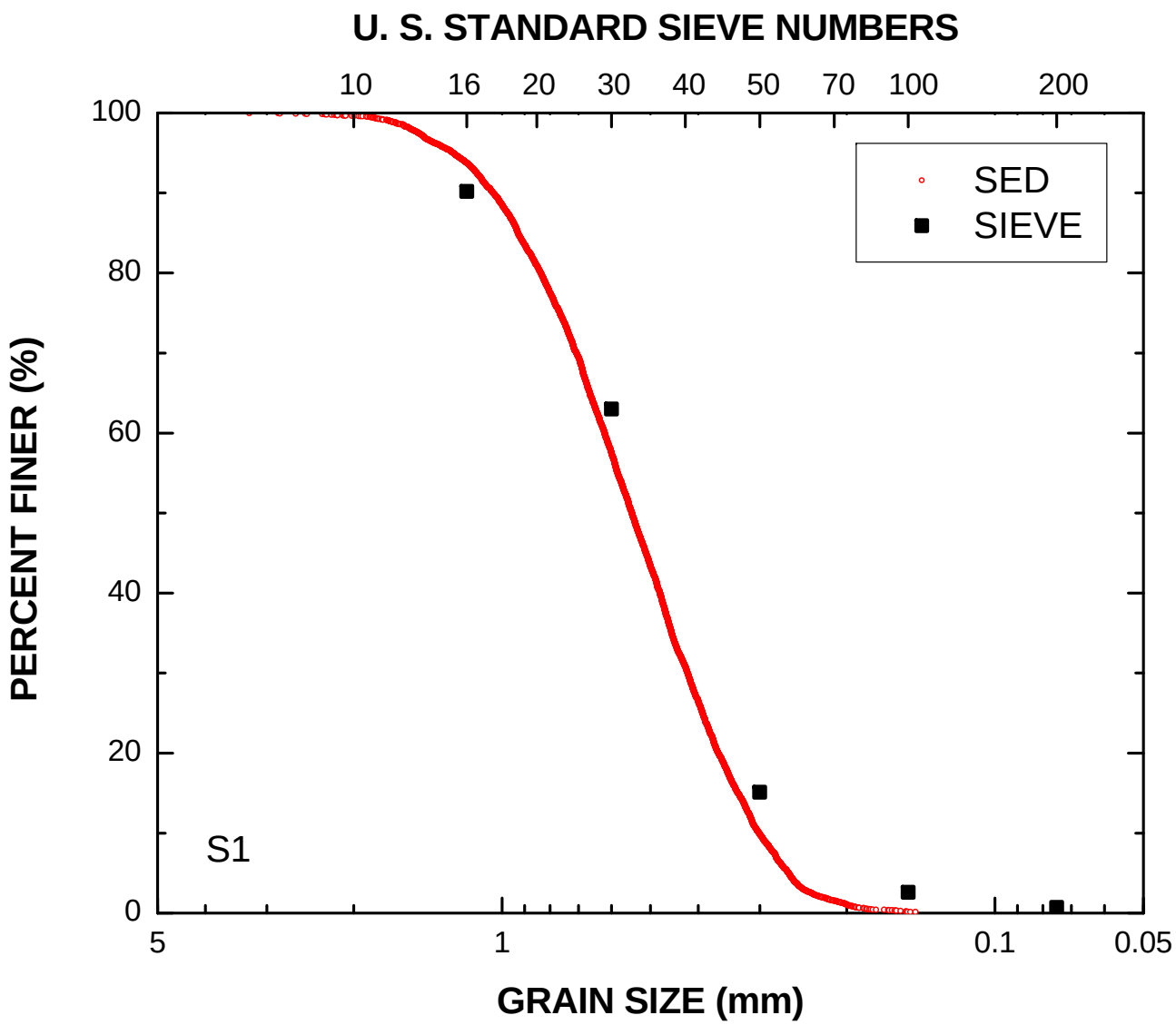
U. S. STANDARD SIEVE NUMBERS
10
16
20
30
40
50
70
100
200
100
80
60
40
20
0
PERCENT FINER (%)
SED
SIEVE
S1
5
1
0.1
0.05
GRAIN SIZE (mm)

SEDIMAGING (SED) TEST

GEOTECHNICAL ENGINEERING

UNIVERSITY OF MICHIGAN

MATERIAL: S2

DATE TESTED: 22-Sep-2011 15:38:54

TESTED BY: Ohm, H.S.

D_{60} (mm): 0.67

D_{30} (mm): 0.45

D_{10} (mm): 0.31

C_u: 2.15

C_g: 0.99

PF (%): 0.2

MAGNIFICATION (pix/mm): 36.9

IMAGE SIZE (pix): 4584 x 1280

IMAGE SIZE (mm): 124.2 x 34.7

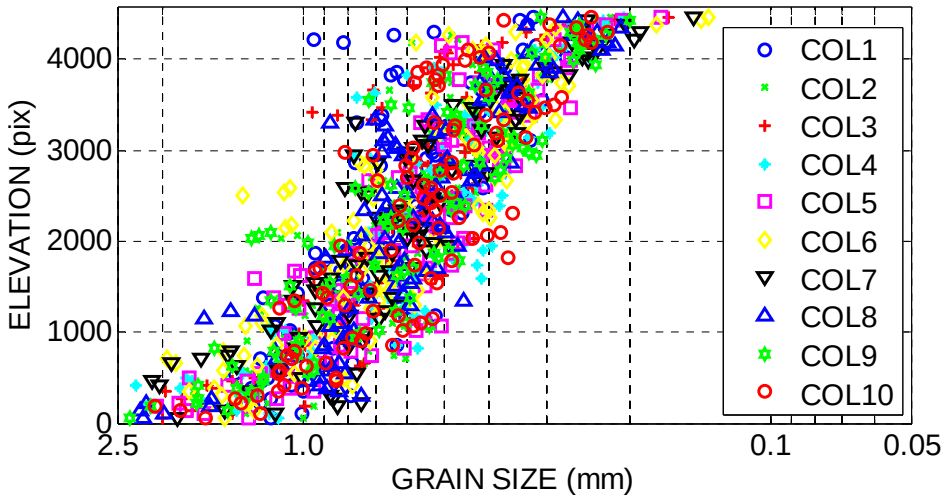

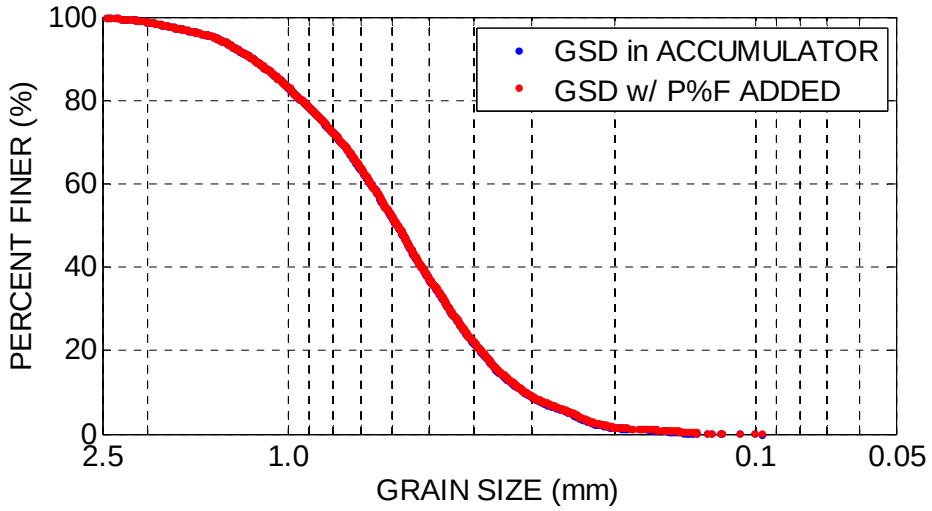

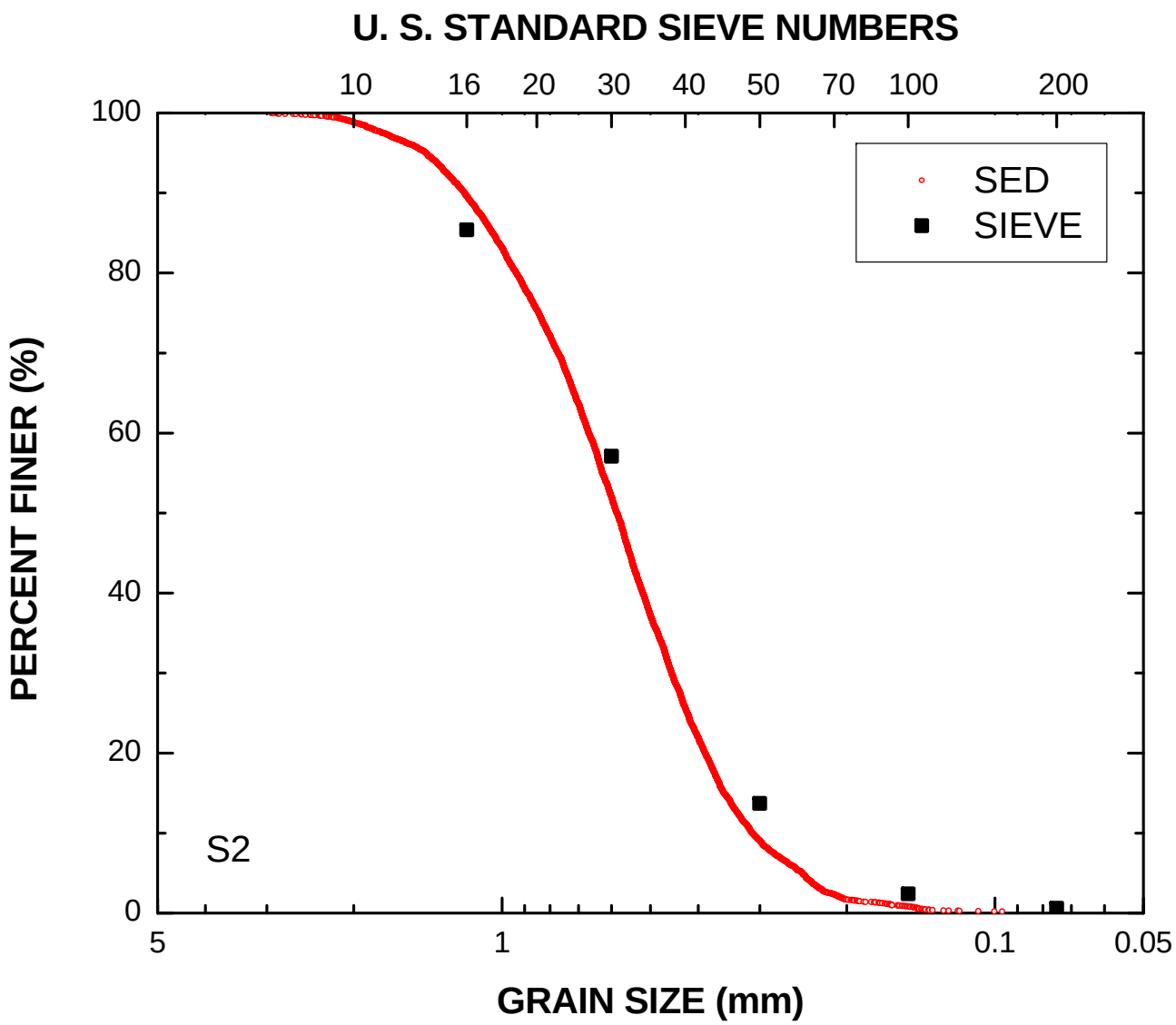
U. S. STANDARD SIEVE NUMBERS
10
16
20
30
40
50
70
100
200
100
80
60
40
20
0
PERCENT FINER (%)
SED
SIEVE
S2
5
1
0.1
0.05
GRAIN SIZE (mm)

SEDIMAGING (SED) TEST

GEOTECHNICAL ENGINEERING

UNIVERSITY OF MICHIGAN

MATERIAL: S3

DATE TESTED: 23-Sep-2011 10:53:24

TESTED BY: Ohm, H.S.

D_{60} (mm): 0.79

D_{30} (mm): 0.52

D_{10} (mm): 0.34

C_u: 2.28

C_g: 0.99

PF (%): 0.0

MAGNIFICATION (pix/mm): 36.9

IMAGE SIZE (pix): 4680 x 1280

IMAGE SIZE (mm): 126.8 x 34.7

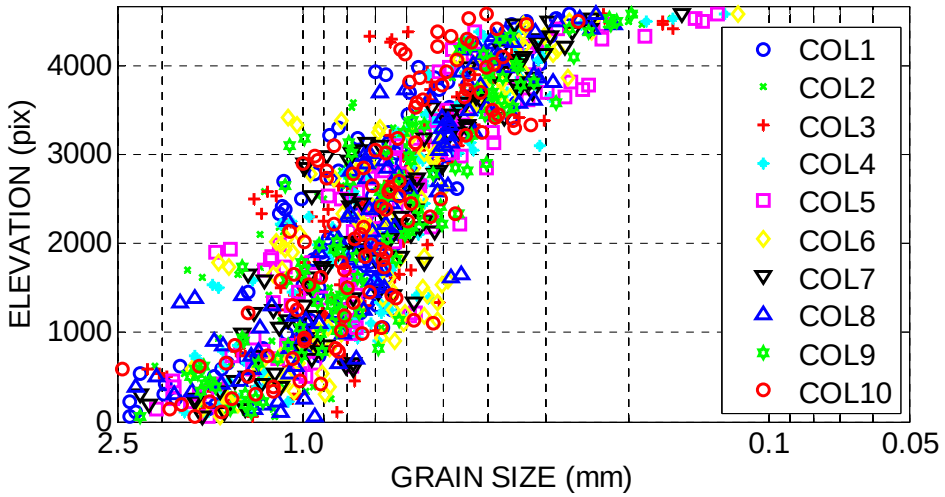

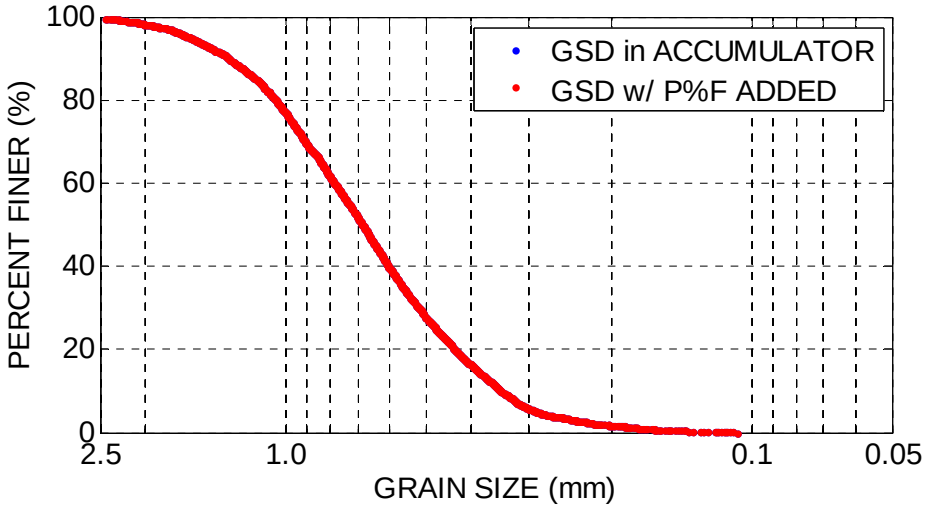

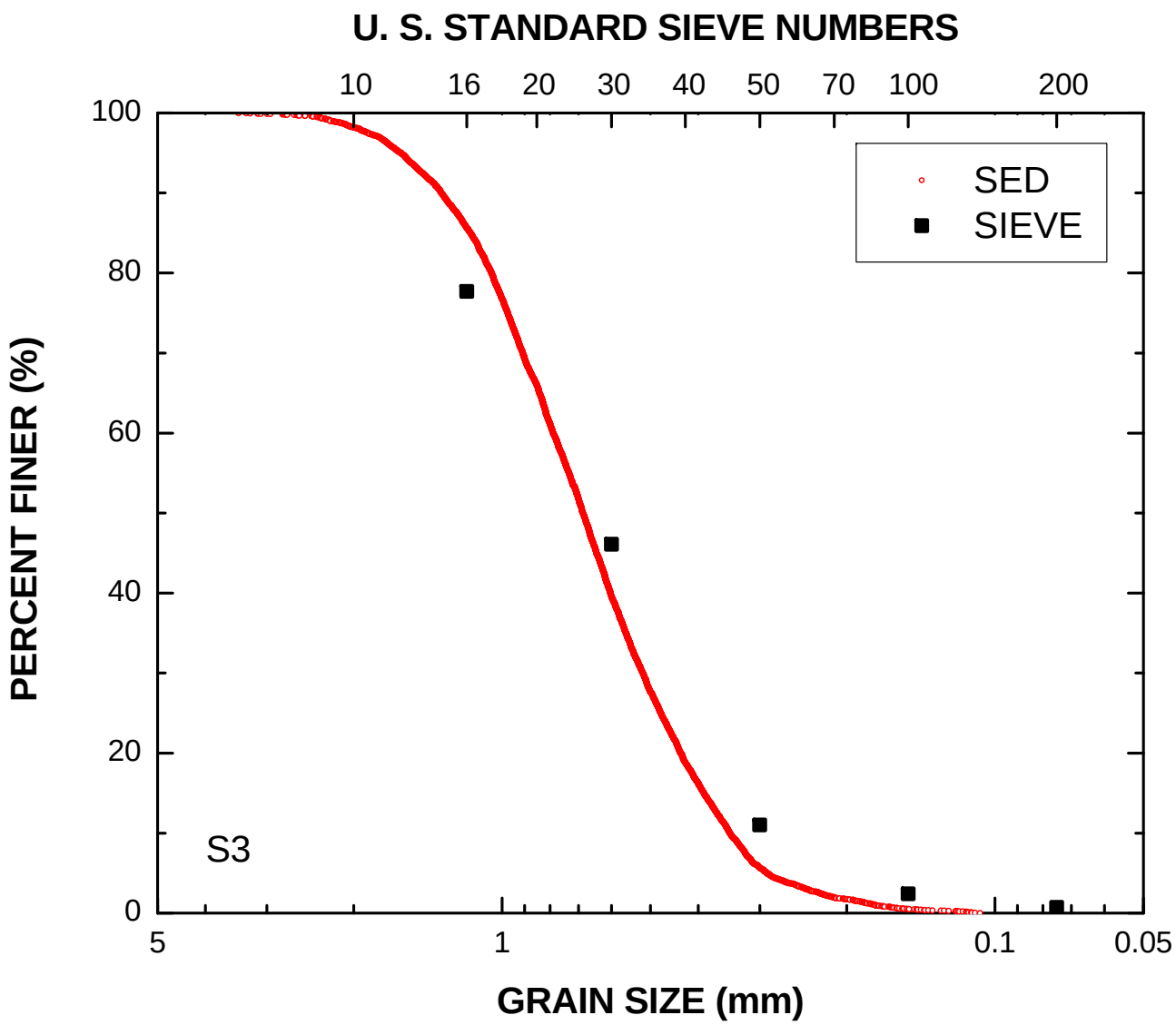
U. S. STANDARD SIEVE NUMBERS
10
16
20
30
40
50
70
100
200
100
80
60
40
20
0
PERCENT FINER (%)
SED
SIEVE
S3
5
1
0.1
0.05
GRAIN SIZE (mm)

SEDIMAGING (SED) TEST

GEOTECHNICAL ENGINEERING

UNIVERSITY OF MICHIGAN

MATERIAL: S4

DATE TESTED: 23-Sep-2011 10:23:34

TESTED BY: Ohm, H.S.

D_{60} (mm): 0.70

D_{30} (mm): 0.47

D_{10} (mm): 0.29

C_u: 2.39

C_g: 1.07

PF (%): 0.8

MAGNIFICATION (pix/mm): 36.9

IMAGE SIZE (pix): 4672 x 1280

IMAGE SIZE (mm): 126.6 x 34.7

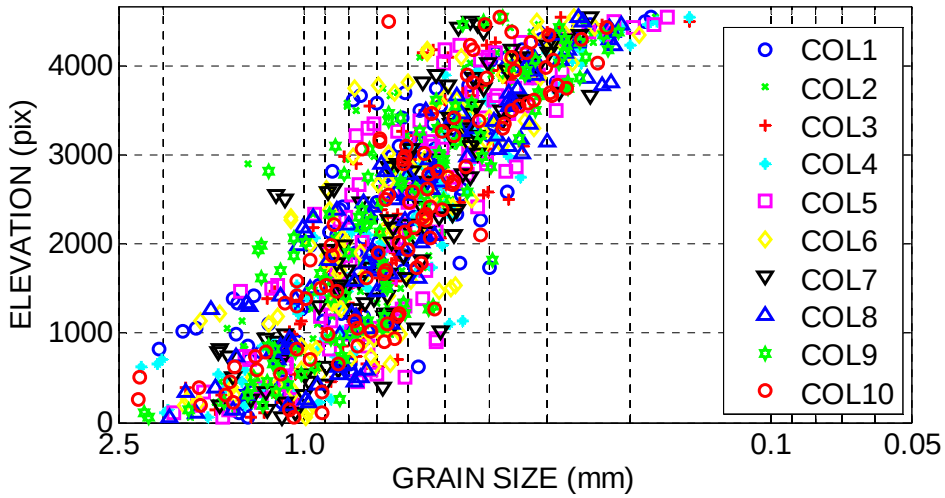

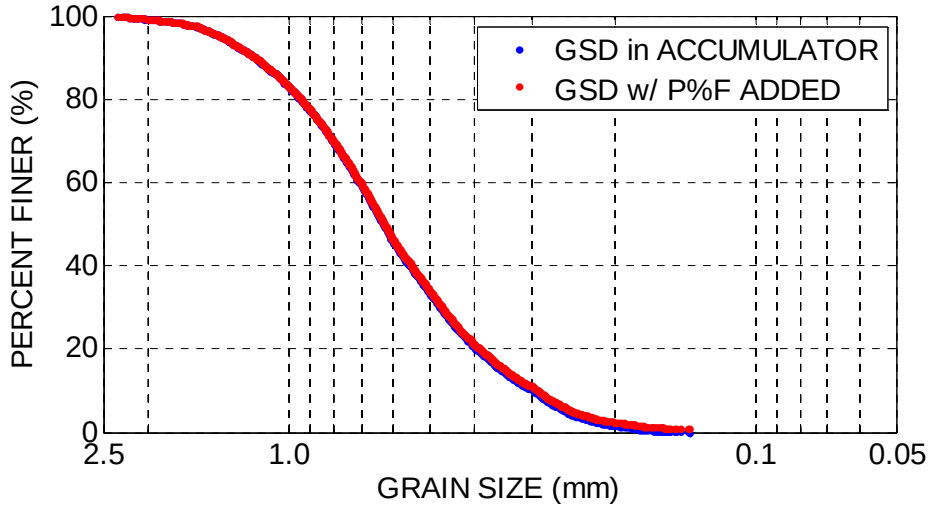

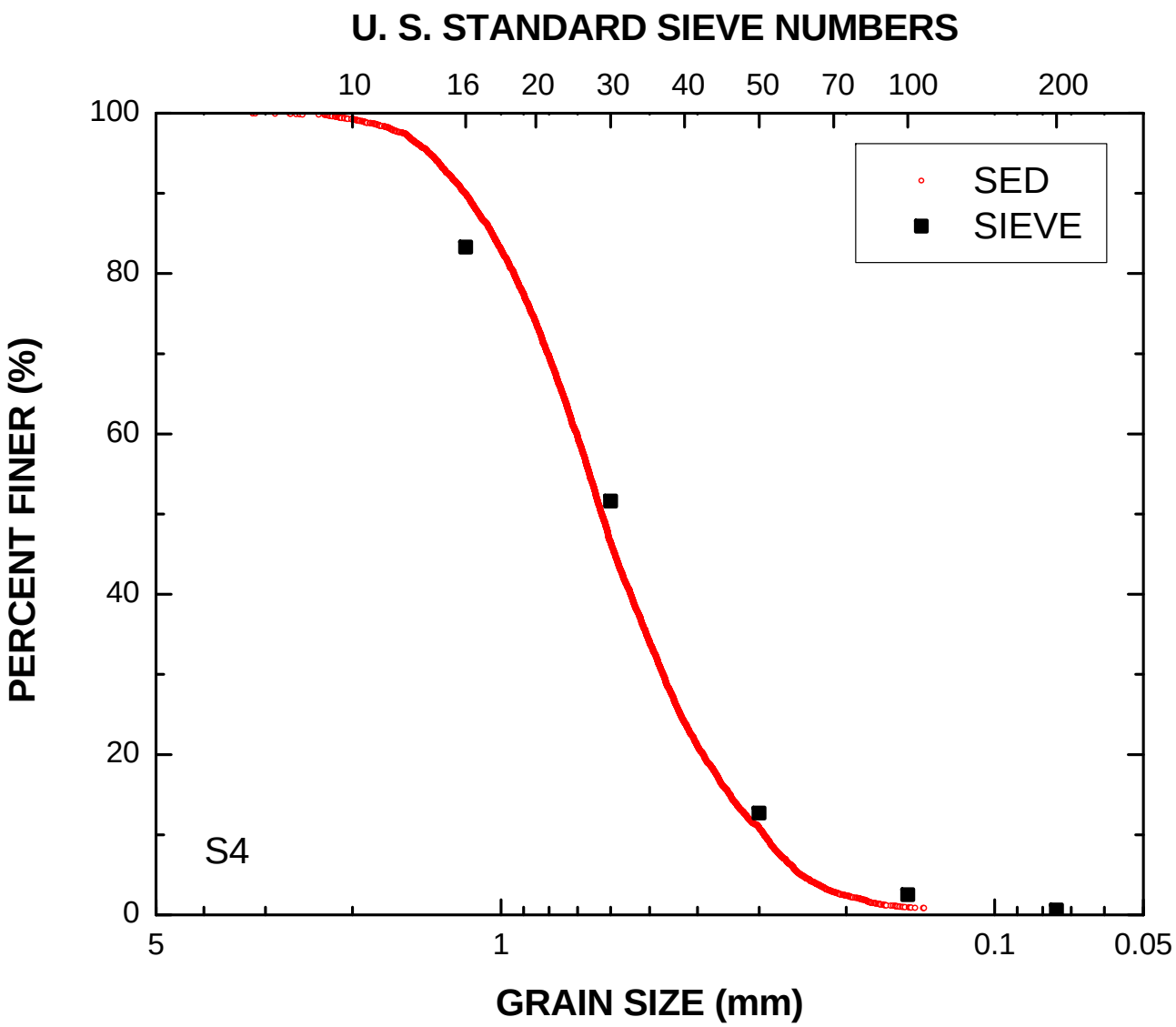
U. S. STANDARD SIEVE NUMBERS
10
16
20
30
40
50
70
100
200
100
80
60
40
20
0
PERCENT FINER (%)
SED
SIEVE
S4
5
1
0.1
0.05
GRAIN SIZE (mm)

SEDIMAGING (SED) TEST

GEOTECHNICAL ENGINEERING

UNIVERSITY OF MICHIGAN

MATERIAL: S4

DATE TESTED: 23-Sep-2011 10:23:34

TESTED BY: Ohm, H.S.

D_{60} (mm): 0.70

D_{30} (mm): 0.47

D_{10} (mm): 0.29

C_u: 2.39

C_g: 1.07

PF (%): 0.8

MAGNIFICATION (pix/mm): 36.9

IMAGE SIZE (pix): 4672 x 1280

IMAGE SIZE (mm): 126.6 x 34.7

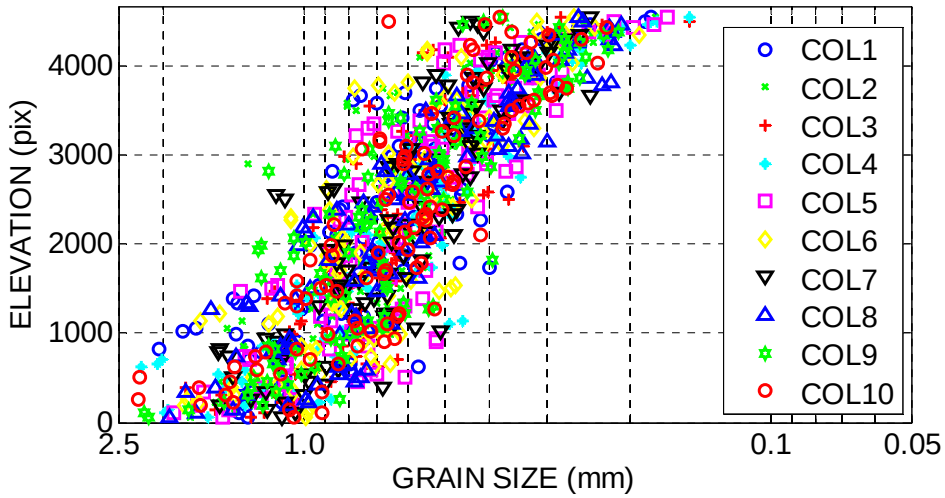

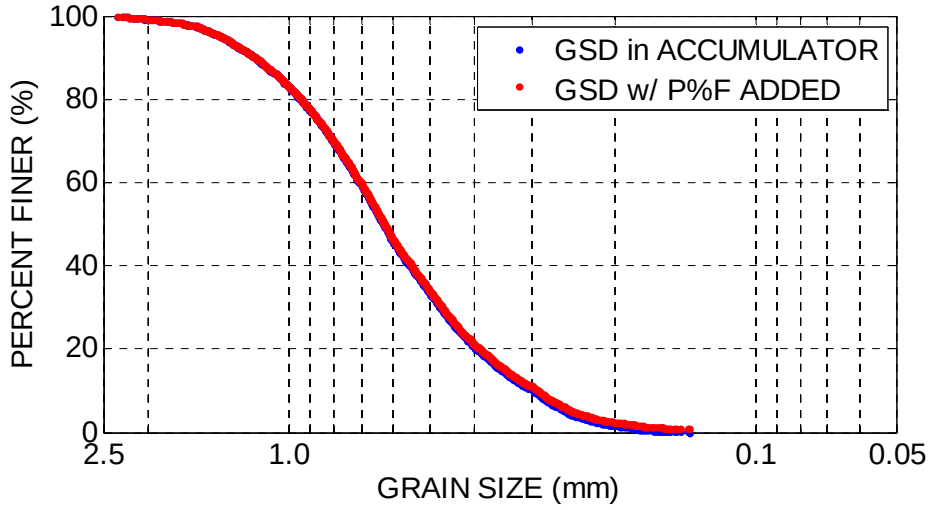

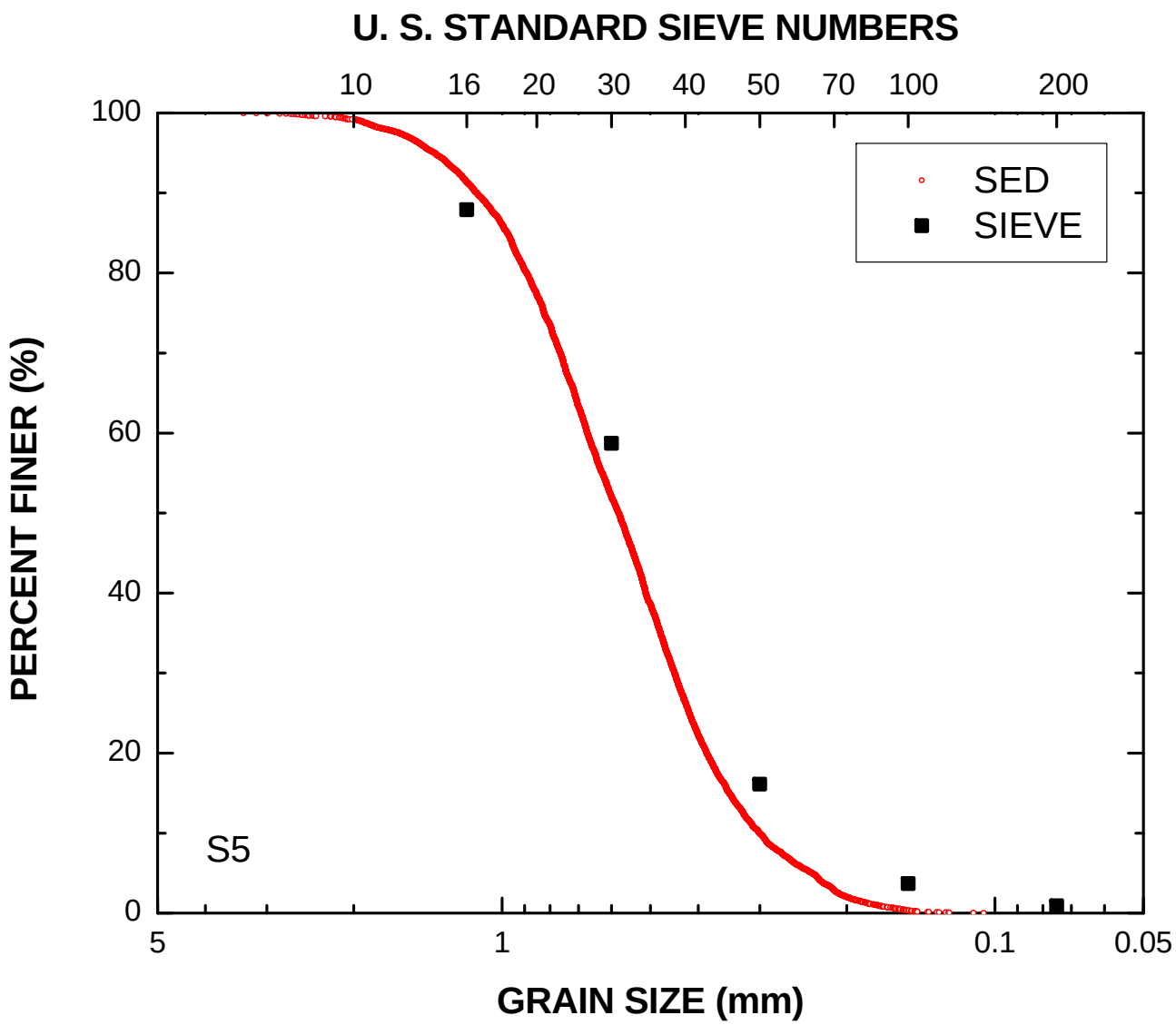
U. S. STANDARD SIEVE NUMBERS
10
16
20
30
40
50
70
100
200
100
80
60
40
20
0
PERCENT FINER (%)
SED
SIEVE
S5
5
1
0.1
0.05
GRAIN SIZE (mm)

SEDIMAGING (SED) TEST

GEOTECHNICAL ENGINEERING

UNIVERSITY OF MICHIGAN

MATERIAL: S6

DATE TESTED: 23-Sep-2011 11:58:32

TESTED BY: Ohm, H.S.

D_{60} (mm): 0.76

D_{30} (mm): 0.52

D_{10} (mm): 0.33

C_u: 2.28

C_g: 1.05

PF (%): 0.1

MAGNIFICATION (pix/mm): 36.9

IMAGE SIZE (pix): 4760 x 1280

IMAGE SIZE (mm): 129.0 x 34.7

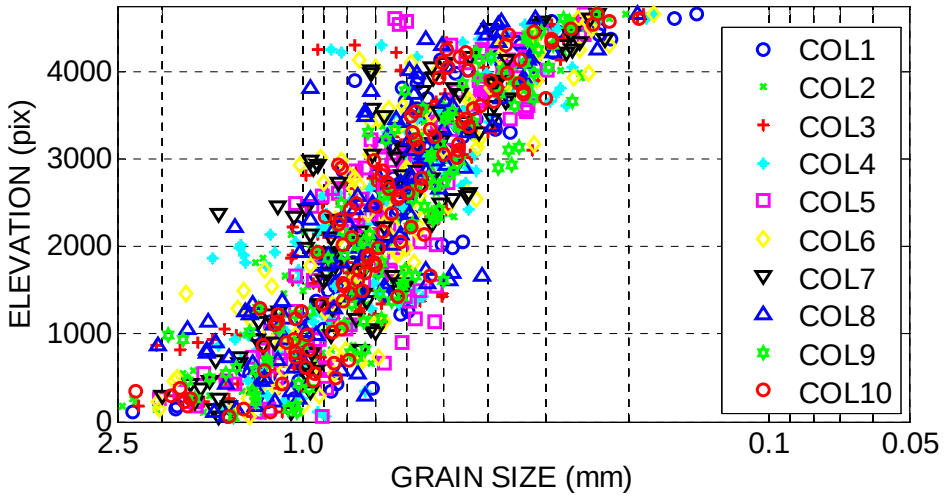

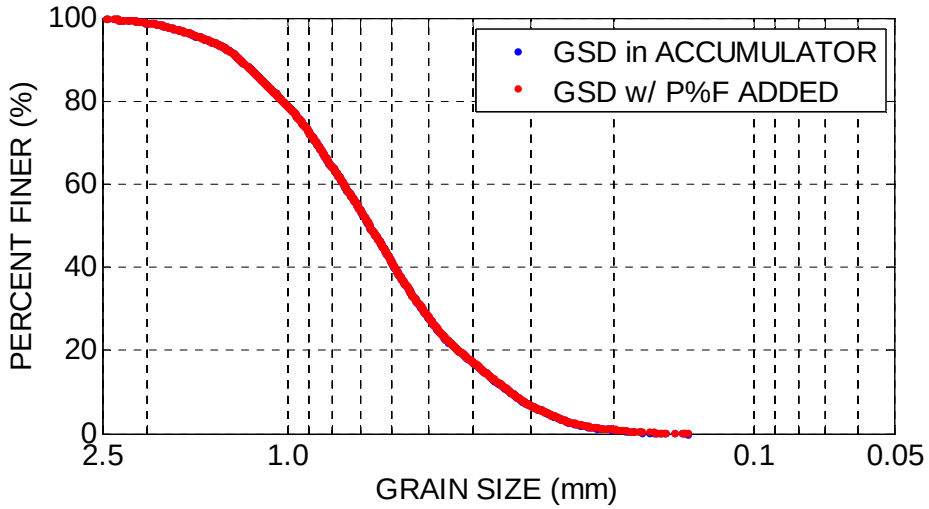

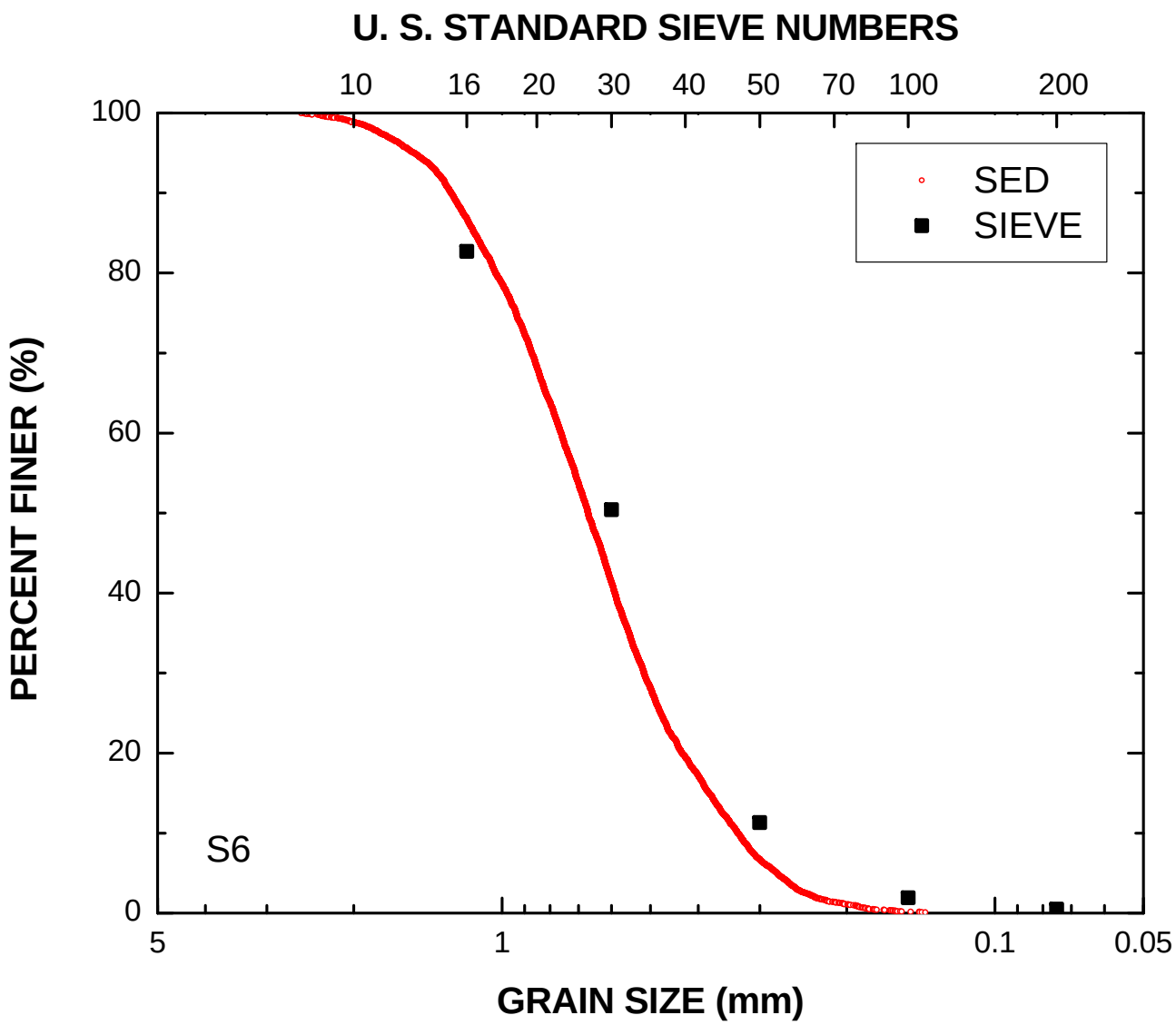
U. S. STANDARD SIEVE NUMBERS
10
16
20
30
40
50
70
100
200
100
80
60
40
20
0
PERCENT FINER (%)
SED
SIEVE
S6
5
1
0.1
0.05
GRAIN SIZE (mm)

SEDIMAGING (SED) TEST
GEOTECHNICAL ENGINEERING
UNIVERSITY OF MICHIGAN

MATERIAL: S7
DATE TESTED: 22-Sep-2011 12:50:34
TESTED BY: Ohm, H.S.

D_{60} (mm): 0.78
D_{30} (mm): 0.52
D_{10} (mm): 0.34
C_u: 2.29
C_g: 1.02
PF (%): 0.1

MAGNIFICATION (pix/mm): 36.9
IMAGE SIZE (pix): 4568 x 1280
IMAGE SIZE (mm): 123.8 x 34.7

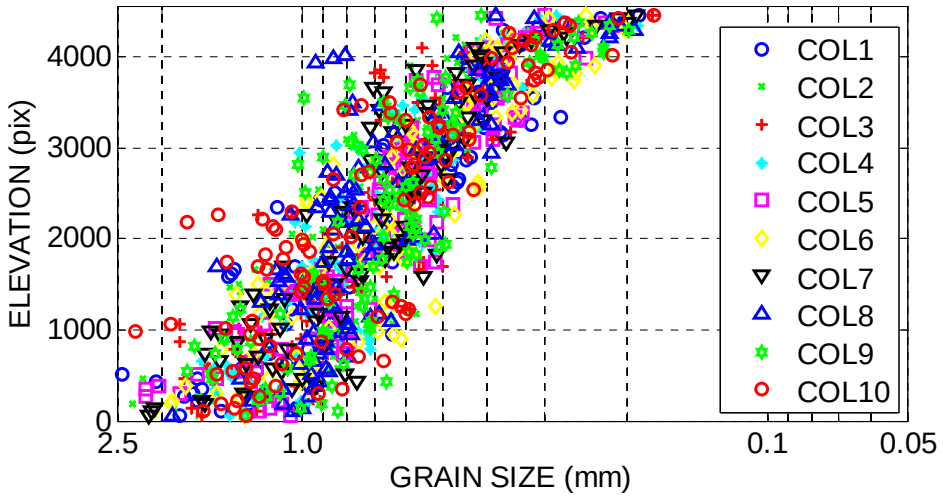

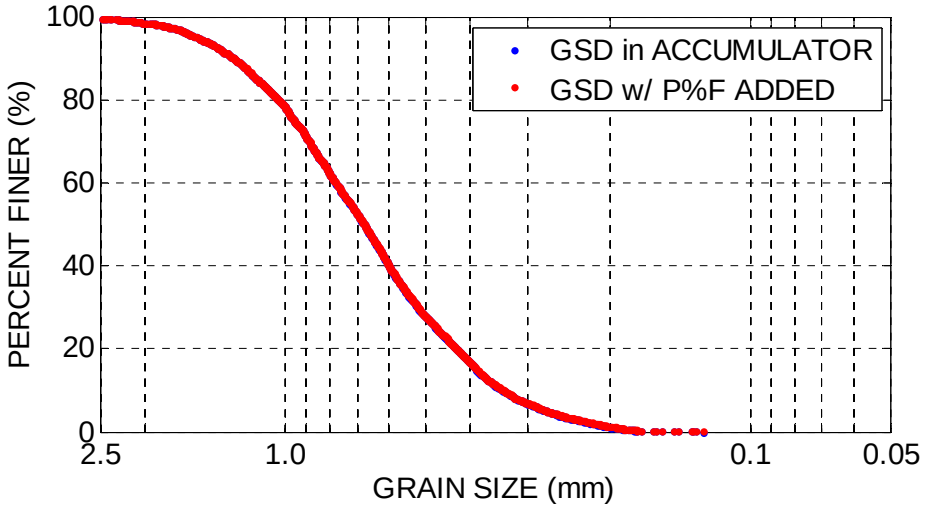

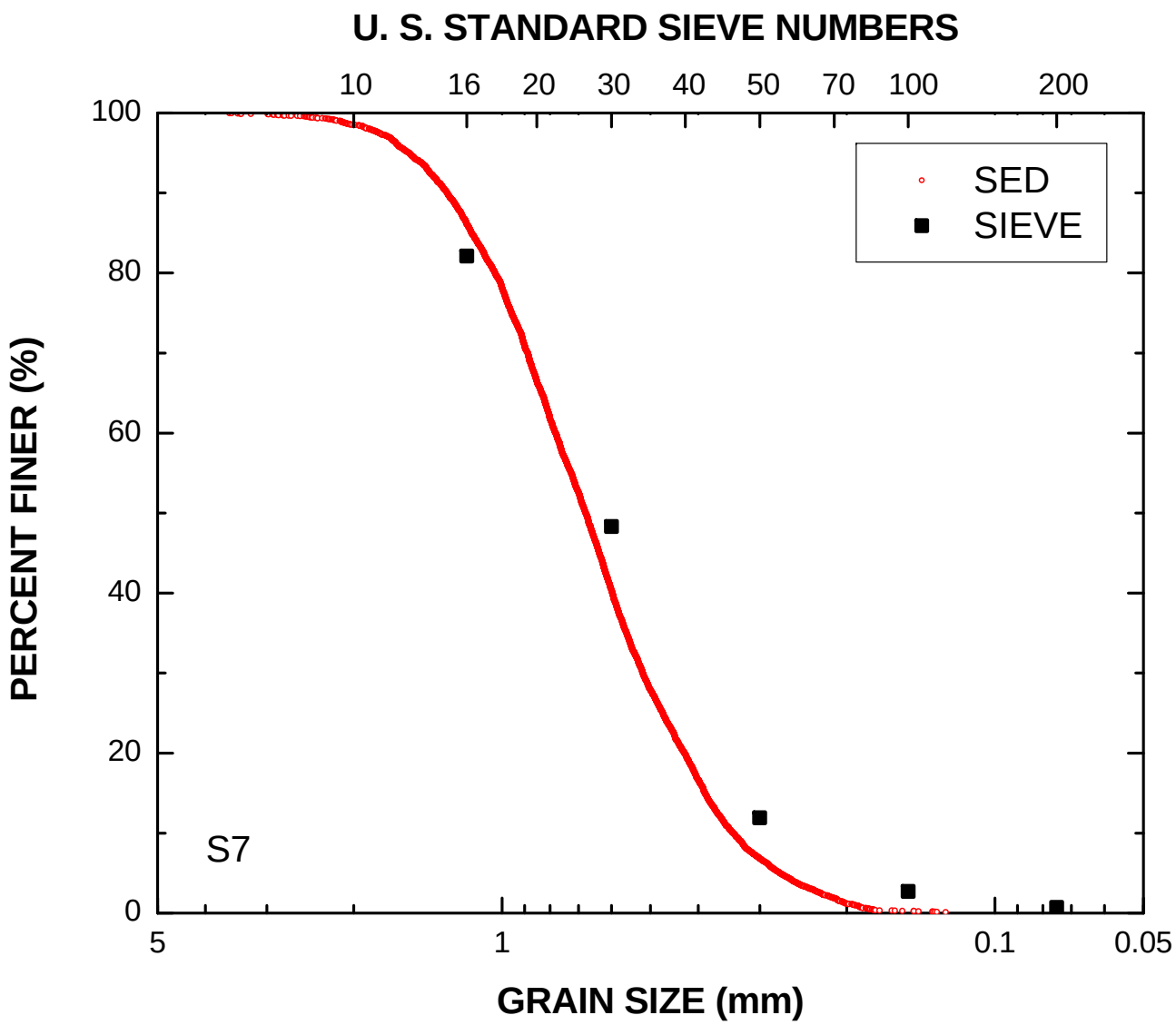
U. S. STANDARD SIEVE NUMBERS
10
16
20
30
40
50
70
100
200
100
80
60
40
20
0
PERCENT FINER (%)
SED
SIEVE
S7
5
1
0.1
0.05
GRAIN SIZE (mm)

SEDIMAGING (SED) TEST

GEOTECHNICAL ENGINEERING

UNIVERSITY OF MICHIGAN

MATERIAL: S8

DATE TESTED: 23-Sep-2011 11:24:14

TESTED BY: Ohm, H.S.

D_{60} (mm): 0.76

D_{30} (mm): 0.50

D_{10} (mm): 0.31

C_u: 2.43

C_g: 1.04

PF (%): 0.0

MAGNIFICATION (pix/mm): 36.9

IMAGE SIZE (pix): 4728 x 1280

IMAGE SIZE (mm): 128.1 x 34.7

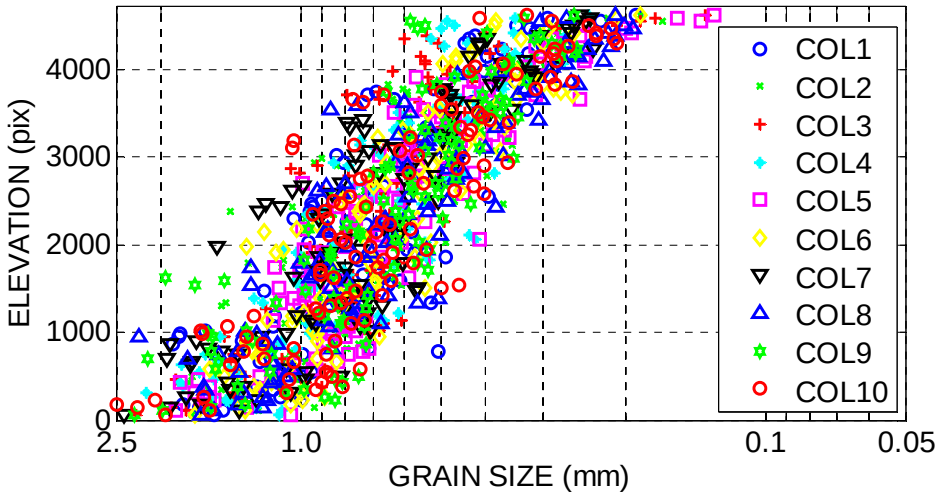

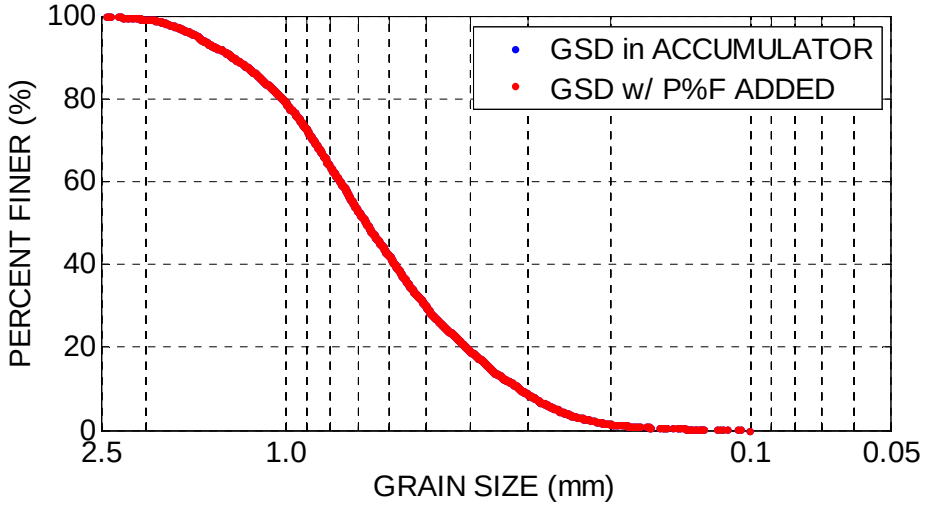

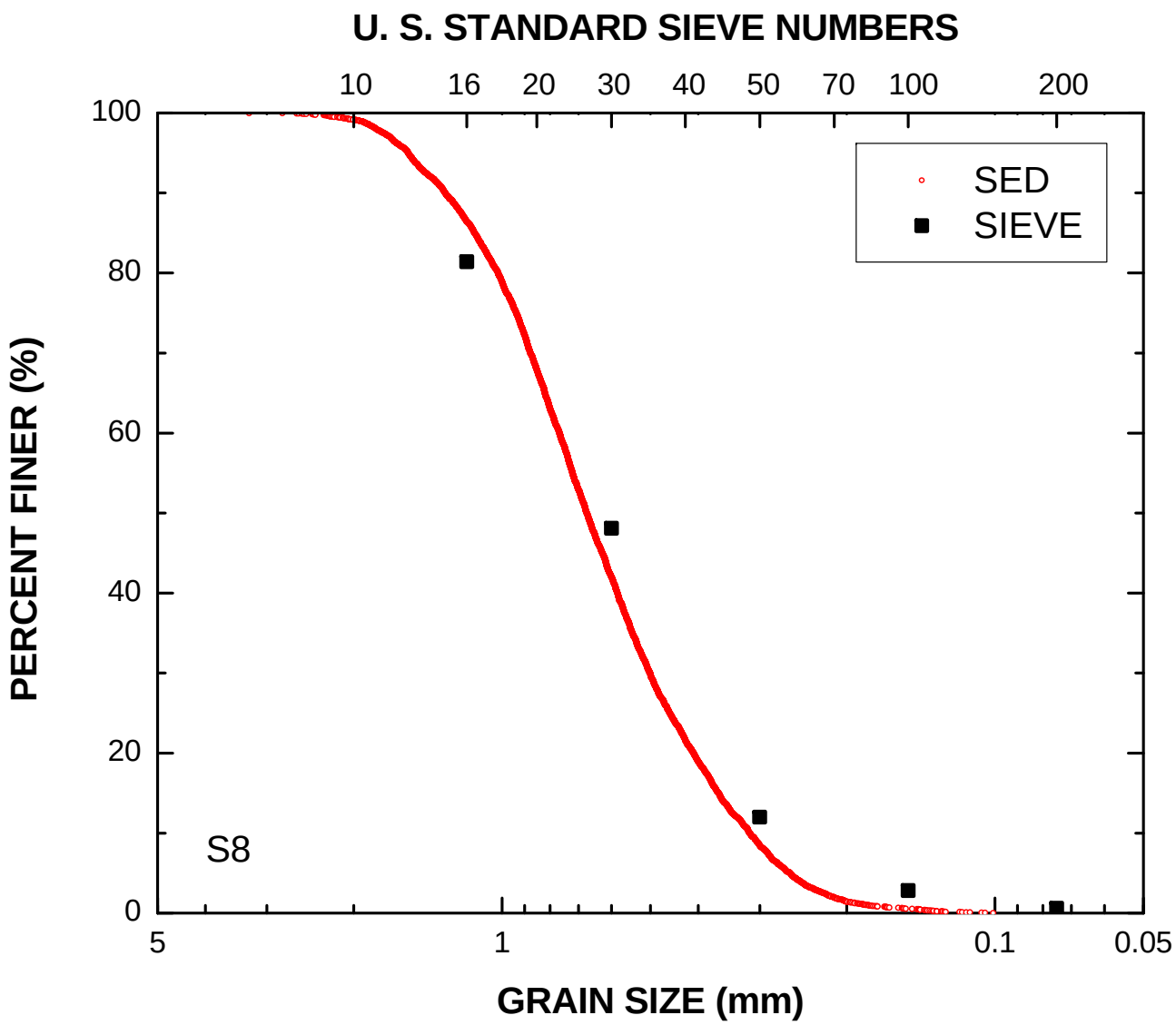
U. S. STANDARD SIEVE NUMBERS
10
16
20
30
40
50
70
100
200
100
80
60
40
20
0
PERCENT FINER (%)
SED
SIEVE
S8
5
1
0.1
0.05
GRAIN SIZE (mm)

SEDIMAGING (SED) TEST
GEOTECHNICAL ENGINEERING
UNIVERSITY OF MICHIGAN

MATERIAL: S9
DATE TESTED: 23-Sep-2011 12:30:08
TESTED BY: Ohm, H.S.

D_{60} (mm): 0.88
D_{30} (mm): 0.57
D_{10} (mm): 0.39
C_u: 2.26
C_g: 0.96
PF (%): 0.0

MAGNIFICATION (pix/mm): 36.9
IMAGE SIZE (pix): 4808 x 1280
IMAGE SIZE (mm): 130.3 x 34.7

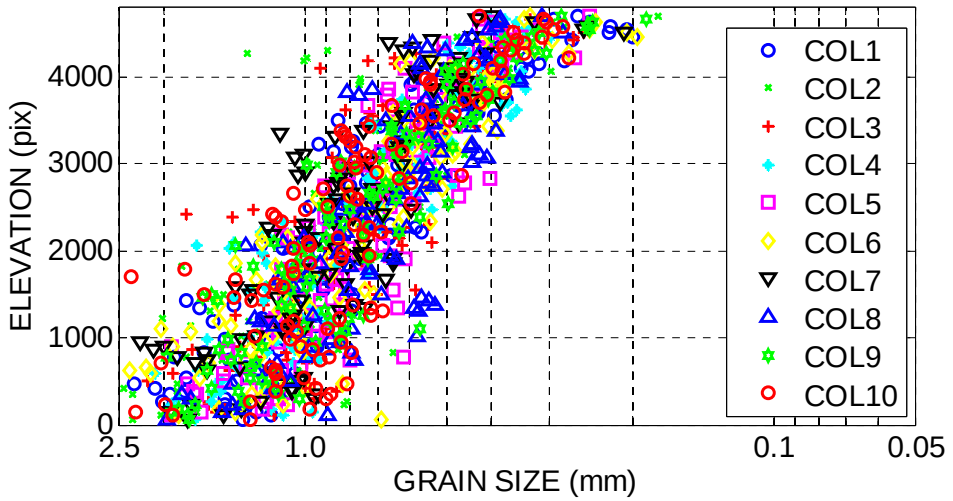

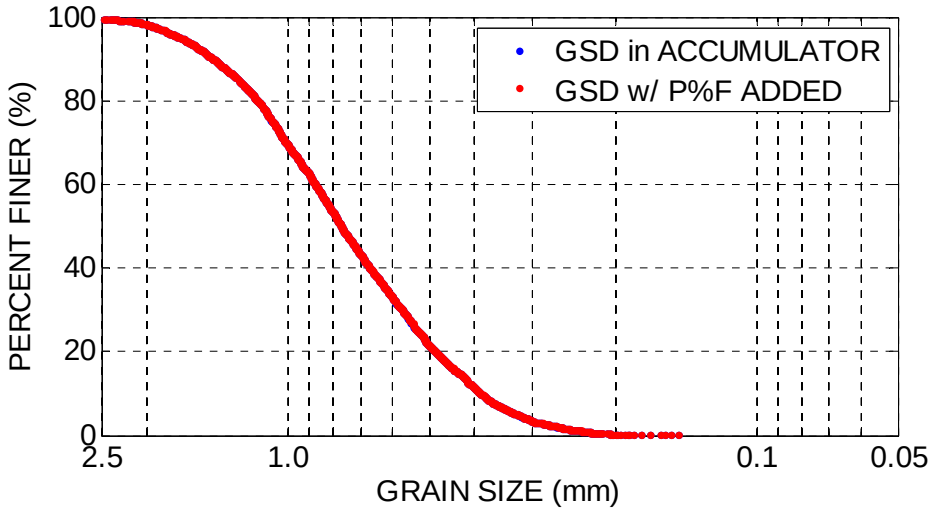

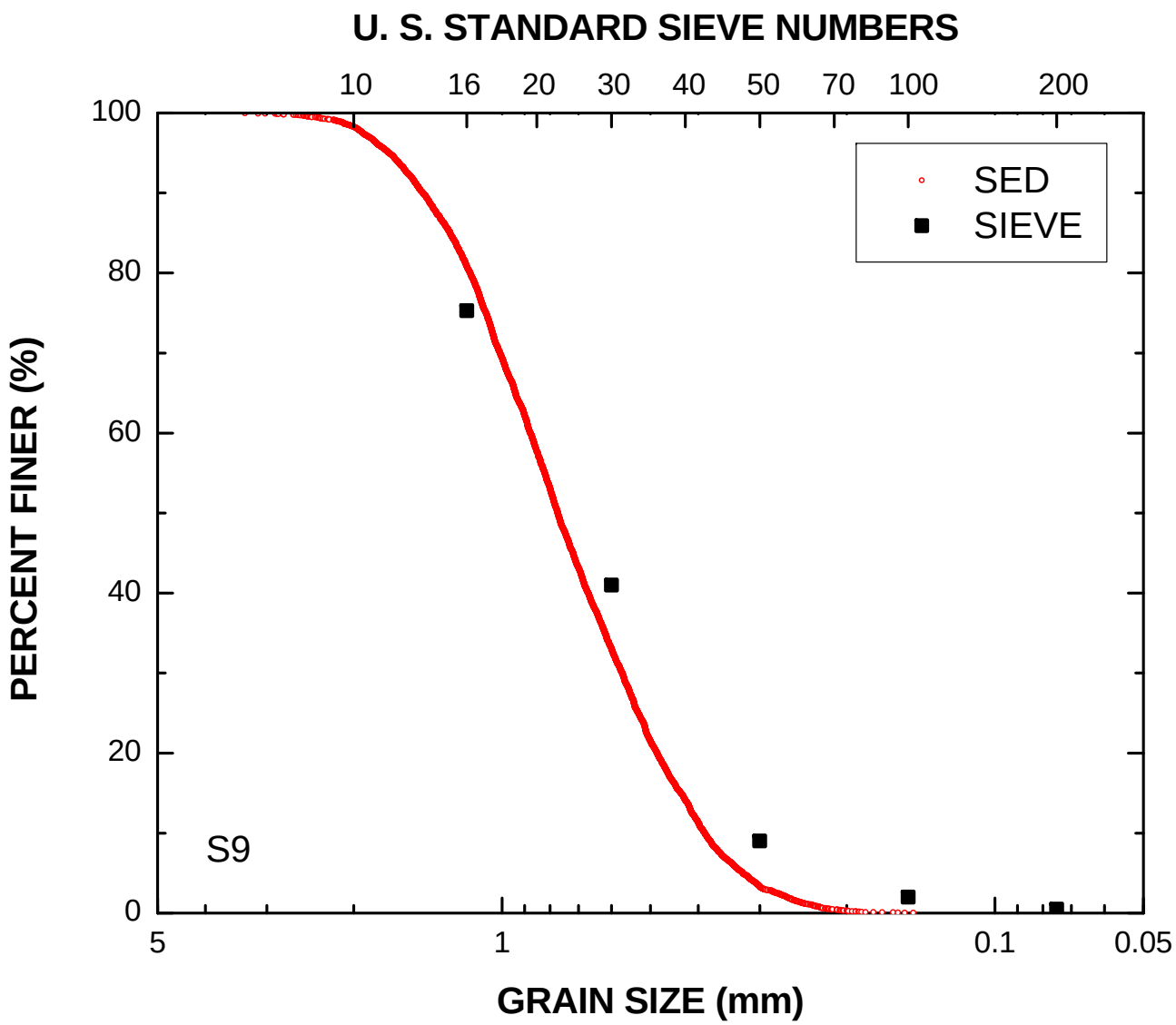
U. S. STANDARD SIEVE NUMBERS
10
16
20
30
40
50
70
100
200
100
80
60
40
20
0
PERCENT FINER (%)
SED
SIEVE
S9
5
1
0.1
0.05
GRAIN SIZE (mm)

SEDIMAGING (SED) TEST
GEOTECHNICAL ENGINEERING
UNIVERSITY OF MICHIGAN

MATERIAL: S10
DATE TESTED: 21-Sep-2011 16:31:40
TESTED BY: Ohm, H.S.

D_{60} (mm): 0.82
D_{30} (mm): 0.55
D_{10} (mm): 0.34
C_u: 2.45
C_g: 1.08
PF (%): 0.0

MAGNIFICATION (pix/mm): 36.9
IMAGE SIZE (pix): 4544 x 1280
IMAGE SIZE (mm): 123.1 x 34.7

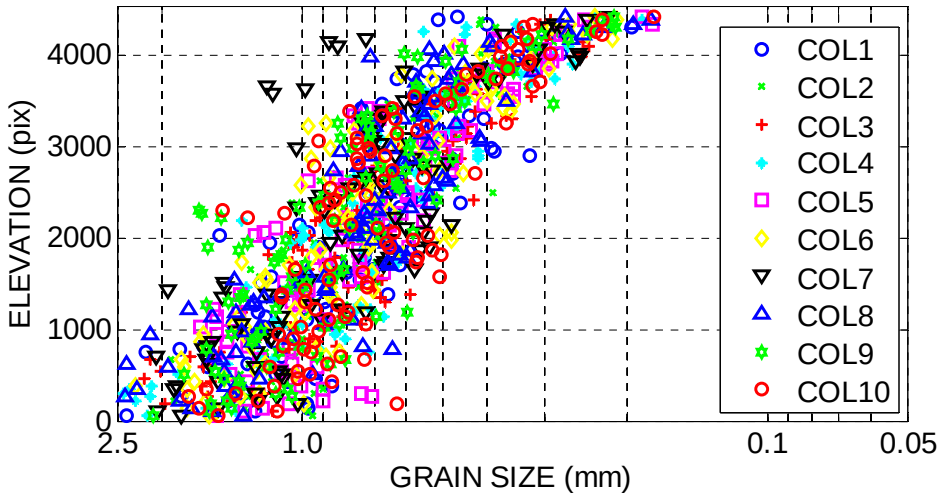

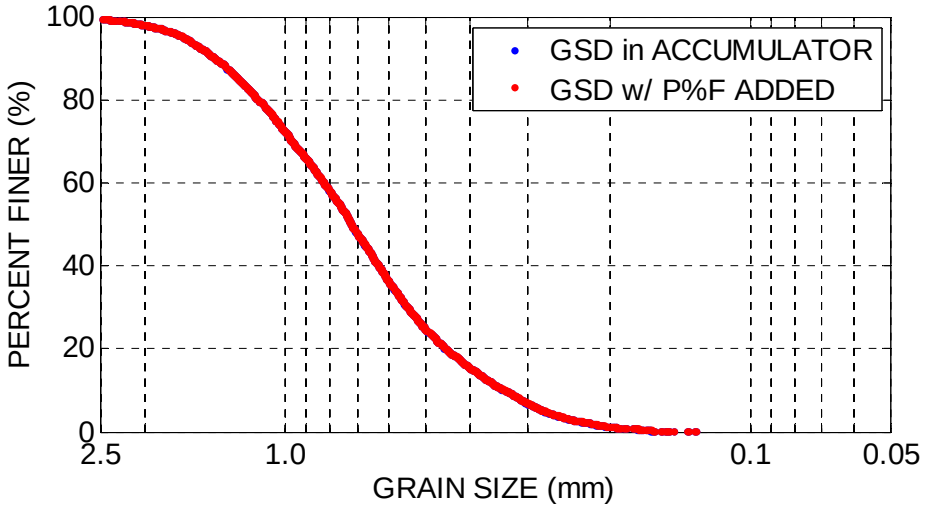

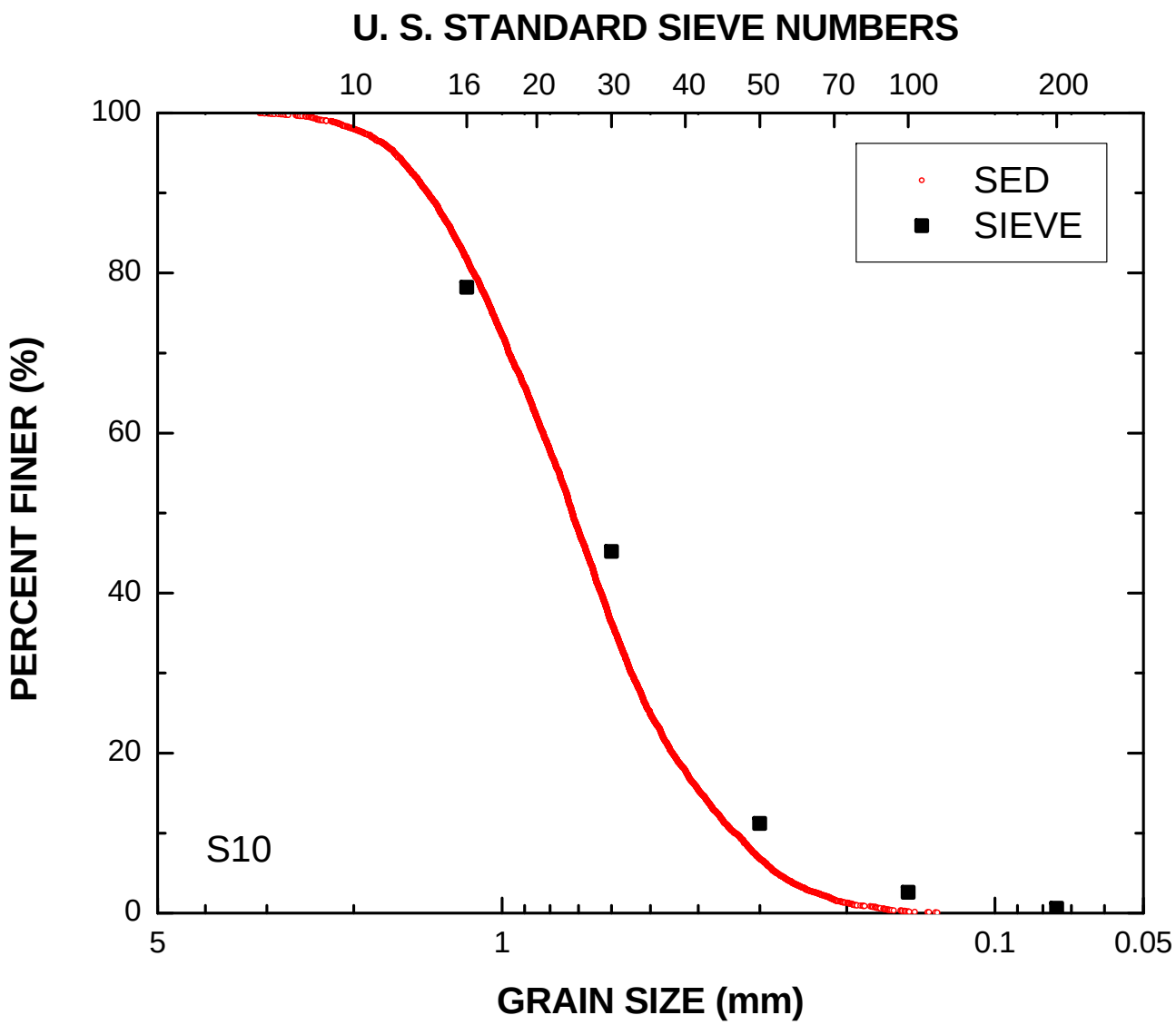
U. S. STANDARD SIEVE NUMBERS
10
16
20
30
40
50
70
100
200
100
80
60
40
20
0
PERCENT FINER (%)
SED
SIEVE
S10
5
1
0.1
0.05
GRAIN SIZE (mm)

SEDIMAGING (SED) TEST
GEOTECHNICAL ENGINEERING
UNIVERSITY OF MICHIGAN

MATERIAL: S11
DATE TESTED: 21-Sep-2011 15:55:26
TESTED BY: Ohm, H.S.

D_{60} (mm): 0.70
D_{30} (mm): 0.36
D_{10} (mm): 0.23
C_u: 3.05
C_g: 0.80
PF (%): 0.4

MAGNIFICATION (pix/mm): 36.9
IMAGE SIZE (pix): 4488 x 1280
IMAGE SIZE (mm): 121.6 x 34.7

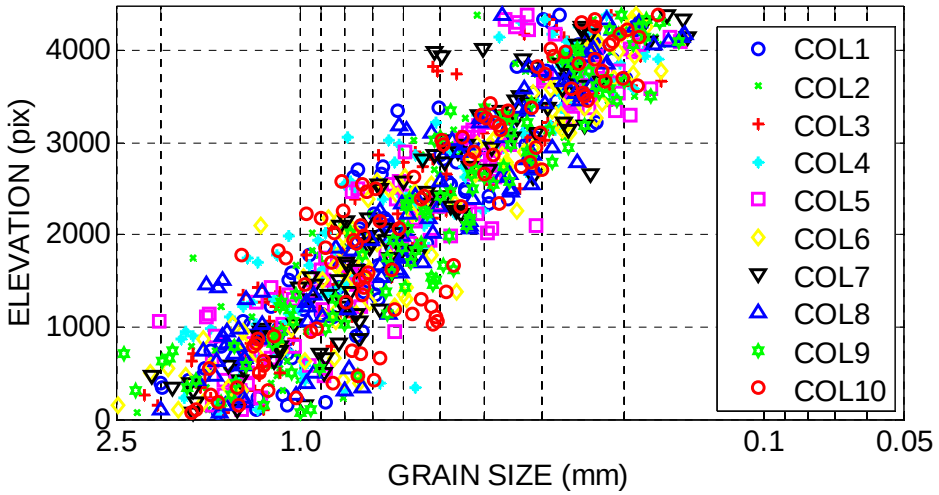

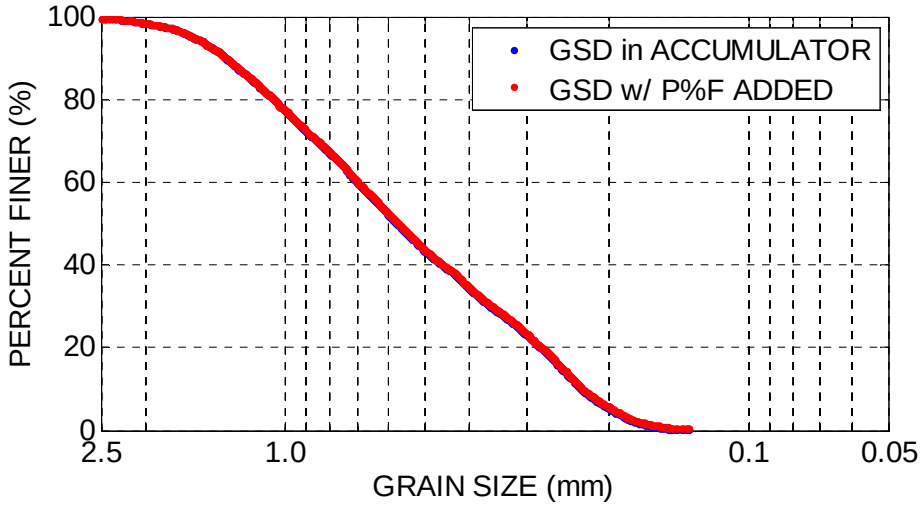

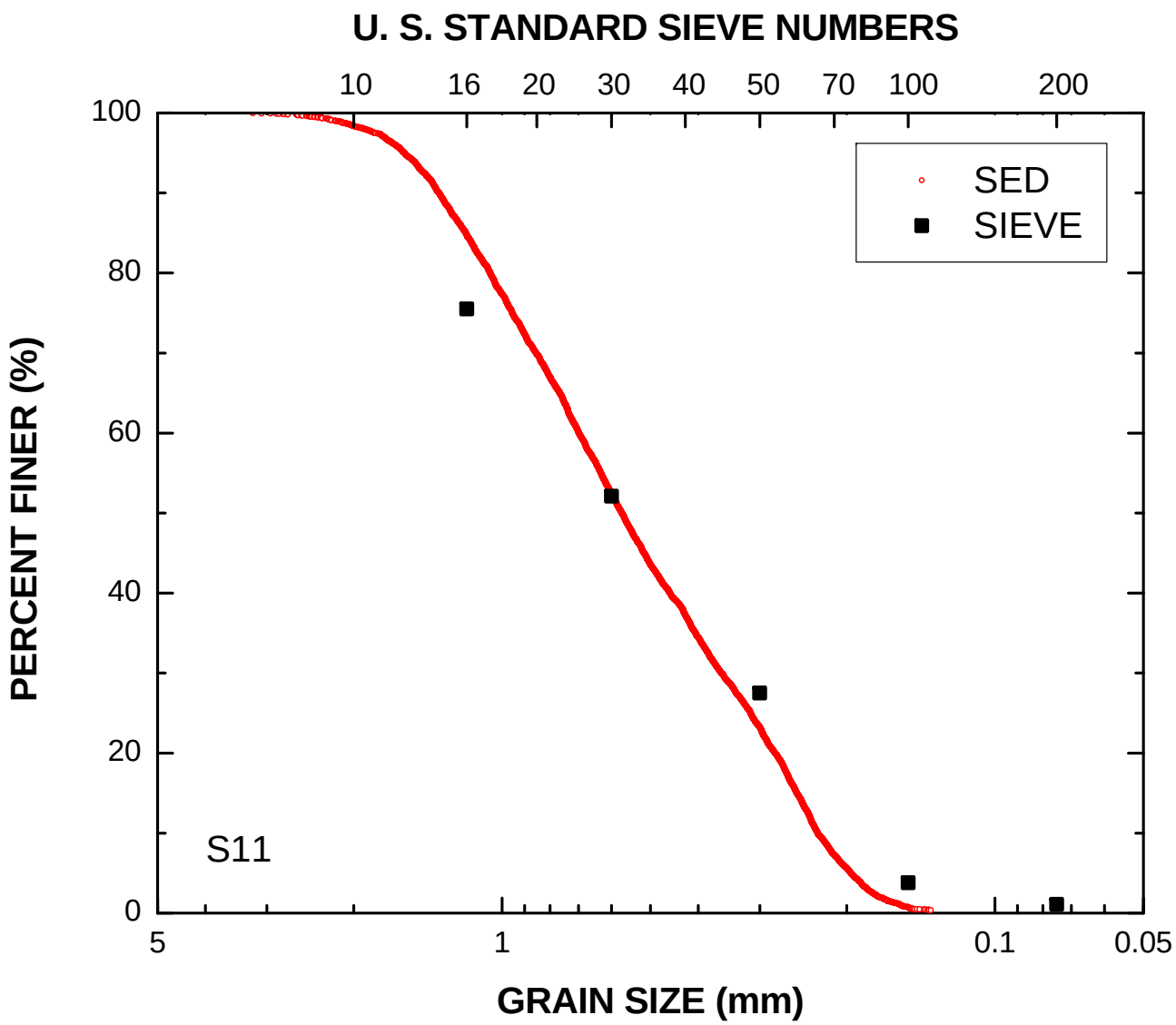
U. S. STANDARD SIEVE NUMBERS
10
16
20
30
40
50
70
100
200
100
80
60
40
20
0
PERCENT FINER (%)
SED
SIEVE
S11
5
1
0.1
0.05
GRAIN SIZE (mm)

SEDIMAGING (SED) TEST
GEOTECHNICAL ENGINEERING
UNIVERSITY OF MICHIGAN

MATERIAL: S12
DATE TESTED: 22-Sep-2011 16:10:38
TESTED BY: Ohm, H.S.

D_{60} (mm): 1.09
D_{30} (mm): 0.40
D_{10} (mm): 0.23
C_u: 4.82
C_g: 0.65
PF (%): 0.5

MAGNIFICATION (pix/mm): 36.9
IMAGE SIZE (pix): 4576 x 1280
IMAGE SIZE (mm): 124.0 x 34.7

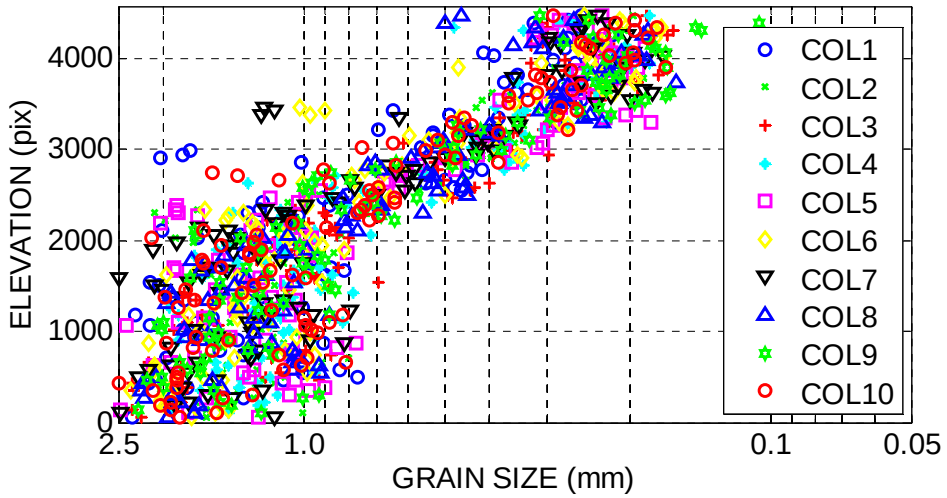

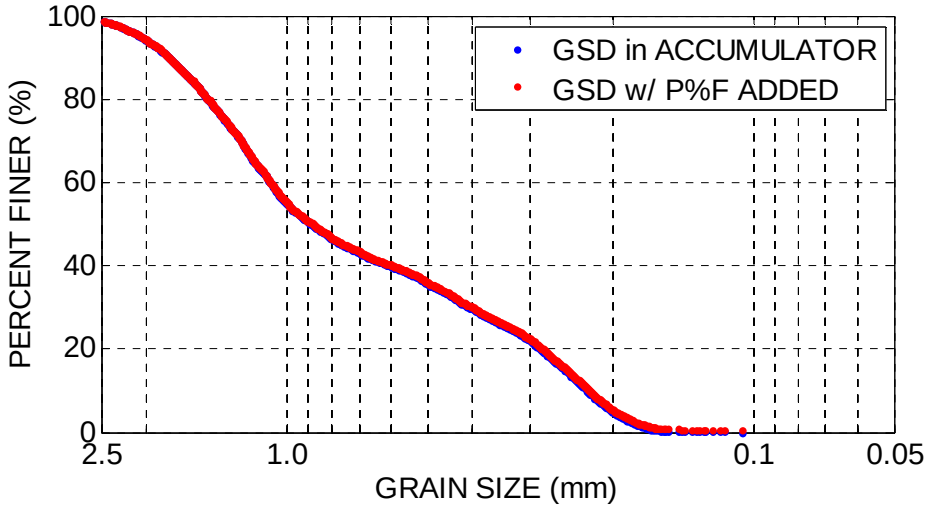

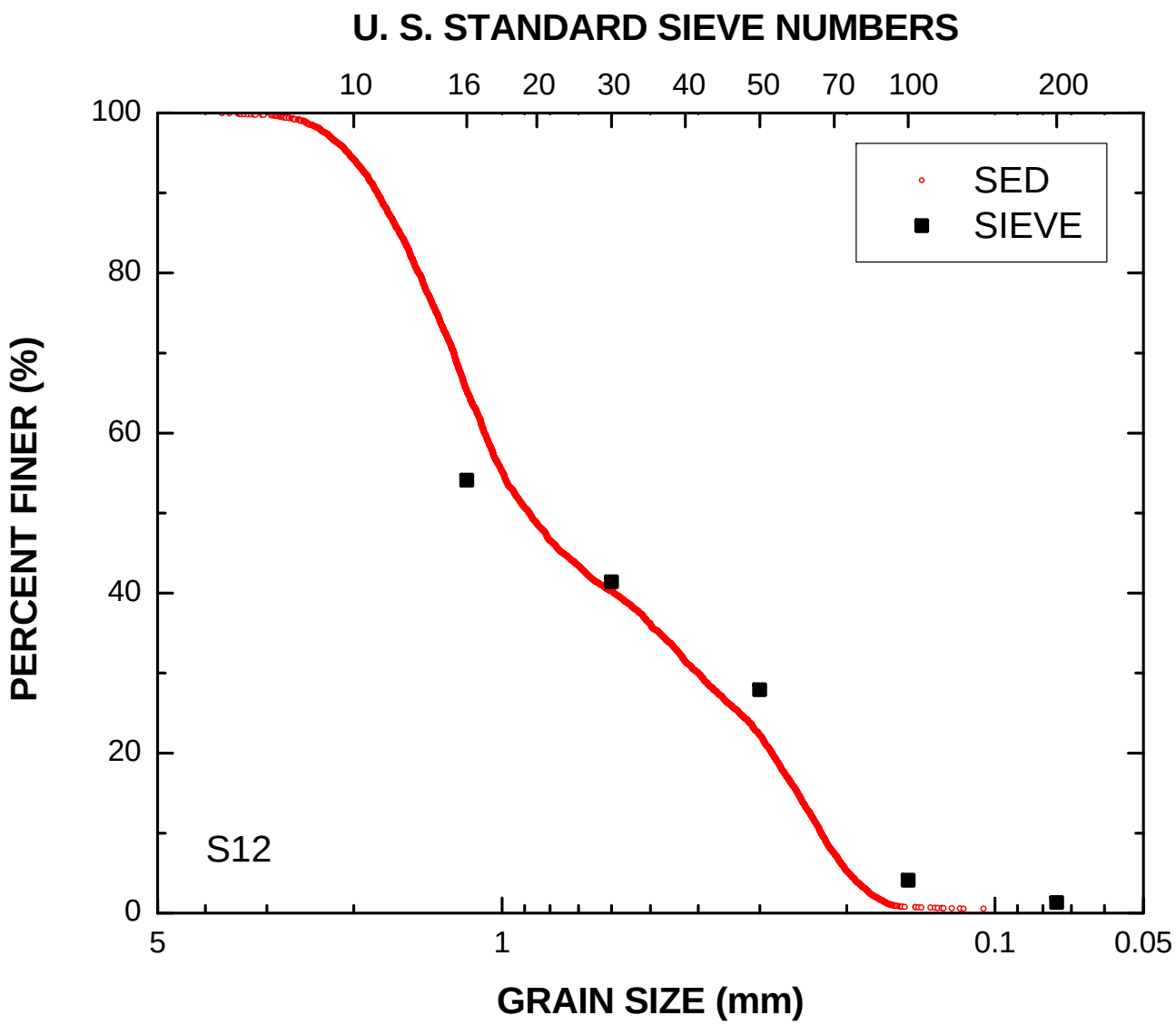
U. S. STANDARD SIEVE NUMBERS
10
16
20
30
40
50
70
100
200
100
80
60
40
20
0
PERCENT FINER (%)
SED
SIEVE
S12
5
1
0.1
0.05
GRAIN SIZE (mm)

SEDIMAGING (SED) TEST

GEOTECHNICAL ENGINEERING

UNIVERSITY OF MICHIGAN

MATERIAL: S13

DATE TESTED: 20-Sep-2011 17:46:38

TESTED BY: Ohm, H.S.

D_{60} (mm): 0.80

D_{30} (mm): 0.46

D_{10} (mm): 0.23

C_u: 3.42

C_g: 1.12

PF (%): 0.0

MAGNIFICATION (pix/mm): 36.9

IMAGE SIZE (pix): 4472 x 1280

IMAGE SIZE (mm): 121.2 x 34.7

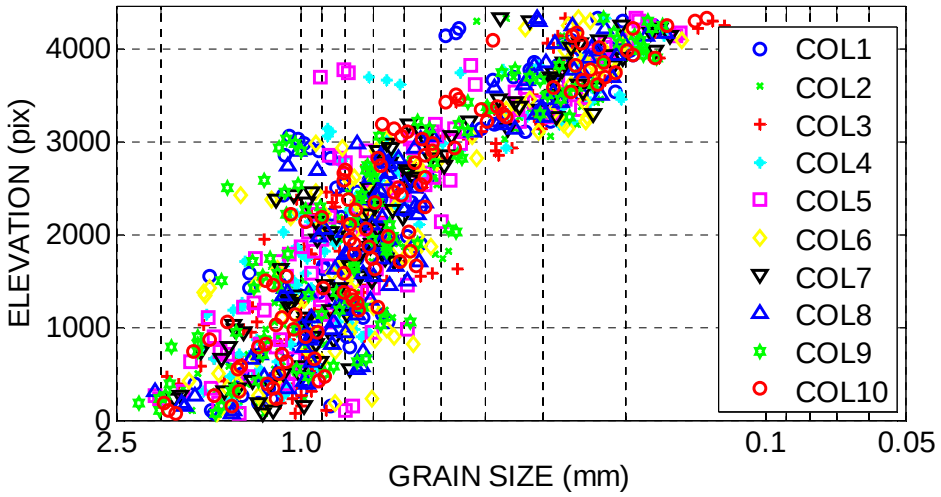

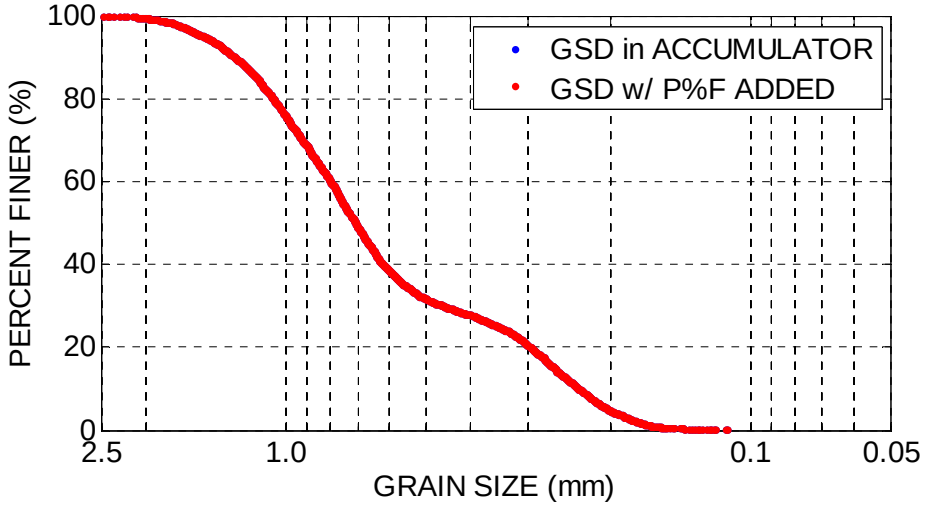

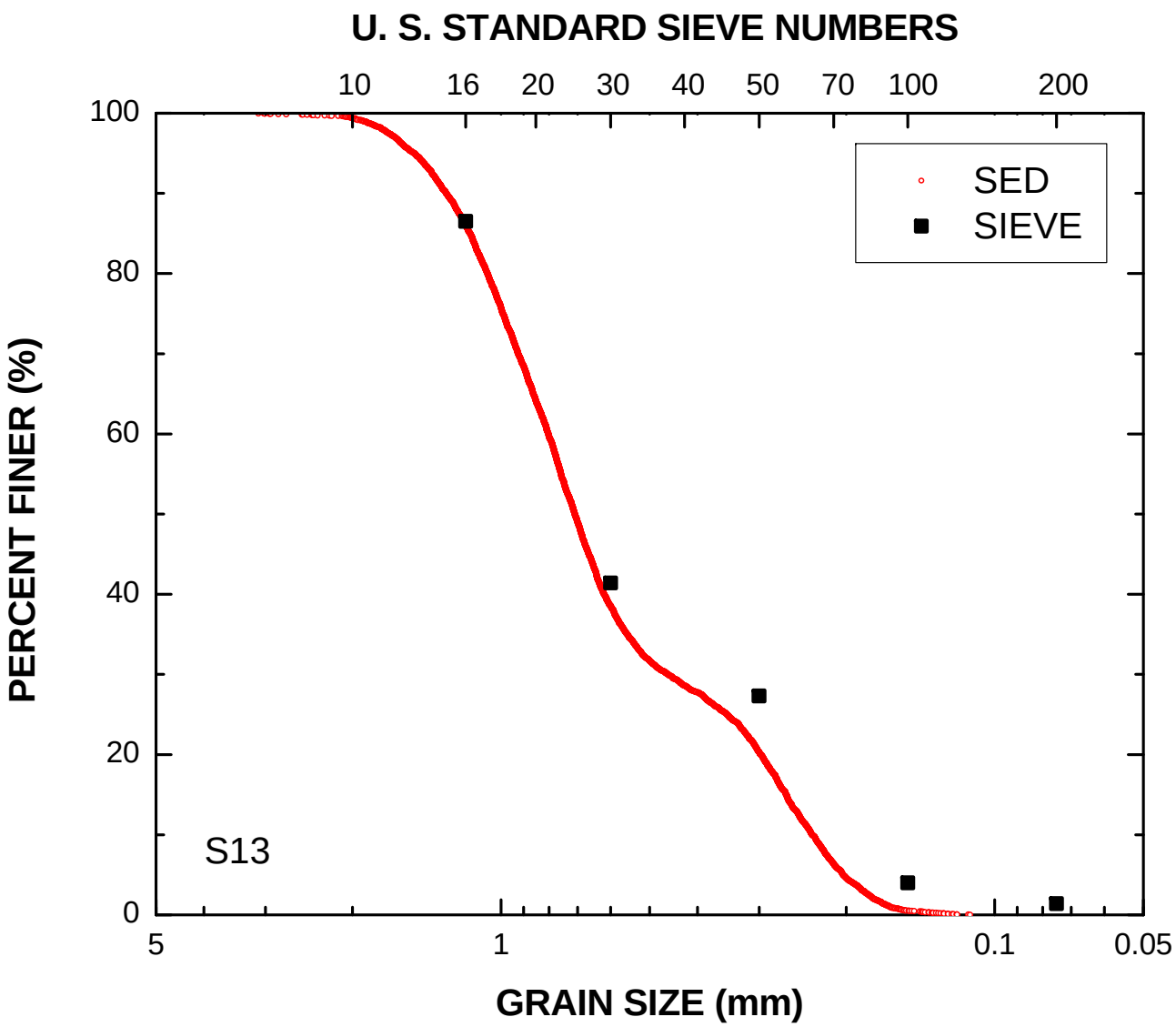
U. S. STANDARD SIEVE NUMBERS
10
16
20
30
40
50
70
100
200
100
80
60
40
20
0
PERCENT FINER (%)
SED
SIEVE
S13
5
1
0.1
0.05
GRAIN SIZE (mm)

SEDIMAGING (SED) TEST
GEOTECHNICAL ENGINEERING
UNIVERSITY OF MICHIGAN

MATERIAL: S14
DATE TESTED: 23-Sep-2011 09:53:04
TESTED BY: Ohm, H.S.

D_{60} (mm): 0.53
D_{30} (mm): 0.33
D_{10} (mm): 0.23
C_u: 2.26
C_g: 0.91
PF (%): 1.2

MAGNIFICATION (pix/mm): 36.9
IMAGE SIZE (pix): 4592 x 1280
IMAGE SIZE (mm): 124.4 x 34.7

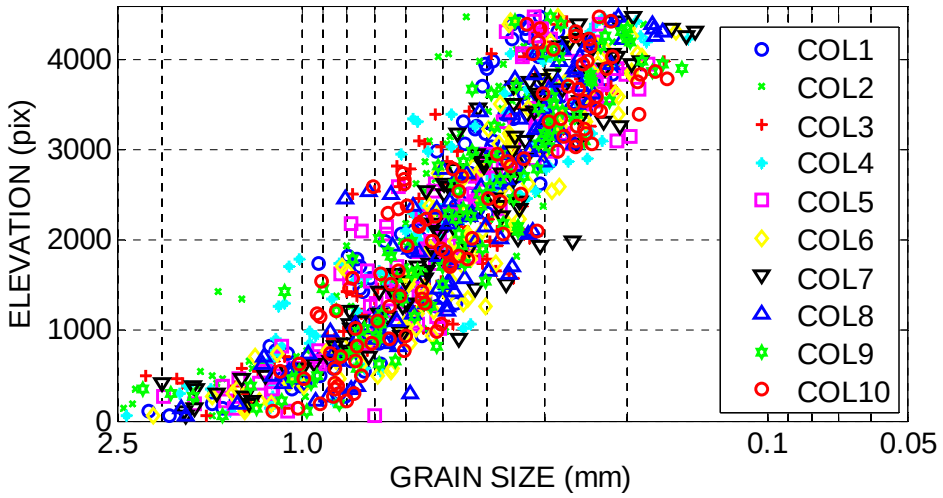

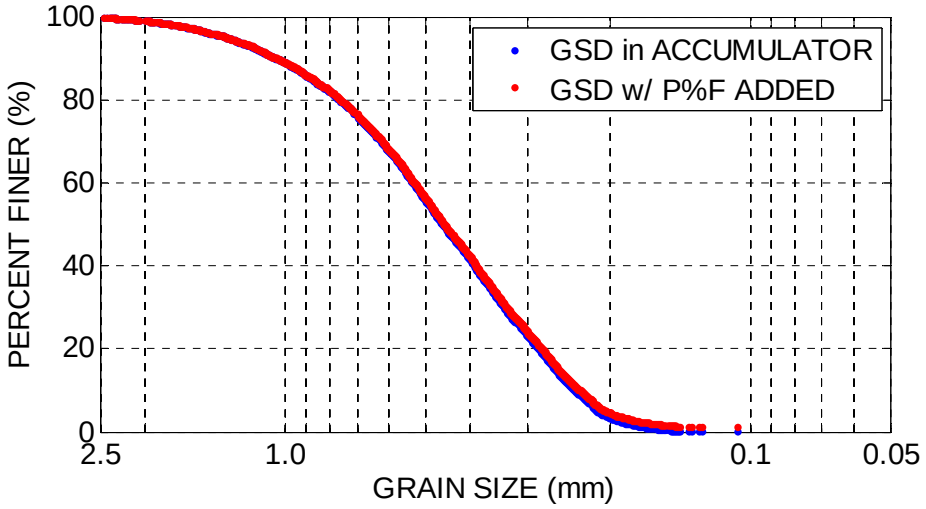

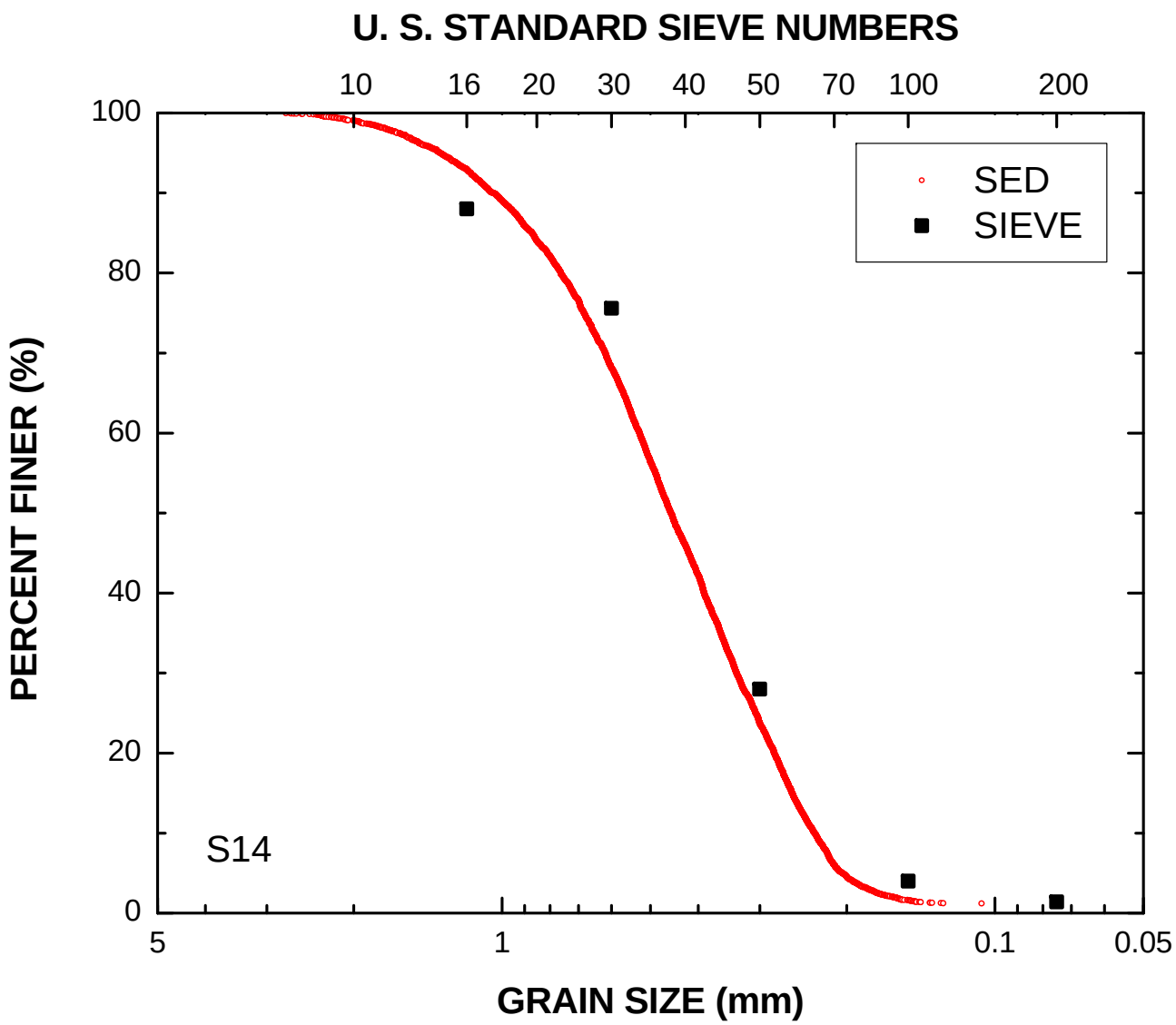
U. S. STANDARD SIEVE NUMBERS
10
16
20
30
40
50
70
100
200
100
80
60
40
20
0
PERCENT FINER (%)
SED
SIEVE
S14
5
1
0.1
0.05
GRAIN SIZE (mm)

SEDIMAGING (SED) TEST
GEOTECHNICAL ENGINEERING
UNIVERSITY OF MICHIGAN

MATERIAL: S15
DATE TESTED: 22-Sep-2011 12:18:50
TESTED BY: Ohm, H.S.

D_{60} (mm): 0.64
D_{30} (mm): 0.29
D_{10} (mm): 0.22
C_u: 2.93
C_g: 0.58
PF (%): 1.0

MAGNIFICATION (pix/mm): 36.9
IMAGE SIZE (pix): 4608 x 1280
IMAGE SIZE (mm): 124.9 x 34.7

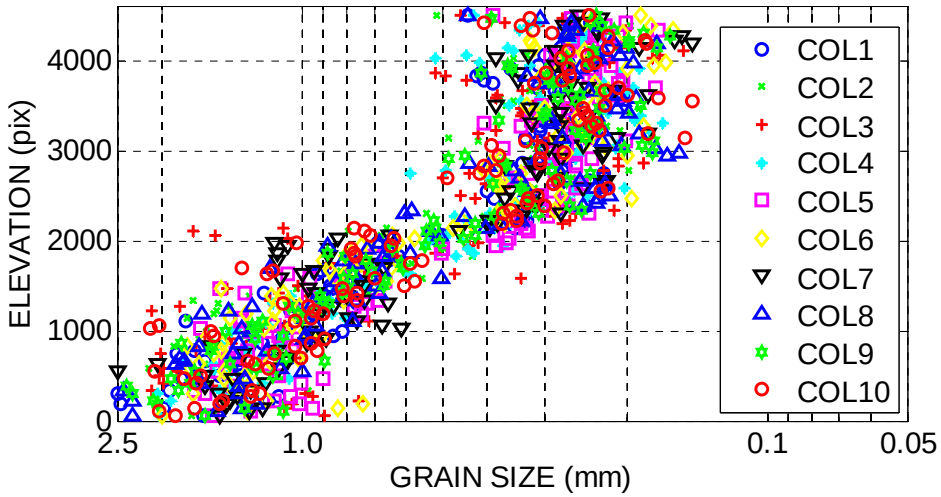

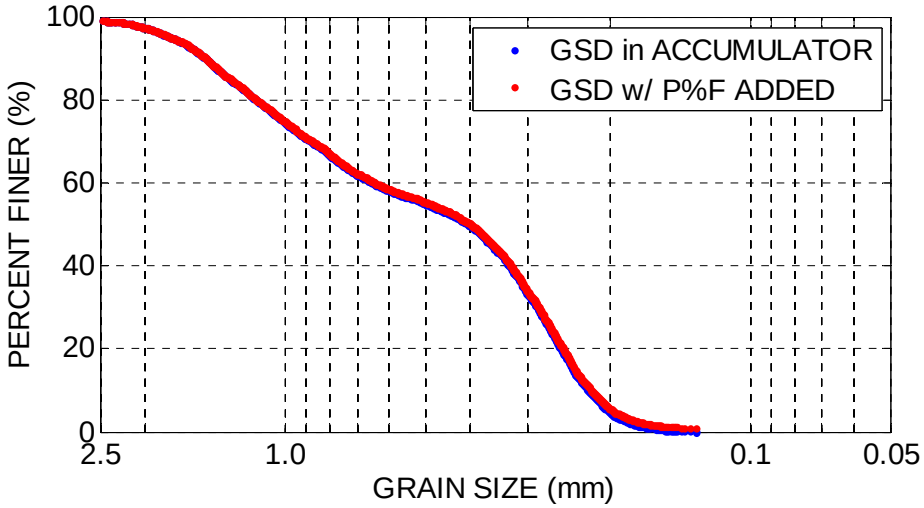

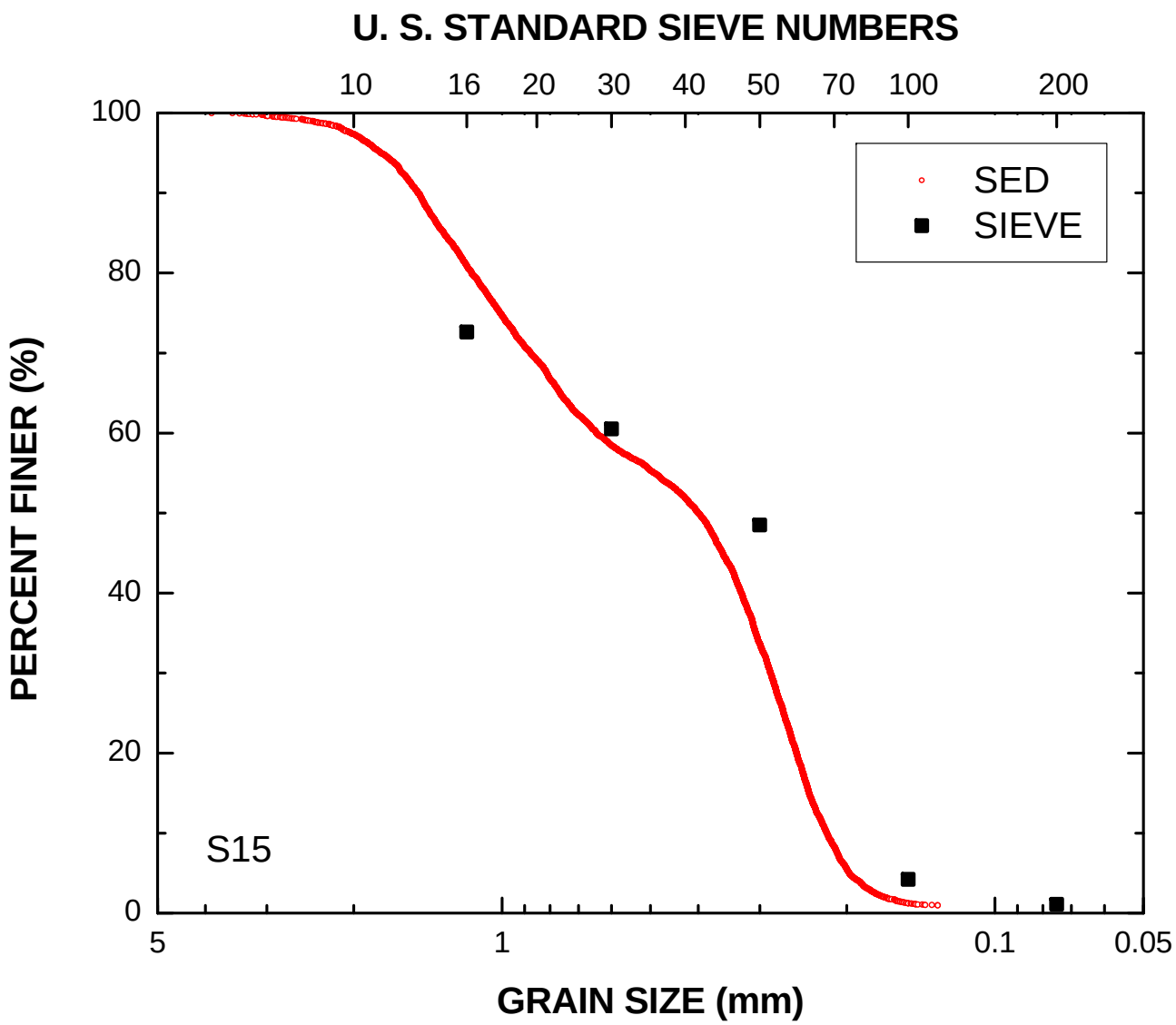
U. S. STANDARD SIEVE NUMBERS
10
16
20
30
40
50
70
100
200
100
80
60
40
20
0
PERCENT FINER (%)
SED
SIEVE
S15
5
1
0.1
0.05
GRAIN SIZE (mm)

SEDIMAGING (SED) TEST
GEOTECHNICAL ENGINEERING
UNIVERSITY OF MICHIGAN

MATERIAL: S16
DATE TESTED: 15-Sep-2011 15:48:42
TESTED BY: Ohm, H.S.

D_{60} (mm): 0.43
D_{30} (mm): 0.18
D_{10} (mm): 0.12
C_u: 3.72
C_g: 0.64
PF (%): 1.1

MAGNIFICATION (pix/mm): 36.9
IMAGE SIZE (pix): 4472 x 1280
IMAGE SIZE (mm): 121.2 x 34.7

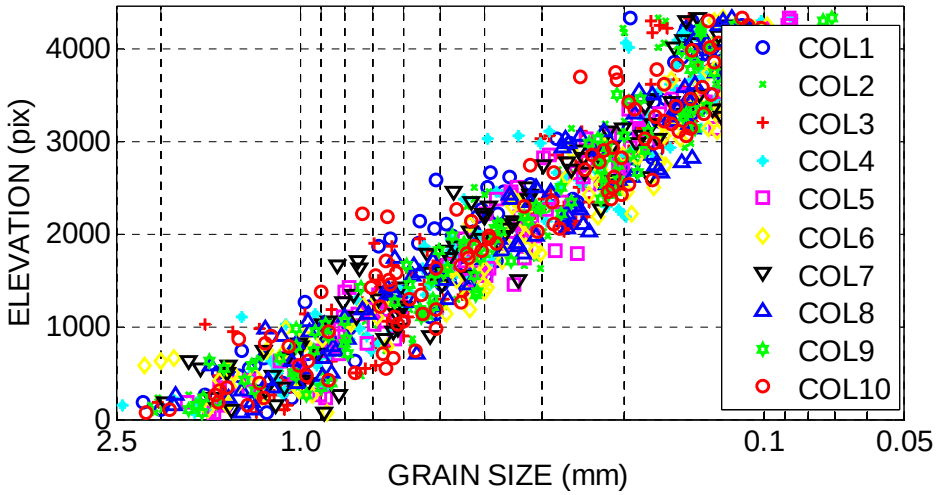

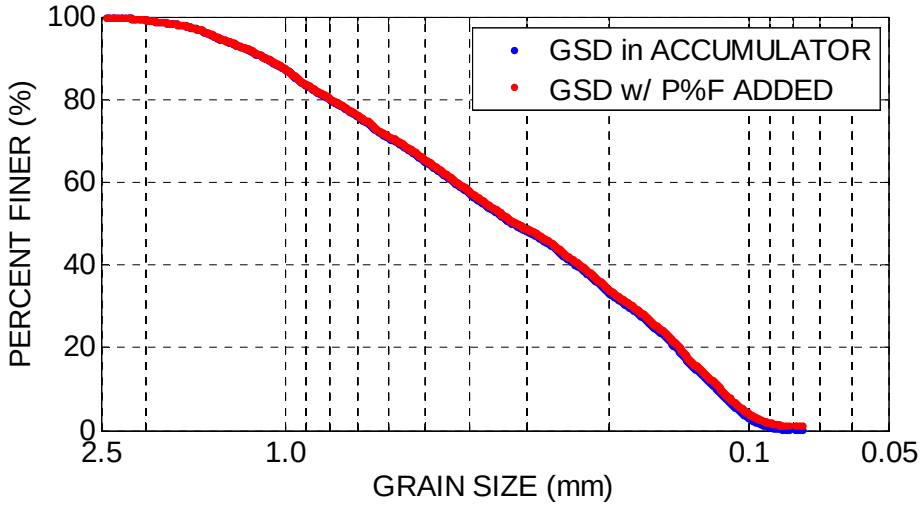

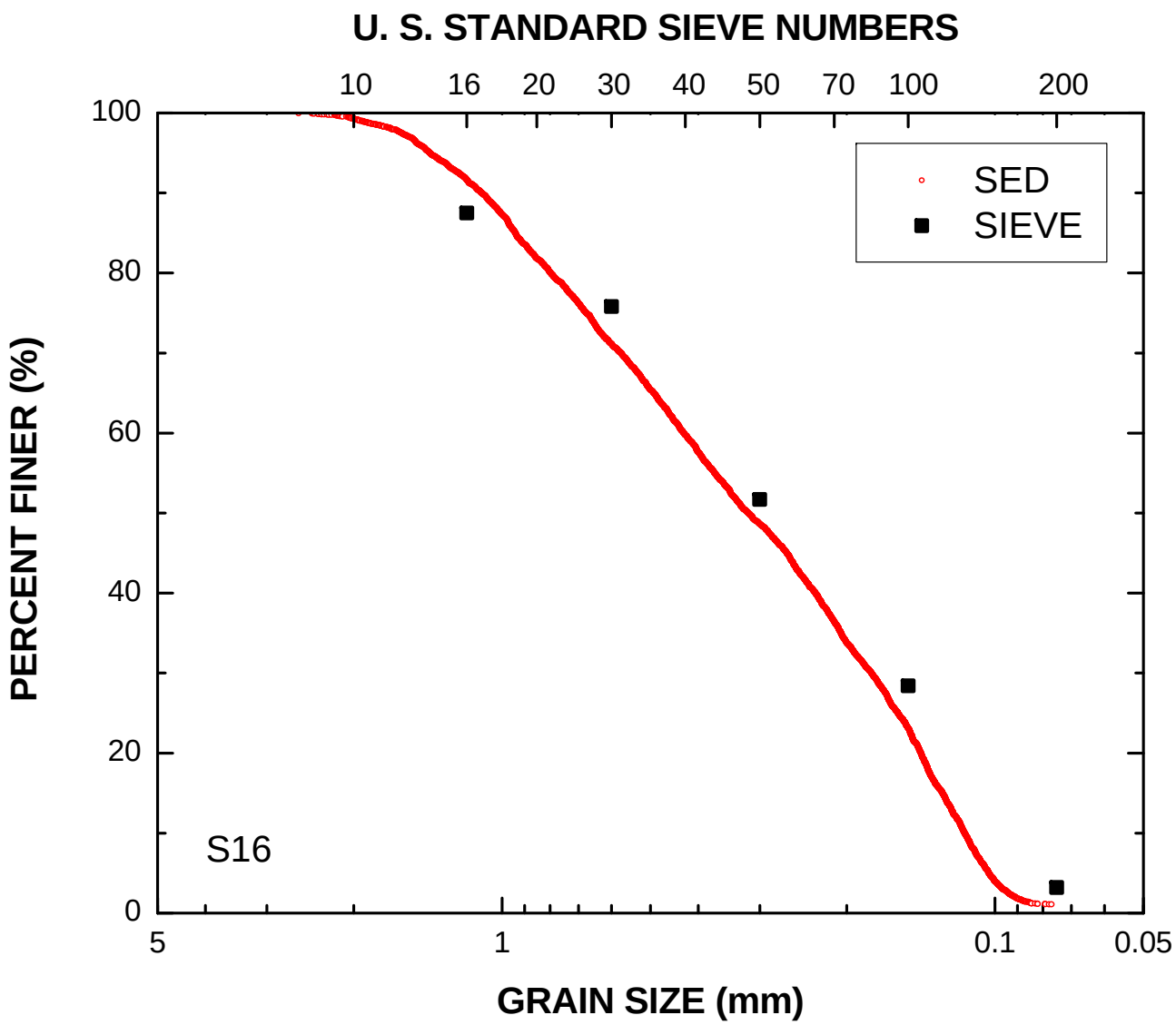
U. S. STANDARD SIEVE NUMBERS
10
16
20
30
40
50
70
100
200
100
80
60
40
20
0
PERCENT FINER (%)
SED
SIEVE
S16
5
1
0.1
0.05
GRAIN SIZE (mm)

SEDIMAGING (SED) TEST
GEOTECHNICAL ENGINEERING
UNIVERSITY OF MICHIGAN

MATERIAL: S17
DATE TESTED: 21-Sep-2011 17:17:06
TESTED BY: Ohm, H.S.

D_{60} (mm): 0.93
D_{30} (mm): 0.57
D_{10} (mm): 0.31
C_u: 2.97
C_g: 1.10
PF (%): 0.5

MAGNIFICATION (pix/mm): 36.9
IMAGE SIZE (pix): 4464 x 1280
IMAGE SIZE (mm): 121.0 x 34.7

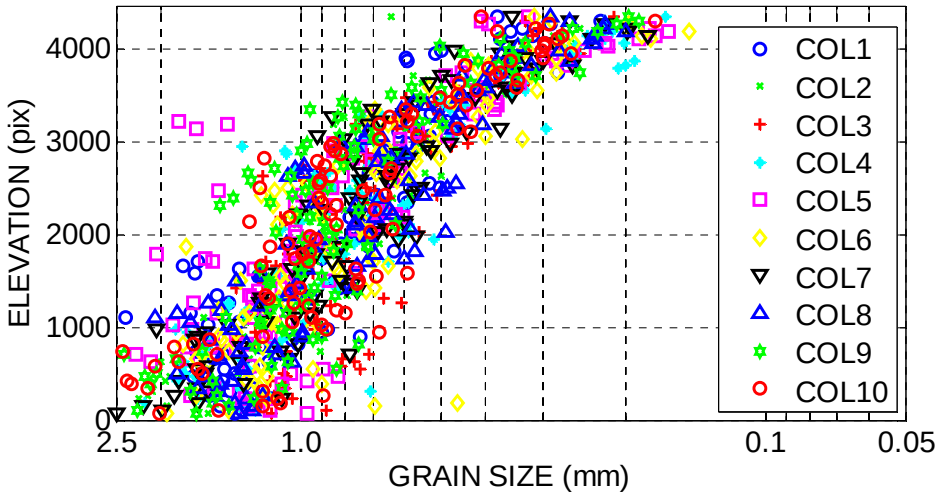

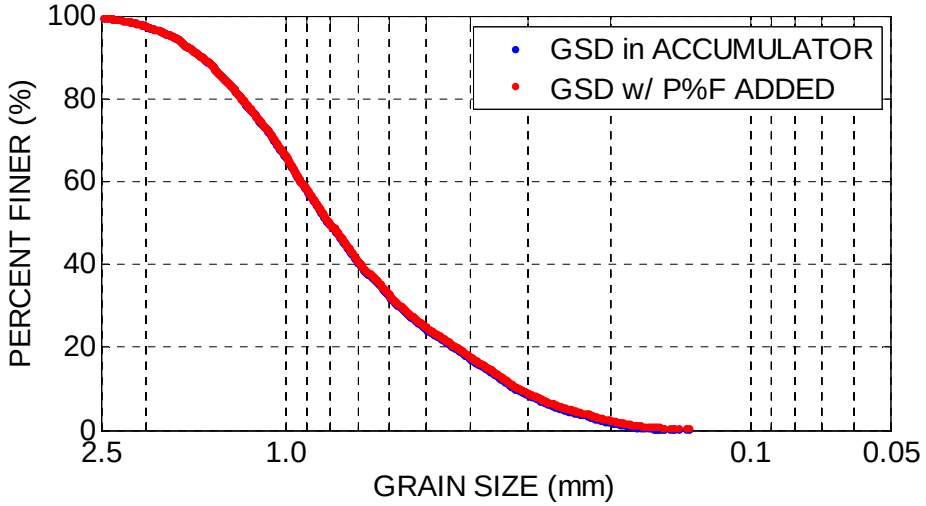

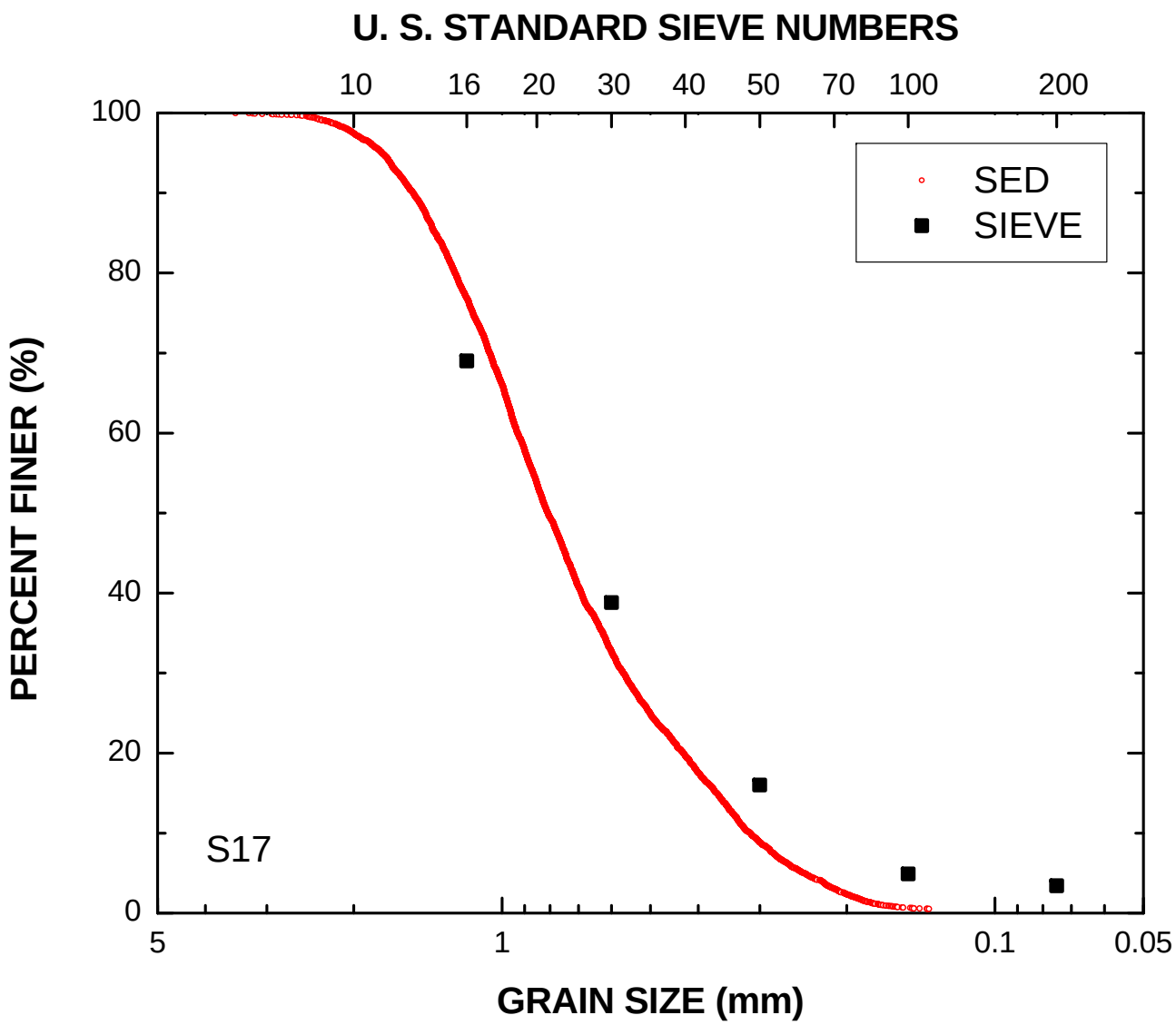
U. S. STANDARD SIEVE NUMBERS
10
16
20
30
40
50
70
100
200
100
80
60
40
20
0
PERCENT FINER (%)
SED
SIEVE
S17
5
1
0.1
0.05
GRAIN SIZE (mm)

SEDIMAGING (SED) TEST
GEOTECHNICAL ENGINEERING
UNIVERSITY OF MICHIGAN

MATERIAL: S18
DATE TESTED: 21-Sep-2011 13:16:30
TESTED BY: Ohm, H.S.

D_{60} (mm): 0.51
D_{30} (mm): 0.27
D_{10} (mm): 0.18
C_u: 2.90
C_g: 0.81
PF (%): 1.3

MAGNIFICATION (pix/mm): 36.9
IMAGE SIZE (pix): 4544 x 1280
IMAGE SIZE (mm): 123.1 x 34.7

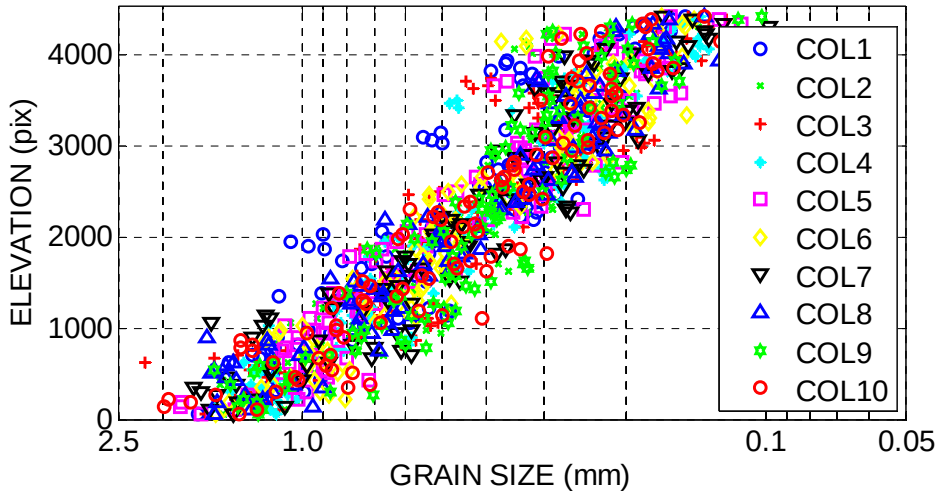

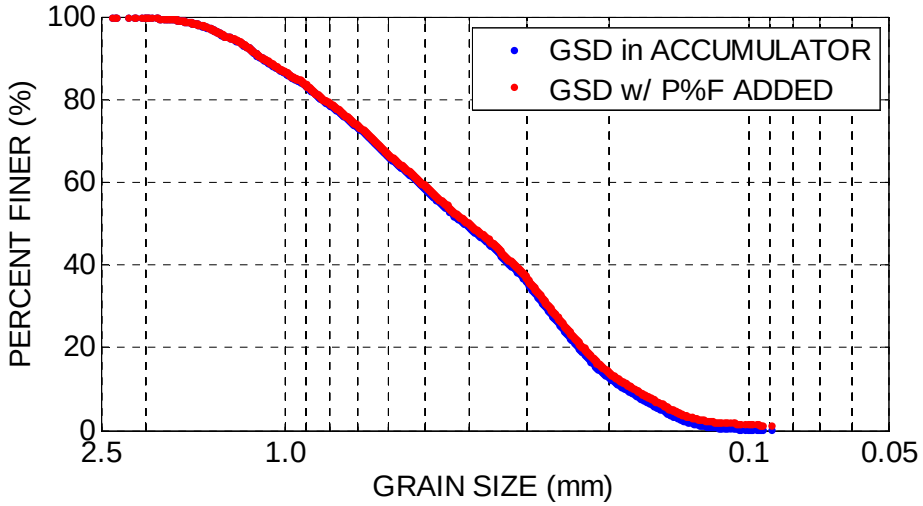

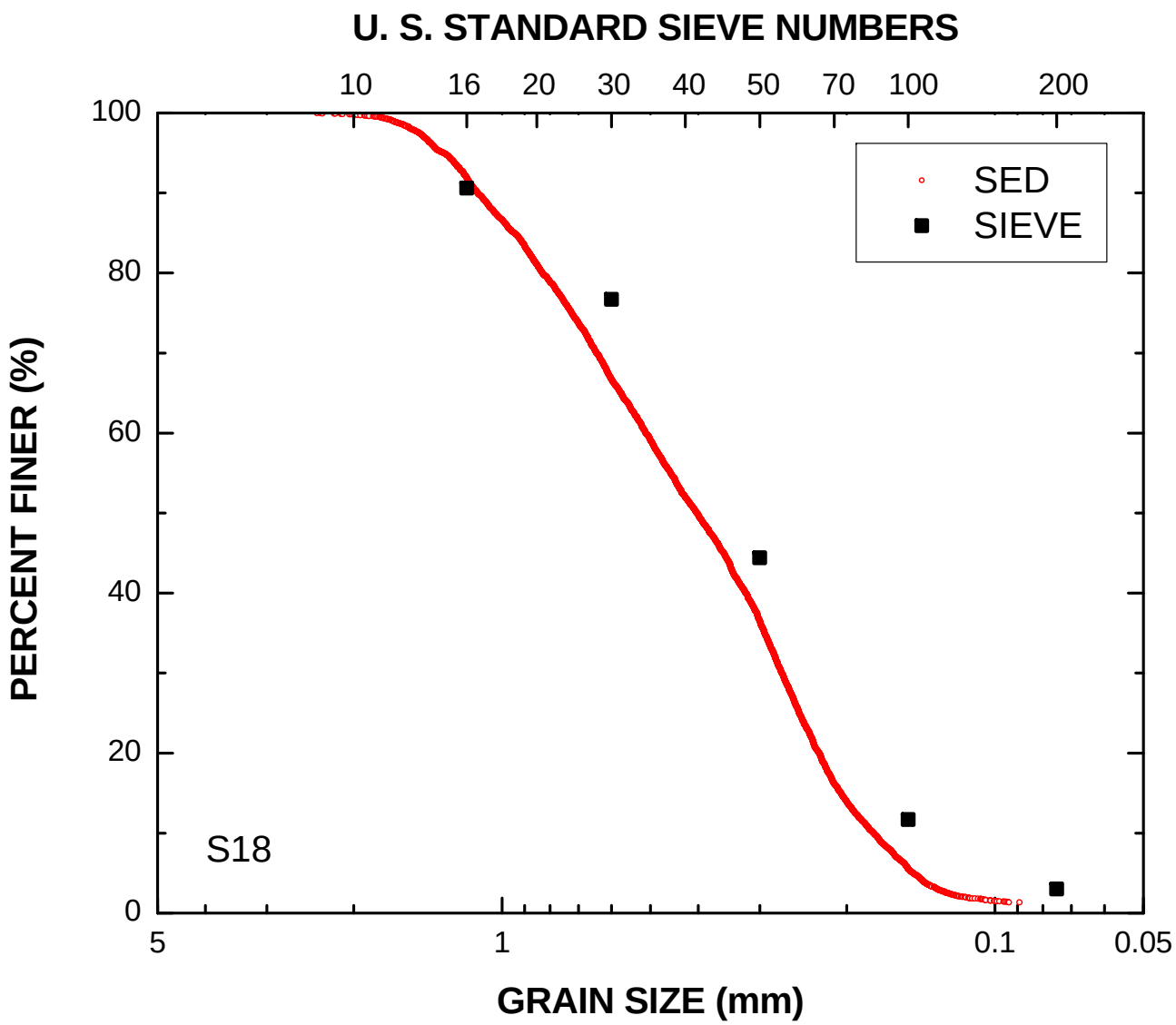
U. S. STANDARD SIEVE NUMBERS
10
16
20
30
40
50
70
100
200
100
80
60
40
20
0
PERCENT FINER (%)
SED
SIEVE
S18
5
1
0.1
0.05
GRAIN SIZE (mm)

SEDIMAGING (SED) TEST

GEOTECHNICAL ENGINEERING

UNIVERSITY OF MICHIGAN

MATERIAL: S19

DATE TESTED: 22-Sep-2011 11:43:26

TESTED BY: Ohm, H.S.

D_{60} (mm): 0.25

D_{30} (mm): 0.15

D_{10} (mm): 0.11

C_u: 2.22

C_g: 0.78

PF (%): 2.1

MAGNIFICATION (pix/mm): 36.9

IMAGE SIZE (pix): 4672 x 1280

IMAGE SIZE (mm): 126.6 x 34.7

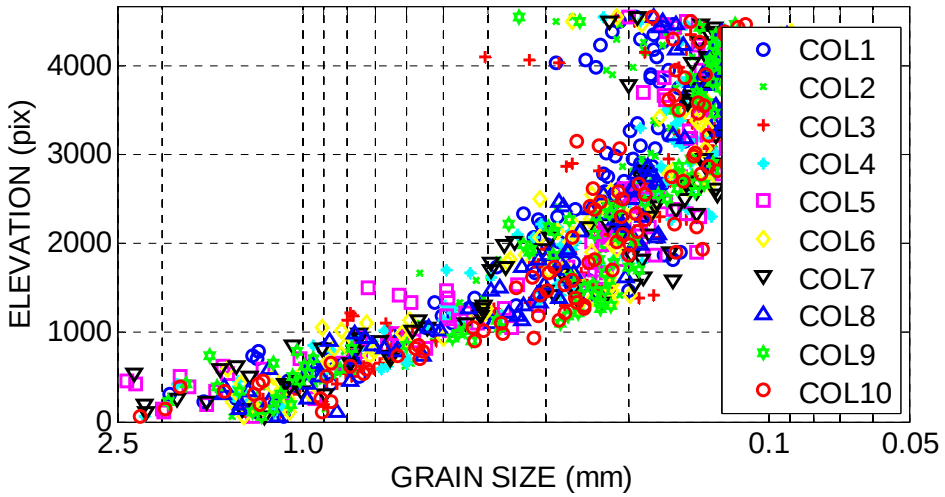

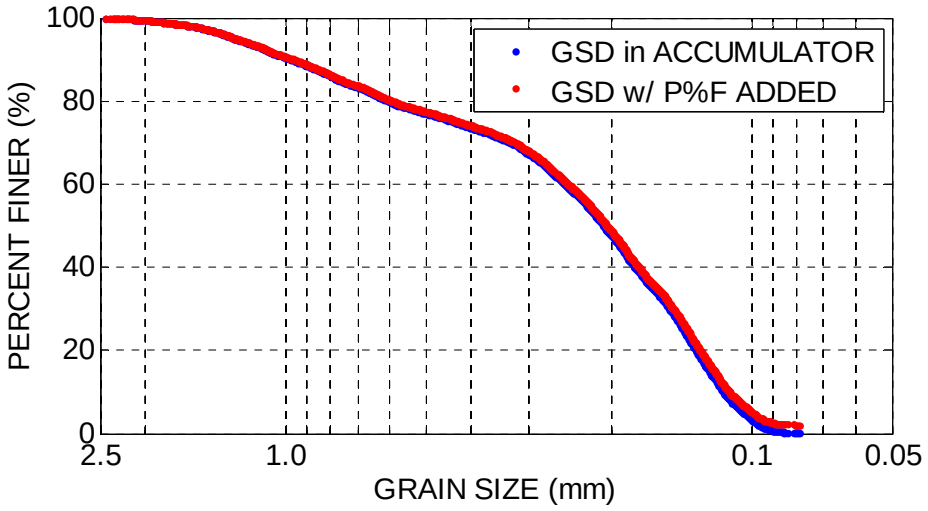

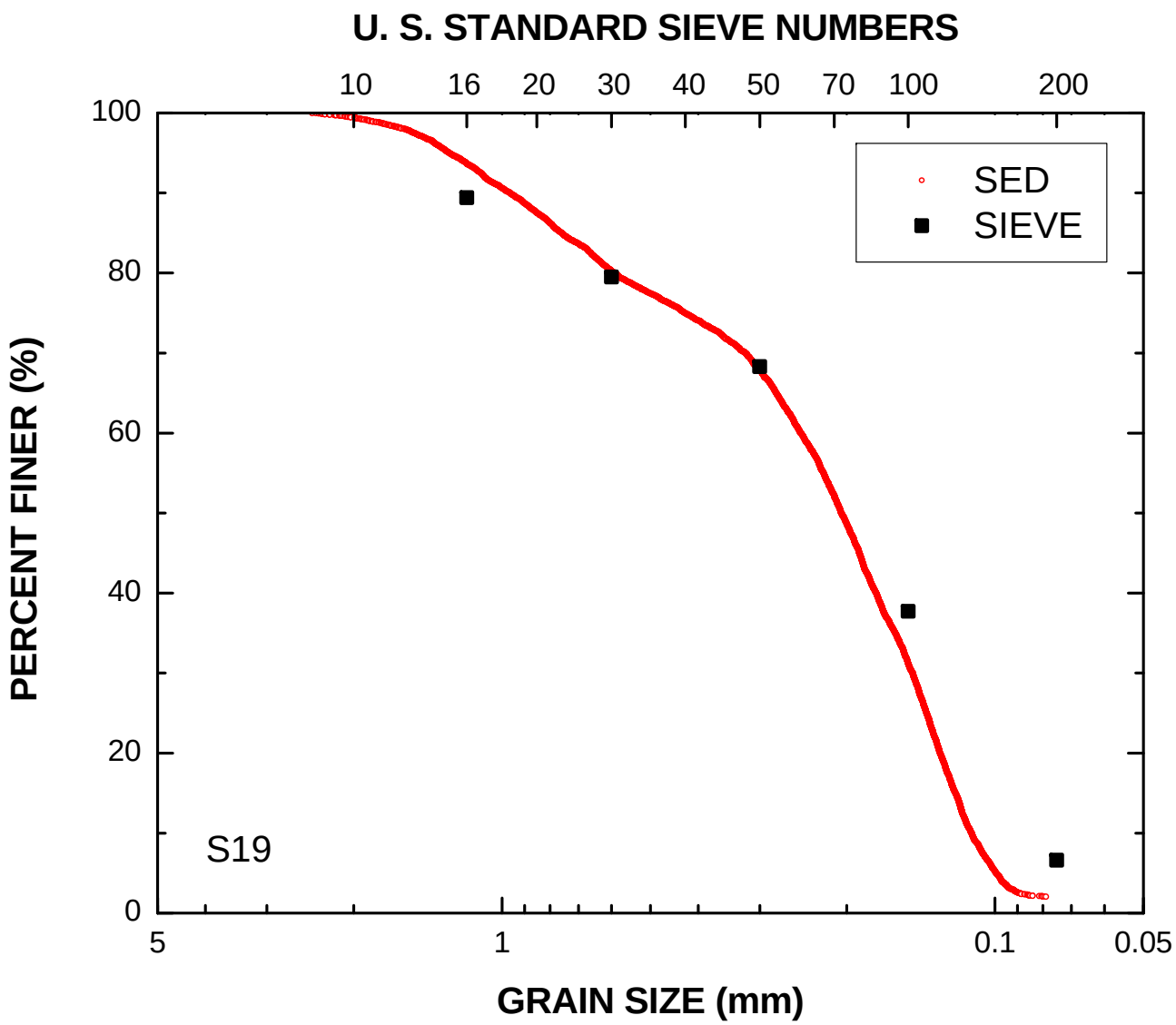
U. S. STANDARD SIEVE NUMBERS
10
16
20
30
40
50
70
100
200
100
80
60
40
20
0
PERCENT FINER (%)
SED
SIEVE
S19
5
1
0.1
0.05
GRAIN SIZE (mm)

SEDIMAGING (SED) TEST
GEOTECHNICAL ENGINEERING
UNIVERSITY OF MICHIGAN

MATERIAL: S20
DATE TESTED: 20-Sep-2011 16:49:08
TESTED BY: Ohm, H.S.

D_{60} (mm): 0.61
D_{30} (mm): 0.25
D_{10} (mm): 0.12
C_u: 5.21
C_g: 0.85
PF (%): 0.4

MAGNIFICATION (pix/mm): 36.9
IMAGE SIZE (pix): 4512 x 1280
IMAGE SIZE (mm): 122.3 x 34.7

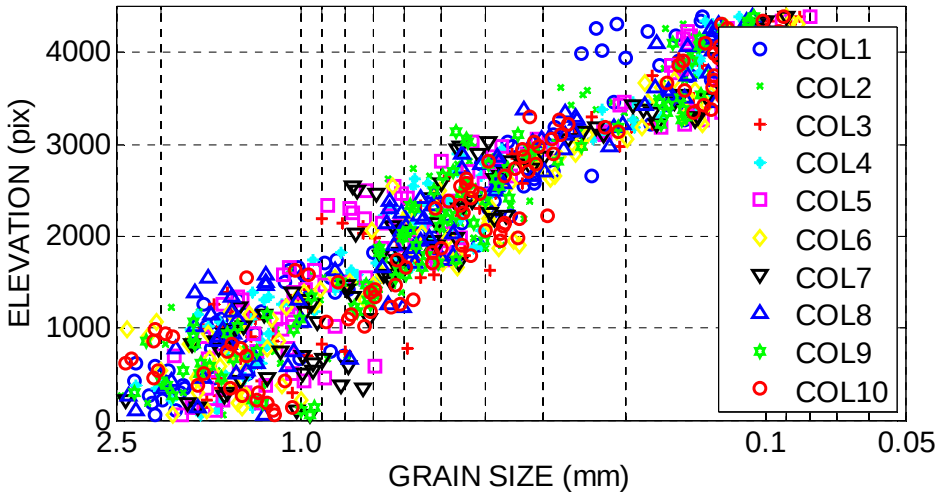

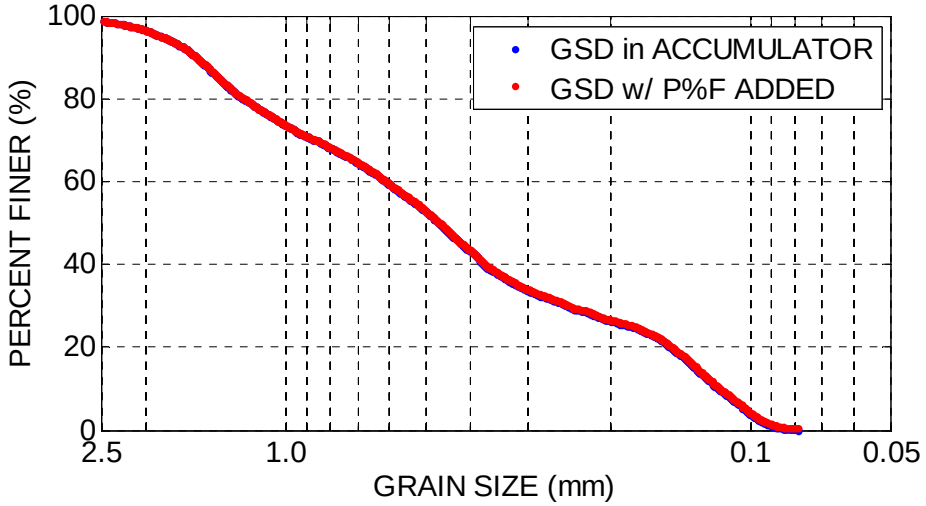

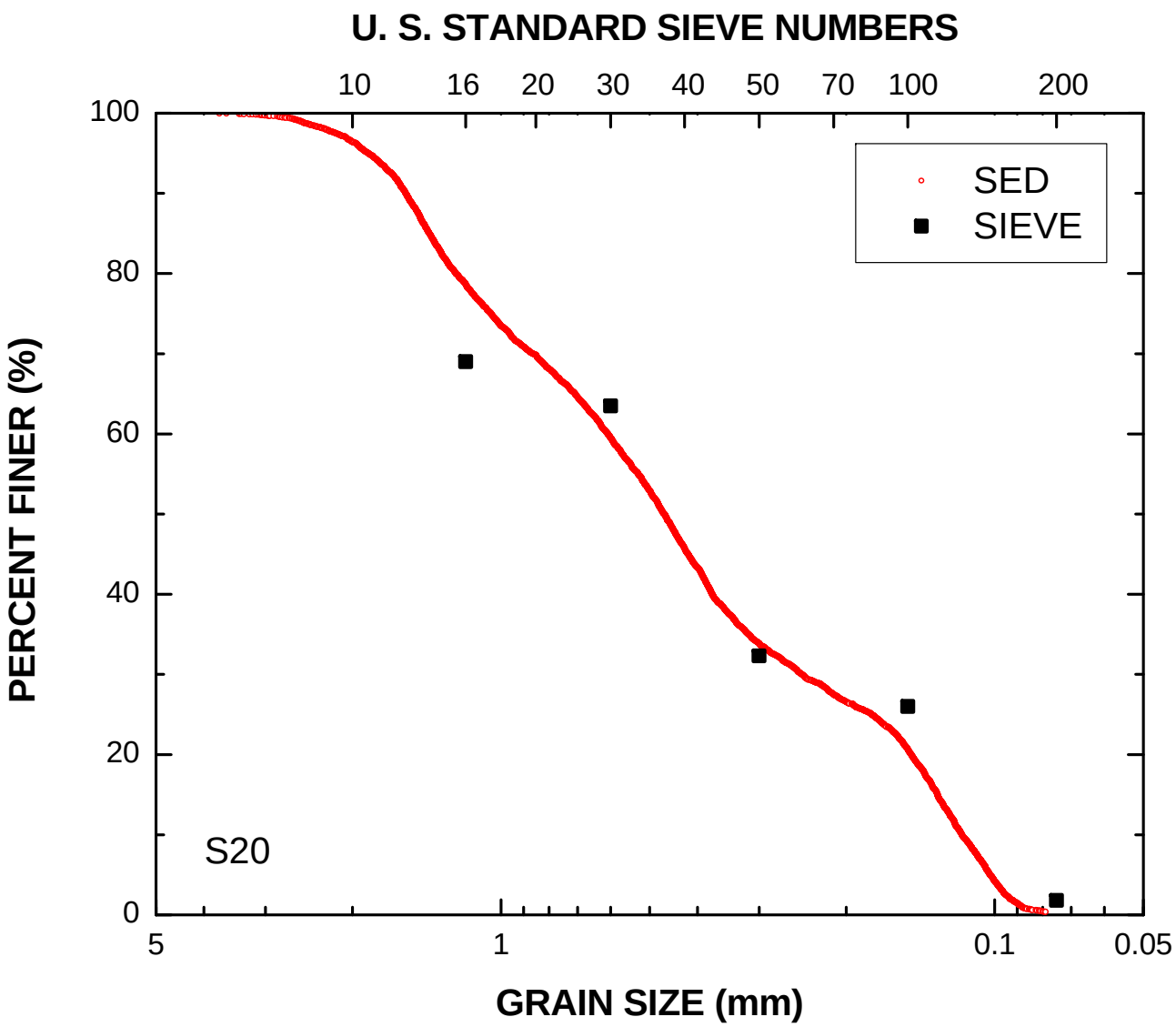
U. S. STANDARD SIEVE NUMBERS
10
16
20
30
40
50
70
100
200
100
80
60
40
20
0
PERCENT FINER (%)
SED
SIEVE
S20
5
1
0.1
0.05
GRAIN SIZE (mm)

Appendix D. Complete Translucent Segregation Table Results

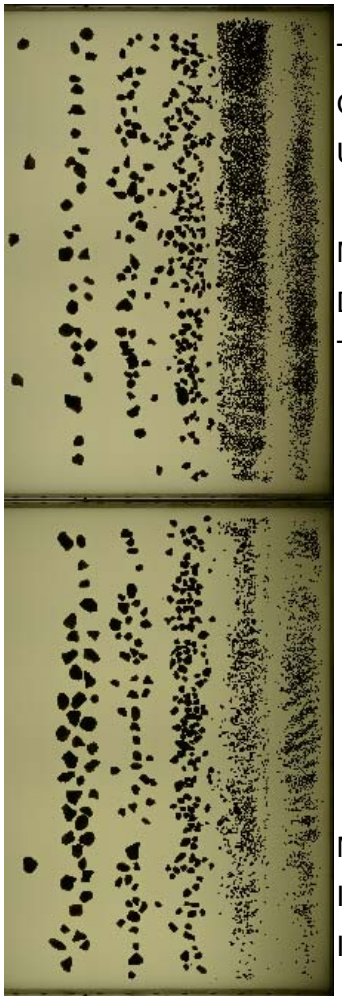

TRANSLUCENT SEGREGATION TABLE (TST)

GEOTECHNICAL ENGINEERING

UNIVERSITY OF MICHIGAN

MATERIAL: T1

DATE TESTED: 12-Jun-2012 11:29:08

TESTED BY: Ohm, H.S.

MAGNIFICATION (pix/mm): 5.4

IMAGE SIZE (pix): 9856 x 3264

IMAGE SIZE (mm): 1825.2 x 604.4

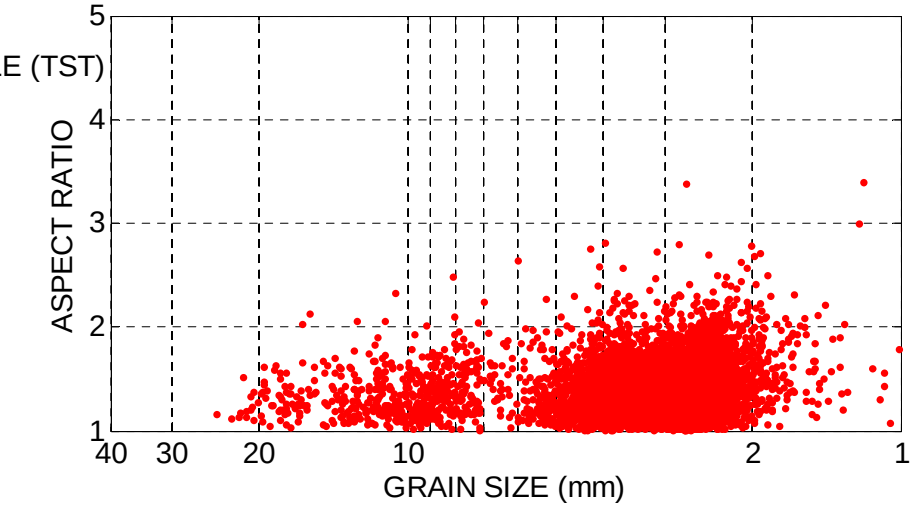

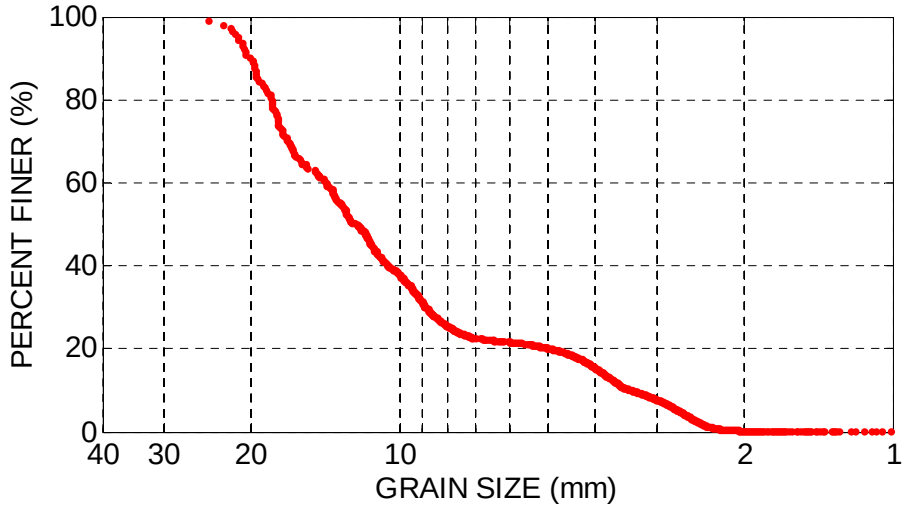

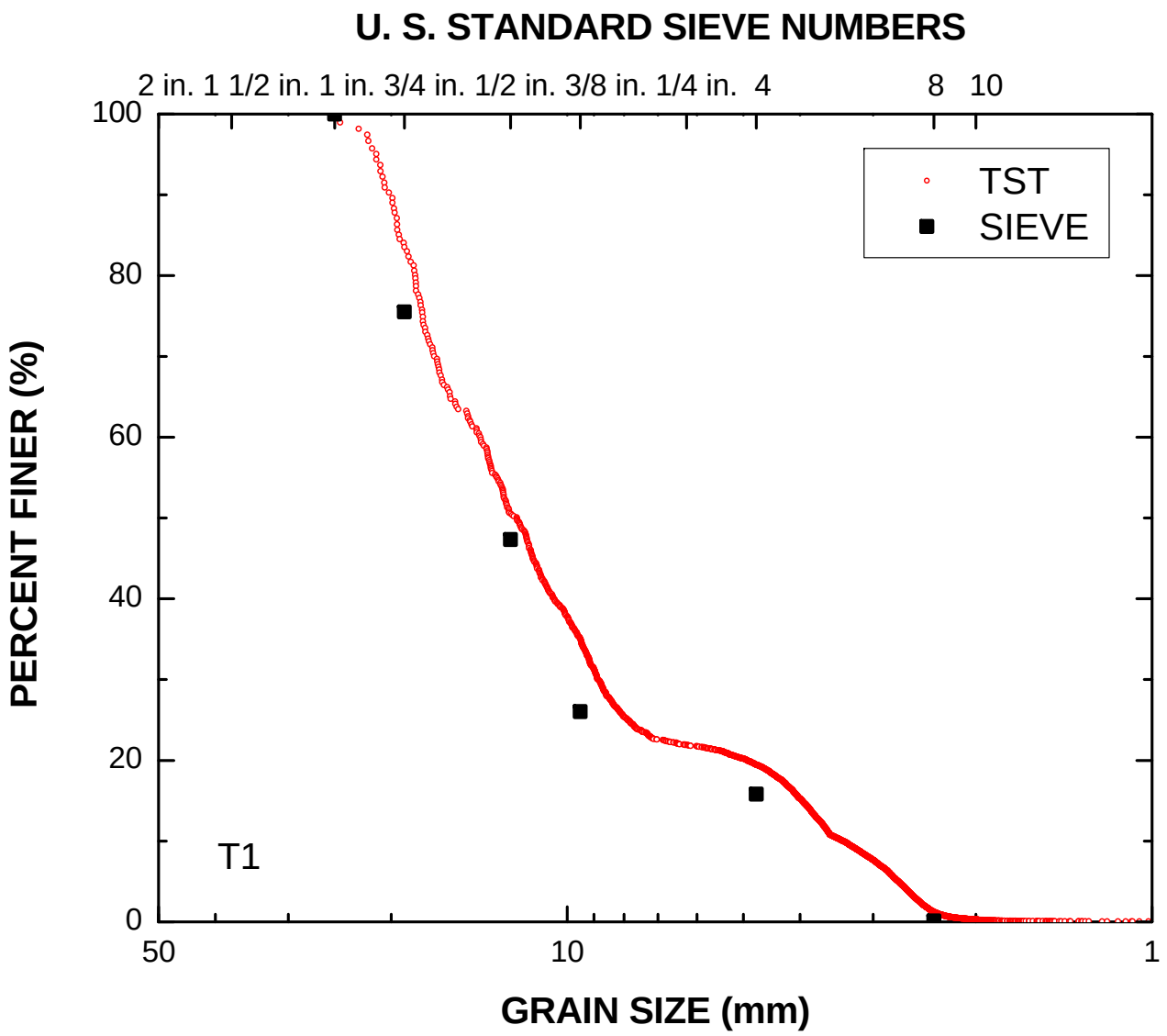
U. S. STANDARD SIEVE NUMBERS
2 in. 1 1/2 in. 1 in. 3/4 in. 1/2 in. 3/8 in. 1/4 in. 4 8 10
100
80
60
40
20
0
PERCENT FINER (%)
TST
SIEVE
T1
50
10
1
GRAIN SIZE (mm)

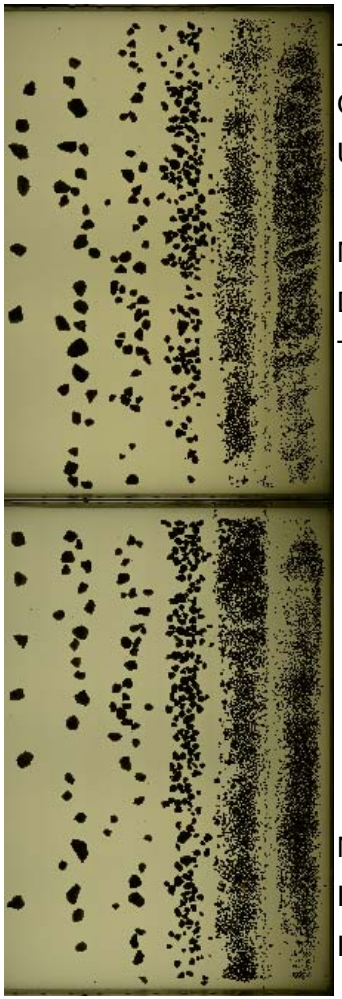

TRANSLUCENT SEGREGATION TABLE (TST)
GEOTECHNICAL ENGINEERING
UNIVERSITY OF MICHIGAN

MATERIAL: T2
DATE TESTED: 12-Jun-2012 13:08:00
TESTED BY: Ohm, H.S.

MAGNIFICATION (pix/mm): 5.4
IMAGE SIZE (pix): 9856 x 3264
IMAGE SIZE (mm): 1825.2 x 604.4

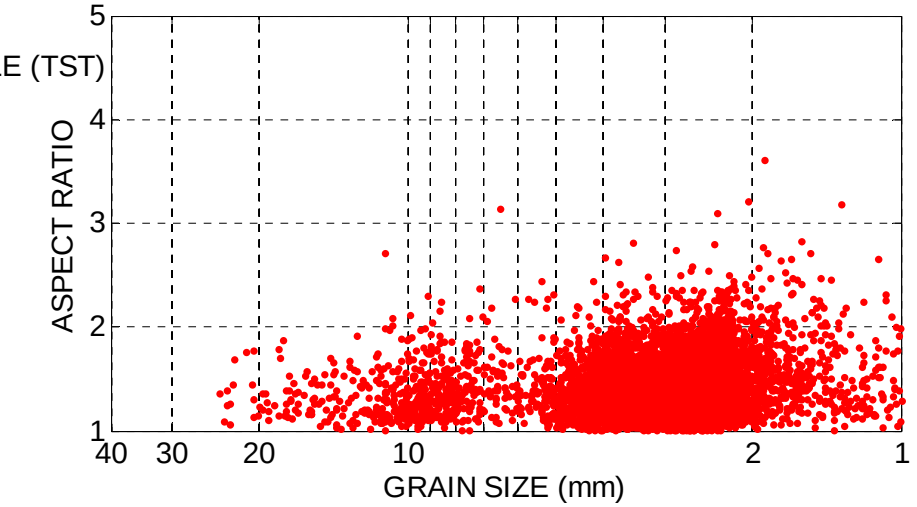

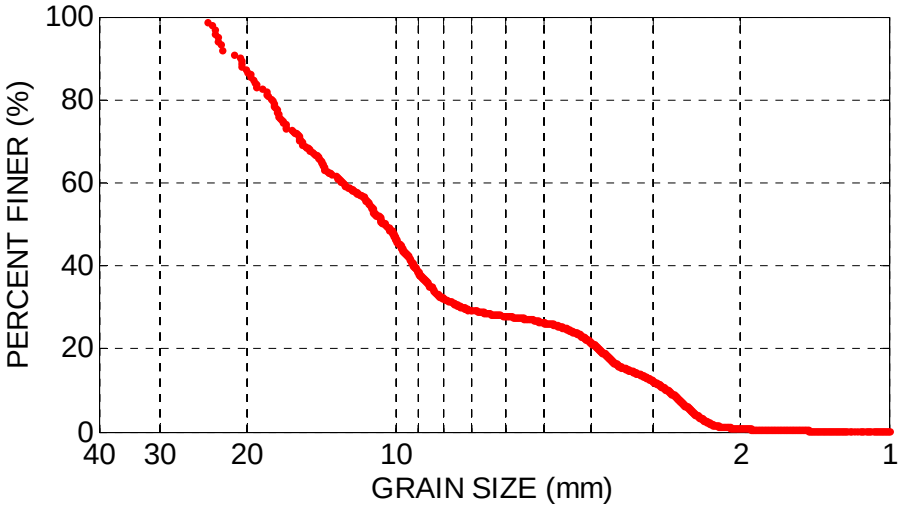

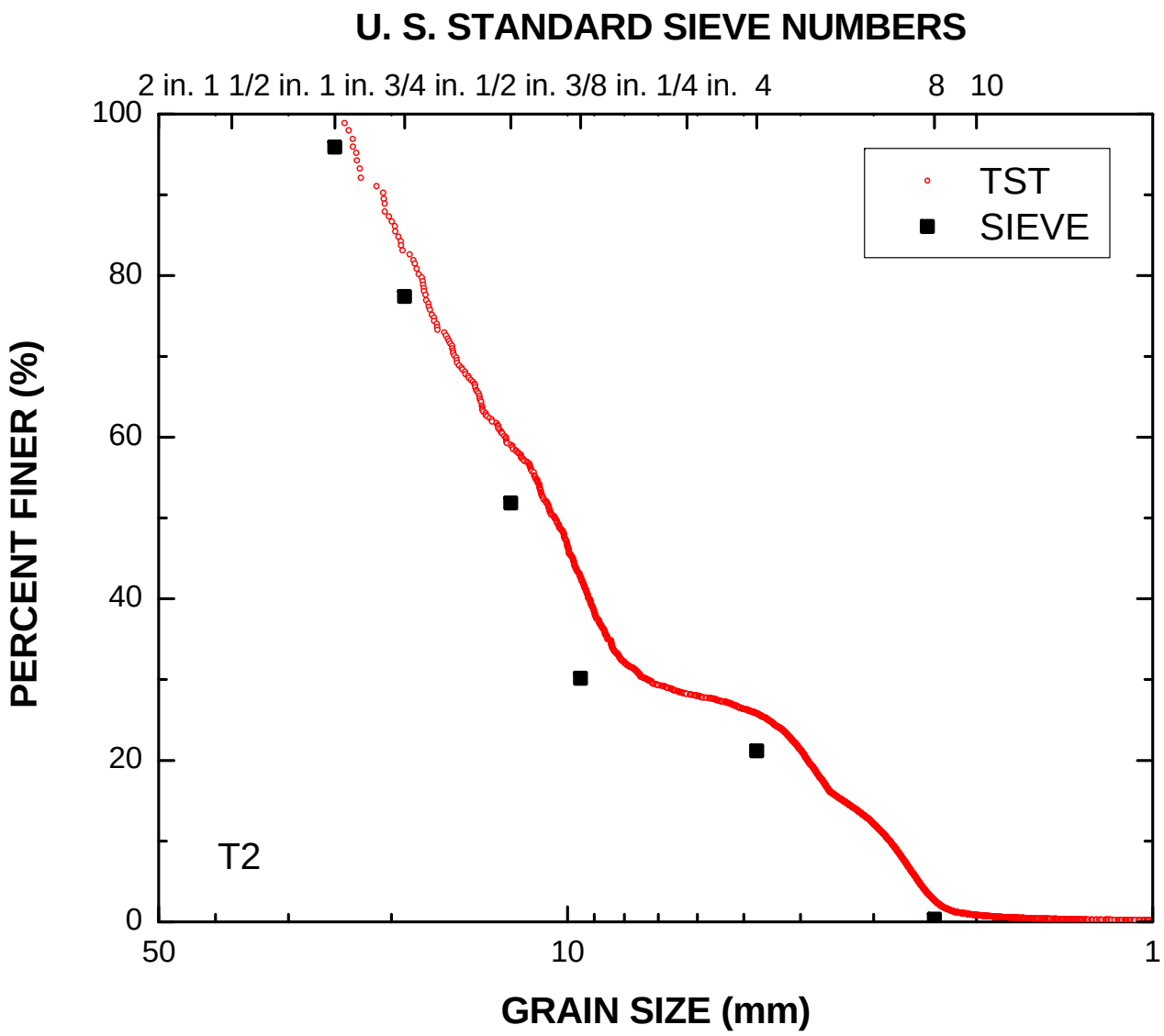
U. S. STANDARD SIEVE NUMBERS
2 in. 1 1/2 in. 1 in. 3/4 in. 1/2 in. 3/8 in. 1/4 in. 4 8 10
100
80
60
40
20
0
PERCENT FINER (%)
TST
SIEVE
T2
50
10
1
GRAIN SIZE (mm)

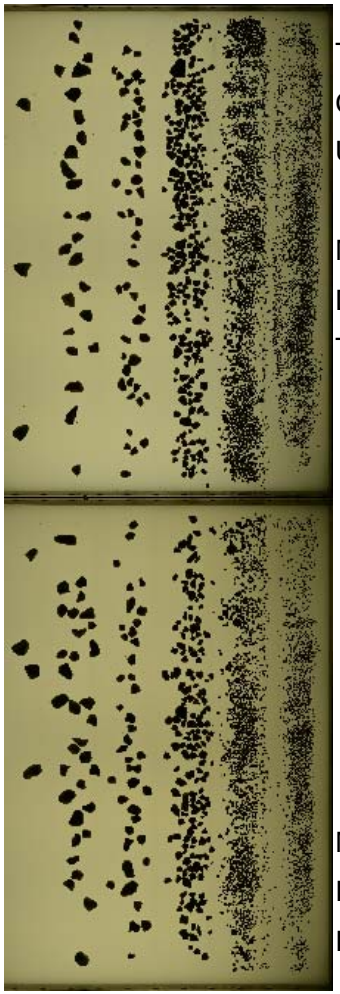

TRANSLUCENT SEGREGATION TABLE (TST)

GEOTECHNICAL ENGINEERING

UNIVERSITY OF MICHIGAN

MATERIAL: T3

DATE TESTED: 12-Jun-2012 13:39:50

TESTED BY: Ohm, H.S.

MAGNIFICATION (pix/mm): 5.4

IMAGE SIZE (pix): 9856 x 3264

IMAGE SIZE (mm): 1825.2 x 604.4

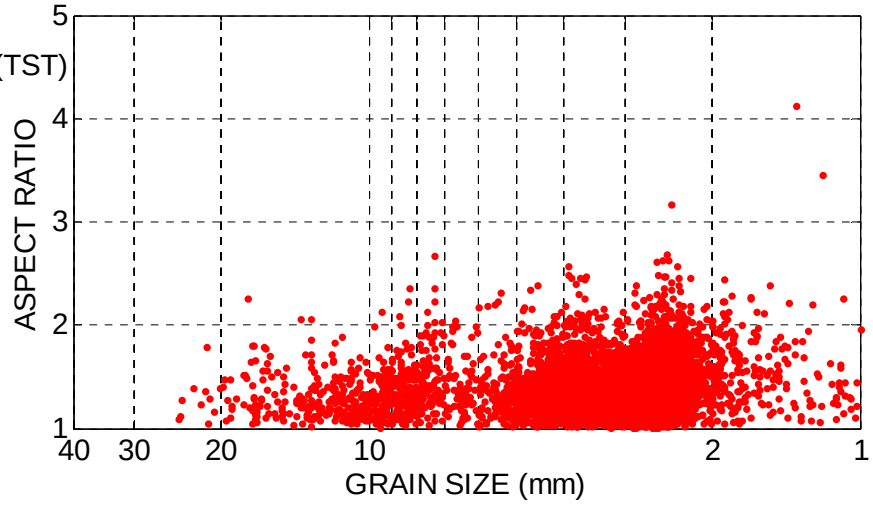

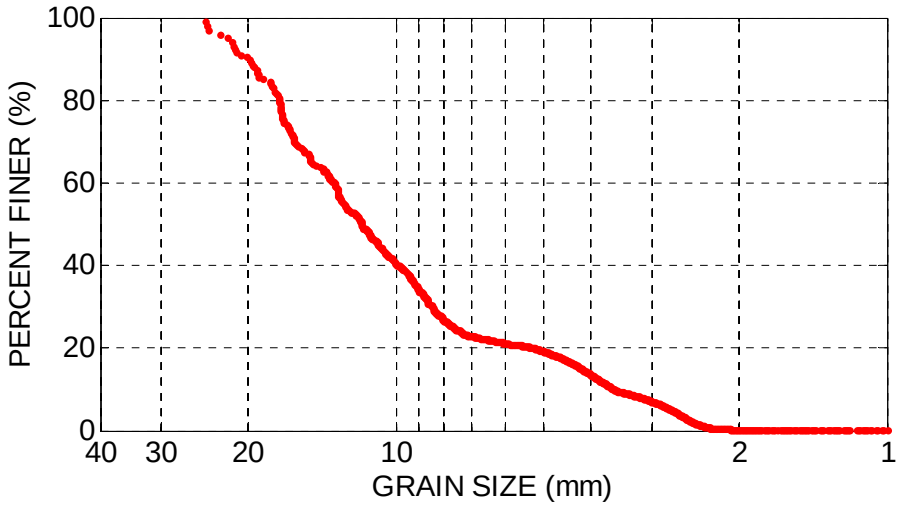

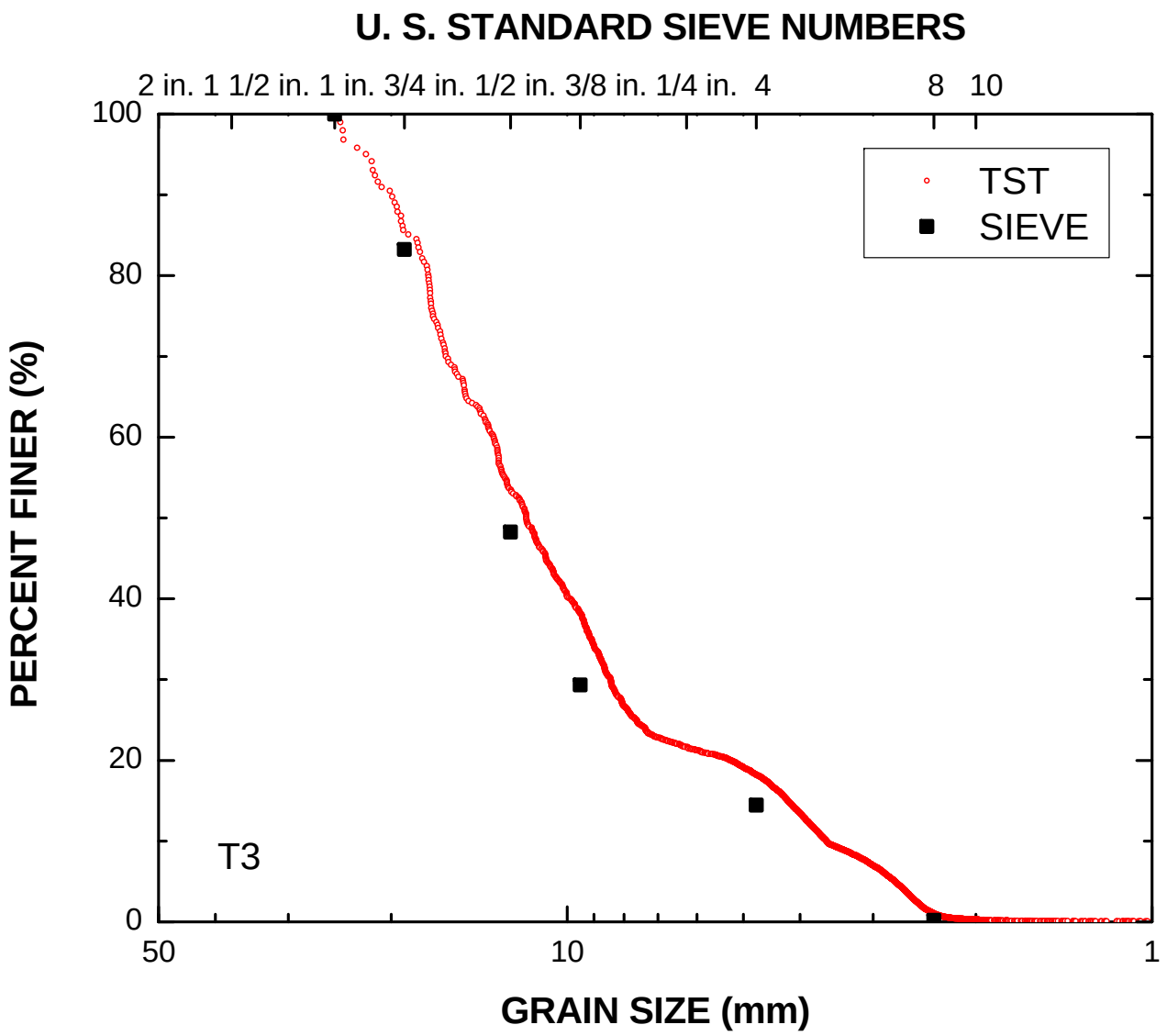
U. S. STANDARD SIEVE NUMBERS
2 in. 1 1/2 in. 1 in. 3/4 in. 1/2 in. 3/8 in. 1/4 in. 4 8 10
100
80
60
40
20
0
PERCENT FINER (%)
TST
SIEVE
T3
50
10
1
GRAIN SIZE (mm)

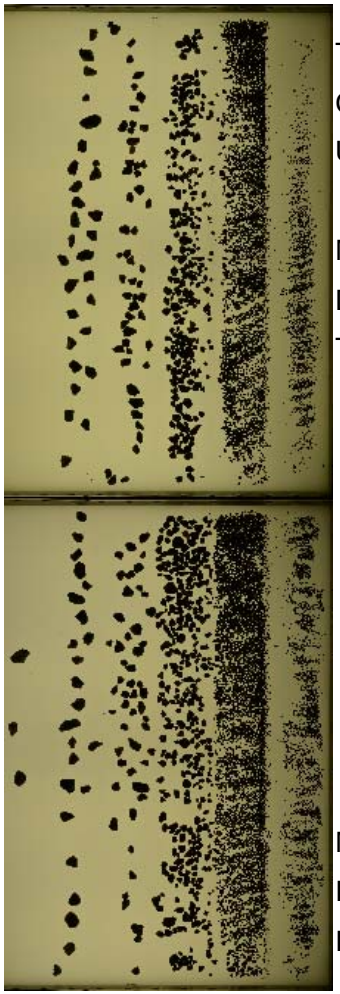

TRANSLUCENT SEGREGATION TABLE (TST)

GEOTECHNICAL ENGINEERING

UNIVERSITY OF MICHIGAN

MATERIAL: T4

DATE TESTED: 02-Jul-2012 12:56:52

TESTED BY: Ohm, H.S.

MAGNIFICATION (pix/mm): 5.4

IMAGE SIZE (pix): 9856 x 3264

IMAGE SIZE (mm): 1825.2 x 604.4

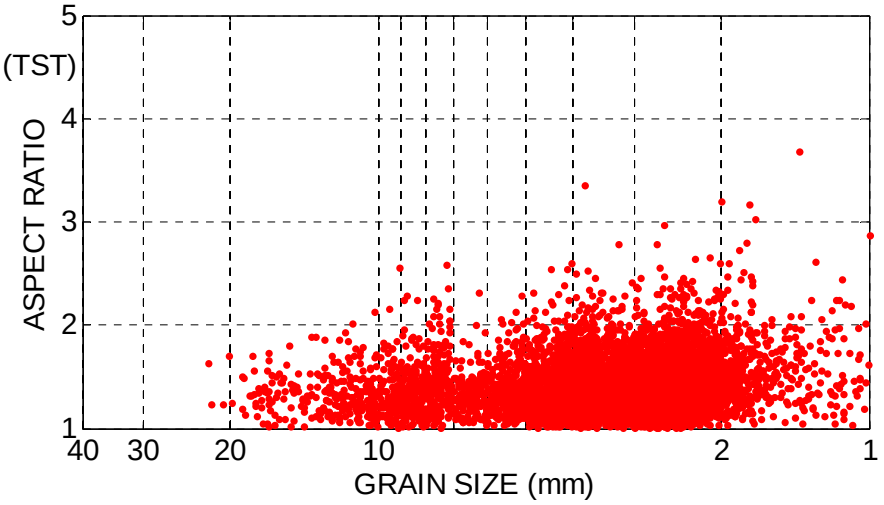

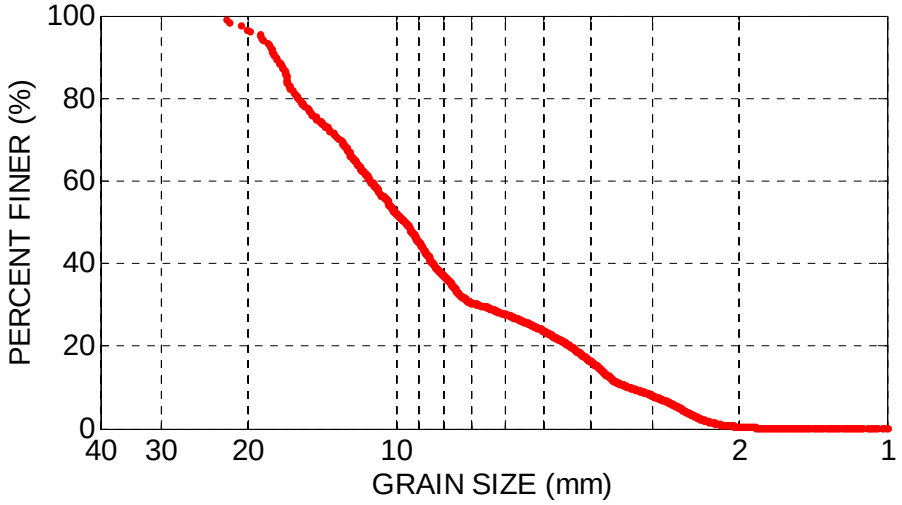

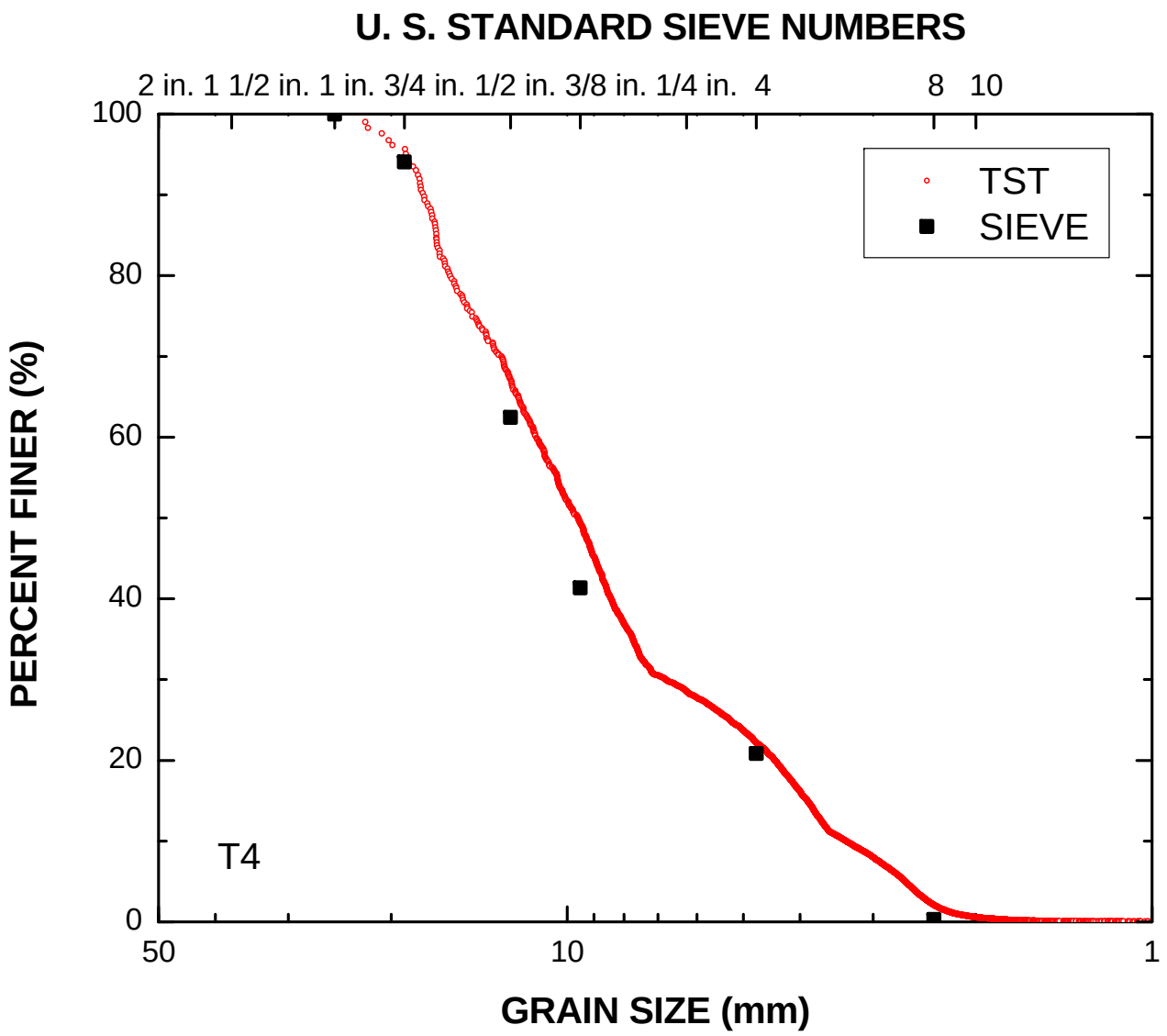
U. S. STANDARD SIEVE NUMBERS
2 in. 1 1/2 in. 1 in. 3/4 in. 1/2 in. 3/8 in. 1/4 in. 4 8 10
100
80
60
40
20
0
PERCENT FINER (%)
TST
SIEVE
T4
50
10
1
GRAIN SIZE (mm)

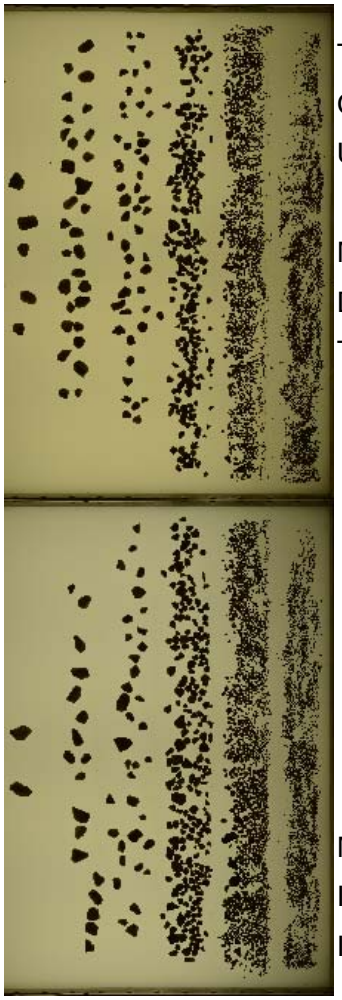

TRANSLUCENT SEGREGATION TABLE (TST)

GEOTECHNICAL ENGINEERING

UNIVERSITY OF MICHIGAN

MATERIAL: T5

DATE TESTED: 02-Jul-2012 14:02:22

TESTED BY: Ohm, H.S.

MAGNIFICATION (pix/mm): 5.4

IMAGE SIZE (pix): 9856 x 3264

IMAGE SIZE (mm): 1825.2 x 604.4

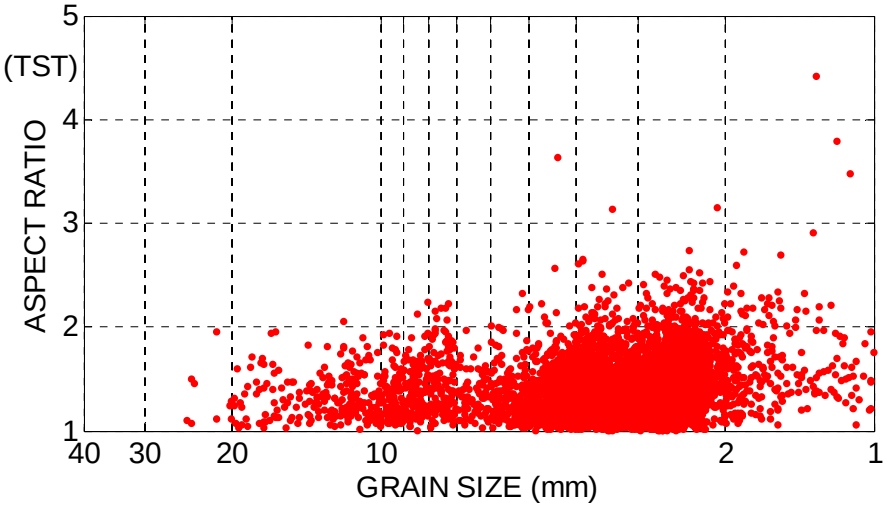

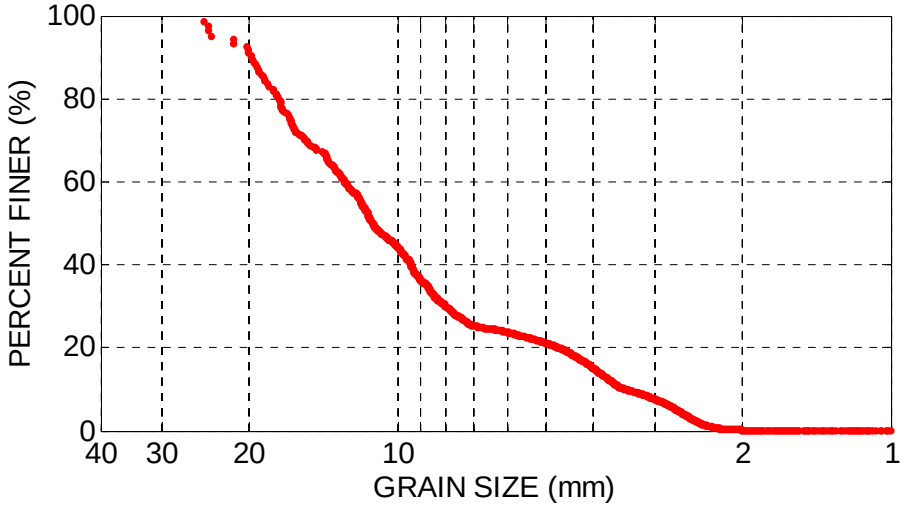

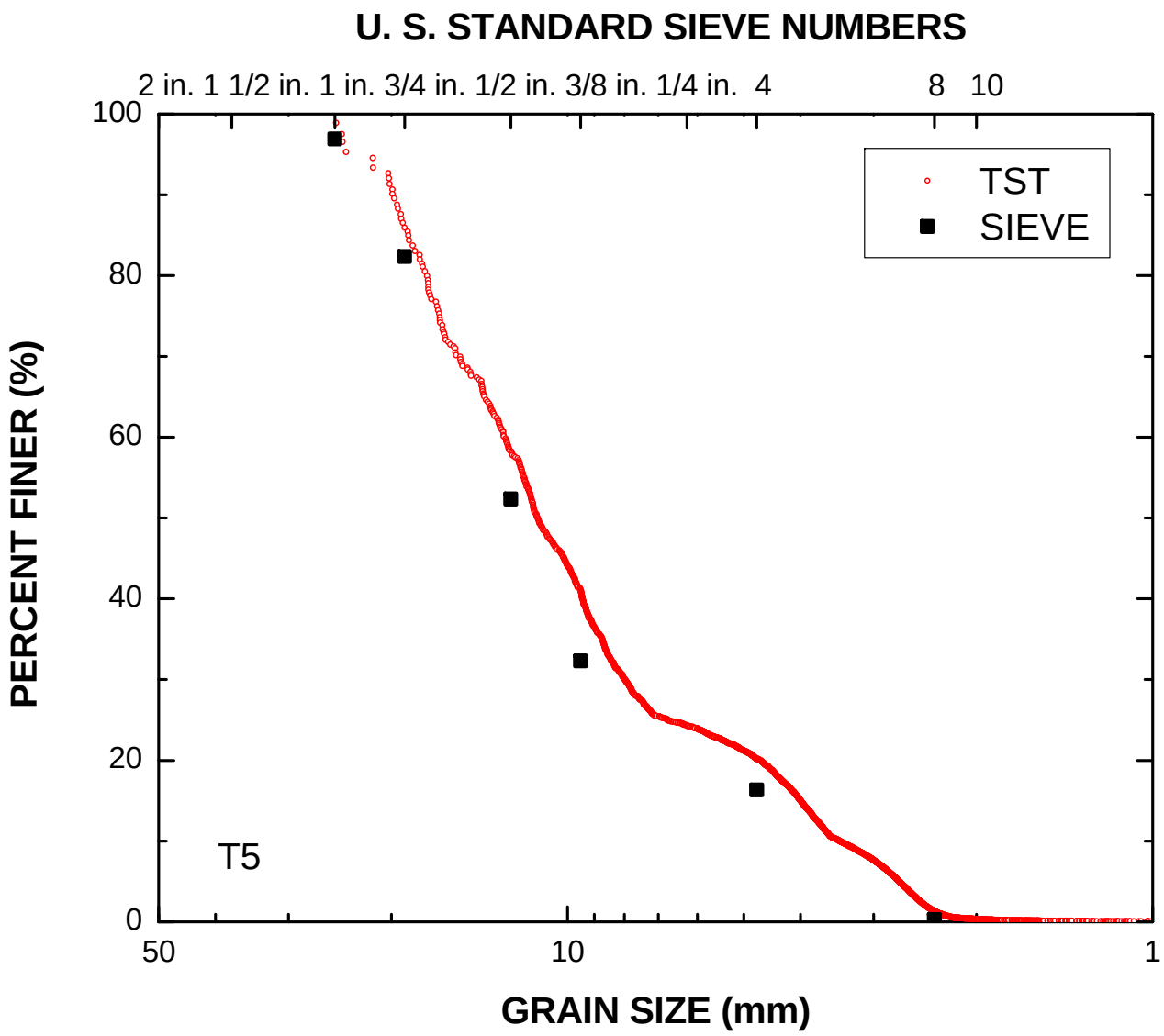
U. S. STANDARD SIEVE NUMBERS
2 in. 1 1/2 in. 1 in. 3/4 in. 1/2 in. 3/8 in. 1/4 in. 4 8 10
100
80
60
40
20
0
PERCENT FINER (%)
TST
SIEVE
T5
50
10
1
GRAIN SIZE (mm)

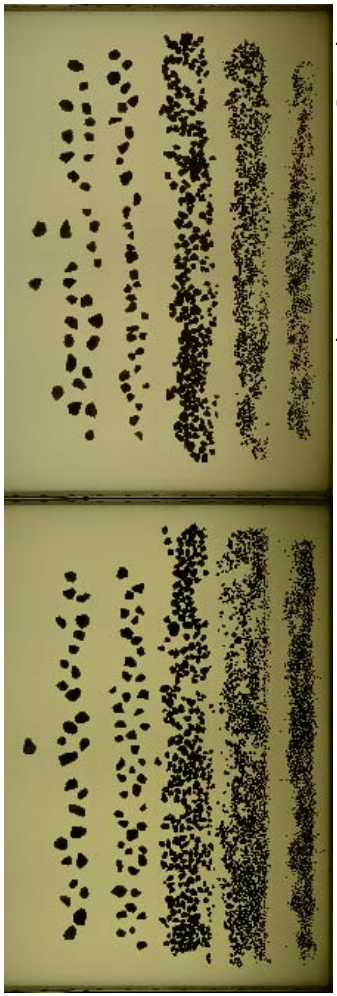

TRANSLUCENT SEGREGATION TABLE (TST)
GEOTECHNICAL ENGINEERING
UNIVERSITY OF MICHIGAN

MATERIAL: T6
DATE TESTED: 02-Jul-2012 15:01:56
TESTED BY: Ohm, H.S.

MAGNIFICATION (pix/mm): 5.4
IMAGE SIZE (pix): 9856 x 3264
IMAGE SIZE (mm): 1825.2 x 604.4

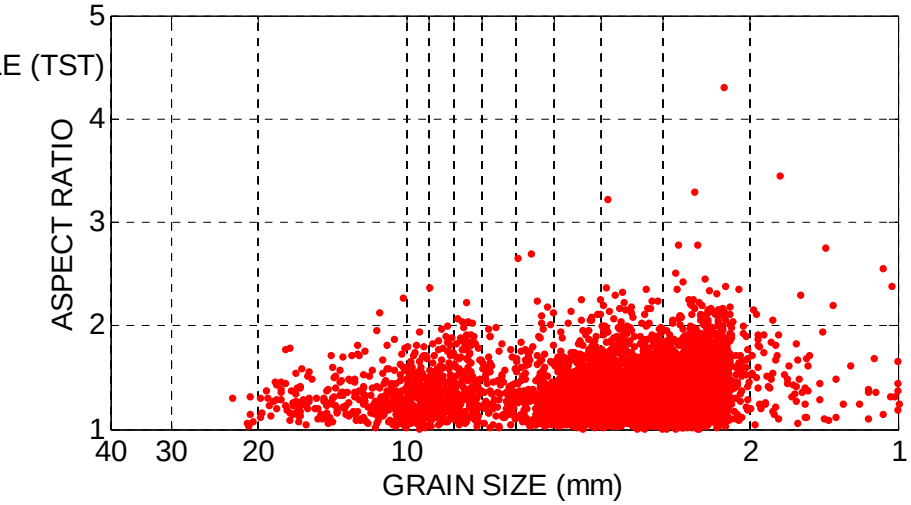

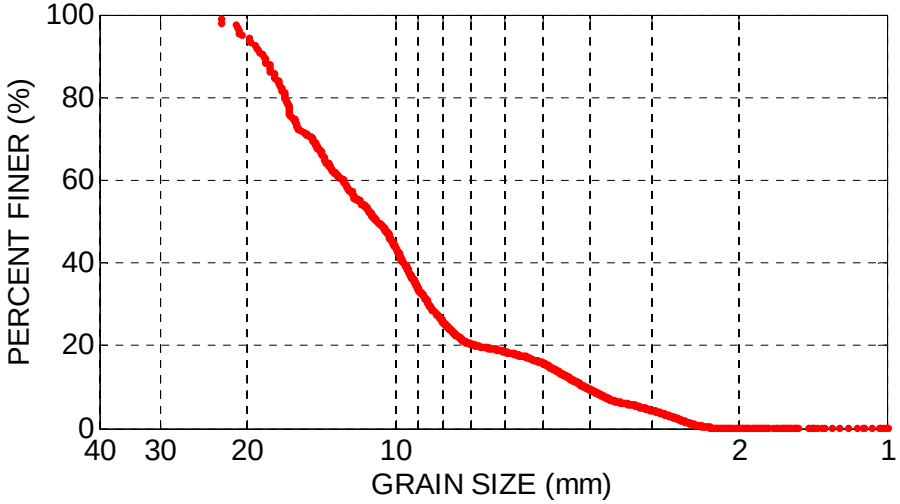

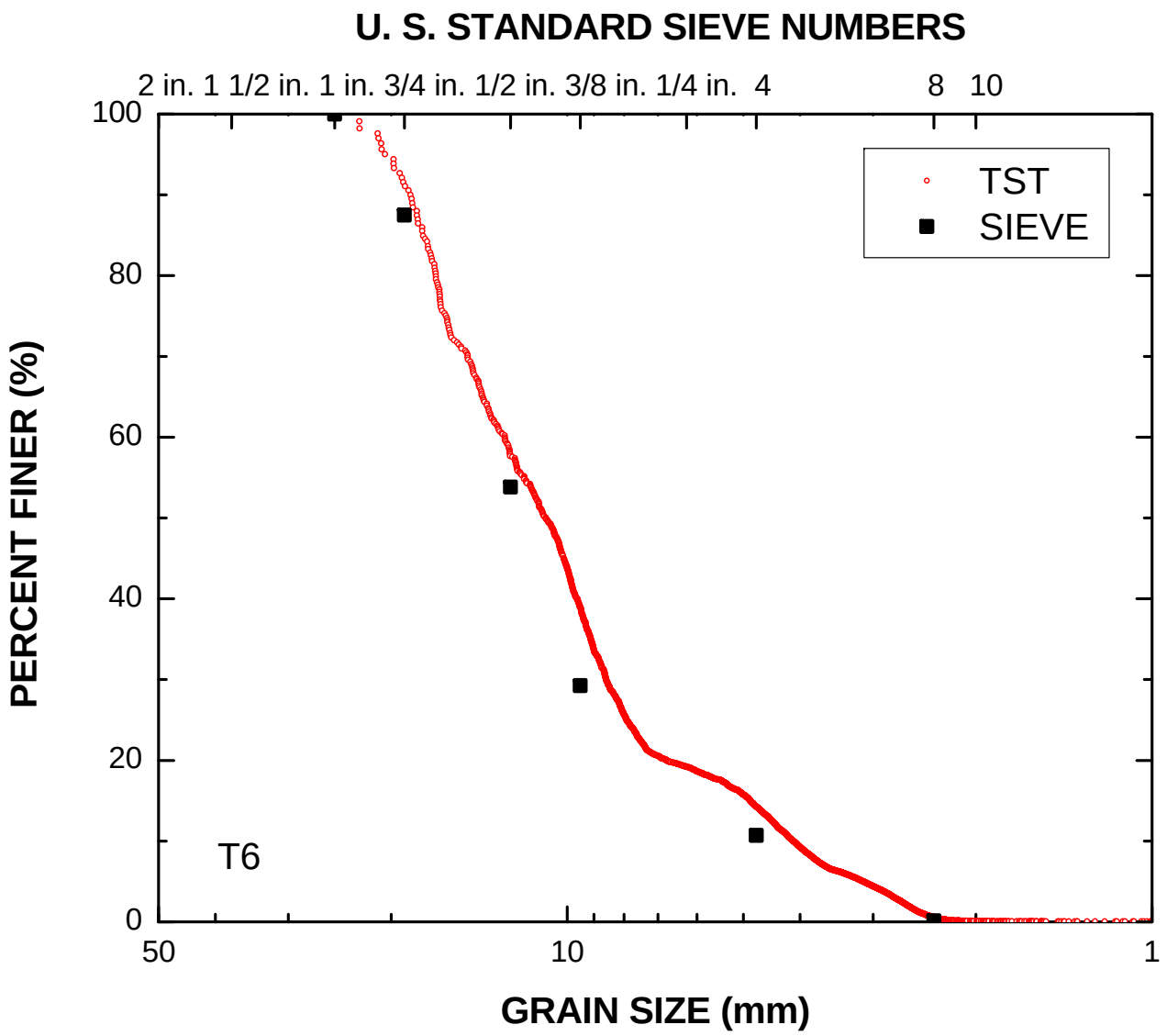
U. S. STANDARD SIEVE NUMBERS
2 in. 1 1/2 in. 1 in. 3/4 in. 1/2 in. 3/8 in. 1/4 in. 4 8 10
100
80
60
40
20
0
PERCENT FINER (%)
TST
SIEVE
T6
50
10
1
GRAIN SIZE (mm)

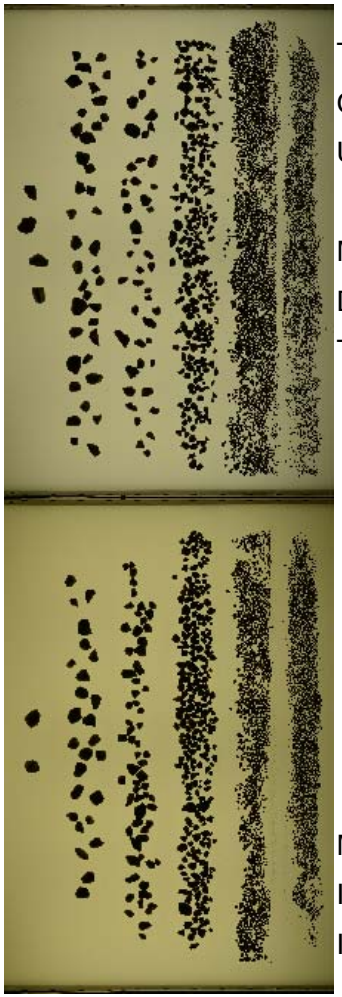

TRANSLUCENT SEGREGATION TABLE (TST)

GEOTECHNICAL ENGINEERING

UNIVERSITY OF MICHIGAN

MATERIAL: T7

DATE TESTED: 03-Jul-2012 11:41:56

TESTED BY: Ohm, H.S.

MAGNIFICATION (pix/mm): 5.4

IMAGE SIZE (pix): 9856 x 3264

IMAGE SIZE (mm): 1825.2 x 604.4

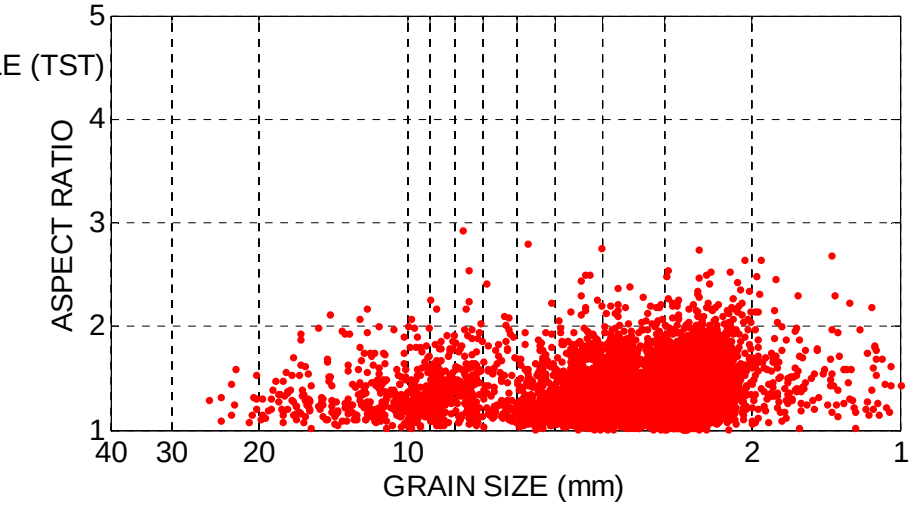

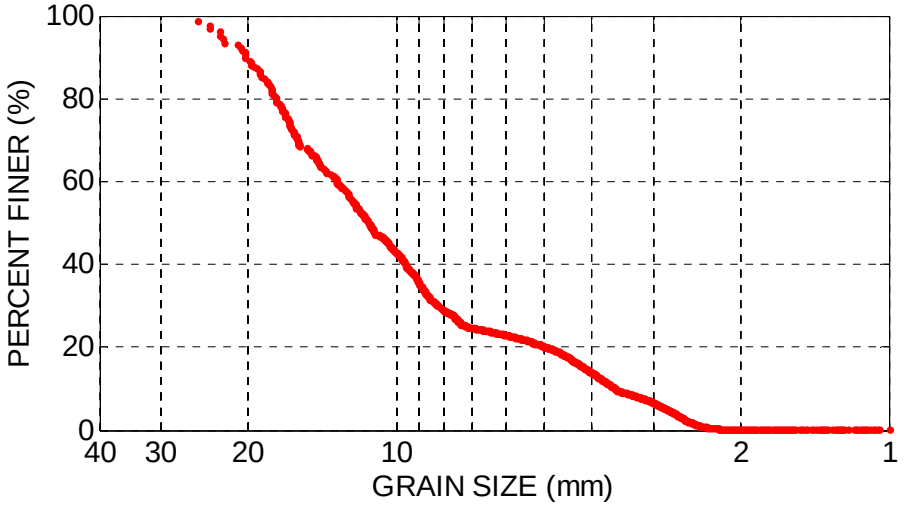

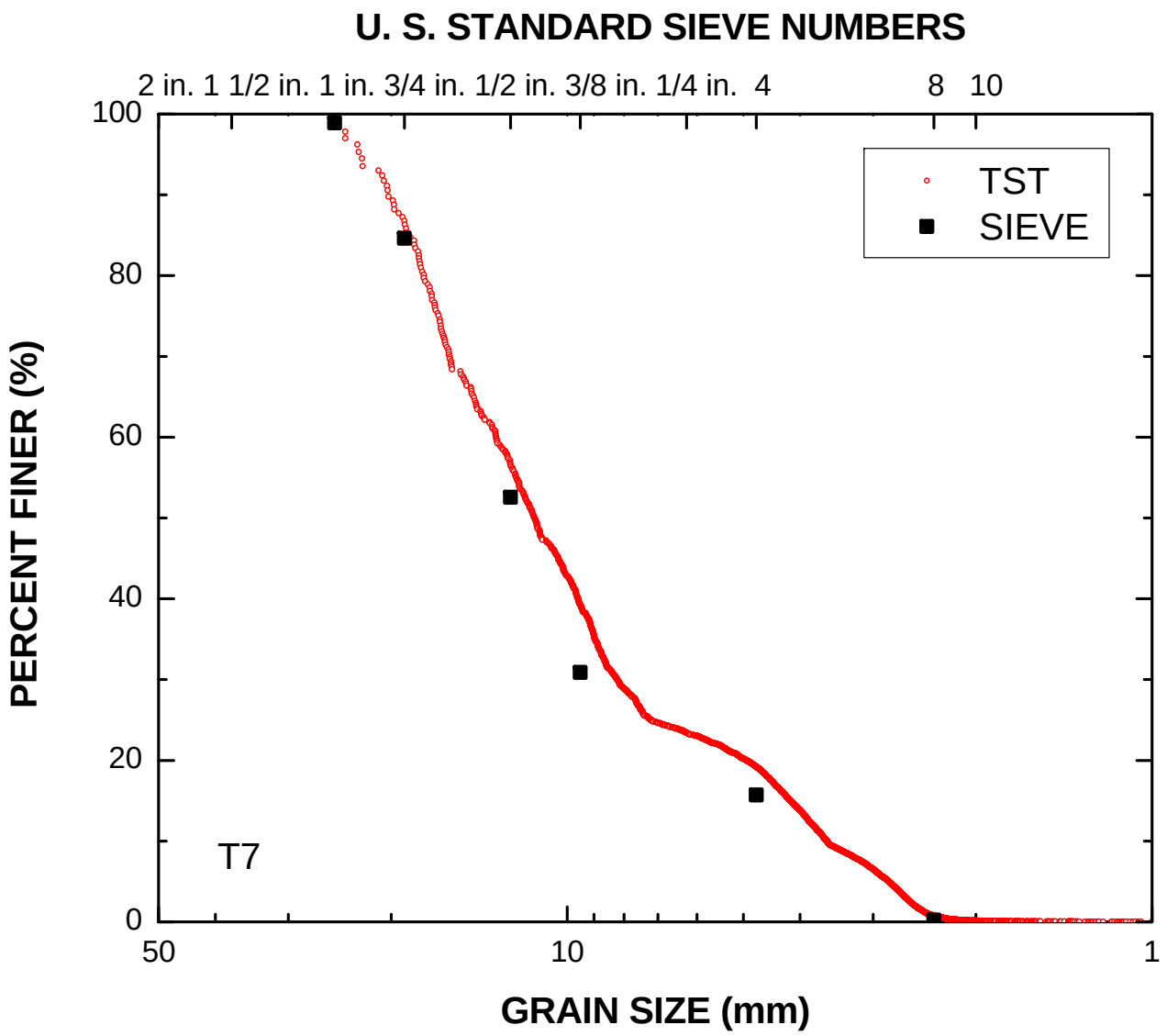
U. S. STANDARD SIEVE NUMBERS
2 in. 1 1/2 in. 1 in. 3/4 in. 1/2 in. 3/8 in. 1/4 in. 4 8 10
100
80
60
40
20
0
PERCENT FINER (%)
TST
SIEVE
T7
50
10
1
GRAIN SIZE (mm)

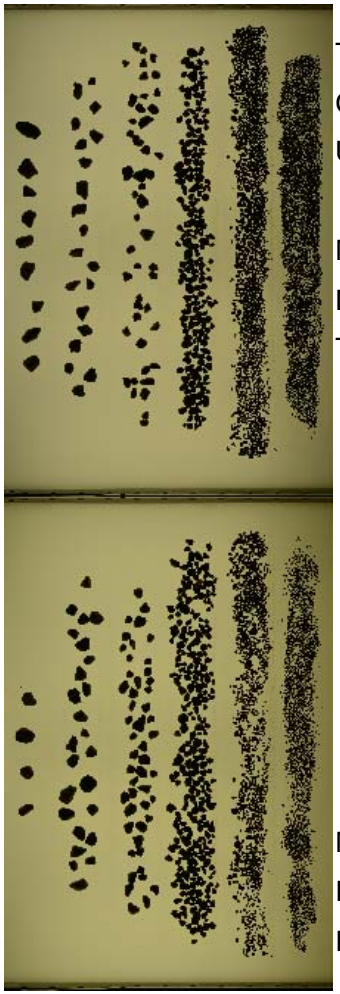

TRANSLUCENT SEGREGATION TABLE (TST)

GEOTECHNICAL ENGINEERING

UNIVERSITY OF MICHIGAN

MATERIAL: T8

DATE TESTED: 03-Jul-2012 13:02:58

TESTED BY: Ohm, H.S.

MAGNIFICATION (pix/mm): 5.4

IMAGE SIZE (pix): 9856 x 3264

IMAGE SIZE (mm): 1825.2 x 604.4

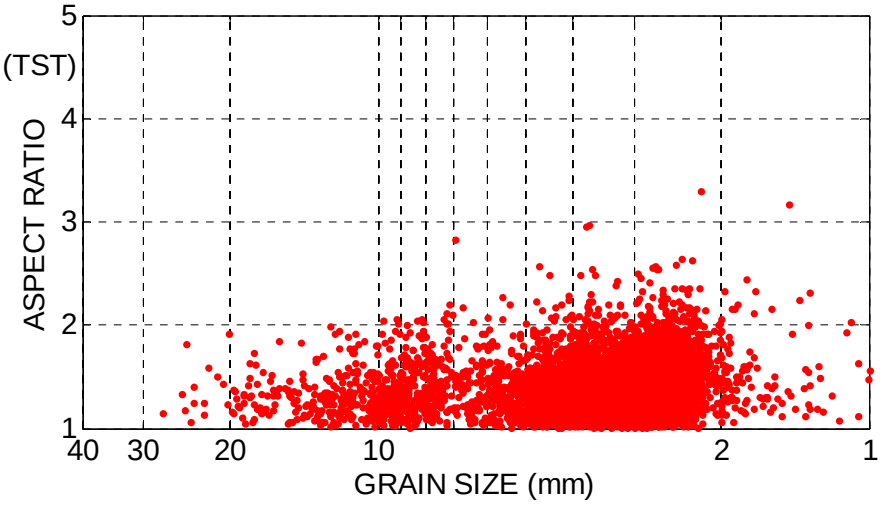

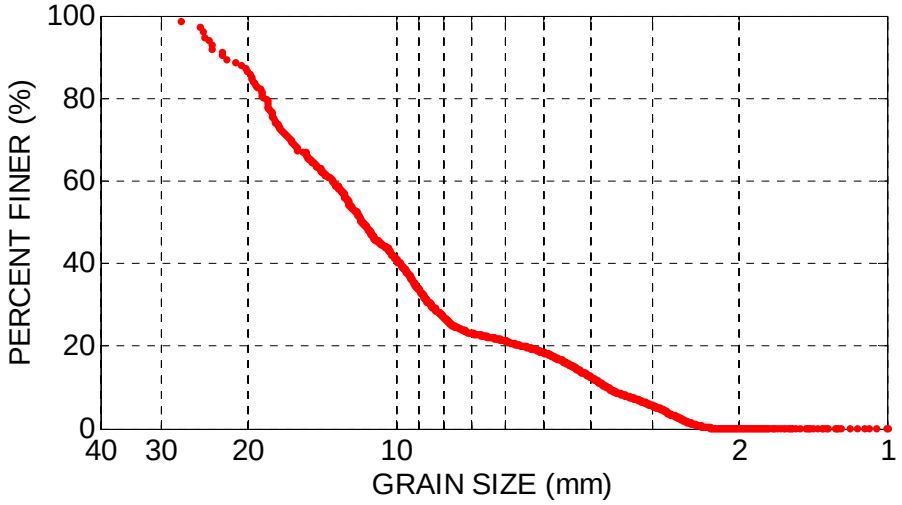

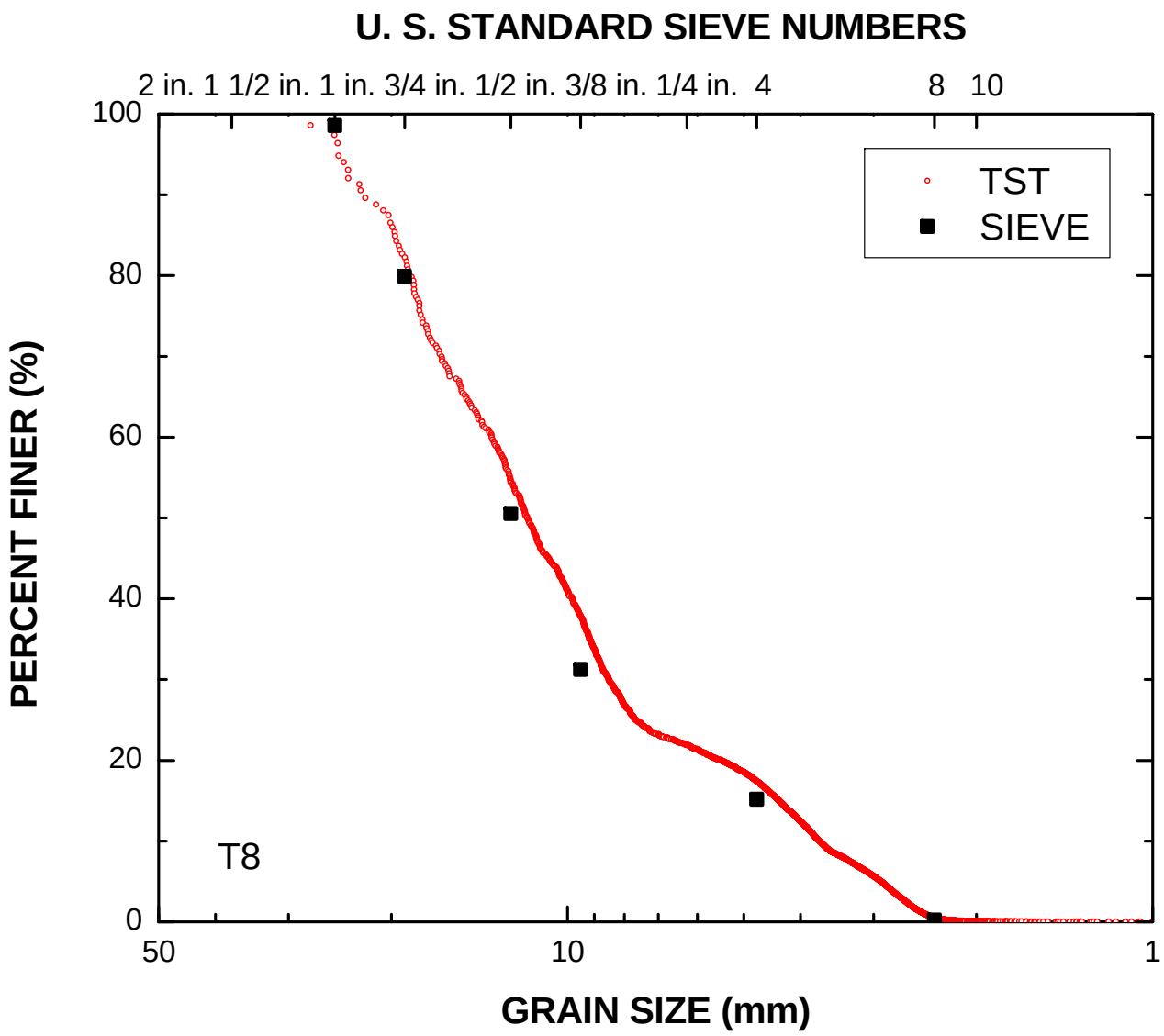
U. S. STANDARD SIEVE NUMBERS
2 in. 1 1/2 in. 1 in. 3/4 in. 1/2 in. 3/8 in. 1/4 in. 4 8 10
100
80
60
40
20
0
PERCENT FINER (%)
TST
SIEVE
T8
50
10
1
GRAIN SIZE (mm)

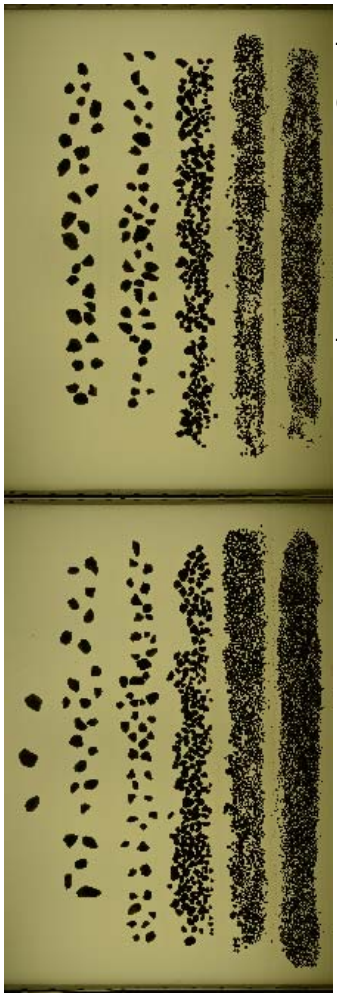

TRANSLUCENT SEGREGATION TABLE (TST)

GEOTECHNICAL ENGINEERING

UNIVERSITY OF MICHIGAN

MATERIAL: T9

DATE TESTED: 03-Jul-2012 14:17:16

TESTED BY: Ohm, H.S.

MAGNIFICATION (pix/mm): 5.4

IMAGE SIZE (pix): 9856 x 3264

IMAGE SIZE (mm): 1825.2 x 604.4

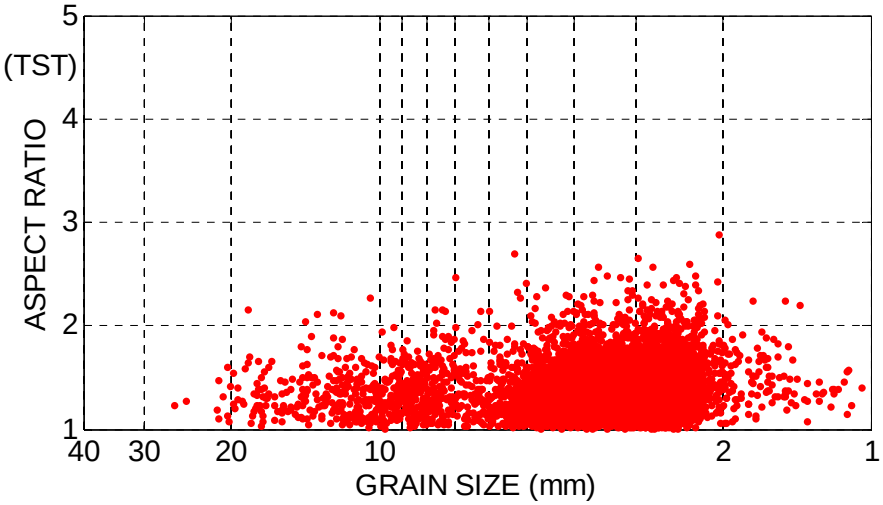

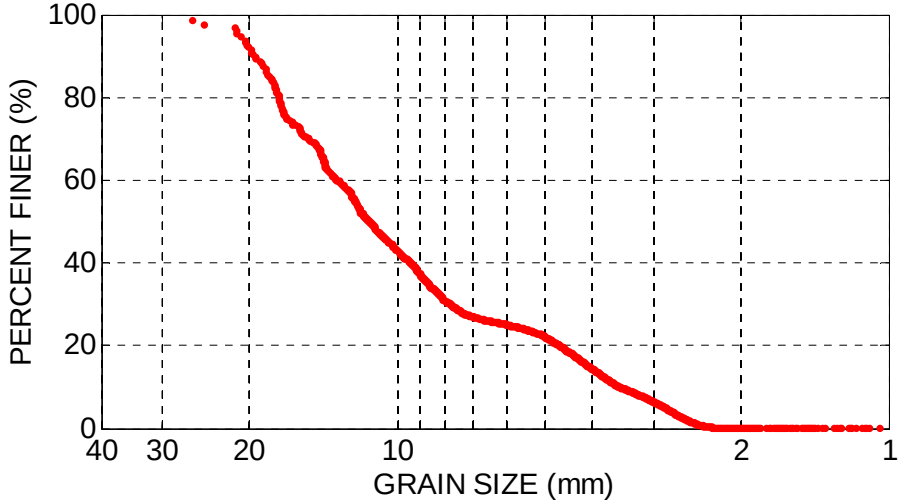

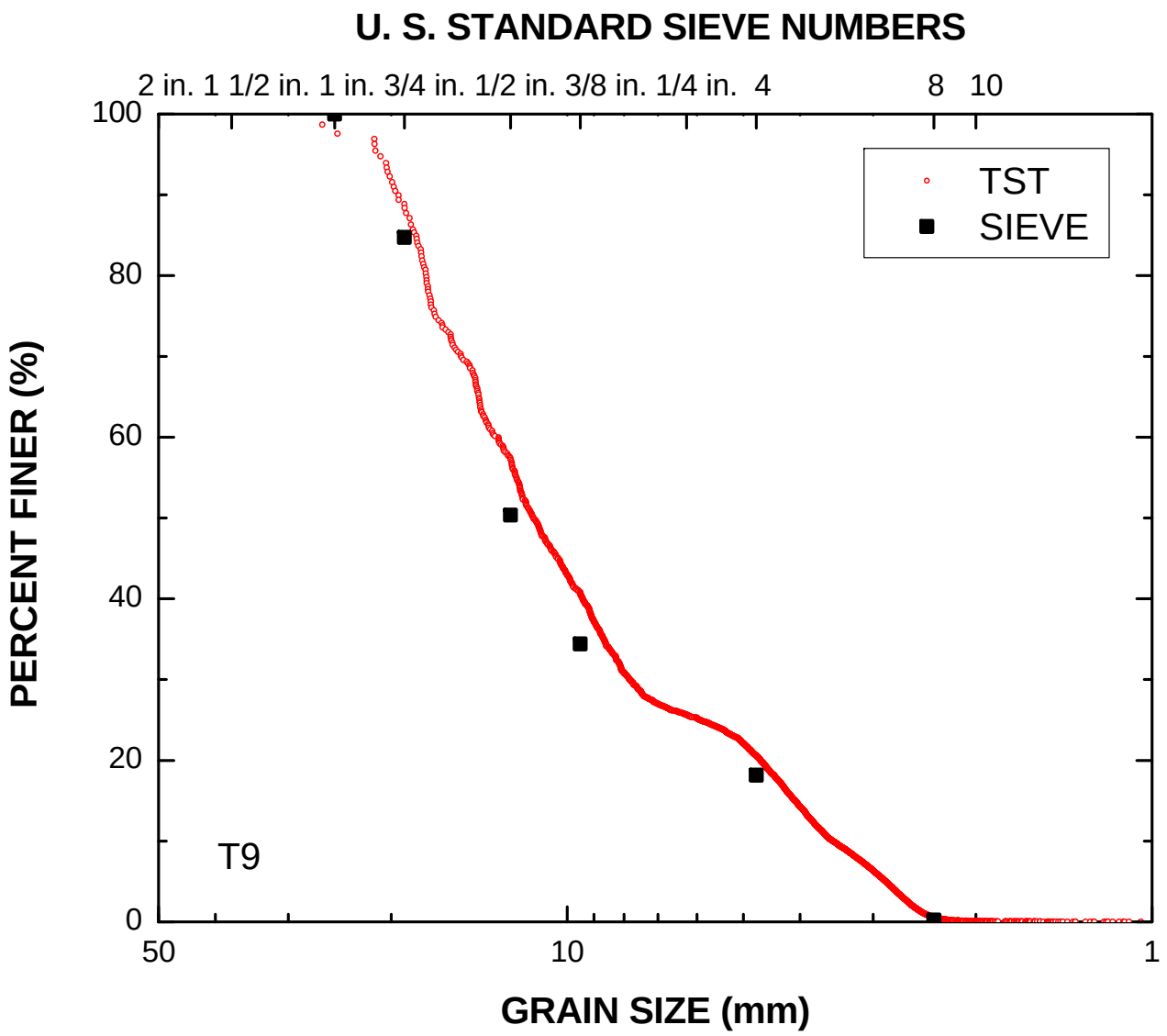
U. S. STANDARD SIEVE NUMBERS
2 in. 1 1/2 in. 1 in. 3/4 in. 1/2 in. 3/8 in. 1/4 in. 4 8 10
100
80
60
40
20
0
PERCENT FINER (%)
TST
SIEVE
T9
50
10
1
GRAIN SIZE (mm)

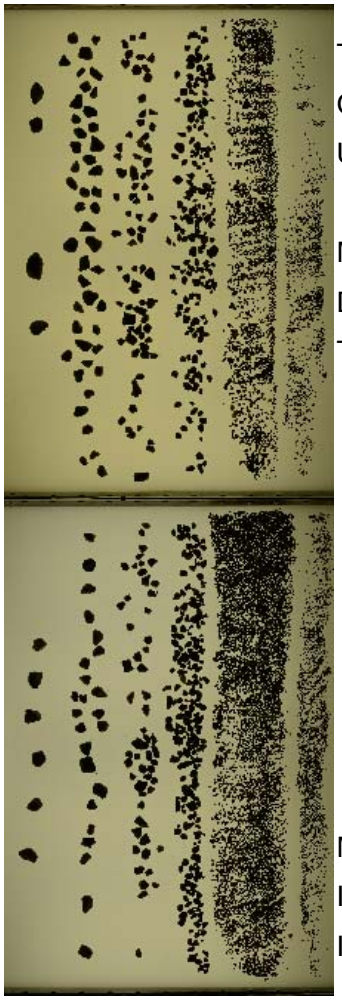

TRANSLUCENT SEGREGATION TABLE (TST)
GEOTECHNICAL ENGINEERING
UNIVERSITY OF MICHIGAN

MATERIAL: T10
DATE TESTED: 04-Jul-2012 10:55:12
TESTED BY: Ohm, H.S.

MAGNIFICATION (pix/mm): 5.4
IMAGE SIZE (pix): 9856 x 3264
IMAGE SIZE (mm): 1825.2 x 604.4

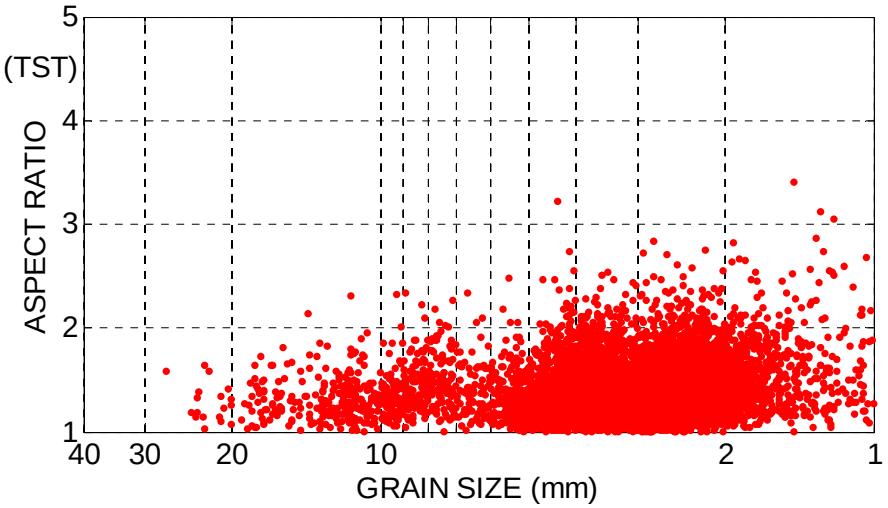

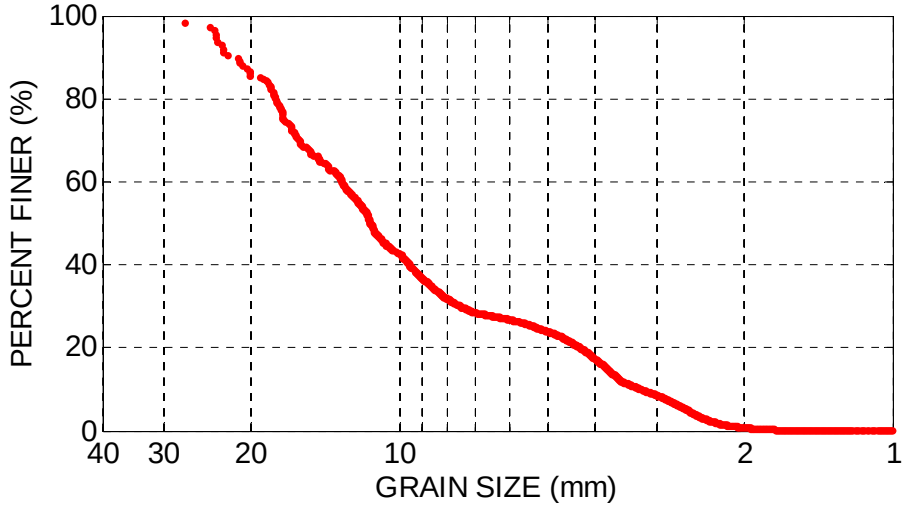

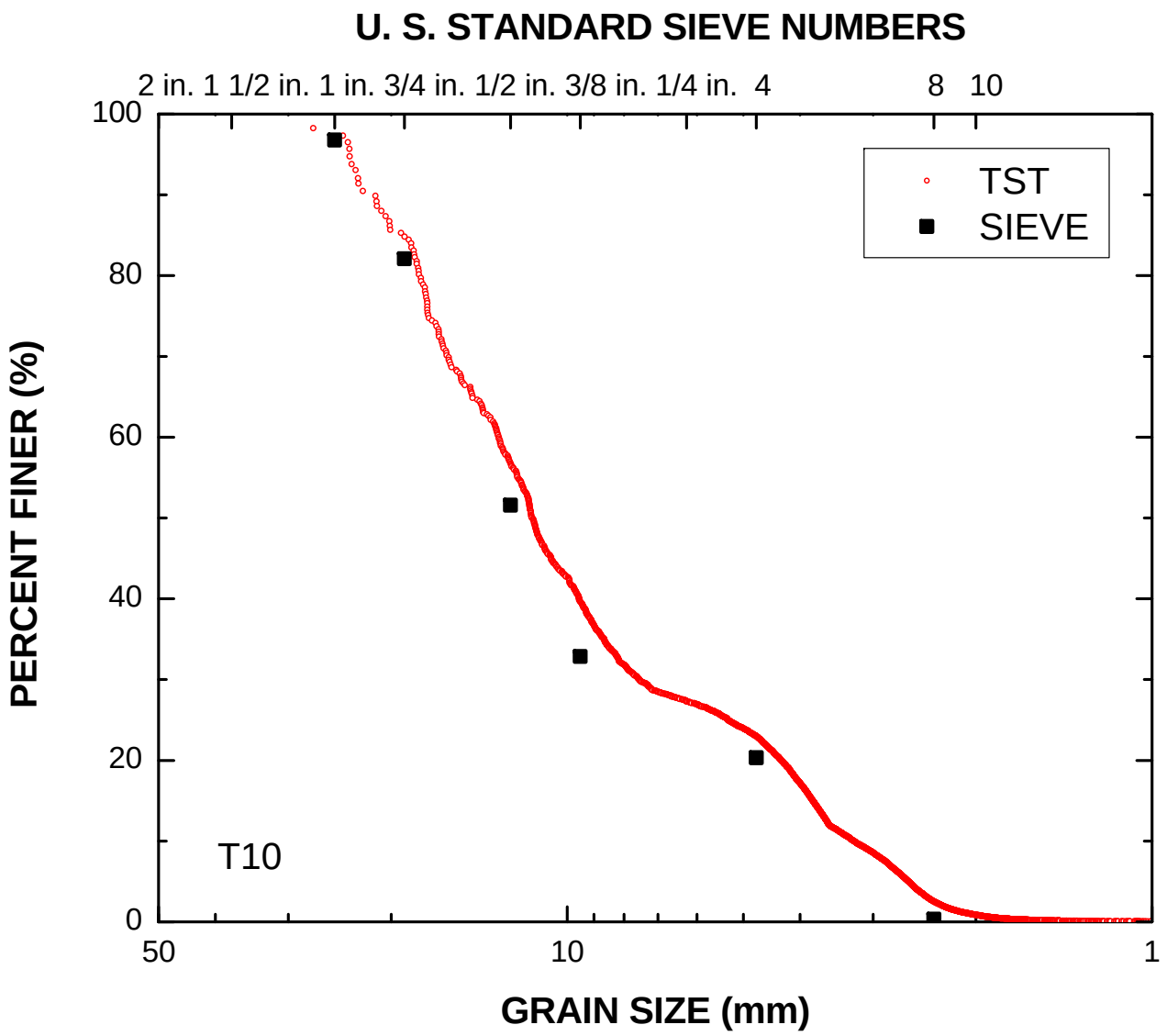
U. S. STANDARD SIEVE NUMBERS
2 in. 1 1/2 in. 1 in. 3/4 in. 1/2 in. 3/8 in. 1/4 in. 4 8 10
100
80
60
40
20
0
50
10
1
PERCENT FINER (%)
GRAIN SIZE (mm)
TST
SIEVE
T10

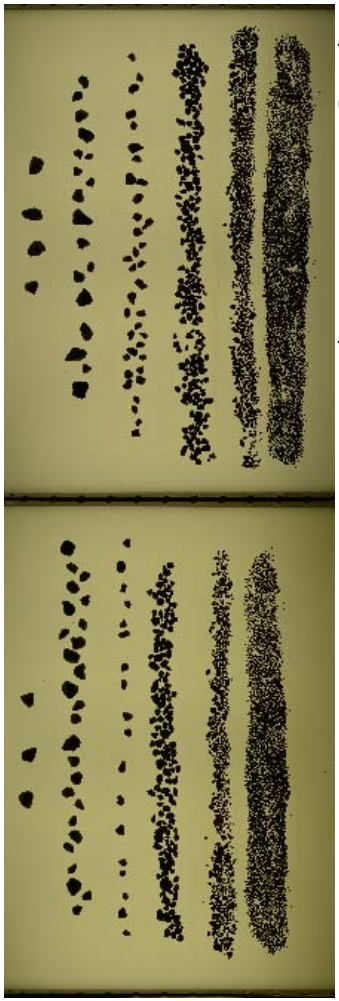

TRANSLUCENT SEGREGATION TABLE (TST)

GEOTECHNICAL ENGINEERING

UNIVERSITY OF MICHIGAN

MATERIAL: T11

DATE TESTED: 05-Jul-2012 12:24:56

TESTED BY: Ohm, H.S.

MAGNIFICATION (pix/mm): 5.4

IMAGE SIZE (pix): 9856 x 3264

IMAGE SIZE (mm): 1825.2 x 604.4

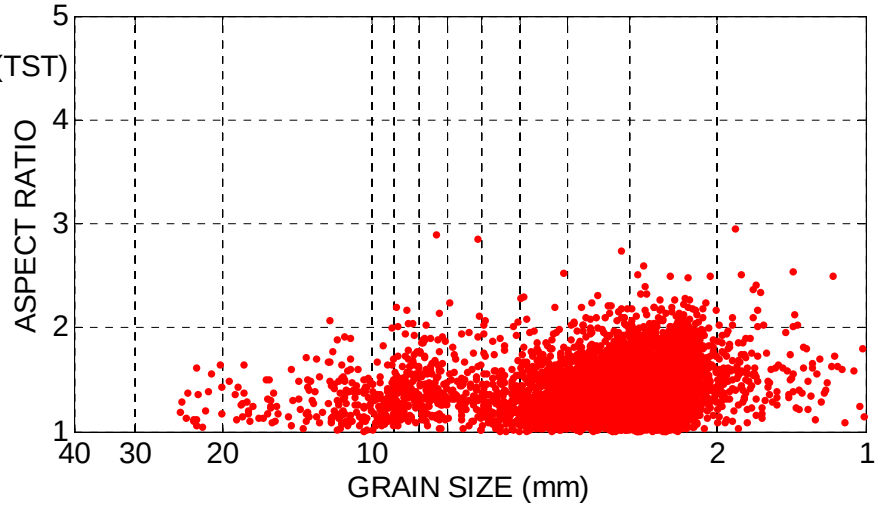

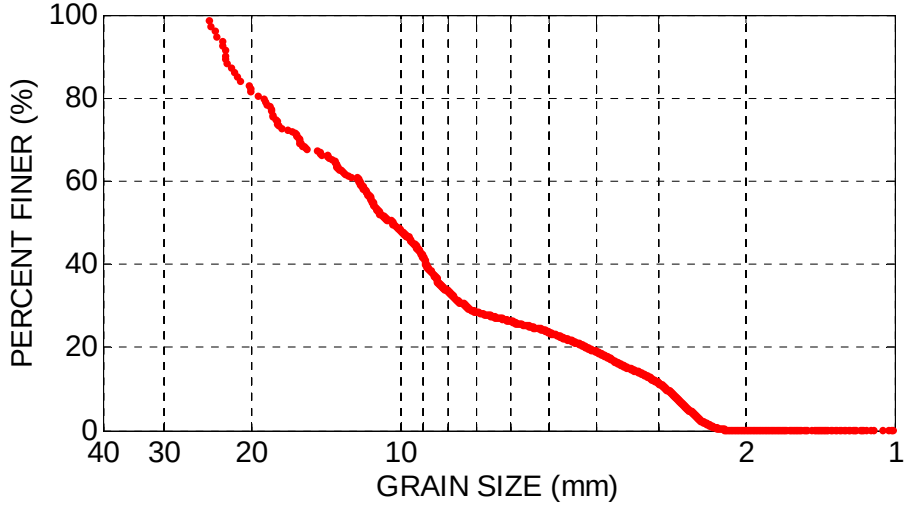

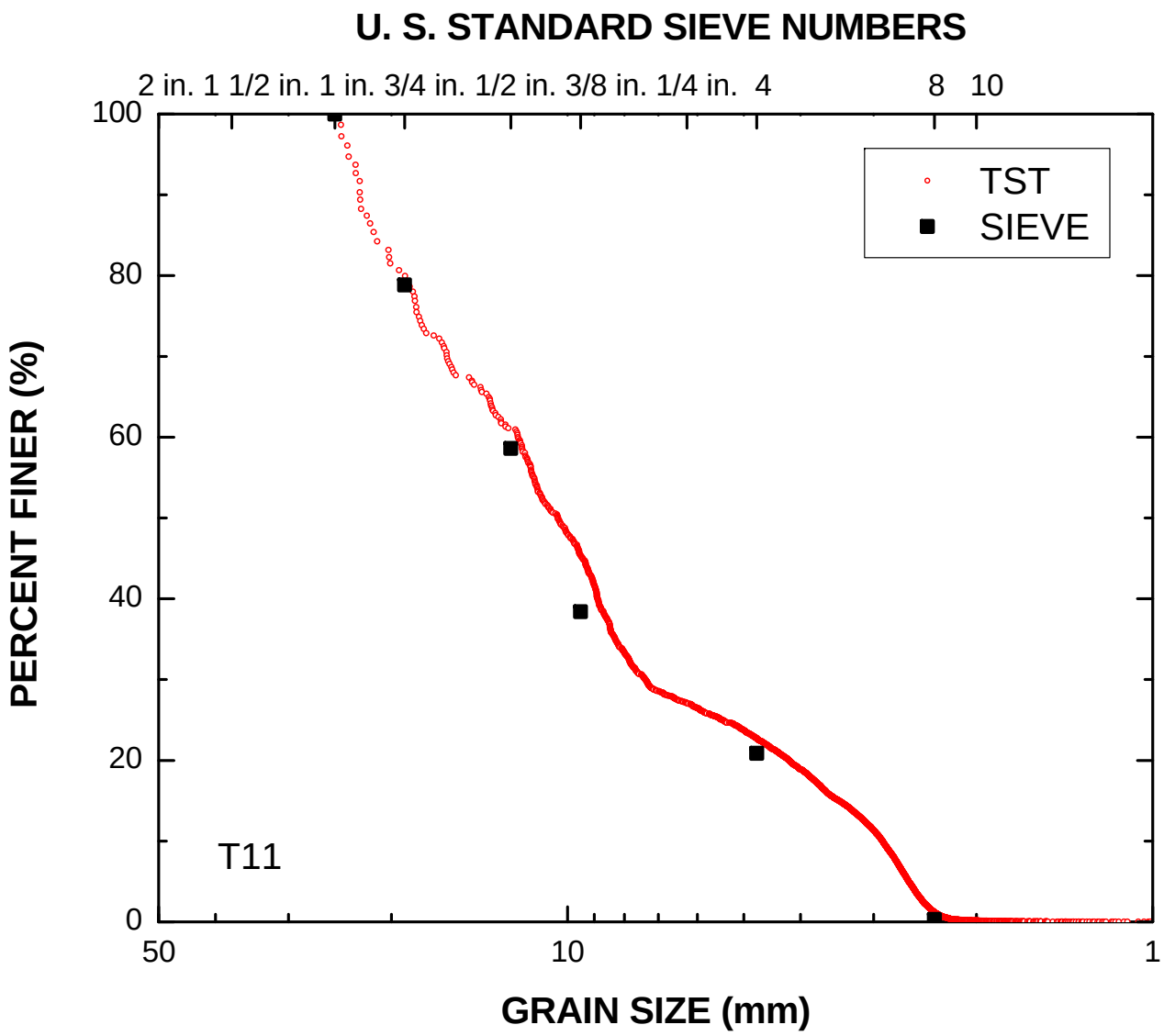
U. S. STANDARD SIEVE NUMBERS
2 in. 1 1/2 in. 1 in. 3/4 in. 1/2 in. 3/8 in. 1/4 in. 4 8 10
100
80
60
40
20
0
PERCENT FINER (%)
TST
SIEVE
T11
50
10
1
GRAIN SIZE (mm)

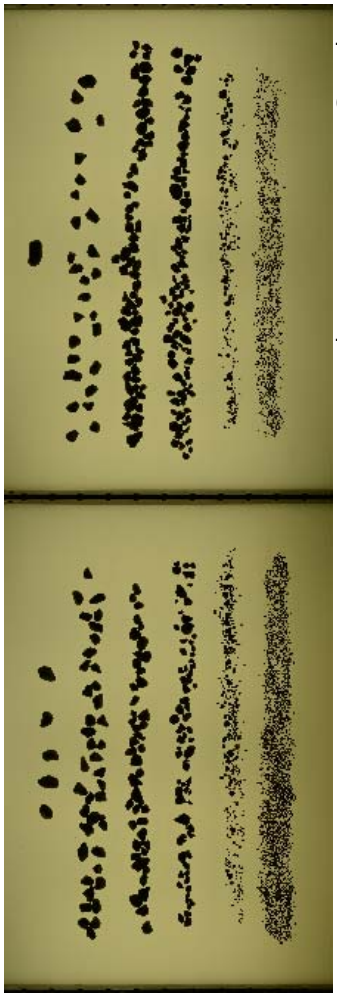

TRANSLUCENT SEGREGATION TABLE (TST)

GEOTECHNICAL ENGINEERING

UNIVERSITY OF MICHIGAN

MATERIAL: T12

DATE TESTED: 05-Jul-2012 13:26:12

TESTED BY: Ohm, H.S.

MAGNIFICATION (pix/mm): 5.4

IMAGE SIZE (pix): 9856 x 3264

IMAGE SIZE (mm): 1825.2 x 604.4

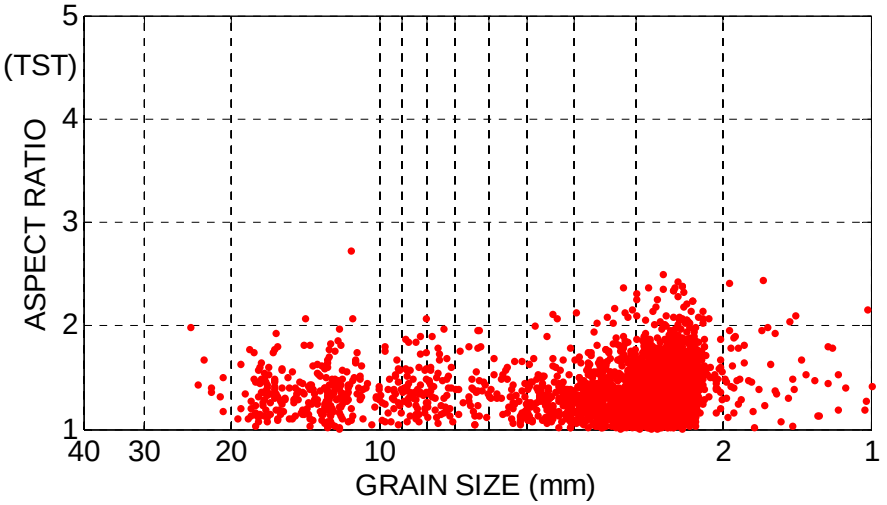

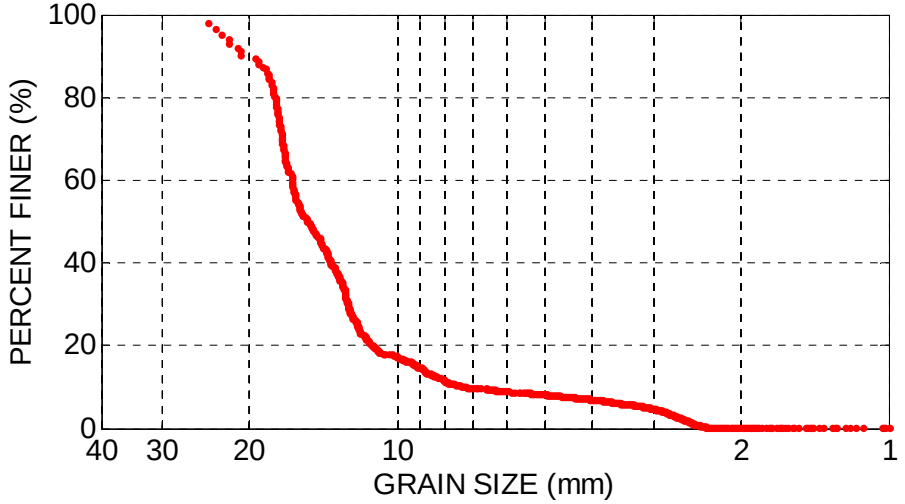

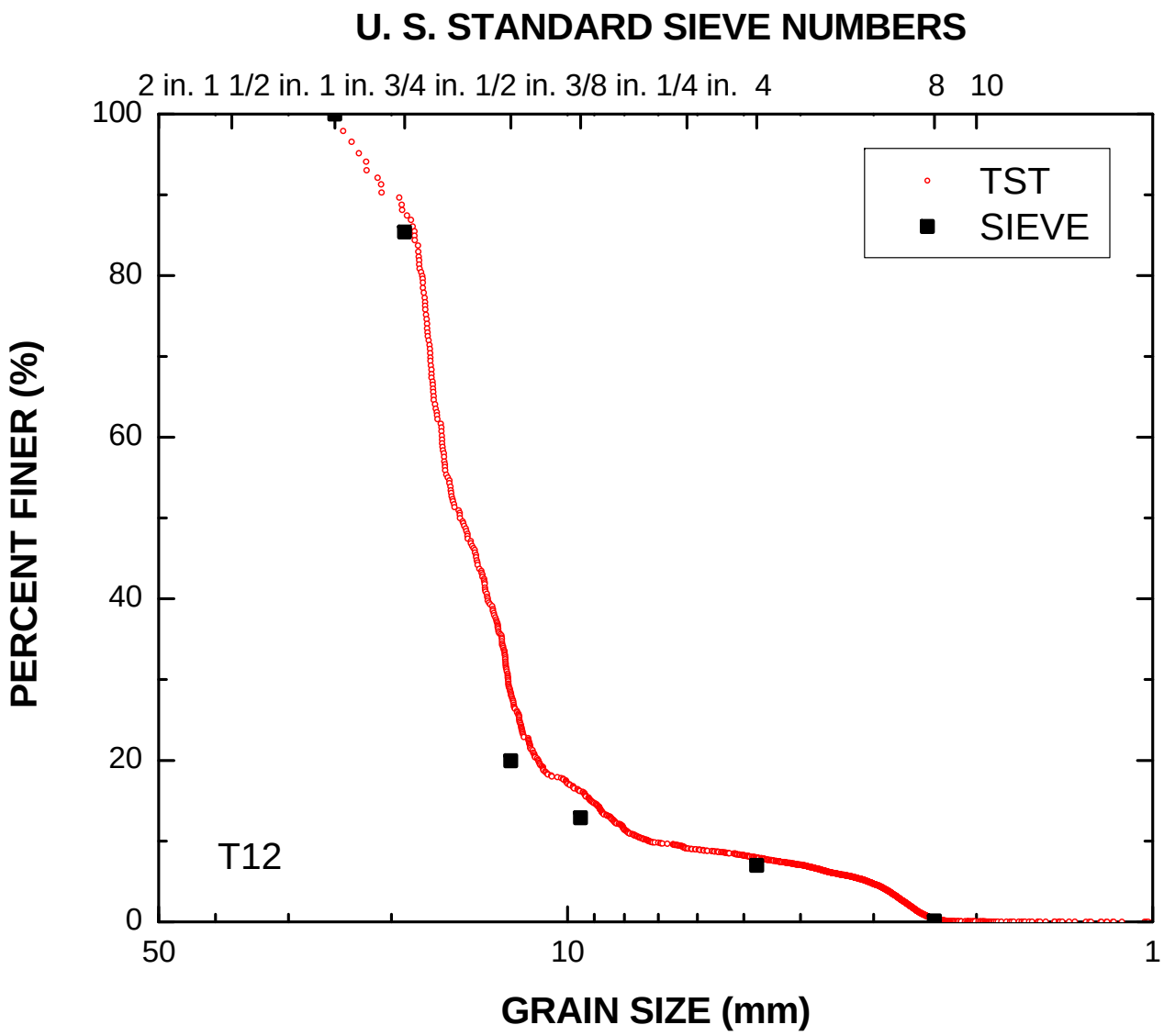
U. S. STANDARD SIEVE NUMBERS
2 in. 1 1/2 in. 1 in. 3/4 in. 1/2 in. 3/8 in. 1/4 in. 4 8 10
100
80
60
40
20
0
PERCENT FINER (%)
TST
SIEVE
T12
50
10
1
GRAIN SIZE (mm)

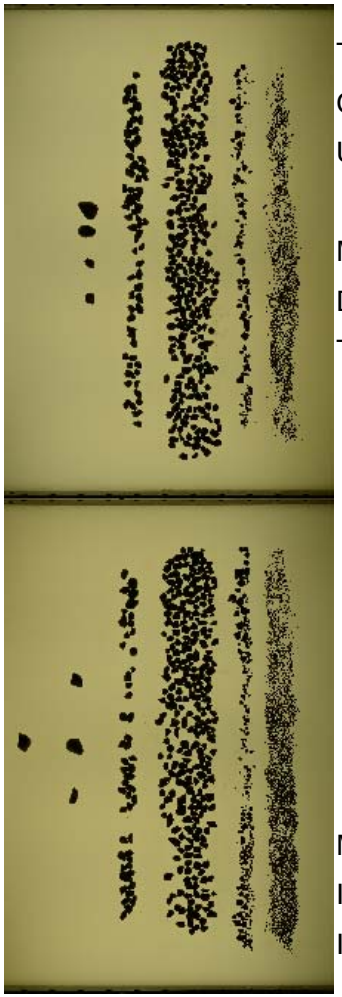

TRANSLUCENT SEGREGATION TABLE (TST)
GEOTECHNICAL ENGINEERING
UNIVERSITY OF MICHIGAN

MATERIAL: T13
DATE TESTED: 05-Jul-2012 14:25:14
TESTED BY: Ohm, H.S.

MAGNIFICATION (pix/mm): 5.4
IMAGE SIZE (pix): 9856 x 3264
IMAGE SIZE (mm): 1825.2 x 604.4

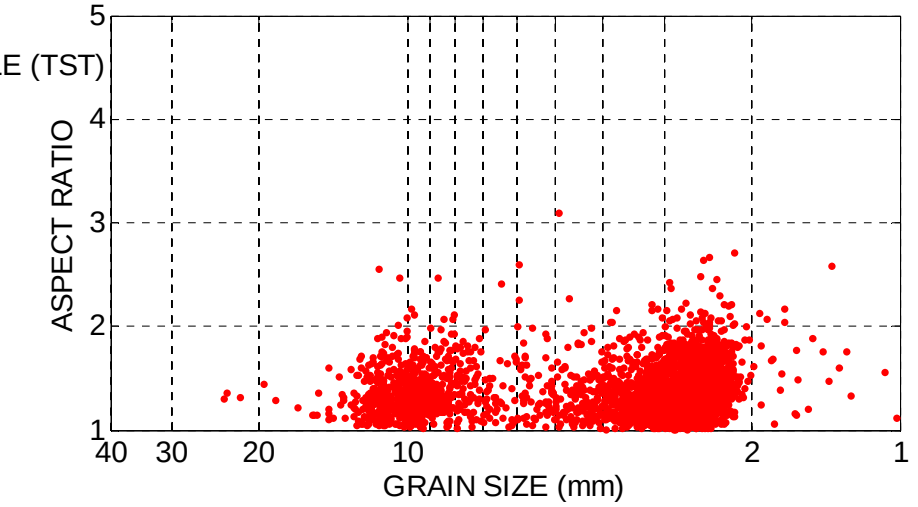

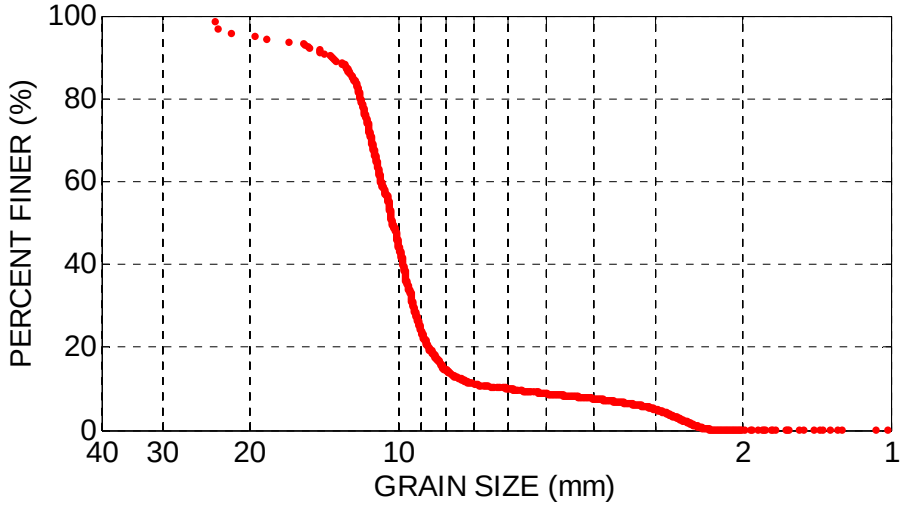

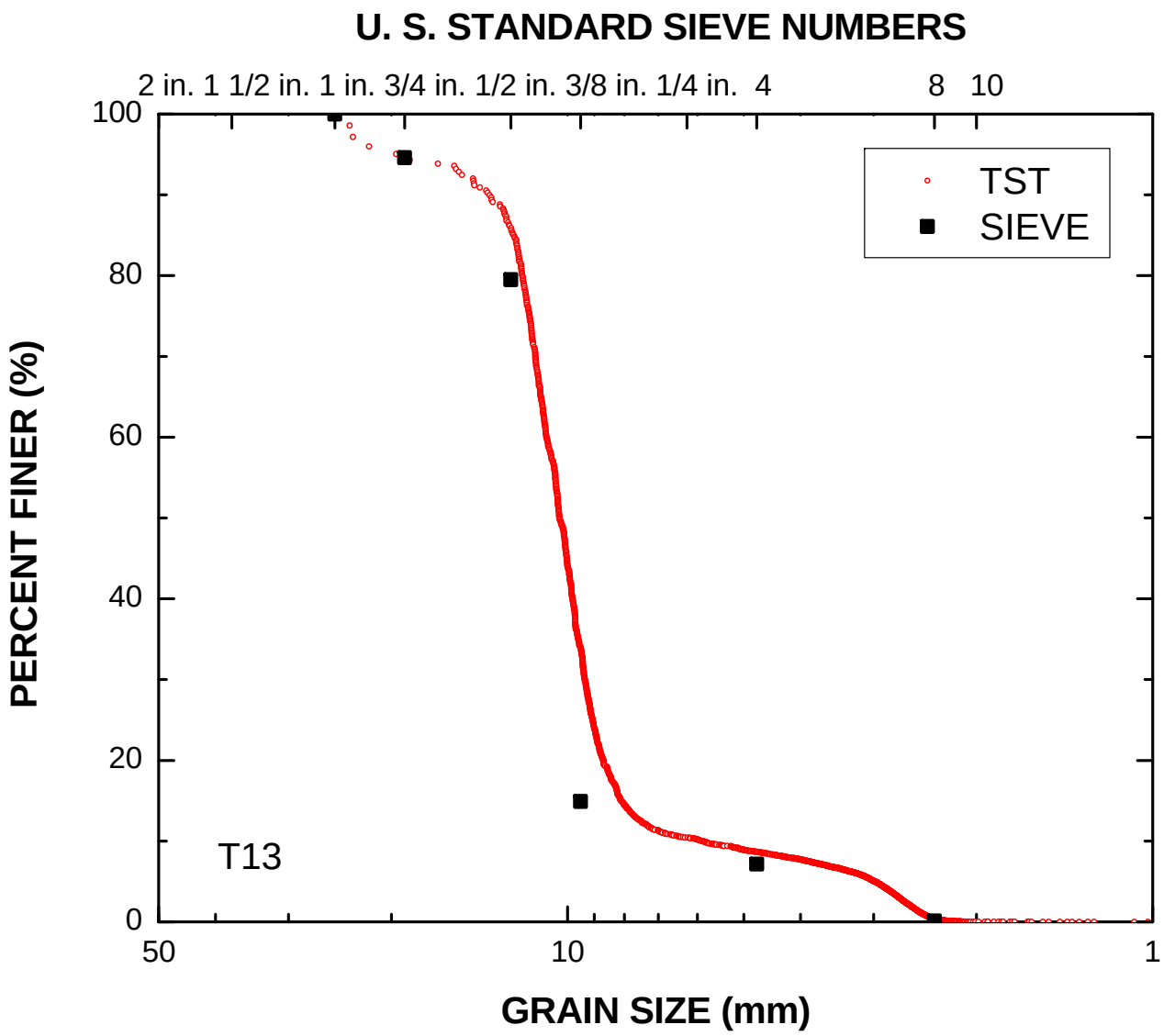
U. S. STANDARD SIEVE NUMBERS
2 in. 1 1/2 in. 1 in. 3/4 in. 1/2 in. 3/8 in. 1/4 in. 4 8 10
100
80
60
40
20
0
50
10
1
PERCENT FINER (%)
GRAIN SIZE (mm)
TST
SIEVE
T13

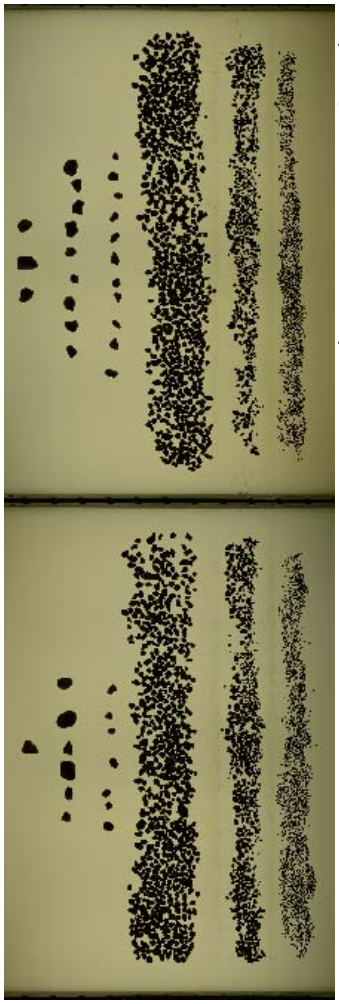

TRANSLUCENT SEGREGATION TABLE (TST)
GEOTECHNICAL ENGINEERING
UNIVERSITY OF MICHIGAN

MATERIAL: T14
DATE TESTED: 06-Jul-2012 11:33:56
TESTED BY: Ohm, H.S.

MAGNIFICATION (pix/mm): 5.4
IMAGE SIZE (pix): 9856 x 3264
IMAGE SIZE (mm): 1825.2 x 604.4

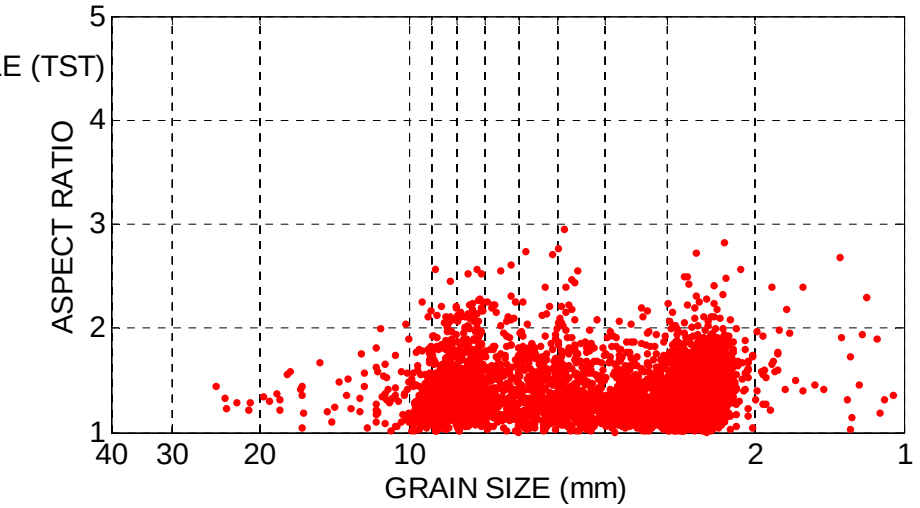

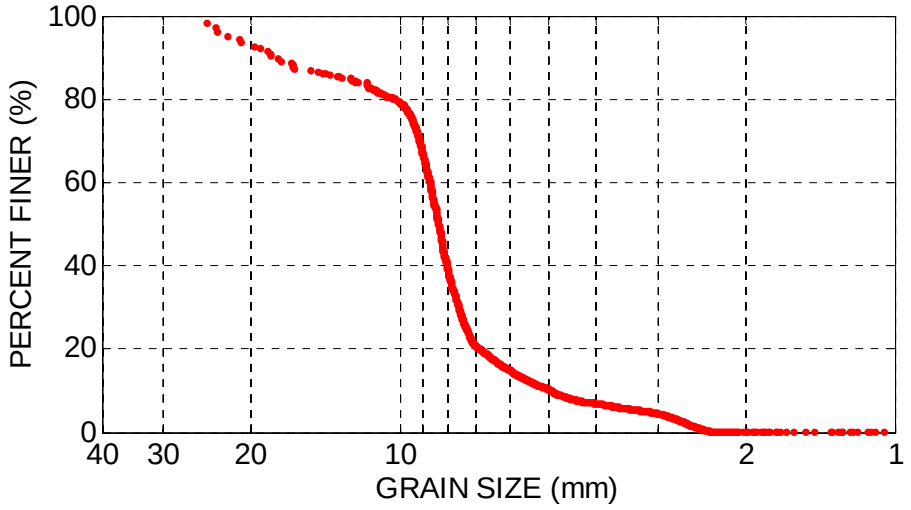

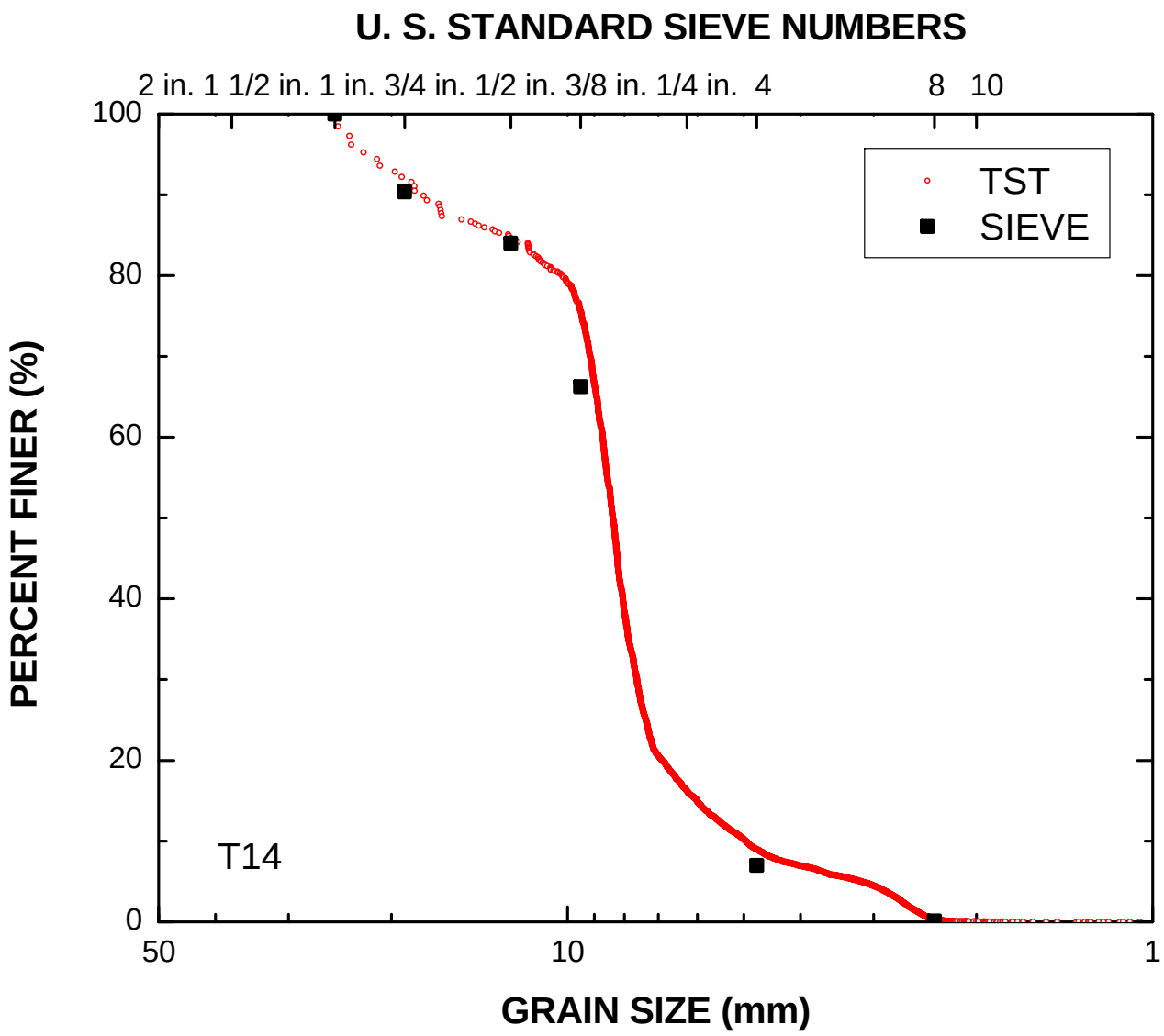
U. S. STANDARD SIEVE NUMBERS
2 in. 1 1/2 in. 1 in. 3/4 in. 1/2 in. 3/8 in. 1/4 in. 4 8 10
100
80
60
40
20
0
50
10
1
PERCENT FINER (%)
GRAIN SIZE (mm)
TST
SIEVE
T14

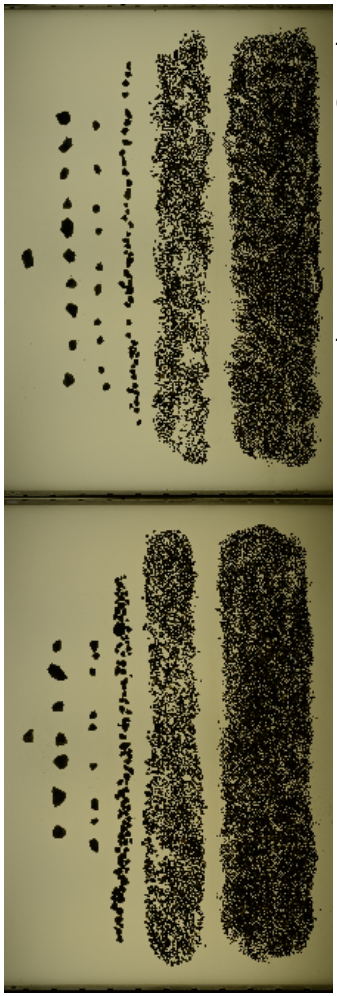

TRANSLUCENT SEGREGATION TABLE (TST)

GEOTECHNICAL ENGINEERING

UNIVERSITY OF MICHIGAN

MATERIAL: T15

DATE TESTED: 06-Jul-2012 13:01:30

TESTED BY: Ohm, H.S.

MAGNIFICATION (pix/mm): 5.4

IMAGE SIZE (pix): 9856 x 3264

IMAGE SIZE (mm): 1825.2 x 604.4

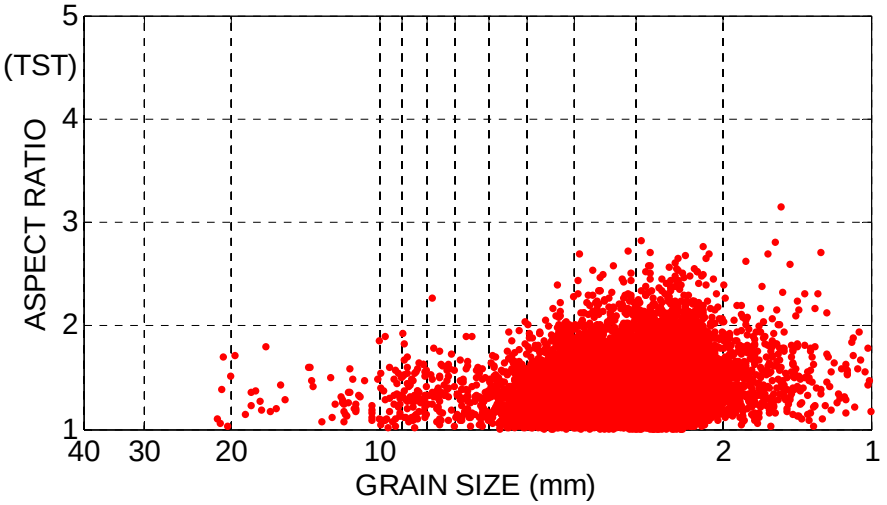

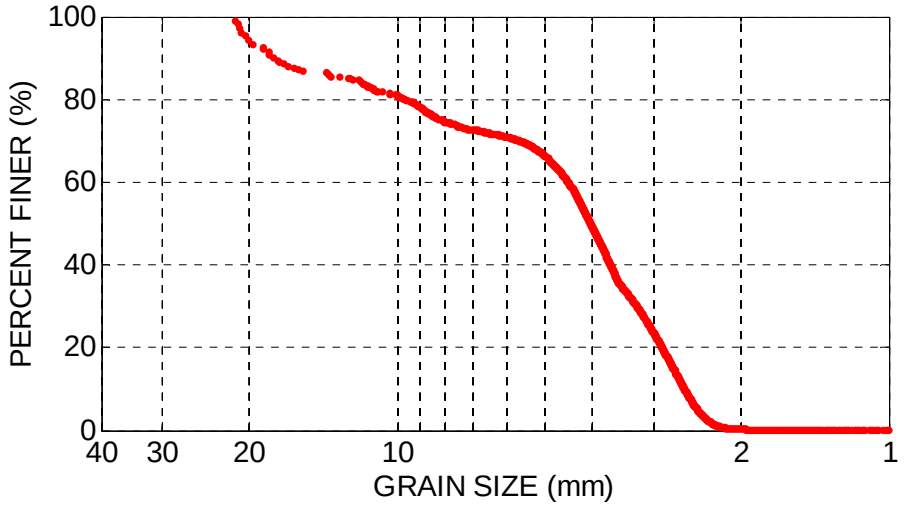

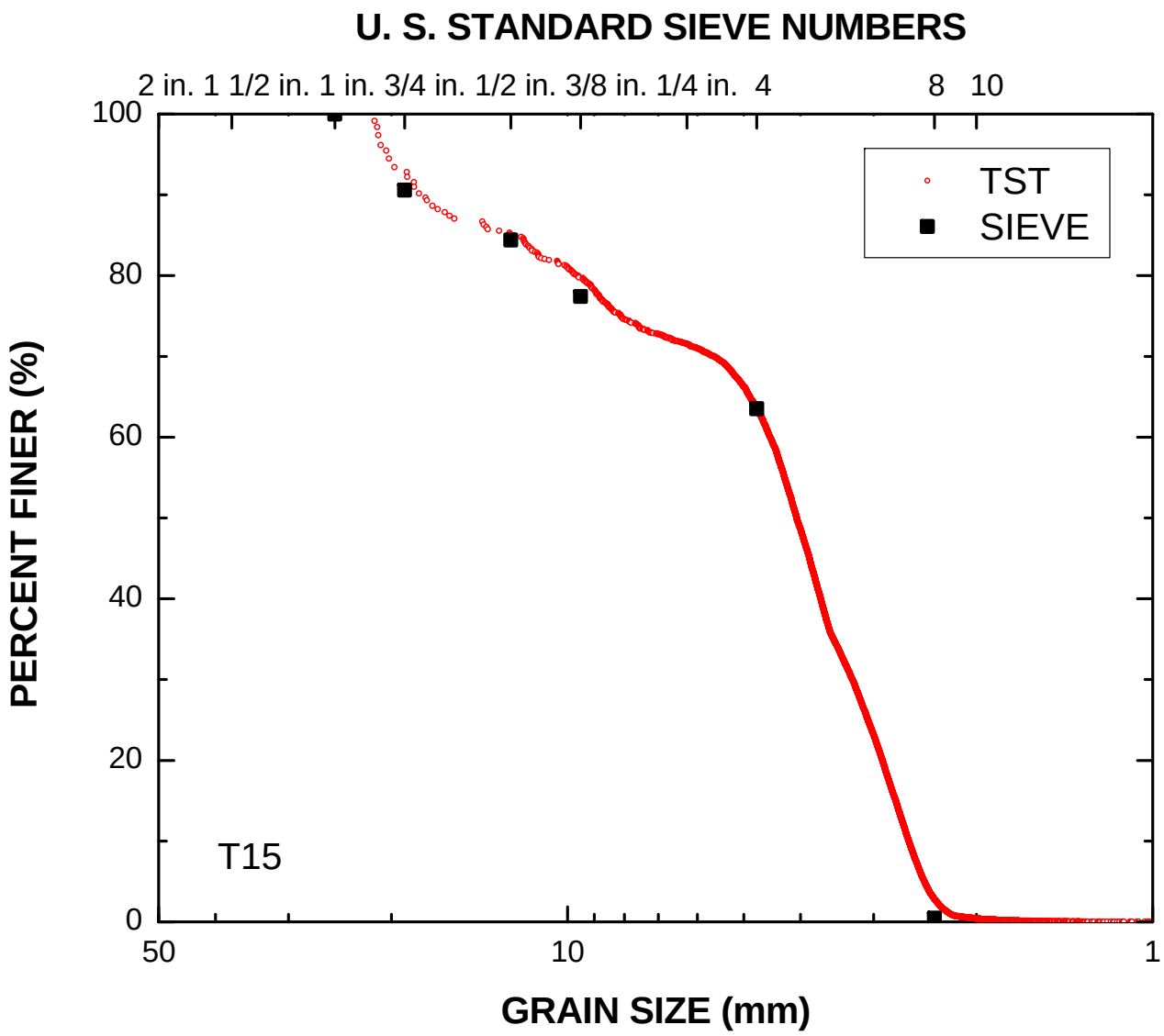
U. S. STANDARD SIEVE NUMBERS
2 in. 1 1/2 in. 1 in. 3/4 in. 1/2 in. 3/8 in. 1/4 in. 4 8 10
100
80
60
40
20
0
PERCENT FINER (%)
TST
SIEVE
T15
50
10
1
GRAIN SIZE (mm)

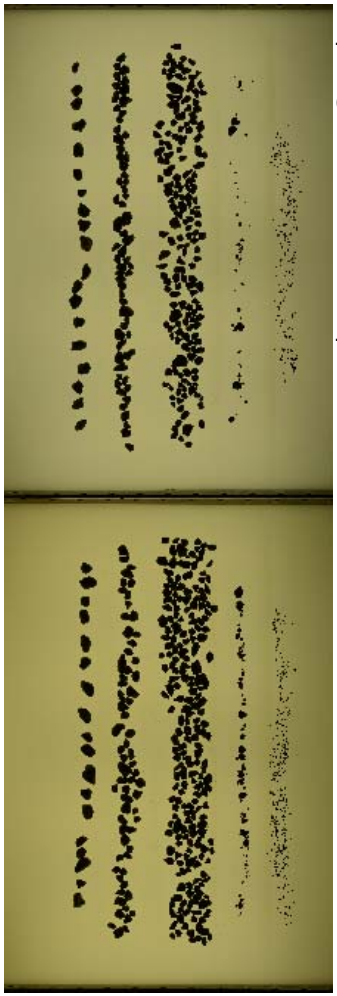

TRANSLUCENT SEGREGATION TABLE (TST)
GEOTECHNICAL ENGINEERING
UNIVERSITY OF MICHIGAN

MATERIAL: T16
DATE TESTED: 06-Jul-2012 14:25:42
TESTED BY: Ohm, H.S.

MAGNIFICATION (pix/mm): 5.4
IMAGE SIZE (pix): 9856 x 3264
IMAGE SIZE (mm): 1825.2 x 604.4

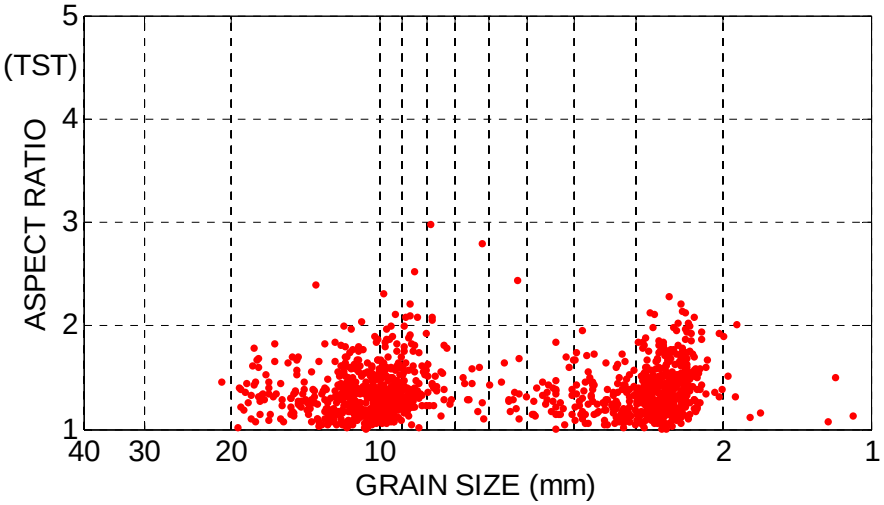

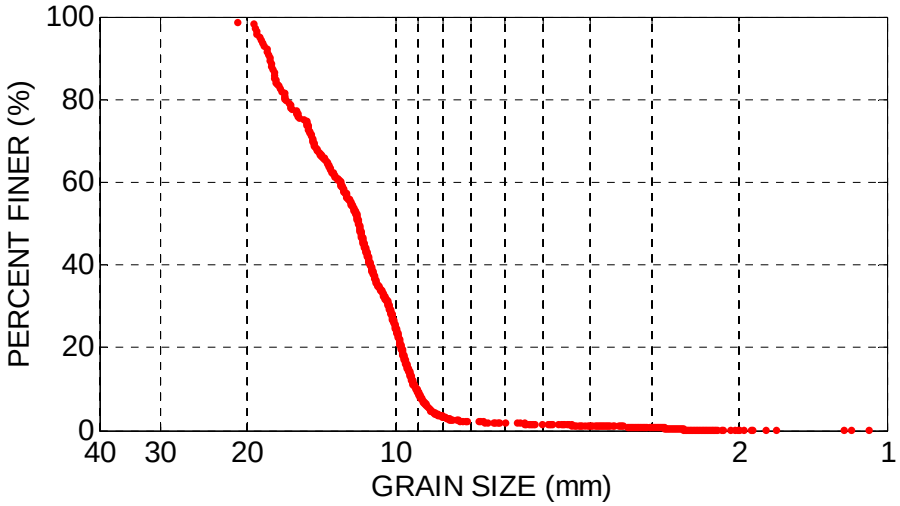

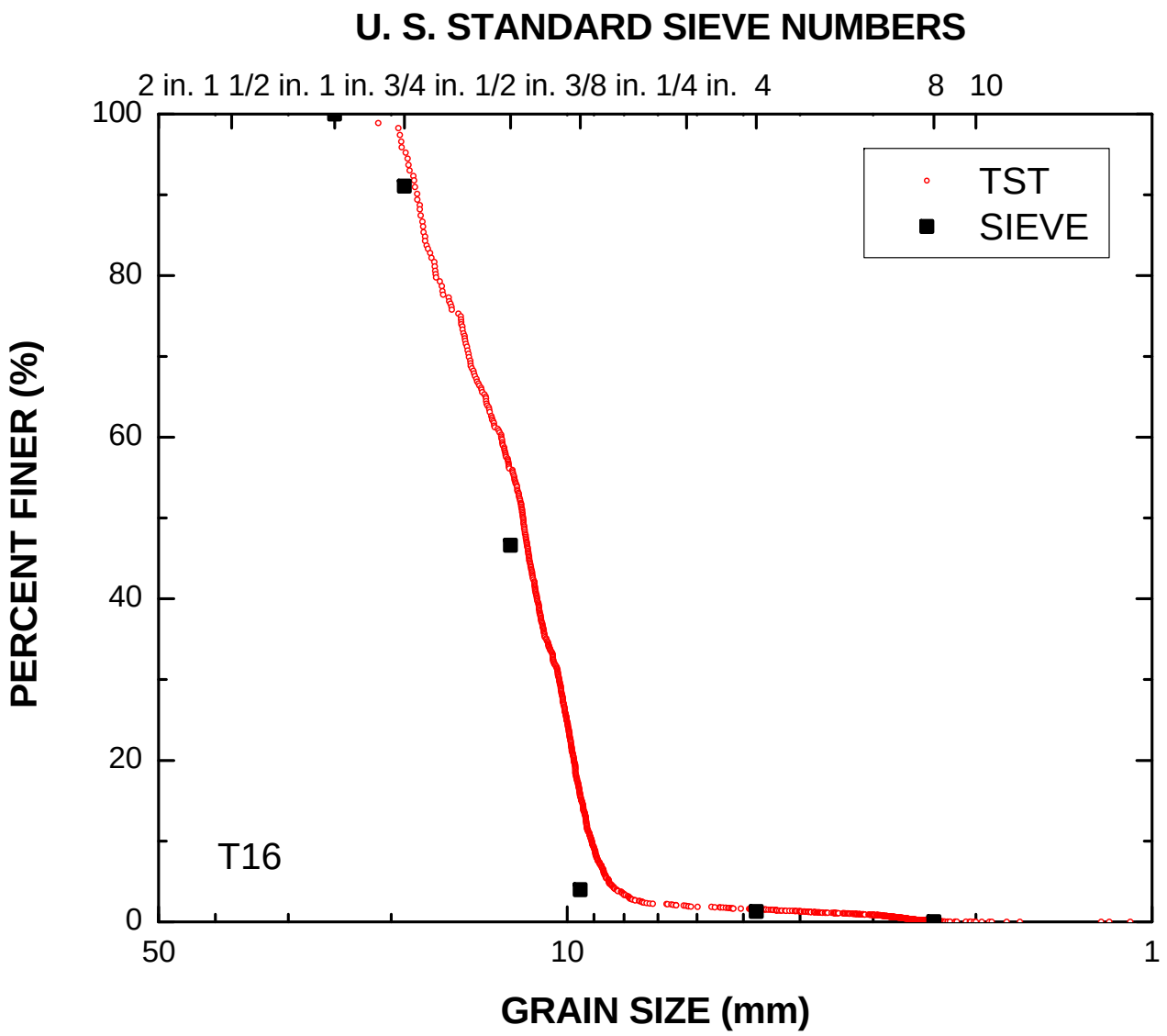
U. S. STANDARD SIEVE NUMBERS
2 in. 1 1/2 in. 1 in. 3/4 in. 1/2 in. 3/8 in. 1/4 in. 4 8 10
100
80
60
40
20
0
PERCENT FINER (%)
TST
SIEVE
T16
50
10
1
GRAIN SIZE (mm)

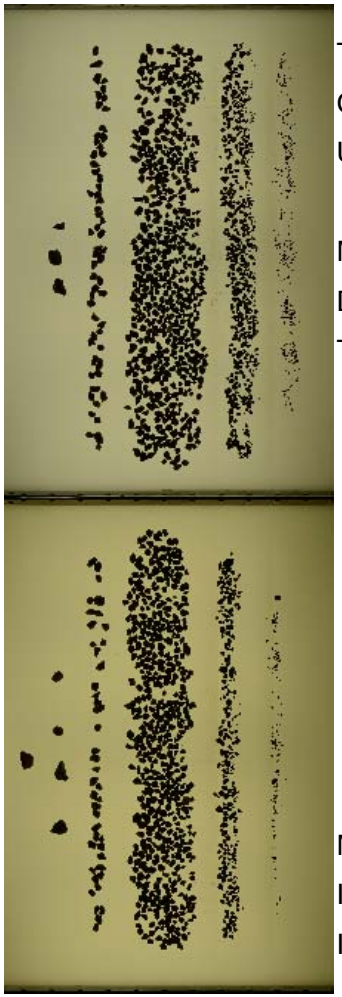

TRANSLUCENT SEGREGATION TABLE (TST)
GEOTECHNICAL ENGINEERING
UNIVERSITY OF MICHIGAN

MATERIAL: T17
DATE TESTED: 09-Jul-2012 11:27:54
TESTED BY: Ohm, H.S.

MAGNIFICATION (pix/mm): 5.4
IMAGE SIZE (pix): 9856 x 3264
IMAGE SIZE (mm): 1825.2 x 604.4

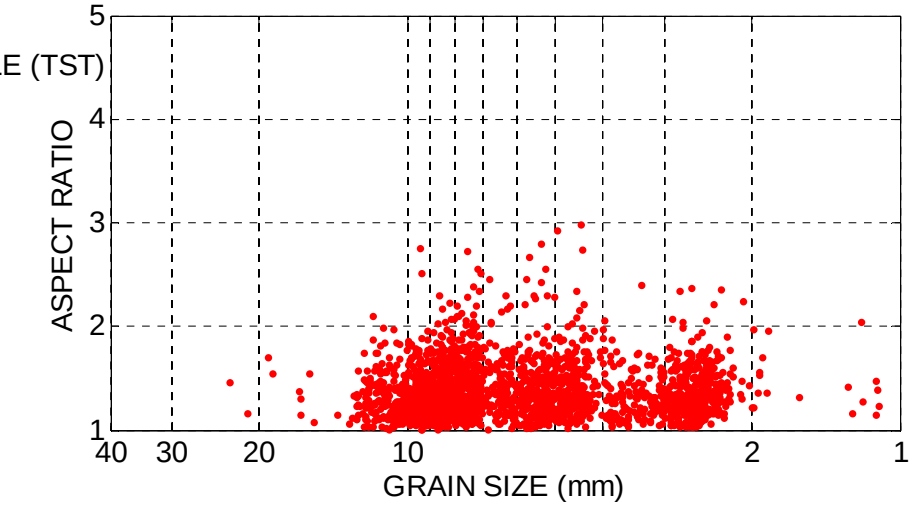

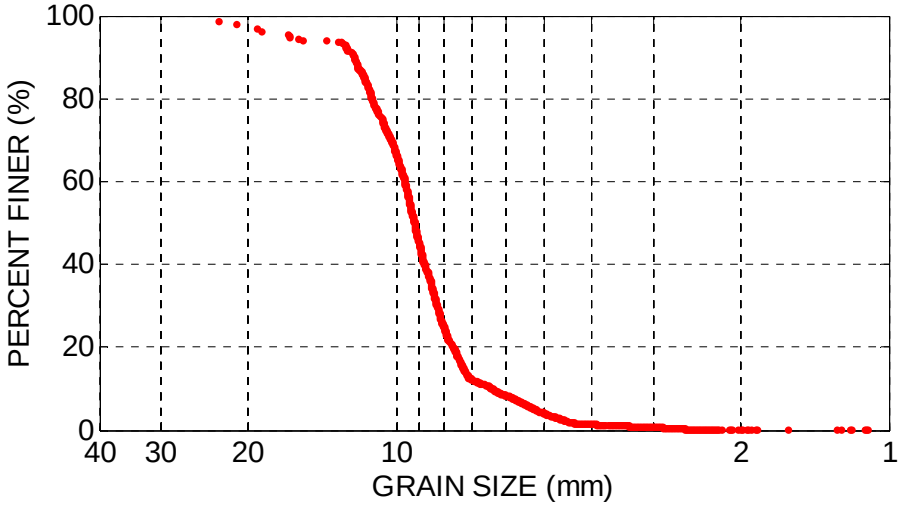

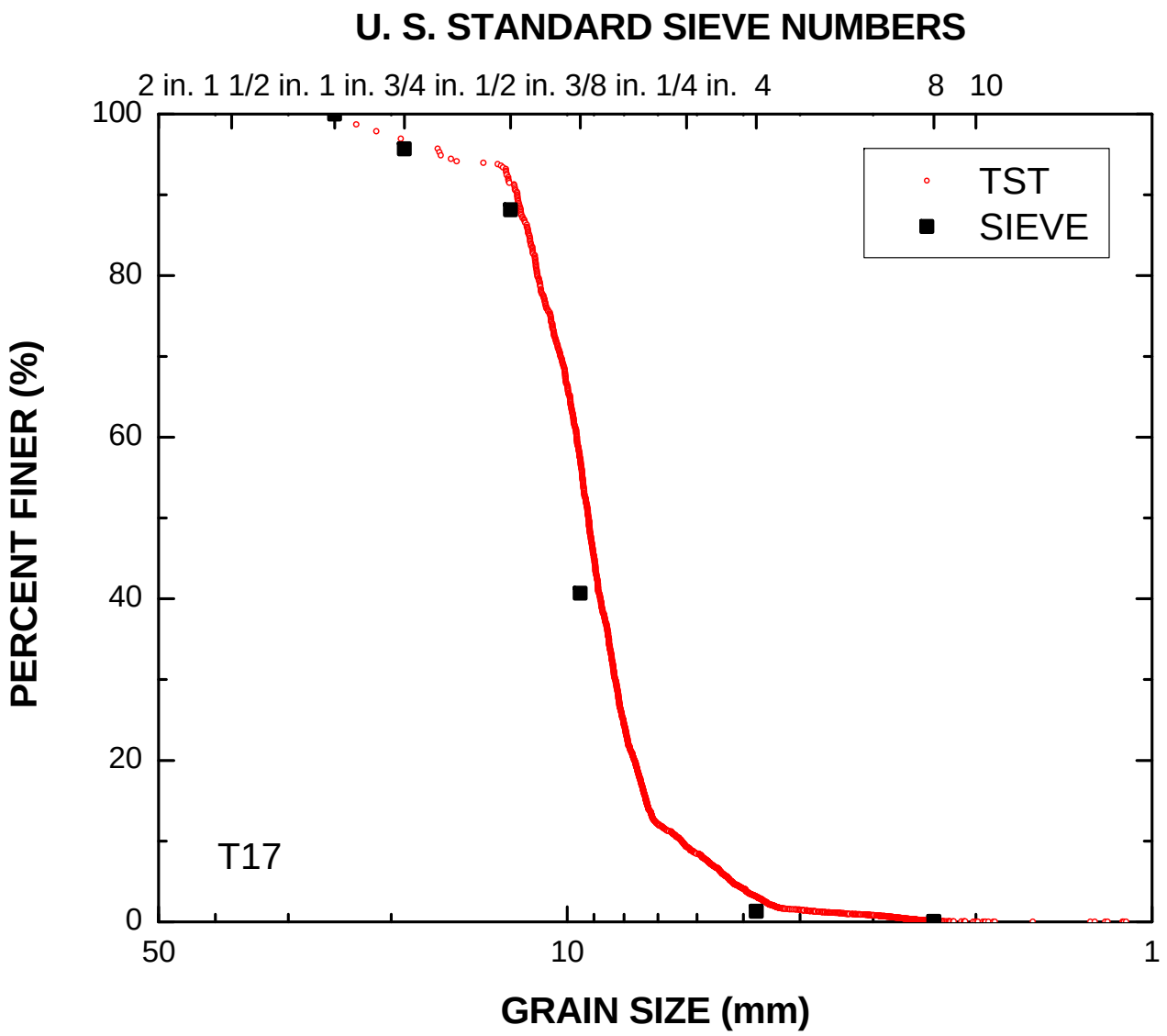
U. S. STANDARD SIEVE NUMBERS
2 in. 1 1/2 in. 1 in. 3/4 in. 1/2 in. 3/8 in. 1/4 in. 4 8 10
100
80
60
40
20
0
PERCENT FINER (%)
50
10
1
GRAIN SIZE (mm)
TST
SIEVE
T17

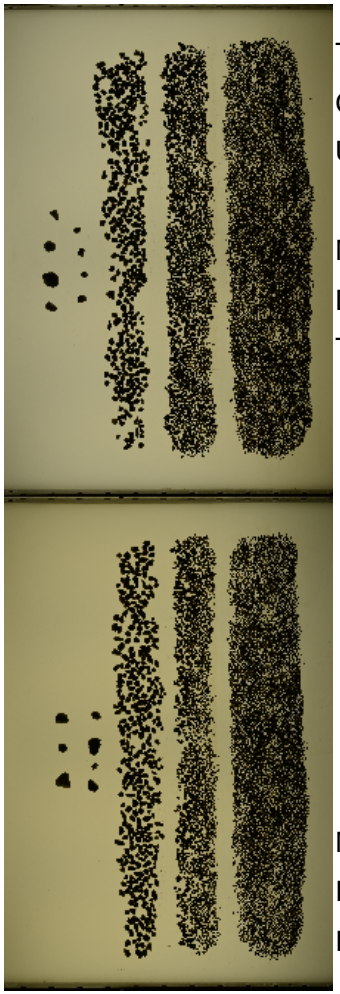

TRANSLUCENT SEGREGATION TABLE (TST)
GEOTECHNICAL ENGINEERING
UNIVERSITY OF MICHIGAN

MATERIAL: T18
DATE TESTED: 09-Jul-2012 12:58:52
TESTED BY: Ohm, H.S.

MAGNIFICATION (pix/mm): 5.4
IMAGE SIZE (pix): 9856 x 3264
IMAGE SIZE (mm): 1825.2 x 604.4

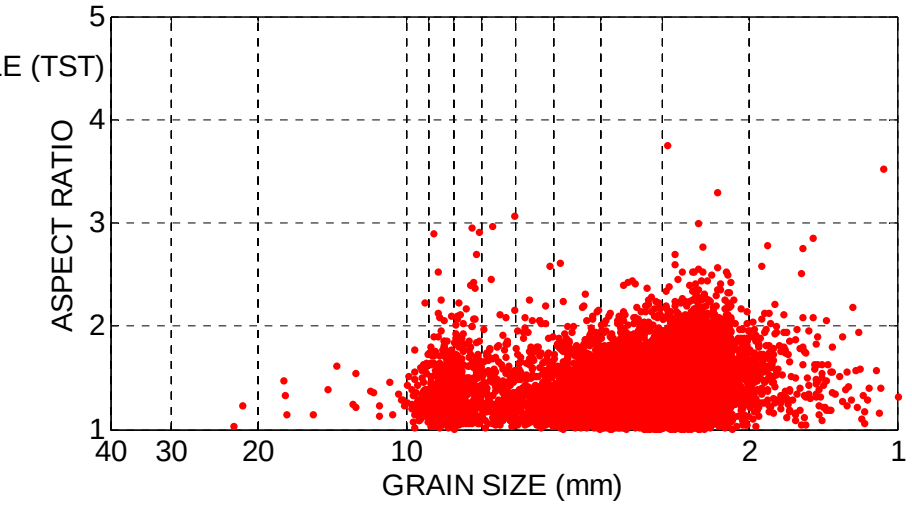

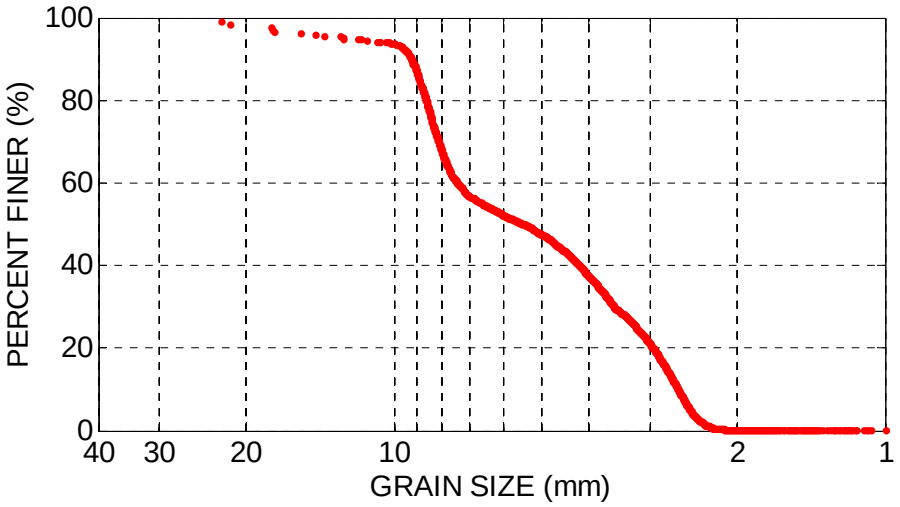

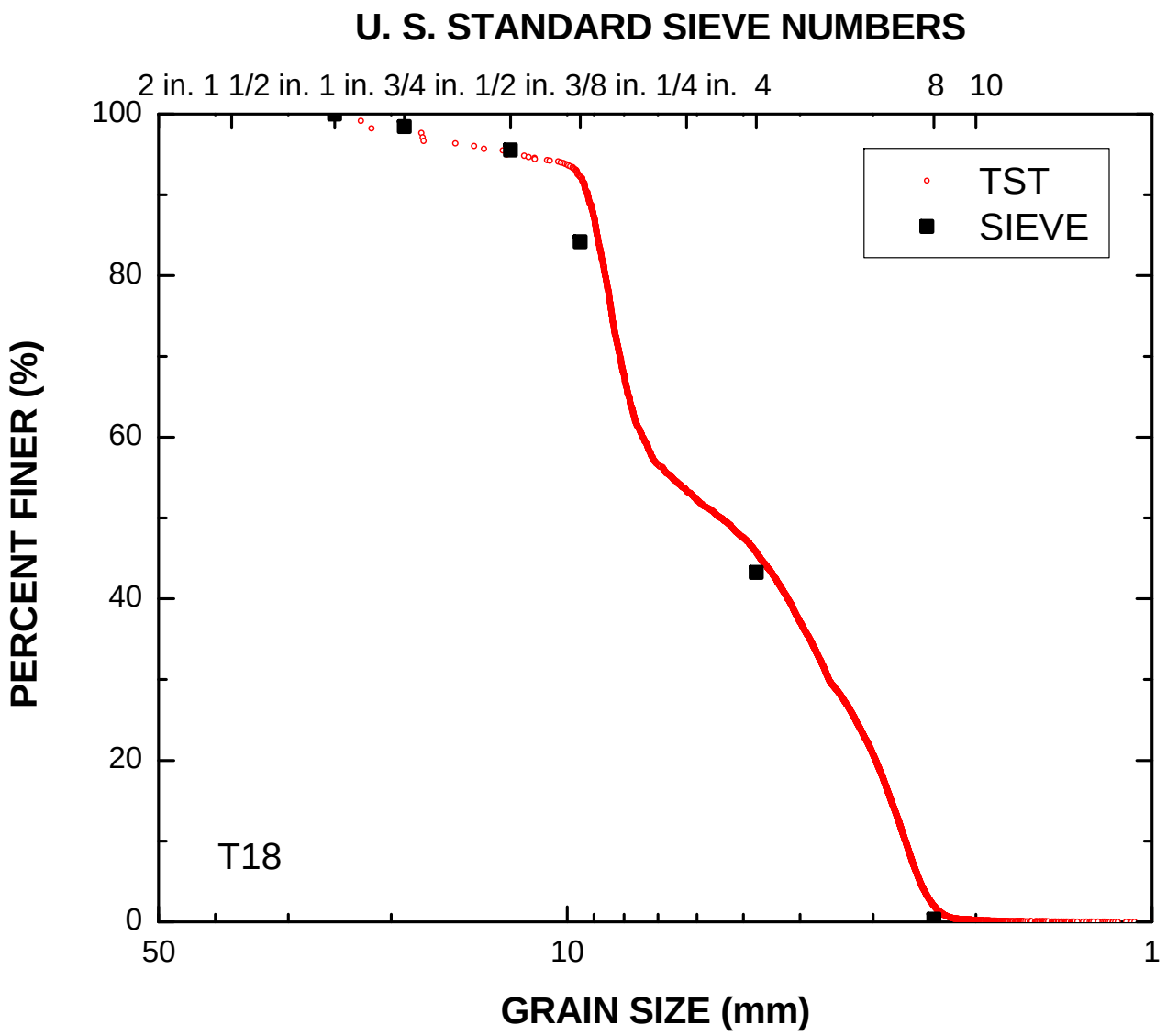
U. S. STANDARD SIEVE NUMBERS
2 in. 1 1/2 in. 1 in. 3/4 in. 1/2 in. 3/8 in. 1/4 in. 4 8 10
100
80
60
40
20
0
PERCENT FINER (%)
50
10
1
GRAIN SIZE (mm)
TST
SIEVE
T18

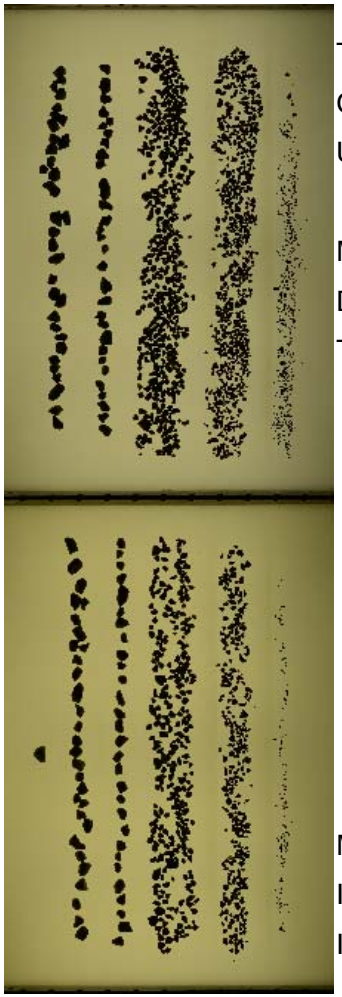

TRANSLUCENT SEGREGATION TABLE (TST)
GEOTECHNICAL ENGINEERING
UNIVERSITY OF MICHIGAN

MATERIAL: T19
DATE TESTED: 09-Jul-2012 14:23:18
TESTED BY: Ohm, H.S.

MAGNIFICATION (pix/mm): 5.4
IMAGE SIZE (pix): 9856 x 3264
IMAGE SIZE (mm): 1825.2 x 604.4

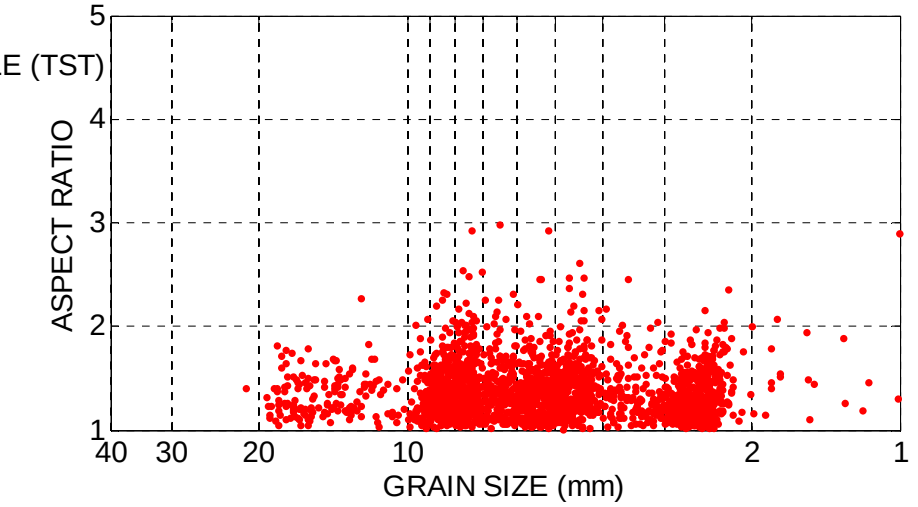

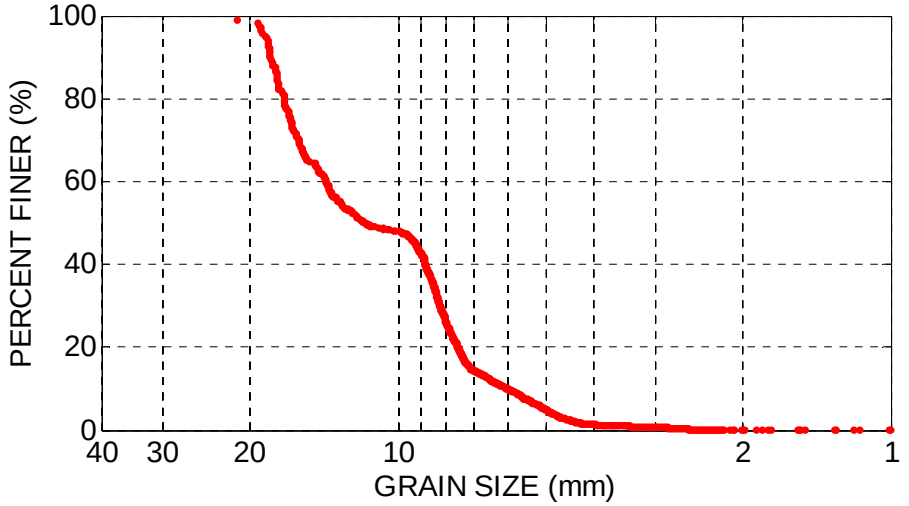

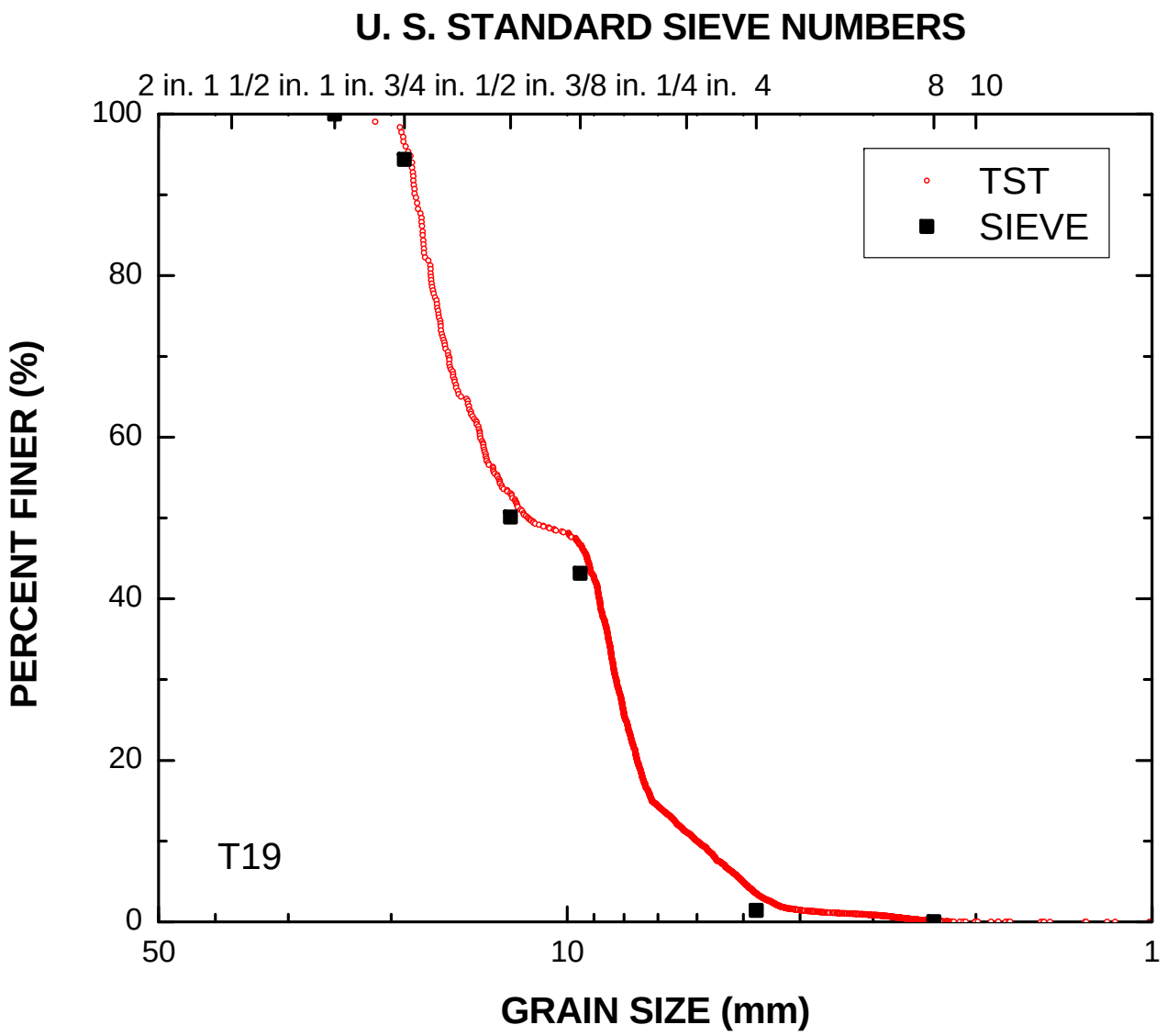
U. S. STANDARD SIEVE NUMBERS
2 in. 1 1/2 in. 1 in. 3/4 in. 1/2 in. 3/8 in. 1/4 in. 4 8 10
100
80
60
40
20
0
PERCENT FINER (%)
TST
SIEVE
T19
50
10
1
GRAIN SIZE (mm)

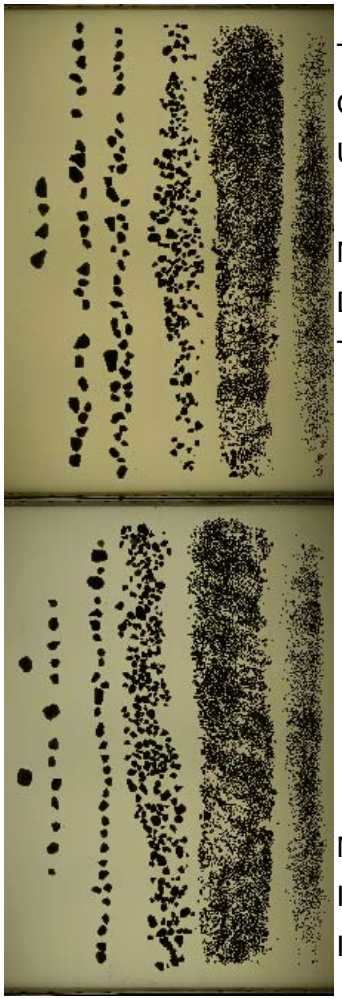

TRANSLUCENT SEGREGATION TABLE (TST)

GEOTECHNICAL ENGINEERING

UNIVERSITY OF MICHIGAN

MATERIAL: T20

DATE TESTED: 12-Jul-2012 12:01:50

TESTED BY: Ohm, H.S.

MAGNIFICATION (pix/mm): 5.4

IMAGE SIZE (pix): 9856 x 3264

IMAGE SIZE (mm): 1825.2 x 604.4

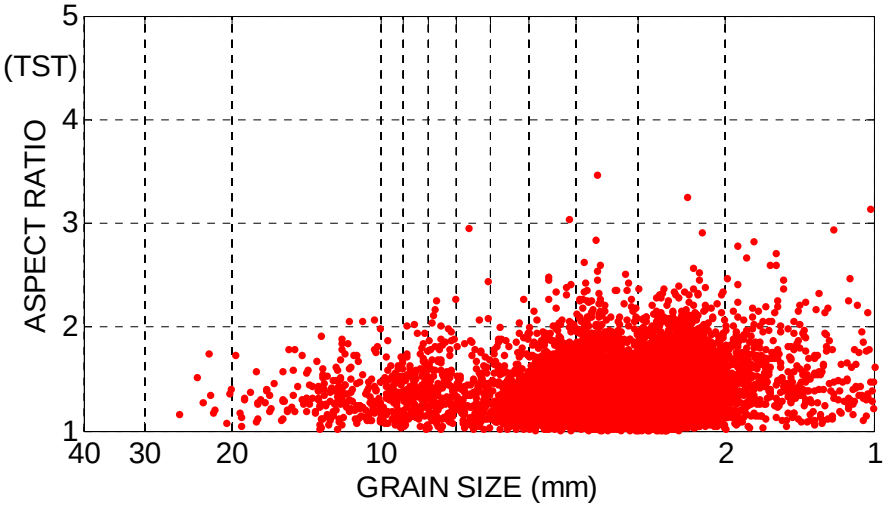

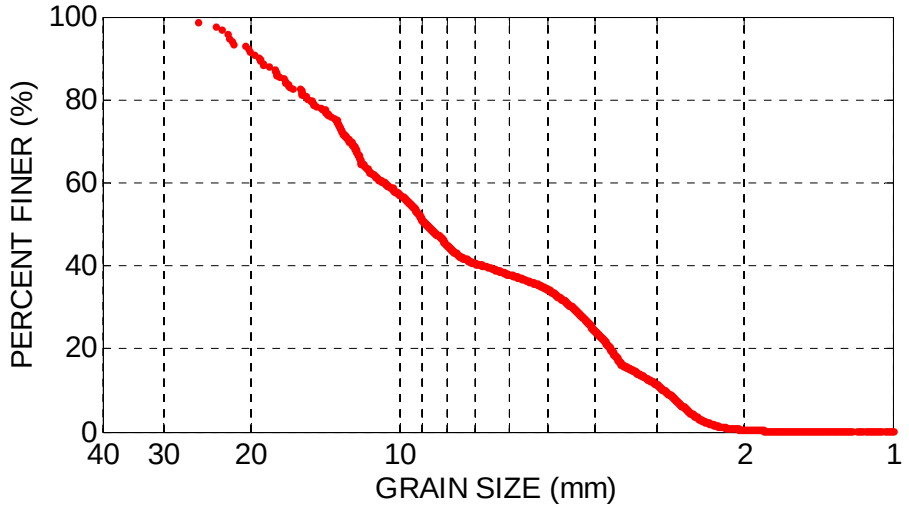

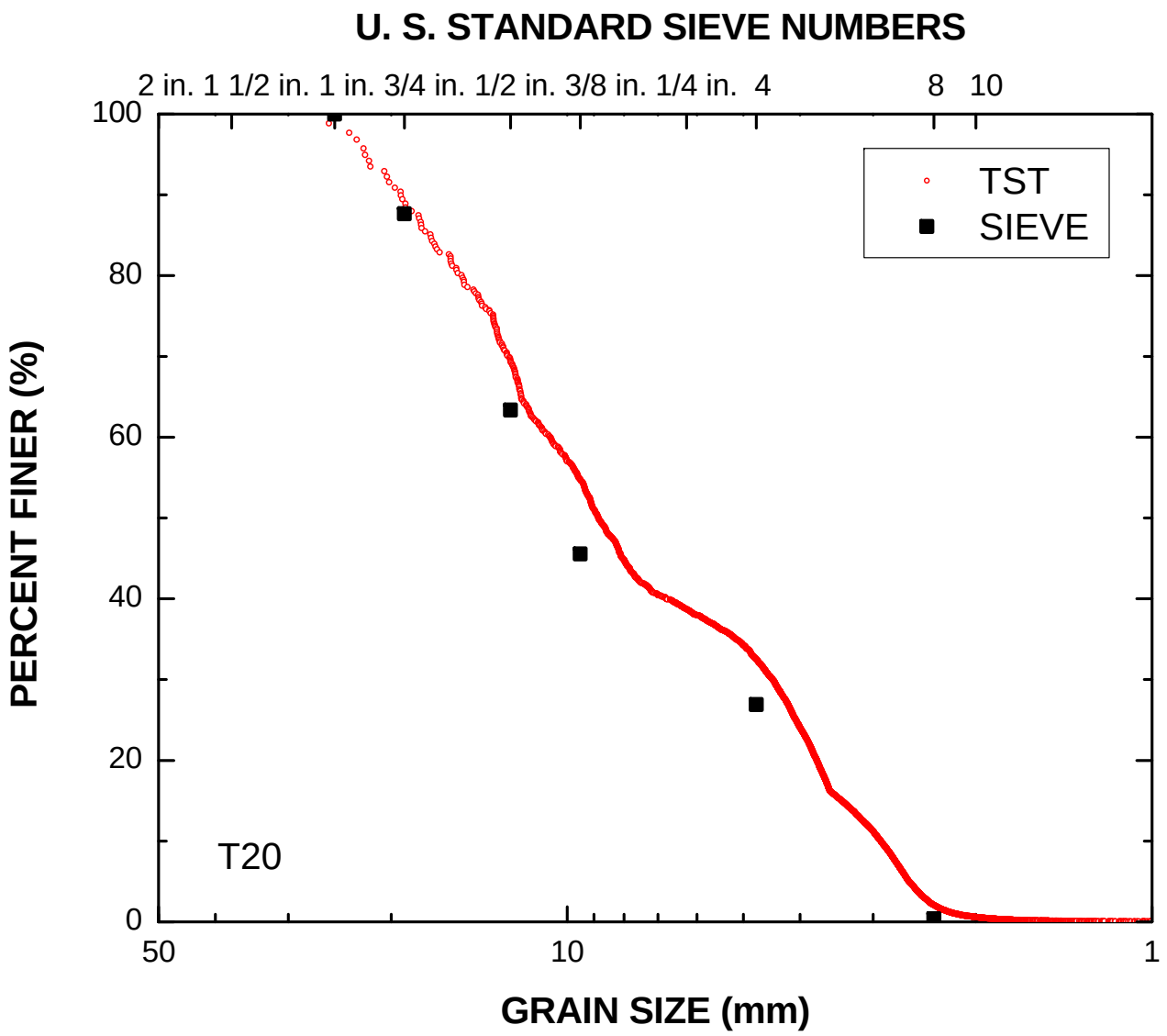
U. S. STANDARD SIEVE NUMBERS
2 in. 1 1/2 in. 1 in. 3/4 in. 1/2 in. 3/8 in. 1/4 in. 4 8 10
100
80
60
40
20
0
PERCENT FINER (%)
TST
SIEVE
T20
50
10
1
GRAIN SIZE (mm)

REFERENCES

Abbireddy, C.O.R., and Clayton, C.R.I. (2009). "A Review of Modern Particle Sizing Methods." Proceedings of the Institution of Civil Engineers - Geotechnical Engineering, 162(GE4), 193-201.

Al-Rousan, Masad, E., Tutumluer, E., and Pan, T. (2007). "Evaluation of Image Analysis Techniques for Quantifying Aggregate Shape Characteristics." Construction and Building Materials, 21(5), 978-990.

Al-Rousan, T., Masad, E., Myers, L., and Speigelman, C. (2005). "New Methodology for Shape Classification of Aggregates." Transportation Research Record: Journal of the Transportation Research Board, No. 1913, 11-23.

Alshibli, K.A., and Alsaleh, M.I. (2004). "Characterizing Surface Roughness and Shape of Sands Using Digital Microscopy." Journal of Computing in Civil Engineering, 18(1), 36-45.

Alshibli, K.A., Macari, E.J., and Sture, S. (1996). "Digital Imaging Techniques for Assessment of Homogeneity of Granular Materials." Transportation Research Record: Journal of the Transportation Research Board, No. 1526, 121-128.

Altuhafi, F., O'Sullivan, C., and Cavarretta, I. (2012). "Analysis of an Image Based Method to Quantify the Size and Shape of Sand Particles." Journal of Geotechnical and Geoenvironmental Engineering, Accepted.

Amankwah, A., and Aldrich, C. (2011). "Estimation of Particulate Fines on Conveyor Belts by Use of Wavelets and Morphological Image Processing." International Journal of Machine Learning and Computing, 1(2), 132-137.

Ashmawy, A.K., Sukumaran, B., and Hoang, V.V. (2003). "Evaluating the Influence of Particle Shape on Liquefaction Behavior Using Discrete Element Modeling." Annual International Society of Offshore and Polar Engineering Conference, Kyushu, Japan.

Bardet, J.-P., and Young, J. (1997). "Grain-Size Analysis by Buoyancy Method." Geotechnical Testing Journal, 20(4), 481-485.

Bareither, C.A., Edil, T.B., Benson, C.H., and Mickelson, D.M. (2008). "Geological and Physical Factors Affecting the Friction Angle of Compacted Sands." Journal of Geotechnical and Geoenvironmental Engineering, 134(10), 1476-1489.

Barrett, P.J. (1980). "The Shape of Rock Particles, A Critical Review." Sedimentology, 27(3), 291-303.

Beucher, S., and Lantuejoul, C. (1979). "Use of Watersheds in Contour Detection." Proceedings of the International Workshop on Image Processing: Real-Time Edge and Motion Detection/Estimation, Rennes, France.

Bowman, E.T. (2002). "Ageing and Creep of Dense Granular Materials." Ph.D. Dissertation, University of Cambridge.

Bowman, E.T., and Soga, K. (2003). "Creep, Ageing and Microstructural Change in Dense Granular Materials." Soils and Foundations, 43(4), 107-117.

Bowman, E.T., Soga, K., and Drummond, W. (2001). "Particle Shape Characterisation Using Fourier Descriptor Analysis." Géotechnique, 51(6), 545-554.

Breul, P., and Gourves, R. (2006). "In Field Soil Characterization: Approach Based on Texture Image Analysis." Journal of Geotechnical and Geoenvironmental Engineering, 132(1), 102-107.

Brzezicki, J.M., and Kasperkiewicz, J. (1999). "Automatic Image Analysis in Evaluation of Aggregate Shape." Journal of Computing in Civil Engineering, 13(2), 123-128.

Chandan, C., Sivakumar, K., Masad, E., and Fletcher, T. (2004). "Application of Imaging Techniques to Geometry Analysis of Aggregate Particles." Journal of Computing in Civil Engineering, 18(1), 75-82.

Chang, T.-S., and Woods, R.D. (1992). "Effect of Particle Contact Bond on Shear Modulus." Journal of Geotechnical Engineering, 118(8), 1216-1233.

Cho, G.C., Dodds, J., and Santamarina, J.C. (2006). "Particle Shape Effects on Packing Density, Stiffness, and Strength: Natural and Crushed Sands." Journal of Geotechnical and Geoenvironmental Engineering, 132(5), 591-602.

Clark, M.W. (1981). "Quantitative Shape Analysis: A Review." Mathematical Geology, 13(4), 303-320.

Comaniciu, D., and Meer, P. (2002). "Mean Shift: A Robust Approach Toward Feature Space Analysis." IEEE Transactions on Pattern Analysis and Machine Intelligence, 24(5), 603-619.

Das, N., Thomas, S., Kopmann, J., Donovan, C., Hurt, C., Daouadji, A., Ashmawy, A.K., and Sukumaran, B. (2011). "Modeling Granular Particle Shape Using Discrete Element Method." Geo-Frontiers 2011, 4293-4302.

Devaux, M.F., Robert, P., Melcion, J.P., and Le Deschault de Monredon, F. (1997). "Particle Size Analysis of Bulk Powders Using Mathematical Morphology." Powder Technology, 90(2), 141-147.

Dodds, J. (2003). "Particle Shape and Stiffness - Effects on Soil Behaviour." Master's Thesis, Georgia Institute of Technology.

Dur, J.C., Elsass, F., Chaplain, V., and Tessier, D. (2004). "The Relationship between Particle-Size Distribution by Laser Granulometry and Image Analysis by Transmission Electron Microscopy in a Soil Clay Fraction." European Journal of Soil Science, 55(2), 265-270.

Fernlund, J.M.R. (1998). "The Effect of Particle Form on Sieve Analysis: A Test by Image Analysis." Engineering Geology, 50, 111-124.

Fernlund, J.M.R. (2005). "Image Analysis Method for Determining 3-D Size Distribution of Coarse Aggregates." Bulletin of Engineering Geology and the Environment, 64(2), 159-166.

Fletcher, T., Chandan, C., Masad, E., and Sivakumar, K. (2002). "Measurement of Aggregate Texture and its Influence on Hot Mix Asphalt (HMA) Permanent Deformation." Journal of Testing and Evaluation, 30(6), 524-531.

Fletcher, T., Chandan, C., Masad, E., and Sivakumar, K. (2003). "Aggregate Imaging System for Characterizing the Shape of Fine and Coarse Aggregates." Transportation Research Record: Journal of the Transportation Research Board, No. 1832, 67-77.

Forsyth, D.A., and Ponce, J. (2003). "Computer Vision: A Modern Approach." Prentice Hall, New Jersey.

Gates, L., Masad, E., Pyle, R., and Bushee, D. (2011). "Aggregate Imaging Measurement System 2 (AIMS2): Final Report." Final Report Submitted to Fedral Highway Administration, FHWA-HIF-11-030.

Gelinas, V., and Vidal, D. (2010). "Determination of Particle Shape Distribution of Clay Using an Automated AFM Image Analysis Method." Powder Technology, 203(2) 254-264.

Ghalib, A.M. (2001). "Laboratory and In-Situ Soil Characterization by Computer Vision." Ph.D. Dissertation, University of Michigan.

Ghalib, A.M., and Hryciw, R.D. (1999). "Soil Particle Size Distribution by Mosaic Imaging and Watershed Analysis." Journal of Computing in Civil Engineering, 13(2), 80-87.

Ghalib, A.M., Hryciw, R.D., and Shin, S.C. (1998). "Image Texture Analysis and Neural Networks for Characterization of Uniform Soils." Proceedings of the International Computing Congress, Boston, 671-682.

Hanson, C.E., Towers, D.A., and Meister, L.D. (2006). "Transit Noise and Vibration Impact Assessment." Final Report Submitted to Federal Transit Administration, FTA-VA-90-1003-06.

Harris, C., and Stephens, M. (1988). "A Combined Corner and Edge Detector." Proceedings of the 4th Alvey Vision Conference, 147-151.

Hayton, S., Nelson, C.S., Ricketts, B.D., Cooke, S., and Wedd, M.W. (2001). "Effect of Mica on Particle-Size Analyses Using the Laser Diffraction Technique." Journal of Sedimentary Research, 71(3), 507-509.

Hryciw, R.D., and Jung, Y. (2008). "Accounting for Void Ratio Variation in Determination of Grain Size Distribution by Soil Column Image Processing." Proceedings of the GeoCongress 2008, New Orleans, 966-973.

Hryciw, R.D., and Jung, Y. (2009). "Three-Point Imaging Test for AASHTO Soil Classification." Transportation Research Record: Journal of the Transportation Research Board, No. 2101, 27-33.

Hryciw, R.D., and Ohm, H.-S. (2012). "Feasibility of Digital Imaging to Characterize Earth Materials." Final Report Submitted to Michigan Department of Transportation.

Hryciw, R.D., Jung, Y., Susila, E., and Ibrahim, A. (2009). "Thin Soil Layer Detection by VisCPT and FEM Simulations." Proceedings of the 17th International Conference on Soil Mechanics and Geotechnical Engineering (ICSMGE 2009), Alexandria, Egypt , 1052-1055.

Hryciw, R.D., Ohm, H.-S., and Zhou, J. (2013). "The Theoretical Basis for Optical Granulometry by Wavelet Transformation." Journal of Computing in Civil Engineering (Submitted).

Hryciw, R.D., Shin, S., Jung, Y. (2006). "Soil Image Processing – Single Grains to Particle Assemblies" Proceedings of the GeoCongress 2006, Atlanta, GA, 1-6.

Jackson, G.A., Logan, B.E., Alldredge, A.L., and Dam, H.G. (1995). "Combining Particle Size Spectra from a Memocosm Experiment Measured Using Photographic and Aperture Impedance (Coulter and Elzone) Techniques." Deep-Sea Research II, 42(1), 139-157.

Jung, Y. (2010). "Determination of Soil Grain Size Distribution by Soil Sedimentation and Image Processing." Ph.D. Dissertation, University of Michigan.

Kim, H., Haas, C.T., Rauch, A.F., and Browne, C. (2002). "Wavelet-Based Three-Dimensional Descriptors of Aggregate Particles." Transportation Research Record: Journal of the Transportation Research Board, No. 1787, 109-116.

Koerner, R.M. (1969). "Limiting Density Behavior of Quartz Powders." Powder Technology, 3(1), 208-212.

Koerner, R.M. (1970). "Effect of Particle Characteristics on Soil Strength." Journal of the Soil Mechanics and Foundations Division, 96(4), 1221-1234.

Kokusho, T., Hara, T., and Hiraoka, R. (2004). "Undrained Shear Strength of Granualr Soils with Different Particle Gradations." Journal of Geotechnical and Geoenvironmental Engineering, 130(6), 621-629.

Krumbein, W.C. (1941). "Measurement and Geological Significance of Shape and Roundness of Sedimentary Particles." Journal of Sedimentary Petrology, 11(2), 64-72.

Krumbein, W.C., and Sloss, L.L. (1963). "Stratigraphy and Sedimentation." W.H. Freeman and Company, San Francisco.

Kumara, G.H.A.J.J., Hayano, K., and Ogiwara, K. (2012). "Image Analysis Techniques on Evaluation of Particle Size Distribution of Gravel." International Journal of GEOMATE, 3(1), 290-297.

Kuo, C.-Y. (2002). "Correlating Permanent Deformation Characteristics of Hot Mix Asphalt with Aggregate Geometric Irregularities." Journal of Testing and Evaluation, 30(2), 136-144.

Kuo, C.-Y., and Freeman, R.B. (1998). "Image Analysis Evaluation of Aggregates for Asphalt Concrete Mixtures." Transportation Research Record: Journal of the Transportation Research Board, No. 1615, 65-71.

Kuo, C.-Y., and Freeman, R.B. (2000). "Imaging Indices for Quantification of Shape, Angularity, and Surface Texture of Aggregates." Transportation Research Record: Journal of the Transportation Research Board, No. 1721, 57-65.

Kuo, C.-Y., Frost, J.D., Lai, J.S., and Wang, L.B. (1996). "Three-Dimensional Image Analysis of Aggregate Particles from Orthogonal Projections." Transportation Research Record: Journal of the Transportation Research Board, No. 1526, 98-103.

Kuo, C.-Y., Rollings, R.S., and Lynch, L.N. (1998). "Morphological Study of Coarse Aggregates Using Image Analysis." Journal of Materials in Civil Engineering, 10(3), 135-142.

Lee, J.R.J., Smith, M.L., and Smith L.N. (2007). "A New Approach to the Three-Dimensional Quantification of Angularity Using Image Analysis of the Size and Form of Coarse Aggregates." Engineering Geology, 91(2-4), 254-264.

Likos, W.J., and Lu, N. (2001). "A Laser Technique to Quantify the Size, Porosity, and Density of Clay Clusters During Sedimentation." Geotechnical Testing Journal, 24(1), 83-91.

Lindeberg, T. (1998). "Feature Detection with Automatic Scale Selection." International Journal of Computer Vision, 30(2), 79-116.

Maerz, N.H. (2004). "Technical and Computational Aspects of the Measurement of Aggregate Shape by Digiatal Image Analysis." Journal of Computing in Civil Engineering, 18(1), 10-18.

Mahmoud, E., and Masad, E. (2007). "Experimental Methods for the Evaluation of Aggregate Resistance to Polishing, Abrasion, and Breakage." Journal of Materials in Civil Engineering, 19(11), 977-985.

Mahmoud, E., Gates, L., Masad, E., Erdogan, S., and Garboczi, E. (2010). "Comprehensive Evaluation of AIMS Texture, Angularity, and Dimension Measurements." Journal of Materials in Civil Engineering, 22(4), 369-379.

Mahmoud, E., Masad, E., and Nazarian, S. (2010). "Discrete Element Analysis of the Influences of Aggregate Properties and Internal Structure on Fracture in Asphalt Mixtures." Journal of Materials in Civil Engineering, 22(1), 10-20.

Masad, E., and Tutumluer, E. (2007). "Test Methods for Characterizing Aggregate Shape, Texture, and Angularity." Transportation Research Board, NCHRP Report 555.

Masad, E., Button, J.W., and Papagiannakis, T. (2000). "Fine-Aggregate Angularity." Transportation Research Record: Journal of the Transportation Research Board, No. 1721, 66-72.

Masad, E., Olcott, D., White, T., and Tashman, L. (2001). "Correlation of Fine Aggregate Imaging Shape Indices with Asphalt Mixture Performance." Transportation Research Record: Journal of the Transportation Research Board, No. 1757, 148-156.

Matheron, G. (1975). "Random Sets and Intergral Geometry." John Wiley, New York.

Matthews, M.D. (1991). "The Effect of Grain Shape and Density on Size Measurement." Principles, Methods and Application of Particle Size Analysis, Cambridge University Press, Cambridge, UK, 22-33.

Meloy, T.P. (1977). "Fast Fourier Transforms Applied to Shape Analysis of Particle Silhouettes to obtain Morphological Data." Powder Technology, 17(1), 27-35.

Meyer, F., and Beucher, S. (1990). "Morphological Segmentation." Journal of Visual Communications and Image Representation, 1(1), 21-46.

Mikolajczyk, K., and Schmid, C. (2001). "Indexing Based on Scale Invariant Interest Points." Proceedings of the 8th IEEE International Conference on Computer Vision, 525-531.

Mishra, D., Tutumluer, E., and Xiao, Y. (2010). "Particle Shape, Type and Amount of Fines, and Moisture Affecting Resilient Modulus Behavior of Unbound Aggregates." Proceedings of the GeoShanghai 2010 International Conference, 279-287.

Mitchell, J. K. and Soga, K. (2005). "Fundamentals of Soil Behavior." John Wiley & Sons, New Jersey.

Mlynarczuk, M. (2009). "Description and Classification of Rock Surfaces by Means of Laser Profilometry and Mathematical Morphology." International Journal of Rock Mechanics and Mining Sciences, 47(1), 138-149.

Motoi, T., Ohira, Y., and Obata, E. (2010). "Measurement of the Floating Particle Size Distribution by a Buoyance Weighing-Bar Method." Powder Technology, 201(3), 283-288.

Ohm, H.-S., and Hryciw, R.D. (2012). "Particle Shape Determination in a Sedimaging Device." Proceedings of the 2012 World Congress on Advances in Civil, Environmental, and Materials Research, Seoul, Korea, 637-643.

Ohm, H.-S., and Hryciw, R.D. (2013a). "Enhanced Soil Characterization through Advances in Imaging Technology." Proceedings of the 18th International Conference on Soil Mechanics and Geotechnical Engineering, Paris, France (Submitted).

Ohm, H.-S., and Hryciw, R.D. (2013b). "Size Distribution of Coarse-Grained Soil by Sedimaging." Journal of Geotechnical and Geoenvironmental Engineering (Submitted).

Ohm, H.-S., and Hryciw, R.D. (2013c). "The Translucent Segregation Table Test for Sand and Gravel Particle Size Distribution." Geotechnical Testing Journal (Submitted).

Ohm, H.-S., Jung, Y., and Hryciw, R.D. (2014). "Morphological Opening to Determine Particle Size Distributions of Sedimented Soil Images." Powder Technology (Prepared for submission).

Ohm, H.-S., and Hryciw, R.D. (2014). "Soil Fabric Characterization by Wavelet Transformation of Images." Geo-Congress 2014, Atlanta (Abstract Submitted).

Ohm, H.-S., Sahadewa, A., Hryciw, R.D., Zekkos, D., and Brant, N. (2012). "Sustainable Soil Particle Size Characterization through Image Analysis." Proceedings of the 17th Great Lakes Geotechnical and Geoenvironmental Conference, Cleveland, Ohio, 26-33.

Ozgurel, H.G., and Vipulanandan, C. (2005). "Effect of Grain Size and Distribution on Permeability and Mechanical Behavior of Acrylamide Grouted Sand." Journal of Geotechnical and Geoenvironmental Engineering, 131(12), 1457-1465.

Pan, T. (2002). "Fine Aggregate Characterization Using Digital Image Analysis." Master's Thesis, Louisiana State University.

Pan, T., and Tutumluer, E. (2006). "Quantification of Coarse Aggregate Surface Texture Using Image Analysis." Journal of Testing and Evaluation, 35(2), 1-10.

Pan, T., Tutumluer, E., and Anochie-Boateng, J. (2006). "Aggregate Morphology Affecting Resilient Behavior of Unbound Granular Materials." Transportation Research Record: Journal of the Transportation Research Board, No. 1952, 12-20.

Pan, T., Wang, L., and Tutumluer, E. (2011). "Experimental Investigation of Aggregate-Mortar Interface Affecting the Early Fracture Toughness of Portland Cement Concrete." Internaional Journal of Pavement Research and Technology, Chinese Society of Pavement Engineering, 4(3), 168-175.

Qian, Y., Tutumluer, E., and Huang, H. (2011). "A Validated Discrete Element Modeling Approach for Studying Geogrid-Aggregate Reinforcement Mechanisms." Geo-Frontiers 2011, 4653-4662.

Rao, C., and Tutumluer, E. (2000). "Determination of Volume of Aggregates." Transportation Research Record: Journal of the Transportation Research Board, No. 1721, 73-80.

Rao, C., Tutumluer, E., and Kim, I.T. (2002). "Quantification of Coarse Aggregate Angularity Based on Image Analysis." Transportation Research Record: Journal of the Transportation Research Board, No. 1787, 117-124.

Rao, C., Tutumluer, E., and Stefanski, J.A. (2001). "Coarse Aggregate Shape and Size Properties Using a New Image Analyzer." Journal of Testing and Evaluation, 29(5), 461-471.

Raschke, S.A. (1996). "Computer Vision for Experimental Soil Micromechanics and Soil Characterization." Ph.D. Dissertation, University of Michigan.

Raschke, S.A., and Hryciw, R.D. (1997). "Grain-Size Distribution of Granular Soils by Computer Vision." Geotechnical Testing Journal, 20(4), 433-442.

Raschke, S.A., and Hryciw, R.D. (1997). "Vision Cone Penetrometer for Direct Subsurface Soil Observation." Journal of Geotechnical and Geoenvironmental Engineering, 123(11), 1074-1076.

Sallam, A.M. (2004). "Studies on Modeling Angular Soil Particles Using the Discrete Element Method." Ph.D. Dissertation, University of South Florida.

Sallam, A.M., and Ashmawy, A.K. (2009). "Effect of Particle Shape and Angularity on Dilation of Granular Soils: A Discrete Element Approach." Proceedings of the XVII International Conference on Soil Mechanics and Geotechnial Engineering, Alexandria, Egypt.

Santamarina, J.C., and Cho, G.C. (2001). "Determination of Critical State Parameters in Sandy Soils: Simple Procedure." Geotechnical Testing Journal, 24(2), 185-192.

Santamarina, J.C., and Cho, G.C. (2004). "Soil Behaviour: The Role of Particle Shape." The Proceedings of Skempton Conference, London, 604-617.

Shin, S. (2005). "High-Resolution Subsurface Soil Characterization by Image Analysis and Vision CPT." Ph.D. Dissertation, University of Michigan.

Shin, S., and Hryciw, R.D. (2004). "Wavelet Analysis of Soil Mass Images for Particle Size Determination." Journal of Computing in Civil Engineering, 18(1), 19-27.

Solomon, C., and Breckon, T. (2011). "Fundamentals of Digital Image Processing." Wiley-Blackwell, UK.

Stein, R. (1985). "Rapid Grain-Size Analyses of Clay and Silt Fraction by Sedigraph 5000D: Comparison with Coulter Counter and Atterberg Methods." Journal of Sedimentary Petrology, 55(4), 590-615.

Sukumaran, B., and Ashmawy, A.K. (2001). "Quantitative Characterisation of the Geometry of Discrete Particles." Géotechnique, 51(7), 619-627.

Sukumaran, B., and Ashmawy, A.K. (2003). "Influence of Inherent Particle Characteristics on Hopper Flow Rate." Powder Technology, 138(1), 46-50.

Tutumluer, E., and Pan, T. (2008). "Aggregate Morphology Affecting Strength and Permanent Deformation Behavior of Unbound Aggregate Materials." Journal of Materials in Civil Engineering, 20(9), 617-627.

Tutumluer, E., Pan, T., and Carpenter, S.H. (2005). "Investigation of Aggregate Shape Effects on Hot Mix Performance Using an Image Analysis Approach." Final Report Submitted to Federal Highway Administration.

Tutumluer, E., Rao, C., and Stefanski, J.A. (2000). "Video Image Analysis of Aggregates." Final Report Submitted to Federal Highway Administration, FHWA-IL-UI-278.

Vincent, L., and Soille, P. (1991). "Watersheds in Digital Spaces: An Efficient Algorithm Based on Immersion Simulations." IEEE Transactions on Pattern Analysis and Machine Intelligence, 13(6), 583-598.

Vipulanandan, C., and Ozgurel, H.G. (2009). "Simplified Relationships for Particle-Size Distribution and Permeation Groutability Limits for Soils." Journal of Geotechnical and Geoenvironmental Engineering, 135(9), 1190-1197.

Wadell, H. (1932). "Volume, Shape, and Roundness of Rock Particles." Journal of Geology, 40(5), 443-451.

Wang, L., Lane, S., Lu, Y., and Druta, C. (2009). "Portable Image Analysis System for Characterizing Aggregate Morphology." Transportation Research Record: Journal of the Transportation Research Board, No. 2104, 3-11.

Wang, L., Wang, X., Mohammad, L., and Abadie, C. (2005). "Unified Method to Quantify Aggregate Shape Angularity and Texture Using Fourier Analysis." Journal of Materials in Civil Engineering, 17(5), 498-504.

Wen, B., Aydin, A., and Duzgoren-Aydin, N.S. (2002). "A Comparative Study of Particle Size Analyses by Sieve-Hydrometer and Laser Diffraction Methods." Geotechnical Testing Journal, 25(4), 434-442.

Wettimuny, R., and Penumadu, D. (2004). "Application of Fourier Analysis to Digital Imaging for Particle Shape Analysis." Journal of Computing in Civil Engineering, 18(1), 2-9.

White, D.J. (2003). "PSD Measurement Using the Single Particle Optical Sizing (SPOS) Method." Géotechnique, 53(3), 317-326.

Wilson, J.D., and Klotz, L.D. (1996). "Quantitative Analysis of Aggregate Based on Hough Transform." Transportation Research Record: Journal of the Transportation Research Board, No. 1530, 111-115.

Xiao, Y., Tutumluer, E., and Siekmeier, J. (2011). "Resilient Modulus Behavior Estimated from Aggregate Source Properties." Geo-Frontiers 2011, 4843-4852.